DEVELOPMENT OF NANOSIZE LIPID BASED VESICULAR DELIVERY SYSTEM OF ZIDOVUDINE TO CROSS BLOOD BRAIN BARRIER

Thesis submitted by

LOPAMUDRA DUTTA

DOCTOR OF PHILOSOPHY (PHARMACY)

Department of Pharmaceutical Technology,
Faculty Council of Engineering & Technology
Jadavpur University
Kolkata, India

2018

JADAVPUR UNIVERSITY

KOLKATA-700 032, INDIA

INDEX NO. 230/15/Ph.

1. Title of the thesis: Development of nanosize lipid based vesicular delivery system of Zidovudine to cross blood brain barrier

2. Name, Designation & Institution of the Supervisor:

Prof. (Dr.) Biswajit Mukherjee,
Professor
Department of Pharmaceutical Technology
Jadavpur University
Kolkata-700 032

3. List of publications:

- **Lopamudra Dutta**, Biswajit Mukherjee, Tapash Chakraborty, Malay Kumar Das, Laboni Mondal, Sanchari Bhattacharya, Raghuvir H. Gaonkar and Mita Chatterjee Debnath. Lipid-based nanocarrier efficiently delivers highly water soluble drug across the blood-brain barrier into brain. Drug Delivery, 2018; 25(1): 504-516. **(Impact factor: 6.402)**.

- Sanchari Bhattacharya, Laboni Mondal, Biswajit Mukherjee, **Lopamudra Dutta**, Iman Ehsan, Mita C. Debnath, Raghuvir H. Gaonkar, Murari M. Pal and Subrata Majumdar. Apigenin loaded nanoparticle delayed development of hepatocellular carcinoma in rats. Nanomedicine: Nanotechnology, Biology and Medicine, 2018; 14(6): 1905-1917. **(Impact factor: 5.720)**.

- Biswajit Mukherjee, Paramita Paul, **Lopamudra Dutta**, Samrat Chakraborty, Moumita Dhara, Laboni Mondal and Soma Sengupta. Pulmonary administration of biodegradable drug nanocarriers for more efficacious treatment of fungal infections in lungs: insights based on recent findings. In: Grumezescu AM, eds. Multifunctional Systems for Combined Delivery, Biosensing and Diagnostics. Elsevier: Netherlands, United Kingdom, United States, 2017; pp 261-280.

- Biswajit Mukherjee, Samrat Chakraborty, Laboni Mondal, Bhabani Sankar Satapathy, Soma Sengupta, **Lopamudra Dutta**, Ankan Choudhury and Dipika Mandal. Multifunctional drug nanocarriers facilitate more specific entry of therapeutic payload into tumors and control multiple drug resistance in cancer. In: Grumezescu AM, eds. Nanobiomaterials in Cancer Therapy. Elsevier: United Kingdom, United States, 2016; pp 203-251.

- Biswajit Mukherjee, Paramita Paul, Ankan Choudhury, Sanchari Bhattacharya, Ruma Maji and **Lopamudra Dutta**. Variation of pharmacokinetic profiles of some antidiabetic drugs from nanostructured formulations administered through pulmonary route. Current Drug Metabolism, 2016; 17(3): 271-278. **(Impact factor: 2.659)**.

- Biswajit Mukherjee, **Lopamudra Dutta**, Laboni Mondal, Niladri Shekhar Dey, Samrat Chakraborty, Ruma Maji and Tapan Kumar Shaw. Nanoscale formulations and diagnostics with their recent trends: a major focus of future nanotechnology. Current Pharmaceutical Design, 2015; 21(36): 5172-5186. **(Impact factor: 3.052)**.

4. List of Patents: NIL

5. List of Presentations in National/ International/ Conferences/ Workshops

National

- Participated and presented paper in 3rd annual national seminar of All India Association of Medical Social Work Professionals on "**Social Work Practices in Health Care: Emerging Health Issues among Women**" at Safdarjung Hospital, New Delhi from 26th March to 27th March, 2016.

- Participated and presented poster in national seminar on "**Current Perspective of Nano-Technology for Drug Delivery**" held in College of Pharmaceutical Sciences, Puri, odisha on 19th February, 2016.

- Participated and presented poster in JU IAPST national seminar on "**Drug and Diseases: Role of Pharmacists and Doctors**" organized jointly by the Centre for Advance Research in Pharmaceutical Sciences, Department of Pharmaceutical Technology, Jadavpur University, Kolkata and Indian Association of Pharmaceutical Scientists and Technologists, Kolkata on 16th January, 2016.

- Participated and presented poster National seminar on "**Novel Pharmaceutical Technologies: Challenges and Opportunities**" held in Manipal college of Pharmaceutical Sciences, Manipal University, Manipal on 15th November, 2015.

International

- Participated and presented poster 4th international conference on "**Nanomedicine and Tissue Engineering**" organized by International and Interuniversity Centre for Nanoscience and Nanotechnology, Mahatma Gandhi University, Kottayam, Kerala, India and Wuhan University, China and Nicholas Copernicus University, Poland from 12th August to 14th August, 2016. (Achieved 2nd prize).

CERTIFICATE FROM THE SUPERVISOR

This is to certify that the thesis entitled **"Development of nanosize lipid based vesicular delivery system of Zidovudine to cross blood brain barrier"** submitted by **Mrs. Lopamudra Dutta**, who got her name registered on 07/04/2015 for the award of Ph.D. (Pharmacy) degree of Jadavpur University is absolutely based upon her own work under the supervision of **Prof. (Dr.) Biswajit Mukherjee**, Department of Pharmaceutical Technology, Jadavpur University, Kolkata - 700 032 and that neither her thesis nor any part of the thesis has been submitted for any degree/diploma or any other academic award anywhere before.

_____

Signature of the Supervisor
and date with Office Seal

DEDICATED

TO

MY RESPECTED PARENTS

&

BELOVED HUSBAND

ACKNOWLEDGEMENT

At this moment, that I am at the verge of accomplishing one of my dreams to achieve the doctorate degree in my field of academics, I would like to grab this occasion to express my thanks and gratitude to them without whom I couldn't have made it. I bow down to the omnipotent divine for manifesting itself through me and guiding me through the challenges and vagaries of life.

First of all, I would like to express my thanks, sincere gratitude and respect to my guide Prof. Biswajit Mukherjee, Department of Pharmaceutical Technology, Jadavpur University, Kolkata-700 032, India, who was behind me all along this work, supporting and guiding me in every possible way throughout the research work from title's selection to finding the results. Indeed, his valuable suggestions, insightful ideas, motivation and patience have provided me more power and spirit to excel a successful end on this research work. Conducting the research activities regarding such a difficult and valuable topic could not be possible without him. Not only he has been my mentor and advisor in academic supervision, but also his broad mind and immense knowledge about other fields has helped me to go forward in my life.

I extend my heartfelt thanks to Department of Biotechnology (DBT), Govt. of India, for providing the financial support to execute this research work. I would like to express my gratitude to the authorities of Jadavpur University and Head of the Department of Pharmaceutical Technology whose role, directly or indirectly during this research tenure, could never be ignored.

It gives me great pleasure in acknowledging Indian Institute of Chemical Biology (IICB), Kolkata; Indian Association for the Cultivation of Science (IACS), Kolkata; Indian School of Mines, Dhanbad; and Ballygunge Science College, Kolkata; for their cooperation and giving me the opportunity to use their facilities during this research period.

Besides, I would like to thank my fellow labmates too for their valuable help, the fun-time we spent together that gave me the courage to complete the research and for stimulating the discussions. I express my

thanks to seniors for their impressive practical suggestions and the friends and acquaintances who were with me all along this journey.

I am grateful to my parents and elder sister, who remembered me in their prayers for the ultimate success. I consider myself nothing without them. They gave me enough moral support, encouragement and motivation to accomplish this milestone.

Last but not the least, I am indebted to my husband, for his continuous motivation, sacrifice, positive attitude, support and understanding, that made the completion of this journey possible.

Pardon me for any inadvertent omission. However, I sincerely believe if my contributions in this thesis can better their life in some unforeseen ways, then perhaps that would be the best expression of gratitude from my part.

Date:

Place: Jadavpur, Kolkata *(Lopamudra Dutta)*

LIST OF ABBREVIATIONS

AFM	Atomic force microscopy
AIDS	Acquired immunodeficiency syndrome
AJs	Adherens junctions
AUC_{0-t}	Area under the concentration-time curve from time of injection to a determined time point
$AUMC_{0-t}$	Area under the first moment curve
AZT	Zidovudine
AZT-M	AZT myristate
AZT-SLNs	AZT loaded SLNs
AZTTP	AZT 5'-triphosphate
BBB	Blood-brain barrier
BHT	Butylated hydroxytoluene
CDS	Chemical delivery system
CHO	Cholesterol
Cl	Clearance
CNS	Central nervous system
Cryo-TEM	Cryo-transmission electron microscopy
CSF	Cerebrospinal fluid
DNL-PE	DSPE incorporated NLs
DSPE	Phosphotidylethanolamine
DTPA	Diethylenetriamine pentaacetic acid
FBS	Fetal bovine serum
FESEM	Field emission scanning electron microscopy

FITC	Fluorescein isothiocyanate (Isomer I)
FTIR	Fourier-transform infrared spectroscopy
HAART	Highly active antiretroviral treatment
HIV	Human immunodeficiency virus
i.v.	Intravenous
JAMs	Junctional adhesion molecules
LUVs	Large unilamellar vesicles
MEM	Minimum Essential Medium Eagle
ML	Fatty acid combination
MLVs	Multilamellar vesicles
MMA-SPM	Methylmethacrylate-sulfopropylmethacrylate
MRP	Multidrug resistance-associated protein
MRT	Mean residence time
n	Release exponent
NL	Nanoliposome
NLs	Nanoliposomes
NPs	Nanoparticles
OA	Oleic acid
PA	Palmitic acid
PBCA	Polybutylcyanoacrylate
PBS	Phosphate buffered saline
PDI	Polydispersity index
PEG	Polyethylene glycol
PEI	Polyethyleneimine
PLGA	Poly(lactic-co-glycolic acid)

PLNs	Polymer-lipid hybrid NPs
R^2	Correlation coefficient
SA	Stearic acid
SE	Surface engineered
SEM	Scanning electron microscopy
SL	Soya lecithin
SLM	Solidified reverse micellar microparticulate
SLMs	Solid lipid microparticles
SLNs	Solid lipid NPs
SUVs	Small unilamellar vesicles
$t_{1/2}$	Time taken for maximum blood concentration to drop in half-life
TJs	Tight junctions
UDCA	Ursodeoxycholic acid
USFDA	United States Food and Drug Administration
Vss	Steady state volume of distribution
ZO	Zonula occludens
3TC	Lamivudine
^{99m}Tc	Technetium-99m
λ_{max}	Absorption maxima

CONTENTS

LIST OF FIGURES

LIST OF TABLES

Chapter 1

Introduction

1. Introduction

1.1. Background

Blood-brain barrier (BBB), a complex tight endothelial vascular lining, is the main hindrance of most chemicals for free diffusion and penetration into the brain from blood stream of body for maintaining homeostasis in brain (Seju et al., 2011; Martins et al., 2012). BBB acts as a safeguard of brain from exogenous toxic agents as well as rejecter of essential therapeutic agents (Hu et al., 2009). Nearly 100 % of large molecular drugs and about 98 % of drugs consisting of small molecules are unable to cross BBB to provide therapeutic outcome (Wilson et al., 2008; Hu et al., 2017). Various novel drug delivery systems such as nanoparticles (NPs), nanoliposomes (NLs), micelles, dendrimers, quantum dots, and nanoemulsions are applied to overcome the limitations (Li et al., 2017). Nowadays, nanosize drug delivery into brain across BBB is an emerging field of pharmaceutical research. In the current study, we have selected lipid-based nanoliposomal drug carrier to deliver drug into brain. It is always an enormous challenge for formulation scientists to deliver highly water soluble drug into brain across BBB and the same is true for many other large molecules.

1.2. BBB - a dynamic interface

Structural, biochemical and highly selective barrier which is known as BBB serves as a safeguard against environmental impacts and detrimental exterior agents and keeps maintaining the nutrients supply through intracerebral milieu into the brain (Tajes et al., 2014). BBB shields brain from the molecules which are present in systemic circulation and it is the foremost obstacle during the treatment to get proper therapeutic efficacy in various diseases such as neurodegenerative diseases, brain cancer, psychiatric disorders, and microbial pathogenesis such as acquired immunodeficiency syndrome (AIDS), etc. (Tajes et al., 2014; Alyautdin et al., 2014).

In 1885, Paul Ehrlich revealed the presence of hematoencephalic barrier at first. He applied a dye named trypan blue through intravenous (i.v.) route in animals and explained that peripheral tissues were stained due to the dye after extruding from blood capillaries as well as the brain was not stained. A property of lower affinity of dye to brain was established by Ehrlich. Further, Edwin Goldmann confirmed the existence of a barrier between the blood and cerebrospinal fluid (CSF) after the investigation where only brain was stained due to inject of dye in CSF where as other tissues were not stained. Lewandowsky created or applied the word "BBB" ("Blut-Hirn-Schranke") in 1900. In 1929, LS Stern first announced the word "histohematic barrier". After 1960, scientists recognized extensively the presence of BBB (Ribatti et al., 2006; Alyautdin et al., 2014). In early 1970s, Oldendorf coined the term "brain uptake index (BUI)" using to quantify BBB permeability (Oldendorf, 1971). Various characteristics such as molecular weight, lipid solubility, physico-chemical characteristics, etc. of compounds may predict the entrance rate of such compounds through BBB applying this method (Banks et al., 1999). Initiation and improvement of *in vitro*, *in situ*, *in vivo* experiments in this era were extensively performed in 1970s and 1980s (Patlak et al, 1983; Blasberg et al, 1983; Takasato et al,1984; Zlokovic et al, 1986; Raeissi and Audus, 1989; Barrera et al, 1991).

Human brain capillaries are approximately 650 km in length along with about 20 m^2 of total surface area (Pardridge, 2002; Cecchelli et al., 2007). BBB generates ionic homeostasis for the functions of neuron (Abbott, 2002) and utilizing intricate transport systems BBB supplies nutrients in Central nervous system (CNS) as well as shields it from any kind of toxic agents (Abbott et al., 2006). Hydrophilic drugs and molecules having mass greater than 400 Da are unable to cross BBB due to lower degree of paracellular flux along with transendothelial vesicular trafficking. On the other hand, lipophilic drugs and xenobiotics are restricted to

enter in brain by the efficacious efflux transporters present in luminal membrane of endothelial cells of brain (Deli, 2011).

1.3. Structure of BBB

BBB comprises of blood vessels that construct by expert endothelial cells, basal lamina, astrocytes, pericytes and neurons (Risau and Wolburg, 1990; Abbott and Romero, 1996; Abbott et al., 2006; Weiss et al., 2009).

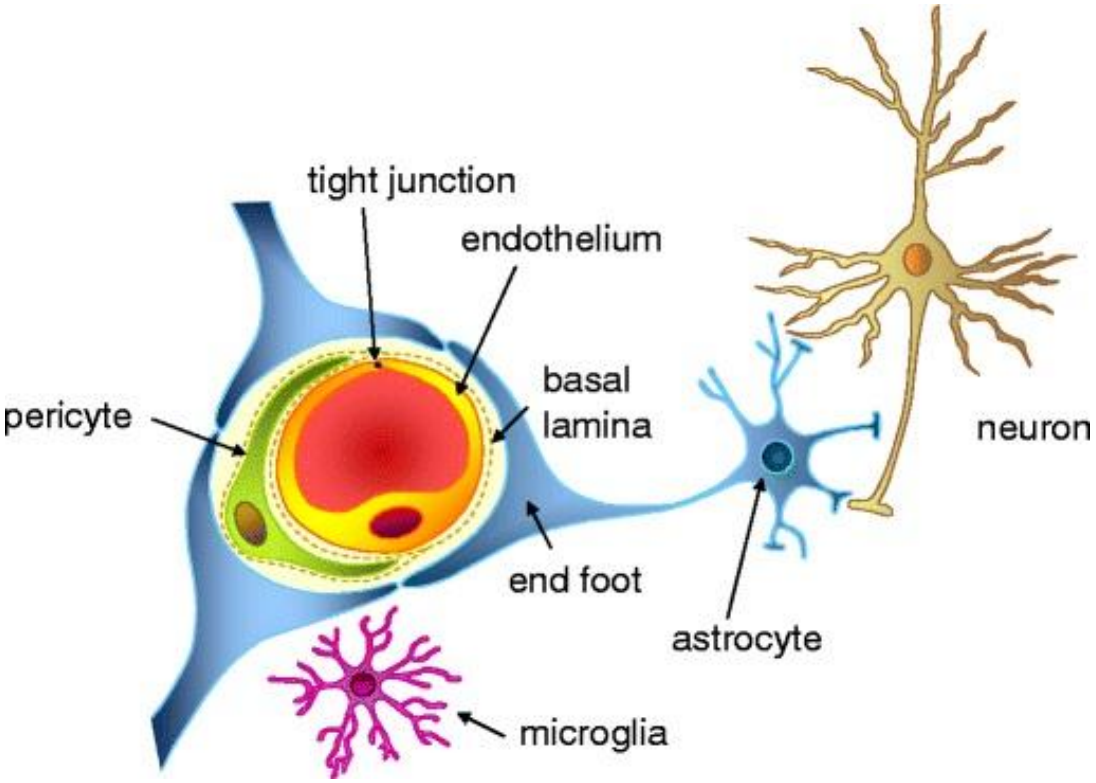

Figure 1.1: The neurovascular unit of brain consisting of endothelium, basal lamina, astrocyte, pericyte and neuron (Abbott, 2013).

1.3.1. Endothelial cells

Brain endothelial cells are different than the peripheral endothelial cells. Lack of endocytic vesicles restricts the transcellular flux. Absence of fenestrations is also special characteristics of endothelial cells. Tight junctions of endothelial cells are responsible for high electrical resistance which limits the paracellular flux. Higher amount of cytosolic mitochondria

increases cellular metabolism. Superior transport mechanism is also special attractiveness of brain endothelial cells (Brightman and Kadota, 1992; Rubin and Staddon, 1999; Abbott, 2005; Ballabh et al., 2004; Chaudhuri, 2000). Alkaline phosphatase, γ-glutamyl-transpeptidase (GGTP), glucose transporter-1 (GLUT-1) and von Willebrand factor (vWf) are the special characteristic markers of brain endothelial cells. P-glycoprotein (Pgp) and multidrug resistance-associated protein (MRP) are remarkable two N-glycosylated phosphoproteins of brain endothelial cells (Balkovetz et al., 1989; Bernacki et al., 2008).

1.3.2. Basal lamina

Three layers are gathered together side by side to form basal lamina. One layer is generated by brain endothelial cells and contains laminin-4 and laminin-5. Another one, containing laminin-1 and laminin-2, is a resultant of astrocyte. Both the cells help to form middle layer containing collagen IV. Various glycoproteins, collagens, proteoglycans are present in these three layers. Basal lamina has a great contribution to maintain the integrity of BBB (Wolburg and Lippoldt, 2002; Perlmutter and Chui, 1990; Abrahamson, 1986; Berzin et al., 2000).

1.3.3. Astrocytes

Ectoderm of neural tube produces astrocytes and about 11 phenotypes attributed for astrocytes. Functional polarity generates due to cross cellular interactions of astrocytes. In brain mainly two types of cells of astrocytes are observed. They are protoplasmic cells and fibrillary cells. Protoplasmic cells which are present in grey matter contain several dense cytoplasmic appendices whereas in white matter fibrillary cells are localized. The term “end feet” means cap like structure formed by endings of appendices. These end feets attach strongly with blood vessels and also with neurons and produce a definite transmit place between blood and neurons (Abbott et al., 2006; Abbott, 2007; Reichenbach and Wolburg, 2004). Astrocytes have significant contribution in metabolism of neurons, excretion of

utilized substrate and nutrition and also perform an important role in transcytosis as well as active ion transport (Bernacki et al., 2008). To maintain the integrity of BBB, astrocytes play a vital part which was already published earlier (Janzer and Raff, 1987).

1.3.4. Pericytes

A specific type of mesenchymal cell is known as pericytes which is present in large amount in brain microvessels. The space in the middle of the astrocytes end feet and capillary wall is engaged by pericytes. Pericytes play very important activities such as integrity maintaining of vessels, sustaining vasculature stability, angiogenesis, and stability and also performing BBB permeability restriction and brain homeostasis (Lindahl et al. 1997; Peppiatt et al., 2006; Kutcher and Herman, 2009).

1.3.5. Neurons

Various projections of neurons are closely associated with endothelial cells, astrocytes and also with pericytes to form BBB and it has impacts on vessel dynamics and cerebral blood flow (Hellstrom et al., 2001; Kacem et al., 1998; Weiss et al., 2009)

1.4. BBB endothelial junctions

Tissue integrity as well as vascular permeability maintenance is a fundamental work of intercellular junctions. There are two junctions such as “tight junctions (TJs) and adherens junctions (AJs) which are associated with BBB (Zlokovic, 2008; Tietz and Engelhardt, 2015; Wallez and Huber, 2008).

1.4.1. TJs

TJs exist in the most outside part of two endothelial cells junctions and act as a margin among basolateral and apical plasma membrane areas (Bednarczyk and Lukasiuk, 2011). TJs restrict protein diffusion within compartments of membrane and manage cell trafficking

between blood and CNS by sealing the paracellular space among the endothelial cells of brain capillary (Zlokovic, 2008; Tietz and Engelhardt, 2015) with sealing proteins such as transmembrane molecules (claudin, occludin) and junctional adhesion molecules (JAMs). Integrity of TJs is influenced by the concentration of extracellular Ca^{2+} ion and depending on high electrical resistance (1500-2000 Ωcm^2) TJs are categorized. Stability of TJs is disturbed by a drop of electrical resistance. Fusion points are formed by increasing amount of intracellular cATP resulting tightness of TJs. Opposite incidents appear due to phorbol esters (Ballabh et al., 2004). Additionally cytoplasmic proteins such as various zonula occludens (ZO) like ZO-1, ZO-2, ZO-3 and cingulin (Ballabh et al., 2004) that create link between actin and transmembrane proteins have been distinguished.

1.4.1.1. Claudins

Claudins, 22 kDa phosphoproteins, contain four transmembrane domains and act as a backbone of TJs. The primary closure of TJs takes place by the connection between claudin of a brain-endothelial cell with an analogous claudin of another adjacent brain endothelial cell (Bernacki et al., 2008). Claudins 1, 3, 5 and 12 have been found to express in cerebral microvascular endothelium (Liebner et al., 2000; Nitta et al., 2003; Wolburg et al., 2003).

1.4.1.2. Occludin

Occludin, phosphoprotein, containing four transmembrane domains is greater as compared to claudin (60 kDa). Paracellular part of TJ is made by two extracellular loops elongated from claudin and occludin. On the other hand, cytoplasmic domain is compactly associated with ZO proteins (Balda et al., 2000; Furuse et al., 1993; Schneeberger and Lynch, 2004). Occludin plays normally regulatory activities along with maintaining paracellular transport (Hirase et al., 1997). Hydrophilic molecules and various ions are selectively transported by heteropolymers as well as transcellular tracts associated with various channels formed by

occludins and claudins (Balda et al., 2003). Occludins also try to maintain electrical resistance of blood barrier and to form aqueous pore (Tsukita et al., 2001).

1.4.1.3. JAMs

JAMs are especially immunoglobulins which help to construct TJs dynamically. They are third group of membrane proteins having about 40 kDa molecular mass. Single transmembrane domain of them is attached along with extracellular portion which contains twice immunoglobulin-like loops (Petty and Lo, 2002). There are three modifications which identified till now. They are JAM-1, JAM-2 and JAM-3. In brain vessels, JAM-1 and JAM-3 are observed strictly whereas JAM-1 is confined as a single or clustered form in interendothelial junctions randomly. JAMs actively work in monocyte extravasation and cell adhesion activities (Palmeri et al., 2000) and also maintain transendothelial migration process of leukocytes (Hawkins and Davis, 2005).

1.4.2. AJs

AJs are formed by large family of cadherin which is a type of transmembrane glycoprotein. AJs play a vital role in tightening of junctional complex of brain endothelial cells and also in maintenance of TJs. The main cadherin in this cadherin superfamily is vascular endothelium cadherin which produces homotypic adhesive complexes in presence of calcium ion by interacting with adjacent cells (Takeichi, 1995; Petty and Lo, 2002). The anchor proteins belonging to Armadillo superfamily such as α-catenin, γ-catenin, β-catenin, etc. produce linkage through a cytoplasmic plaque between glycoproteins and cytoskeleton (Nagafuchi and Takeichi, 1989; McCrea and Gumbiner, 1991). The α-catenin, β-catenin and γ-catenin form a complex together that links with actin cytoskeleton by α-catenin (Lampugnani et al., 1995). The newly discovered p120-catenin has highly binding affinity with vascular

endothelium cadherin to maintain permeability activity as well as function of BBB (Hatzfeld, 2005; Bazzoni, 2006).

1.5. Transport across the BBB

1.5.1 Passive transcellular transport for lipophilic molecules

Small molecules with molecular weight 400 to 500 and having lipophilic nature take entry into brain through lipid-mediated free diffusion process. Alcohol, nicotine, heroin, caffeine, etc. which belong under drugs of abuse category and neurotherapeutics containing small molecules easily cross BBB by this process. If molecules are highly lipophilic, problem is also arised due to increasing uptake of them through peripheral tissues and also seclusion of the molecules in microvasculature of brain resulting insufficient delivery of that molecule into brain (Pardridge, 2002; Banks, 2009). High polar surface area of compounds is also a cause of restriction of entry in CNS. More than six hydrogen bond forming inclination is a vital factor in this area (Clark, 2003; Gleeson, 2008). Penetration in CNS is pointedly reduced by high plasma protein binding affinity with a low off-rate. But there are also some examples of exception (Bodor and Buchwald, 2003).

1.5.2. Passive paracellular transport for hydrophilic molecules

Tight endothelial junctions of BBB inhibit hydrophilic substances to enter freely in brain by restricting the paracellular pathway. They also restrict the entry of peptides, polysaccharides, proteins, etc. into brain through crossing BBB freely. As many of drugs related to CNS disease are hydrophilic, low penetration of those drugs into brain via BBB occurs (Pardridge, 2002).

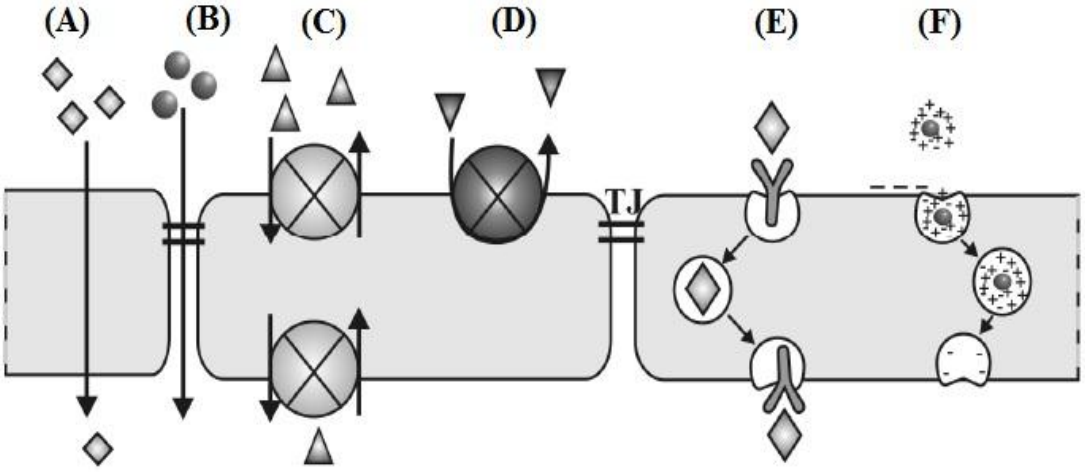

Figure 1.2: Different transport process across BBB. (A) Passive transcellular transport for lipophilic molecules, (B) Passive paracellular transport for hydrophilic molecules, (C) Carrier mediated transport, (D) Efflux transport, (E) Receptor mediated transcytosis, (F) Adsorptive mediated transcytosis (Deli, 2011).

1.5.3. Carrier mediated transport

The carrier-mediated transport is an energy dependent or independent saturable process. This transport procedure facilitates the substance-exchange phenomenon among brain parenchyma and systemic circulation (Brasnjevic et al., 2009).Various nutrients, minerals and vitamins are transported through this process into brain across the BBB (Abbott et al., 2010). Using consecutive gene expression analysis, solute carrier (SLC) family (approximately 40 members) was recognised in microvessels of brain for transportation (Enerson and Drewes, 2006). Various carrier systems express actively as a vehicle of many molecules in brain endothelial cells (Tamai and Tsuji, 2000). Proteins for glucose transportation such as GLUT-1 (SLC2A1), GLUT-3 (SLC2A3) are known as glucose transporters and SGLT2 (SLC5A2) is identified as sodium glucose co-transporter. Monocarboxylic acids transporters such as MCT-1, -2, and -6 (SLC16A1, 2, 6) are expressed in absence of glucose in endothelial cells of brain. N- or L- system helps for transportation of neutral, aromatic and large amino acids where as neutral small amino acid is transported in brain by A-system (Cancilla and DeBault, 1983).

1.5.4. Efflux transport

It is already established that a rising quantity of efflux transporters are present in the region of BBB (Enerson and Drewes, 2006; Fricker and Miller, 2004; Terasaki and Ohtsuki, 2005). The efflux transporters regulate active transport process by removing of substrates from CNS as well as transferring them into systemic circulation to avoid accumulation of compounds for crossing BBB (Loscher and Potschka, 2005; Newton, 2006). Due to efflux pumps the drugs which are able to cross BBB are unable to reach in therapeutically effective concentrations as the drugs are carried from parenchyma to luminal membrane and sent to systemic circulation. This makes those drugs inefficacious in various disease conditions. So, drug penetration in brain is restricted by the efflux transporters and thus, it is a crucial problem to treat various diseases such as brain tumours, neurodegenerative disorders, AIDS, stroke, etc. The ATP binding cassette which is known as ABC transporters. P-glycoprotein (ABCB1), brain multidrug resistance proteins such as BCRP / ABCG2 / BMDP, and multidrug resistance proteins such as MRP-1, MRP-4, MRP-5 and MRP-6 (ABCC1-6) belong to the ABC transporters and express in brain capillaries. High concentration of P-glycoprotein restricts the toxins or drugs accumulation in brain and protects the neuron viability (Schinkel et al., 1994; Schinkel et al., 1996). Dauchy and his groups revealed the expression of MRP-12 in BBB (Dauchy et al., 2005). Various efflux transporters regulate excitatory neurotransmitter glutamate level in brain. Excitatory amino acid transporters such as EAAT-1, EAAT-2, EAAT-3 and EAAT-4 existing in endothelial cells of brain maintain the magnitude variation up to 2-3 orders among blood and CNS in respect of glutamate concentration (O'Kane et al., 1999; Hosoya et al., 1999).

1.5.5. Receptor mediated transcytosis

For selective uptake of macromolecules receptor-mediated transcytosis is the excellent choice of BBB. Various receptors to take up different types of ligands, enzymes, plasma proteins, growth factors are present in brain endothelial cells (Chen and Leu et al., 2012). Transcytosis has three phases. At the first phase, receptor-mediated endocytosis takes place at the luminal membrane of endothelial cells of brain. Then transcytosis takes place by cytoplasm of cells. At last, at the abluminal side of endothelium, exocytosis occurs to complete this total process (Pardridge, 2002). Caveolae helps to regulate endocytosis and transcytosis (Zlokovic, 2008). Receptor-mediated transport is influenced by temperature (Tajes et al., 2014). Penetration of protein and peptides and also their clearance are ensured by receptor-mediated transcytosis in brain. Insulin, transferrin, leptin, melanotransferrin, low density lipoproteins, ghrelin, etc. are reached in brain through this mechanism (Pardridge, 2002; Banks, 1999; Zlokovic, 2008). For transferrin it follows bidirectional path i.e. blood to brain as well as brain to blood. But in case of immunoglobulin G, unidirectional transport is caused by Fc receptor of BBB from brain to blood only (Pardridge, 2002). This receptor-mediated transcytosis does not depend on lipophilicity as well as size of molecules (Tajes et al., 2014).

1.5.6. Adsorptive mediated transcytosis

The unregulated outflow of serum proteins into brain due to deficiency of endothelial fenestrations and decreasing pinocytosis rate are inhibited by restricted paracellular pathway in physiological conditions and it, thereby, protects neurons from toxicity. In peripheral endothelial cells, albumin is transferred by adsorptive-mediated transcytosis which is suppressed in brain. This transport process again continues in various diseased conditions such as oedema in brain, seizures and due to presence of pathological mediators (Deli, 2011).

1.6. Functions of BBB

BBB performs several functions which are mentioned below (Abbott, 2013; Shatzmiller et al., 2016).

i. BBB is able to protect the brain by restricting the entry of foreign substances which is already in systemic circulation at various disease states.
ii. BBB protects the brain from neurotransmitters as well as hormones from rest of the body.
iii. BBB regulates properly molecular traffic and shields the brain from toxins.
iv. BBB is able to minimize the death of neuronal cells and maintains neural connectivity.
v. BBB has a contribution in maintaining ion homeostasis for optimum neural signalling.
vi. Central and peripheral neurotransmitter pools are separated by BBB. It decreases cross-talk and permits non-synaptic signalling in CNS.
vii. Low protein atmosphere in CNS is sustained by BBB.
viii. BBB tolerates immune investigation and gives response in cell damage condition as well as minimum inflammation.

1.7. Nanocarriers for drug transport across BBB into brain

Using different methods the therapeutic or preventive or diagnostic molecules can be dissolved, adsorbed, encapsulated or entrapped, attached covalently with nanomaterials to provide nanosize drug carrier systems in various forms such as NPs, micelles, nanogels, quantum dots, nanoemulsions, dendrimers, liposomes, etc. Nanosize (1-1000 nm) makes these formulations unique on the basis of activities and properties. Due to very small size (6-9 µm) of blood capillaries in respect to diameter and small size (10-20 µm) of cells in human body, nanocariers are easily able to enter in different organs through blood and are adsorded or taken up by the cells for delivering drugs at proper site of action. Specially, nanocarriers

are also able to cross BBB to deliver drugs into brain after applying some modifications (Li et al., 2017).

1.7.1. NPs

NPs, spherical submicron size structures, are capable to deliver drug in targeted and / or controlled manner resulting enhanced therapeutic efficacy and minimize side-effects. Natural polymers such as chitosan, heparin, dextran, alginates, collagen and gelatin, and synthetic polymers, such as polycaprolactone (PCL), polylactic acid (PLA), polyethylene glycols (PEGs), N-(2-hydroxypropyl)-methacrylamide copolymer, polystyrene-maleic anhydride copolymer, poly-L-glutamic acid (PGA) are utilized to formulate the polymeric NPs. NPs can be conjugated with antibody such as monoclonal antibodies (mAbs) for selective binding with specific antigens to enhance intracellular stability and cellular uptake. The United States Food and Drug Administration (USFDA) approved the polymer poly(lactic-co-glycolic acid) (PLGA) for systemic application (Mukherjee et al., 2016; Mukherjee et al., 2015). Autoxidation-mediated toxicity in brain is decreased and neurobehavioral and neurochemical deficits are reversed by application of dopamine containing PLGA NPs in parkinsonian rats (Pahuja et al., 2015). Protein based formulations are also recognised because of their potentiality, biocompatibility, biodegradability, lower toxicity. Ferritin / apoferritin protein cage, the small heat-shock protein cage, plant-derived viral capsids, collagen, albumin, gelatin etc. are under investigation for delivering drug at desired site of action (Mukherjee et al., 2016). The permeability of polymeric NPs across BBB are increased by application of surfactants such as polysorbate 80 coated poly(butylcyanoacrylate) (PBCA) NPs to successfully deliver drugs such as rivastigmine, leu-enkephalin dalargin, tacrine, met-enkephalin kyotorphin across BBB (Alyautdin et al., 1997; Schroder and Sabel, 1996; Schroeder et al., 1998; Wilson et al., 2008; Wilson et al., 2008) .

Solid lipid NPs (SLNs), nanosize dispersion, are prepared from biocompaticle lipids such as fatty acids or waxes, triglycerides and stabilized using surfactants which have hydrophile-lipophile balance (HLB) values below 12. Atazanavir reaches in human brain endothelial cells *in vitro* after applying it through SLNs which is prepared using stearic acid (SA) and stabilized by pluronic®F68. Using ligands with SLNs, the NPs can be used to deliver drug into brain across BBB (Mehnert and Mader, 2001; Blasi et al., 2007; Chattopadhyay et al., 2008).

1.7.2. Polymeric micelles

Polymeric micelles are nanodimentional (normally 5-100 nm) colloidal structures which are formulated using an amphiphilic polymer consisting hydrophobic as well as hydrophilic units. The amphiphiles are normally belongs as monomers in an aqueous media at low concentration. But they are aggregated and self-assembled at a range of certain concentration to produce special structure called micelles. Micelles are applied for delivery of hydrophobic drugs as two distinctive regions such as hydrophilic head-group and hydrophobic core are present (Mukherjee et al., 2015). Drug loading in polymeric micelles is easily done by physical encapsulation and or by chemical covalent attachment. Various external stimuli such as temperature, ultrasound, enzymes, pH may be capable to regulate the release of drug from micelles (Mukherjee et al., 2016). The transcriptional activator peptide TAT conjugated polymeric micelles fabricated from cholesterol (CHO)-conjugated PEG are established to deliver antibiotics in brain across BBB (Liu et al., 2008). The polymeric mixed micelles were formulated by using pluronic F127 and D-α-tocopheryl polyethylene glycol succinate (TPGS) and they are shown to efficiently deliver dyes and proteins in brain through BBB (Meng et al., 2017).

1.7.3. Nanogels

Nanosize particles, physical or chemical crosslinked networks formed by polymer, are able to swell in a proper solvent known as nanogels. The crosslinked bifunctional networks between a non-ionic and polyionic polymer was first familiarized as “nanogel” for delivering polynucleotides (cross-linked polyethyleneimine (PEI) and PEG or PEG-*cl*-PEI) (Sultana et al., 2013). Nanogels deliver drugs by sustained, controlled as well as targetable manner. It is already well-known that lipophilic molecules easily cross the BBB as compared to hydrophilic molecules. To enhance the transportation of encapsulated drug across BBB, surface modification of nanogels has been established (Li et al., 2017). Methotrexate encapsulated chitosan nanogels were shown to remarkably deliver the drug in brain (Azadi et al., 2013). Vinogradov and his co-workers proved that nanogels worked as a favourable system to deliver oligonucleotide into brain (Vinogradov et al., 2004).

1.7.4. Quantum dots

Quantum dots which are inorganic tiny semiconductor crystals having diameter ranging from 2 to 10 nm and they consist of 10-50 atoms of elements belonging to the group II to IV or III to V of the periodic table. They have mainly two units such as crystalline metalloid core and shell for protecting core. Various modifications of quantum dots are possible through conjugation by specific ligands or bioactive moieties such as antibodies, receptors, and ligands. The light emission and absorption properties of quantum dots are regulated by their shape and size which can be adjusted as per requirement. Quantum dots are preferably utilized due to some of their special characteristics such as long standing stability, and higher sensitivity. But toxicity level of them should be under limitation as well as investigation which occurs due to the presence of hazardous heavy metals (Walling et al., 2009; Kim, 2007; Mukherjee et al., 2016). The theranostic quantum dots offer an approach for expressively improving dosage efficacy level of drugs to traverse through BBB (Xu et al.,

2013). The asparagines-glycine-arginine peptide modified PEGylated quantum dots under non-toxic concentration are able to cross BBB and target the CD13-overexpressing glioma as well as tumor vasculature (Huang et al., 2017).

1.7.5. Nanoemulsions

The stabilized biphasic dispersion formed by two types of immiscible liquids such as oil-in-water (O/W) and water-in-oil (W/O) is known as nanoemulsion. The stabilization of this dispersion is done using amphiphilic surfactant. The ultrafine emulsions possess some favourable significant properties such as visual properties, viscoelasticity, differential drug loading capacity, etc. which is helpful for drug delivery (Singh et al., 2017). Droplets sizes are regulated by the structure of surfactant phase at inversion point initiated by composition or temperature. Nanoemulsion is protected from creaming or sedimentation due to their small droplet size (droplet diameter 10-500 nm). Nanoemulsions may create a new era for novel drug delivery due to their controlled and sustained drug release properly (Sharma et al., 2013). Indinavir loaded tween 80 containing lipid nanoemulsion showed that it is capable to deliver indinavir into brain across BBB (Prabhakar et al., 2013).

1.7.6. Dendrimers

Dendrimer having tree-like closely packed dense structure is synthetic polymer-based macromolecular nanocarrier. They have extraordinary molecular uniformity, nanosize (about 1-10 nm), lower polydispersity index and they possess three units such as principal central core, peripheral terminal groups and repeating units. The drug delivery through dendrimers is performed by physical entrapment of drug inside the dendrimeric cavity or by conjugation at the peripheral terminal groups. This is applicable for delivering hydrophilic as well as hydrophobic drugs. Nonpolar cavities of dendrimers are utilized for incorporation of

hydrophobic drugs. On the other hand, hydrophilic drug delivery is possible by the appropriate modifications of the internal dendrimeric cavities. This type of nanocarrier offers some advantages such as better pharmacokinetic and pharmacodynamics profile, controlled drug release profile etc. (Mukherjee et al., 2015; Mukherjee et al., 2016; Srinageshwar et al., 2017). It has been already established that poly-amidoamine (PAMAM) dendrimers crossed BBB after administering through carotid artery in mice (Srinageshwar et al., 2017). Transferrin bearing polypropylenimine dendrimer is a successful carrier system for targeted gene delivery into brain (Somani et al., 2014).

1.7.7. Liposomes

Very well-known nanocarriers, liposomes, are inspected in details for targeting various drugs. They are able to stabilize therapeutic agents, avoid the difficulties of cellular and tissue uptake and progress the biodistribution process of therapeutic agents in a site specific way (Sercombe et al., 2015). At Babraham Institute in Cambridge, Dr. Alec D Bangham, British haematologist, first described regarding liposomes. During the testing of electron microscope by adding of negative stain to phospholipids, Dr. Bangham and R. W. Home discovered liposomes (Pawar et al., 2013). At the beginning, liposomes were utilized for observing of physical characteristics of biological membranes such as orientation of lipids in bilayer, transportation of ions through bio-membranes, etc. but at present it is extensively tried to use for drug delivery purpose (Pandey et al., 2016).

The nanosize version of liposome is a spherical, nanosize, closed colloidal structure having lipid bilayer with a unilamellar or multilamellar vesicle having aqueous core. It has surrounded by bilayered lipid. Different phospholipids such as phosphatidylcholine, phosphatidylglycerol, phosphatidylethanolamine, phosphatidylserine, etc. and other component such as CHO are normally used for preparation of liposomes. Inside the lipid

bilayer, hydrophobic tail of lipid is remained inwards whereas hydrophilic head is positioned towards the surface. By altering various factors such as composition of lipids, size, surface charge, liposomes can be used in drug delivery purposes efficiently as they are able to incorporate hydrophobic as well as hydrophilic drugs (Mukherjee et al., 2016). Hydrophilic molecules are entrapped in aqueous core whereas hydrophobic molecules can be placed into lipid bilayer (Koning and Storm, 2003; Ding et al., 2006; Hua and Wu, 2013). Various macromolecules such as proteins, DNA, imaging agents, etc. can be delivered due to huge aqueous core and biocompatible external lipid parts (Ulrich, 2002; Monteiro et al., 2014).

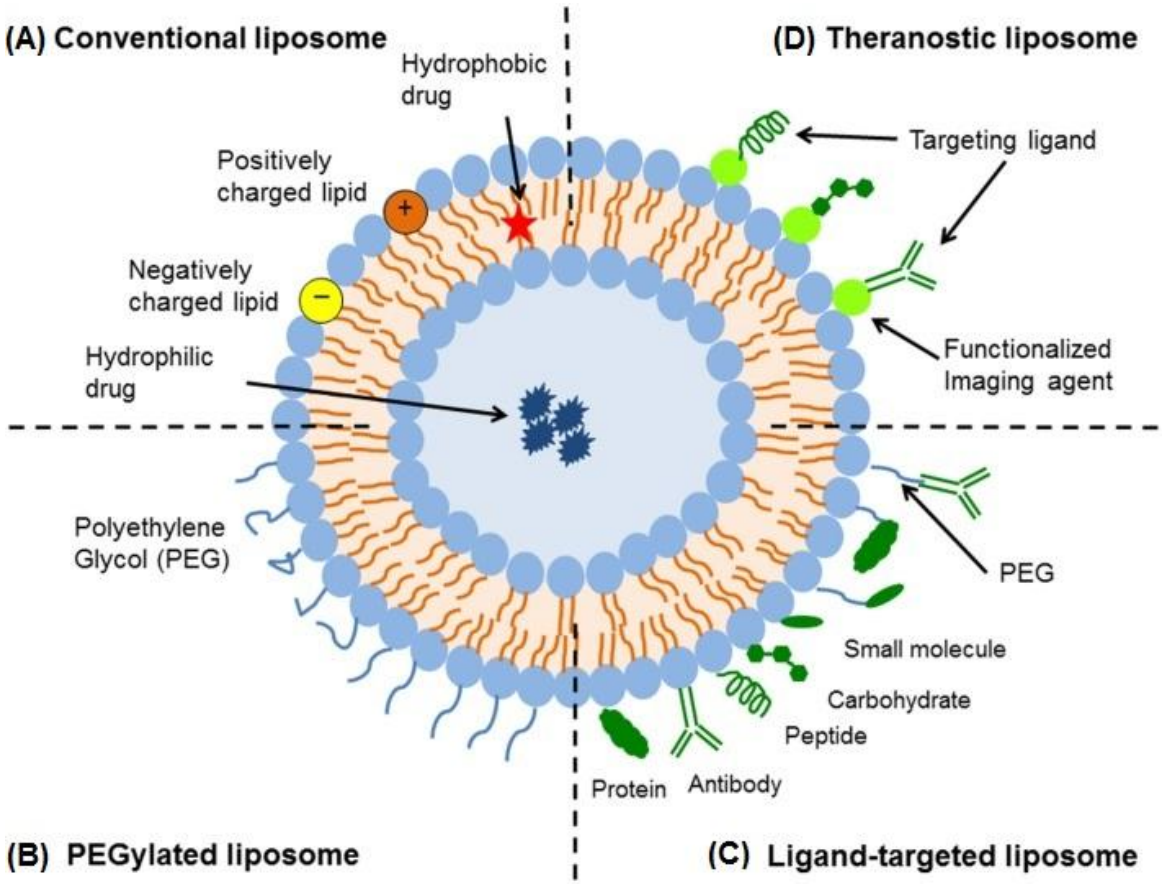

Figure 1.3: Schematic diagram of liposomal drug delivery system. (A) Conventional liposome, (B) PEGylated liposome, (C) Ligand-targeted liposome, (D) Theranostic liposome (Sercombe et al., 2015).

Liposomes have several advantages such as flexibility, devoid of toxicity, biocompatibility, complete biodegradability, non-immunogenicity during non-systemic as well as systemic administrations. It is capable to increase the efficiency and therapeutic index of encapsulated drug, reduce toxicity of entrapped therapeutic agent and improve pharmacokinetic effects by decreasing elimination and enhancing blood circulation time (Akbarzadeh et al., 2013; Dua et al., 2012).

1.7.7.1. Types of liposomes

There are three types of parameters based on which are normally classified. They include size and number of lipid bilayer, composition and method of preparation.

(a) Based on size and number of bilayers:

Liposomes possess single or more bilayer membranes. Half-life of liposomes in blood circulation depends on the size of vesicular liposomes. On the other hand, drug entrapment capability of liposomes depends on the number of bilayers as well as size of vesicles. Based on the size and number of bilayers or lamellarity liposomes are of three types, namely multilamellar vesicles (MLVs), large unilamellar vesicles (LUVs), small unilamellar vesicles (SUVs) (Figure 1.4).

(i) MLVs

This kind of liposomes has an onion like structure. MLVs are formed by the numerous unilamellar vesicles which are accumulated to develop on the inside of the other having small structure in size. In MLVs, several concentric lipid bilayers are separated to each other by aqueous layers (Shaheen et al., 2006; Lasic, 2001). They are comparatively larger in size up to 5 μm (Pandey et al., 2016). The lipid hydration using excess organic solvent or thin film hydration technique is normally utilized to formulate this type of liposomes. Due to

comparatively larger size, they are quickly cleared by reticulo-endothelial system that may be applied in targeted drug delivery directed to the organs of reticulo-endothelial system. The drug entrapment efficiency of these MLVs can be improved by slowing the hydration procedure as well as gentle mixing process. They are normally mechanically stable during extended storage and have adequate trapped volume (Sharma and Sharma 1997; Olson et al., 1979).

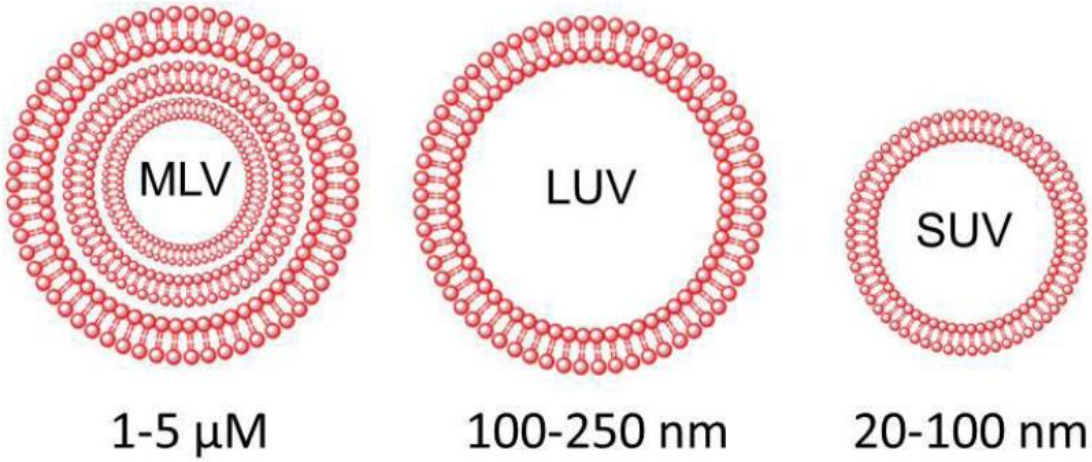

Figure 1.4: Types of liposomes classified on the basis of size and number of bilayers. MLV: Multilamellar vesicle, LUV: Large unilamellar vesicle, SUV: Small unilamellar vesicle (Pandey et al., 2016).

(ii) LUVs

LUVs consist of a single lipid bilayer surrounding aqueous phase. Normally the size range of these liposomes is 100-250 nm (Pandey et al., 2016). As LUVs are capable to grip a higher volume of solution in the cavity in them, they have greater efficiency of drug encapsulation (Vemuri and Rhodes, 1995). They are utilized for encapsulation of hydrophilic therapeutic agents and possess high trapped volume. The benefit of this type of liposomes is that they use smaller amount of lipid for encapsulation of drug. Due to their bigger size, they are cleared easily through reticulo-endothelial system. Detergent dialysis, ether injection and reverse

phase evaporation are applied for the preparation of LUVs formulation (Sharma and Sharma, 1997; Tirrell et al., 1976).

(iii) SUVs

They consist of aqueous chamber encircled by a single lipid bilayer. They are smaller in size than that of LUVs. The size of them is within the range of 20-100 nm (Pandey et al., 2016). They contain lower entrapped volume along with long circulation half-life. Solvent injection technique using ethanol or ether is applied for SUVs preparation (Deamer and Bangham, 1976). Using sonication or extrusion technique along with maintaining atmosphere fully inert, the size of LUVs can be decreased to convert them as SUVs. SUVs may be obtained through transferring MLVs within a narrow orifice applying higher pressure (Hamilton et al., 1980).

(b) Based on composition

We can divide liposomes into four types such as conventional liposomes, sterically-stabilized liposomes, ligand-targeted liposomes and combination of all (Figure 1.3).

(i) Conventional liposomes

They are known as first generation liposomes. Usually they contain lipid bilayer which is formed by CHO and anionic, cationic and or neutral lipids surrounding the aqueous phase. From 1980s, research on this conventional type of liposomes has been started and it is fruitfully established for the drugs such as amphotericin and doxorubicin regarding improvement of therapeutic index (Koning and Storm, 2003; Ding et al., 2006; Hua and Wu, 2013). They are able to increase pharmacokinetic and biodistribution efficacy and to reduce toxicity as compared to free drug. But quick elimination of them from blood circulation restricts the therapeutic effect due to formulation (Gabizon et al., 1991; Gabizon et al., 1994).

Uptake by macrophages and opsonisation of plasma components are mainly responsible for such kind of rapid clearance (Hua and Wu, 2013).

(ii) Sterically-stabilized liposomes

The sterically-stabilized liposomes have the capacity to improve stability and prolong circulation time in blood stream. To get sterically-stabilized liposomes, hydrophilic polymer PEG is applied as a constituent. Uptake of such liposomes by macrophages and opsonisation of plasma components are minimized due to steric barrier (Torchilin et al., 1992; Northfelt et al., 1996). By varying in particle size or using coating polymer, liposomes may vary half-life from 2 to 24 hour (h) in rodents and as high as 45 h in case of humans (Allen, 1994; Moghimi and Szebeni, 2003).

(iii) Ligand-targeted liposomes

For site-specific drug delivery in targeted cells or organs ligand-targeted liposomes may be used. Different types of ligands such as peptides or proteins, antibodies, carbohydrates, etc. can be utilized depending on the target. Monoclonal antibodies, multipurpose ligands, are attached to the surface of liposomes to form immunoliposomes (Hua, 2013; Bendas, 2001; Puri et al., 2009). The benefits of monoclonal antibodies include their satisfactory stability and two binding sites (Willis and Forssen, 1998). But immunogenicity and pharmacokinetic efficacy are the major hindrances of using such kind of liposomes (Puri et al., 2009).

(iv) Combination of all

To avoid above-said problems, a combination of all the above-said designs may be utilized for further improvement such as immunoliposomes having integrating target-specific binding along with PEG for steric stabilization. It may increase circulation time of immunoliposome in blood stream and improve pharmacokinetic efficacy of them (Maruyama, 2002).

(c) Based on method of preparation

Depending on the methods of preparation of liposomes, they are mainly three types such as reverse phase evaporation vesicles (REVs), ether injection vesicles (EIVs), French press vesicles (FPVs) (Kalepu et al., 2013).

1.7.7.2. Methods of preparation

Liposomes can be formulated by various methods. The types of methods of preparations have an influence on the some properties of liposomes such as size, shape, stability as well as drug loading efficiency (Pandey et al., 2016).

Different methods utilized for preparation of liposomes are mentioned below as a schematic diagram.

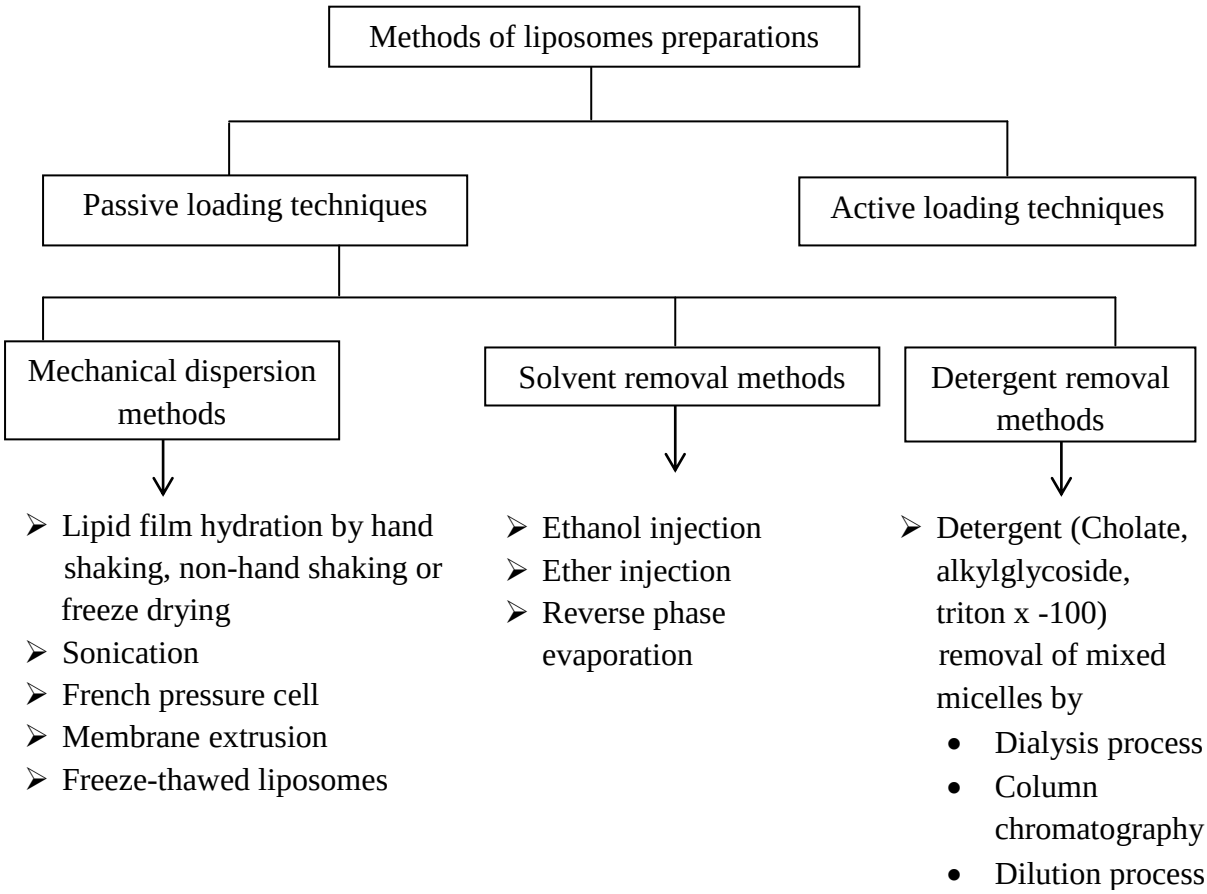

Figure 1.5: Different methods of liposomes preparation (Dua et al., 2012).

Drug encapsulation technique during the liposome preparation is mainly two types such as active loading and passive loading. The encapsulation of drug during the process of vesicle formation is known as passive loading. On the other hand, when drug is encapsulated after vesicle formation is called active loading (Pandey, 2016).

(a) Passive loading

The hydrophilic drugs are mixed with hydrating buffer which is essential for hydration of thin film during liposomal formation and are loaded in liposomal internal core. At the time of thin film formation of lipids, lipophilic drugs are mixed with the lipidic components of liposomes for loading into lipid layers. Using gel-filtration chromatography or dialysis techniques free drug molecules can be removed from liposomal suspension (Tyagi et al., 2011; Tyagi et al., 2013). Various factors that affect the encapsulation capacity of liposomes are size of liposome, other physico-chemical characteristics and concentration of lipids, etc. For hydrophilic drugs, passive loading technique gives comparatively lower encapsulation efficiency. Larger vesicles normally have greater entrapment capacity than the smaller one (Tyagi et al., 2013; Akbarzadeh et al., 2013). Lipophilic drugs have the ability to have physical interaction / chemical interaction with lipid layers which provide high encapsulation efficiency.

(i) Mechanical dispersion methods

***Lipid film hydration method*:** This conventional method has been used for formulating liposomes since the beginning of its development (Laouini et al., 2012). Required components (such as CHO, lipids, etc.) are added in required organic solvent. The organic solvent is evaporated by using rotary evaporator under reduced pressure to form a thin film. This dry film is hydrated using aqueous medium by agitation. MLVs (200 to 1000 nm in size)

are formed after hydration. These liposomes are reduced in terms of size as per requirement by using sonication for SUVs or extrusion for LUVs (Olson et al., 1979; Mui et al., 2003; Akbarzadeh et al. 2013).

***Sonication*:** Sonication is most useful method for preparation of SUVs from MLVs (Riaz, 1996; Jesorka and Orwar, 2008). There are two types of sonicators such as probe sonicator and bath sonicator (Akbarzadeh et al., 2013). The tip of sonicator is placed in the flask containing MLVs for sonication under probe sonication (Prabhu et al., 2010). But in case of bath sonication, liposomal dispersion containing cylinder is kept into bath sonicator. This is comparatively an easier method than probe sonication (Kataria et al., 2011).

***French pressure cell method*:** French pressure cell method is a process of extrusion which helps the MLVs to convert to LUVs or SUVs (Berger et al., 2001). Extrusion process is carried out at 20000 psi at 4°C (Dua et al., 2012). In this method, proteins are not affected significantly due to sonication (Mayer et al., 1986). Unstable materials are gently handled by this technique (Hamilton and Guo, 1984). Small working volume and achieving high temperature are the drawbacks of this process (Riaz, 1996; Anwekar et al., 2011).

***Membrane extrusion*:** Using uniform pore size containing polycarbonate membranes liposomal vesicles are extruded under pressure. Liposomes with different size can be made by using this technique as membranes with different pore size are applied here. Liposomes having very narrow size range are made by repeating extrusion of same material applying membrane with selective porosity. In large scale processing it creates problems (Swami, 2015).

***Freeze-thawed liposomes*:** In this process, SUVs are frozen quickly and defrosted gradually. The aggregated things are dispersed in LUVs due to sonication of short duration. During the

continuous freezing and thawing process the fusion of SUVs forms unilamellar vesicles (Pick, 1981; Ohsawa et al., 1985; Liu and Yonetaini, 1994). The enhanced concentration of phospholipid and ionic strength of medium obstruct intensely the preparation by this process (Pick, 1981).

(i) Solvent removal methods

***Ethanol injection*:** The lipid solution containing ethanol is injected at a fast speed into an excess quantity of buffer. As a result of this, formation of MLVs takes place quickly. The heterogeneous productions (30-110 nm) as well as less in quantity of liposomes are the main drawbacks of this process. The elimination of total ethanol is very tough as it turns into azeotrope in presence of water. The inactivation of different biologically active macromolecules is probably higher due to presence of ethanol (Batzri and Korn, 1973).

***Ether injection*:** Ether and methanol mixture or diethyl ether is used to dissolve lipids to prepare solution. This solution is injected slowly into the aqueous solution containing the materials which is needed to encapsulate. This total process is performed under reduced pressure within a temperature range from 55°C to 65°C. Liposomes are produced due to the removal of ether using vacuum. There are few disadvantages such as obtained product has wide range of size distribution (70 to 200 nm) and at high temperature the material to be encapsulated is exposed within organic solvents before encapsulation in liposomes which could degrade the material (Deamer and Bangham, 1976; Schieren et al., 1978).

***Reverse phase evaporation method*:** This technique gives a new era in the field of liposome formulation which is capable to encapsulate large amount of existing aqueous substances. Inverted micelles are the starting form of this procedure. Such inverted micelles are formed by the sonication process of a mixture containing an organic part which solubilizes amphiphilic molecules and an aqueous phase as in form of buffer in which water soluble

molecules are solubilized for encapsulation into liposomal formulation. These inverted micelles are converted into viscous phase and gel form due to gentle removal of organic solvent. Some of these micelles are in distress due to collapsing of gel state at a critical point during this procedure. The complete bilayer around the rest of the micelles is formed by the extra quantity of lipids present in the entire process and liposomes are produced as a result of this technique (Anwekar et al., 2011; Kataria et al., 2011).

At first, biphasic system consisting of aqueous buffer and diethyl ether or isopropyl ether or a mixture of chloroform and isopropyl ether is sonicated to form water-in-oil emulsion. Viscous gel is produced due to elimination of remaining solvent by reducing pressure. Reverse phase evaporation method is useful for encapsulation of small and large molecules. The material to be encapsulated is exposed to organic solvent(s) before encapsulation and it is a major disadvantage of this process (Szoka and Papahadjopoulos, 1978; Dua et al., 2012).

(ii) Detergent removal methods

***Dialysis process*:** Detergent is used for solubilizing lipids at their critical micelle concentration (CMC). The comfortability of micelles with lipids is enhanced after removal of detergents though dialysis and the result is formation of LUVs (Daemen et al., 1995; Alpes et al., 1986; Kirby et al., 1984). A dialysis system or device called LipoPrep (Diachema AG, Switzerland) can be used for eliminating of detergents or dialysis is also carried out using dialysis bags in buffers which is absolutely free from detergents (Shaheen et al., 2006).

***Column chromatography*:** In this procedure, removal of detergents is performed by a special type of column chromatography called gel permeation chromatography which is able to separate materials as per the size. In this column, liposomes are not able to enter into the packed beads. The inter bead spaces are filled by liposomes. From detergent monomers attached to the beads, liposomes are separated maintaining a gentle flow rate of aqueous

solvent for getting good results. The pre-treatment is essential as significant quantity of amphiphilic lipids are adsorbed by swollen beads of polysaccharide. This pre-treatment can be performed by applying liposomal suspension to pre-saturate the gel filtration column by lipids (Akbarzadeh et al., 2013).

***Dilution process*:** The polydispersity as well as micellar size profoundly enhances due to the effect of dilution of aqueous mixed solution of micelles containing detergent and lipids along with buffer. Liposomal vesicles are formed from polydispersed micelles through impulsive alteration due to dilution beyond the mixed micellar phase periphery (Akbarzadeh et al., 2013).

(b) Active loading

The active loading process for liposomal formulation is utilized for some weakly alkaline or acidic drug molecules. The electrochemical potential which is the resultant of pH or ion gradients of lipid bilayer of liposome is the main motorist of this process (Akbarzadeh et al. 2013; Bozzuto and Molinari, 2015). The buffer of specific pH used for liposome preparation creates such pH or ion gradients. Variable pH or ion concentration is applied for exchanging the external pH of liposomes with the help of dialysis and size exclusion chromatography. At a specific temperature which is above the phase transition temperature of the utilized lipids, drug is loaded through mixing along with liposomes. This helps for fluidity and effective transportation of drug molecules across lipid bilayer. Drug molecules are getting charged through the interaction with ions and as a result, drug molecules are entrapped within the core of liposome as well as unable to come out. Active loading techniques applied for a commercially available liposomal formulation, Doxil™ (Lasic et al. 1992; Haran et al. 1993).

1.8. AIDS and zidovudine

AIDS, one of the vital health complications of human throughout the world, occurs due to human immunodeficiency virus (HIV) which is able to destroy lymphocyte (Rao et al., 2009). HIV is able to enter into the brain utilizing the "Trojan horse" strategy (Ivey et al., 2009). In HIV infected patients, at very early stage such as 10 days of post HIV infection neuro-invasion can arise and HIV infected circulated monocytes in blood stream can easily enter into brain (Ivey et al., 2009). Zidovudine (AZT), nucleoside reverse transcriptase inhibitor, was the first approved drug by the USFDA for the treatment of AIDS (Mu et al., 2016). AZT is also a part of combination therapy popularly known as "highly active antiretroviral treatment (HAART)" for anti-HIV treatment (Mu et al., 2016; Bergshoeff et al., 2004). AZT for its strong hydrophilicity is unable to cross BBB sufficiently to reach brain to provide an adequate concentration of AZT for therapeutic efficacy (Rautio et al., 2008; Weiss et al., 2009).

In the present study, we have selected a highly water soluble drug zidovudine (AZT) as a model water-soluble drug to deliver across BBB into brain. AZT is a highly water soluble drug (25 mg/ml at 25ºC). Therefore, it has been used as a representative water soluble active pharmaceutical ingredient or drug in a number of reports (Jain et al., 2008; Nayak et al., 2009; Singh et al., 2010; Christoper et al., 2014). It is expected that the physical characteristics provided by AZT would be similar for many other hydrophilic drugs. Hence, we have considered AZT as a water soluble model drug in the present study.

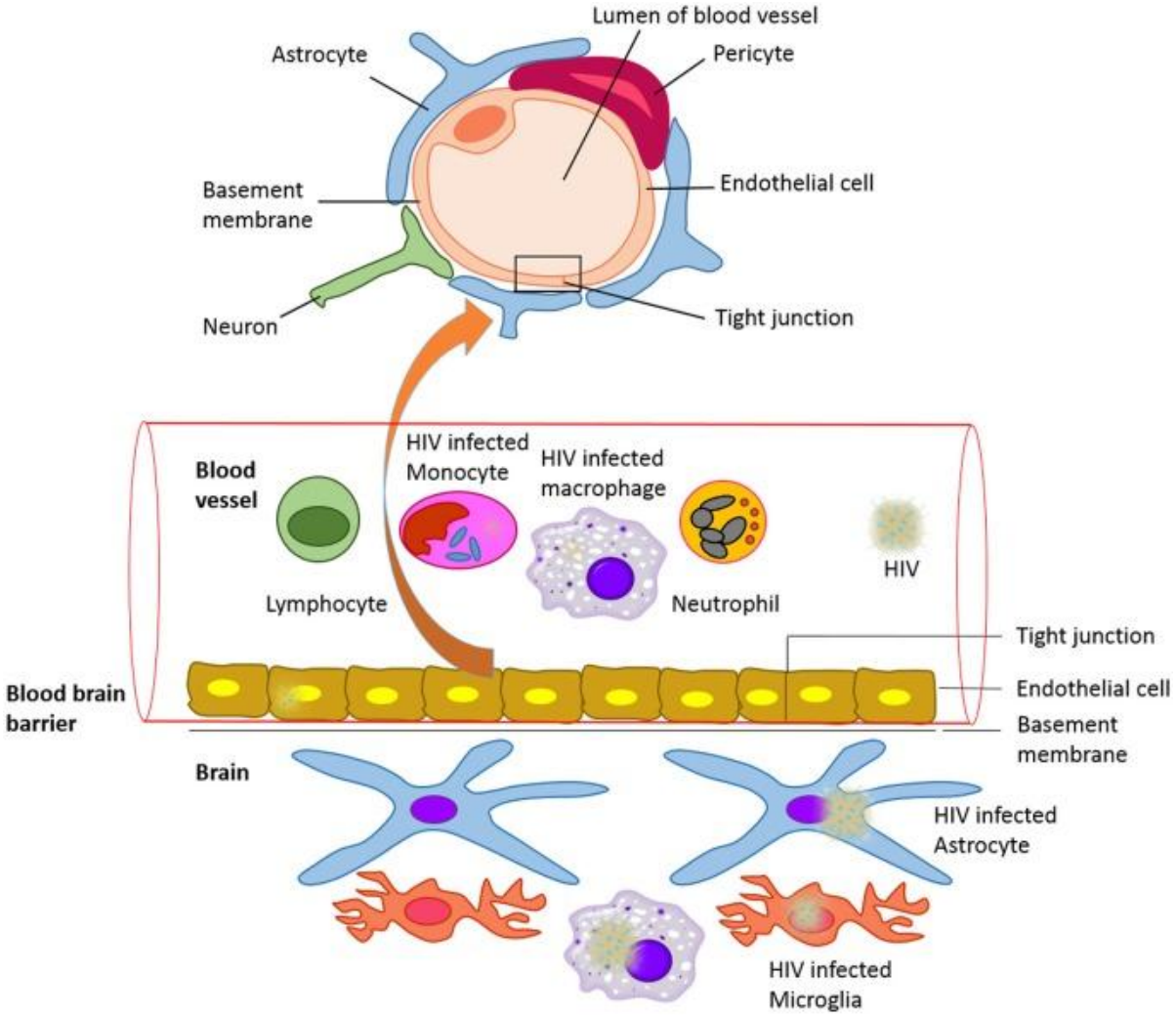

Figure 1.6: The blood-brain barrier (BBB) with human immunodeficiency virus (HIV) infected condition (Atluri et al., 2015).

Chapter 2

Objectives

2. Objectives of the research work

The prime objective of this investigation was to evaluate the capability of a newly developed fatty acid combination (ML) as base component for the development of nanocarrier to deliver highly water soluble drug into brain across BBB. Further, its efficiency was evaluated by comparing with soya lecithin (SL)-based drug nanocarrier. In details, the objectives of this present work are mentioned below.

- Development of ML lipid by mixing selective fatty acids
- Development of ML-based nanosize vesicular delivery system [nanoliposome (NL)] by using lipid layer hydration technique
- Characterization of ML-based nanosize formulations on the basis of physicochemical parameters such as drug loading, yield, size distribution and zeta potential and surface morphology
- Development of SL-based NLs by using same procedure
- Physicochemical characterization of SL-based nanosize vesicles in terms of drug loading, yield, size distribution and zeta potential and surface morphology
- Comparative *in vitro* drug release pattern study of ML-based formulation and SL-based formulation in freshly prepared PBS (pH 7.4) and in 50 % human serum
- Performing *in vitro* drug release kinetic study of ML-based nanosize vesicles and SL-based nanosize formulation
- Investigation of *in vitro* cellular uptake of both the type of nanosize formulations by U-87 MG human glioblastoma cells applying confocal microscopy

- Determination of stability of ML-based formulation and SL-based formulation
- Determination of ability of both the types of NLs as compared to free drug to reach brain across BBB using gamma scintigraphy
- Investigation of biodistribution of radiolabeled ML-based formulation, SL-based formulation and free drug (AZT) in Sprague-Dawley rats
- Determination of *in vivo* plasma pharmacokinetic parameters in rats after i.v. administration of both the types of nanosize vesicles and free drug (AZT) suspension
- Investigation of AZT level from ML-based nanosize vesicles as well as SL-based NLs in brain and determination of *in vivo* brain pharmacokinetic profile in rats

Chapter 3

Literature Review

3. Literature review

Brain is possibly considered as a very tough organ to access for delivering active pharmacological agents due to BBB (Pavan et al., 2008). BBB, diffusion barrier, performs its crucial role through protection and maintain the homeostasis of brain (Ballabh et al., 2004; Marianecci et al., 2017). Drug delivery into brain is obstructed due to BBB for treatment of several diseases such as brain tumors, acute ischemic stroke, viral infection like AIDS, psychiatric disorders, etc. Inadequate concentrations of drugs in brain fail to give proper therapeutic efficacy. The efficient drug delivery into brain to get fruitful therapeutic outcome is a vital challenge for formulation scientists (Shah et al., 2017; Kuo and Chung, 2012; Tajes et al., 2014).

AIDS is spreading as a life-threatening disease worldwide and particularly morbidity and mortality rates of this disease causing by HIV is very high (Rao et al., 2009; Alyautdin, 2014). Devastation of lymphocytes spoils immune defence of body and at the advanced stage of AIDS immune suppression takes place (Lange et al., 2003). After first 10 days of HIV infection neuro-invasion can ensue in patients and HIV infected circulated monocytes enter in a very easy way into brain as HIV infected monocytes have the capacity to enter into brain across BBB more efficiently than the normal or non-infected monocytes (Davis et al., 1992; Lackner et al., 1994; Persidsky et al., 1999).

AZT, first licensed drug for treatment of AIDS and a constituent of HAART, acts as a nucleoside reverse transcriptase inhibitor (Bergshoeff et al., 2004; Kuo and Chung, 2012). Quality of life of HIV infected patients are improved and elongated due to suppression of various difficulties causing by AIDS through the usage of AZT. CD4 counts are enhanced by AZT and AZT decreases the quantity of HIV RNA at an undetectable stage which is the cause improved immune system by decreasing the chance of opportunistic infections

(Christoper et al., 2014). AZT can be also useful for post exposure prophylaxis and it is recommended to inhibit the transmission of HIV from mother to child (Mugavero and Hicks, 2004). High dose of AZT used in chronic therapy produces severe toxic effects such as neutropenia, anaemia, cardiomyopathy, hepatotoxicity, etc. (Fischl et al., 1987). The highly hydrophilic drug AZT is unable to reach efficiently in HIV infected brain cells which act as a pool of HIV to produce continuous infection (Weiss et al., 2009; Singh et al. 2010; Nath et al., 2011).

Structure of BBB impedes during drug delivery as treatment of various diseases related to brain (Huang et al., 2013). The endothelial cells present in BBB have lack of fenestrations as well as presence of extra extensive TJs which makes the BBB endothelial cells different as compared to the endothelial cells present in rest of the body. These endothelial TJs restrict the entry of hydrophilic molecules in brain across BBB (Ballabh et al., 2004; Kusuhara et al., 1997). Compounds having higher lipophilicity and small size or low molecular weight can diffuse superiorly through BBB and reach in brain easily. On the other hand, membrane permeability can be increased by the reduction in hydrogen bond in a substance (Lawther, 2011). Physico-chemical characteristics such as ionisation, lipophilicity and polarity of compounds have an effect on regulation of intracellular passage of those compounds by TJs. Some higher lipophilic drugs or other substances with lower molecular size can able to enter in brain across BBB through passive diffusion (Jouyban and Soltani, 2012). Jouyban and Soltani also discussed the characters of substances such as small molecular weight, higher lipophilicity and lower hydrogen binding for easily crossing BBB to reach brain in a faster way (Jouyban and Soltani, 2012).

Nanotechnology is an emergent arena to solve the problem regarding drug delivery across BBB. Various investigations have been carried out applying nanocarriers as brain drug

delivery system for a long time. By applying some modifications in surface through ligands such as monoclonal antibodies, peptides, modified proteins, peptidomimetic antibodies, etc. or changing physico-chemical properties of such carriers, brain uptake activities of these nanocarriers are executed (Comoglu et al., 2017; Marianecci et al., 2017). NLs which are considered as eye catching transportation system for brain drug delivery across BBB among different types of nanocarriers can be utilized to transport hydrophilic as well as lipophilic drugs (Alyautdin et al., 2014; Upadhyay, 2014). Upadhyay already mentioned regarding the usage of liposomal drug delivery for controlling retention of loaded drugs in biological fluids. As a result of this, regulated residence of vesicles within systemic circulation and increased targeted cellular uptake are noticed. Hence, it is anticipated that they are able to transport the drug avoiding rapid degradation along with least side effects in patients (Upadhyay, 2014). Longer circulation time of NLs can be obtained through using particle size reduction approach (< 100 nm) (Lu et al., 2014).

Various methods were available for preparation of NLs. Among them lipid layer hydration technique is most common as a conventional method from the earlier days. Rudra and his co-workers utilized the lipid layer hydration method for preparation of hydrophilic drug doxorubicin loaded NLs as well as doxorubicin entrapped phosphatidylethanolamine conjugated NLs. They were successful to get nanosize vesicles (32-37 nm). Field emission scanning electron microscopy (FESEM) was applied to examine surface morphology of nanovesicles (Rudra et al., 2010).

Shaw et al. worked on hydrophobic drug docetaxel against brain tumor. They also applied lipid layer hydration method for preparation of NLs (< 50 nm in size). NLs were prepared using SL and CHO. Cryo-transmission electron microscopy (Cryo-TEM) study was performed to observe lamellarity of nanosize vesicles. These docetaxel loaded NLs without

any ligands were capable to cross BBB fruitfully. Sustained drug release profile was observed from the NLs. NLs were proved as an efficient vehicle to reach anticancer drug docetaxel in brain as a therapy of brain tumor and it was established that these docetaxel loaded NLs had better *in vivo* pharmacokinetic profile as compared to the free drug as well as marketed formulation (Shaw et al., 2017).

Christoper and his group prepared AZT loaded PLGA NPs by using nanoprecipitation method and these particles were coated with tween 80 to obtain effective brain targeting. NPs were less than 100 nm in size. *In vitro* drug release was measured up to 12 h and cumulative 70.67 % to 85.67 % AZT released from different formulations. Mice was utilized for *in vivo* evaluation and it was observed that tween 80 coated NPs attained higher concentration in brain as compared to free drug in solution as well as uncoated formulation but data was taken only for 1 h (Christoper, 2014).

Kuo and Chung investigated the ability of cross-reacting material 197 grafted polybutylcyanoacrylate NPs for delivering AZT through BBB. Human brain-microvascular endothelial cells were utilized for *in vitro* study. Decreasing diameter of such NPs improved the permeability coefficient of AZT across BBB. The uptake of these NPs was also enhanced by human brain-microvascular endothelial cells (Kuo and Chung, 2012). So, size of nanocarrier is a vital factor for brain targeting across BBB.

Permeability through BBB is very poor for hydrophilic drugs and peptides. Different drug delivery systems along with diverse surfacial individualities are already reported for transferring drug in brain through BBB. Applying ultra-emulsification method and chemical cross linking process using glutaraldehyde Mishra and his co-workers were prepared water soluble AZT loaded PEGylated albumin NPs having long systemic circulating capability. The

modification of these PEGylated albumin NPs was done by attaching transferrin as a ligand for brain targeted drug delivery. The physico-chemical characterization of these particles were performed by various investigations such as average diameter of particle, polydispersity, zeta potential, entrapment efficiency, *in vitro* drug release study, etc. Albino rats were utilized for *in vivo* evaluation. From fluorescence studies it was established that brain uptake predominantly increased in case of transferrin-anchored NPs as compared to unmodified NPs. Tissue distribution was carried out after i.v. administration of plain AZT solution, unmodified and modified NPs. The localization of AZT in brain was enhanced significantly for transferrin anchored PEGylated albumin NPs. Through this study they proved the efficacy of transferrin ligand for drug delivery in brain across BBB (Mishra et al., 2006).

Kuo and Chen prepared nanosize AZT loaded and lamivudine (3TC) loaded NPs individually by utilization of polybutylcyanoacrylate (PBCA) and again applying methylmethacrylate-sulfopropylmethacrylate (MMA-SPM). The effect of size of respective types of NPs such as AZT loaded PBCA NPs, 3TC entrapped PBCA NPs, AZT loaded MMA-SPM NPs and 3TC entrapped MMA-SPM NPs on the relative drug loading efficiency, absolute drug loading efficiency and permeability of drug across BBB were investigated. Impact of alcohol on permeation of AZT and 3TC through BBB was also investigated in case of two different polymeric NPs. The relative drug loading efficiency, absolute drug loading efficiency and permeability of AZT and 3TC across BBB were reduced with the enhancing diameter or size of both the types of NPs. For AZT loaded PBCA NPs permeability of AZT across BBB increased 8 to 20 folds. About 10 to 18 folds enhanced permeation capability of 3TC through BBB was observed in case of 3TC loaded PBCA NPs. The permeability through BBB increased twice for AZT loaded MMA-SPM NPs as well as 3TC entrapped MMA-SPM NPs.

The permeation capabilities of AZT and 3TC were greater for PBCA-based NPs as compared to MMA-SPM-based NPs due to electrical repulsion between bovine brain-microvascular endothelial cells and negative charged MMA-SPM NPs. BBB permeabilities were also enhanced 4 % to 12 % for the drugs AZT as well as 3TC entrapped in two different nanoparticulate carriers by influence of alcohol. Hence, alcohol addition in pharmaceutical formulations may be useful as a permeability enhancer for drug delivery in brain across BBB. This utilized BBB model further could be investigated for the relation study among drug and carrier by infrared spectroscopy and also for interaction study between cell and carrier using confocal microscopy. These NPs could be inspected in terms of biodegradation in physiochemical and physiological conditions (Kuo and Chen, 2006).

Joshy et al. indicated that therapeutic usage of AZT faces drawbacks due to aqueous solubility, short half-life, and vital side effect for repeated administration. This is a tough job for making formulations with AZT avoiding such problems. AZT entrapped SLNs modified by gelation were prepared as unique formulation using two different lipids such as SA and compritol. The modified double emulsion solvent evaporation method was utilized to prepare NPs. These polymer-lipid hybrid NPs (PLNs) had efficient drug loading as well as sustained drug release profile. The haemolysis and aggregation investigations were carried out to check the interactions of NPs with the content of blood and the results showed that PLNs were haemocompatible. From *in vitro* cytotoxicity studies it was confirmed that PLNs were non-toxic in MCF-7 cells as well as neuro 2a brain cells. In both the cell lines the excellent cellular internalization of drug loaded PLNs were observed by utilization of fluorescence microscopy. AZT loaded PLNs can be used as a nanocarrier for anti-HIV drug delivery as safe and efficient therapy (Joshy et al., 2017).

Purvin et al. worked on AZT loaded SLNs (AZT-SLNs). The pharmacokinetic and tissue distribution investigations of these AZT-SLNs were performed. Actually a comparison study between AZT-SLNs and AZT solution was carried out in Charles Foster strain albino rats (200–230 gm) after oral administration of AZT-SLNs and AZT solution individually. Reverse phase high performance liquid chromatography was utilized for quantification of AZT in plasma and tissues. About 31.25 % greater area under curve of concentration versus time (AUC) was obtained for AZT-SLNs than that of AZT solution. Pharmacokinetics parameters gave comparatively better results in AZT-SLNs than AZT solution. Tissue distribution study also provided the same supporting data. The AUC values of AZT in liver and brain were about 1.77 and 2.73 times higher respectively in case of AZT-SLNs as compared to AZT solution. This proved that AZT-SLNs can enter into brain through BBB. The researchers of this research work stated that AZT-SLNs can able to improve *in vivo* pharmacokinetic parameters as well as biodistribution of AZT after oral administration (Purvin et al., 2014).

Kumar and its group of co-workers formulated AZT entrapped lactoferrin NPs to improve oral delivery of AZT. They were successful to make the NPs within 50 nm to 60 nm in size along with 67 % encapsulation efficiency of drug. These particles are stable in simulated gastric as well as intestinal fluids. In acute infectious condition, the anti-HIV property of AZT still remained unchanged in the form of nanoformulation. Higher bioavailability was noticed in blood and the high amount of AZT was obtained in liver and kidney as tissue distribution. The pharmacokinetic profile of AZT loaded lactoferrin NPs was established as better than that of soluble AZT. In case of these NPs the maximum serum concentration was enhanced about 30 % and time to reach maximum concentration (T_{max}) was increased about 2 fold. Approximate 2 fold reduced toxicity was recognized by bone marrow micronucleus

assay as compared to soluble AZT. A lesser amount or no significant toxicity in organ was further established through the results of histopathological as well as biochemical investigation. Hence, nanoformulations can be used as safe and targeted drug delivery (Kumar, 2015).

To overcome the first-pass metabolism of AZT, drug administration through nasal route is a promising path along with enhancing therapeutic efficacy of AZT. Using sodium tripolyphosphate Barbi et al. prepared AZT loaded chitosan NPs through modified ionotropic gelation technique. Small NPs (260 nm in size) (NP1 10:01 (w/w)) were formed by enhancing proportion of chitosan but particle size (330 nm) was increased with the increasing proportion of tripolyphosphate anions (NP2 5:1 w/w). The size of NP1 and NP2 were increased by the incorporation of AZT. In AZT loaded NP1 the electrophoretic mobility was not changed due to incorporation of AZT but a significant increase in electrophoretic mobility was followed for AZT loaded NP2. For obtaining mucoadhesive properties positive surface of NPs is very crucial through interaction with sialic groups of mucin. Chitosan with higher concentration in NPs favouring ionic interaction of limited phosphate units (pyrophosphate) was determined by nuclear resonance magnetic data. The spherical structures along with porous surface properties of NPs were shown through scanning electron microscopy (SEM). The entrapment efficiency of AZT was higher in NP1 as compared to NP2. The results were 2.12 and 4.62 for NP1 and NP2 respectively during the mucoadhesion force measurement with the help of nasal tissue and mucin discs. NPs encouraged enhancement in the flux of drug by nasal mucosa which was revealed by *in vitro* permeation study. The chitosan NPs can be an efficient approach for entrapment of hydrophilic drugs along with expressive potentiality of nasal administration (Barbi et al., 2014).

Dalpiaz et al. obtained prodrug of AZT through conjugation between AZT and ursodeoxycholic acid (UDCA). As they already proved that the prodrug (UDCA-AZT) can be used as a useful carrier of AZT to reach into CNS (Dalpiaz et al., 2012). Again solid lipid microparticles (SLMs) of this prodrug (UDCA-AZT) were prepared by them for increasing the amount of AZT in brain as brain targeting drug delivery through nasal administration. Tristearins and SA were utilized individually as lipid carrier to prepare SLMs by using hot emulsion procedure. SA-based SLMs were comparatively small in size than that of tristearin-based formulations. In case of SA-based SLMs, the prodrug loading efficiency as well as negative zeta potential value was higher as compared to tristearin-based SLMs. But release of prodrug was controlled by tristearin SLMs and was increased significantly for SA SLMs. Hydrolysis of free prodrug was occurred in liver of rat homogenates more quickly in case of SA SLMs than that of tristearin SLMs. In this respect, SA SLMs had lesser stabilization effect on prodrug. After the i.v. administration of prodrug no trace of AZT and UDCA-AZT was found in CSF of rat. When SA-based SLMs was administered through nasal route, permeation of prodrug was detected in CSF by quantification of UDCA-AZT. In this case permeation of prodrug occurred via nose to CNS pathway. Further, the uptake of UDCA-AZT from SA-based SLMs in CSF increased six times through nasal administration in presence of chitosan. For selective brain uptake of AZT SA-based SLMs can be an encouraging nasal formulation (Dalpiaz et al., 2014).

Nasal formulation of AZT is a new approach to transfer AZT in brain. It was prepared by Ved and Kim to inspect olfactory transfer of AZT after administration via intranasal route as well as to evaluate the absorption and brain uptake activity due to the usage of thermoreversible gelling system. Using thermoreversible gelling agent such as about 20 % poly (ethylene oxide / propylene oxide) (Poloxamer 407) and permeation enhancer n-tridecyl-

β-D-maltoside (TDM) (1 %), AZT containing nasal formulation was prepared. At 27ºC to 30ºC temperature the formulation was very stable along with optimum gelation profile. About 53 % enhancing permeability of AZT was noticed by using the formulation in *in vitro* permeation studies. In case of *in vivo* experiments male New Zealand white rabbits were utilized. The concentration of AZT was determined in plasma, six different areas of brain tissue (such as cerebellum, anterior, posterior and middle segments of cerebrum, olfactory tract and olfactory bulb) and CSF. About 29.4 % systemic bioavailability was obtained for this Poloxamer 407 containing nasal formulation. On the other hand, absorption process was 4 times slower in this case as compared to control. The concentrations of AZT in brain and CSF were greater in case of intranasal administration of this formulation as compared AZT i.v. injection. Polar drug AZT could transfer into brain and CSF through probably olfactory pathway from nasal cavity after the administration of formulation intranasal way (Ved and Kim, 2011).

Frequent administration of conventional formulation of AZT is necessary due to poor bioavailability and short elimination half-life of this drug which results dose dependent haematological toxicity. To solve the crucial problem Jain et al. prepared AZT loaded poly (propyl ether imine) (PETIM) dendrimer having sustained drug release property. *In vitro* drug release study was performed using dialysis bag. For evaluation of sustained drug release pattern and biosafety, pharmacokinetic and biodistribution as well as haemolytic toxicity study were performed. The cumulative drug release from AZT loaded dendrimer was 6.5 ± 0.3 % at 1 h and it was 94.3 ± 3.8 % within 14 h that indicated sustained drug release ability of formulation. On the other hand, cumulative amount of AZT 95.8 ± 4.1 % released in 1 h from drug solution used as control. Haemolytic toxicity due to AZT was reduced due to stable AZT loaded dendrimer as compared to drug solution of pure AZT. Sustained drug

release profile was also observed from *in vivo* pharmacokinetic profile of AZT-dendrimer complex. They estimated the quantity of AZT in various organs (liver, spleen, kidney and heart) of rats but they did not evaluate the amount of AZT in brain of rats (Jain et al., 2013).

Uronnachi et al. prepared AZT loaded solidified reverse micellar microparticulate (SLM) and investigated release profile, pharmacokinetic, biodistribution as well as stability of this formulation. Phospholipon® 90H and fat of goat at various ratios were utilized for preparation of AZT loaded SLM. *In vitro* drug release study was carried out in simulated intestinal fluid (pH 7.2) and simulated gastric fluid (pH 1.2). Wister albino rats were used as experimental animal for *in vivo* study. Lipid ratio 1:1 was proved as best for preparation of most stable AZT loaded SLM. The concentration dependent growth was followed from various formulations for concentration maximum (C_{max}). Biodistribution studies gave good results as compared to pure AZT but maximum concentration of AZT was found in liver and least in brain. Fluctuation of AZT level in blood which is normally observed for administration of conventional tablets can be resolved by using such formulations (Uronnachi et al., 2013).

Brewster and his co-workers stated that treatment of HIV induced infection is challenging due to the limitation of penetration of vital antiretroviral drugs in brain across BBB. Using redox trapping, chemical delivery system (CDS) was prepared for AZT by them. Healthy mongrel dogs (20 kg to 35 kg) were utilized for this research work. Fast systemic elimination and poor uptake of AZT in brain was observed after parenteral administration of AZT. But quick uptake by tissue and conversation of CDS to its quaternary salt along with successive production of AZT were noticed by the administration of AZT-CDS. The results showed 1.75 to 3.3 fold higher AZT level in brain in case of AZT-CDS as compared to conventional AZT (Brewster et al., 1997).

Jin et al. indicated that liposomes can be a fruitful vehicle for improvement of therapeutic index of AZT. Due to lower entrapment efficiency of AZT in liposomes they synthesized AZT myristate (AZT-M) which is a prodrug of AZT and prepared AZT-M loaded NLs. The average size of these NLs 90 nm and they have higher drug encapsulation efficiency about 98 %. The AZT-M loaded NLs and AZT solution were administered in Wistar rats via i.v. route and pharmacokinetic parameters and biodistribution of AZT were performed. For NLs formulation it was shown that AZT level in plasma was expressively higher than that of AZT solution. Biodistribution data which was carried out for only 4 h also gave the considerably higher amount of AZT in various organs like kidney, heart, spleen, liver and lung but the amount of AZT in brain up to 4 h was slightly higher for liposomal formulation than that of AZT solution (Jin et al., 2005).

Antiretroviral therapy is unable to cross BBB that results inadequate concentration of drug in brain to produce proper therapeutic outcome. Antiretroviral drugs can deliver in brain through active targeting of drugs to enhance therapeutic efficacy. Magnetic nanoliposomal formulation of AZT 5'-triphosphate (AZTTP) was prepared and by applying an external magnetic field the capacity of formulation to move across *in vitro* BBB model was investigated. It is assumed that magnetic nanocarriers can reach brain via crossing BBB though monocyte mediated transport or direct transport. These magnetic NLs of AZTTP were 150 nm in size along with extreme magnetite and drug loading capacity of 45.3 % and 54.5 % respectively. Through the applied externally magnetic field, magnetic NLs were evaluated for transmigration across BBB model *in vitro* by utilizing of monocyte mediated transport or direct transport. It was noticed that about 3 fold higher apparent permeability occurred for magnetic AZTTP NLs as compared to free AZTTP. The magnetic AZTTP NLs were competently picked up by monocytes. But in magnetic field, magnetic monocytes displayed

increased transendothelial migration than nonmagnetic or normal monocytes. From there, Saiyed et al. anticipated that applying external magnetic force magnetic nanoformulation can be useful for active targeting of nucleotide analog reverse transcriptase inhibitors into brain across BBB to eliminate HIV reservoir from brain (Saiyed et al., 2010).

Doijad et al. tried to formulate stable liposomal drug delivery system of AZT along with its improved therapeutic index. Here, AZT used as a model drug. AZT loaded NLs were prepared using thin film hydration procedure for drug targeting. Various concentrations of excipients such as dipalmitoyl phosphatidylcholine (DPPC) and egg phosphatidylcholine (EPC) were utilized to formulate four different nanoliposomal formulations. Several investigations such as particle size distribution, drug loading, SEM analysis, zeta potential, *in vitro* drug release study, etc. were performed for evaluation of physico-chemical characterization of these formulations to optimize. *In vivo* biodistribution study was performed with the best formulation. The quantity of AZT was determined in liver, speen, kidney and lung. No brain uptake was measured in biodistribution process. Accumulation of AZT was higher in liver among the all experimental tissues (Doijad et al., 2009).

Kaur et al. worked on AZT entrapped NLs modified by surface engineering. Charges incorporation such as positive charge or negative charge and attaching the ligand such as mannose for site specificity were performed for achieving surface engineered (SE) NLs to increase accumulation in lymphatics (spleen and lymph nodes). Stearylamine or dicetyl phosphate individually was utilized to prepare positively charged or negatively charged SE NLs respectively. But mannose-terminated stearylamine (mannose conjugate) was applied to formulate ligand coated SE NLs. The liposomal formulations were examined in terms of size, shape, surface morphology, drug entrapment efficiency and *in vitro* drug release profile. Biphasic release of AZT was observed for all SE NLs but AZT release significantly

decreased for mannose coated NLs as compared to conventional NLs. From biodistribution study of SE NLs it was revealed that significantly enhanced amount of AZT was present in lymph nodes and spleen where as predominantly reduced quantity of AZT was observed in serum. Applying fluorescent microscopy, the increased uptake and localization of SE NLs was noticed in spleen and lymph nodes. The mannose coated NLs showed high performance in this purpose. The SE NLs proved itself as an efficient drug delivery system for increasing targeting of AZT in lymphatics to treat AIDS (Kaur et al., 2008).

Gurturk and his co-workers stated that presence of BBB creates problem in crossing of the CNS acting drugs administered through i.v. route which results incapability of drugs for expressing their proper therapeutic effect. Levodopa, a hydrophilic drug, is applied for treatment in Parkinson's disease. For enhancing the transport of drug across BBB as well as for targeted drug delivery, levodopa loaded unique nanoliposomal formulations were prepared along with modification through maltodextrin. In NLs the ability of glutathione was evaluated in respect of delivery and stability as it was co-loaded in NLs as antioxidant and supportive agent. In SH-SY5Y and 3T3 cells, co-loaded glutathione showed positive effect on cell viabilities. The parallel artificial membrane permeability assay revealed that there was high *in vitro* levodopa passage and having higher binding ability with MDCK cells in case of maltodextrin modified targeted NLs. Hence, maltodextrin modified NLs can be utilized for improving the drug delivery in brain as it is able to target BBB efficiently (Gurturk et al., 2017).

Satapathy and his co-workers investigated the efficiency of 1,2-distearoyl-*sn*-glycero-3-phosphotidylethanolamine (DSPE) incorporated NLs (DNL-PE) of hydrophobic drug docetaxel for brain delivery across BBB. DNL-PE formulation was of nano size having average diameter 82.1 ± 2.2 nm with drug loading 7.8 ± 0.4 %. It had negative zeta potential,

smooth surface and sustained drug release profile. To visualize the brain uptake across BBB gamma scintigraphy study was performed by using radiolabeled NLs as well as free drug with technetium-99m (^{99m}Tc). The results revealed that drug loaded DNL-PE reached in brain in a time dependent manner. Brain pharmacokinetic profile data again established the presence of docetaxel quantitatively from DNL-PE in brain (Satapathy et al., 2016).

Soni et al. worked on transferrin coupled liposomes for enhancing the delivery of doxorubicin into brain. The cast film method was utilized for preparation of liposomal formulations. The physico-chemical characteristics of liposomes were determined through some experiments in terms of size, surface morphology, drug encapsulation efficiency and *in vitro* drug release study. ^{99m}Tc-DTPA (diethylenetriamine pentacetic acid) was used for radiolabeling of doxorubicin through redox reaction and it was optimized for obtaining maximum efficiency of radiolabeling. The suitability of radiolabeled system for applying *in vivo* experiments was determined by *in vitro* stability study through checking of their efficiency. Biodistribution studies were executed by i.v. administration of ^{99m}Tc-DTPA labeled doxorubicin loaded transferrin coupled and non-coupled liposomes in albino rats. In various organs such as liver, kidney, spleen, lung and brain, doxorubicin distribution through transferrin coupled and non-coupled liposomal formulations was established by radioactivity measured with the help of gamma scintillation unit. Brain uptake of doxorubicin enhanced about 10 fold and 7 fold for transferrin coupled and non-coupled liposomes respectively. Therefore, transferrin coupled liposomal formulation can be useful for drug delivery into brain to get the therapeutic efficacy in brain related diseases (Soni et al., 2007).

Chapter 4

Materials and Equipment

4. Materials and equipment

4.1. Materials

Drug and various chemicals which were utilized in this research work are enlisted below with their corresponding source (Table 4.1).

Table 4.1: List of materials and their sources

Material	Source
Zidovudine	Cipla Ltd., Goa, India
Lecithin Soya, 30 %	HiMedia Laboratories Pvt. Ltd., Mumbai, India
Cholesterol	HiMedia Laboratories Pvt. Ltd., Mumbai, India
Stearic acid	Sigma-Aldrich, Bangalore, India
Oleic acid	Sigma-Aldrich, Bangalore, India
Palmitic acid	Sigma-Aldrich, Bangalore, India
Butylated hydroxytoluene (BHT)	Qualigens Fine Chemicals, Mumbai, India
Fluorescein isothiocyanate (Isomer I) (FITC)	HiMedia Laboratories Pvt. Ltd., Mumbai, India
Fetal bovine serum (FBS)	HiMedia Laboratories Pvt. Ltd., Mumbai, India
Minimum Essential Medium Eagle (MEM)	HiMedia Laboratories Pvt. Ltd., Mumbai, India
U-87 MG cells (Human glioblastoma cells)	National Centre for Cell Science, Pune, India
Human serum	KPC Medical College and Hospital, Kolkata, India
Sodium chloride	Merck Life Science Pvt. Ltd., Mumbai, India
Disodium hydrogen phosphate	Merck Life Science Pvt. Ltd., Mumbai, India

anhydrous	
Potassium dihydrogen phosphate	Merck Specialities Pvt. Ltd., Mumbai, India
Chloroform	Merck Life Science Pvt. Ltd., Mumbai, India
Ethanol	Merck KGaA, Darmstadt, Germany
Dialysis membrane - 110	HiMedia Laboratories Pvt. Ltd., Mumbai, India
Paraformaldehyde	Merck Specialities Pvt. Ltd., Mumbai, India
Acetonitrile (for chromatography HPLC)	Merck Life Science Pvt. Ltd., Mumbai, India
Water (for chromatography HPLC)	Merck Life Science Pvt. Ltd., Mumbai, India

4.2. Drug profile

4.2.1. Zidovudine

Chemical Name: 1-[(2R,4S,5S)-4-azido-5-(hydroxymethyl)oxolan-2-yl]-5-methylpyrimidine -2,4-dione

Synonym: Azidothymidine

Molecular formula: $C_{10}H_{13}N_5O_4$

Chemical structure:

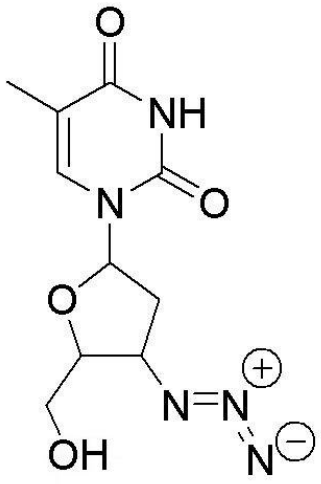

Molecular weight: 267.24 g/mol

Description: White or slightly off white in colour, odourless, solid powdery in nature

Melting point: 122ºC to 126ºC

Solubility: Soluble in water (25 mg/ml at 25ºC), ethanol and dimethyl sulfoxide

Mechanism of action: It acts as nucleoside reverse transcriptase inhibitor. The cellular enzymes activate AZT by formation of its mono, di and triphosphates in HIV infected as well as uninfected cells. AZT triphosphate, active metabolite, inhibits HIV-1 reverse transcriptase which results the inhibition of production of viral double stranded DNA from single stranded RNA (Sperling, 1998; Mainardes et al., 2010).

Pharmacokinetics: In oral administration of this drug, rapid absorption is followed from gastrointestinal tract and bioavailability is 60 % to 65 %. Excretion route of unchanged drug and metabolite is through urine. The $t_{1/2}$ is 1 h and plasma protein binding is about 30 %.

Uses: AZT, antiretroviral medication, is used for treatment of patients suffering from AIDS.

Adverse effect: High dose of AZT produces severe toxic effects such as neutropenia, cardiomyopathy, anaemia, hepatotoxicity, thrombocytopenia, etc. (Fischl et al., 1987; Mainardes et al., 2010).

4.3. Profile of excipients

4.3.1. Lecithin Soya, 30 %

Synonym: L-α-Lecithin, from Soyabean; L-α-Phosphatidylcholine, 30 %;

Soya lecithin, 30 %

Source: Soyabean

Description: Yellow to brown coloured powder

Solubility: Soluble in chloroform (100 mg/ml), benzene, and hexane

Uses: It is utilized as emulsifying agent, food additive, and dietary supplement and also as an excipient for preparation of liposomal nanocarrier for encapsulating of various drugs.

4.3.2. Cholesterol

Chemical Name: 5-Cholesten-3β-ol

Synonym: Cholesterin, Cholesteryl alcohol

Molecular formula: $C_{27}H_{46}O$

Chemical structure:

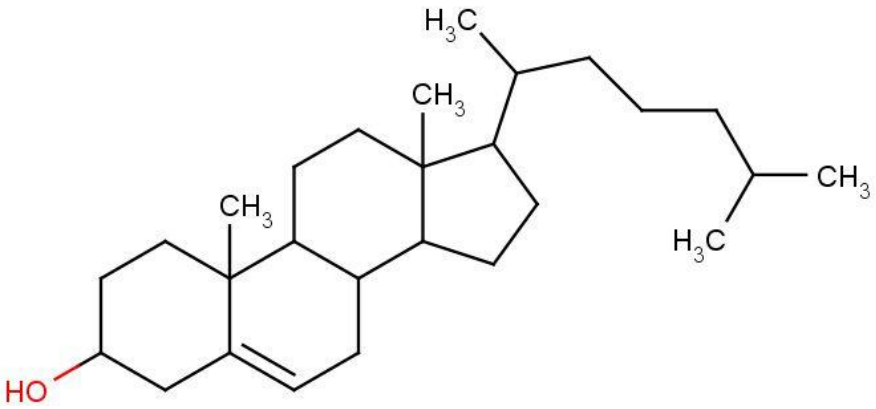

Molecular weight: 386.65 g/mol

Description: White coloured pearly solid powder in nature, almost odourless

Melting point: 142ºC to 150ºC

Solubility: Soluble in chloroform (100 mg/ml), benzene and moderately soluble in hot alcohol

Uses: As therapeutic aid (emulsifying agent), for preparation of liposomes in which it acts as stabilizer.

4.3.3. Stearic acid

Chemical Name: Octadecanoic acid

Molecular formula: $C_{18}H_{36}O_2$

Molecular weight: 284.48 g/mol

Chemical structure:

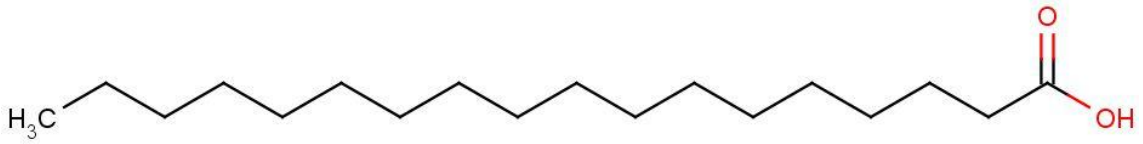

Description: White solid crystals along with characteristic or mild odour

Melting point: 67ºC to 72ºC

Solubility: Soluble in chloroform, acetone and carbon disulphide and slightly soluble in benzene and ethanol

Uses: It is used as lubricant, surfactant, corrosion inhibitor, anti-scaling agent, and filler etc.

4.3.4. Oleic acid

Chemical Name: cis-9-Octadecenoic acid

Molecular formula: $C_{18}H_{34}O_2$

Chemical structure:

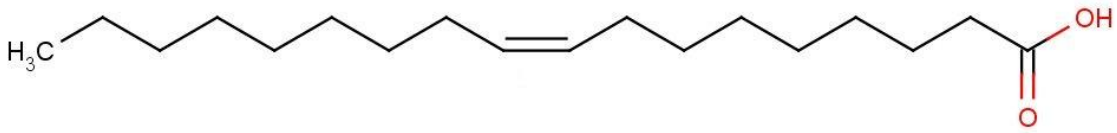

Molecular weight: 282.47 g/mol

Description: Pale yellow coloured liquid with peculiar lard-like odour

Melting point: 13ºC to 14ºC

Solubility: Insoluble in water and soluble in ether, chloroform and benzene

Uses: It is utilized as surfactant, flavouring agent, plant growth regulator, and lubricant etc.

4.3.5. Palmitic acid

Chemical Name: Hexadecanoic acid

Molecular formula: $C_{16}H_{32}O_2$

Chemical structure:

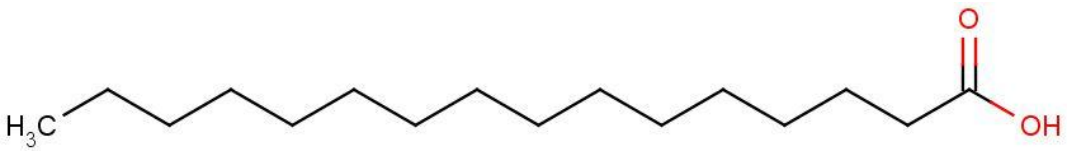

Molecular weight: 256.43 g/mol

Description: White solid crystalline scales

Melting point: 61ºC to 62.5ºC

Solubility: Very soluble in chloroform and soluble in benzene, ethanol and acetone

Uses: It is used as lubricant, surfactant, and flavouring agent etc.

4.4. Equipment or instruments

The list of equipment or instruments with their sources is mentioned below (Table 4.2).

Table 4.2: List of equipment and source

Name of equipment or instrument	Name of company
Digital balance	Sartorius, Goettingen, Germany
pH meter	Eutech Instruments Pte. Ltd., Singapore
UV/VIS spectrophotometer (Model: Intech-295)	Intech, Gentaur GmbH, Aachen, Germany
FTIR instrument (FTIR 4200)	JASCO International Co. Ltd., Tokyo, Japan
Rotary vacuum evaporator (Rotavap, model PBU-6)	Superfit Continental Pvt. Ltd., Mumbai, India
Aspirator A3S	Eyela, Rikakikaic Co. Ltd., Taguig City, Philippines
Cold circulating water bath	Spac N service, Kolkata, India
Vacuum desiccator	Tarson, Kolkata, India

Bath type sonicator	Trans-o-Sonic, Mumbai, India
Cold centrifuge	3K30 Sigma Lab Centrifuge, Merrington Hall Farm, Shrewsbury, UK
Freeze dryer	Instrumentation (India) Ltd., Kolkata, India
Zetasizer Nano ZS90	Malvern Instrument, Malvern, UK
Cyclo Mixer	Remi Equipments, Mumbai, India
Field emission scanning electron microscope (Model-JSM-6700F)	JSM-6700F; JEOL, Tokyo, Japan
Cryo-transmission electron microscope (Version: 4.6 FEI Tecnai G2)	Tecnai Polara G2, FEI Company, Eindhoven, Netherlands
Atomic force microscope	Dimension Icon, Bruker, Karlsruhe, Germany
Magnetic stirrer	Remi Equipments, Mumbai, India
Confocal laser scanning microscope (Model: IX81)	Olympus Singapore Pte Ltd., Singapore
Gamma counter (Model: LV4755)	Electronic Corporation of India, Hyderabad, India
LC–MS/MS system (LC: Shimadzu, Model 20AC; MS: AB-SCIEX, Model: API4000; Software: Analyst 1.6)	Shimadzu, North America; AB Sciex Pte. Ltd., Singapore

4.5. Animals

Sprague-Dawley rats (male: female ratio 2:1) having body weight 200-250 g were utilized for biodistribution investigation, plasma and brain pharmacokinetic study and only male Sprague-Dawley rats of body weight 200-250 g were used for gamma scintigraphy study. Animal experiments were carried out upon receiving approval of the Animal Ethics Committee, Jadavpur University, Kolkata. Animals were accommodated in the university animal house after keeping them in polypropylene cages. The temperature (22 ± 1ºC) and humidity (55 ± 5 %) were maintained of the room of animal house with 12 h dark / light circle. The animals had free access of standard diet (Dey et al., 2016) and drinking water.

Chapter 5

Methodology

5. Methodology

5.1. Development of calibration curve of AZT in phosphate buffered saline (PBS) (pH 7.4) and in the mixture of PBS (pH 7.4) and ethanol (5:1)

5.1.1. Preparation of PBS (pH 7.4)

For preparation of PBS (pH 7.4) as per Indian Pharmacopoeia (2007), 2.38 g of disodium hydrogen phosphate, 0.19 g of potassium dihydrogen phosphate and 8.0 g of sodium chloride were weighed accurately and were dissolved in sufficient double distilled water to produce 1000 ml. By using a pre-calibrated pH meter, the pH of this prepared solution was adjusted to 7.4.

5.1.2. Scanning for determination of absorption maxima (λ_{max}) of AZT in PBS (pH 7.4) and in the mixture of PBS (pH 7.4) and ethanol (5:1)

Two different solutions of AZT (10 µg/ml) in PBS (pH 7.4) as well as in the mixture of PBS (pH 7.4) and ethanol (5:1) were prepared individually to determine the λ_{max} of AZT in these two different respective solutions. The two different solutions of AZT were scanned from wave length 200 nm to 400 nm by UV/VIS spectrophotometer using PBS (pH 7.4) and mixture of PBS (pH 7.4) and ethanol respectively as blank, as per requirement. For *in vitro* drug release study, PBS (pH 7.4) was used individually as drug release media and the mixture of PBS (pH 7.4) and ethanol at a ratio 5:1 was utilized as a medium for evaluation of drug loading of NLs.

5.1.3. Preparation of calibration curve of AZT in PBS (pH 7.4)

About 5 mg of AZT was weighed accurately by using a digital balance. A stock solution (100 µg/ml) of AZT in PBS (pH 7.4) was prepared by dissolving this 5 mg of AZT in 50 ml of PBS (pH 7.4) using sonication for about 10 min. From this stock solution nine different

dilutions were made by using PBS (pH 7.4) to prepare nine different solutions having different concentrations of AZT such as 1µg/ml, 2 µg/ml, 4 µg/ml, 6 µg/ml, 8 µg/ml, 10 µg/ml, 15 µg/ml, 20 µg/ml and 25 µg/ml. Absorbance of these solutions were determined by UV/VIS spectrophotometer at 265 nm using PBS (pH 7.4) as blank. This experiment was performed thrice and the average values of absorbance were taken for each of nine different solutions containing different concentrations of AZT. From these data, calibration curve was prepared by plotting the drug concentration in X - axis against drug absorbance in Y - axis.

5.1.4. Preparation of calibration curve of AZT in the mixture of PBS (pH 7.4) and ethanol (5:1)

At first a mixture of PBS (pH 7.4) and ethanol at a ratio 5:1 was prepared. Accurately weighed 5 mg of AZT was dissolved in 50 ml of this mixture homogeneously by utilization of sonication for about 10 min to prepare a stock solution (100 µg/ml). Nine different dilutions such as 1 µg/ml, 2 µg/ml, 4 µg/ml, 6 µg/ml, 8 µg/ml, 10 µg/ml, 15 µg/ml, 20 µg/ml and 25 µg/ml were prepared. By using UV/VIS spectrophotometer absorbance of each diluted solutions was measured against the mixture of PBS (pH 7.4) and ethanol (5:1) as blank at 265 nm. This total procedure was repeated thrice and the average absorbance for each was considered to plot data. From these data, calibration curve was prepared as mentioned above.

5.2. Development of calibration curve of AZT in 50 % human serum

5.2.1. Preparation of 50 % human serum

Human serum and PBS (pH 7.4) were mixed homogeneously in aseptic condition at a ratio 1:1 to prepare 50 % serum.

5.2.2. Scanning for determination of λ_{max} of AZT in 50 % human serum

AZT containing 50 % human serum solution was prepared. Protein was precipitated of drug

containing solution as well as 50 % human serum without drug solution by protein precipitation method as mentioned under LC-MS/MS study. The supernatant of each sample was collected. With the help of UV/VIS spectrophotometer, the supernatant of drug solution was scanned from wave length 200 nm to 400 nm using supernatant of only 50 % human serum as blank to determine λ_{max}. Aseptic condition in all respect was maintained throughout the study.

5.2.3. Preparation of calibration curve of AZT in 50 % human serum

A stock solution (100 µg/ml) was prepared by dissolving accurately weighed 5 mg of AZT in 50 ml of 50 % human serum. From this stock solution, ten dilutions were made to prepare ten different concentrations of AZT containing solutions such as 10 µg/ml, 20 µg/ml, 30 µg/ml, 40 µg/ml, 50 µg/ml, 60 µg/ml, 70 µg/ml, 80 µg/ml, 90 µg/ml and 100 µg/ml. Before measuring of the absorbance, protein was precipitated of each solution including blank (50 % human serum) as mentioned under LC-MS/MS study. The supernatant for each sample was collected. Then absorbance of these individual supernatant was determined by UV/VIS spectrophotometer using supernatant of protein precipitated 50 % human serum as blank. This experiment was conducted thrice maintaining aseptic condition in all respect under laminar air flow hood and average absorbance was considered for each dilution. The calibration curve was prepared from the resulting data.

5.3. Preparation of ML

Here, by trial and error method we developed several lipids using various mixtures of three fatty acids present in many edible lipids (Kittiphoom, 2012). Out of them we have selected the best combination [SA:oleic acid (OA):palmitic acid (PA) = 8.08:4.13:1] (ML) on the basis of its consistency to develop the nanocarrier. Fatty acids at the selected ratio were

dissolved in small quantity of chloroform and chloroform was evaporated under vacuum to get the lipid formed from the fatty acids.

5.4. Fourier-transform infrared spectroscopy (FTIR)

FTIR was conducted to determine possible interaction (if any) between the drug and the excipients. For ML based formulation, pure drug (AZT), CHO, ML, BHT, physical mixture (PM) of CHO, ML, BHT, physical mixture (PMD) of CHO, ML, BHT and drug AZT, lyophilized formulation without drug (MGB) and lyophilized formulation with drug (MGF) and for SL based formulation, AZT, CHO, SL, BHT, physical mixture (PM-1) of CHO, SL, BHT, physical mixture (PMD-1) of CHO, SL, BHT and AZT, lyophilized formulation without drug (SYB) and lyophilized formulation with drug (SYF) were scanned at 4000 cm^{-1} to 400 cm^{-1} using FTIR instrument using their pellets formed by mixing with potassium bromide (KBr) at 1:100 ratio and compressing with a hydraulic press (Sahana et al., 2010).

5.5. Preparation of NLs

NLs were prepared by lipid layer hydration technique by varying different process parameters (Rudra et al., 2010). Specific weighed amounts of excipients CHO, lipids (ML for ML-based formulations / SL for SL-based formulations, respectively) (Table 5.1) and BHT (1 % w/v as antioxidant) were taken in 250 ml round bottom flask and adequate quantity of chloroform was added within the flask with vigorous shaking to dissolve the excipients. The flask was set up in a rotary vacuum evaporator fitted with an A3S aspirator and a circulating water-bath at 5ºC and was rotated at 145 rpm rotation speed at 40ºC in water-bath to evaporate the organic solvent and to form thin film of lipid layer on the inside-wall of the flask. For complete elimination of the residual chloroform, the flask was kept overnight in a vacuum desiccator. The weighed amount of AZT was dissolved in PBS (pH 7.4), and the mixture was taken in the flask. The flask was then fitted in a rotary vacuum evaporator with rotation speed at 145

rpm and at 40ºC in a water-bath for complete dispersion of thin lipid film in the aqueous phase. The dispersion was sonicated at 30 ± 3 KHz in a bath type sonicator for 1 h with cold water. To form vesicles, the round bottom flask was kept at room temperature for 1.5 h and stored overnight at 4ºC. The preparation was centrifuged at 5000 rpm for 15 min at 4ºC to separate the larger vesicles and the obtained supernatant was again centrifuged (at 16000 rpm for 45 min in a cold centrifuge at 4ºC) to precipitate NLs. The obtained precipitate was re-suspended in fresh PBS (pH 7.4) and precipitated again number of times to wash the NLs. NLs were collected in a petridish and lyophilized for 12 h to get dry product. Blank NLs (MGB, SYB) were prepared by the same procedure without using AZT.

Table 5.1: Composition of experimental formulations[b]

Formulation code	Composition	Ratio (w/w)
MGF_1	CHO, ML, AZT	5:5:3
MGF	CHO, ML, AZT	5:15:3
MGF_2	CHO, ML, AZT	5:25:3
SYF_1	CHO, SL, AZT	5:5:3
SYF	CHO, SL, AZT	5:15:3
SYF_2	CHO, SL, AZT	5:25:3

[a] Data were expressed as mean ± SD (n = 3). SD: Standard deviation.
[b] MGF_1, MGF, MGF_2: Lipid (ML)-based formulation, SYF_1, SYF, SYF_2: Soya lecithin (SL)-based formulation.

Fluorescent NLs were prepared using the same process as described above except the step where fluorescent marker FITC was used. FITC stock solution (0.4 % w/v) was prepared in a mixture of chloroform and ethanol at volume 3:1 ratio and a volume of 100 µl was mixed into the organic phase (chloroform) during the initial mixing of preparation (Shaw et al., 2017).

5.6. Characterization of NLs

5.6.1. Evaluation of drug loading

NLs (5 mg) were taken in a mixture of PBS (pH 7.4) and ethanol at a ratio of 5:1 and

sonicated and vortex-mixed. After centrifugation (at 16000 rpm for 15 min at 4ºC), the supernatant was collected and measured at 265 nm using UV/VIS spectrophotometer. The same procedure was performed for all the experimental formulations. Absorbance for drug was obtained by deducting the absorbance obtained from NLs without drug and from that of NLs with drug (Satapathy et al., 2016). Each study was conducted thrice. The percentage of drug loading was calculated using the following formula.

Percentage of drug loading = (Amount of AZT in NLs / Amount of NLs taken) x 100 (1)

5.6.2. Percentage of yield determination

To determine the yield of NLs from the utilized total amount of raw materials of NLs preparation, lyophilized dried NLs of each batch were weighed and the percentage of yield was calculated by using the following equation as mentioned earlier (Sahana et al., 2010).

Percentage of yield = (Amount of NLs obtained / Total amount of drug and excipients used)

x 100 (2)

5.6.3. Evaluation of size distribution and zeta potential

By utilizing the dynamic light scattering (DLS) technology in a Zetasizer Nano ZS90, average size of NLs, size distribution pattern, PDI and zeta potential of the experimental formulations were determined.

5.6.4. FESEM for surface morphology analysis

FESEM was used to investigate the surface morphology of NLs. The lyophilized NLs were placed on an adhesive tape of carbon over a stub by spreading smoothly and then dried through vacuum and coated with platinum using a platinum coater instrument. After that the

samples were observed at various magnifications with the help of field emission scanning electron microscope (Dey et al., 2016).

5.6.5. Cryo-TEM study

Cryo-TEM study was performed to observe morphology and lamellarity of NLs. About 1.5 mg lyophilized formulation was taken in a microcentrifuge tube and 1 ml of Milli-Q water was added into it. The suspension was vortexed followed by sonication for a few minutes to prevent agglomeration. The NLs suspension (4 µl) was put on a clean grid, blotted away the excess (if any) with the help of filter paper and vitrified instantly by dipping into liquid ethane. The grid was stored in liquid nitrogen till shifting under the electron microscope which was operated at 300 kV equipped with an FEI Eagle 4K x 4K charge-coupled device (CCD) camera for capturing the images (Fox et al., 2014).

5.6.6. Atomic force microscopy (AFM) study

AFM study was performed to understand the three-dimensional measurement and surface morphology of NLs. MGF / SYF was dispersed in Milli-Q water by vortexor and followed by brief sonication. One drop of dispersed NLs solution was placed on the surface of a well cleaned glass slide and dried by using vacuum drying. In ambient conditions through mode PeakForce QNM (Quantitative Nanomechanical mapping) applying silicon nitride probe along with a force constant 0.4 N/m and a resonance frequency 150–350 kHz the morphology of the NLs was observed using atomic force microscope.

5.7. *In vitro* investigations

5.7.1. *In vitro* drug release study

In vitro drug release study was conducted in freshly prepared PBS (pH 7.4) and in 50 % human serum individually as drug release media at room temperature [for PBS (pH 7.4) as

media] and at 37ºC (for 50 % human serum as media) (in physiological mimicking condition), respectively for 24 h. Drug release media (50 ml) was taken in a glass beaker (100 ml). Lyophilized formulation (5 mg) was weighed accurately and reconstituted in 1 ml of the respective drug release media and was placed into a dialysis bag (dialysis membrane – 110) (Dey et al., 2016). The dialysis bag was tightly knotted at the two ends with cotton thread and hanged centrally into the beaker containing drug release medium (in such a way so that the formulation portion inside the bag immersed within the media) using a laboratory ring stand with clamp kit. The beaker was put on a magnetic stirrer maintaining stirring at 300 rpm using a magnetic bead. From the beaker, 1 ml media was withdrawn at various predetermined time intervals and same volume of fresh media was replaced immediately into the beaker. All the collected samples were analysed using UV/VIS spectrophotometer at 265 nm with PBS or 50 % human serum as blank according to requirement. In case of human serum sample protein was precipitated as mentioned under LC-MS/MS study. The drug concentration at any individual time point was calculated with the help of calibration curve. For 50 % human serum as drug release media, total experiment was conducted maintaining aseptic condition in all respect under laminar air flow hood.

5.7.2. *In vitro* drug release kinetic study

In vitro drug release data were applied in various kinetic models such as zero order (percentage cumulative drug release versus time), first order (log of percentage cumulative amount of drug remained to release versus time), Higuchi model (percentage cumulative drug release versus square root of time), Hixson–Crowell model (cube root of percentage cumulative amount of drug remained to release versus time), Korsmeyer-Peppas model (log of percentage cumulative drug release versus log of time) to predict the drug release pattern

of the optimized formulations. The highest correlation coefficient value (R^2) from all the tested models was utilized to select the suitable kinetic pattern (Das et al., 2015).

5.7.3. *In vitro* cellular uptake study

To investigate the cellular uptake ability of NLs by U-87 MG cells, confocal laser scanning microscopy study was executed. In six well culture plates U-87 MG cells were seeded on coverslips (3×10^4) and cultivated using MEM containing 10 % FBS for 24 h. These cells were treated with FITC-MGF / FITC-SYF suspension at a concentration of 100 μg/ml. At different time points (i.e., 0.25 h, 1 h, 3 h) of incubation, the cells were washed thrice and fixed applying paraformaldehyde aqueous solution (4 %). They were cleaned by using freshly prepared PBS (pH 7.4) after 5 min of fixation. Then, coverslips were collected cautiously and mounted on the glass slide. After complete air drying, the slides were placed individually under a confocal laser scanning microscope and the images were snapped (Maji et al., 2014).

5.8. Stability study

Stability testing of the lyophilized formulations was performed as per ICH guidelines as done earlier (Sahana et al., 2010).

5.9. *In vivo* investigations

5.9.1. Radiolabeling of AZT and AZT loaded NLs

According to the tin (II) chloride reduction method as described earlier (Satapathy et al., 2016; Das et al., 2015) radiolabeling of AZT and AZT loaded MGF / SYF was performed with ^{99m}Tc. At first 5 mg of AZT was dissolved in 0.5 ml ethanol and AZT loaded NLs (equivalent to 5 mg of AZT) were suspended in 0.5 ml of nitrogen purged water. The aqueous ^{99m}Tc-pertechnetate ($^{99m}TcO4^-$) (40–100 MBq) was incorporated to them followed by addition of 25 μl of aqueous stannous chloride dihydrate ($SnCl_2.2H_2O$) (2 mg/ml) solution.

At room temperature, they were incubated for 15 min. The radiolabeled efficiencies were then assessed with the help of ascending thin layer chromatography by applying silica gel coated aluminium strips as stationary phase and methyl ethyl ketone as mobile phase. The sheets were dried after developing the spots and they were cut into 5 strips (1 cm each). These were analysed quantitatively through counting using a well type gamma counter at 140 keV.

5.9.2. Gamma Scintigraphy

For providing direct evidence of location of radiolabeled NLs as well as free drug within the body of experimental rats, gamma scintigraphy imaging was performed. Only male Sprague-Dawley rats (body weight 200-250 g) were utilized in this study. After dividing the total rats into three groups, ^{99m}Tc labeled AZT / ^{99m}Tc labeled MGF / ^{99m}Tc labeled SYF was injected (100 µl) through femoral vein of rats of the respective group. Using the intramuscular injection of ketamine hydrochloride (1 ml) rats were anesthetized and fixed on a board in the posterior position for imaging. At predetermined time interval (1 h and 5 h of post injection) static images were snapped with the help of planar gamma camera (GE Infinia Gamma Camera equipped with Xeleris Workstation, GE, Cleveland, OH, USA).

5.9.3. Biodistribution study

Sprague-Dawley rats (body weight 200-250 g) were utilized for performing the biodistribution of radiolabeled AZT and NLs (MGF, SYF). By applying ketamine (30-50 mg/kg) intramuscularly, rats were anesthetized and cannulation was done in the femoral vein of animals using polyethylene (PE-50) catheter tubes. All the experimental animals were well-hydrated by administering (2 ml) normal saline (0.9 % NaCl (w/v) in water) through intraperitoneal route for 1 h. ^{99m}Tc labeled AZT / ^{99m}Tc labeled MGF / ^{99m}Tc labeled SYF was injected at 0.03 ml volume (10-15 MBq/kg) via i.v. route through the cannula. The

animals were sacrificed at 1 h and 5 h post injection. The organs and tissues such as heart, liver, lung, spleen, muscle, intestine, stomach, kidney and brain were removed followed by washing using normal saline. The collected organs and tissues were dried up immediately using blotting paper (if applicable) and taken into the preweighed counting vials. Blood was collected using heart puncture process. With the help of a well-type gamma scintillation counter along with an injection standard, the corresponding radioactivity of the samples was measured and percentage of injected dose per gram (% ID per g) of tissue or organ was utilized for expressing the results.

5.9.4. *In vivo* plasma and brain pharmacokinetic study

In vivo plasma and brain pharmacokinetic study was performed to compare the distribution of AZT from free drug suspension and NLs (MGF, SYF) and observe the ability of NLs to cross BBB in Sprague-Dawley rats. The animals were distributed into four groups. AZT suspension was injected in animals of one group through i.v. route as per dose. Another group of animals was injected MGF and the third group was treated with SYF intravenously with an equivalent amount of AZT with respect to free drug in suspension. Tail vein was selected to administer the injection for all animals of each batch. The fourth group remained as control (untreated). For plasma pharmacokinetic study, blood samples were collected by terminal cardiac puncture of each animal following anaesthesia, at a predetermined time interval such as 0.25 h, 0.5 h, 1 h, 2 h, 4 h, 6 h, 8 h, 10 h, 12 h, 24 h and 48 h of post i.v. injection and kept the sample immediately into a microcentrifuge tube having EDTA solution. For plasma collection, the blood samples were centrifuged at 5000 rpm for 6 min using cold centrifuge and the plasma was preserved at -80ºC till further analysis (Dey et al., 2016).

For brain kinetic study, at a predetermined time interval (0.5 h, 1 h, 2 h, 4 h, 6 h, 8 h, 10 h, 12

h and 24 h of post i.v. injection), rats were dissected and brains were separated followed by washing with Milli-Q water. *In situ* blood perfusion (Takasato et al., 1984) was done before collection of brain in the experiment. Then the collected brains were kept into cryogenic tubes and stored at -80ºC till LC-MS/MS study.

5.9.5. LC-MS/MS study

Evaluation of AZT concentration in plasma and brain was performed by using LC-MS/MS technique (Shaw et al, 2017). Briefly, plasma sample / homogenized brain tissue was first mixed with ice cold acetonitrile (plasma / tissue homogenate:cold acetonitrile was 1:3 by volume) containing internal standard followed by vortex-mixed for 10 min and centrifuged (at 4000 rpm for 15 min at 4ºC) for efficient extraction of AZT by protein precipitation method (Gautam et al., 2013). The supernatant for each sample was collected. The supernatant (100 µl) of each sample was mixed with 100 µl water and loaded into LC-MS/MS. Elution was done with the help of YMC Triat C18 column (2.1 x 30 mm, 5 µ). Gradient elution technique of two mobile phases (mobile phase A: 0.1 % formic acid in water and mobile phase B: 0.1 % formic acid in 80:20 acetonitrile / water) was conducted with injection volume: 20 µl, flow rate 0.8 ml/min and total run time was 3.0 min in each case.

5.9.6. Calculation of PK parameter

AZT concentrations in plasma and brain were plotted against time. By utilizing of NCA toolbox of Phoenix-Winnonlin software (Certara, UK), various PK parameters such as area under the concentration-time curve from time of injection to a determined time point (AUC_{0-t}), area under the first moment curve ($AUMC_{0-t}$), clearance (Cl), time taken for maximum blood concentration to drop in half-life ($t_{1/2}$), steady state volume of distribution (Vss), mean residence time (MRT) etc. were determined.

5.9.7. Statistical analysis

Statistical calculations of various data were conducted by applying one-way analysis of variance (ANOVA) through Tukey-Kramer multiple comparisons test with the help of GraphPad InStat (version 3.06) software (California, USA). The probability value ($P<0.05$ at 95 % confidence interval was recognised as statistically significant.

Chapter 6

Results

6. Results

6.1. Determination of λ_{max} of AZT in PBS (pH 7.4) and in the mixture of PBS (pH 7.4) and ethanol (5:1)

The λ_{max} of AZT in different working solutions such as PBS (pH 7.4) and the mixture of PBS (pH 7.4) and ethanol (5:1) was determined by using UV/VIS spectrophotometer. The λ_{max} of AZT was found to be at 265 nm in PBS (pH 7.4) (Figure 6.1A) as well as in the mixture of PBS (pH 7.4) and ethanol (5:1) (Figure 6.1B) and this value was selected for further analysis as per requirement. The first peaks in the figures were responsible for solvent(s).

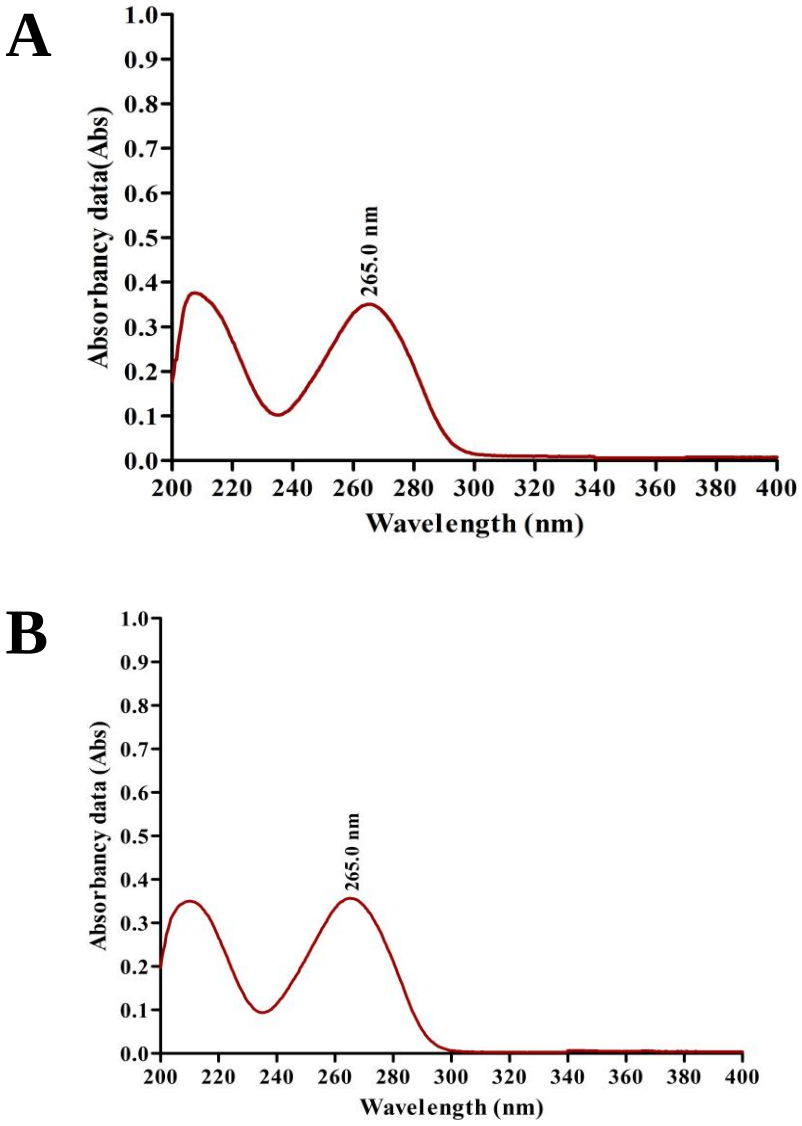

Figure 6.1: (A) Absorption maxima (λ_{max}) of AZT in PBS (pH 7.4) showed at 265 nm. (B) Absorption maxima (λ_{max}) of AZT in the mixture of PBS (pH 7.4) and ethanol (5:1) showed at 265 nm.

6.2. Preparation of calibration curve of AZT in PBS (pH 7.4)

The following absorbance values against different concentrations of AZT (as mentioned in Table 6.1) were determined in PBS (pH 7.4) at λ_{max} 265 nm. The calibration curve was drawn using these data by plotting absorbance values against respective concentrations (Figure 6.2).

Table 6.1: Absorbance data for calibration curve of AZT in PBS (pH 7.4) at 265 nm

Concentration (µg/ml)	Absorbance*
1	0.04167 ± 0.000577
2	0.08533 ± 0.000577
4	0.15267 ± 0.004163
6	0.22267 ± 0.000577
8	0.29367 ± 0.001155
10	0.36467 ± 0.008083
15	0.56500 ± 0.001732
20	0.73900 ± 0.002000
25	0.89733 ± 0.002082

* Data were expressed as mean ± SD (n = 3). SD: Standard deviation.

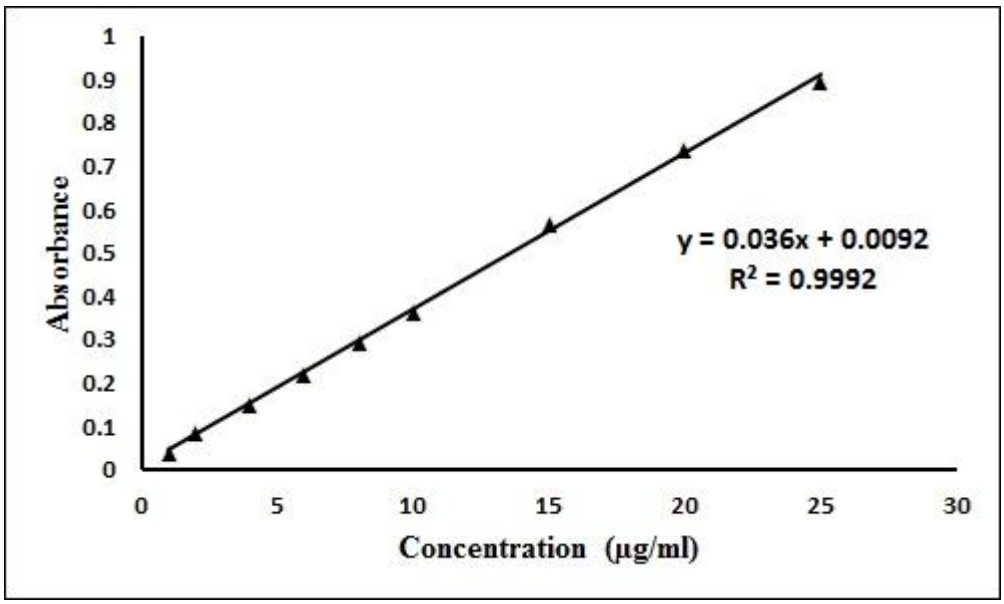

Figure 6.2: Calibration curve of AZT in PBS (pH 7.4). Data show mean (n = 3).

6.3. Preparation of calibration curve of AZT in the mixture of PBS (pH 7.4) and ethanol (5:1)

Absorbance of various concentrations of AZT in the mixture of PBS (pH 7.4) and ethanol (5:1) was measured at λ_{max} 265 nm and given in Table 6.2. The calibration curve was prepared by plotting AZT concentrations in X - axis against absorbance in Y- axis (Figure 6.3).

Table 6.2: Absorbance data for calibration curve of AZT in the mixture of PBS (pH 7.4) and ethanol (5:1)

Concentration (µg/ml)	Absorbance*
1	0.03600 ± 0.001000
2	0.07300 ± 0.001732
4	0.14367 ± 0.003786
6	0.21233 ± 0.003055
8	0.28400 ± 0.001000
10	0.36267 ± 0.001528
15	0.55433 ± 0.003786
20	0.72267 ± 0.002309
25	0.89200 ± 0.001732

* Data were expressed as mean ± SD (n = 3). SD: Standard deviation.

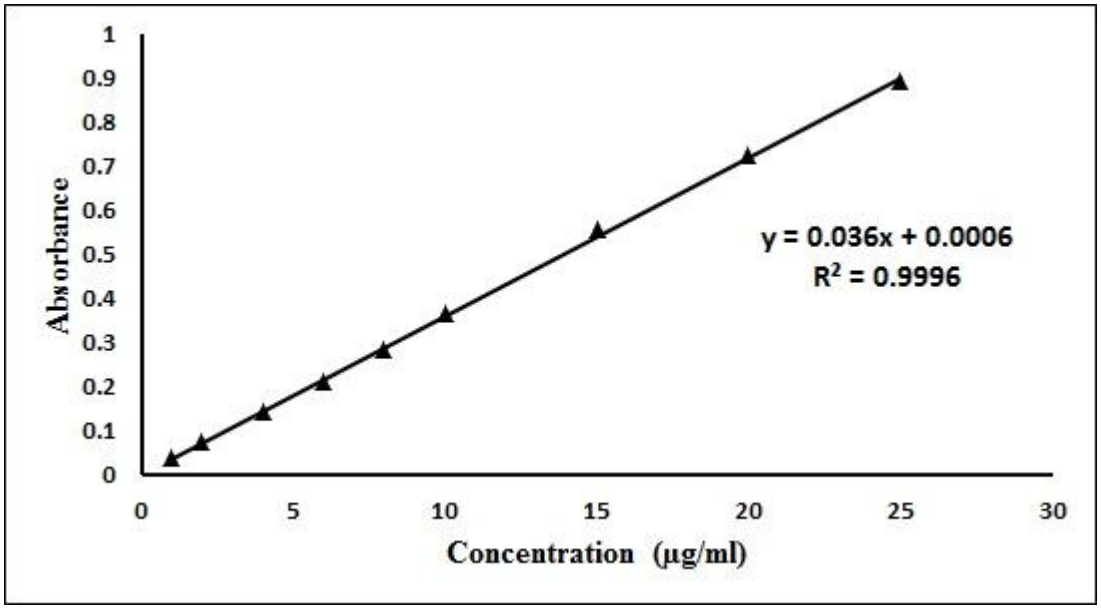

Figure 6.3: Calibration curve of AZT in the mixture of PBS (pH 7.4) and ethanol (5:1). Data show mean (n = 3).

6.4. Determination of λ_{max} of AZT in 50 % human serum

The λ_{max} of AZT was observed at 265 nm in 50 % human serum with the help of UV/VIS spectrophotometer (Figure 6.4). As per requirement this value was utilized for further analysis.

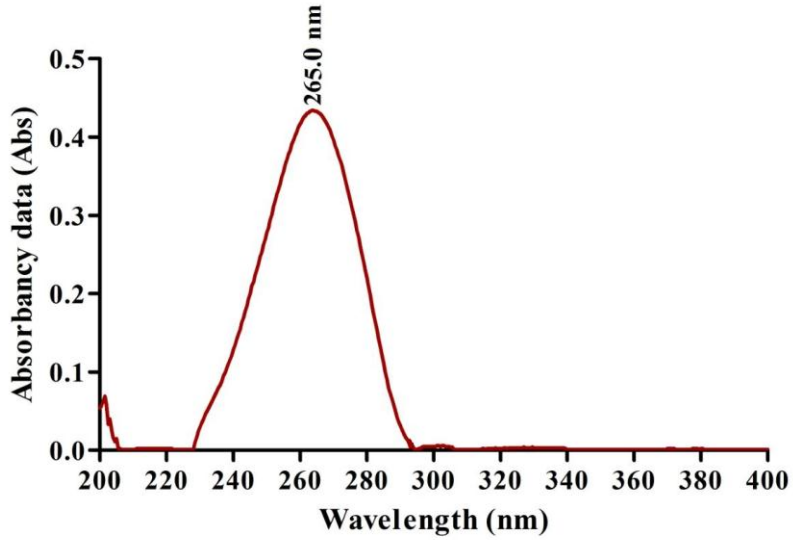

Figure 6.4: Absorption maxima (λ_{max}) of AZT in 50 % human serum showed at 265 nm.

6.5. Preparation of calibration curve of AZT in 50 % human serum

Absorbance values of different concentrations of AZT in 50 % human serum were determined at λ_{max} 265 nm against 50 % human serum as blank and given in Table 6.3. The calibration curve of AZT in 50 % human serum was prepared using these data as mentioned above (Figure 6.5).

Table 6.3: Absorbance data for calibration curve of AZT in 50 % human serum

Concentration (µg/ml)	Absorbance*
10	0.08633 ± 0.007638
20	0.16533 ± 0.012423
30	0.25467 ± 0.017898
40	0.34000 ± 0.029816
50	0.42533 ± 0.029023
60	0.51267 ± 0.033546
70	0.60100 ± 0.047286
80	0.68200 ± 0.048539
90	0.76533 ± 0.061256
100	0.84567 ± 0.059543

* Data were expressed as mean ± SD (n = 3). SD: Standard deviation.

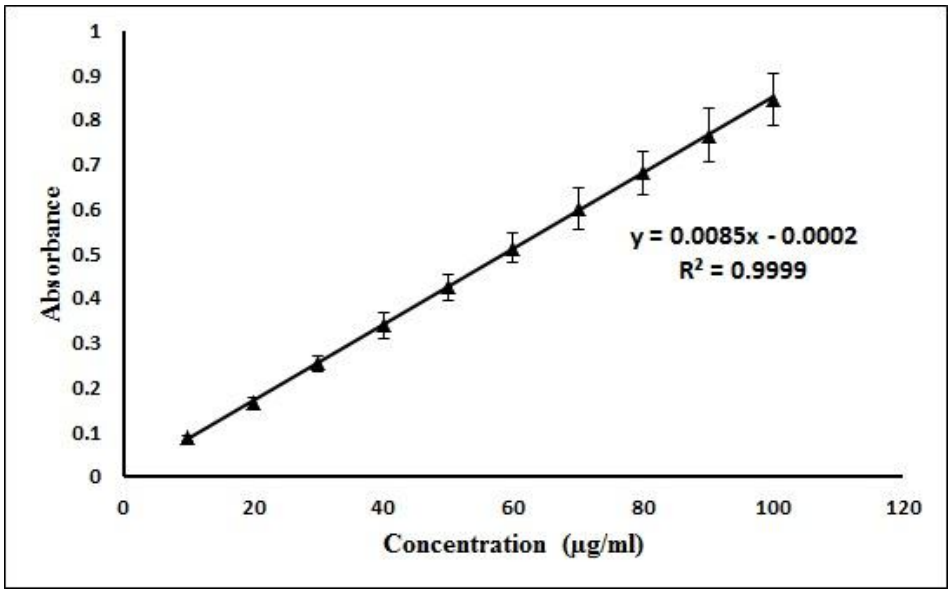

Figure 6.5: Calibration curve of AZT in 50 % human serum. Data show mean ± SD (n = 3). SD: Standard deviation.

6.6. FTIR analysis

Drug-excipient interaction was investigated through FTIR spectroscopy to determine any interaction between the functional groups of drug (AZT) and the excipients of a formulation (Basu et al., 2012). When the FTIR spectra of the physical mixture of the drug and the excipients (ML, CHO) were compared with those of the physical mixture of the excipients without drug, the lyophilized formulation with or without drug and each of the excipients, the presence of the characteristic peaks of the drug (at 2083 cm^{-1}), ML (at 2922 cm^{-1}, at 2852 cm^{-1} and at 721 cm^{-1}) and CHO (at 1373 cm^{-1}) was observed (Figure 6.6).

Likewise, during the comparison of the FTIR spectra of the drug, SL and CHO, the presence of the characteristic peak of the drug was observed at 2083 cm^{-1} in the physical mixture. The characteristic peaks of SL (at 2928 cm^{-1} and at 1462 cm^{-1}) and CHO (at 1373 cm^{-1}) were also observed in the physical mixture of the drug and the excipients (Figure 6.6).

The findings suggest the absence of any chemical interaction between the drug and the excipients for both the formulations (ML based, MGF and SL based, SYF). However, minor shifting of some of the peaks of the excipients in formulations (from 2922 cm^{-1} to 2920 cm^{-1}, 2852 cm^{-1} to 2851 cm^{-1} and from 721 cm^{-1} to 719 cm^{-1} in ML-based formulation and CHO from 3415 cm^{-1} to 3436 cm^{-1} in case of SL-based formulation) was observed. The observations suggest that physical interactions existed between the molecules of the excipients. The interaction might be responsible to provide the structure of the formulation and for sustained drug release from the formulations. In case of the ML formulation, the peak of the drug was not observed. The finding suggests that the drug was encapsulated entirely in the formulation and there was the absence of drug molecules on the surface of the

formulation. For SL formulation, presence of the peak of the drug was found to shift from 2084 cm^{-1} to 2096 cm^{-1}. The finding indicates that the shifting of the peak of the drug might be due to physical interaction between the drug and the excipients. Further, the drug molecules were also present in the lipid bilayers and might retain in the formulation due to the physical interaction between the drug and the excipients.

In case of SL formulation, a shifting of wave number from 2084 cm^{-1} to 2096 cm^{-1} might be due to the formation of weak bond (such as hydrogen bond, van der Waals force of attraction or dipole moment) between methyl group of the drug and OH group of CHO. The wave number ranging from 3415 cm^{-1} to 3436 cm^{-1} is the strong intensity stretching vibration zone of OH group. The wave number ranging from 2084 cm^{-1} to 2096 cm^{-1} is the stretching vibration zone of C-C=C of the drug. Further, the wave number regions, 2922 cm^{-1} to 2920 cm^{-1} and 2852 cm^{-1} to 2851 cm^{-1}, are the strong intensity stretching vibration regions of CH_2, CH and CH_3 and the region 721 cm^{-1} to 719 cm^{-1} is the variable to weak intensity bending vibration region of out of plane OH bending. Hence, there might be physical interaction by formation of weak bonds (hydrogen bond, van der Waals force of attraction or dipole moment) responsible for minor shifting of peaks.

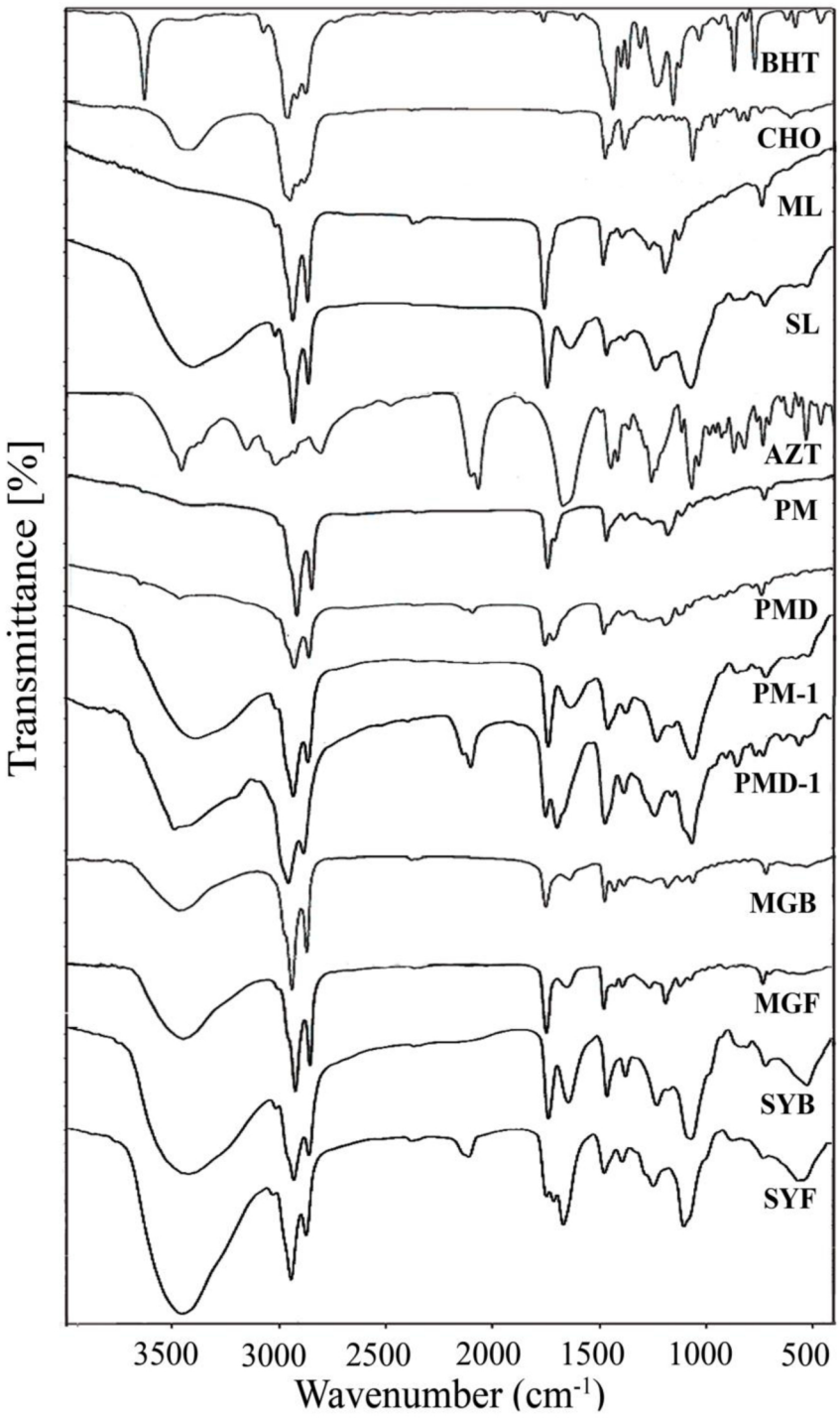

Figure 6.6: Fourier transform infrared spectroscopy (FTIR)-spectra of BHT (butylated hydroxytoluene), CHO (cholesterol), ML (lipid), SL (soya lecithin), AZT (zidovuine), PM (physical mixture of BHT, CHO, ML), PMD (physical mixture of BHT, CHO, ML and drug), PM-1 (physical mixture of BHT, CHO, SL), PMD-1 (physical mixture of BHT, CHO, SL and drug), MGB (ML-based lyophilized formulation without drug), MGF (ML-based lyophilized formulation with drug), SYB (SL-based lyophilized formulation without drug) and SYF (SL-based lyophilized formulation with drug).

6.7. Physico-chemical characterization of NLs

We initially varied the different process parameters such as temperature and speed of hydration, duration of sonication, time and speed of centrifugation, duration of freeze drying and ratio of the constituents to optimize the preparation process and to select the formulations. The best two formulations (MGF, SYF) were selected based on drug loading, particle size, PDI and zeta potential data (Table 6.4) and investigated for further study.

Table 6.4: % drug loading, % yield, particle size, PDI, zeta potential of experimental formulations[b]

Formulation code	Practical % drug loading[a]	% yield[a]	Particle size[a] (d. nm)	PDI[a]	Zeta potential[a] (mV)
MGF_1	0.2 ± 0.21	59.65 ± 5.11	81.23 ± 3.1	0.27 ± 0.05	-53.0 ± 4.1
MGF	5.7 ± 0.37	60.87 ± 5.92	24.37 ± 2.2	0.26 ± 0.02	-71.5 ± 6.5
MGF_2	1.8 ± 0.23	59.79 ± 4.82	65.21 ± 4.0	0.29 ± 0.04	-63.0 ± 7.3
SYF_1	1.3 ± 0.47	58.18 ± 5.01	95.58 ± 5.1	0.37 ± 0.02	-57.4 ± 3.5
SYF	7.0 ± 0.23	54.34 ± 4.79	33.75 ± 3.7	0.25 ± 0.06	-70.8 ± 7.0
SYF_2	2.5 ± 0.51	45.57 ± 5.62	60.21 ± 3.1	0.25 ± 0.02	-72.0 ± 6.2

[a] Data were expressed as mean ± SD (n = 3). SD: Standard deviation.
[b] MGF_1, MGF, MGF_2: Lipid (ML)-based formulation, SYF_1, SYF, SYF_2: Soya lecithin (SL)-based formulation.

6.7.1. Percentage of drug loading and yield

The percentage of drug loading of MGF was 5.7 ± 0.37 % with 60.87 ± 5.92 % yield capacity but SYF had 7.00 ± 0.23 % drug loading with yield capacity of 54.34 ± 4.79 % (Table 6.4). Every experiment was repeated thrice to establish the reproducibility.

6.7.2. Size, size distribution and zeta potential

Liposomal size, surface morphology and the lamellarity of liposome have been assessed by particle size analyser, FESEM and Cryo-TEM, respectively. FESEM figures showed that the

average size of the lyophilized liposome varied for MGF and SYF. When the liposomes were assessed by particle size analyser it showed the average size 24.37 ± 2.2 nm for MGF (Figure 6.7A) and 33.75 ± 3.7 nm for SYF (Figure 6.7B), respectively with their PDI 0.26 ± 0.02 and 0.25 ± 0.06 respectively (Table 6.4).

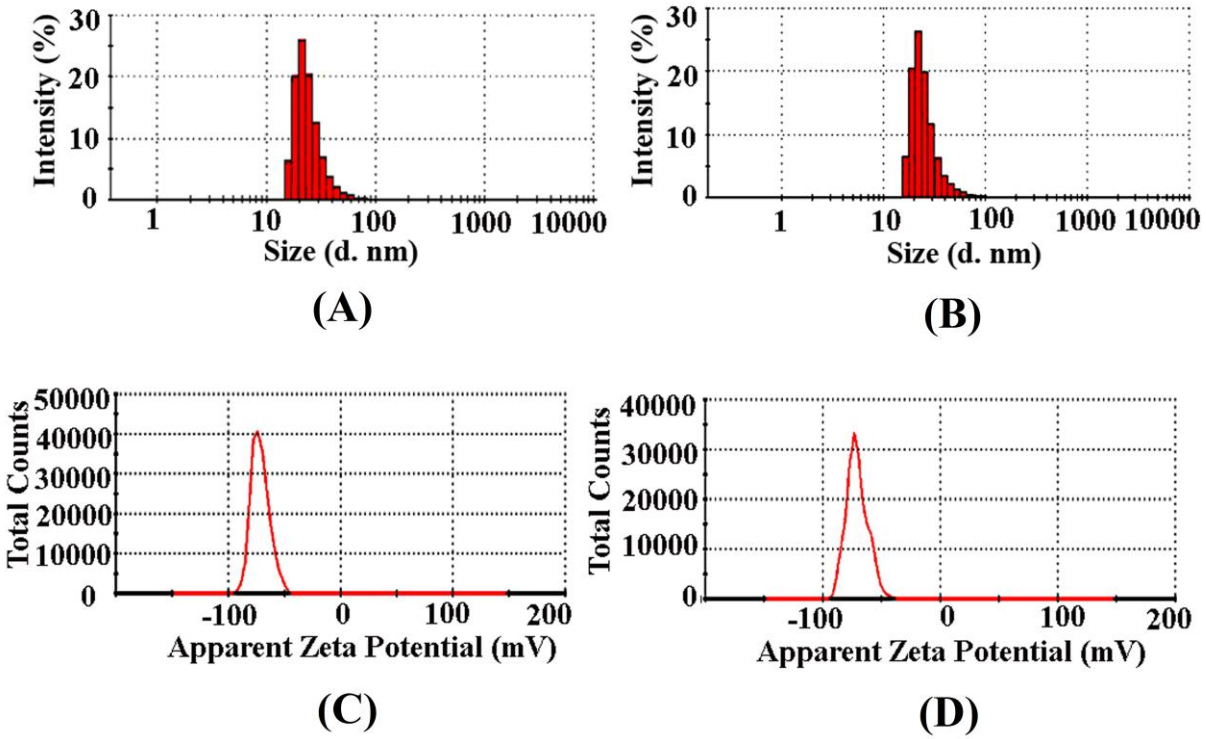

Figure 6.7: Particle size distribution of (A) MGF, (B) SYF. Zeta potential of (C) MGF, (D) SYF.

When the lamellarity was checked by Cryo-TEM, average size of the vesicles was found to be 30.75± 1.8 nm for MGF and 40.43± 2.4 nm for SYF with the intact lamellarity. The size was little bit higher as compared to the lyophilized liposome and the liposome analysed by particle size analyser. Since for Cryo-TEM analysis, the lyophilized liposomes were suspended for longer time as compared to particle size analysis by particle size analyser, the average size was enhanced marginally due to the entrapment of water in the core area of the liposomal vesicles. However, all the methods of analysis showed that the size were below 50

nm. Zeta potential of both the formulations were observed as negative, -71.5 ± 6.5 mV (Figure 6.7C) and -70.8 ± 7.0 mV (Figure 6.7D) for MGF and SYF, respectively. The statistical analysis of data of average size for both the formulations and the variation in PDI showed that there was an insignificant variation ($P>0.05$) in size distribution, but a significant variation of particle size between MGF and SYF. MGF showed smaller size particles compared to SYF. Zeta potential showed nearly same value for both the formulations.

6.7.3. FESEM study

Three images of FESEM at different magnifications namely 60000x, 120000x, 300000x were captured for MGF to establish the shape, size and distribution pattern of the formulation. The MGF had nanosize structure with smooth surface and was homogenously distributed at 60000x and 120000x magnification (Figure 6.8A, Figure 6.8B). At 300000x magnification, MGF was found to be spherical structure having nanosize with smooth surface and a homogeneous distribution pattern (Figure 6.8C). The FESEM image at 100000x magnification of SYF revealed that the liposomes were also in nanosize (about 30 nm), spherical shape with smooth surface and homogenous distribution (Figure 6.8D).

6.7.4. Cryo-TEM study

Cryo-TEM study was performed to visualize the internal structure of NLs. Nanosize unilamellar vesicles were found in the Cryo-TEM images for both the types of NLs (Figure 6.8E, Figure 6.8F). MGF had smaller size lyophilized vesicles than the size of SYF vesicles.

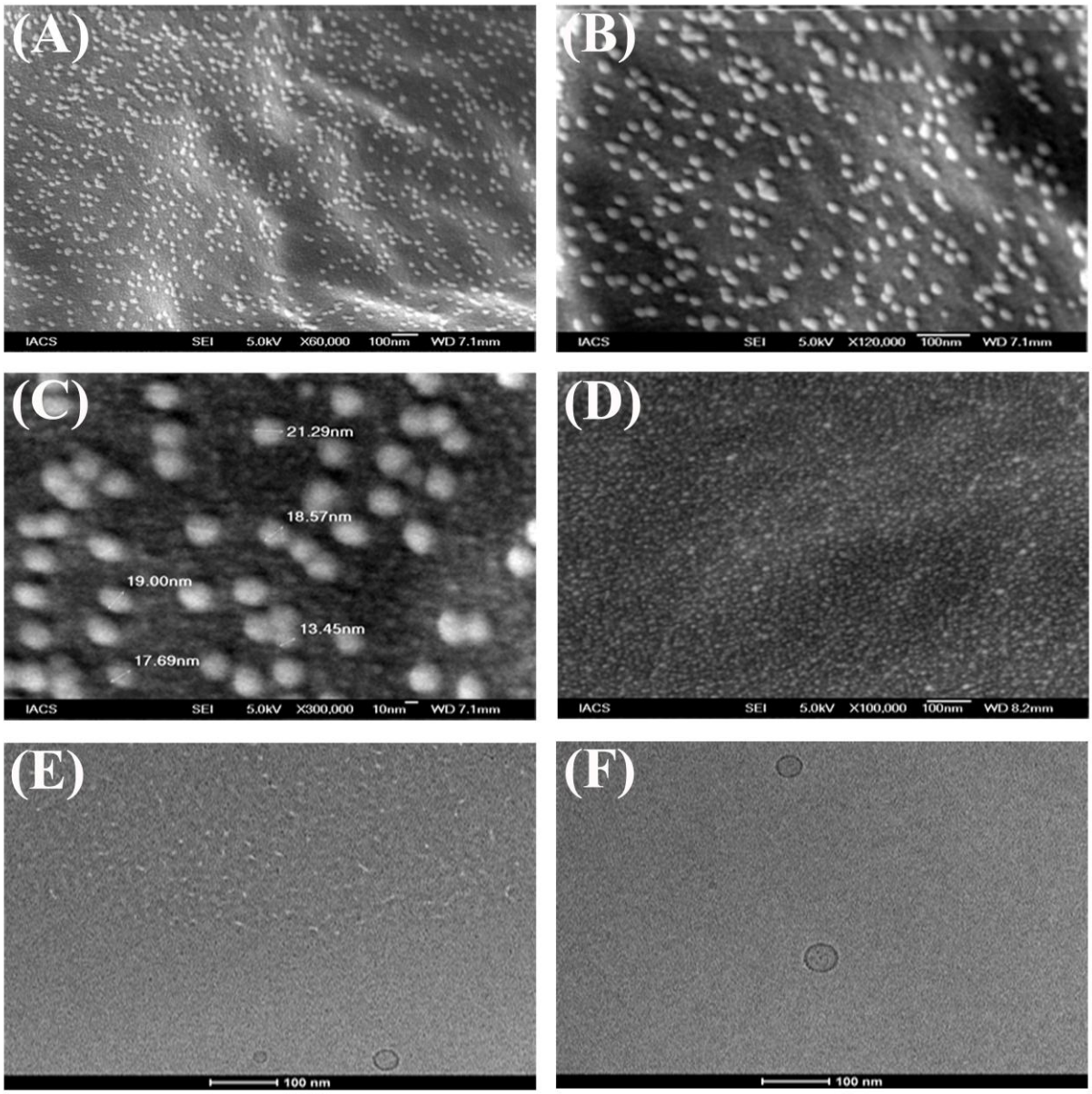

Figure 6.8: Morphological characterization of MGF and SYF. Field emission scanning electron microscopy (FESEM) images of (A) MGF at magnification of 60000x, (B) MGF at magnification of 120000x, (C) MGF at magnification of 300000x, (D) SYF at magnification of 100000x. Cryo-transmission electron microscopy (Cryo-TEM) images of (E) MGF, (F) SYF. Scale bar for Cryo-TEM image: 100 nm.

6.7.5. AFM study

From the AFM study it was observed that MGF / SYF was homogeneously distributed throughout the field. MGF / SYF was in nanosize along with a maximum height varied between 9.6 nm for MGF (Figure 6.9A) and 14.4 nm for SYF (Figure 6.9B).

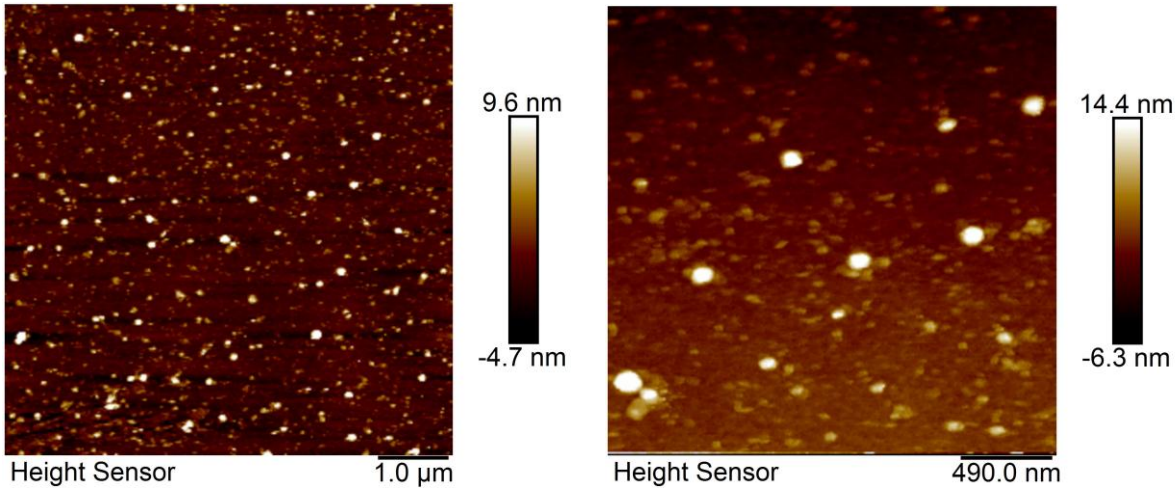

Figure 6.9: Atomic force microscopy (AFM) images of (A): MGF and (B): SYF.

6.8. *In vitro* investigations

6.8.1. *In vitro* drug release study

In vitro drug release study was conducted for both the formulations (MGF and SYF) to compare *in vitro* drug release patterns of both the formulations in two different release media. The data were plotted as percentage of cumulative drug release against time measured in hour (h) (Figure 6.10, Figure 6.11). From the results it appeared that cumulative 73.43 % and cumulative 82.21 % of AZT released from MGF in PBS media and in 50 % human serum respectively, whereas cumulative 82.48 % (PBS as media) and cumulative 84.51 % (50 % human serum as media) of AZT released from SYF over a period of 24 h. Drug release was to an extent slower from MGF than SYF. However, a steady and sustained drug release pattern was observed for both the formulations.

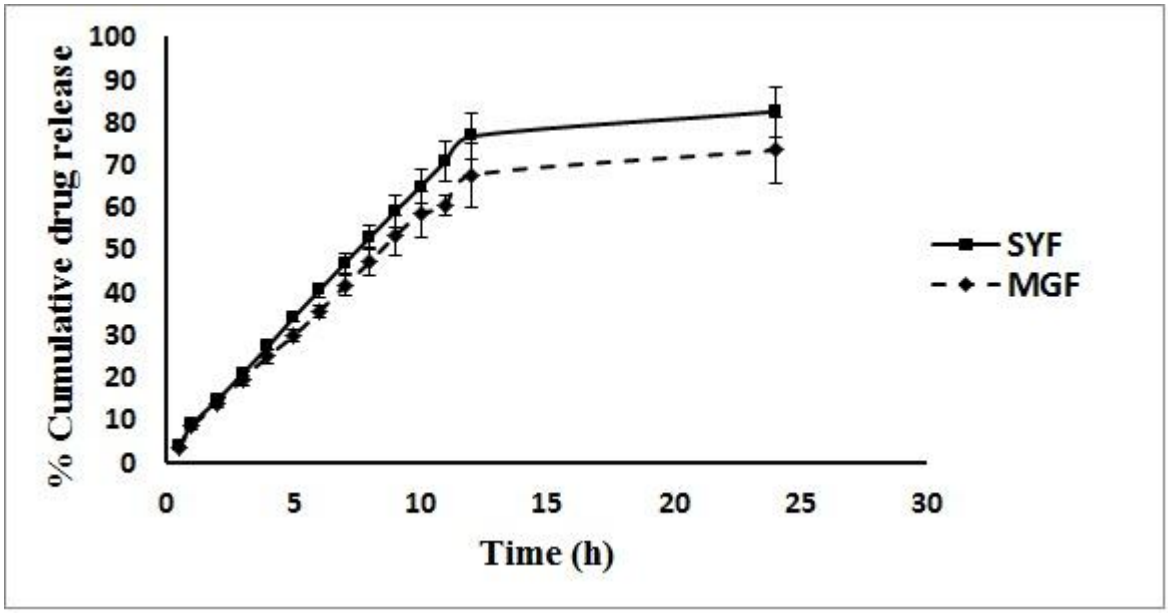

Figure 6.10: *In vitro* drug release profiles of MGF and SYF in PBS (pH 7.4). Data show mean ± SD (n = 3). SD: Standard deviation.

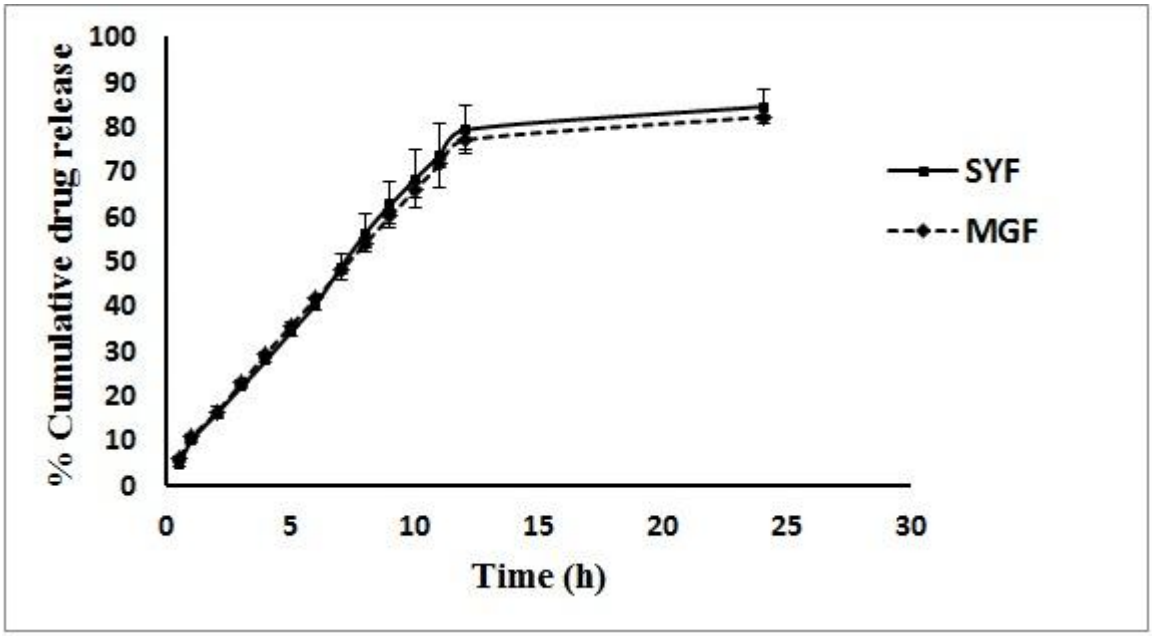

Figure 6.11: *In vitro* drug release profiles of MGF and SYF in 50 % human serum. Data show mean ± SD (n = 3). SD: Standard deviation.

6.8.2. Drug release kinetics analysis

To understand the drug release kinetic patterns, data were plotted using various kinetic equations and the corresponding correlation coefficients (represented here as R^2 values) were

determined (Table 6.5, Figure 6.12 to Figure 6.15). Data gave good linearity in Korsmeyer-Peppas kinetic model for both the formulations [R^2 = 0.9742 (PBS as drug release media) and R^2 = 0.9780 (50 % human serum as drug release media) for MGF and R^2 = 0.9752 (PBS as drug release media) and R^2 = 0.9751 (50 % human serum as drug release media) for SYF] as compared to the other kinetic models tested. The release exponent values (n) were 0.8387 and 0.8561 for MGF and SYF in PBS drug release media where as in 50 % human serum "n" values were 0.7539 for MGF and 0.8179 for SYF respectively. The "n" values indicated non-Fickian diffusion pattern of release of drug from NLs in both types of drug release media.

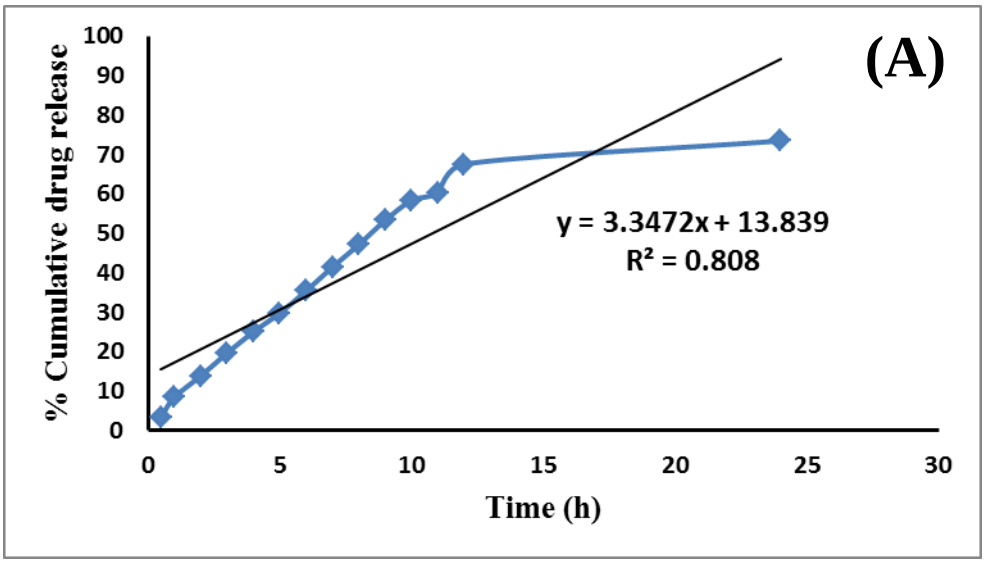

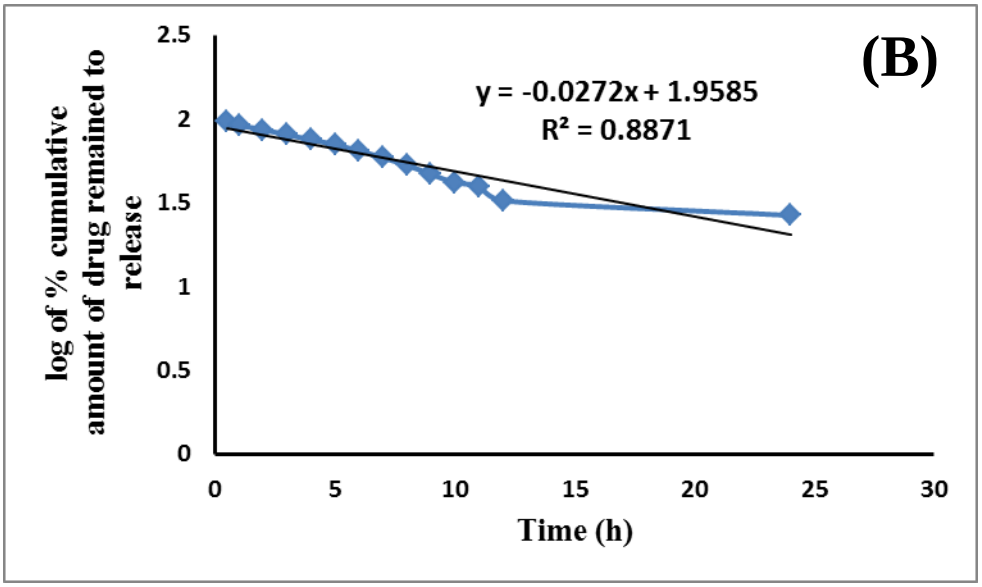

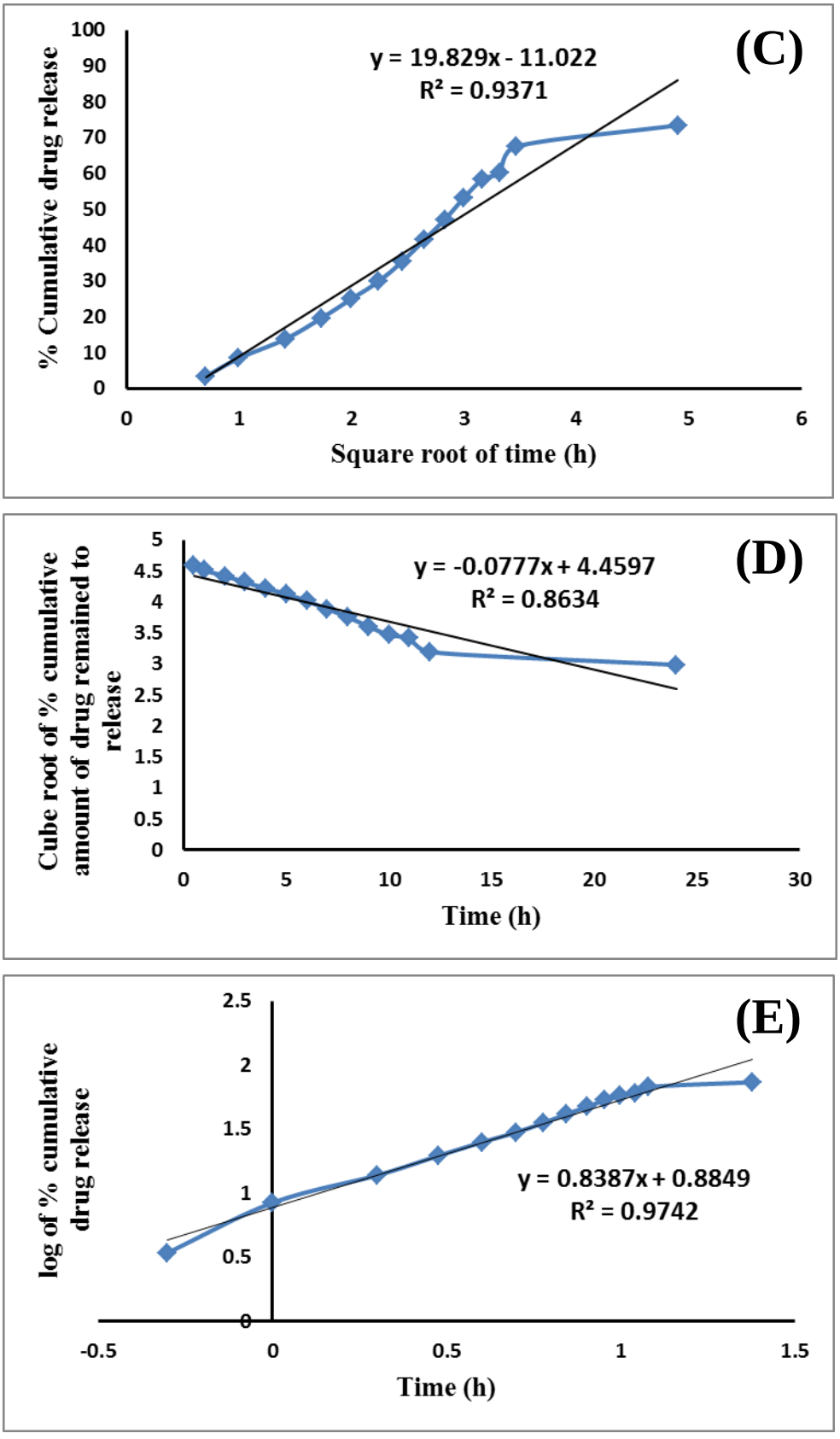

Figure 6.12: Graphical representation of various kinetic models of drug release from MGF in PBS (pH 7.4) as drug release media. (A) Zero order kinetics, (B) First order kinetics, (C) Higuchi kinetics, (D) Hixson-Crowell kinetics, (E) Korsmeyer-Peppas kinetics.

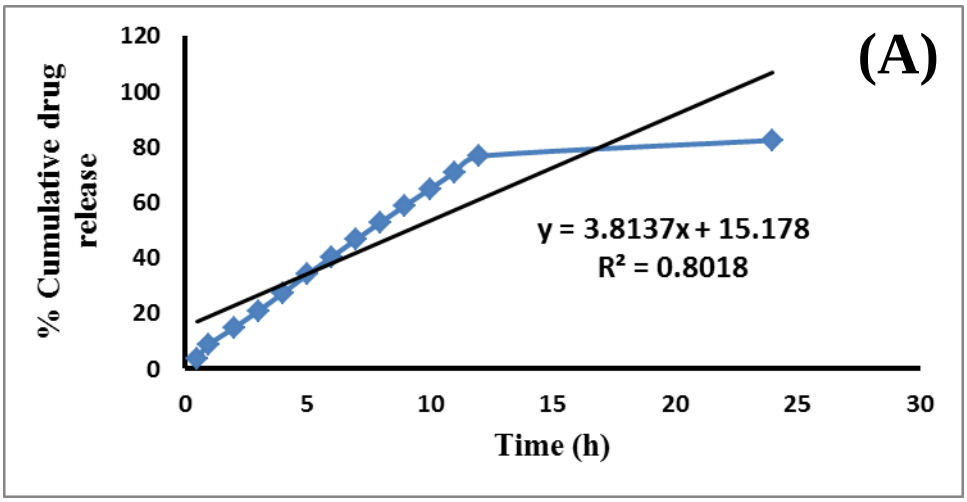
(A)
% Cumulative drug release
120
100
80
60
40
20
0
0
5
10
15
20
25
30
Time (h)
y = 3.8137x + 15.178
R² = 0.8018

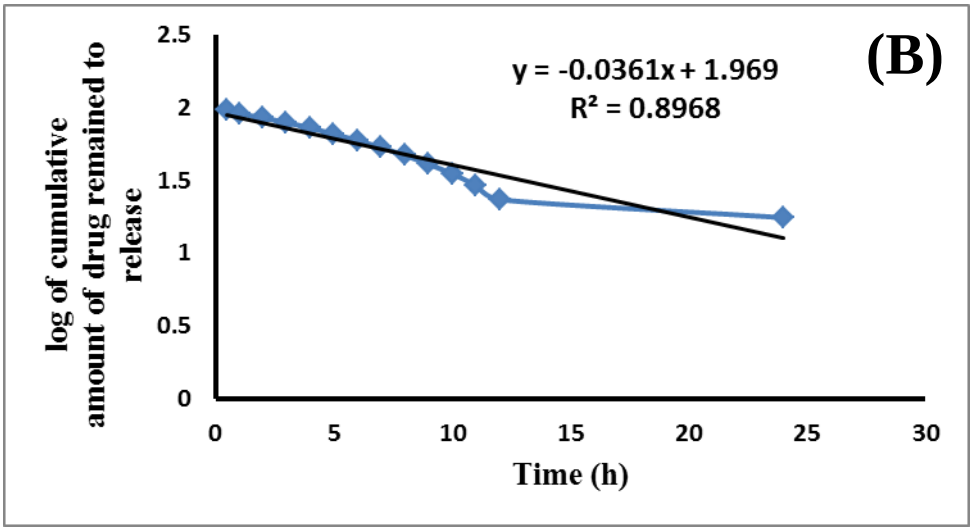
(B)
log of cumulative amount of drug remained to release
2.5
2
1.5
1
0.5
0
0
5
10
15
20
25
30
Time (h)
y = -0.0361x + 1.969
R² = 0.8968

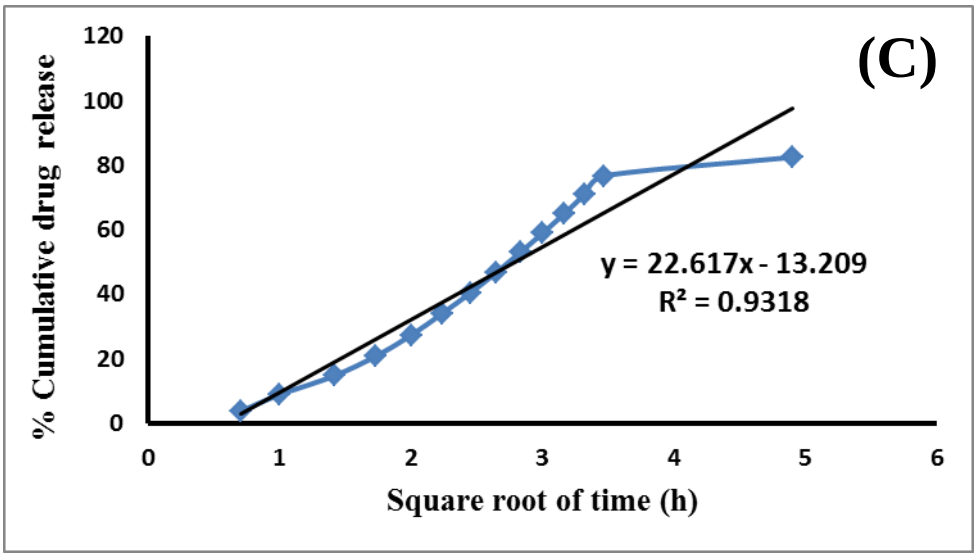
(C)
% Cumulative drug release
120
100
80
60
40
20
0
0
1
2
3
4
5
6
Square root of time (h)
y = 22.617x - 13.209
R² = 0.9318

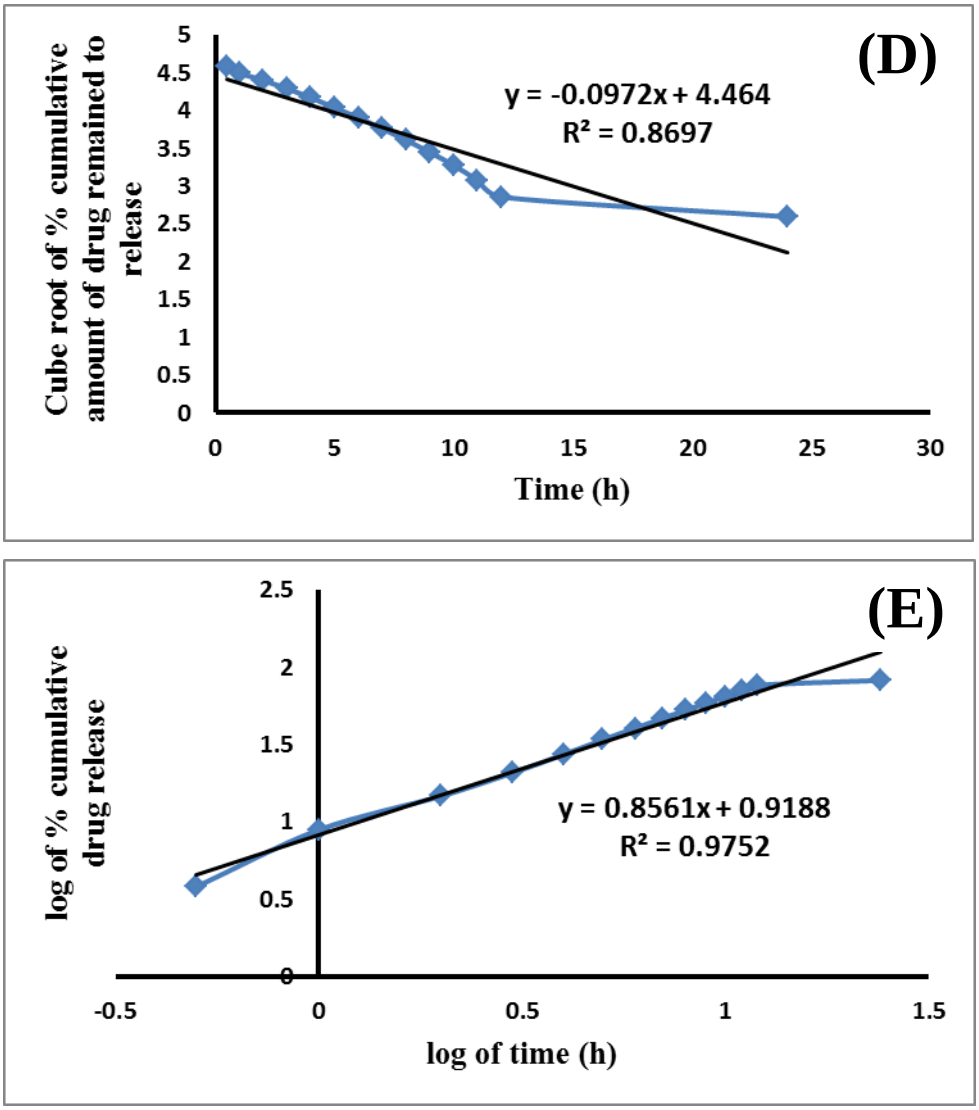

Figure 6.13: Graphical representation of various kinetic models of drug release from SYF in PBS (pH 7.4) as drug release media. (A) Zero order kinetics, (B) First order kinetics, (C) Higuchi kinetics, (D) Hixson-Crowell kinetics, (E) Korsmeyer-Peppas kinetics.

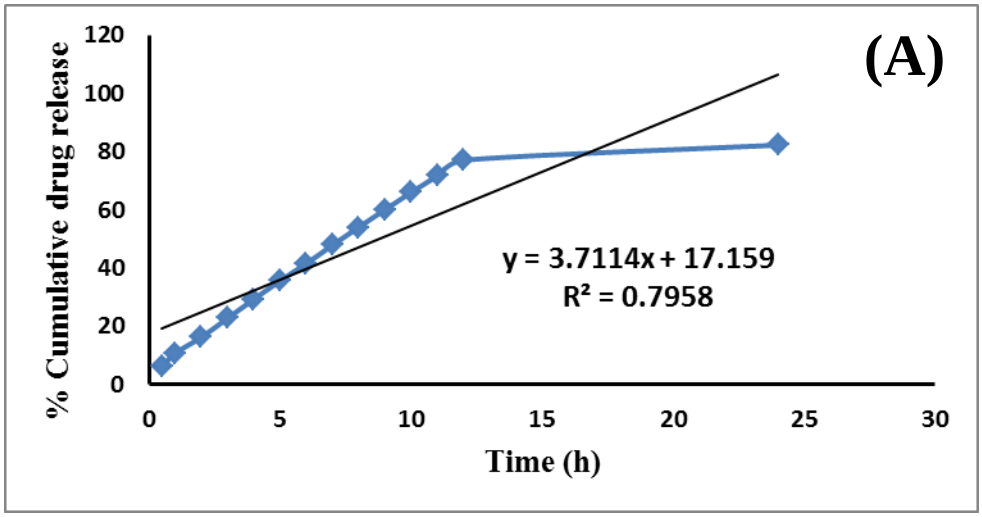

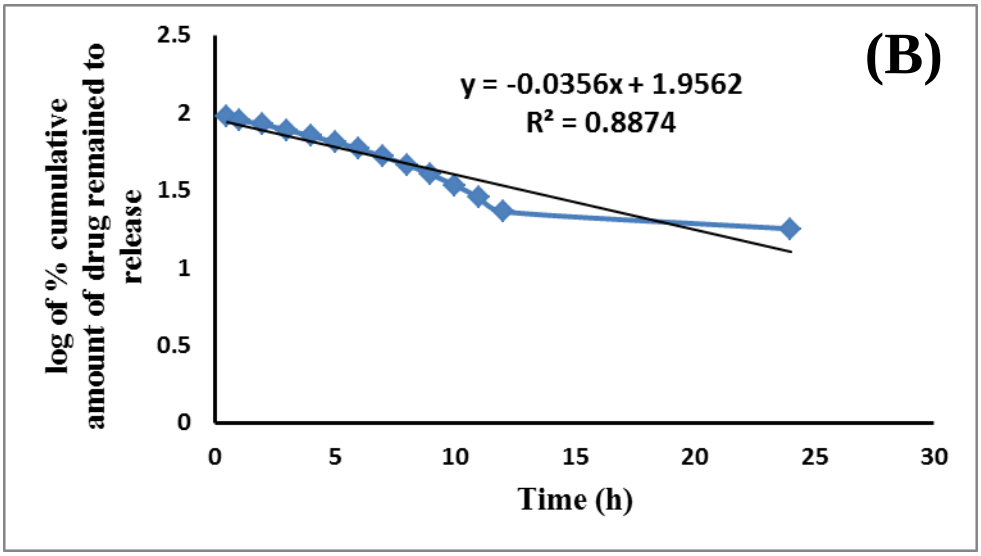
(B)
y = -0.0356x + 1.9562
R² = 0.8874
log of % cumulative amount of drug remained to release
Time (h)
2.5
2
1.5
1
0.5
0
0
5
10
15
20
25
30

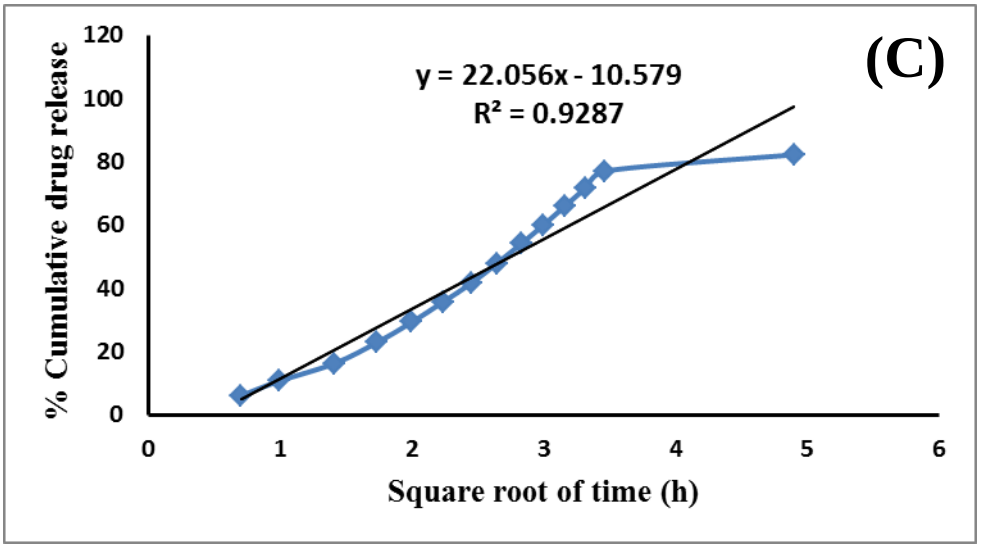
(C)
y = 22.056x - 10.579
R² = 0.9287
% Cumulative drug release
Square root of time (h)
120
100
80
60
40
20
0
0
1
2
3
4
5
6

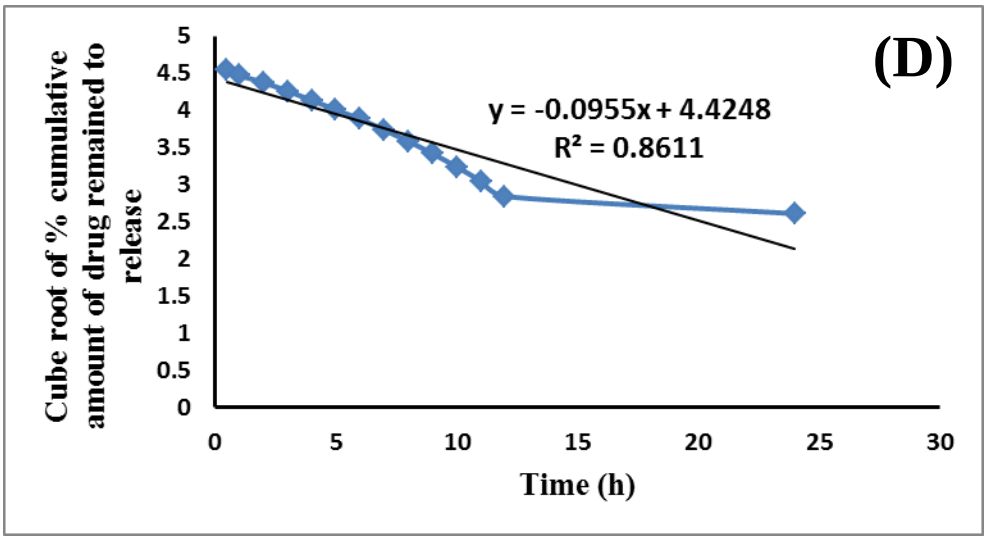
(D)
y = -0.0955x + 4.4248
R² = 0.8611
Cube root of % cumulative amount of drug remained to release
Time (h)
5
4.5
4
3.5
3
2.5
2
1.5
1
0.5
0
0
5
10
15
20
25
30

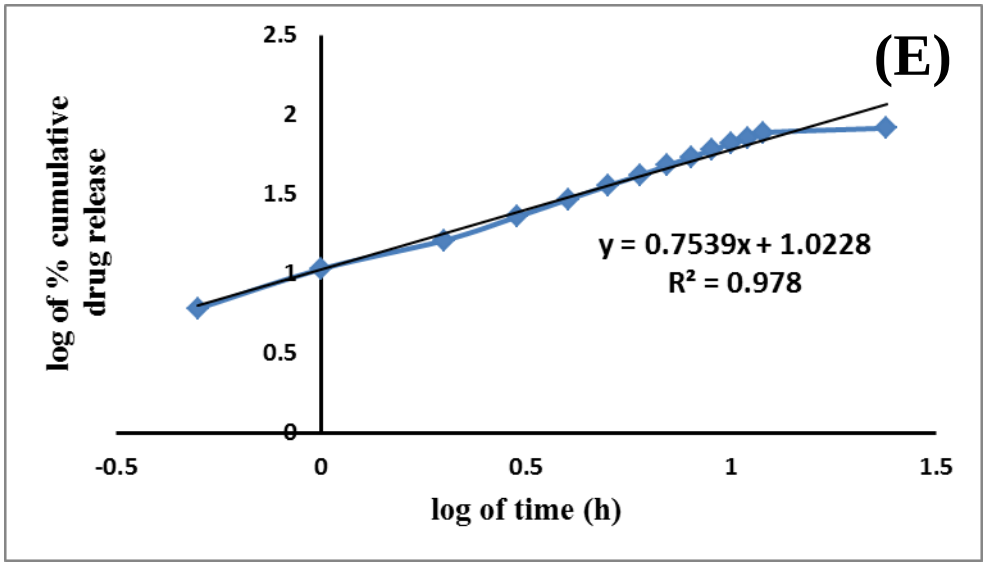

Figure 6.14: Graphical representation of various kinetic models of drug release from MGF in 50 % human serum as drug release media. (A) Zero order kinetics, (B) First order kinetics, (C) Higuchi kinetics, (D) Hixson-Crowell kinetics, (E) Korsmeyer-Peppas kinetics.

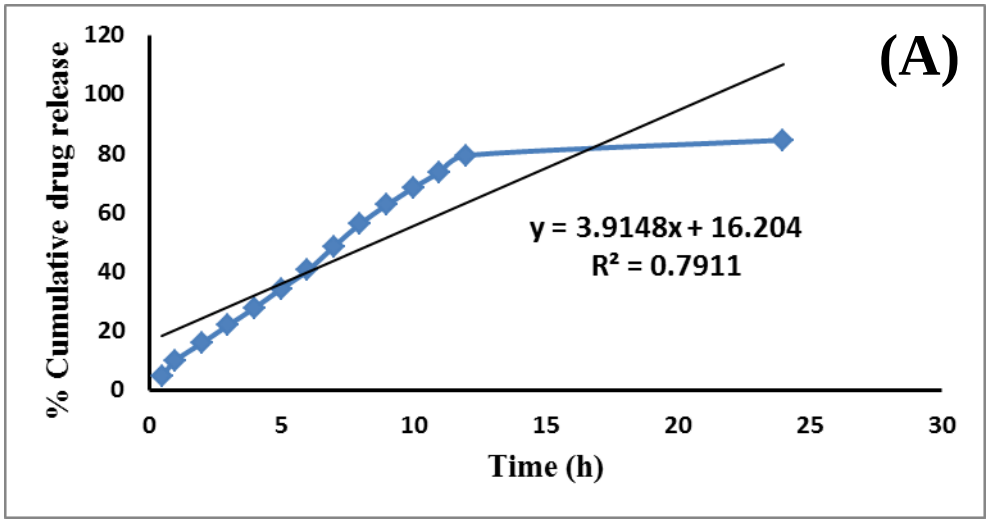

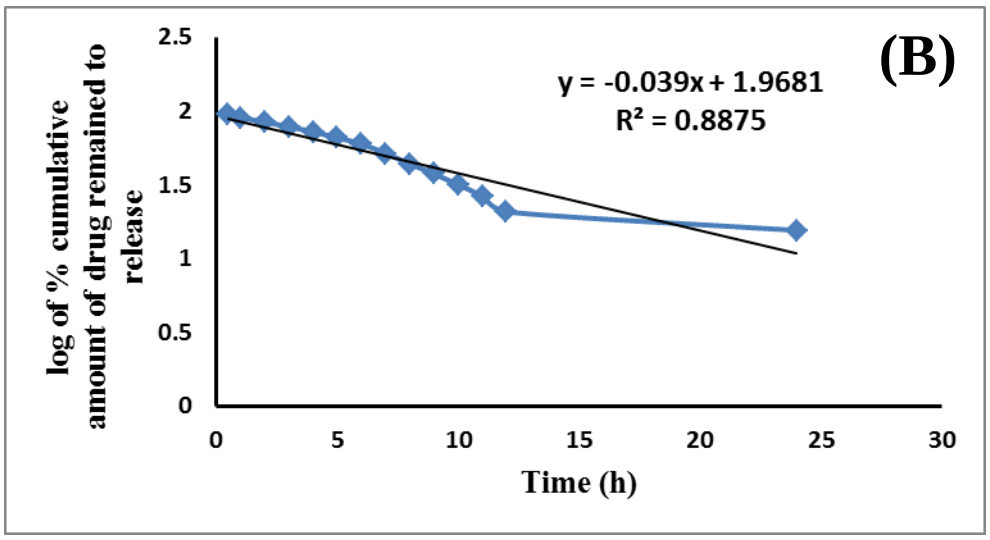

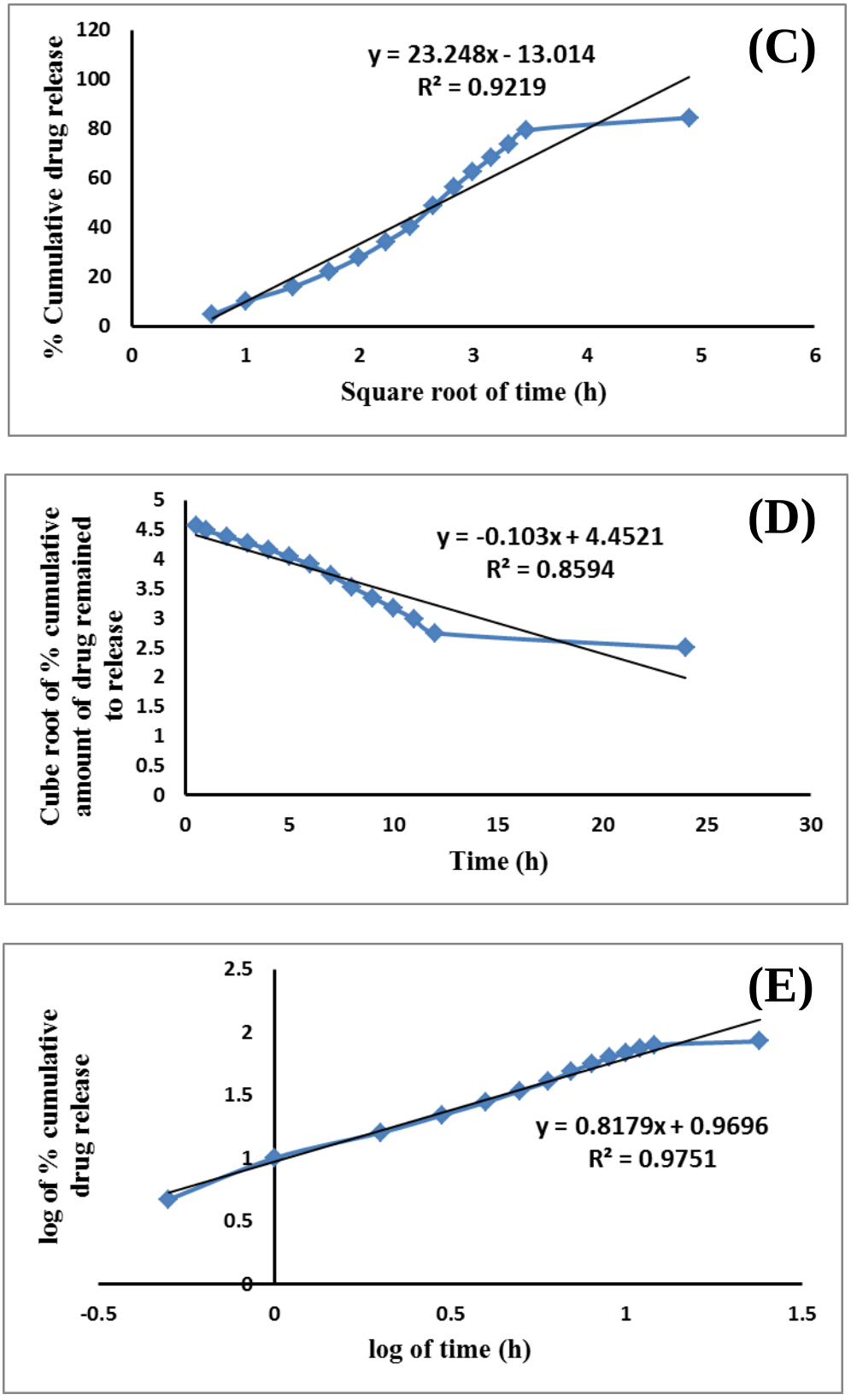

Figure 6.15: Graphical representation of various kinetic models of drug release from SYF in 50 % human serum as drug release media. (A) Zero order kinetics, (B) First order kinetics, (C) Higuchi kinetics, (D) Hixson-Crowell kinetics, (E) Korsmeyer-Peppas kinetics.

Table 6.5: *In vitro* drug release kinetics of MGF and SYF with R^2 and "n" values

PBS (pH 7.4) using as drug release media		
Kinetic model	**MGF**	**SYF**
	Kinetic equation	**Kinetic equation**
Zero order kinetics	y = 3.3472x + 13.839	y = 3.8137x + 15.178
	R^2 = 0.8080	R^2 = 0.8018
First order kinetics	y = -0.0272x + 1.9585	y = -0.0361x + 1.969
	R^2 = 0.8871	R^2 = 0.8968
Higuchi kinetics	y = 19.829x - 11.022	y = 22.617x - 13.209
	R^2 = 0.9371	R^2 = 0.9318
Hixson-Crowell kinetics	y = -0.0777x + 4.4597	y = -0.0972x + 4.464
	R^2 = 0.8634	R^2 = 0.8697
Korsmeyer-Peppas kinetics	y = 0.8387x + 0.8849	y = 0.8561x + 0.9188
	R^2 = 0.9742	R^2 = 0.9752
	n = 0.8387	n = 0.8561
50 % human serum using as drug release media		
Kinetic model	**MGF**	**SYF**
	Kinetic equation	**Kinetic equation**
Zero order kinetics	y = 3.7114x + 17.159	y = 3.9148x + 16.204
	R^2 = 0.7958	R^2 = 0.7911
First order kinetics	y = -0.0356x + 1.9562	y = -0.039x + 1.9681
	R^2 = 0.8874	R^2 = 0.8875
Higuchi kinetics	y = 22.056x - 10.579	y = 23.248x - 13.014
	R^2 = 0.9287	R^2 = 0.9219
Hixson-Crowell kinetics	y = -0.0955x + 4.4248	y = -0.103x + 4.4521
	R^2 = 0.8611	R^2 = 0.8594
Korsmeyer-Peppas kinetics	y = 0.7539x + 1.0228	y = 0.8179x + 0.9696
	R^2 = 0.9780	R^2 = 0.9751
	n = 0.7539	n = 0.8179

R^2: Correlation coefficient; n: Release exponent; PBS: Phosphate buffered saline.

6.8.3. *In vitro* cellular uptake study

In vitro cellular uptake study of NLs was conducted in U-87 MG human glioblastoma cells by using fluorescent NLs to inspect the uptake ability of NLs in brain cells using confocal microscopy. From the results it revealed that both the types of fluorescent NLs (FITC-MGF,

FITC-SYF) were internalized by the cells (Figure 6.16A, Figure 6.16B) and were localized in cytoplasm as well as nucleus. Cellular uptake of FITC-MGF increased with time till 3 h of the study (Figure 6.16A). However, for FITC-SYF, the cellular uptake was more in 1 h than 0.25 h and then decreased at 3 h (total duration of the study) (Figure 6.16B).

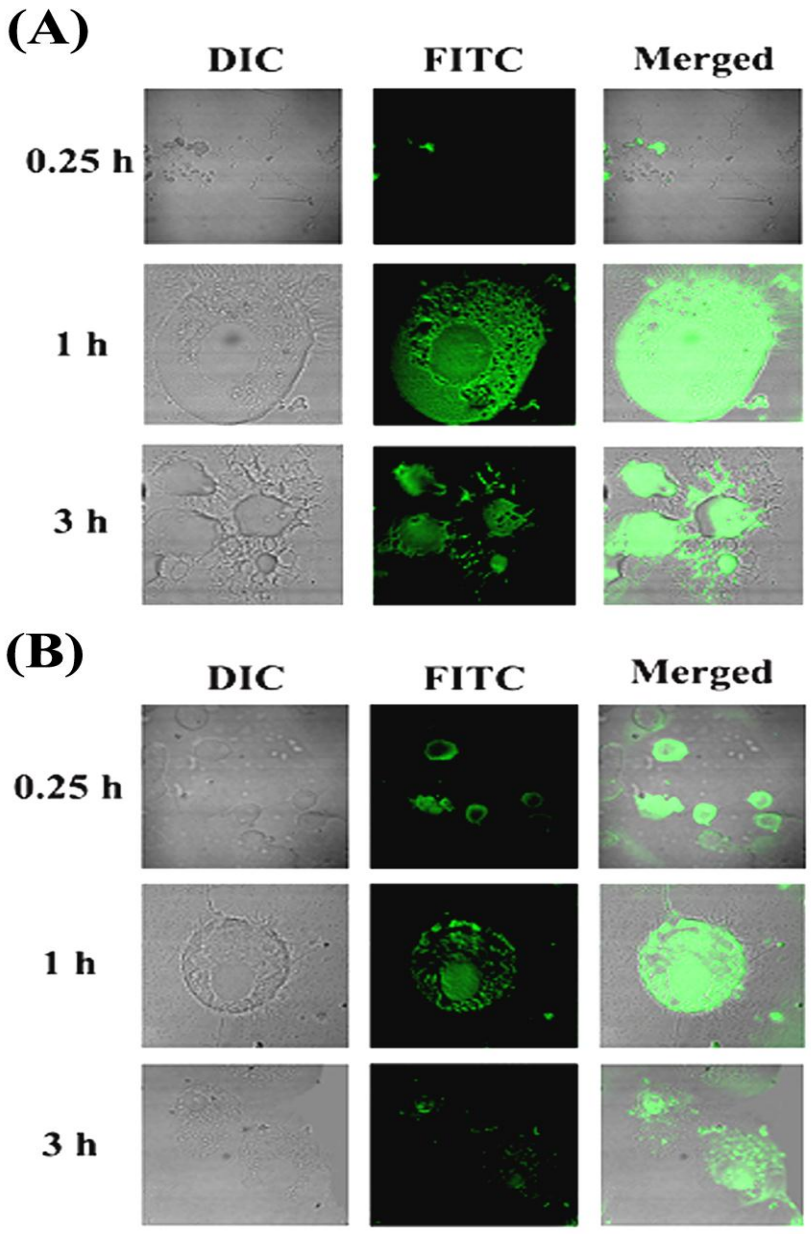

Figure 6.16: Investigation of *in vitro* cellular uptake of MGF and SYF by confocal microscopy. (A) *In vitro* cellular uptake study of fluorescein isothiocyanate labeled MGF (FITC-MGF) in U-87 MG human glioblastoma cells at various time points (0.25 h, 1 h, 3 h). (B) *In vitro* cellular uptake study of fluorescein isothiocyanate labeled SYF (FITC-SYF) in U-87 MG human glioblastoma cells at various time points (0.25 h, 1 h, 3 h). DIC: Differential interference contrast images of U-87 MG human glioblastoma cells.

By both confocal and conventional fluorescence microscopies, FITC treated cells were shown to internalize FITC in a time dependant manner (Cole et al., 1990). Thus, addition of FITC in media alone as a control sample to treat cells would provide results which can mislead the actual findings of the FITC-labeled formulations. Hence, no FITC control was run.

6.9. Stability study

FTIR spectra of the stored NLs (MGF, SYF) (Figure 6.17) were compared with those of the freshly prepared formulations. No distinguish changes in spectrum were observed for the formulations stored at 4ºC as compared to the freshly prepared formulation. From the FESEM image of the formulations (MGF, SYF) stored at 4ºC it was determined that they had spherical structure with smooth surface (Figure 6.18). Structures of the freshly prepared formulations have been given in Figure 6.8. However, NLs stored at 25ºC showed some deformations of structure (data not shown). Further, upon drug assay, similar drug contents were found for NLs stored at 4ºC and 25ºC.

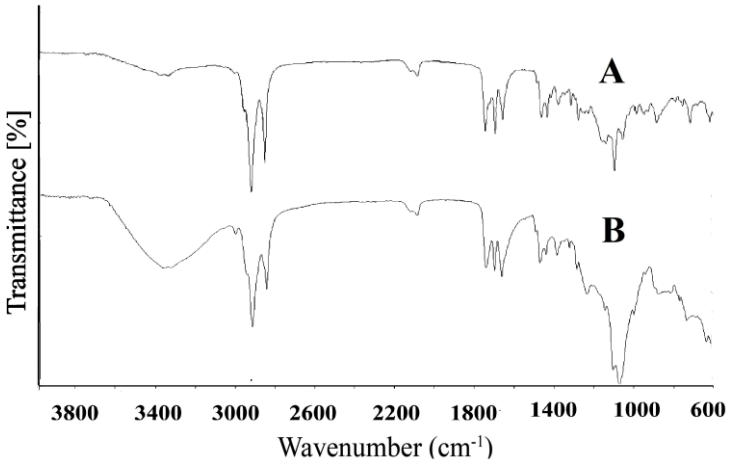

Figure 6.17: Fourier transform infrared spectroscopy (FTIR)-spectra of (A) MGF stored at 4ºC for 90 days, (B) SYF stored at 4ºC for 90 days.

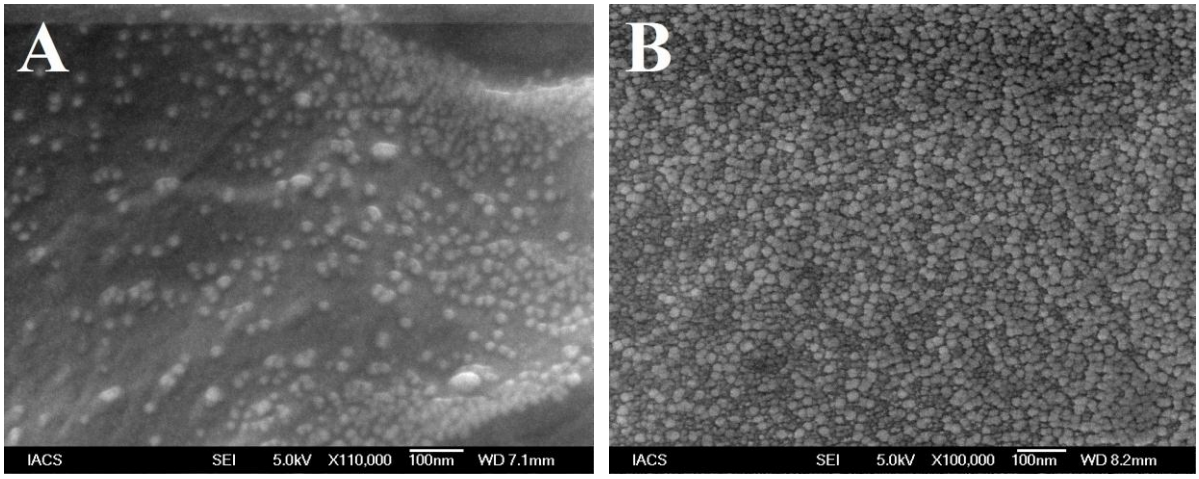

Figure 6.18: Field emission scanning electron microscopy (FESEM) images of (A) MGF stored at 4ºC for 90 days, (B) SYF stored at 4ºC for 90 days.

6.10. *In vivo* analysis

6.10.1. Gamma Scintigraphy

The gamma scintigraphy was performed to investigate the ability of the NLs to cross BBB after the administration of ^{99m}Tc labeled MGF, ^{99m}Tc labeled SYF and ^{99m}Tc labeled free drug (AZT) in different groups of Sprague-Dawley rats respectively. The radioactivity signals were observed (Figure 6.19) and assessed in brain as well as in different organs (Table 6.6) of the experimental animals which received radiolabeled NLs / AZT. The study showed that NLs were able to cross BBB and reached in brain. In animals treated with radiolabeled MGF, the intensity of signals in brain tissue was higher at 1 h as compared to 5 h (Figure 6.19[I]). The signals were stronger in brain at 1 h than 5 h in the animals received radiolabeled SYF (Figure 6.19[II]). At 5 h the signals were stronger in the brain tissue of animals treated with radiolabeled MGF compared to radiolabeled SYF. In ^{99m}Tc labeled free drug (AZT)-treated animals, very weak signal was noticed at 1 h and 5 h in brain tissue (Figure 6.19[III]) which indicated poor permeation of free AZT through BBB.

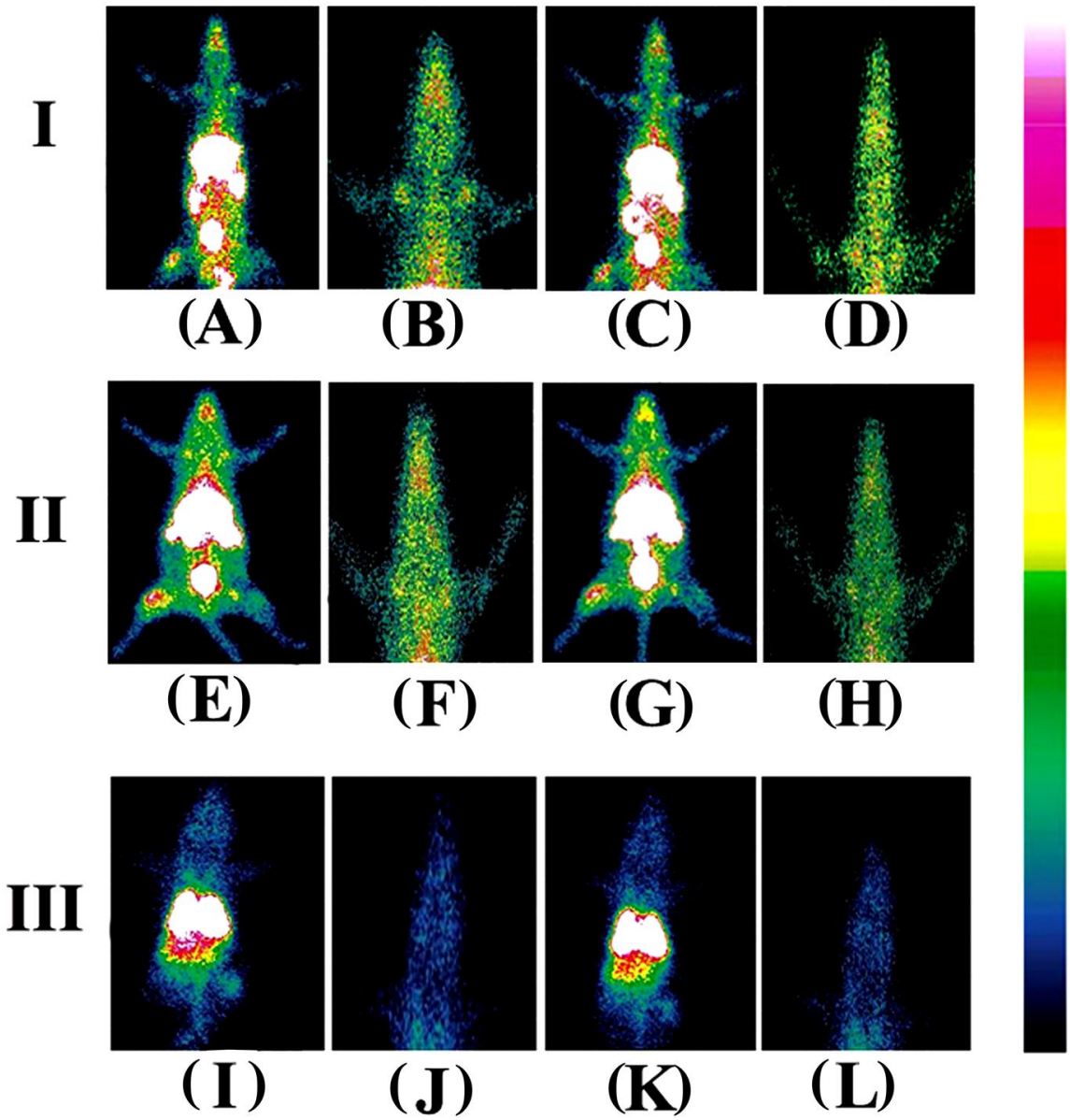

Figure 6.19: Gamma scintigraphy images of rats after receiving radiolabeled MGF / radiolabeled SYF / radiolabeled AZT. (I) rats received ^{99m}Tc labeled MGF at 1 h (A, B) and at 5 h (C, D) post i.v. injection; (II) rats received ^{99m}Tc labeled SYF at 1 h (E, F) and at 5 h (G, H) post i.v. injection; (III) rats received ^{99m}Tc labeled free drug at 1 h (I, J) and at 5 h (K, L) post i.v. injection. A, C, E, G, I, K are whole animal image; B, D, F, H, J, L are magnified brain part.

6.10.2. Biodistribution study

Biodistribution studies were conducted by administering ^{99m}Tc labeled MGF, ^{99m}Tc labeled SYF and ^{99m}Tc labeled free drug (AZT) in Sprague-Dawley rats through i.v. route at 1 h and 5 h after injection. In different organs including brain, accumulation of radiolabeled NLs as

well as free drug were measured and data were reported as percentage of injected dose per gram (% ID per g) of tissue or organ (Table 6.6). The values of residence time of radiolabeled formulation MGF / SYF in blood were 2.90 fold, 3.09 fold higher at 1 h and 4.08 fold, 3.94 fold greater than that of radiolabeled AZT at 5 h respectively. On the other hand, kidney accumulation was distinctively more in free drug than NLs at 1 h as well as 5 h. Further, at 1 h, kidney accumulation of radiolabeled SYF was 2.75 time less than MGF but at 5 h this was 31.91 % higher as compared to MGF. Enhancement of brain uptake values (by 18 folds and 19 folds, respectively, at 1 h and 36 times and 23 times, respectively, at 5 h, for MGF and SYF) was observed as compared to the brain uptake values of labeled AZT at those respective time points. Although brain uptake of ^{99m}Tc labeled MGF was slightly less in values than those of SYF at 1 h but it was 56.52 % higher compared to SYF at 5 h (Table 6.6). For this reason, brain / blood ratio was 0.48 for MGF at 5 h which was greater than the value at 1 h whereas it was 0.32 for SYF at 5 h. Brain / blood ratio was predominantly higher for NLs compared to free AZT (Table 6.6).

Table 6.6: Biodistribution studies of ^{99m}Tc labeled MGF / SYF and ^{99m}Tc labeled free drug (AZT) in rats at 1 h and 5 h post i.v. injection time period

Organ	**MGF**		**SYF**		**AZT**	
	1h	**5h**	**1h**	**5h**	**1h**	**5h**
Heart	0.06 ± 0.02	0.18 ± 0.04	0.05 ± 0.01	0.14 ± 0.03	0.31 ± 0.01	0.15 ± 0.03
Blood	1.97 ± 0.18	1.51 ± 0.15	2.10 ± 0.21	1.46 ± 0.11	0.68 ± 0.19	0.37 ± 0.13
Liver	27.61 ± 2.78	36.25 ± 2.43	25.22 ± 2.34	38.21 ± 2.31	32.28 ± 3.21	38.23 ± 3.11
Lung	2.93 ± 1.33	1.63 ± 1.43	3.51 ± 1.26	2.63 ± 1.55	1.66 ± 1.36	2.15 ± 1.35
Spleen	2.65 ± 0.26	1.51 ± 0.19	3.99 ± 0.19	1.91 ± 0.21	1.53 ± 0.24	2.23 ± 0.27
Muscle	0.06 ± 0.01	0.09 ± 0.01	0.03 ± 0.00	0.06 ± 0.01	0.15 ± 0.02	0.19 ± 0.05
Intestine	1.64 ± 0.29	2.07 ± 0.26	1.56 ± 0.31	2.96 ± 0.23	1.11 ± 0.28	2.23 ± 0.29
Stomach	0.68 ± 0.17	0.75 ± 0.13	0.38 ± 0.09	0.56 ± 0.07	0.45 ± 0.09	0.57 ± 0.11
Kidney	0.33 ± 0.11	0.47 ± 0.12	0.12 ± 0.05	0.62 ± 0.08	4.56 ± 0.19	6.45 ± 0.21
Brain	0.90 ± 0.16	0.72 ± 0.09	0.95 ± 0.21	0.46 ± 0.11	0.05 ± 0.01	0.02 ± 0.00
Brain / Blood	0.46	0.48	0.45	0.32	0.07	0.05

Results are expressed in % mean of injected dose per gram of organ / tissue ± SD (n = 5).
SD: Standard deviation.

6.10.3. *In vivo* plasma pharmacokinetic study

The plasma pharmacokinetic study was performed to observe the changes of pharmacokinetic parameters in Sprague-Dawley rats after i.v. administration of MGF / SYF / free AZT suspension. The mean plasma concentration of drug from MGF / SYF was higher than that of AZT in animals which had received AZT suspension, at the different experimental time points. The plasma concentration of AZT from MGF was comparatively higher than that of SYF after 4 h (Figure 6.20A). AUC_{0-t} value for MGF was reasonably greater than those of SYF as well as free drug suspension, respectively (Table 6.7). $AUMC_{0-t}$ values of drug in rats received MGF / SYF were 13.76 fold / 8.25 fold respectively greater than $AUMC_{0-t}$ value as detected in animals received free drug suspension. Half-life ($t_{1/2}$) value of AZT from MGF was 8.44 fold higher than that of free AZT suspension and 1.27 fold higher than that of SYF, suggesting a predominantly sustained drug release from MGF. MRT values were 5.10 fold and 3.25 fold higher for MGF and SYF respectively than the MRT value found in rats treated with AZT suspension. This suggests maximally prolonged blood residence time of MGF among the experimental formulations. A predominant variation in V_{ss} values was also noticed for MGF (about 2 times greater than the value obtained from rat treated with AZT suspension and 1.5 times greater than the value obtained from rat treated with SYF). There was 63.21 % decreased clearance of AZT from MGF as compared to free AZT suspension. Data revealed that MGF provided most favourable pharmacokinetic profile of AZT as compared to SYF and free AZT suspension.

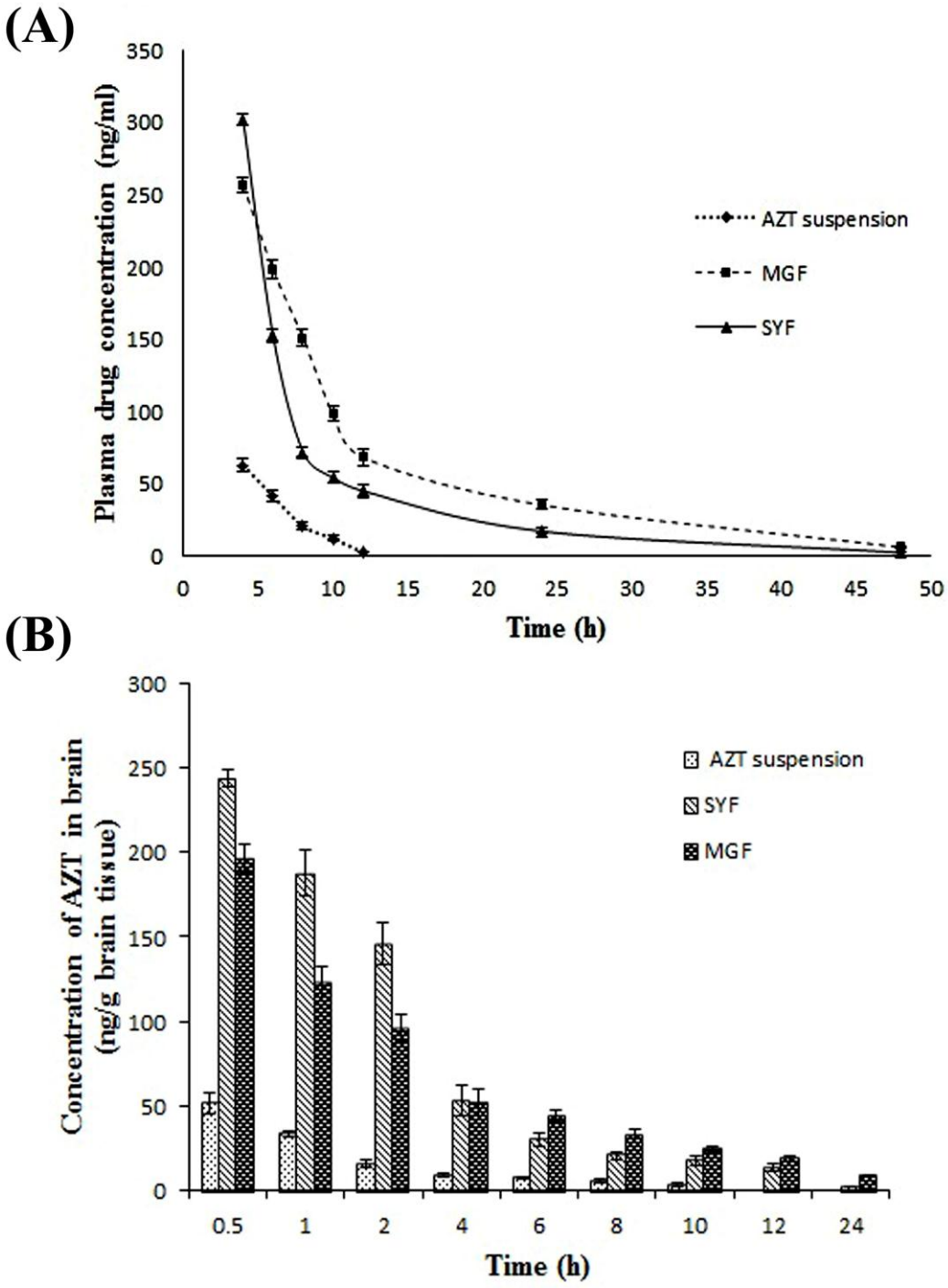

Figure 6.20: *In vivo* pharmacokinetic determination in plasma and brain. (A) Plasma concentration of AZT-time profiles after i.v. administration of MGF / SYF / free drug (AZT) suspension in rats. (B) Concentration of AZT in brain after i.v. administration of MGF / SYF / AZT suspension in rats represented by bar diagram. Data showed mean ± SD (n = 3). SD of each point was represented by error bar. SD: Standard deviation represented by deviation bar.

Table 6.7: Plasma and brain pharmacokinetic parameters of AZT after i.v. administration of MGF / SYF / free drug (AZT) suspension in rats

Plasma pharmacokinetic profile			
Pharmacokinetic parameters	**AZT suspension**	**MGF**	**SYF**
$t_{1/2}$ (h)	1.15 ± 0.04	9.71 ± 0.21[a,b]	7.64 ± 0.08[a]
AUC_{0-t} (h ng ml^{-1})	2003.27 ± 24.63	5405.57 ± 151.03[a]	5107.23 ± 153.91[a]
$AUMC_{0-t}$ (h^2 ng ml^{-1})	2529.70 ± 188.70	34806.50 ± 2475.71[a,b]	20881.90 ± 1198.92[a]
Cl (L h^{-1} Kg^{-1})	2.99 ± 0.04	1.10 ± 0.03[a]	1.17 ± 0.03[a]
MRT (h)	1.26 ± 0.08	6.43 ± 0.28[a,b]	4.09 ± 0.24[a]
Vss (L Kg^{-1})	3.83 ± 0.19	7.88 ± 0.19[a,b]	5.03 ± 0.38[a]
Brain pharmacokinetic profile			
Pharmacokinetic parameters	**AZT suspension**	**MGF**	**SYF**
AUC_{0-t} (h ng ml^{-1})	141.17 ± 12.08	888.23 ± 28.67[a]	875.73 ± 53.86[a]
$AUMC_{0-t}$ (h^2 ng ml^{-1})	386.53 ± 35.11	5396.33 ± 236.87[a,b]	3574.03 ± 290.51[a]
MRT (h)	2.73 ± 0.06	6.07 ± 0.15[a,b]	4.07 ± 0.06 [a]
Cl (L h^{-1} Kg^{-1})	37.33 ± 4.66	5.9 ± 0.17[a]	6.73 ± 0.35 [a]

Data were expressed as mean ± SD of three separate observations.
[a]Data were significantly different (P<0.05) where MGF and SYF were compared with AZT suspension. It was assessed by one-way analysis of variance (ANOVA) through Tukey-Kramer multiple comparisons test.
[b]Data were significantly different (P<0.05) where MGF was compared with SYF. It was assessed by one-way analysis of variance (ANOVA) through Tukey-Kramer multiple comparisons test.
$t_{1/2}$, time taken for maximum blood concentration to drop in half-life; AUC_{0-t}, area under the concentration-time curve from time of injection (t = 0) to a determined time point; $AUMC_{0-t}$, area under the first moment curve; Cl, clearance; MRT, mean residence time; Vss, steady state volume of distribution.

6.10.4. *In vivo* brain pharmacokinetic study

Till 24 h (the total duration of the study), AZT level was detectable in brain from MGF / SYF (Figure 6.20B). However, AZT could not be detected in the brain of rats treated with AZT suspension after 10 h of the study. AZT level in brain was found to be maximum from SYF followed by MGF in 0.5 h. The values were five and four fold higher respectively as compared to the values detected in animals treated with AZT suspension at 0.5 h. AZT level

was 25 % higher in the brain of rats treated with SYF as compared to MGF at 0.5 h. With the increasing duration of time, AZT levels were decreasing in all the cases. Interestingly, at 4 h of the investigation the values of AZT concentration in brain were almost same in rats treated with SYF / MGF. However, from then on, till 24 h of the study, AZT levels in brain were found to be more (46.76 % more in value at 6 h, 263.75 % more in value at 24 h) in rats treated with MGF as compared to those treated with SYF. Treatment of AZT through MGF enhanced $AUMC_{0\text{-}t}$ value by 50.99 % and MRT value by 49.14 % as compared to the rats treated with SYF. The data were also substantiated by clearance values (Table 6.7).

Chapter 7

Discussion

The present investigation was intended to understand the capability of ML to act as base material of lipid nanocarrier to deliver water soluble drug through BBB to brain. Continuous TJs of endothelial cells of brain capillaries and several transmembrane proteins seal the paracellular pathways and effectively block the free diffusion of polar solutes (such as AZT) from blood along these potential paracellular pathways, causing denial of access to brain interstitial fluid (Ballabh et al., 2004; Abbott, 2005). Blood-brain barrier predominantly impedes entry from blood to brain of virtually all molecules, other than those that are small and lipophilic (example, NL) or those (such as essential nutrients, precursors and cofactors) that enter the brain through active transport mechanism (Alavijeh et al., 2005; Agrawal et al., 2017). Thus, lipophilicity and size of NL tend to lead higher permeation across BBB as compared to the polar drug or comparatively polar phospholipid vesicles. Since AZT is a highly water soluble drug that does not cross BBB efficiently (Rautio et al., 2008; Weiss et al., 2009) and the nanosize lipid vesicles have been shown to permeate through BBB effectively (Li et al., 2017; Vieira et al., 2016; Masserini, 2013), we developed two types of optimized NLs (MGF and SYF) applying lipid layer hydration technique by using ML / SL. A comparative physico-chemical and biopharmaceutical analysis on those two types of formulations were also performed.

FTIR data analysis revealed that there was no chemical interaction between the drug and the excipients. However, there were some physical interactions between the drug and excipients and between the molecules of excipients. Such physical interactions might have a role to form the spherical nanostructure of the drug carrier (Rudra et al., 2010) and to retain the drug in the lipid layer, causing slower diffusion of drug through the membrane (Rudra et al., 2010). Again, absence of peak of AZT in the lyophilized ML-based NLs was due to the reason of entire encapsulation of AZT in the formulation. Presence of peak of AZT in SYF

suggests the availability of free drug on the surface of the formulation.

Various process parameters such as temperature and speed of hydration, duration of sonication, time and speed of centrifugation, duration of freeze drying and ratio of the constituents were optimized to develop formulations with maximum drug loading, homogeneous and uniform particle size, desirable zeta potential value and smooth surface structure, among the experimental formulations. Out of the various experimental formulations, the best optimized formulation of each category (MGF / SYF) was selected and reported here.

Lower drug loading was observed in MGF as compared to SYF. AZT is a highly water soluble drug (Nath et al., 2011; Singh et al., 2010). SYF had hydrophobic phospholipid and cholesterol. Presence of phosphate group in SL makes it comparatively more hydrophilic than ML (Jones, 2008). Presence of SA, OA, PA possibly caused comparatively less partitioning of drug into the lipid layer causing less drug loading in MGF. Yield of SYF was near about 6 % less as compared to MGF and the possible reason may be the recovery problem due to slightly stickiness of SYF for presence of SL (Das et al., 2015).

Nanosize SYF had larger size (38.49 % larger) than MGF. This could be because of the presence of phospholipid in SYF. Phospho moiety owing to the hydrophilic nature of the phosphate group (Jones, 2008) might have been pulled with more tension by water molecules toward the bulk of the liquid during the formation of the liposomal structure, resulting in comparatively larger size. PDI values of both the formulations were nearly similar. PDI value is a very crucial indicator for size distribution, stability and uniformity of NLs (Masarudin et al., 2015). Lower PDI value signifies more monodisperse pattern with better stability of NLs. On the other hand, higher PDI value indicates aggregation of particles with low stability (Masarudin et al., 2015). The PDI value 0.1 to 0.25 is desirable for uniform distribution but

the value more than 0.5 is an indication of poor homogeneity (Gharib et al., 2014). In our study both the formulations were mostly uniform in size and homogeneously distributed. Zeta potential is also considered as a parameter for confirmation of physical stability (Dey et al., 2016; Shaw et al., 2017). If electric charge of NLs surface is high, then zeta potential of NLs will also show high value. This means strong repellent forces among the vesicles of NLs are able to inhibit agglomeration of NLs in suspension. Normally, zeta potential value (more than +30 mV or less than -30 mV) indicates good stability of NLs in colloidal dispersion (Dey et al., 2016). In our study, nearly similar zeta potential values (about -70 mV) were achieved for MGF and SYF. This denotes that both the formulations had prolonged and better physical stability in colloidal suspension. The negatively charged NLs are removed slowly than the positive one, which suggests longer blood residence time of negatively charged drug carriers (Satapathy et al., 2016). Thus, both the experimental formulations are expected to possess extended blood residence time.

FESEM provides information related to 3D structure as well as surface property (Tripathi et al., 2017). FESEM study reveals that both the formulations had spherical structure with smooth surface and they were homogeneously distributed with non-appearance of any agglomerate.

The cryo-TEM images show that MGF / SYF had unilamellar spherical nanosize structure with an intact lamellarity. Lipid layer was present at the external side and aqueous part was enclosed by the lipid layer. Dark spot in the inner aqueous core and dark outer layer revealed the presence of hydrophilic drug in a suspended condition in the aqueous core as well as in the outer lipid layer.

Morphology of MGF / SYF was obtained from AFM data. The findings showed that there

was discrete particulate distribution for both the cases. Moreover, MGF / SYF was of nanosize with smooth surface.

Drug was found to release in a slower and more sustained manner from MGF compared to SYF in both types of drug release media. This could be due to the lipid composition of the NLs. SYF fundamentally consisted of phospholipid which contains polar phosphoryl and basic groups and they make the phospholipid more hydrophilic (Jones, 2008) than the ML which does not contain any phospholipid. Since AZT is a highly water soluble drug (Nath et al., 2011; Singh et al., 2010), it seems to permeate more through phospholipid than the ML.

The drug release pattern from both the NLs in PBS (pH 7.4) media as well as 50 % human serum was best fitted (based on R^2 value) with Korsmeyer-Peppas kinetic model. Release component (n) value suggests for an anomalous non-Fickian diffusion pattern of drug molecules (Pattnaik et al., 2012). Further, Korsmeyer-Peppas kinetic model suggests that AZT release from the experimental NLs followed diffusion and erosion process (Pattnaik et al., 2012).

Cellular uptake of both the NLs in U-87 MG human glioblastoma cells showed that NLs were localized in the cytoplasm and in the nucleus after internalization by the cells. But FITC-MGF was intense in cells in a time dependent manner whereas FITC-SYF concentration in cells initially increased (at 1 h as investigated) and then decreased with the time (at 3 h, total duration of the investigation). Possibly phospholipid vesicles were metabolized faster than MGF by glioma cells (Klein, 2002; Carnielli et al., 1998).

At 4ºC, absence of changes in spectra for formulations indicates that there was no physico-chemical reaction occurred between the drug and the excipients in the storage condition. Further, drug remained stable in stored formulation during storage condition at 4ºC. At 25ºC,

although FTIR spectra did not significantly vary for the experimental formulations, the deformity of some structures of NLs forced us to reject the consideration to store at 25ºC.

We performed gamma scintigraphic investigation and brain pharmacokinetic study to compare the capability of MGF and SYF to cross BBB. Gamma scintigraphic images gave clear picture of localization of radiolabeled NLs / radiolableled AZT in whole body of the experimental rats. From the gamma scintigraphic images, it revealed that both the radiolableled NLs were capable to cross BBB and reached in brain. The intensity of signal in brain was stronger at 1 h as compared to 5 h for both MGF and SYF (as observed from signal intensity bar given with the photograph). At 5 h, the signal intensity of MGF in brain was more pronounced than that of SYF, suggesting longer retention of radiolabeled MGF than radiolabeled SYF in brain after crossing BBB. Very weak signal at 1 h and 5 h for ^{99m}Tc labeled free drug (AZT) signifies poor ability of AZT to cross BBB. Both the NLs successfully crossed BBB possibly due to their nano-vesicular structure (Li et al., 2017) and longer retention of MGF in brain compared to SYF might be due to the variable lipid characteristics of MGF than SYF which had phospholipid in its structure.

In biodistribution study, radiolabeled MGF obtained from brain / blood ratio maintained its level persistently as compared to radiolabeled SYF, suggesting MGF was able to provide sustaining drug level in brain and blood better than SYF. Application of MGF showed presence of more amount of drug in brain with the increasing duration of the experiment as compared to that of SYF owing to an increased presence of MGF in brain. The presence of more MGF in brain / blood ratio as compared to SYF might be due to the sustained drug release and less clearance of drug through liver and kidney as compared to those of SYF. Predominant hepatic clearance of free AZT is also noteworthy to mention. The investigation reported that it is possible for a compound to possess a long half-life in blood, but a short

half-life in brain or even not to permeate BBB at all (Dawson et al., 2001). Hence, if a drug or formulation remains longer time in blood, it does not necessarily provide enhanced brain level of the drug (Dawson et al., 2001; Vieira et al., 2016). On the other hand, almost all things injected in blood must go into liver and liver does not have any barrier like BBB. Hence, the access of drug / formulation takes place much faster with a greater amount in liver than brain. Thus, MGF can tackle the short elimination half-life, low bioavailability, frequent dosing and dose dependent toxicity of AZT (Blum et al., 1988; Mandal and Tenjarla, 1996; Oh et al., 1998; Thomas and Panchagnula, 2003) more effectively than SYF.

After i.v. administration, at 4 h, SYF showed more drug level in blood as compared to MGF. It dropped sharply with the increasing duration till 8 h which indicates rapid distribution of SYF compared to MGF. However, MGF showed slow distribution and significantly ($P<0.05$) longer blood residence time as compared to SYF which also increased $t_{1/2}$ value of AZT. AUC_{0-48} and $AUMC_{0-48}$ were significantly more for MGF. It could be due to the longer MRT and less renal clearance of MGF compared to SYF. Reports suggest that longer MRT and less renal clearance increase AUMC and AUC (Dey et al., 2016; Satapathy et al., 2016).

Drug concentration in brain was initially 25 % more for SYF than MGF. The drug level in brain from MGF / SYF eventually reduced with the duration. At 4 h, the drug level in brain from MGF / SYF was more or less same. Interestingly brain drug concentration from SYF dropped sharply after 4 h whereas it dropped in a much slower manner for MGF till 24 h of the study where brain drug level was about 260 % more than that obtained from SYF. One of the most important features of brain is that it is completely separated from blood by blood brain barrier. In our study, blood perfusion was done before collection of brain from the animals to estimate drug in brain. Blood perfusion precludes the presence of drug in brain vasculatures and rather suggests its accumulation in brain, as drug has to cross blood brain

barrier to reach brain endothelial cells (Alavijeh et al., 2005; Ballabh et al., 2004; Abbott, 2005). Thus, *in situ* perfusion provides a measure of brain uptake and the brain / plasma ratio of the drug (as done in the present study) provides a partial measure (Alavijeh et al., 2005; Abbott, 2005; Takasato et al., 1984). Since both the studies have been done, it supports that drug reached in brain. It is also an indicative of cross of the drug-loaded formulations through blood brain barrier. Sustained drug release, less clearance and enhanced MRT of MGF in brain could be responsible for such enhancement. These further reflected in the enhanced availability of drug in brain from MGF compared to SYF. Lipid composition of MGF might be responsible for such variation.

Chapter 8

Summary and Conclusion

8. Summary and conclusion

Delivering highly water soluble drugs across BBB is a crucial and tough challenge for the formulation scientists. A successful therapeutic intervention by developing a suitable drug delivery system may revolutionize treatment across BBB. In AIDS, brain cells are also infected by HIV and it becomes a pool of HIV. Efforts were given here to unravel the capability of a newly developed ML as fundamental component of nanocarrier to deliver highly water soluble AZT as a model drug into brain across BBB. A comparison was made with an experimentally developed standard phospholipid based nanocarrier containing AZT. Due to lipophilic nature and nanosize, NLs were selected as a nanocarrier in the delivery of AZT to obtain the desired outcome.

To investigate the interaction between AZT and the excipients, FTIR study was performed and no chemical interaction between the drug and excipients was observed. NLs were prepared by applying the lipid layer hydration procedure through changing different process parameters. Depending on several physicochemical characteristics of the different experimental nanoliposomal formulations, MGF and SYF were selected for further investigation.

MGF and SYF were both in nanosize with nearly similar PDI and zeta potential values. From FESEM study, it revealed that they were spherical with smooth surface and were distributed homogenously without any agglomeration. Unilamellar nanovesicular structure was observed clearly in Cryo-TEM images for both the formulations. Discrete particulate distributions were observed for MGF / SYF in AFM study. In drug release study *in vitro*, comparatively slower and more sustained drug release pattern was noticed from MGF than that of SYF in PBS (pH 7.4) and also in 50 % human serum. In both the drug release media, AZT release pattern from MGF as well as SYF followed Korsmeyer-Peppas kinetic model that denoted the diffusion

and erosion release mechanism of AZT from the MGF / SYF. The cellular uptake study in U-87 MG human glioblastoma cells showed that FITC-MGF was internalised by cells in a time dependent manner where as concentration of FITC-SYF in glioma cells enhanced initially and then reduced with time (at 3 h, total duration of the investigation). Further, as stability aspects, 4ºC is perfect for storage of MGF and SYF.

Gamma scintigraphic images showed both the radiolabeled formulations successfully crossed BBB, but longer retention in brain was observed for ML-based formulation as compared to SL-based drug carrier. As a part of *in vivo* studies, gamma scintigraphy study, biodistribution study and plasma and brain pharmacokinetic studies were performed. Gamma scintigraphic images showed both the radiolabeled formulations successfully crossed BBB, but longer retention in brain was observed for ML-based formulation as compared to SL-based drug carrier. From the brain / blood ratio data of biodistribution study, it revealed that radiolabeled MGF was capable to retain its level persistently than that of SYF. This signifies that the capability of MGF for providing sustained drug level in brain and blood is better as compared to SYF. Plasma and brain pharmacokinetic data showed less clearance, prolonged residence time, more bioavailability and sustained release of AZT from MGF in rats compared to those data of the rats treated with SYF / AZT suspension.

In conclusion of this research work, nanosize drug delivery systems were developed successfully utilizing ML / SL to deliver AZT in brain across BBB. Both the formulations had sustained drug release profiles. *In vivo* gamma scintigraphy study and brain pharmacokinetic investigation revealed that both the formulations sufficiently reached brain through BBB, but MGF had better pharmacokinetic profile than that of SYF with respect to sustained drug release, prolonged blood residence time as well as brain residence time and increased $t_{1/2}$. Thus, ML may be utilized to successfully develop drug nanocarrier to deliver

drug into brain across BBB, in a sustained manner for a prolong period of time and may provide an effective therapeutic strategy for many diseases of brain. Further, many anti-HIV drugs cannot cross BBB sufficiently. Hence, the developed formulation may be a suitable option to carry those drugs into brain for better therapeutic management of HIV. ML could be an emerging carrier system for developing various therapeutic strategies to deliver drugs to brain and other organs. However, further studies are warranted in the area.

Chapter 9

References

9. References

Abbott NJ. (2002). Astrocyte-endothelial interactions and blood-brain barrier permeability. J Anat 200:629-38.

Abbott NJ. (2005). Dynamics of the CNS barriers: evolution, differentiation, and modulation. Cell Mol Neurobiol 25:5-23.

Abbott NJ. (2007). The bipolar astrocyte: polarized features of astrocytic glia underlying physiology, with particular reference to the blood-brain barrier. In: Dermietzel R, Spray DC, Nedergaard M, eds. Blood-Brain Barriers: From Ontology to Artificial Interfaces. Wiley-VCH Verlag GmbH and Co. KGaA, Weinheim. p 189-208.

Abbott NJ. (2013). Blood-brain barrier structure and function and the challenges for CNS drug delivery. J Inherit Metab Dis 36:437-49.

Abbott NJ, Patabendige AA, Dolman DE, et al. (2010). Structure and function of the blood-brain barrier. Neurobiol Dis 37:13-25.

Abbott NJ, Romero IA. (1996). Transporting therapeutics across the blood-brain barrier. Mol Med Today 2:106-13.

Abbott NJ, Rönnbäck L, Hansson E. (2006). Astrocyte-endothelial interactions at the blood-brain barrier. Nat Rev Neurosci 7:41-53.

Abrahamson DR. (1986). Recent studies on the structure and pathology of basement membranes. J Pathol 149:257-78.

Agrawal M, Ajazuddin, Tripathi DK, et al. (2017). Recent advancements in liposomes targeting strategies to cross blood-brain barrier (BBB) for the treatment of alzheimer's disease. J Control Release 260:61-77.

Akbarzadeh A, Rezaei-Sadabady R, Davaran S, et al. (2013). Liposome: classification, preparation, and applications. Nanoscale Res Lett 8:102.

Alavijeh MS, Chishty M, Qaiser MZ, Palmer AM. (2005). Drug metabolism and pharmacokinetics, the blood-brain barrier, and central nervous system drug discovery. NeuroRx 2:554-71.

Allen TM. (1994). Long-circulating (sterically stabilized) liposomes for targeted drug delivery. Trends Pharmacol Sci 15:215-20.

Alpes H, Allmann K, Plattner H, et al. (1986). Formation of large unilamellar vesicles using alkyl maltoside detergents. Biochim Biophys Acta 862:294-302.

Alyautdin R, Khalin I, Nafeeza MI, et al. (2014). Nanoscale drug delivery systems and the blood-brain barrier. Int J Nanomedicine 9:795-811.

Alyautdin RN, Petrov VE, Langer K, et al. (1997). Delivery of loperamide across the blood-brain barrier with polysorbate 80-coated polybutylcyanoacrylate nanoparticles. Pharm Res 14:325-8.

Anwekar H, Patel S, Singhai AK. (2011). Liposomes as drug carriers. IJPLS 2:945-51.

Atluri VS, Hidalgo M, Samikkannu T, et al. (2015). Effect of human immunodeficiency virus on blood-brain barrier integrity and function: an update. Front Cell Neurosci 9:212.

Azadi A, Hamidi M, Rouini MR. (2013). Methotrexate-loaded chitosan nanogels as 'trojan horses' for drug delivery to brain: preparation and *in vitro*/*in vivo* characterization. Int J Biol Macromol 62:523-30.

Balda MS, Flores-Maldonado C, Cereijido M, Matter K. (2000). Multiple domains of occludin are involved in the regulation of paracellular permeability. J Cell Biochem 78:85-96.

Balkovetz DF, Tiruppatchi C, Leibach FH, et al. (1989). Evidence for an impiramine-sensitive serotonin transporter in human placental brush-border membranes. J Biol Chem 264:2195-8.

Ballabh P, Braun A, Nedergaard M. (2004). The blood-brain barrier: an overview: structure, regulation, and clinical implications. Neurobiol Dis 16:1-13.

Banks WA. (1999). Physiology and pathology of the blood-brain barrier: implications for microbial pathogenesis, drug delivery and neurodegenerative disorders. J Neurovirol 5:538-55.

Banks WA. (2009). Characteristics of compounds that cross the blood-brain barrier. BMC Neurol 9:S3.

Barbi Mda S, Carvalho FC, Kiill CP, et al. (2014). Preparation and characterization of chitosan nanoparticles for AZT nasal delivery. J Nanosci Nanotechnol 14:1-10.

Barrera CM, Kastin AJ, Fasold MB, Banks WA. (1991). Bidirectional saturable transport of LHRH across the blood-brain barrier. Am J Physiol 261:E312-18.

Basu S, Mukherjee B, Chowdhury SR, et al. (2012). Colloidal gold-loaded, biodegradable, polymer-based stavudine nanoparticle uptake by macrophages: an *in vitro* study. Int J Nanomedicine 7:6049-61.

Batzri S, Korn ED. (1973). Single bilayer liposomes prepared without sonication. Biochim Biophys Acta 298:1015-19.

Bazzoni G. (2006). Endothelial tight junctions: permeable barriers of the vessel wall. Thromb Haemost 95:36-42.

Bednarczyk J, Lukasiuk K. (2011). Tight junctions in neurological diseases. Acta Neurobiol Exp 71:393-408.

Bendas G. (2001). Immunoliposomes: a promising approach to targeting cancer therapy. Bio Drugs 15:215-24.

Berger N, Sachse A, Bender J, et al. (2001). Filter extrusion of liposomes using different devices: comparison of liposome size, encapsulation efficiency, and process characteristics. Int J Pharm 223:55-68.

Bergshoeff AS, Fraaij PLA, Verweij C, et al. (2004). Plasma levels of zidovudine twice daily compared with three times daily in six HIV-1-infected children. J Antimicrob Chemother 54:1152-4.

Bernacki J, Dobrowolska A, Nierwińska K, Małecki A. (2008). Physiology and pharmacological role of the blood-brain barrier. Pharmacol Rep 60:600-22.

Berzin TM, Zipser BD, Rafii MS, et al. (2000). Agrin and microvascular damage in Alzheimer's disease. Neurobiol Aging 21:349-55.

Blasberg RG, Fenstermacher JD, Patlak CS. (1983). Transport of alpha-aminoisobutyric acid across brain capillary and cellular membranes. J Cereb Blood Flow Metab 3:8-32.

Blasi P, Giovagnoli S, Schoubben A, et al. (2007). Solid lipid nanoparticles for targeted brain drug delivery. Adv Drug Deliv Rev 59:454-77.

Blum MR, Liao SH, Good SS, Miranda P. (1988). Pharmacokinetics and bioavailability of zidovudine in humans. Am J Med 85:189-94.

Bodor N, Buchwald P. (2003). Brain-targeted drug delivery: experiences to date. Am J Drug Targ 1:13-26.

Bozzuto G, Molinari A. (2015). Liposomes as nanomedical devices. Int J Nanomedicine 10:975-99.

Brasnjevic I, Steinbusch HW, Schmitz C, Martinez-Martinez P. (2009). Delivery of peptide and protein drugs over the blood-brain barrier. Prog Neurobiol 87:212-51.

Brewster ME, Anderson WR, Webb AI, et al. (1997). Evaluation of a brain-targeting zidovudine chemical delivery system in dogs. Antimicrob Agents Chemother 41:122-8.

Brightman MW, Kadota Y. (1992). Nonpermeable and permeable vessels of the brain. NIDA Res Monogr 120:87-107.

Cancilla PA, DeBault LE. (1983). Neutral amino acid transport properties of cerebral endothelial cells *in vitro*. J Neuropathol Exp Neurol 42:191-9.

Carnielli VP, Verlato G, Pederzini F, et al. (1998). Intestinal absorption of long-chain polyunsaturated fatty acids in preterm infants fed breast milk or formula. Am J Clin Nutr 67:97-103.

Cecchelli R, Berezowski V, Lundquist S, et al. (2007). Modelling of the blood-brain barrier in drug discovery and development. Nat Rev Drug Discov 6:650-61.

Chattopadhyay N, Zastre J, Wong HL, et al. (2008). Solid lipid nanoparticles enhance the delivery of the HIV protease inhibitor, atazanavir, by a human brain endothelial cell line. Pharma Res 25:2262-71.

Chaudhuri JD. (2000). Blood-brain barrier and infection. Med Sci Monit 6:1213-22.

Chen Y, Liu L. (2012). Modern methods for delivery of drugs across the blood-brain barrier. Adv Drug Deliv Rev 64:640-65.

Christoper GVP, Raghavan CV, Siddharth K, et al. (2014). Formulation and optimization of coated PLGA – zidovudine nanoparticles using factorial design and *in vitro in vivo* evaluations to determine brain targeting efficiency. Saudi Pharm J 22:133-40.

Clark DE. (2003). In silico prediction of blood-brain barrier permeation. Drug Discov Today 8:927-933.

Cole L, Coleman J, Evans D, Hawes C. (1990). Internalisation of fluorescein isothiocyanate and fluorescein isothiocyanate-dextran by suspension-cultured plant cells. J Cell Sci 96:721-30.

Comoglu T, Arisoy S, Akkus ZB. (2017). Nanocarriers for Effective Brain Drug Delivery. Curr Top Med Chem 17:1490-506

Daemen T, Hofstede G, Ten Kate MT, et al. (1995). Liposomal doxorubicin induced toxicity: depletion and impairment of phagocytic activity of liver macrophages. Int J Cancer 61:716-21.

Dalpiaz A, Paganetto G, Pavan B, et al. (2012). Zidovudine and ursodeoxycholic acid conjugation: design of a new prodrug potentially able to bypass the active efflux transport systems of the central nervous system. Mol Pharm 9:957-68.

Dalpiaz A, Ferraro L, Perrone D, et al. (2014). Brain uptake of a zidovudine prodrug after nasal administration of solid lipid microparticles. Mol Pharm 11:1550-61.

Das PJ, Paul P, Mukherjee B, et al. (2015). Pulmonary delivery of voriconazole loaded nanoparticles providing a prolonged drug level in lungs: a promise for treating fungal infection. Mol Pharm 12:2651-64.

Dauchy S, Dutheil F, Weaver RJ, et al. (2008). ABC transporters, cytochromes P450 and their main transcription factors:expression at the human blood-brain barrier. J Neurochem 107:1518-28.

Davis LE, Hjelle BL, Miller VE, et al. (1992). Early viral brain invasion in iatrogenic human immunodeficiency virus infection. Neurology 42:1736-9.

Dawson DA, Wadsworth G, Palmer AM. (2001). A comparative assessment of the efficacy and side effect liability of neuroprotective compounds in experimental stroke. Brain Res 892:344-50.

Deamer D, Bangham AD. (1976). Large volume liposomes by an ether vaporization method. Biochim Biophys Acta 443:629-34.

Deli MA. (2011). Drug transport and the blood-brain barrier. In: Tihanyi K, Vastag M, eds. Solubility, Delivery and ADME Problems of Drugs and Drug-Candidates. Bentham Science Publishers Ltd., United Arab Emirates. p 144-65.

Dey NS, Mukherjee B, Maji R, Satapathy BS. (2016). Development of linker-conjugated nanosize lipid vesicles: A strategy for cell selective treatment in breast cancer. Curr Cancer Drug Targets 16:357-72.

Ding BS, Dziubla T, Shuvaev VV, et al. (2006). Advanced drug delivery systems that target the vascular endothelium. Mol Interv 6:98-112.

Doijad RC, Bhambere DS, Manvi FV, Deshmukh NV. (2009). Formulation and characterization of vesicular drug delivery system for anti-HIV drug. JGPT:94-100.

Dua JS, Rana AC, Bhandari AK. (2012). Liposome: methods of preparation and applications. IJPSR III:14-20.

Enerson BE, Drewes LR. (2006). The rat blood-brain barrier transcriptome. J Cereb Blood Flow Metab 26:959-73.

Fischl MA, Richman DD, Grieco MH, et al. (1987). The efficacy of azidothymidine (AZT) in the treatment of patients with AIDS and AIDS-related complex. A double-blind, placebocontrolled trial. N Engl J Med 317:185-91.

Fox CB, Mulligan SK, Sung J, et al. (2014). Cryogenic transmission electron microscopy of recombinant tuberculosis vaccine antigen with anionic liposomes reveals formation of flattened liposomes. Int J Nanomedicine 9:1367-77.

Fricker G, Miller DS. (2004). Modulation of drug transporters at the blood-brain barrier. Pharmacology 70:169-76.

Furuse M, Hirase T, Itoh M, et al. (1993). Occludin: a novel integral membrane protein localizing at tight junctions. J Cell Biol 123:1777-88.

Gabizon A, Catane R, Uziely B, et al. (1994). Prolonged circulation time and enhanced accumulation in malignant exudates of doxorubicin encapsulated in polyethylene-glycol coated liposomes. Cancer Res 54:987-92.

Gabizon A, Chisin R, Amselem S, et al. (1991). Pharmacokinetic and imaging studies in patients receiving a formulation of liposome-associated adriamycin. Br J Cancer 64:1125-32.

Gautam N, Bathena SPR, Chen Q, et al. (2013). Pharmacokinetics, protein binding, and metabolism of a quinoxaline urea analog as a NF-κB inhibitor in mice and rats by LC-MS/MS. Biomed Chromatogr 27:900-9.

Gharib A, Faezizadeh Z, Namin SARM, Saravani R. (2014). Preparation, characterization and *in vitro* efficacy of magnetic nanoliposomes containing the artemisinin and transferrin. Daru 22:44.

Gleeson MP. (2008). Generation of a set of simple, interpretable ADMET rules of thumb. J Med Chem 51:817-34.

Gurturk Z, Tezcaner A, Dalgic AD, et al. (2017). Maltodextrin modified liposomes for drug delivery through the blood-brain barrier. Med Chem Commun 8:1337-45.

Hamilton RL Jr, Goerke J, Guo L, et al. (1980). Unilamellar liposomes made with the French pressure cell: a simple preparative and semi-quantitative technique. J Lipid Res 21:981-92.

Hamilton RL, Guo LSS. (1984). Liposomes preparation methods. J Clin Biochem Nut 7:175.

Haran G, Cohen R, Bar LK, Barenholz Y. (1993). Transmembrane ammonium sulfate gradients in liposomes produce efficient and stable entrapment of amphipathic weak bases. Biochim Biophys Acta 1151:201-15.

Hatzfeld M. (2005). The p120 family of cell adhesion molecules. Eur J Cell Biol 84:205-14.

Hawkins BT, Davis TP. (2005). The blood-brain barrier/neurovascular unit in health and disease. Pharmacol Rev 57:173-85.

Hellstrom M, Gerhardt H, Kalen M, et al. (2001). Lack of pericytes leads to endothelial hyperplasia and abnormal vascular morphogenesis. J Cell Biol 153:543-53.

Hirase T, Staddon JM, Saitou M, et al. (1997). Occludin as a possible determinant of tight junction permeability in endothelial cells. J Cell Sci 110:1603-13.

Hosoya K, Sugawara M, Asaba H, Terasaki T. (1999). Blood-brain barrier produces significant efflux of L-aspartic acid but not D-aspartic acid: *in vivo* evidence using the brain efflux method. J Neurochem 73:1206-11.

Hu K, Li J, Shen Y, et al. (2009). Lactoferrin-conjugated PEG-PLA nanoparticles with improved brain delivery: *in vitro* and *in vivo* evaluations. J Control Release 134:55-61.

Hu X, Yang F, Liao Y, et al. (2017). Cholesterol-PEG comodified poly (N-butyl) cyanoacrylate nanoparticles for brain delivery: *in vitro* and *in vivo* evaluations. Drug Deliv 24:121-32.

Hua S, Wu SY. (2013). The use of lipid-based nanocarriers for targeted pain therapies. Front Pharmacol 4:143.

Hua S. (2013). Targeting sites of inflammation: intercellular adhesion molecule-1 as a target for novel inflammatory therapies. Front Pharmacol 4:127.

Huang FY, Chen WJ, Lee WY, et al. (2013). *In vitro* and *in vivo* evaluation of lactoferrin-conjugated liposomes as a novel carrier to improve the brain delivery. Int J Mol Sci 14:2862-74.

Huang N, Cheng S, Zhang X, et al. (2017). Efficacy of NGR peptide-modified PEGylated quantum dots for crossing the blood-brain barrier and targeted fluorescence imaging of glioma and tumor vasculature. Nanomedicine 13:83-93.

Ivey NS, MacLean AG, Lackner AA. (2009). AIDS and the blood-brain barrier. J Neurovirol 15:111-22.

Jain S, Tiwary AK, Jain NK. (2008). PEGylated elastic liposomal formulation for lymphatic targeting of zidovudine. Curr Drug Deliv 5:275-81.

Jain SK, Sharma A, Mahajan M, Sankar R. (2013). *In-vitro* and *in-vivo* evaluation of poly (propyl ether imine) (PETIM) dendrimer for sustained delivery of zidovudine. J Antivir Antiretrovir S10-004.

Janzer RC, Raff MC. (1987). Astrocytes induce blood-brain barrier properties in endothelial cells. Nature 325:253-7.

Jesorka A, Orwar O. (2008). Liposomes: technologies and analytical applications. Annu Rev Anal Chem 1:801-32.

Jin SX, Bi DZ, Wang J, et al. (2005). Pharmacokinetics and tissue distribution of zidovudine in rats following intravenous administration of zidovudine myristate loaded liposomes. Pharmazie 60:840-3.

Jones ML. (2008). Lipids. In: Bancroft JD, Gamble M, eds. Theory and Practice of Histological Techniques. Churchill Livingstone Elsevier, Philadelphia. p 187-216.

Joshy KS, Snigdha S, Kalarikkal N, et al. (2017). Gelatin modified lipid nanoparticles for anti-viral drug delivery. Chem Phys Lipids 207:24-37.

Jouyban A, Soltani S. (2012). Blood brain barrier permeation. In: Acree B, eds. Toxicity and Drug Testing. InTech, Europe. p 1-24.

Kacem K, Lacombe P, Seylaz J, Bonvento G. (1998). Structural organization of the perivascular astrocyte endfeet and their relationship with the endothelial glucose transporter: a confocal microscopy study. Glia 23:1-10.

Kalepu S, Sunilkumar KT, Betha S, Mohanvarma M. (2013). Liposomal drug delivery system - a comprehensive review. Int J Drug Dev & Res 5:62-75.

Kataria S, Sandhu P, Bilandi A, et al. (2011). Stealth liposomes: a review. IJRAP 2:1534-8.

Kaur CD, Nahar M, Jain NK. (2008). Lymphatic targeting of zidovudine using surface-engineered liposomes. J Drug Target 16:798-805.

Kim KY. (2007). Nanotechnology platforms and physiological challenges for cancer therapeutics. Nanomed Nanotech Biol Med 3:103-10.

Kirby CJ, Gregoriadis G. (1984). A simple procedure for preparing liposomes capable of high encapsulation efficiency under mild conditions. In: Gregoriadis G, eds. Liposome Technology. CRC Press Inc, Boca Raton. p 19-28.

Kittiphoom S. (2012). Utilization of mango seed. Int Food Res J 19:1325-35.

Klein CJ. (2002). Nutrient requirements for preterm infant formulas. J Nutr 132:1395S-577S.

Koning GA, Storm G. (2003). Targeted drug delivery systems for the intracellular delivery of macromolecular drugs. Drug Discov Today 8:482-3.

Kumar P, Lakshmi YS, Bhaskar C, et al. (2015). Improved safety, bioavailability and pharmacokinetics of zidovudine through lactoferrin nanoparticles during oral administration in rats. PLoS One 10:e0140399.

Kuo YC, Chen HH. (2006). Effect of nanoparticulate polybutylcyanoacrylate and methylmethacrylate-sulfopropylmethacrylate on the permeability of zidovudine and lamivudine across the *in vitro* blood-brain barrier. Int J Pharm 327:160-9.

Kuo YC, Chung CY. (2012). Transcytosis of CRM197-grafted polybutylcyanoacrylate nanoparticles for delivering zidovudine across human brain-microvascular endothelial cells. Colloids Surf B Biointerfaces 91:242-9.

Kusuhara H, Suzuki H, Terasaki T, et al. (1997). P-Glycoprotein mediates the efflux of quinidine across the blood-brain barrier. J Pharmacol Exp Ther 283:574-80.

Kutcher ME, Herman IM. (2009). The pericyte: cellular regulator of microvascular blood flow. Microvasc Res 77:235-46.

Lackner AA, Vogel P, Ramos RA, et al. (1994). Early events in tissues during infection with pathogenic (SIVmac239) and nonpathogenic (SIVmac1A11) molecular clones of simian immunodeficiency virus. Am J Pathol 145:428-39.

Lampugnani MG, Corada M, Caveda L, et al. (1995). The molecular organization of endothelial cell to cell junctions: differential association of plakoglobin, beta-catenin, and alpha-catenin with vascular endothelial cadherin (VE-cadherin). J Cell Biol 129:203-17.

Lange CG, Lederman MM, Medvik K, et al. (2003). Nadir CD4+ T-cell count and numbers of CD28+ CD4+ T-cells predict functional responses to immunizations in chronic HIV-1 infection. AIDS 17:2015-23.

Laouini A, Jaafar-Maalej C, Limayem-Blouza I, et al. (2012). Preparation, characterization and applications of liposomes: state of the art. J Colloid Sci Biotechnol 1:147-68.

Lasic DD, Frederik PM, Stuart MC, et al. (1992). Gelation of liposome interior. A novel method for drug encapsulation. FEBS Lett 312:255-8.

Lasic DD, Joannic R, Keller BC, et al. (2001). Spontaneous vesiculation. Adv Colloid Interface Sci 89-90:337-49.

Lawther BK, Kumar S, Krovvidi H. (2011). Blood-brain barrier. Contin Educ Anaesth, Crit Care Pain 11:128-32.

Li X, Tsibouklis J, Weng T, et al. (2017). Nano carriers for drug transport across the blood-brain barrier. J Drug Target 25:17-28.

Liebner S, Fischmann A, Rascher G, et al. (2000). Claudin-1 and claudin-5 expression and tight junction morphology are altered in blood vessels of human glioblastomamultiforme. Acta Neuropathol 100:323-31.

Lindahl P, Johansson BR, Leveen P, Betsholtz C. (1997). Pericyte loss and microaneurysm formation in PDGF-B-deficient mice. Science 277:242-5.

Liu L, Yonetani T. (1994). Preparation and characterization of liposome encapsulated haemoglobin by a freeze-thaw method. J Microencapsulation 11:409-21.

Liu L, Venkatraman SS, Yang YY, et al. (2008). Polymeric micelles anchored with TAT for delivery of antibiotics across the blood-brain barrier. Biopolymers 90:617-23.

Loscher W, Potschka H. (2005). Role of drug efflux transporters in the brain for drug disposition and treatment of brain diseases. Prog Neurobiol 76:22-76.

Lu CT, Zhao YZ, Wong HL, et al. (2014). Current approaches to enhance CNS delivery of drugs across the brain barriers. Int J Nanomedicine 9:2241-57.

Mainardes RM, Khalil NM, Gremião MPD. (2010). Intranasal delivery of zidovudine by PLA and PLA-PEG blend nanoparticles. Int J Pharm 395:266-71.

Maji R, Dey NS, Satapathy BS, et al. (2014). Preparation and characterization of tamoxifen citrate loaded nanoparticles for breast cancer therapy. Int J Nanomedicine 9:3107-18.

Mandal TK, Tenjarla S. (1996). Preparation of biodegradable microcapsules of zidovudine using solvent evaporation: Effect of the modification of aqueous phase. Int J Pharm 137:187-97.

Marianecci C, Rinaldi F, Hanieh PN, et al. (2017). Drug delivery in overcoming the blood-brain barrier: role of nasal mucosal grafting. Drug Des Devel Ther 11:325-35.

Martins S, Tho I, Reimold I, et al. (2012). Brain delivery of camptothecin by means of solid lipid nanoparticles: formulation design, *in vitro* and *in vivo* studies. Int J Pharm 439:49-62.

Maruyama K. (2002). PEG-immunoliposome. Biosci Rep 22:251-66.

Masarudin MJ, Cutts SM, Evison BJ, et al. (2015). Factors determining the stability, size distribution, and cellular accumulation of small, monodisperse chitosan nanoparticles as candidate vectors for anticancer drug delivery: application to the passive encapsulation of [^{14}C]-doxorubicin. Nanotechnol Sci Appl 8:67-80.

Masserini M. (2013). Nanoparticles for brain drug delivery. ISRN Biochem 2013:1-18.

Matter K, Balda MS. (2003). Signalling to and from tight junctions. Mol Cell Biol 4:225-36.

Mayer LD, Bally MB, Hope MJ, Cullis PR. (1986). Techniques for encapsulating bioactive agents in to liposomes. Chem Phys Lipids 40:333-45.

McCrea PD, Gumbiner BM. (1991). Purification of a 92-kDa cytoplasmic protein tightly associated with the cell-cell adhesion molecule E-cadherin (uvomorulin). Characterization and extractability of the protein complex from the cell cytostructure. J Biol Chem 266:4514-20.

Mehnert W, Mader K. (2001). Solid lipid nanoparticles: production, characterization and applications. Adv Drug Deliv Rev 47:165-96.

Meng X, Liu J, Yu X, et al. (2017). Pluronic F127 and D-α-tocopheryl polyethylene glycol succinate (TPGS) mixed micelles for targeting drug delivery across the blood brain barrier. Sci Rep 7:2964.

Mishra V, Mahor S, Rawat A, et al. (2006). Targeted brain delivery of AZT via transferrin anchored pegylated albumin nanoparticles. J Drug Target 14:45-53.

Moghimi SM, Szebeni J. (2003). Stealth liposomes and long circulating nanoparticles: critical issues in pharmacokinetics, opsonization and protein-binding properties. Prog Lipid Res 42:463-78.

Monteiro N, Martins A, Reis RL, Neves NM. (2014). Liposomes in tissue engineering and regenerative medicine. J R Soc Interface 11:20140459.

Mu L, Zhou R, Tang F, et al. (2016). Intracellular pharmacokinetic study of zidovudine and its phosphorylated metabolites. Acta Pharm Sin B 6:158-62.

Mugavero MJ, Hicks CB. (2004). HIV resistance and the effectiveness of combination antiretroviral treatment. Drug Discov Today 1:529-35.

Mui B, Chow L, Hope MJ. (2003). Extrusion technique to generate liposomes of defined size. Methods Enzymol 367:3-14.

Mukherjee B, Chakraborty S, Mondal L, et al. (2016). Multifunctional drug nanocarriers facilitate more specific entry of therapeutic payload into tumors and control multiple drug resistance in cancer. In: Grumezescu AM, eds. Nanobiomaterials in Cancer Therapy. Elsevier, UK; USA. p 203-51.

Mukherjee B, Dutta L, Mondal L, et al. (2015). Nanoscale formulations and diagnostics with their recent trends: a major focus of future nanotechnology. Curr Pharm Des 21:5172-86.

Nagafuchi A, Takeichi M. (1989). Transmembrane control of cadherinmediated cell adhesion: a 94 kDa protein functionally associated with a specific region of the cytoplasmic domain of E-cadherin. Cell Regul 1:37-44.

Nath B, Nath LK, Kumar P. (2011). Preparation and *in vitro* dissolution profile of zidovudine loaded microspheres made of Eudragit RS 100, RL 100 and their combinations. Acta Pol Pharm 68:409-15.

Nayak UY, Gopal S, Mutalik S, et al. (2009). Glutaraldehyde cross-linked chitosan microspheres for controlled delivery of zidovudine. J Microencapsul 26: 214-22.

Newton HB. (2006). Advances in strategies to improve drug delivery to brain tumors. Expert Rev Neurother 6:1495-1509.

Nitta T, Hata M, Gotoh S, et al. (2003). Size-selective loosening of the blood-brain barrier in claudin-5-deficient mice. J Cell Biol 161:653-60.

Northfelt DW, Martin FJ, Working P, et al. (1996). Doxorubicin encapsulated in liposomes containing surface-bound polyethylene glycol: pharmacokinetics, tumor localization, and safety in patients with AIDS-related Kaposi's sarcoma. J Clin Pharmacol 36:55-63.

O'Kane RL, Martínez-López I, DeJoseph MR, et al. (1999). Na(+)-dependent glutamate transporters (EAAT1, EAAT2, and EAAT3) of the blood-brain barrier. A mechanism for glutamate removal. J Biol Chem 274:31891-95.

Oh SY, Jeong SY, Park TG, Lee JH. (1998). Enhanced transdermal delivery of AZT (zidovudine) using iontophoresis and penetration enhancer. J Control Release 51:161-8.

Ohsawa T, Miura H, Harada K. (1985). Improvement of encapsulation efficiency of water-soluble drugs in liposomes formed by the freeze-thawing method. Chem Pharm Bull 33:3945-52.

Oldendorf WH. (1971). Brain uptake of radio-labelled amino acids, amines and hexoses after arterial injection. Am J Physiol 221:1629-39.

Olson F, Hunt CA, Szoka FC, et al. (1979). Preparation of liposomes of defined size distribution by extrusion through polycarbonate membranes. Biochim Biophys Acta 557:9-23.

Pahuja R, Seth K, Shukla A, et al. (2015). Trans-blood brain barrier delivery of dopamine-loaded nanoparticles reverses functional deficits in Parkinsonian rats. ACS Nano 9:4850-71.

Palmeri D, van Zante A, Huang CC, et al. (2000). Vascular endothelial junction-associated molecule, a novel member of the immunoglobulin superfamily, is localized to intercellular boundaries of endothelial cells. J Biol Chem 275:19139-45.

Pandey H, Rani R, Agarwal V. (2016). Liposome and their applications in cancer therapy. Braz Arch Biol Technol 59:e16150477.

Pardridge WM. (2002). Drug and gene targeting to brain with molecular Trojan horses. Nat Rev Drug Discov 1:131-9.

Patlak CS, Blasberg RG, Fenstermacher JD. (1983). Graphical evaluation of blood-to-brain transfer constants from multiple-time uptake data. J Cereb Blood Flow Metab 3:1-7.

Pattnaik G, Sinha B, Mukherjee B, et al. (2012). Submicron-size biodegradable polymer-based didanosine particles for treating HIV at early stage: an *in vitro* study. J Microencapsul 29:666-76.

Pavan B, Dalpiaz A, Ciliberti N, et al. (2008). Progress in drug delivery to the central nervous system by the prodrug approach. Molecules 13:1035-65.

Pawar V, Mishra SK, Yadav M, Tiwari A. (2013). Liposome: a powerful approach festinates drug delivery system. IJDDT 3:4-7.

Peppiatt CM, Howarth C, Mobbs P, Attwell D. (2006). Bidirectional control of CNS capillary diameter by pericytes. Nature 443:700-4.

Perlmutter LS, Chui HC. (1990). Microangiopathy, the vascular basement membrane and Alzheimer's disease: a review. Brain Res Bull 24:677-86.

Persidsky Y, Ghorpade A, Rasmussen J, et al. (1999). Microglial and astrocyte chemokines regulate monocyte migration through the blood-brain barrier in human immunodeficiency virus-1 encephalitis. Am J Pathol 155:1599-611.

Petty MA, Lo EH. (2002). Junctional complexes of the bloodbrain barrier: permeability changes in neuroinflammation. Prog Neurobiol 68:311-23.

Pick U. (1981). Liposomes with a large trapping capacity prepared by freezing and thawing of sonicated phospholipid mixtures. Arch Biochem Biophys 212:186-94.

Prabhakar K, Afzal SM, Surender G, Kishan V. (2013). Tween 80 containing lipid nanoemulsions for delivery of indinavir to brain. Acta Pharm Sin B 3:345-53.

Prabhu P, Nitish KR, Koland M, et al. (2010). Preparation and evaluation of nano-vesicles of brimonidine tartrate as an ocular drug delivery system. J Young Pharm 2:356-61.

Puri A, Loomis K, Smith B, et al. (2009). Lipid-based nanoparticles as pharmaceutical drug carriers: from concepts to clinic. Crit Rev Ther Drug Carrier Syst 26:523-80.

Raeissi S, Audus KL. (1989). *In-vitro* characterization of blood-brain barrier permeability to delta sleep-inducing peptide. J Pharm Pharmacol 41:848-52.

Rao KS, Ghorpade A, Labhasetwar V. (2009). Targeting anti-HIV drugs to the CNS. Expert Opin Drug Deliv 6:771-84.

Rautio J, Laine K, Gynther M, Savolainen J. (2008). Prodrug approaches for CNS delivery. AAPS J 10:92-102.

Reichenbach A, Wolburg H. (2004). Morphology and ultrastructure of glial cells, astrocytes and ependymal glia. In: Kettemann H, Ransom BR, eds. Neurologia (2nd edn). Oxford University Press, New York. p 19-35.

Riaz M. (1996). Liposome preparation method. Pak J Pharm Sci 9:65-77.

Ribatti D, Nico B, Crivellato E, Artico M. (2006). Development of the blood-brain barrier: a historical point of view. Anat Rec B New Anat 289:3-8.

Risau W, Wolburg H. (1990). Development of the blood-brain barrier. Trends Neurosci 13:174-8.

Rubin LL, Staddon JM. (1999). The cell biology of the blood-brain barrier. Annu Rev Neurosci 22:11-28.

Rudra A, Deepa RM, Ghosh MK, et al. (2010). Doxorubicin-loaded phosphatidylethanolamine-conjugated nanoliposomes: *in vitro* characterization and their accumulation in liver, kidneys, and lungs in rats. Int J Nanomedicine 5:811-23.

Sahana B, Santra K, Basu S, Mukherjee B. (2010). Development of biodegradable polymer based tamoxifen citrate loaded nanoparticles and effect of some manufacturing process parameters on them: a physicochemical and *in-vitro* evaluation. Int J Nanomedicine 5:621-30.

Saiyed ZM, Gandhi NH, Nair MP. (2010). Magnetic nanoformulation of azidothymidine 5'-triphosphate for targeted delivery across the blood-brain barrier. Int J Nanomedicine 5:157-66.

Satapathy BS, Mukherjee B, Baishya R, et al. (2016). Lipid nanocarrier-based transport of docetaxel across the blood brain barrier. RSC Adv 6:85261-74.

Schieren H, Rudolph S, Finkelstein M, et al. (1978). Comparison of large unilamellar vesicles prepared by a petroleum ether vaporization method with multilamellar vesicles: ESR, diffusion and entrapment analyses. Biochim Biophys Acta 542:137-53.

Schinkel AH, Smit JJ, van Tellingen O, et al. (1994). Disruption of the mouse mdr1a P-glycoprotein gene leads to a deficiency in the blood-brain barrier and to increased sensitivity to drugs. Cell 77:491-502.

Schinkel AH, Wagenaar E, Mol CA, van Deemter L. (1996). P-glycoprotein in the blood-brain barrier of mice influences the brain penetration and pharmacological activity of many drugs. J Clin Invest 97:2517-24.

Schneeberger EE, Lynch RD. (2004). The tight junction: a multifunctional complex. Am J Physiol Cell Physiol 286:C1213-28.

Schroder U, Sabel BA. (1996). Nanoparticles, a drug carrier system to pass the blood-brain barrier, permit central analgesic effects of i.v. dalargin injections. Brain Res 710:121-4.

Schroeder U, Sommerfeld P, Ulrich S, Sabel BA. (1998). Nanoparticle technology for delivery of drugs across the blood-brain barrier. J Pharm Sci 87:1305-7.

Seju U, Kumar A, Sawant KK. (2011). Development and evaluation of olanzapine-loaded PLGA nanoparticles for nose-to-brain delivery: *in vitro* and *in vivo* studies. Acta Biomater 7:4169-76.

Sercombe L, Veerati T, Moheimani F, et al. (2015). Advances and challenges of liposome assisted drug delivery. Front Pharmacol 6:286.

Shah MR, Imran M, Ullah S. (2017). Nano suspensions. In: Lipid-based Nanocarriers for Drug Delivery and Diagnosis. Elsevier, UK; US. p 139-72.

Shah Purvin, Vuddanda PR, Singh SK, et al. (2014). Pharmacokinetic and tissue distribution study of solid lipid nanoparticles of zidovudine in rats. J Nanotechnol 2014: 854018.

Shaheen SM, Ahmed FRS, Hossen MN, et al. (2006). Liposome as a carrier for advanced drug delivery. Pak J Biol Sci 9:1181-91.

Sharma A, Sharma US. (1997). Liposomes in drug delivery: progress and limitations. Int J Pharm 154:123-40.

Sharma N, Mishra S, Sharma S, et al. (2013). Preparation and optimization of nanoemulsions for targeting drug delivery. Int J Drug Dev & Res 5:37-48.

Shatzmiller S, Lapidot I, Zats G. (2016). Blood brain barrier crossing for therapeutic and diagnostic agents. SM J Neurol Disord Stroke 2:1012.

Shaw TK, Mandal D, Dey G, et al. (2017). Successful delivery of docetaxel to rat brain using experimentally developed nanoliposome: a treatment strategy for brain tumor. Drug Deliv 24:346-57.

Singh S, Dobhal AK, Jain A, et al. (2010). Formulation and evaluation of solid lipid nanoparticles of a water soluble drug: zidovudine. Chem Pharm Bull 58:650-5.

Singh Y, Meher JG, Raval K, et al. (2017). Nanoemulsion: concepts, development and applications in drug delivery. J Control Release 252:28-49.

Somani S, Blatchford DR, Millington O, et al. (2014). Transferrin-bearing polypropylenimine dendrimer for targeted gene delivery to the brain. J Control Release 188:78-86.

Soni V, Kohli DV, Jain SK. (2007). Transferrin coupled liposomes for enhanced brain delivery of doxorubicin. Vascular Disease Prevention 4:31-8.

Sperling R. (1998). Zidovudine. Infect Dis Obstet Gynecol 6:197-203.

Srinageshwar B, Peruzzaro S, Andrews M, et al. (2017). PAMAM dendrimers cross the blood-brain barrier when administered through the carotid artery in C57BL/6J mice. Int J Mol Sci 18:E628.

Sultana F, Manirujjaman, Imran-Ul-Haque M, et al. (2013). An overview of nanogel drug delivery system. JAPS 3:S95-105.

Swami H, Kataria MK, Bilandi A, et al. Liposome: an art for drug delivery. IJPSL 5:523-30.

Szoka F Jr, Papahadjopoulos D. (1978). Procedure for preparation of liposomes with large internal aqueous space and high capture by reverse-phase evaporation. Proc Natl Acad Sci 75:4194-8.

Tajes M, Ramos-Fernández E, Weng-Jiang X, et al. (2014). The blood-brain barrier: structure, function and therapeutic approaches to cross it. Mol Membr Biol 31:152-67.

Takasato Y, Rapoport SI, Smith QR. (1984). An *in situ* brain perfusion technique to study cerebrovascular transport in the rat. Am J Physiol 247:H484-93.

Takeichi M. (1995). Morphogenetic roles of classic cadherins. Curr Opin Cell Biol 7:619-27.

Tamai I, Tsuji A. (2000). Transporter-mediated permeation of drugs across the blood-brain barrier. J Pharm Sci 89:1371-88.

Terasaki T, Ohtsuki S. (2005). Brain-to-blood transporters for endogenous substrates and xenobiotics at the blood-brain barrier: an overview of biology and methodology. NeuroRx 2:63-72.

Thomas NS, Panchagnula R. (2003). Transdermal delivery of zidovudine: effect of vehicles on permeation across rat skin and their mechanism of action. Eur J Pharm Sci 18:71-9.

Tietz S, Engelhardt B. (2015). Brain barriers: crosstalk between complex tight junctions and adherens junctions. J Cell Biol 209:493-506.

Torchilin VP, Klibanov AL, Huang L, et al. (1992). Targeted accumulation of polyethylene glycol-coated immunoliposomes in infarcted rabbit myocardium. FASEB J 6:2716-9.

Tripathi KM, Castro M, Feller JF, Sankar SK. (2017). Characterization of metal, semiconductor, and metal-semiconductor core-shell nanostructures. In: Gupta RK, Misra M, eds. Metal Semiconductor Core-Shell Nanostructures for Energy and Environmental Applications. Elsevier, Netherlands. p 51-78.

Tsukita S, Furuse M, Itoh M. (2001). Multifunctional strands in tight junctions. Nat Rev Mol Cell Biol 2:285-93.

Tyagi N, Rathore SS, Ghosh PC. (2011). Enhanced killing of human epidermoid carcinoma (KB) cells by treatment with ricin encapsulated into sterically stabilized liposomes in combination with monensin. Drug Deliv 18:394-404.

Tyagi N, Rathore SS, Ghosh PC. (2013). Efficacy of liposomal monensin on the enhancement of the antitumour activity of liposomal ricin in human epidermoid carcinoma (KB) Cells. Indian J Pharm Sci 75:16-22.

Tyrrell DA, Heath TD, Colley CM, Ryman BE. (1976). New aspects of liposomes. Biochim Biophys Acta 457:259-302.

Ulrich AS. (2002). Biophysical aspects of using liposomes as delivery vehicles. Biosci Rep 22:129-50.

Upadhyay RK. (2014). Drug delivery systems, CNS protection, and the blood brain barrier. Biomed Res Int 2014:869269.

Uronnachi EM, Ogbonna JDN, Kenechukwu FC, et al. (2013). Pharmacokinetics and biodistribution of zidovudine loaded in a solidified reverse micellar delivery system. IJDD 5:73-80.

Ved PM, Kim K. (2011). Poly(ethylene oxide/propylene oxide) copolymer thermo-reversible gelling system for the enhancement of intranasal zidovudine delivery to the brain. Int J Pharm 411:1-9.

Vemuri S, Rhodes CT. (1995). Preparation and characterization of liposomes as therapeutic delivery systems: a review. Pharm Acta Helv 70:95-111.

Vieira DB, Gamarra LF. (2016). Getting into the brain: liposome-based strategies for effective drug delivery across the blood–brain barrier. Int J Nanomedicine 11:5381-414.

Vinogradov SV, Batrakova EV, Kabanov AV. (2004). Nanogels for oligonucleotide delivery to the brain. Bioconjug Chem 15:50-60.

Wallez Y, Huber P. (2008). Endothelial adherens and tight junctions in vascular homeostasis, inflammation and angiogenesis. Biochim Biophys Acta 1778:794-809.

Walling MA, Novak JA, Shepard JRE. (2009). Quantum dots for live cell and *in vivo* imaging. Int J Mol Sci 10:441-91.

Weiss N, Miller F, Cazaubon S, Couraud PO. (2009). The blood-brain barrier in brain homeostasis and neurological diseases. Biochim Biophys Acta 1788:842-57.

Willis M, Forssen E. (1998). Ligand-targeted liposomes. Adv Drug Deliv Rev 29:249-71.

Wilson B, Samanta MK, Santhi K, et al. (2008). Poly(n-butylcyanoacrylate) nanoparticles coated with polysorbate 80 for the targeted delivery of rivastigmine into the brain to treat Alzheimer's disease. Brain Res 1200:159-68.

Wilson B, Samanta MK, Santhi K, et al. (2008). Targeted delivery of tacrine into the brain with polysorbate 80-coated poly(n-butylcyanoacrylate) nanoparticles. Eur J Pharm Biopharm 70:75-84.

Wolburg H, Lippoldt A. (2002). Tight junctions of the blood-brain barrier: development, composition and regulation. Vascul Pharmacol 38:323-37.

Wolburg H, Wolburg-Buchholz K, Kraus J, et al. (2003). Localization of claudin-3 in tight junctions of the blood-brain barrier is selectively lost during experimental autoimmune encephalomyelitis and human glioblastoma multiforme. Acta Neuropathol 105:586-92.

Xu G, Mahajan S, Roy I, Yong KT. (2013). Theranostic quantum dots for crossing blood-brain barrier *in vitro* and providing therapy of HIV-associated encephalopathy. Front Pharmacol 4:140.

Zlokovic BV. (2008). The blood-brain barrier in health and chronic neurodegenerative disorders. Neuron 57:178-201.

Zlokovic BV, Begley DJ, Djuricic BM, Mitrovic DM. (1986). Measurement of solute transport across the blood-brain barrier in the perfused guinea pig brain: method and application to N-methyl-α-aminoisobutyric acid. J Neurochem 46:1444-51.

Chapter 10

Annexure

যাদবপুর বিশ্ববিদ্যালয়
কলকাতা-৭০০০৩২, ভারত

JADAVPUR UNIVERSITY
KOLKATA-700032, INDIA

Ref. No.: P. 1/Rs/192/14.
Dated : 10.06.2014.

Smt. Lopamudra Dutta
Begunia Para Bye Lane(Badra Para)
P.O. Nabadwip, Dist. Nadia,
Pin - 741 302
West Bengal

Madam,

I am pleased to inform you that you have been selected Senior Research Fellow to work in the DBT sponsored research Scheme entitled on "Development of Nano Structured Lipid Carriers…..of Zidovudine " under the supervision of Prof.(Dr.)Biswajit Mukherjee, Principal Investigator of the Project, Department of Pharmaceutical Technology, of this University.

You will be paid a fellowship of Rs.18,000/= per month with HRA as per DBT norms.The tenure of your fellowship is up to the termination of the scheme provided you work satisfactorily and exhibit good conduct. You are to take classes up to six periods a week. The fellowship will be paid to you only on receipt of the fund from the sponsoring authority.

You may have to register your name for the Ph.D. Degree within one year from the date of your joining the post and the registration documents to be submitted to the Research Section.

Your service will be governed by the same terms and conditions of the University Service Rules as may be applicable to the temporary staff of the University and you will be under the administrative control of the undersigned.

You are requested to join the post within ten days from the date of receipt of this letter and submit your joining report in duplicate through proper channel to the undersigned with a declaration stating that you are not a recipient of any emoluments from any other source from the date of your joining the fellowship.

Yours faithfully,

REGISTRAR 6/6/14

Dr. Biswajit Mukherjee

M.Pharm., Ph.D., F.I.C., F.I.C.S.
Professor in Pharmaceutics
Coordinator, QIP Nodal Cell (Pharmacy)
Joint Coordinator,
Centre for Advance Research in Pharmaceutical Sciences,
Jadavpur University, Kolkata
Former DAAD Fellow (Germany) and Ex-guest Scientist,
German Cancer Research Center (DKFZ)
Heidelberg, Germany
Indo-Hungarian Education Exchange Fellow,
Budapest, Hungary
Former Fellow Scientist, School of Pharmacy,
University of London, London, U.K.
Ex. Biotechnology Overseas Associate,
Department of Biotechnology
(Government of India) and Worked in DKFZ
Heidelberg, Germany

Department of Pharmaceutical Technology
JADAVPUR UNIVERSITY
Kolkata - 700 032, India
Phone : +91-33-2414 6677 / 2414 6666 ext. 2588
Resi. : +91-33-2427 6026
Fax : +91-33-2414 6677 / 6396 (O)
E-mail : biswajit55@yahoo.com

To,
Lopamudra Dutta
c/o- Prof. Biswajit Mukherjee
Dept. of Pharm. Tech.
Jadavpur University
Kolkata-700032, India.

Project title: Development of nanosize lipid based vesicular delivery system of Zidovudine to cross blood brain barrier.

Ref No.: AEC/PHARM/1601/14/2016
Date: 21.04.2016

Dear Sir/Madam,

As per the meeting of Animal Ethics Committee (AEC), Jadavpur University, held on 21.04.2016, I am pleased to inform you that the AEC, Jadavpur University, has approved your project for fresh /renewal applied to the respective funding agencies. However, you are requested to abide by the following guidelines-

1) All the animal experiments should be conducted strictly following the guidelines of CPCSEA (Govt. of India) and the UGC, New Delhi.
2) Animals are to be purchased from registered breeders only and record should be maintained and required to be submitted to the convenor, AEC, Jadavpur University.
3) Details of animals housed and sacrifice of animals being carried out should be given to the AEC time to time.

Furthermore, you are requested to submit the project no. to the AEC once the project is sanctioned. Moreover, you are requested to note further that the expenditure regarding maintenance of the animals has to be made from your project only. **Special attention should be provided to prohibit any unlawful cruelty to the animals.**

Thanking you
Yours sincerely,

21/04/2016
(Dr. Biswajit Mukherjee)

Dr. Biswajit Mukherjee
Convener
Animal Etheics Committee
JADAVPUR UNIVERSITY
Kolkata-700 032

Chapter 11

Paper Presentations

3rd Annual National Seminar of All India Association of
Medical Social Work Professionals
On
"Social Work Practices in Health Care: Emerging Health Issues among Women"

26th to 27th March, 2016

Organized by
Medical Social Workers, Vardhman Mahavir Medical College & Safdarjung Hospital, New Delhi
At
Old Lecture Theater, Vardhman Mahavir Medical College & Safdarjung Hospital, New Delhi

Certificate Of Honour

This is to certify that Prof / Dr / Mr / Ms. LOPAMUDRA DUTTA *has participated in the 3rd National Seminar of AIAMSWP on "Social Work Practices in Health Care: Emerging Health Issues among Women", at Vardhman Mahavir Medical College & Safdarjung Hospital, New Delhi from 26th to 27th March, 2016 & delivered a Guest Lecture / Chaired a Scientific Session / Presented Paper(s)/Poster(s) titled* Zidovudine Loaded Nanoliposomes Enable the Drug to cross Blood Brain Barriers for Better HIV management in Patients

Rashmi Sharma
Organizing Chairperson
& President, AIAMSWP

Sushil Kumar Mishra
Organizing Secretary &
Jt. Secy. AIAMSWP

Dr. O P Giri
Hony. General Secretary
AIAMSWP

19th February 2016

Certificate

This to certified that Prof./Dr./Sri/Smt. Lopamudra Dutta of _____ has participated in the NATIONAL SEMINAR on " CURRENT PERSPECTIVE OF NANO-TECHNOLOGY FOR DRUG DELIVERY" held in College of Pharmaceutical Sciences, Puri, Odisha on 19th February 2016 as a participant / Speaker / Poster Presenter / Member of organizing committee.

Prof. Amiya Ka. Mishra	**Prof. Biswajit Mukherjee**	**Prof.(Dr.) P.N. Murthy**
Organizing Secretary	Secretary	President
National Seminar-2016	IAPST	OPA

PT-001

NANOLIPOSOMES CONTAINING ANTI-HIV DRUG CROSS BLOOD BRAIN BARRIER: AN IN VITRO STUDY

Lopamudra Dutta and Biswajit Mukherjee

Department of Pharmaceutical Technology, Jadavpur University, Kolkata-700032, India

Presenting author email: lopamudra2008@yahoo.com

Effective treatment of acquired immunodeficiency syndrome (AIDS) remains as a tough challenge for the scientists all over the world. The causative organism of this dreadful disease is human immunodeficiency virus (HIV) which is responsible for high mortality in humans. In this disease, HIV easily crosses the blood brain barrier.(BBB) to reach into the brain and creates this disease more painful, vulnerable and critical. BBB is the main barrier of fruitful drug delivery of anti-HIV agent into the brain. Two types of nanoliposomes containing anti-HIV drug were prepared by using lipid layer hydration method. Soya-L-?-lecithin was used in one type of formulation, whereas in other case mango lipid was utilized. These two types of formulations were characterized by field emission scanning electron microscopy (FESEM), particle size, zeta potential, in vitro drug loading, transmission electron microscopy (TEM), in vitro drug release study etc. Both types of nanoliposomes had higher negative zeta potentials suggesting their stability in solution form and had distinct smooth surface also. Cryo-TEM images showed the presence of intact bilayer in these nanoformulations. The developed formulations had 35-40% drug loading efficiency with sustained drug release profile. Further in vitro studies will be carried out in future. The in vivo studies will be performed in suitable animal model depending upon the results of in vitro study. At last, the correlation between the results of in vitro and in vivo study will be scrutinized to prove the efficiency of the formulated nanoliposomes for treating AIDS in human.

PT-002

LIGAND CONJUGATED ANTICANCER DRUG LOADED POLYMERIC NANOPARTICLES FOR TARGETED CANCER THERAPY

Vimal Prakash Mishra, Biswajit Mukherjee*, Samrat Chakraborty, B.S. Satapathy, Laboni Mondal

Department of Pharmaceutical Technology, Jadavpur

E-mail: vimalju6@gmail.com

Targeted drug delivery is a kind of advanced drug delivery system in which the drug is delivered to a particular body part (organs / tissues / cells), in a sequential and controlled manner. Drug loaded polymeric nanoparticles (NPs)-aptamer conjugates represent a promising technology in the field of targeted chemotherapy. It facilitates controlled release of chemotherapeutics to the desired sites, avoiding concomitant toxicity to the neighboring tissues. By properly integrating the benefits of NPs with the unique cell-targeting capabilities of aptamers, aptamer-functionalized NPs may provide a better option of designing solutions for critical diseases like cancer. The objective of this research work was the development and in vitro investigation of aptamer modified anticancer drug loaded PLGA nanoparticles for breast cancer therapy. Multiple emulsion-solvent evaporation method was used to prepare the NPs using PLGA 50:50 with carboxylic acid termination. To assure the mutual compatibility between the drug and excipients, FTIR study was performed as a preformulation study. The prepared formulations were characterized by scanning electron microscopy (SEM), particle size analysis, zeta potential, in vitro drug loading, in vitro drug release study etc. The optimized formulations were within nano size range, spherical shape, and smooth surface with a narrow size distribution pattern. The drug loading was found to be around 8% with a sustained drug release profile over an extended period of time. The ligand conjugated formulation showed higher cytotoxicity in tested breast cancer cells than unconjugated formulation and free drug.

JU IAPST National Seminar on

Drug and Diseases: Role of Pharmacists and Doctors

16th January, 2016

Certificate

This Certificate is awarded to Ms./ Mr./ Dr./ Prof. Lopamudra Dutta

for participation as Delegate /~~Resource Person~~ /~~Chairing a Session~~ /Presenting a Paper (Research/~~Review~~).

16/01/2016

Prof. Biswajit Mukherjee
Organizing Secretary

16.01.2016

Mr. Anup Pal
Hon. Secretary, IAPST

16/1/16

Dr. Ketousetuo Kuotsu
Chairperson, Scientific Committee

16/1/2016

Dr. Saikat Dewanjee
Chairperson, Scientific Committee

16/01/2016

Prof. Banasri Hazra
Chairperson, Scientific Committee

Jointly Organized by:

The Centre for Advance Research in Pharmaceutical Sciences, Department of Pharmaceutical Technology, Jadavpur University, Kolkata

Indian Association of Pharmaceutical Scientists and Technologists, Kolkata

IAPST/ABS/P-77

Nanoliposome containing zidovudine crosses BBB for HIV treatment

Lopamudra Dutta, Biswajit Mukherjee*
Department of Pharmaceutical Technology, Jadavpur University, Kolkata-700032, India
*E-mail: biswajit55@yahoo.com

The human immunodeficiency virus (HIV) is the causative organism of the dreadful disease called acquired immunodeficiency syndrome (AIDS) in human. In this disease suffering condition, HIV easily reaches into the brain to create infection and makes this disease more critical, vulnerable and painful. Though pervasiveness of AIDS is raised in worldwide but fruitful drug delivery of anti-HIV agent into the brain is difficult to treat this disease due to blood brain barrier (BBB). This BBB allows selective entry of molecules and maintains homeostasis of brain. By using lipid layer hydration method anti-HIV drug loaded two types of nanoliposomes were formulated. In one case, soya-L-α-lecithin was used, whereas mango lipid was utilized in other case. Both formulations were characterized by particle size, field emission scanning electron microscopy (FESEM), zeta potential, *in vitro* drug loading, transmission electron microscopy (TEM), *in vitro* drug release study etc. Both types of nano size formulations had distinct smooth surface with stable negative zeta potential. Cryo TEM study proved the good formulation of nanoliposomes with intact bilayer. In future, further *in vitro* studies will be carried out and depending upon the *in vitro* study results, relevant *in vivo* study will be conducted in suitable animal model. Finally, the co-relation between the results of *in vitro* and *in vivo* study will be investigated to establish the efficacy of the developed nanoliposomes for HIV infection.

IAPST/ABS/P-78

Development of PLGA Based Nanoparticles Loaded with a Chemoprotective Plant Flavonoid Apigenin and their Various Characterization Studies Intended to Treat Hepatocellular Carcinoma in Future

Sanchari Bhattacharya, Biswajit Mukherjee*
Department of Pharmaceutical Technology, Jadavpur University, Kolkata-700032
*E-mail: biswajit55@yahoo.com

Polymeric nanoparticle based drug delivery technology has been extensively studied to combat various kinds of diseases especially which are to be addressed in molecular level. Targeted drug delivery can be achieved easily using this technology. In our study, we are preparing biodegradable poly (lactic-co-glycolic acid) (PLGA) nanoparticles of apigenin and they will be studied against hepatocellular carcinoma. Nanoparticles were prepared using multiple emulsion and solvent evaporation method. Characterization studies such as drug excipients interactions, particle surface morphology, particle size, zeta potential and polydispersity index, drug loading, drug release study of selected nanoparticles *etc*. have been done. The SEM/FESEM data revealed that particles were in nano-range, round in shape with smooth surface. There were no chemical interactions between the drug and the excipients as confirmed by FTIR data. Drug release study shows that a controlled release pattern was maintained over a period of time and further *in-vitro* and *in-vivo* experiments will be performed to achieve the goal of this study.

Manipal College of Pharmaceutical Sciences

Manipal University, Manipal 576 104.

प्रज्ञानं ब्रह्म
Manipal
INSPIRED BY LIFE

Certificate

This is to certify that

Mr/Ms Lopamudra Dutta

has participated / presented poster in the National Seminar on

"Novel Pharmaceutical Technologies: Challenges and Opportunities" held on 15 November 2015

in Manipal College of Pharmaceutical Sciences, Manipal University, Manipal.

Dr N Udupa
Convener

Dr C Mallikarjuna Rao
Organizing Secretary

Dr M Sreenivasa Reddy
Coordinator

Fourth International Conference on Nanomedicine and Tissue Engineering

ICNT 2016

12-14 August 2016

Organized By:

International and Interuniversity Centre for Nanoscience and Nanotechnology (IIUCNN)
Mahatma Gandhi University, Kottayam, Kerala, India
&
Wuhan University,
Wuchang Dist., Hubei, China 430072.
&
Nicholas Copernicus University
ul. Wile ska 4, 87-100 Torun, Poland

Certificate

This is to certify that Prof./Dr./Ms./Mrs./Mr. Lopamudra Dutta
Jadavpur University, Kolkata
has won ~~First~~/ Second/ ~~Third~~ prize in Poster presentation for the poster entitled
"Phosphoethanolamine Conjugated Nanosize Lipid Vesicles Containing Tamoxifen Citrate for Treating Breast Cancer" *at the* ***Fourth International Conference on Nanomedicine and Tissue Engineering (ICNT - 2016)*** *held at Mahatma Gandhi University, Kottayam, Kerala, India from 12-14 August 2016.*

M.G. UNIVERSITY KOTTAYAM

Prof. (Dr.) Sabu Thomas
Chairman

DIRECTOR
International & Inter University Centre
for Nanoscience & Nano Technology

Chapter 12

Paper Publications

DRUG DELIVERY, 2018
VOL. 25, NO. 1, 504–516
https://doi.org/10.1080/10717544.2018.1435749

Taylor & Francis
Taylor & Francis Group

RESEARCH ARTICLE

OPEN ACCESS Check for updates

Lipid-based nanocarrier efficiently delivers highly water soluble drug across the blood–brain barrier into brain

Lopamudra Dutta[a], Biswajit Mukherjee[a], Tapash Chakraborty[b], Malay Kumar Das[b], Laboni Mondal[a], Sanchari Bhattacharya[a], Raghuvir H. Gaonkar[c] and Mita Chatterjee Debnath[c]

[a]Department of Pharmaceutical Technology, Jadavpur University, Kolkata, India; [b]Department of Pharmaceutical Sciences, Dibrugarh University, Dibrugarh, India; [c]Infectious Diseases and Immunology Division, CSIR-Indian Institute of Chemical Biology, Kolkata, India

ABSTRACT

Delivering highly water soluble drugs across blood–brain barrier (BBB) is a crucial challenge for the formulation scientists. A successful therapeutic intervention by developing a suitable drug delivery system may revolutionize treatment across BBB. Efforts were given here to unravel the capability of a newly developed fatty acid combination (stearic acid:oleic acid:palmitic acid = 8.08:4.13:1) (ML) as fundamental component of nanocarrier to deliver highly water soluble zidovudine (AZT) as a model drug into brain across BBB. A comparison was made with an experimentally developed standard phospholipid-based nanocarrier containing AZT. Both the formulations had nanosize spherical unilamellar vesicular structure with highly negative zeta potential along with sustained drug release profiles. Gamma scintigraphic images showed both the radiolabeled formulations successfully crossed BBB, but longer retention in brain was observed for ML-based formulation (MGF) as compared to soya lecithin (SL)-based drug carrier (SYF). Plasma and brain pharmacokinetic data showed less clearance, prolonged residence time, more bioavailability and sustained release of AZT from MGF in rats compared to those data of the rats treated with SYF/AZT suspension. Thus, ML may be utilized to successfully develop drug nanocarrier to deliver drug into brain across BBB, in a sustained manner for a prolong period of time and may provide an effective therapeutic strategy for many diseases of brain. Further, many anti-HIV drugs cannot cross BBB sufficiently. Hence, the developed formulation may be a suitable option to carry those drugs into brain for better therapeutic management of HIV.

ARTICLE HISTORY
Received 7 December 2017
Revised 23 January 2018
Accepted 29 January 2018

KEYWORDS
Nanosize lipid carrier; blood–brain barrier; gamma scintigraphy; pharmacokinetics; biodistribution

Introduction

Blood–brain barrier (BBB), a complex tight endothelial vascular lining, is the main hindrance of most chemicals for free diffusion and penetration into the brain from blood stream of body for maintaining homeostasis in brain (Seju et al., 2011; Martins et al., 2012). BBB acts as a safeguard of brain from exogenous toxic agents as well as rejecter of essential therapeutic agents (Hu et al., 2009). Nearly 100% of large molecular drugs and about 98% of drugs consisting of small molecules are unable to cross BBB to provide therapeutic outcome (Wilson et al., 2008; Hu et al., 2017). Various novel drug delivery systems such as nanoparticles, nanoliposomes (NLs), micelles, dendrimers, quantum dots, and nanoemulsions are applied to overcome the limitations (Li et al., 2017). Nowadays, nanosize drug delivery into brain across BBB is an emerging field of pharmaceutical research. In the current study, we have selected lipid-based nanoliposomal drug carrier to deliver drug into brain. NLs can deliver hydrophobic as well as hydrophilic drug efficiently due to their special structure. Due to some important properties such as biodegradability, biocompatibility, low toxicity, ability of enhancement of therapeutic index and efficacy of drug, enhancement of stability of drug through encapsulation, and non-immunogenicity, the liposomal drug delivery is a choice as a drug carrier (Akbarzadeh et al., 2013).

It is always an enormous challenge for formulation scientists to deliver highly water soluble drug into brain across BBB and the same is true for many other large molecules. In the present study, we have selected a highly water soluble drug zidovudine (AZT), 1-[(2R,4S,5S)-4-azido-5-(hydroxymethyl)oxolan-2-yl]-5-methylpyrimidine-2,4-dione (Figure 1(A)), as a model water-soluble drug to deliver across BBB into brain. AZT is a highly water soluble drug (25 mg/ml at 25 °C). Therefore, it has been used as a representative water soluble active pharmaceutical ingredient or drug in a number of reports (Jain et al., 2008; Nayak et al., 2009; Singh et al., 2010; Christoper et al., 2014). It is expected that the physical characteristics provided by AZT would be similar for many other hydrophilic drugs. Hence, we have considered AZT as a water soluble model drug in the present study. AZT, nucleoside reverse transcriptase inhibitor, is also a part of combination therapy 'highly active antiretroviral treatment (HAART)' for anti-HIV treatment (Bergshoeff et al., 2004; Mu et al., 2016).

CONTACT Biswajit Mukherjee biswajit.mukherjee@jadavpuruniversity.in, biswajit55@yahoo.com Department of Pharmaceutical Technology, Jadavpur University, Kolkata 700032, West Bengal, India

Supplemental data for this article can be accessed here.

AZT due to its strong hydrophilicity is unable to cross BBB sufficiently to reach brain, resulting in inadequate concentration of AZT for therapeutic efficacy (Rautio et al., 2008; Weiss et al., 2009). Thus, delivering AZT in brain could be utilized for better management of HIV as in HIV infected patients, at very early stage (up to 10 days of post HIV infection), neuroinvasion can arise and HIV infected circulated monocytes in blood stream can easily enter into brain (Ivey et al., 2009).

Here, by trial and error method we developed several lipids using various mixtures of three fatty acids present in many edible lipids (Kittiphoom, 2012). Out of them we have selected the best combination [stearic acid (SA):oleic acid (OA):palmitic acid (PA) = 8.08:4.13:1] (ML) on the basis of its consistency to develop the nanocarrier. We also compared the efficacy of this formulation with soya lecithin (SL)-based formulation developed by us.

The prime objective of this investigation was to evaluate the capability of ML as base component for the development of nanocarrier to deliver highly water soluble drug into brain across BBB. Further, its efficiency was evaluated by comparing with SL-based drug nanocarrier.

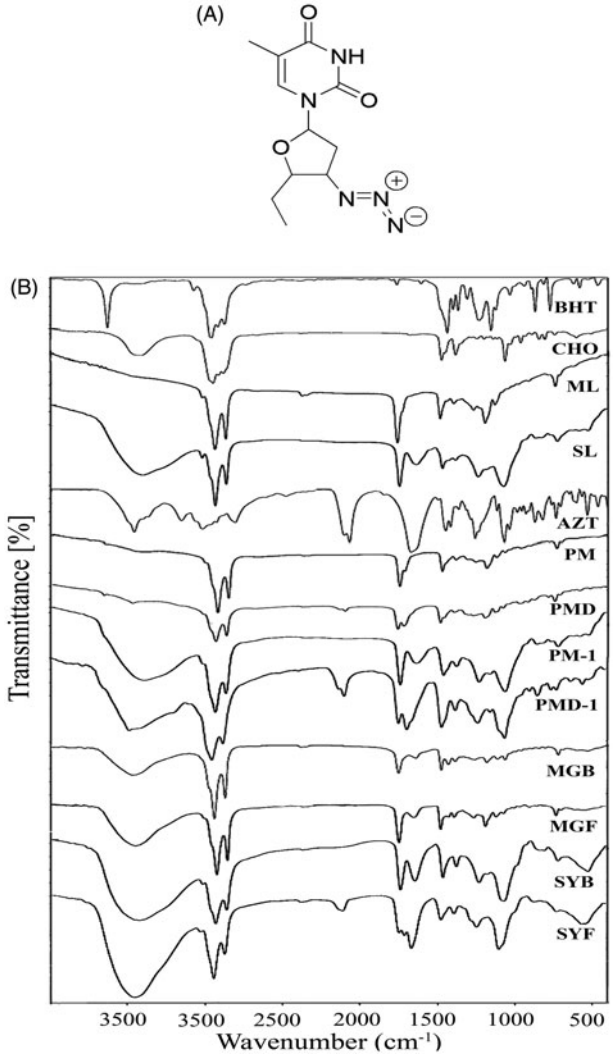

Figure 1. (A) Chemical structure of zidovudine (AZT). (B) Fourier transform infrared spectroscopy (FTIR)-spectra of BHT (butylated hydroxytoluene), CHO (cholesterol), ML (lipid), SL (soya lecithin), AZT (zidovudine), PM (physical mixture of BHT, CHO, ML), PMD (physical mixture of BHT, CHO, ML, and drug), PM-1 (physical mixture of BHT, CHO, SL), PMD-1 (physical mixture of BHT, CHO, SL, and drug), MGB (ML-based lyophilized formulation without drug), MGF (ML-based lyophilized formulation with drug), SYB (SL-based lyophilized formulation without drug), and SYF (SL-based lyophilized formulation with drug).

Materials and methods

AZT was obtained as a gift sample from Cipla Ltd. (Goa, India). Cholesterol (CHO), fluorescein isothiocyanate (Isomer I) (FITC), SL, fetal bovine serum (FBS) and minimum essential medium Eagle (MEM) were procured from HiMedia Laboratories Pvt. Ltd. (Mumbai, India). SA, OA, and PA were purchased from Sigma-Aldrich (Bangalore, India) and butylated hydroxytoluene (BHT) was obtained from Qualigens Fine Chemicals (Mumbai, India). U-87 MG cells were procured from National Center for Cell Science (Pune, India). All other chemicals used were of analytical grade.

Animals

Sprague-Dawley rats (male:female ratio 2:1) having body weight 200–250 g were utilized for biodistribution investigation, plasma and brain pharmacokinetic study and only male Sprague-Dawley rats of body weight 200–250 g were used for gamma scintigraphy study. Animal experiments were carried out upon receiving approval of the Animal Ethics Committee, Jadavpur University, Kolkata. Animals were accommodated in the university animal house after keeping them in polypropylene cages. The temperature (22 ± 1 °C) and humidity (55 ± 5%) were maintained in the animal house with 12 h light/dark circle. The animals had free access of standard diet (Dey et al., 2016) and drinking water.

Fourier-transform infrared spectroscopy (FTIR)

FTIR was conducted to determine possible interaction (if any) between the drug and the excipients. For ML-based formulation, pure drug (AZT), CHO, ML, BHT, physical mixture (PM) of CHO, ML, BHT, physical mixture (PMD) of CHO, ML, BHT and drug AZT, lyophilized formulation without drug (MGB) and lyophilized formulation with drug (MGF) and for SL-based formulation, AZT, CHO, SL, BHT, physical mixture (PM-1) of CHO, SL, BHT, physical mixture (PMD-1) of CHO, SL, BHT and AZT, lyophilized formulation without drug (SYB) and lyophilized formulation with drug (SYF) were scanned at 4000–400 cm^{-1} using FTIR instrument (JASCO International Co. Ltd., FTIR 4200, Tokyo, Japan) using their pellets formed by mixing with potassium bromide (KBr) at 1:100 ratio and compressing with a hydraulic press (Sahana et al., 2010).

Preparation of NLs

Fatty acids at the selected ratio were dissolved in small quantity of chloroform and chloroform was evaporated under vacuum to get the lipid formed from the fatty acids.

NLs were prepared by lipid layer hydration technique by varying different process parameters (Rudra et al., 2010). Specific weighed amounts of excipients CHO, lipids (ML for MGF/SL for SYF, respectively) (Supplementary Table 1) and

BHT (1% w/v as antioxidant) were taken in 250 ml round bottom flask and adequate quantity of chloroform was added within the flask with vigorous shaking to dissolve the excipients. The flask was set up in a rotary vacuum evaporator (Rotavap, model PBU-6, Superfit Continental Pvt. Ltd., Mumbai, India) fitted with an A3S aspirator (Eyela, Rikakikaic, Ltd., Taguig City, Philippines) and a circulating water bath (Spac N service, Kolkata, India) at 5 °C and was rotated at 145 rpm rotation speed at 40 °C in water bath to evaporate the organic solvent and to form thin film of lipid layer on the inside-wall of the flask. For complete elimination of the residual chloroform, the flask was kept overnight in a vacuum desiccator. The weighed amount of AZT was dissolved in phosphate buffer (pH 7.4), and the mixture was taken in the flask. The flask was then fitted in a rotary vacuum evaporator with rotation speed at 145 rpm and at 40 °C in a water-bath for complete dispersion of thin lipid film in the aqueous phase. The dispersion was sonicated at 30 ± 3 kHz in a bath type sonicator (Trans-o-Sonic, Mumbai, India) for 1 h with cold water. To form vesicles, the round bottom flask was kept at room temperature for 1.5 h and stored overnight at 4 °C. The preparation was centrifuged at 5000 rpm for 15 min at 4 °C to separate the larger vesicles and the obtained supernatant was again centrifuged (at 16,000 rpm for 45 min in a cold centrifuge at 4 °C) (3K30 Sigma Lab Centrifuge, Merrington Hall Farm, Shrewsbury, UK) to precipitate NLs. The obtained precipitate was re-suspended in fresh phosphate buffer (pH 7.4) and precipitated again number of times to wash the NLs. NLs were collected in a petridish and lyophilized for 12 h (Laboratory Freeze Dryer, Instrumentation India Ltd., Kolkata, India) to get dry product. Blank NLs (MGB, SYB) were prepared by the same procedure without using AZT. Fluorescent NLs were prepared using the same process as described above except the step where fluorescent marker FITC was used. FITC stock solution (0.4% w/v) was prepared in a mixture of chloroform and ethanol at volume 3:1 ratio and a volume of 100 µl was mixed into the organic phase (chloroform) during the initial mixing of preparation (Shaw et al., 2017).

Characterization of NL

Evaluation of drug loading

MGF/SYF (5 mg) was taken in a mixture of phosphate buffer (pH 7.4) and ethanol at a ratio of 5:1 and sonicated and vortex-mixed. After centrifugation (at 16,000 rpm for 15 min at 4 °C), the supernatant was collected and measured at 265 nm using UV/VIS spectrophotometer (Model Intech-295, Gentaur GmbH, Aachen, Germany). The same procedure was performed for MGB/SYB. Absorbance for drug was obtained by deducting the absorbance obtained from NLs without drug and from that of NLs with drug (Satapathy et al., 2016). Each study was conducted thrice. The percentage of drug loading was calculated using the following formula:

$$\text{Percentage of drug loading} = (\text{Amount of AZT in NLs}/\text{Amount of NLs taken}) * 100 \quad (1)$$

Percentage of yield determination

To determine the yield of NLs from the utilized total amount of raw materials of NLs preparation, lyophilized dried NLs of each batch were weighed and the percentage of yield was calculated by using the following equation as mentioned earlier (Sahana et al., 2010).

$$\text{Percentage of yield} = (\text{Amount of NLs obtained}/\text{Total amount of drug and excipients used}) * 100 \quad (2)$$

Evaluation of size distribution and zeta potential

By utilizing the dynamic light scattering (DLS) technology in a Zetasizer Nano ZS90 (Malvern Instrument, Malvern, UK), average size of NLs, size distribution pattern, polydispersity index (PDI) and zeta potential of the experimental formulations were determined.

Field emission scanning electron microscopy (FESEM) for surface morphology analysis

FESEM was used to investigate the surface morphology of NLs. The lyophilized NLs were placed on an adhesive tape of carbon over a stub by spreading smoothly and then dried through vacuum and coated with platinum using a platinum coater instrument (JEOL, Tokyo, Japan). After that the samples were observed at various magnifications with the help of FESEM (Model-JSM-6700F; JEOL, Tokyo, Japan) (Dey et al., 2016).

Cryo-transmission electron microscopy (Cryo-TEM) study

Cryo-TEM study was performed to observe morphology and lamellarity of NLs. About 1.5 mg lyophilized formulation was taken in a microcentrifuge tube and 1 ml of Milli-Q water was added into it. The suspension was vortexed followed by sonication for a few minutes to prevent agglomeration. The NLs suspension (4 µl) was put on a clean grid, blotted away the excess (if any) with the help of filter paper and vitrified instantly by dipping into liquid ethane. The grid was stored in liquid nitrogen till shifting under the electron microscope (Tecnai Polora, version 4.6 FEI Tecnai G2, Eindhoven, Netherlands) which was operated at 300 kV equipped with an FEI Eagle 4 K × 4 K charge-coupled device (CCD) camera for capturing the images (Fox et al., 2014).

In vitro *investigations*

In vitro *drug release study*

In vitro drug release study was conducted in freshly prepared phosphate buffer (pH 7.4) and in 50% serum [serum:phosphate buffer (pH 7.4) = 1:1] individually as drug release media at room temperature (for phosphate buffer as media) and at 37 °C (for 50% serum as media) (in physiological mimicking condition), for 24 h. Drug release media (50 ml) were taken in a glass beaker (100 ml). Lyophilized formulation (5 mg) was weighed accurately and reconstituted in 1 ml of the

respective drug release media and was placed into a dialysis bag (Himedia Dialysis Membrane – 110, Mumbai, India) (Dey et al., 2016). The dialysis bag was tightly knotted at the two ends with cotton thread and hanged centrally into the beaker containing drug release medium (in such a way so that the formulation portion inside the bag immersed within the media) using a laboratory ring stand with clamp kit. The beaker was put on a magnetic stirrer maintaining stirring at 300 rpm using a magnetic bead. From the beaker, 1 ml media was withdrawn at various predetermined time intervals and same volume of fresh media was replaced immediately into the beaker. All the collected samples were analyzed using UV-VIS spectrophotometer at 265 nm with phosphate buffer or 50% serum as blank according to requirement. In case of serum sample, protein was precipitated as mentioned under LC-MS/MS study. The drug concentration at any individual time point was calculated with the help of calibration curve. For 50% serum as drug release media, total experiment was conducted maintaining aseptic condition in all respect under laminar air flow hood.

In vitro *drug release kinetic study*

In vitro drug release data were applied in various kinetic models such as zero order (percentage cumulative drug release versus time), first order (log of percentage cumulative amount of drug remained to release versus time), Higuchi model (percentage cumulative drug release versus square root of time), Hixson–Crowell's model (cube root of percentage cumulative amount of drug remained to release versus time), Korsmeyer–Peppas's model (log of percentage cumulative drug release versus log of time) to predict the drug release pattern of the optimized formulations. The highest correlation coefficient value (R^2) from all the tested models was utilized to select the suitable kinetic pattern (Das et al., 2015).

In vitro *cellular uptake study*

To investigate the cellular uptake ability of NLs by U-87 MG cells, confocal laser scanning microscopy study was executed. In six well culture plates, U-87 MG cells were seeded on coverslips (3×10^4) and cultivated using MEM containing 10% FBS for 24 h. These cells were treated with FITC-MGF/FITC-SYF suspension at a concentration of 100 μg/ml. At different time points (i.e. 0.25 h, 1 h, 3 h) of incubation, the cells were washed thrice and fixed applying paraformaldehyde aqueous solution (4%). They were cleaned by using freshly prepared phosphate buffer (pH 7.4) after 5 min of fixation. Then, coverslips were collected cautiously and mounted on the glass slide. After complete air drying, the slides were placed individually under a confocal laser scanning microscope (Model: IX81, Olympus Singapore Pte Ltd., Singapore) and the images were snapped (Maji et al., 2014).

Stability study

Stability testing of the lyophilized formulations was performed as per ICH guidelines (Sahana et al., 2010).

In vivo *investigations*

Radiolabeling of AZT and AZT loaded NLs

According to the tin (II) chloride reduction method as described earlier (Das et al., 2015; Satapathy et al., 2016), radiolabeling of AZT and AZT loaded MGF/SYF was performed with technetium-99m (^{99m}Tc). At first, 5 mg of AZT was dissolved in 0.5 ml ethanol and AZT loaded NLs (equivalent to 5 mg of AZT) were suspended in 0.5 ml of nitrogen purged water. The aqueous ^{99m}Tc-pertechnetate ($^{99m}TcO4^-$) (40–100 MBq) was incorporated to them followed by addition of 25 μl of aqueous stannous chloride dihydrate ($SnCl_2{\cdot}2H_2O$) (2 mg/ml) solution. At room temperature, they were incubated for 15 min. The radiolabeled efficiencies were then assessed with the help of ascending thin layer chromatography by applying silica gel coated aluminum strips (Merck, Darmstadt, Germany) as stationary phase and methyl ethyl ketone as mobile phase. The sheets were dried after developing the spots and they were cut into five strips (1 cm each). These were analyzed quantitatively through counting using a well type gamma counter at 140 keV (Electronic Corporation of India, model LV4755, Hyderabad, India).

Gamma scintigraphy

For providing direct evidence of location of radiolabeled NLs as well as free drug within the body of experimental rats, gamma scintigraphy imaging was performed. Only male Sprague-Dawley rats (body weight 200–250 g) were utilized in this study. After dividing the total rats into three groups, ^{99m}Tc labeled AZT/^{99m}Tc labeled MGF/^{99m}Tc labeled SYF was injected (100 μl) through femoral vein of rats of the respective group. Using the intramuscular injection of ketamine hydrochloride (1 ml), rats were anesthetized and fixed on a board in the posterior position for imaging. At predetermined time interval (1 h and 5 h of post injection), static images were snapped with the help of planar gamma camera (GE Infinia Gamma Camera equipped with Xeleris Workstation, GE, Cleveland, OH).

Biodistribution study

Sprague-Dawley rats (body weight 200–250 g) were utilized for performing the biodistribution of radiolabeled AZT and NLs (MGF, SYF). By applying ketamine (30–50 mg/kg) intramuscularly, rats were anesthetized and cannulation was done in the femoral vein of animals using polyethylene (PE-50) catheter tubes. All the experimental animals were well-hydrated by administering (2 ml) normal saline (0.9% NaCl (w/v) in water) through intraperitoneal route for 1 h. ^{99m}Tc labeled AZT/^{99m}Tc labeled MGF/^{99m}Tc labeled SYF was injected at 0.03 ml volume (10–15 MBq/kg) via intravenous (i.v.) route through the cannula. The animals were sacrificed at 1 h and 5 h post injection. The organs and tissues such as heart, liver, lung, spleen, muscle, intestine, stomach, kidney, and brain were removed followed by washing using normal saline. The collected organs and tissues were dried up immediately using blotting paper (if applicable) and taken into the preweighed counting vials. Blood was collected using heart

puncture process. With the help of a well-type gamma scintillation counter along with an injection standard, the corresponding radioactivity of the samples was measured and percentage of injected dose per gram (% ID per g) of tissue or organ was utilized for expressing the results.

In vivo *plasma and brain pharmacokinetic study*

In vivo plasma and brain pharmacokinetic study was performed to compare the distribution of AZT from free drug suspension and NLs (MGF, SYF) and observe the ability of NLs to cross BBB in Sprague-Dawley rats. The animals were distributed into four groups. AZT suspension was injected in animals of one group through i.v. route as per dose. Another group of animals was injected MGF and the third group was treated with SYF intravenously with an equivalent amount of AZT with respect to free drug in suspension. Tail vein was selected to administer the injection for all animals of each batch. The fourth group remained as control (untreated). For plasma pharmacokinetic study, blood samples were collected by terminal cardiac puncture of each animal following anesthesia, at a predetermined time interval such as 0.25 h, 0.5 h, 1 h, 2 h, 4 h, 6 h, 8 h, 10 h, 12 h, 24 h, and 48 h of post i.v. injection and kept the sample immediately into a microcentrifuge tube having EDTA solution. For plasma collection, the blood samples were centrifuged at 5000 rpm for 6 min using cold centrifuge (HERMLE Labortechnik GmbH, Wehingen, Germany) and the plasma was preserved at −80 °C till further analysis (Dey et al., 2016).

For brain kinetic study, at a predetermined time interval (0.5 h, 1 h, 2 h, 4 h, 6 h, 8 h, 10 h, 12 h, and 24 h of post i.v. injection), rats were dissected and brains were separated followed by washing with Milli-Q water. *In situ* blood perfusion (Takasato et al., 1984) was done before collection of brain in the experiment. Then, the collected brains were kept into cryogenic tubes and stored at −80 °C till LC–MS/MS study.

LC–MS/MS study

Evaluation of AZT concentration in plasma and brain was performed by using LC–MS/MS technique (Shaw et al., 2017). Briefly, plasma sample/homogenized brain tissue was first mixed with ice cold acetonitrile (plasma/tissue homogenate:-cold acetonitrile was 1:3 by volume) containing internal standard followed by vortex-mixed for 10 min and centrifuged (at 4000 rpm for 15 min at 4 °C) for efficient extraction of AZT by protein precipitation method (Gautam et al., 2013). The supernatant for each sample was collected. The supernatant (100 µl) of each sample was mixed with 100 µl water and loaded into LC–MS/MS (LC: Shimadzu Model 20AC, MS: AB-SCIEX, Model: API4000, Software: Analyst 1.6). Elution was done with the help of YMC Triat C18 column (2.1 × 30 mm, 5 µ). Gradient elution technique of two mobile phases (mobile phase A: 0.1% formic acid in water and mobile phase B: 0.1% formic acid in 80:20 acetonitrile/water) was conducted with injection volume: 20 µl, flow rate 0.8 ml/min and total run time was 3.0 min in each case.

Calculation of PK parameter

AZT concentrations in plasma and brain were plotted against time. By utilizing NCA toolbox of Phoenix-Winnonlin software (Certara, Daresbury, UK), various PK parameters such as area under the concentration–time curve from time of injection to a determined time point (AUC_{0-t}), area under the first moment curve ($AUMC_{0-t}$), clearance (Cl), time taken for maximum blood concentration to drop in half-life ($t_{1/2}$), steady state volume of distribution (V_{ss}), mean residence time (MRT), etc. were determined.

Statistical analysis

Statistical calculations of various data were conducted by applying one-way analysis of variance (ANOVA) through Tukey–Kramer's multiple comparisons test with the help of GraphPad InStat (version 3.06) software (La Jolla, CA). The probability value (p) $<.05$ at 95% confidence interval was recognized as statistically significant.

Results

FTIR analysis

Drug–excipient interaction was investigated through FTIR spectroscopy to determine any interaction between the functional groups of drug (AZT) and the excipients of a formulation (Basu et al., 2012). When the FTIR spectra of the physical mixture of the drug and the excipients (ML, CHO) were compared with those of the physical mixture of the excipients without drug, the lyophilized formulation with or without drug and each of the excipients, the presence of the characteristic peaks of the drug (at 2083 cm^{-1}), ML (at 2922 cm^{-1}, at 2852 cm^{-1}, and at 721 cm^{-1}) and CHO (at 1373 cm^{-1}) was observed (Figure 1(B)).

Likewise, during the comparison of the FTIR spectra of the drug, SL and CHO, the presence of the characteristic peak of the drug was observed at 2083 cm^{-1} in the physical mixture. The characteristic peaks of SL (at 2928 cm^{-1} and at 1462 cm^{-1}) and CHO (at 1373 cm^{-1}) were also observed in the physical mixture of the drug and the excipients (Figure 1(B)).

The findings suggest the absence of any chemical interaction between the drug and the excipients for both the formulations (ML based, MGF and SL based, SYF). However, minor shifting of some of the peaks of the excipients in formulations (from 2922 cm^{-1} to 2920 cm^{-1}, 2852 cm^{-1} to 2851 cm^{-1}, and from 721 cm^{-1} to 719 cm^{-1} in ML-based formulation and CHO from 3415 cm^{-1} to 3436 cm^{-1} in case of SL-based formulation) was observed. The observations suggest that physical interactions existed between the molecules of the excipients. The interaction might be responsible to provide the structure of the formulation and for sustained drug release from the formulations. In case of the ML formulation, the peak of the drug was not observed. The finding suggests that the drug was encapsulated entirely in the formulation and there was the absence of drug molecules on the surface of the formulation. For SL formulation, presence of the peak of the drug was found to shift from 2084 cm^{-1}

to 2096 cm^{-1}. The finding indicates that the shifting of the peak of the drug might be due to physical interaction between the drug and the excipients. Further, the drug molecules were also present in the lipid bilayers and might retain in the formulation due to the physical interaction between the drug and the excipients.

In case of SL formulation, a shifting of wave number from 2084 cm^{-1} to 2096 cm^{-1} might be due to the formation of weak bond (such as hydrogen bond, van der Waals force of attraction or dipole moment) between methyl group of the drug and OH group of CHO. The wave number ranging from 3415 cm^{-1} to 3436 cm^{-1} is the strong intensity stretching vibration zone of OH group. The wave number ranging from 2084 cm^{-1} to 2096 cm^{-1} is the stretching vibration zone of C–C=C of the drug. Further, the wave number regions, 2922–2920 cm^{-1} and 2852–2851 cm^{-1}, are the strong intensity stretching vibration regions of CH_2, CH, and CH_3 and the region 721–719 cm^{-1} is the variable to weak intensity bending vibration region of out of plane OH bending. Hence, there might be physical interaction by formation of weak bonds (hydrogen bond, van der Waals force of attraction or dipole moment) responsible for minor shifting of peaks.

Physico-chemical characterization of NLs

We initially varied the different process parameters such as temperature and speed of hydration, duration of sonication, time and speed of centrifugation, duration of freeze drying and ratio of the constituents to optimize the preparation process and to select the formulations. The best two formulations (MGF, SYF) were selected based on drug loading, particle size, zeta potential, FESEM, and Cryo-TEM data and investigated for further study.

Percentage of drug loading and yield

The percentage of drug loading of MGF was 5.7 ± 0.37% with 60.87 ± 5.92% yield capacity but SYF had 7.00 ± 0.23% drug loading with yield capacity of 54.34 ± 4.79% (Supplementary Table 1). Every experiment was repeated thrice to establish the reproducibility.

Size, size distribution, and zeta potential

Liposomal size, surface morphology, and the lamellarity of liposome have been assessed by particle size analyzer, FESEM, and Cryo-TEM, respectively. FESEM figures showed that the average size of the lyophilized liposome varied for MGF and SYF. When the liposomes were assessed by particle size analyzer, it showed the average size 24.37 ± 2.2 nm for MGF (Figure 2(A)) and 33.75 ± 3.7 nm for SYF (Figure 2(B)), with their PDI 0.26 ± 0.02 and 0.25 ± 0.06, respectively. When the lamellarity was checked by Cryo-TEM, average size of the vesicles was found to be 30.75 ± 1.8 nm for MGF and 40.43 ± 2.4 nm for SYF with the intact lamellarity. The size was little bit higher as compared to the lyophilized liposome and the liposome analyzed by particle size analyzer. Since for Cryo-TEM analysis, the lyophilized liposomes were suspended for longer time as compared to particle size analysis by particle size analyzer, the average size was enhanced marginally due to the entrapment of water in the core area of the liposomal vesicles. However, all the methods of analysis showed that the size was below 50 nm. Zeta potential of both the formulations was observed as negative, –71.5 ± 6.5 mV (Figure 2(C)) and –70.8 ± 7.0 mV (Figure 2(D)) for MGF and SYF, respectively. The statistical analysis of data of average size for both the formulations and the variation in PDI showed that there was an insignificant variation ($p > .05$) in size distribution, but a significant variation of particle size between MGF and SYF. MGF showed smaller size particles compared to SYF. Zeta potential showed nearly same value for both the formulations.

FESEM study

Three images of FESEM at different magnifications namely 60,000×, 120,000×, and 300,000× were captured for MGF to establish the shape, size, and distribution pattern of the formulation. The MGF had nanosize structure with smooth surface and was homogenously distributed at 60,000× and 120,000× magnification (Figure 2(E,F)). At 300,000× magnification, MGF was found to be spherical structure having nanosize with smooth surface and a homogeneous distribution pattern (Figure 2(G)). The FESEM image at 100,000× magnification of SYF revealed that the liposomes were also in nanosize (about 30 nm), spherical shape with smooth surface and homogenous distribution (Figure 2(H)).

Cryo-TEM study

Cryo-TEM study was performed to visualize the internal structure of NLs. Nanosize unilamellar vesicles were found in the Cryo-TEM images for both the types of NLs (Figure 2(I,J)). MGF had smaller size lyophilized vesicles than the size of SYF vesicles.

In vitro *investigations*

In vitro *drug release study*

In vitro drug release study was conducted for both the formulations (MGF and SYF) to compare *in vitro* drug release patterns of both the formulations in two different release media. The data were plotted as percentage of cumulative drug release against time measured in hour (h) (Figure 2(K,L)). From the results, it appeared that cumulative 73.43% and cumulative 82.21% of AZT released from MGF in phosphate buffer media and in 50% serum, respectively, whereas cumulative 82.48% (phosphate buffer as media) and cumulative 84.51% (50% serum as media) of AZT released from SYF over a period of 24 h. Drug release was to an extent slower from MGF than SYF. However, a steady and sustained drug release pattern was observed for both the formulations.

Drug release kinetics analysis

To understand the drug release kinetic patterns, data were plotted using various kinetic equations and the

corresponding correlation coefficients (represented here as R^2 values) were determined (Supplementary Table 2). Data gave good linearity in Korsmeyer–Peppas's kinetic model for both the formulations [$R^2 = 0.9742$ (phosphate buffer as drug release media) and $R^2 = 0.9780$ (50% serum as drug release media) for MGF and $R^2 = 0.9752$ (phosphate buffer as drug release media) and $R^2 = 0.9751$ (50% serum as drug release media) for SYF] as compared to the other kinetic models tested. The release exponent values (n) were 0.8387 and 0.8561 for MGF and SYF in phosphate buffer drug release media where as in 50% serum 'n' values were 0.7539 for MGF and 0.8179 for SYF, respectively. The 'n' values indicated non-Fickian diffusion pattern of release of drug from NLs in both types of drug release media.

In vitro *cellular uptake study*

In vitro cellular uptake study of NLs was conducted in U-87 MG human glioblastoma cells by using fluorescent NLs to inspect the uptake ability of NLs in brain cells using confocal microscopy. From the results, it revealed that both the types of fluorescent NLs (FITC-MGF, FITC-SYF) were internalized by the cells (Figure 3(A,B)) and were localized in cytoplasm as well as nucleus. Cellular uptake of FITC-MGF increased with time till 3 h of the study (Figure 3(A)). However, for FITC-SYF, the cellular uptake was more in 1 h than 0.25 h and then decreased at 3 h (total duration of the study) (Figure 3(B)). By both confocal and conventional fluorescence microscopies, FITC treated cells were shown to internalize FITC in a time-dependent manner (Cole et al., 1990). Thus, addition of FITC in media alone as a control

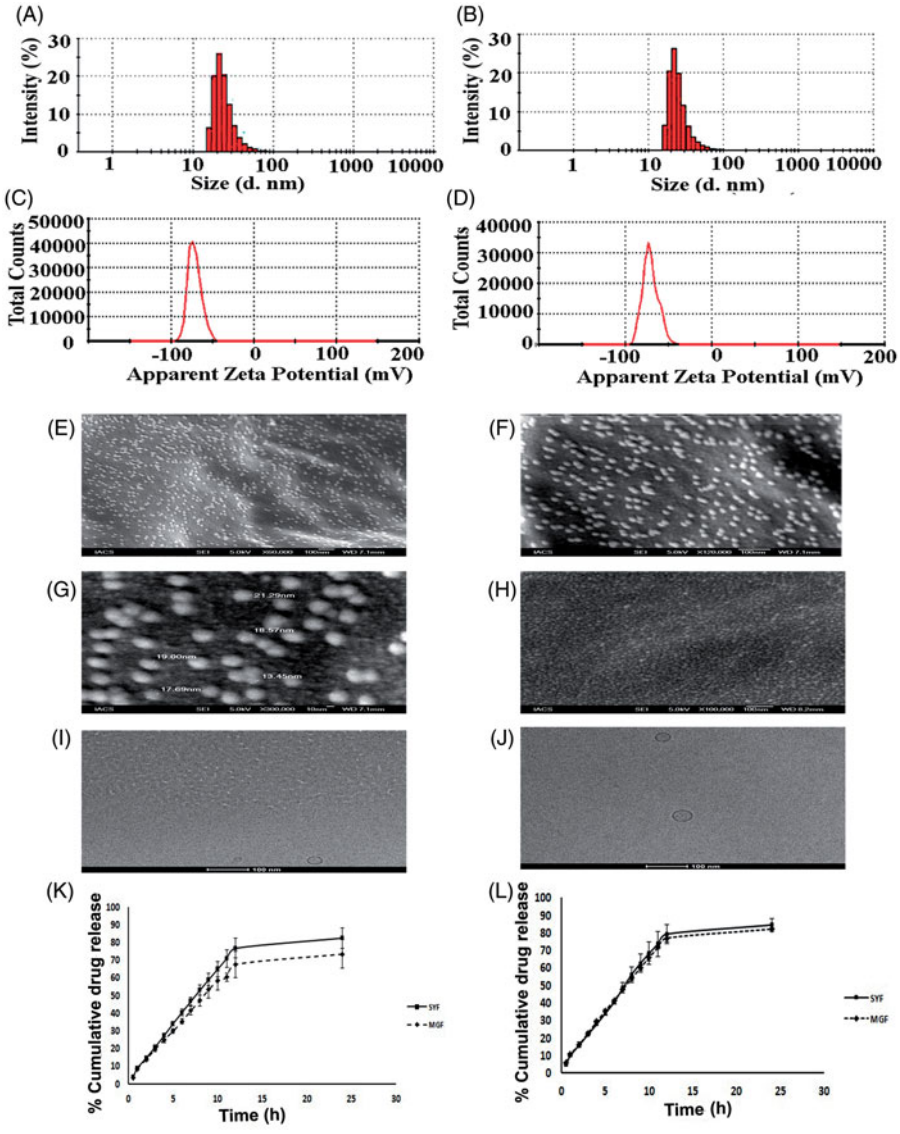

Figure 2. Particle size distribution of (A) MGF and (B) SYF. Zeta potential of (C) MGF and (D) SYF. Field emission scanning electron microscopy (FESEM) images of (E) MGF at magnification of 60,000×, (F) MGF at magnification of 120,000×, (G) MGF at magnification of 300,000×, (H) SYF at magnification of 100,000×. Cryo-transmission electron microscopy (Cryo-TEM) images of (I) MGF and (J) SYF. Scale bar for Cryo-TEM image: 100 nm. (K) *In vitro* drug release profiles of MGF and SYF in phosphate buffer (pH 7.4). (L) *In vitro* drug release profiles of MGF and SYF in 50% serum. Data show mean ± SD ($n = 3$). SD: standard deviation.

sample to treat cells would provide results which can mislead the actual findings of the FITC-labeled formulations. Hence, no FITC control was run.

Stability study

FTIR spectra of the stored NLs (MGF, SYF) were compared with those of the freshly prepared formulations. No distinguish changes in spectrum were observed for the formulations stored at 4 °C. However, NLs stored at 25 °C showed the deformation of structure (data not shown), although drug assay results did not significantly vary the quantity of drug loaded in the formulation. Further, FTIR, DSC (Supplementary Figure 1), UV–visible spectroscopy, LC–MS/MS analysis of free drug, encapsulated drug and drug released showed that drug remained in the active form after encapsulation and released, and in the same active form.

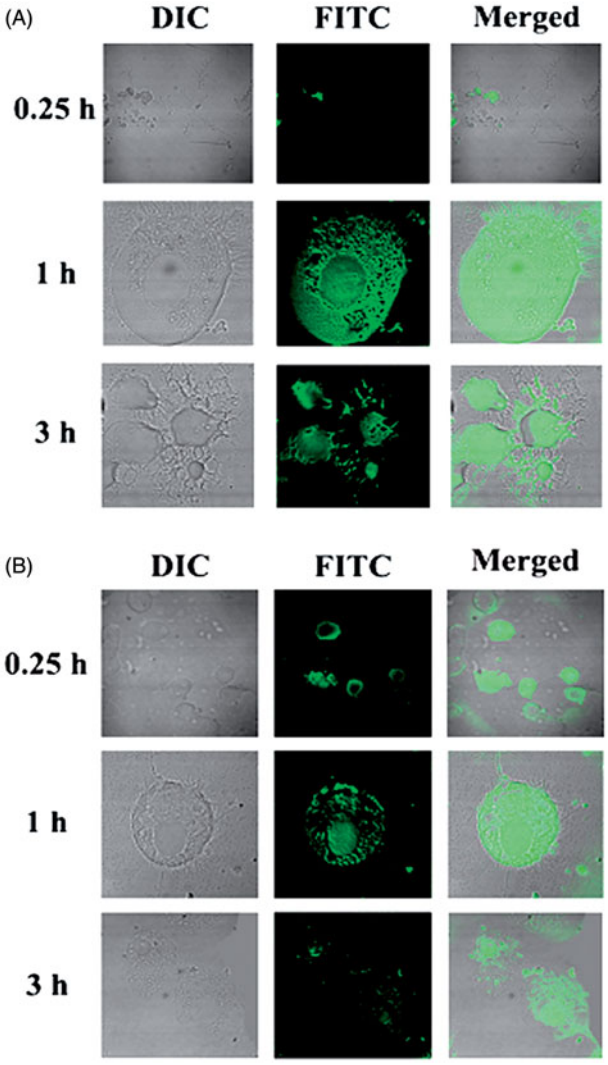

Figure 3. Investigation of *in vitro* cellular uptake of MGF and SYF by confocal microscopy. (A) *In vitro* cellular uptake study of fluorescein isothiocyanate labeled MGF (FITC-MGF) in U-87 MG human glioblastoma cells at various time points (0.25 h, 1 h, 3 h). (B) *In vitro* cellular uptake study of fluorescein isothiocyanate labeled SYF (FITC-SYF) in U-87 MG human glioblastoma cells at various time points (0.25 h, 1 h, 3 h). DIC: differential interference contrast images of U-87 MG human glioblastoma cells.

In vivo *analysis*

Gamma scintigraphy

The gamma scintigraphy was performed to investigate the ability of the NLs to cross BBB after the administration of ^{99m}Tc labeled MGF, ^{99m}Tc labeled SYF and ^{99m}Tc labeled free drug (AZT) in different groups of Sprague-Dawley rats, respectively. The radioactivity signals were observed (Figure 4) and assessed in brain as well as in different organs (Supplementary Table 3) of the experimental animals which received radiolabeled NLs/AZT. The study showed that NLs were able to cross BBB and reached in brain. In animals treated with radiolabeled MGF, the intensity of signals in brain tissue was higher at 1 h as compared to 5 h (Figure 4(I)). The signals were stronger in brain at 1 h than 5 h in the animals received radiolabeled SYF (Figure 4(II)). At 5 h, the signals were stronger in the brain tissue of animals treated with radiolabeled MGF compared to radiolabeled SYF. In ^{99m}Tc labeled free drug (AZT)-treated animals, very weak signal was noticed at 1 h and 5 h in brain tissue (Figure 4(III)) which indicated poor permeation of free AZT through BBB.

Biodistribution study

Biodistribution studies were conducted by administering ^{99m}Tc labeled MGF, ^{99m}Tc labeled SYF, and ^{99m}Tc labeled free drug (AZT) in Sprague-Dawley rats through i.v. route at 1 h and 5 h after injection. In different organs including brain, accumulation of radiolabeled NLs as well as free drug was measured and data were reported as percentage of injected dose per gram (% ID per g) of tissue or organ (Supplementary Table 3). The values of residence time of radiolabeled formulation MGF/SYF in blood were 2.90-fold, 3.09-fold higher at 1 h and 4.08-fold, 3.94-fold greater than that of radiolabeled AZT at 5 h, respectively. On the other hand, kidney accumulation was distinctively more in free drug than NLs at 1 h as well as 5 h. Further, at 1 h, kidney accumulation of radiolabeled SYF was 2.75 time less than MGF but at 5 h this was 31.91% higher as compared to MGF. Enhancement of brain uptake values (by 18 folds and 19 folds, respectively, at 1 h and 36 times and 23 times, respectively, at 5 h, for MGF and SYF) was observed as compared to the brain uptake values of labeled AZT at those respective time points. Although brain uptake of ^{99m}Tc labeled MGF was slightly less in values than those of SYF at 1 h but it was 56.52% higher compared to SYF at 5 h (Supplementary Table 3). For this reason, brain/blood ratio was 0.48 for MGF at 5 h which was greater than the value at 1 h whereas it was 0.32 for SYF at 5 h. Brain/blood ratio was predominantly higher for NLs compared to free AZT (Supplementary Table 3).

In vivo *plasma pharmacokinetic study*

The plasma pharmacokinetic study was performed to observe the changes of pharmacokinetic parameters in Sprague-Dawley rats after i.v. administration of MGF/SYF/free AZT suspension. The mean plasma concentration of

drug from MGF/SYF was higher than that of AZT in animals which had received AZT suspension, at the different experimental time points. The plasma concentration of AZT from MGF was comparatively higher than that of SYF after 4 h (Figure 5(A)). AUC_{0-t} value for MGF was reasonably greater than those of SYF as well as free drug suspension (Table 1). $AUMC_{0-t}$ values of drug in rats received MGF/SYF were 13.76-fold/8.25-fold respectively greater than $AUMC_{0-t}$ value as detected in animals received free drug suspension. Half-life ($t_{1/2}$) value of AZT from MGF was 8.44-fold higher than that of free AZT suspension and 1.27-fold higher than that of SYF, suggesting a predominantly sustained drug release from MGF. MRT values were 5.10-fold and 3.25-fold higher for MGF and SYF respectively than the MRT value found in rats treated with AZT suspension. This suggests maximally prolonged blood residence time of MGF among the experimental formulations. A predominant variation in V_{ss} values was also noticed for MGF (about two times greater than the value obtained from rat treated with AZT suspension and 1.5 times greater than the value obtained from rat treated with SYF). There was 63.21% decreased clearance of AZT from MGF as compared to free AZT suspension. Data revealed that MGF provided most favorable pharmacokinetic profile of AZT as compared to SYF and free AZT suspension.

In vivo *brain pharmacokinetic study*

Till 24 h (the total duration of the study), AZT level was detectable in brain from MGF/SYF (Figure 5(B)). However, AZT could not be detected in the brain of rats treated with AZT suspension after 10 h of the study. AZT level in brain was found to be maximum from SYF followed by MGF in 0.5 h. The values were five- and four-fold higher respectively as compared to the values detected in animals treated with AZT suspension at 0.5 h. AZT level was 25% higher in the brain of rats treated with SYF as compared to MGF at 0.5 h. With the increasing duration of time, AZT levels were decreasing in all the cases. Interestingly, at 4 h of the investigation the values of AZT concentration in brain were almost same in rats treated with SYF/MGF. However, from then on, till 24 h of the study, AZT levels in brain were found to be more (46.76% more in value at 6 h, 263.75% more in value at 24 h) in rats treated with MGF as compared to those treated with SYF. Treatment of AZT through MGF enhanced $AUMC_{0-t}$ value by 50.99% and MRT value by 49.14% as compared to the rats treated with SYF. The data were also substantiated by clearance values (Table 1).

Discussion

The present investigation was intended to understand the capability of ML to act as base material of lipid nanocarrier

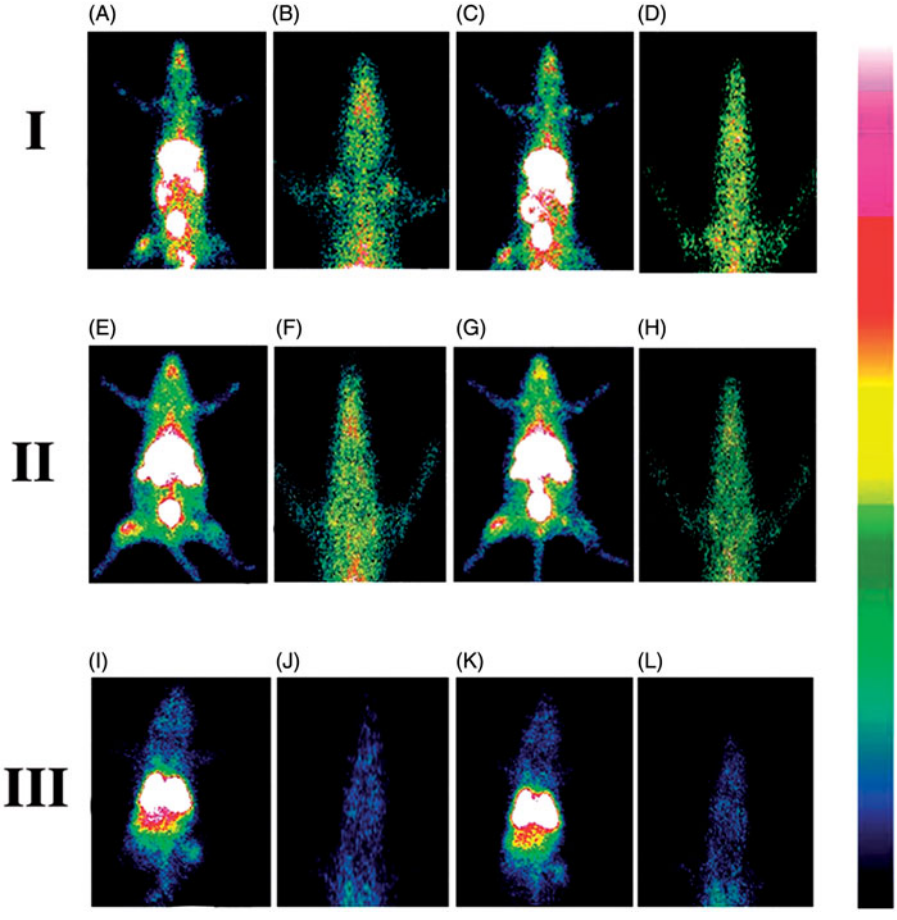

Figure 4. Gamma scintigraphy images of rats after receiving radiolabeled MGF/radiolabeled SYF/radiolabeled AZT. (I) rats received ^{99m}Tc labeled MGF at 1 h (A, B) and at 5 h (C, D) post i.v. injection; (II) rats received ^{99m}Tc labeled SYF at 1 h (E, F) and at 5 h (G, H) post i.v. injection; (III) rats received ^{99m}Tc labeled free drug at 1 h (I, J) and at 5 h (K, L) post i.v. injection. A, C, E, G, I, and K are whole animal image; B, D, F, H, J, and L are magnified brain part.

to deliver water soluble drug through BBB to brain. Continuous tight junctions of endothelial cells of brain capillaries and several transmembrane proteins seal the paracellular pathways and effectively block the free diffusion of polar solutes (such as AZT) from blood along these potential paracellular pathways, causing denial of access to brain interstitial fluid (Ballabh et al., 2004; Abbott, 2005). Blood–brain barrier predominantly impedes entry from blood to brain of virtually all molecules, other than those that are small and lipophilic (e.g. nanoliposome) or those (such as essential nutrients, precursors and cofactors) that enter the brain through active transport mechanism (Alavijeh et al., 2005; Agrawal et al., 2017). Thus, lipophilicity and size of nanoliposome tend to lead higher permeation across BBB as compared to the polar drug or comparatively polar phospholipid vesicles. Since AZT is a highly water soluble drug that does not cross BBB efficiently (Rautio et al., 2008; Weiss et al., 2009) and the nanosize lipid vesicles have been shown to permeate through BBB effectively (Masserini, 2013; Vieira & Gamarra, 2016; Li et al., 2017), we developed two types of NLs (MGF and SYF) applying lipid layer hydration technique by using ML/SL. A comparative physicochemical and biopharmaceutical analysis on those two types of formulations were also performed.

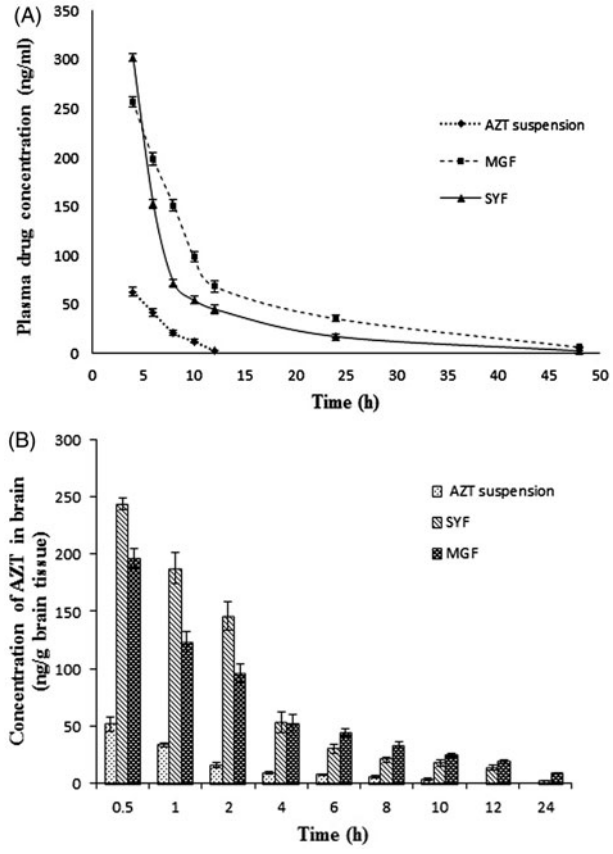

Figure 5. *In vivo* pharmacokinetic parameters in plasma and brain. (A) Plasma concentration of AZT–time profiles after i.v. administration of MGF/SYF/free drug (AZT) suspension in rats. (B) Concentration of AZT in brain after i.v. administration of MGF/SYF/AZT suspension in rats represented by bar diagram. Data showed mean ± SD ($n = 3$). SD of each point was represented by error bar. SD: standard deviation represented by deviation bar.

FTIR data analysis revealed that there was no chemical interaction between the drug and the excipients. However, there were some physical interactions between the drug and excipients and between the molecules of excipients. Such physical interactions might have a role to form the spherical nanostructure of the drug carrier (Rudra et al., 2010) and to retain the drug in the lipid layer, causing slower diffusion of drug through the membrane (Rudra et al., 2010). Again, absence of peak of AZT in the lyophilized ML-based NLs was due to the entire encapsulation of AZT in the formulation. Presence of peak of AZT in SYF suggests the availability of free drug on the surface of the formulation.

Various process parameters such as temperature and speed of hydration, duration of sonication, time and speed of centrifugation, duration of freeze drying and ratio of the constituents were optimized to develop formulations with maximum drug loading, homogeneous and uniform particle size, desirable zeta potential value and smooth surface structure, among the experimental formulations. Out of the various experimental formulations, the best optimized formulation of each category (MGF/SYF) was selected and reported here.

Lower drug loading was observed in MGF as compared to SYF. AZT is a highly water soluble drug (Singh et al., 2010; Nath et al., 2011). SYF had hydrophobic phospholipid

Table 1. Plasma and brain pharmacokinetic parameters of AZT after i.v. administration of MGF/SYF/free drug (AZT) suspension in rats.

Pharmacokinetic parameters	AZT suspension	MGF	SYF
Plasma pharmacokinetic profile			
$t_{1/2}$ (h)	1.15 ± 0.04	9.71 ± 0.21[a,b]	7.64 ± 0.08[a]
AUC_{0-t} (h ng ml^{-1})	2003.27 ± 24.63	5405.57 ± 151.03[a]	5107.23 ± 153.91[a]
$AUMC_{0-t}$ (h^2 ng ml^{-1})	2529.70 ± 188.70	34806.50 ± 2475.71[a,b]	20881.90 ± 1198.92[a]
Cl (L h^{-1} kg^{-1})	2.99 ± 0.04	1.10 ± 0.03[a]	1.17 ± 0.03[a]
MRT (h)	1.26 ± 0.08	6.43 ± 0.28[a,b]	4.09 ± 0.24[a]
V_{ss} (L kg^{-1})	3.83 ± 0.19	7.88 ± 0.19[a,b]	5.03 ± 0.38[a]
Brain pharmacokinetic profile			
AUC_{0-t} (h ng ml^{-1})	141.17 ± 12.08	888.23 ± 28.67[a]	875.73 ± 53.86[a]
$AUMC_{0-t}$ (h^2 ng ml^{-1})	386.53 ± 35.11	5396.33 ± 236.87[a,b]	3574.03 ± 290.51[a]
MRT (h)	2.73 ± 0.06	6.07 ± 0.15[a,b]	4.07 ± 0.06[a]
Cl (L h^{-1} kg^{-1})	37.33 ± 4.66	5.9 ± 0.17[a]	6.73 ± 0.35[a]

$t_{1/2}$: half-life; AUC_{0-t}: area under the concentration–time curve from time of injection ($t = 0$) to a determined time point; $AUMC_{0-t}$: area under the first moment curve; Cl: clearance; MRT: mean residence time; V_{ss}: steady state volume of distribution.
Note: Data were expressed as mean ± SD of three separate observations.
[a]Data were significantly different ($p < .05$) where MGF and SYF were compared with AZT suspension. It was assessed by one-way analysis of variance (ANOVA) through Tukey–Kramer's multiple comparisons test.
[b]Data were significantly different ($p < .05$) where MGF was compared with SYF. It was assessed by one-way analysis of variance (ANOVA) through Tukey–Kramer's multiple comparisons test.

and CHO. Presence of phosphate group in SL makes it comparatively more hydrophilic than ML (Jones, 2008). Presence of SA, OA, and PA possibly caused comparatively less partitioning of drug into the lipid layer causing less drug loading in MGF. Yield of SYF was nearly about 6% less as compared to MGF and the possible reason may be the recovery problem due to slightly stickiness of SYF for presence of SL (Das et al., 2015).

Nanosize SYF had larger size (38.49% larger) than MGF. This could be because of the presence of phospholipid in SYF. Phospho moiety owing to the hydrophilic nature of the phosphate group (Jones, 2008) might have been pulled with more tension by water molecules toward the bulk of the liquid during the formation of the liposomal structure, resulting in comparatively larger size. PDI values of both the formulations were nearly similar. PDI value is a very crucial indicator for size distribution, stability, and uniformity of NLs (Masarudin et al., 2015). Lower PDI value signifies more monodisperse pattern with better stability of NLs. On the other hand, higher PDI value indicates aggregation of particles with low stability (Masarudin et al., 2015). The PDI value 0.1–0.25 is desirable for uniform distribution but the value more than 0.5 is an indication of poor homogeneity (Gharib et al., 2014). In our study, both the formulations were mostly uniform in size and homogeneously distributed. Zeta potential is also considered as a parameter for confirmation of physical stability (Dey et al., 2016; Shaw et al., 2017). If electric charge of NLs surface is high, then zeta potential of NLs will also show high value. This means strong repellent forces among the vesicles of NLs are able to inhibit agglomeration of NLs in suspension. Normally, zeta potential value (more than +30 mV or less than −30 mV) indicates good stability of NLs in colloidal dispersion (Dey et al., 2016). In our study, nearly similar zeta potential values (about −70 mV) were achieved for MGF and SYF. This denotes that both the formulations had prolonged and better physical stability in colloidal suspension. The negatively charged NLs are removed slowly than the positive one, which suggests longer blood residence time of negatively charged drug carriers (Satapathy et al., 2016). Thus, both the experimental formulations are expected to possess extended blood residence time.

FESEM provides information related to 3D structure as well as surface property (Tripathi et al., 2017). FESEM study reveals that both the formulations had spherical structure with smooth surface and they were homogeneously distributed with nonappearance of any agglomerate.

The Cryo-TEM images show that MGF/SYF had unilamellar spherical nanosize structure with an intact lamellarity. Lipid layer was present at the external side and aqueous part was enclosed by the lipid layer. Dark spot in the inner aqueous core and dark outer layer revealed the presence of hydrophilic drug in a suspended condition in the aqueous core as well as in the outer lipid layer.

Drug was found to release in a slower and more sustained manner from MGF compared to SYF in both types of drug release media. This could be due to the lipid composition of the NLs. SYF fundamentally consisted of phospholipid which contains polar phosphoryl and basic groups and they make the phospholipid more hydrophilic (Jones, 2008) than the ML which does not contain any phospholipid. Since AZT is a highly water soluble drug (Singh et al., 2010; Nath et al., 2011), it seems to permeate more through phospholipid than the ML.

The drug release pattern from both the NLs in phosphate buffer media as well as 50% serum was best fitted (based on R^2 value) with Korsmeyer–Peppas's kinetic model. Release component (n) value suggests for an anomalous non-Fickian diffusion pattern of drug molecules (Pattnaik et al., 2012). Further, Korsmeyer–Peppas's kinetic model suggests that AZT release from the experimental NLs followed diffusion and erosion process (Pattnaik et al., 2012).

Cellular uptake of both the NLs in U-87MG human glioblastoma cells showed that NLs were localized in the cytoplasm and in the nucleus after internalization by the cells. But FITC-MGF was intense in cells in a time dependent manner whereas FITC-SYF concentration in cells initially increased (at 1 h as investigated) and then decreased with the time (at 3 h, total duration of the investigation). Possibly phospholipid vesicles were metabolized faster than MGF by glioma cells (Carnielli et al., 1998; Klein, 2002).

At 4 °C, absence of changes in spectra for formulations indicates that there was no physico-chemical reaction occurred between the drug and the excipients during storage condition. So, drug remains as a stable form in stored formulation during storage condition at 4 °C. At 25 °C, although FTIR spectra did not significantly vary for the experimental formulations, the deformity of structures of NLs forced us to reject the consideration of 25 °C to store the formulation. However, drug assay showed that the drug was stable in the formulation at 25 °C.

We performed gamma scintigraphic investigation and brain pharmacokinetic study to compare the capability of MGF and SYF to cross BBB. Gamma scintigraphic images gave clear picture of localization of radiolabeled NLs/radiolableled AZT in whole body of the experimental rats. From the gamma scintigraphic images, it revealed that both the radiolableled NLs were capable to cross BBB and reached in brain. The intensity of signal in brain was stronger at 1 h as compared to 5 h for both MGF and SYF (as observed from signal intensity bar given with the photograph). At 5 h, the signal intensity of MGF in brain was more pronounced than that of SYF, suggesting longer retention of radiolabeled MGF than radiolabeled SYF in brain after crossing BBB. Very weak signal at 1 h and 5 h for ^{99m}Tc labeled free drug (AZT) signifies poor ability of AZT to cross BBB. Both the NLs successfully crossed BBB possibly due to their nano-vesicular structure (Li et al., 2017) and longer retention of MGF in brain compared to SYF might be due to the variable lipid characteristics of MGF than SYF which had phospholipid in its structure.

In biodistribution study, radiolabeled MGF obtained from brain/blood ratio maintained its level persistently as compared to radiolabeled SYF, suggesting MGF was able to provide sustaining drug level in brain and blood better than SYF. Application of MGF showed presence of more amount of drug in brain with the increasing duration of the experiment as compared to that of SYF owing to an increased presence of MGF in brain. The presence of more MGF in brain/blood ratio as compared to SYF might be due to the sustained drug release and less clearance of drug through

liver and kidney as compared to those of SYF. Predominant hepatic clearance of free AZT is also noteworthy to mention. The investigation reported that it is possible for a compound to possess a long half-life in blood, but a short half-life in brain or even not to permeate BBB at all (Dawson et al., 2001). Hence, if a drug or formulation remains longer time in blood, it does not necessarily provide enhanced brain level of the drug (Dawson et al., 2001; Vieira & Gamarra, 2016). On the other hand, almost all things injected in blood must go into liver and liver does not have any barrier like BBB. Hence, the access of drug/formulation takes place much faster with a greater amount in liver than brain. Thus, MGF can tackle the short elimination half-life, low bioavailability, frequent dosing and dose-dependent toxicity of AZT (Mandal & Tenjarla, 1996; Blum et al., 1988; Oh et al., 1998; Thomas & Panchagnula, 2003) more effectively than SYF.

After i.v. administration, at 4 h, SYF showed more drug level in blood as compared to MGF. It dropped sharply with the increasing duration till 8 h which indicates rapid distribution of SYF compared to MGF. However, MGF showed slow distribution and significantly ($p < .05$) longer blood residence time as compared to SYF which also increased $t_{1/2}$ value of AZT. AUC_{0-48} and $AUMC_{0-48}$ were significantly more for MGF. It could be due to the longer MRT and less renal clearance of MGF compared to SYF. Reports suggest that longer MRT and less renal clearance increase AUMC and AUC (Dey et al., 2016; Satapathy et al., 2016).

Drug concentration in brain was initially 25% more for SYF than MGF. The drug level in brain from MGF/SYF eventually reduced with the duration. At 4 h, the drug level in brain from MGF/SYF was more or less same. Interestingly, brain drug concentration from SYF dropped sharply after 4 h whereas it dropped in a much slower manner for MGF till 24 h of the study where brain drug level was about 260% more than that obtained from SYF. One of the most important features of brain is that it is completely separated from blood by BBB. In our study, blood perfusion was done before collection of brain from the animals to estimate drug in brain. Blood perfusion precludes the presence of drug in brain vasculatures and rather suggests its accumulation in brain, as drug has to cross BBB to reach brain endothelial cells (Ballabh et al., 2004; Abbott, 2005; Alavijeh et al., 2005). Thus, *in situ* perfusion provides a measure of brain uptake and the brain/plasma ratio of the drug (as done in the present study) provides a partial measure (Takasato et al., 1984; Abbott, 2005; Alavijeh et al., 2005). Since both the studies have been done, it supports that drug reached in brain. It is also an indicative of cross of the drug-loaded formulations through BBB. Sustained drug release, less clearance, and enhanced MRT of MGF in brain could be responsible for such enhancement. These further reflected in the enhanced availability of drug in brain from MGF compared to SYF. Lipid composition of MGF might be responsible for such variation.

Conclusions

In the study, nanosize drug delivery systems were developed successfully utilizing ML/SL to deliver AZT in brain across BBB. Both the formulations had sustained drug release profiles. *In vivo* gamma scintigraphy study and brain pharmacokinetic investigation revealed that both the formulations sufficiently reached brain through BBB, but MGF had better pharmacokinetic profile than that of SYF with respect to sustained drug release, prolonged blood residence time as well as brain residence time and increased $t_{1/2}$. Thus, ML may be utilized as a new and effective carrier material to deliver AZT effectively in brain. ML could be an emerging pharmaceutical for developing various therapeutic strategies to deliver drugs to brain and other organs. However, further studies are warranted in the area.

Disclosure statement

The authors declare that the content of this article has no conflict of interest.

Funding

The authors are very grateful to the Department of Biotechnology (DBT), Govt. of India, for providing the financial support (sanction no. BT/504/NE/TBP/2013) to execute this work.

ORCID

Biswajit Mukherjee http://orcid.org/0000-0002-7854-9680

References

Abbott NJ. (2005). Dynamics of CNS barriers: evolution, differentiation, and modulation. Cell Mol Neurobiol 25:5–23.

Agrawal M, Ajazuddin, Tripathi DK, et al. (2017). Recent advancements in liposomes targeting strategies to cross blood–brain barrier (BBB) for the treatment of Alzheimer's disease. J Control Release 260:61–77.

Akbarzadeh A, Rezaei-Sadabady R, Davaran S, et al. (2013). Liposome: classification, preparation, and applications. Nanoscale Res Lett 8:102.

Alavijeh MS, Chishty M, Qaiser MZ, et al. (2005). Drug metabolism and pharmacokinetics, the blood–brain barrier, and central nervous system drug discovery. Neurotherapeutics 2:554–71.

Ballabh P, Braun A, Nedergaard M. (2004). The blood–brain barrier: an overview: structure, regulation, and clinical implications. Neurobiol Dis 16:1–13.

Basu S, Mukherjee B, Chowdhury SR, et al. (2012). Colloidal gold-loaded, biodegradable, polymer-based stavudine nanoparticle uptake by macrophages: an *in vitro* study. Int J Nanomedicine 7:6049–61.

Bergshoeff AS, Fraaij PLA, Verweij C, et al. (2004). Plasma levels of zidovudine twice daily compared with three times daily in six HIV-1-infected children. J Antimicrob Chemother 54:1152–4.

Blum MR, Liao SH, Good SS, Miranda P. (1988). Pharmacokinetics and bioavailability of zidovudine in humans. Am J Med 85:189–94.

Carnielli VP, Verlato G, Pederzini F, et al. (1998). Intestinal absorption of long-chain polyunsaturated fatty acids in preterm infants fed breast milk or formula. Am J Clin Nutr 67:97–103.

Christoper GVP, Raghavan CV, Siddharth K, et al. (2014). Formulation and optimization of coated PLGA – zidovudine nanoparticles using factorial design and in vitro in vivo evaluations to determine brain targeting efficiency. Saudi Pharm J 22:133–40.

Cole L, Coleman J, Evans D, Hawes C. (1990). Internalisation of fluorescein isothiocyanate and fluorescein isothiocyanate-dextran by suspension-cultured plant cells. J Cell Sci 96:721–30.

Das PJ, Paul P, Mukherjee B, et al. (2015). Pulmonary delivery of voriconazole loaded nanoparticles providing a prolonged drug level

in lungs: a promise for treating fungal infection. Mol Pharm 12:2651–64.
Dawson DA, Wadsworth G, Palmer AM. (2001). A comparative assessment of the efficacy and side effect liability of neuroprotective compounds in experimental stroke. Brain Res 892:344–50.
Dey NS, Mukherjee B, Maji R, Satapathy BS. (2016). Development of linker-conjugated nanosize lipid vesicles: a strategy for cell selective treatment in breast cancer. Curr Cancer Drug Targets 16:357–72.
Fox CB, Mulligan SK, Sung J, et al. (2014). Cryogenic transmission electron microscopy of recombinant tuberculosis vaccine antigen with anionic liposomes reveals formation of flattened liposomes. Int J Nanomedicine 9:1367–77.
Gautam N, Bathena SPR, Chen Q, et al. (2013). Pharmacokinetics, protein binding, and metabolism of a quinoxaline urea analog as a NF-κB inhibitor in mice and rats by LC–MS/MS. Biomed Chromatogr 27:900–9.
Gharib A, Faezizadeh Z, Namin SARM, Saravani R. (2014). Preparation, characterization and *in vitro* efficacy of magnetic nanoliposomes containing the artemisinin and transferrin. Daru 22:44.
Hu K, Li J, Shen Y, et al. (2009). Lactoferrin-conjugated PEG-PLA nanoparticles with improved brain delivery: in vitro and in vivo evaluations. J Control Release 134:55–61.
Hu X, Yang F, Liao Y, et al. (2017). Cholesterol-PEG comodified poly (N-butyl) cyanoacrylate nanoparticles for brain delivery: in vitro and in vivo evaluations. Drug Deliv 24:121–32.
Ivey NS, MacLean AG, Lackner AA. (2009). Acquired immunodeficiency syndrome and the blood–brain barrier. J Neurovirol 15:111–22.
Jain S, Tiwary AK, Jain NK. (2008). PEGylated elastic liposomal formulation for lymphatic targeting of zidovudine. Curr Drug Deliv 5:275–81.
Jones ML. (2008). Lipids. In: Bancroft JD, Gamble M, eds. Theory and practice of histological techniques. Philadelphia: Churchill Livingstone Elsevier, 187–216.
Kittiphoom S. (2012). Utilization of mango seed. Int Food Res J 19:1325–35.
Klein CJ. (2002). Nutrient requirements for preterm infant formulas. J Nutr 132:1395S–577S.
Li X, Tsibouklis J, Weng T, et al. (2017). Nano carriers for drug transport across the blood–brain barrier. J Drug Target 25:17–28.
Maji R, Dey NS, Satapathy BS, et al. (2014). Preparation and characterization of tamoxifen citrate loaded nanoparticles for breast cancer therapy. Int J Nanomedicine 9:3107–18.
Mandal TK, Tenjarla S. (1996). Preparation of biodegradable microcapsules of zidovudine using solvent evaporation: effect of the modification of aqueous phase. Int J Pharm 137:187–97.
Martins S, Tho I, Reimold I, et al. (2012). Brain delivery of camptothecin by means of solid lipid nanoparticles: formulation design, *in vitro* and *in vivo* studies. Int J Pharm 439:49–62.
Masarudin MJ, Cutts SM, Evison BJ, et al. (2015). Factors determining the stability, size distribution, and cellular accumulation of small, monodisperse chitosan nanoparticles as candidate vectors for anticancer drug delivery: application to the passive encapsulation of [^{14}C]-doxorubicin. Nanotechnol Sci Appl 8:67–80.
Masserini M. (2013). Nanoparticles for brain drug delivery. ISRN Biochem 2013:1–18.
Mu L, Zhou R, Tang F, et al. (2016). Intracellular pharmacokinetic study of zidovudine and its phosphorylated metabolites. Acta Pharm Sin B 6:158–62.
Nath B, Nath LK, Kumar P. (2011). Preparation and *in vitro* dissolution profile of zidovudine loaded microspheres made of Eudragit RS 100, RL 100 and their combinations. Acta Pol Pharm 68:409–15.
Nayak UY, Gopal S, Mutalik S, et al. (2009). Glutaraldehyde cross-linked chitosan microspheres for controlled delivery of zidovudine. J Microencapsul 26:214–22.
Oh SY, Jeong SY, Park TG, Lee JH. (1998). Enhanced transdermal delivery of AZT (zidovudine) using iontophoresis and penetration enhancer. J Control Release 51:161–8.
Pattnaik G, Sinha B, Mukherjee B, et al. (2012). Submicron-size biodegradable polymer-based didanosine particles for treating HIV at early stage: an *in vitro* study. J Microencapsul 29:666–76.
Rautio J, Laine K, Gynther M, Savolainen J. (2008). Prodrug approaches for CNS delivery. AAPS J 10:92–102.
Rudra A, Deepa RM, Ghosh MK, et al. (2010). Doxorubicin-loaded phosphatidylethanolamine-conjugated nanoliposomes: *in vitro* characterization and their accumulation in liver, kidneys, and lungs in rats. Int J Nanomedicine 5:811–23.
Sahana B, Santra K, Basu S, Mukherjee B. (2010). Development of biodegradable polymer based tamoxifen citrate loaded nanoparticles and effect of some manufacturing process parameters on them: a physicochemical and *in-vitro* evaluation. Int J Nanomedicine 5:621–30.
Satapathy BS, Mukherjee B, Baishya R, et al. (2016). Lipid nanocarrier-based transport of docetaxel across the blood brain barrier. RSC Adv 6:85261–74.
Seju U, Kumar A, Sawant KK. (2011). Development and evaluation of olanzapine-loaded PLGA nanoparticles for nose-to-brain delivery: *in vitro* and *in vivo* studies. Acta Biomater 7:4169–76.
Shaw TK, Mandal D, Dey G, et al. (2017). Successful delivery of docetaxel to rat brain using experimentally developed nanoliposome: a treatment strategy for brain tumor. Drug Deliv 24:346–57.
Singh S, Dobhal AK, Jain A, et al. (2010). Formulation and evaluation of solid lipid nanoparticles of a water soluble drug: zidovudine. Chem Pharm Bull 58:650.
Takasato Y, Rapoport SI, Smith QR. (1984). An in situ brain perfusion technique to study cerebrovascular transport in the rat. Am J Physiol 247:H484–93.
Thomas NS, Panchagnula R. (2003). Transdermal delivery of zidovudine: effect of vehicles on permeation across rat skin and their mechanism of action. Eur J Pharm Sci 18:71–9.
Tripathi KM, Castro M, Feller JF, Sankar SK. (2017). Characterization of metal, semiconductor, and metal-semiconductor core–shell nanostructures. In: Gupta RK, Misra M, eds. Metal Semiconductor Core–Shell Nanostructures for Energy and Environmental Applications. Netherlands: Elsevier, 51–78.
Vieira DB, Gamarra LF. (2016). Getting into the brain: liposome-based strategies for effective drug delivery across the blood–brain barrier. Int J Nanomedicine 11:5381–414.
Weiss N, Miller F, Cazaubon S, Couraud PO. (2009). The blood–brain barrier in brain homeostasis and neurological diseases. Biochim Biophys Acta 1788:842–57.
Wilson B, Samanta MK, Santhi K, et al. (2008). Targeted delivery of tacrine into the brain with polysorbate 80-coated poly(n-butylcyanoacrylate) nanoparticles. Eur J Pharm Biopharm 70:75–84.

Nanomedicine: Nanotechnology, Biology, and Medicine
14 (2018) 1905–1917

nanomedjournal.com

Apigenin loaded nanoparticle delayed development of hepatocellular carcinoma in rats

Sanchari Bhattacharya, M.Pharm[a], Laboni Mondal, M.Pharm[a], Biswajit Mukherjee, Ph.D[a,*], Lopamudra Dutta, M.Pharm[a], Iman Ehsan, M.Pharm[a], Mita C. Debnath, Ph.D[b], Raghuvir H. Gaonkar, M.Pharm[b], Murari M. Pal, M.Pharm[a], Subrata Majumdar, Ph.D[c]

[a]*Department of Pharmaceutical Technology, Jadavpur University, Kolkata, West Bengal, India*
[b]*Infectious Diseases and Immunology Division, CSIR-Indian Institute of Chemical Biology, Kolkata, West Bengal, India*
[c]*Division of Molecular Medicine, Bose Institute, Kolkata, West Bengal, India*

Received 30 April 2018; accepted 5 May 2018

Abstract

Hepatocellular carcinoma (HCC) is one of the major causes of cancer related death globally. Apigenin, a dietary flavonoid, possesses anti-tumor activity against HCC cells *in-vitro*. Development, physicochemical characterization of apigenin loaded nanoparticles (ApNp), biodistribution pattern and pharmacokinetic parameters of apigenin upon intravenous administration of ApNp, and effect of ApNp treatment in rats with HCC were investigated. Apigenin loaded nanoparticles had a sustained drug release pattern and successfully reached the hepatic cancer cells *in-vitro* as well as in liver of carcinogenic animals. ApNp predominantly delayed the progress of HCC in chemical induced hepatocarcinogenesis in rats. Quantification of apigenin by liquid chromatography–mass spectroscopy (LC-MS/MS) showed that apigenin availability significantly increased in blood and liver upon ApNp treatment. Apigenin loaded nanoparticle delivery substantially controlled the severity of hepatocellular carcinoma and could be a future hope for lingering the survival in hepatic cancer patients.

Key words: Apigenin nanoparticles; Hepatocellular carcinoma; Pharmacokinetics; Gamma scintigraphy; Histopathology; LC-MS/MS

Hepatocellular carcinoma (HCC) is one of the most common malignant solid tumors with a very poor prognosis[1] and survival rate[2] in humans and HCC-related death has been reported as the second highest among the all cancer related deaths worldwide.[3] Treatment of this life-threatening disease includes surgical (liver resection and transplantation) and non-surgical (chemotherapy) techniques.[4] Liver cirrhosis is the most common underlying cause leading to HCC related deaths in patients.[5] Dietary supplements along with the medicines are always under research to combat this serious health condition and improve patient-compliance.[6] Drug resistance and drug-induced toxicity in patients and often failure of early detection of HCC make it very tough to get cure.[7] Dietary supplements have been reported to improve the condition of HCC in patients as they possess anti-proliferative and anti-tumor effect on malignancies including HCC.[8] Apigenin is a dietary flavonoid found in various vegetable sources such as parsley leaves, chamomile tea, celery, kumquats, dried Mexican oregano, peppermint, vinespinach *etc*.[9] It has effective chemo-preservative and/or tumor-suppressive activity[10] against many kinds of carcinomas such as prostate, oral, skin[11], colon, breast, lung, pancreatic, colo-rectal[9] and hepatic cancer *in-vitro*.[12] Many reports suggest that apigenin induces apoptosis in liver cancer cells and may play a vital role in the treatment of HCC.[13–15] Apigenin, after the oral administration, is cleaved, absorbed and gets distributed inside the gastrointestinal lumen, and thus, bioavailability of apigenin is much less when administered orally.[16] Further, free apigenin has a very high level of protein binding (10,000 times more than the

Funding Source: This work was supported by Department of Science and Technology (Government of India), Grant no. DST/Inspire Fellowship/2012/691.

Disclosure: The authors of this article have no conflicts of interest to declare.

*Corresponding author at: Department of Pharmaceutical Technology, Jadavpur University, Kolkata 700032, India.

E-mail addresses: biswajit.mukherjee@jadavpuruniversity.in, biswajit55@yahoo.com. (B. Mukherjee).

https://doi.org/10.1016/j.nano.2018.05.011
1549-9634/

other flavonoids) and its release from the protein bound stage is extremely slow[17,18] Thus, parenteral administration of free apigenin is also difficult. Nanoparticles are excellent drug delivery systems (DDS) for delivering hydrophobic/hydrophilic drug moieties, flavonoids, vaccines, genes, protein *etc*. to the target site of delivery. Poly lactic co-glycolic acid (PLGA) based polymeric nanoparticles gained most popularity in this field due to their non-toxic and biodegradable nature[19] and PLGA has been approved by the United States Food and Drug Administration[20] (US FDA) for use in intravenous drug delivery in human. Hence we prepared apigenin loaded PLGA-nanoparticle to deliver significant amount of apigenin in liver to inhibit liver cancer growth and the efficacy of apigenin was investigated both *in vitro* and *in vivo*.

Methods

Materials

Apigenin (4′, 5, 7-trihydroxyflavone, M.W 270.24) and PLGA {MW 50,000-75,000; poly (lactide-co-glycolide) ratio 85:15} were procured from Sigma-Aldrich Co, St Louis, MO, USA. Polyvinyl alcohol was purchased from S D Fine-Chemicals limited, Mumbai, India. Fluorescein isothiocyanate 98% (FITC) was purchased from HiMedia Laboratories, Mumbai, India. Dimethylsulfoxide (DMSO) and dicholoro-methane (DCM) were procured from Merck Life Science Pvt. Ltd, Bengaluru, India. All other chemicals used in this study were of analytical grade.

Cell culture and animals

Two different human hepatocellular carcinoma cell lines (HepG2 and Huh-7) were purchased from National Centre for Cell Science (NCCS), Pune, India. Cell lines were maintained in Dulbecco′s Modified Eagle′s Medium (DMEM) supplemented with 10% fetal bovine serum (FBS, Sigma-Aldrich Co), 100 U/ml penicillin, 100 U/ml streptomycin and kept in 5% CO_2 incubator (MCO-15AC; Sanyo, Tokyo, Japan) at 37 °C.

Balb/c mice and Sprague–Dawley rats of either sex were procured from National Institute of Nutrition, Hyderabad, India and all the animal studies were conducted as per the guidelines of the Animal Ethics Committee (AEC), Jadavpur University, Kolkata.

Outline methodologies are given below. Each study protocol in details is given in the supplementary file.

Preparation of nanoparticles

Apigenin loaded nanoparticles (ApNp) were prepared by multiple emulsion solvent evaporation technique as described by Maji et al.[21] For FITC labeled ApNp, FITC was dissolved in the drug solution at a concentration of 5 mg/ml.[21] Blank particles were prepared using the same process without the incorporation of apigenin in the organic phase.

Fourier transform infrared spectroscopy

Fourier transform infrared (FTIR) spectroscopy was used to investigate interactions between apigenin and the excipients selected for the formulation, by the method as described by Maji et al.[21]

Surface characteristics of nanoparticles

Surface morphology of the nanoparticles was investigated by field emission scanning electron microscope (FESEM), transmission electron microscope (TEM) and atomic force microscopy (AFM).

Particle size assessment

A small amount of lyophilized ApNp was taken in 2 ml of Milli-Q water and sonicated for 15 min followed by vortexing for few min. Size distribution, average particle size, polydispersity index (PDI) and zeta potential of the different formulations were determined by Zetasizer nano ZS 90 and analyzed by the instrument Data Transfer Assistance (DTA) software (Malvern Zetasizer Limited, Malvern, UK) by a dynamic light scattering method at 25 °C.

Physicochemical characterization of nanoparticles

Drug loading and loading efficiency were determined in weight % by the procedure described by Maji et al[21] using the following formulas:

$$\text{Actual drug loading (weight \%)} = (\text{Amount of drug present in nanoparticles/Total amount of nanoparticles sample analyzed}) \times 100\ (\%)$$

$$\text{Drug loading efficiency (\%)} = (\text{Actual drug loading}/\text{Theoretical drug loading}) \times 100\ (\%)$$

Stability study

A stability study was performed to understand the effect of temperature and relative humidity (RH) on apigenin loaded nanoparticles. Fixed amounts of ApNp3 were weighed and kept in zone III at 4-8 °C (in refrigerator), 30 °C, 75% RH and 40 °C, 75% RH for 30, 60 and 90 days as per the International Conference on Harmonization (ICH) guidelines (ICH, 2003). Samples were withdrawn and FTIR-spectra, FESEM photograph and drug loading were checked for those samples at 30, 60 and 90 days.

In-vitro drug release study

In-vitro drug release study was performed in phosphate buffer saline (PBS, pH 7.4), citrate buffer (pH 3) and acetate buffer (pH 5) for 60 days using a cumulative drug release method as reported by Abouelmagd et al.[22]

Hydrolytic stability study

Hydrolytic stability of ApNp3 was determined as described by Mandal et al[23] at different pH buffers (citrate buffer pH 3, acetate buffer pH 5, phosphate buffer pH 7.4, bicarbonate buffer pH 10) for 30 days.

Weight variations were measured for each sample over time according to the formula,

$$\text{Weight change } (\%) = (W_0 - W_t)/W_0 \times 100$$

Where W_0 and W_t represent the initial weight and weight at time t, respectively.

In-vitro stability of ApNp3 in mouse serum (blood was collected by heart puncture technique and serum was prepared) was investigated in the above mentioned procedure for 24 h. The actual weight of the nanoparticles in mouse serum was calculated by subtracting control sample (serum without ApNp3) weight from test sample (serum with ApNp3) weight.

Cytotoxicity study by MTT assay

The time-dependent cytotoxic effect of ApNp3 on HepG2 and Huh-7 cells was determined using 3-(4, 5-dimers dimethylthiazol-2-yl)-2, 5-diphenyltetrazolium bromide (MTT dye), (Sigma-Aldrich Co, St. Louis, MO) as per reported method.[24]

$$\%\ \text{cell viability} = (\text{Absorbance of test sample}/\text{absorbance of positive control sample}) \times 100$$

Cellular uptake studies on HepG2 cells in-vitro

Cellular uptake of FITC labeled ApNp3 (ApNp5) was investigated in two types of human hepatocellular carcinoma cells, namely, HepG2 and Huh-7. Internalization of ApNp5 was visualized by confocal microscopy and quantification of the amount of ApNp5 inside the cells was determined by fluorescence activated cell sorter (FACS).

Radiolabeling of apigenin and apigenin loaded nanoparticles and biodistribution and gamma scintigraphy study

Radiolabeling of apigenin and ApNp3 with technetium (^{99m}Tc) chloride was performed according to the procedure described by Gaonkar et al[25] and Satapathy et al.[26] Biodistribution and gamma scintigraphy study of the radiolabeled ApNp3 and radiolabeled apigenin were performed to have direct information about localization of apigenin/ApNp3 in experimental animals.

Pharmacokinetic study and hepatic accumulation of apigenin by LC-MS/MS method

The pharmacokinetic study and hepatic accumulation of apigenin were performed in plasma and liver samples collected from balb/c mice (body weight 25-30 g). Naringenin[27] was used as the internal standard for this study.

Histopathological investigation of carcinogenic rat livers

Male Sprague–Dawley rats (140-150 g bodyweight) were divided into six groups each containing six rats and chemically induced hepatocellular carcinoma in rats was developed as per the protocol published by Ghosh et al.[28] Schematic diagram of hepatocarcinogenesis model along with treatment schedule with free apigenin/ApNp3 (single i.v. dose of 20 mg/kg bodyweight per week) [29] in rats is given in Supplementary Figure 1.

Enzyme assays

Hepatic cytosolic and microsomal fractions were prepared (from both normal/tumor surrounding tissues/ tumor tissues) as reported by Das et al[30] and Ghosh et al[28] and cytochrome P-450 (cyt p-450) content[31], UDP-glucuronyl transferase (UDPGT) and glutathione-S-transferase (GST) activites[32] were determined.

Statistical analysis

The data were statistically analyzed by one-way ANOVA followed by Tukey's multiple comparison test, and statistical significance was considered at $P < 0.05$.

Results

Fourier-transform infrared spectroscopy (FTIR) study

Presence of the characteristic peaks of apigenin [at wave number 1243 cm^{-1}, responsible for C-C (O) –C stretching], PLGA (at wave number 2948 cm^{-1}, responsible for –OH stretching) and PVA (at wave number 3426 cm^{-1}, responsible for –OH stretching) in their physical mixture suggests that no chemical interaction took place between the drug and the excipients. However, absence of the characteristic peak of apigenin (at wave number 1243 cm^{-1}) in apigenin loaded nanoparticles (Supplementary Figure 2) indicates that apigenin distribution occurs inside the polymeric nanoparticle scaffolds and no free apigenin was available on the surface of the nanoparticles.

Determination of surface characteristics

FESEM photographs (Figure 1, *A* and *B*) of ApNp3 showed that prepared particles were in nanosize range, homogeneously and thickly distributed and had smooth outer surface. The surface morphology was further confirmed by 3D AFM picture (Figure 1, *C*) where it showed that height of the particles varied between 10 and 14 nm. TEM images of ApNp3 (Figure 1, *D*) showed that drug particles were scatteredly distributed throughout the polymeric nanoparticle body. Average particle sizes of ApNp3 and ApNp5 were 270 nm (Figure 1, *E*) and 325 nm (Figure 1, *F*) respectively and PDI values for those formulations were 0.260 and 0.409 respectively. The zeta potential values were −4.84 mV (Figure 1, *G*) and −4.1mV (Figure 1, *H*) for ApNp3 and ApNp5 respectively. FESEM images of ApNp3 kept at 30 °C, 75% relative humidity and 40 °C, 75% relative humidity clearly showed the effect of temperature on surface morphology of the particles as the polymeric surface structure softened over time for the samples stored at 30 °C and 40 °C as compared to the freshly prepared samples (Figure 1, *I*). Sample stored at 4-8 °C was found to maintain the structure of the particles.

Drug loading and drug loading efficiency

In this study, percentage of drug loading increased with an increasing amount of apigenin incorporated in nanoparticles. It

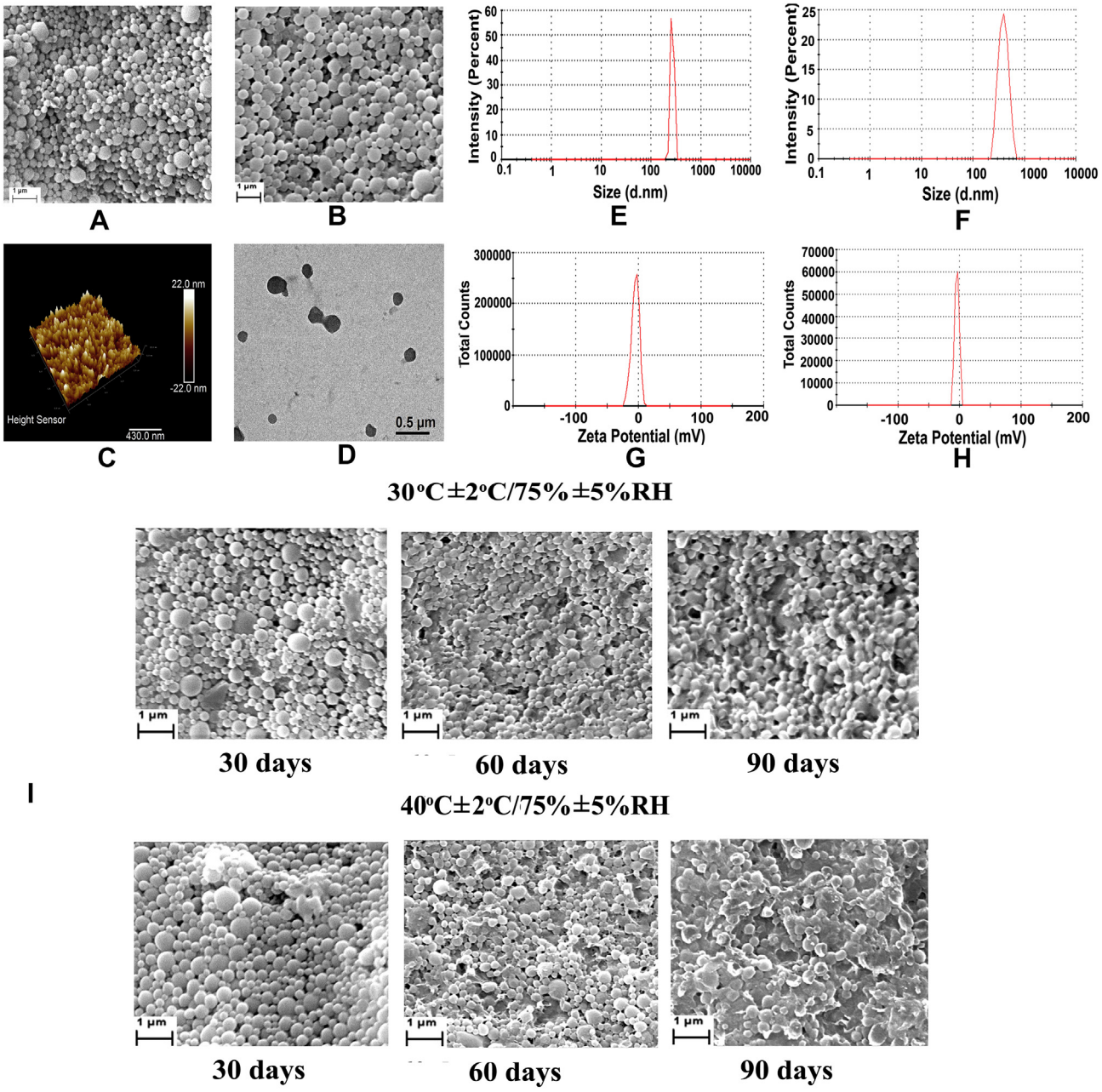

Figure 1. Morphology, size distribution and zeta potential of some selected experimental formulations. Morphology of ApNp3 (stored at 4-8 °C) was showed by FESEM **(A** and **B)**, AFM **(C)** and TEM **(D)**. Particle size distribution of ApNp3 **(E)**, particle size distribution of ApNp5 **(F)** and zeta potential of ApNp3 **(G)**, zeta potential of ApNp5 **(H)**, FESEM images of ApNp3 stored at 30 °C, 75% relative humidity and 40 °C, 75% relative humidity are indicated respectively.

varied from ApNp1 (drug loading, 2.098%) to ApNp3 (drug loading, 19.14%) as shown in Supplementary Table 1. Further, ApNp4 showed a nearly similar drug loading (19.09%) to ApNp3 despite an increase in amount of drug incorporated in the formulation. Drug loading efficiency was found to increase with the increase of amount of drug for ApNp3. Hence we have chosen ApNp3 for further investigation.

Stability of ApNp3 stored at 4-8 °C, 30 °C, 75% RH and 40 °C, 75% RH for 30, 60 and 90 days was evaluated. When the stored samples were compared with the fresh formulation, by FTIR spectroscopy (data not shown) and FESEM, the formulation stored at 4-8 °C was found to have similar FTIR spectra and the formulation structure was found to be maintained. The other formulations were also found to have similar FTIR spectra but deformed structurally due to softening of polymer with higher temperature.

In-vitro drug release and kinetic study

A variable *in-vitro* drug release pattern in different pH buffers was observed (Figure 2, *A*). After 60 days of the study, in PBS (pH 7.4) average percentage cumulative drug release was noted

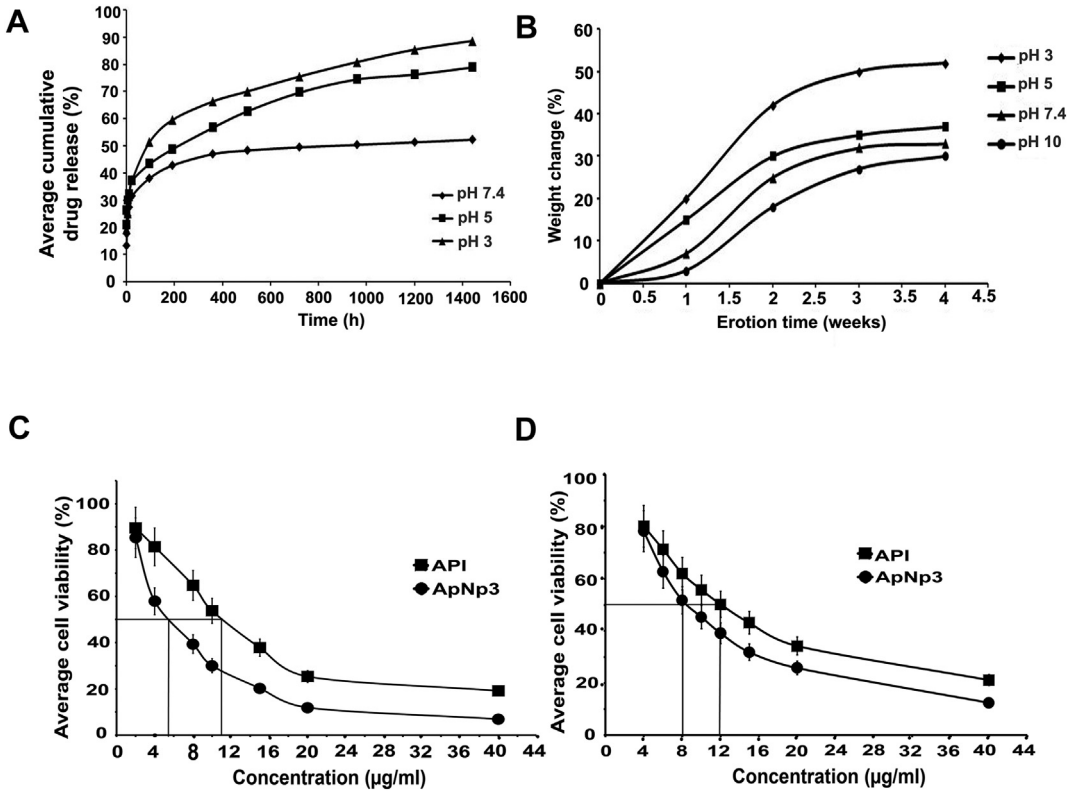

Figure 2. **(A)** *In vitro* drug release profile of ApNp3 in different pH (pH 3, 5 and 7.4) media. **(B)** Weight variation of nanoparticles in buffers of different pH. *In vitro* cytotoxicity of ApNp3 and API was determined in **(C)** HepG2 and **(D)** Huh-7 cells.

as 52.43% from ApNp3. Drug release was more in lower pH mediums. The cumulative drug release was reported as 79.06% and 88.54% in pH 5 and pH 3 respectively. To evaluate the drug-release kinetic pattern in PBS, release data were assessed using zero order, first order, Hixon–Crowell, Korsmeyer–Peppas, and Higuchi kinetic models. Various regression co-efficient (R^2) values for the kinetics were tabulated (Table 1). The corresponding plot (log cumulative percent drug release versus log time) of ApNp3 followed the Korsmeyer–Peppas equation with a good linearity (R^2= 0.9634). The release exponent (n) value for our formulation was 0.17 which suggests apigenin release followed anomalous diffusion pattern.[33]

Hydrolytic stability study

The stability of nanoparticles altered in different pH. Weight loss was found to increase with the decrease pH of medium (Figure 2, B). After 4 weeks of study, the mass loss of ApNp3 in pH 10, pH 7.4, pH 5 and pH 3 was 30.35%±0.48%, 33.87%±0.93%, 37.45%±1.13% and 52.01%±1.97% respectively. The weight loss of ApNp3 was 2.8%±0.13% after 24 h in mouse serum (graph not shown).

In-vitro cytotoxicity

In-vitro cytotoxicity of apigenin suspension (API, free drug) and ApNp3 in hepatocellular carcinoma cells was determined by MTT assay. Earlier reports suggest that apigenin successfully reduced cell viability and proliferation of HepG2[34] and Huh-7 cells.[35] In this study, we found that ApNp3 had an IC_{50} value much lower than that of API. In HepG2 cells, IC_{50} value of ApNp3 was 5.5µg/ml and that of API was 11 µg/ml (Figure 2, *C*). Again, in case of Huh-7 cells, IC_{50} value of ApNp3 was 8.5 µg/ml and that of API was 12 µg/ml (Figure 2, *D*).

Cellular uptake determination and quantification

The confocal images showed time dependent uptake of FITC labeled apigenin loaded formulation (ApNp5) by the HepG2 and Huh-7 cells *in-vitro* **(**Figure 3**)**.

A quantitative measurement by FACS analysis showed that FITC signals were directly proportional to the amount of ApNps incorporated in HepG2 and Huh-7 cells incubated with ApNp5 at 0.5 h, 2 h and 6 h, along with an enhancement of uptake of FITC-nanoparticles in cells with time, as compared to untreated (control) cells (Figure 4). Cellular uptake of drug through ApNp3 in both the cell types was found to be predominantly more as compared to those cells treated with API when analyzed by LC-MS/MS (data not shown).

Gamma scintigraphy and biodistribution

^{99m}Tc-API/^{99m}Tc-ApNp3 was visualized by gamma scintigraphy in different animals (mice/rats) and the investigation showed that labeled ApNp3 accumulated predominantly in liver than ^{99m}Tc-API (Figure 5, *A*). Further, predominant time-dependent accumulations were detected in intestine, thymus gland, stomach and urinary bladder (Figure 5, *A*, *a* and *b*) of mice. However, in case of ^{99m}Tc-ApNp3 administration,

Table 1
Average particle size, PDI and zeta potentials of ApNp3 and drug release data tested on various release kinetics models.

Formulation code	Z-average (d-nm)[a]	PDI[a,b]	Zeta potential (mV)	*In-vitro* kinetic model on which drug release data were assessed	Corresponding kinetic equation with R^2 value
ApNp3	270	0.409±0.05	−4.21±1	Zero Order	y=0.0267x+28.64, **R^2 = 0.6361**
				First Order	y=0.0002x+1.85, **R^2 = 0.6915**
				Higuchi	y=1.0288x+22.79, **R^2=0.8452**
				Hixson–Crowell	y=0.0006x+4.140, **R^2 = 0.6733**
				Korsmeyer–Peppas	y=0.1732x+1.217, **R^2=0.9648 (n=0.17)**[c]

[a] Data show mean ±SD (n = 3).
[b] PDI, polydispersity index.
[c] n=release exponent.

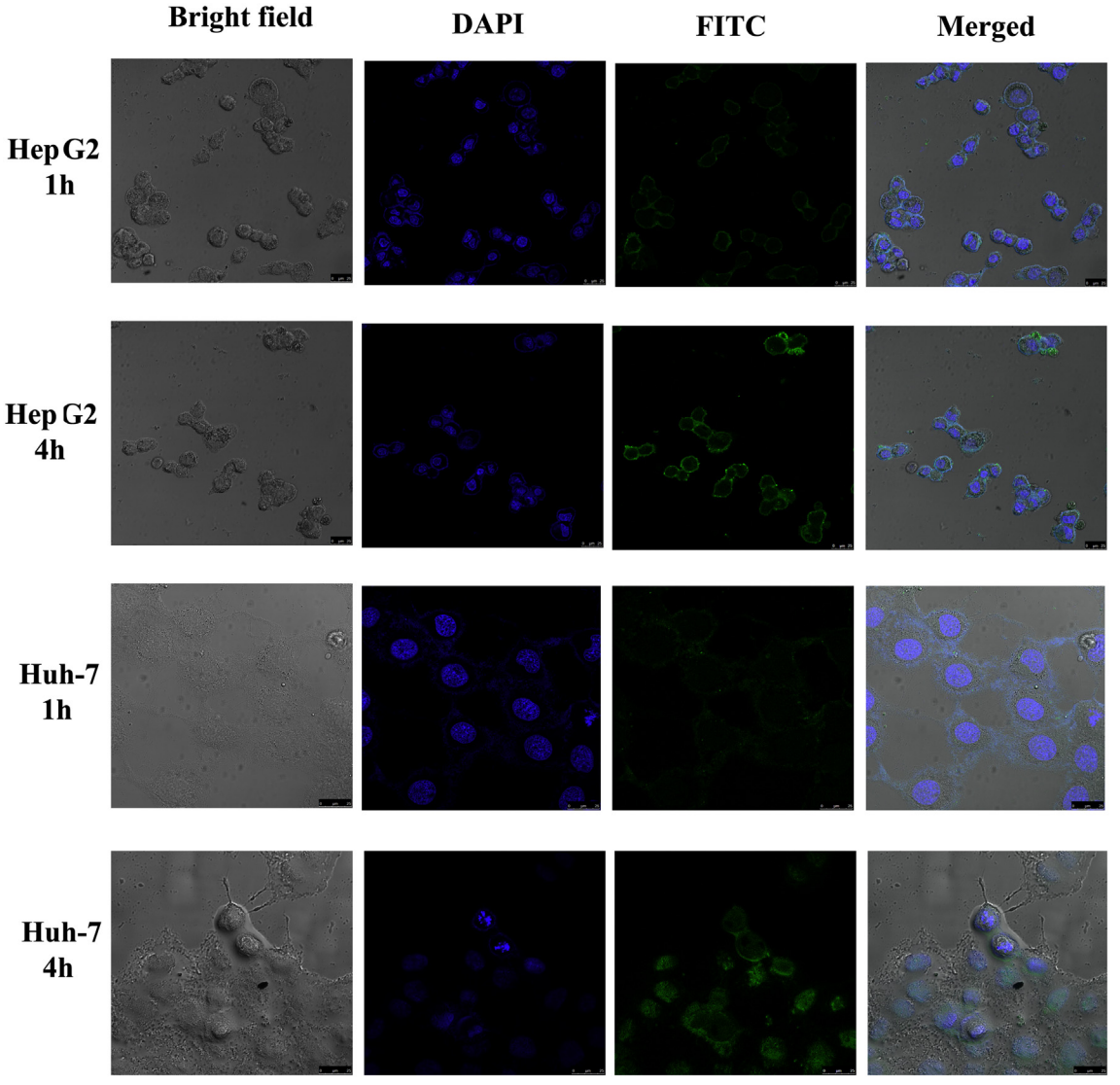

Figure 3. Cellular uptake of FITC labeled ApNp3 (ApNp5) in HepG2 and Huh-7cells observed by confocal microscopy at 1 h and 4 h respectively.

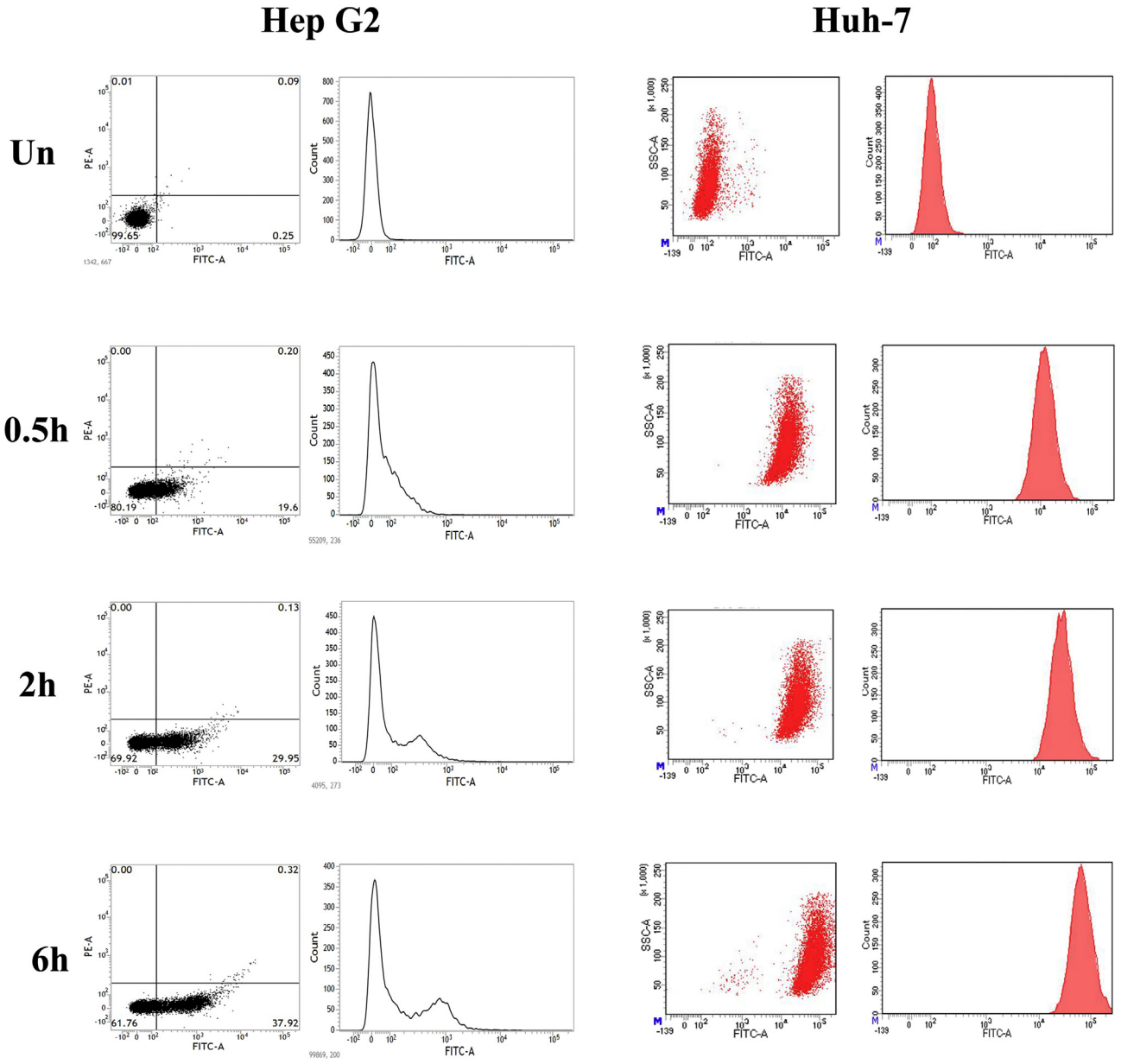

Figure 4. Time-dependent and quantitative measurement of cellular uptake of ApNp5 (FITC-ApNp3) in HepG2 and Huh-7 cells by FACS at 0.5 h, 2 h and 6 h against untreated cells (Un).

prominent time-dependent accumulations in liver, urinary bladder as well as in intestinal region were noticed (Figure 5, *A*, *f* and *g*). When radiolabeled ^{99m}Tc-API /^{99m}Tc-ApNp3 was administered in normal rats by tail vein, a quick and time-dependent distribution of labeled ApNp3 was observed in liver and the clearance of labeled nanoparticles through urinary bladder was very less (Figure 5, *A*, *h* and *i*) as compared to that of ^{99m}Tc-API in mice. Administration of ^{99m}Tc-API in rats showed distribution in kidneys, and elimination through urinary track *via* urinary bladder (Figure 5, *A*, *c* and *d*). When rats with HCC were treated with ^{99m}Tc-ApNp3/ ^{99m}Tc-API, predominant localization of ^{99m}Tc-ApNp3 was seen inside the enlarged (most likely due to inflammation) liver and its surrounding organs (at 4 h) and its clearance through urinary bladder was remarkably low (Figure 5, *A*, *e* and *j*). Biodistribution of ^{99m}Tc-API and ^{99m}Tc-ApNp3 was examined in various organs of balb/c mice. Substantial uptake of ^{99m}Tc- ApNp3 was observed in hepatic region compared to ^{99m}Tc-API. At both the time points (2 h and 6 h), radiolabeled nanoparticles had much higher residence time in blood and lower distribution in kidney than ^{99m}Tc-API (Table 2).

LC-MS/MS study

Graphical representations of the plasma profile and the hepatic accumulation of apigenin upon ApNp3/API administrations were given in Figure 5, *B*, *a* and *B*, *b*, respectively. In case of plasma, ApNp3 was found to maintain a steady blood level of predominantly more amount of drug even up to 72 h (period of the study).

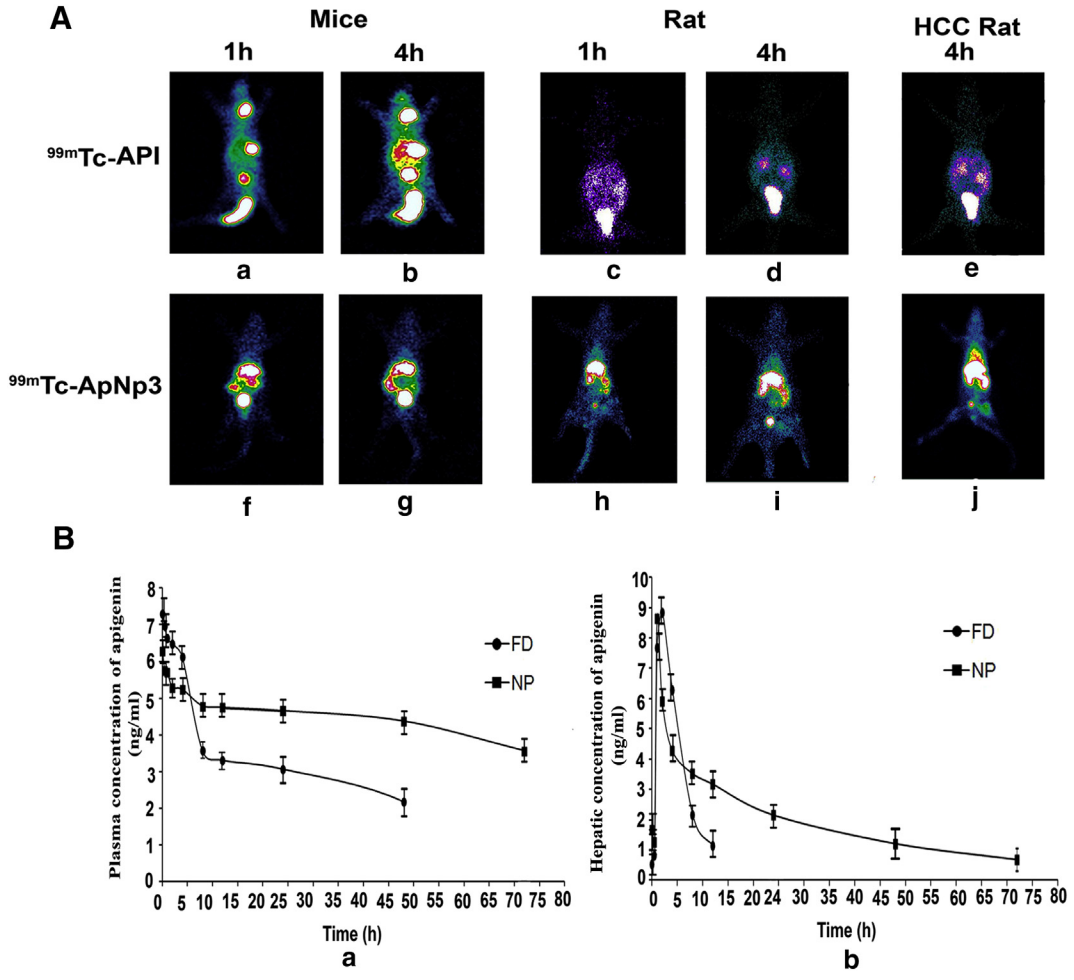

Figure 5. Gamma scintigraphic images of radiolabeled ApNp3/API localization in animals treated with radiolabeled ApNp3/API **(A)** and plasma concentration and hepatic concentration of apigenin in animals treated with ApNp3/API **(B)**. **(A)** Time dependent biodistribution and accumulation of ^{99m}Tc-API in mice at 1 h (a) and 4 h **(b)**; in rats at 1 h **(c)** and 4 h **(d)**; in rats with HCC at 4 h **(e)** along with the accumulation of ^{99m}Tc- ApNp3 in mice at 1 h **(f)** and 4 h **(g)**; in rats at 1 h **(h)** and 4 h **(i)**; rats with HCC at 4 h **(j)**. **(B)** Plasma **(a)** and hepatic **(b)** concentration of apigenin upon i.v bolus injection (at a dose of 1mg/kg body weight) of ApNp3 (NP) and API (FD) were shown.

Table 2
Biodistribution of apigenin in mice that received i.v.[a] injection of ^{99m}Tc-ApNp3/^{99m}Tc-API.[b]

Organ/ Tissue	^{99m}Tc-ApNp3		^{99m}Tc-API	
	2 h	6 h	2 h	6 h
Heart	0.597 ± 0.058[c]	0.421 ± 0.049	0.315 ± 0.051	0.284 ± 0.056
Blood	2.230 ± 0.095	1.806 ± 0.087	0.829 ± 0.099	0.631 ± 0.087
Liver	42.15 ± 1.213	54.151 ± 1.191	22.456 ± 1.311	20.561 ± 1.197
Lung	0.747 ± 0.213	1.285 ± 0.222	1.215 ± 0.192	0.997 ± 0.213
Spleen	0.378 ± 0.054	0.721 ± 0.034	1.531 ± 0.049	1.745 ± 0.057
Kidney	2.912 ± 0.211	2.451 ± 0.189	3.990 ± 0.212	4.785 ± 0.191
Intestine	6.160 ± 1.431	8.751 ± 1.212	21.556 ± 1.198	25.612 ± 1.199
Muscle	0.125 ± 0.003	0.156 ± 0.002	0.287 ± 0.007	0.215 ± 0.002

[a] i.v., intra-venous.
[b] ^{99m}Tc-ApNp3, radiolabeled apigenin loaded nanoparticle; ^{99m}Tc-API, radiolabeled apigenin.
[c] Data show mean ±SD (n = 4).

In case of hepatic concentration of apigenin, apigenin from suspension was detected up to 12 h, but the concentration could not be detected in liver at 24 h. In case of ApNp3, the hepatic concentration of drug was detectable up to 72 h (time period of the investigation) which showed maintenance of a steady level of hepatic concentration of apigenin by ApNp3. Hepatic t_{max} (time to reach maximum concentration) values were very close for ApNp3 and API (about 1-2 h) suggesting rapid uptake of API

Table 3
Plasma and hepatic pharmacokinetic parameters of apigenin from ApNp3[a] and API[b] after intravenous bolus administration of API and ApNp3 with an equivalent amount of drug in balb/c mice.

Parameters	Plasma values of drug upon API administration[c]	Plasma values of drug upon ApNp3 administration	Hepatic values of drug upon API administration	Hepatic values of drug upon ApNp3 administration
Elimination $t_{1/2}$ (h)	39.8 ± 2.1	70.7 ± 4.3	3.8 ± 0.9	25.1 ± 1.
C_{max} (ng/ml)	7.31 ± 1.3	6.29 ± 2.5	8.48 ± 2.78	8.66 ± 1.99
[d]$AUC_{0\text{-}t}$	164.6 ± 12.2	338.6 ± 31.67	47.87 ± 4.9	124.13 ± 2.24
$AUC_{0\text{-inf}}$	289.9 ± 23.5	701.7 ± 55.31	55.9 ± 4.7	168.2 ± 14
CL (L/h/kg)	3.45 ± 0.75	1.43 ± 0.43	17.9 ± 1.54	5.9 ± 0.88
MRT_{last} (h)	20 ± 3.7	33.7 ± 2.24	4.8 ± 1.02	18 ± 2.01
Vss (L/kg)	196.5 ± 17.6	151.5 ± 11	113.9 ± 13.6	209.9 ± 17.8

[a] ApNp3, apigenin loaded nanoparticles.
[b] API, suspension of apigenin.
[c] Data show mean ±SD (n = 4).
[d] Units of AUC in plasma is h ng/ml, and in hepatic tissue h ng/g respectively.

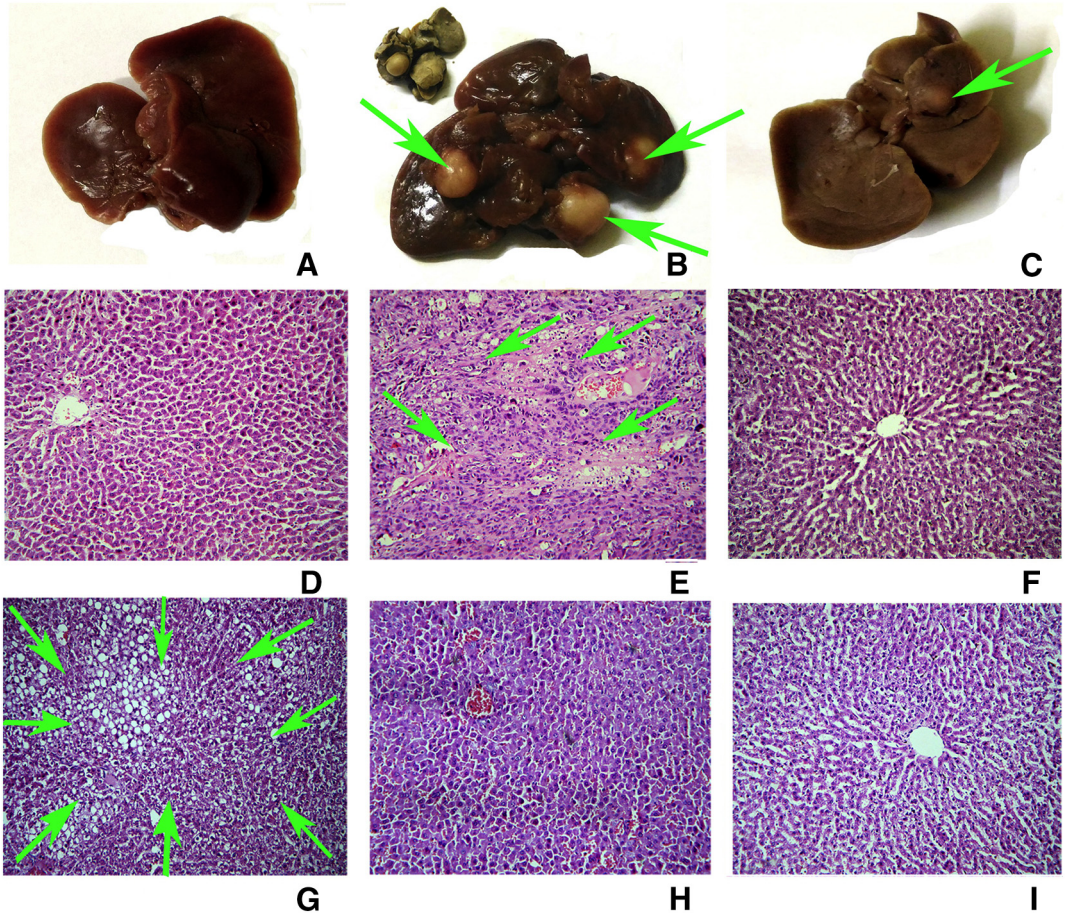

Figure 6. Macroscopic and microscopic images (in 10× magnifications) of liver of the experimental animals. Macroscopic images of livers of normal rats **(A)**, carcinogen control rats **(B)** and carcinogen treated rats treated with ApNp3 **(C)**. Microscopic images of liver section of normal rats **(D)**, carcinogen treated rats **(E)**, carcinogen treated animals treated with ApNp3 **(F)**, carcinogen treated animals treated with API **(G)**, normal animals treated with ApNp3 **(H)**, and normal animals treated with API **(I)**.

and the nanoparticles by liver. The plasma and liver pharmacokinetic data of apigenin from ApNp3 and from API (Table 3) showed that administration of ApNp3 by i.v. route enhanced plasma half-life of drug by 75% and hepatic half-life of it by 6.6 times in the experimental animals. Values of maximum concentration of drug (C_{max}) in plasma and in liver were more or less similar for API and ApNp3. Plasma as well as hepatic AUC values markedly increased upon ApNp3 administration from 1.5 to 3 times respectively as compared to those for API. Further, the values of the mean residence time of apigenin (from ApNp3) in plasma and in liver were found to increase by 1.68 and 3.03 times respectively, compared to API.

Table 4
A quantitative data on the effect of API/ApNp3 treatment of hepatic tumor incidences, number and total area of hepatic altered foci (HAF).

Groups	Number of rats developed HCC per total number of experimental rats per group	Tumor incidences (%)	Number of HAF[a]/cm^2 of hepatic tissue[b]	Total area of lesion (%)
A	0/6	-	-	-
B	6/6	100	79.57 ± 6.08[b]	57.76 ± 1.45
C	2/6	66	21.98 ± 3.34[c]	12.38 ± 0.98[c]
D	-	-	-	-
E	-	-	-	-
F	5/6	83	56.43 ± 5.8[c]	36.73 ± 4.65[c]

[a] HAF: hepatic altered foci.
[b] Values represent mean ±SD (n=6 for each group).
[c] P<0.05 when compared against Group B.

In-vivo HCC model

Macroscopic and histopathology study. Macroscopic images of liver tissues from group A, B and C animals revealed that treatment with apigenin nanoparticles (20 mg/kg single i.v. dose/week) for 12 weeks successfully controlled the tumor development in carcinogen treated rats (Figure 6, *C*). The hyperplasic nodules (HN) and preneoplastic and neoplastic hepatic altered foci lesions (HAF)[30] were clearly visible in HCC rats without any treatment (Figure 6, *B*) and upon intravenous treatment with ApNp3, the sizes of the nodules and number of lesions were markedly reduced (Figure 6, *C*). In the carcinogen control animals (Figure 6, *E*), tumor formation and scattered lesions with cells of ground glass appearance[36] were visible in the liver and normal hepatic architecture was lost. There were focal lesions and tumor formation visible in HCC. Cellular death and cells with pyknotic nucleus were also observed as compared to the normal liver architecture (Figure 6, *D*). Treatment of apigenin nanoparticles (ApNp3) in carcinogenic animals (Figure 6, *F*) was found to hold the hepatocellular architecture predominantly towards normal as compared to the carcinogenic animals treated with free drug (Figure 6, *G*). There was no distinguishable change in hepatocellular architecture in normal animals treated with blank nanoparticle (data not shown), ApNp3 (Figure 6, *H*) and free drug (Figure 6, *I*). A quantitative measurement of the effect of ApNp3 and free apigenin on HAF lesions and total area of the lesions (Table 4**)** showed that ApNp3 predominantly reduced number and total area of lesions and cancer incidence compared to API treatment.

Marker enzyme assay. Cytochrome P-450 (cyt p-450) content, glutathione-S-transferase (GST) activity in cytosolic fraction and, UDP-glucoronyl transferase (UDPGT) activity in microsomal hepatic fraction of the experimental animals were tabulated in Supplementary Table 2. In our study, cyt P-450 content was found to reduce in group B (HCC control) animals both in tumor tissues as well as in tumor surrounding tissue in comparison with the normal rats (Group A). ApNp3 treated HCC animals (Group C) markedly increased cyt P-450 content in the tumor area when compared with group B (HCC) animals. On the other hand, GST and UDPGT activities were found to increase predominantly in tumor areas of group B rats in comparison with the normal rats. Activities of the two enzymes significantly decreased in tumor area after the ApNp3 treatment in group C rats indicating the effect of apigenin nanoparticles in repairing or delaying the progress of HCC in rats.

Discussion

In recent times apigenin has gained much popularity as a naturally occurring flavonoid which has much lower intrinsic toxicity on normal cells compared to cancer cells while used as a tumor-suppressive agent.[37] There are very few reports published to date, which showed tumor suppressive effect of apigenin against HCC *in-vivo*.[14, 38–40] All these studies indicated a much higher dosing of apigenin required to acquire the therapeutic activity. To the best of our knowledge, this is the first report showing that apigenin nanoparticles successfully delayed the progress of HCC. Another uniqueness of our study was that the investigation showed *in-vivo* localization of apigenin-loaded nanoparticle as well as their tissue distribution by gamma scintigraphy. The investigations further support the hypothesis that site specific (liver) delivery of ApNp may ensure a successful treatment to control the progress of HCC.

FTIR data indicated the absence of chemical reaction (electrovalent or covalent type reactions) and rather suggested for physical interactions that might be involved in the formation of structure of the nanoparticles.

Developed nanoparticles were of spherical shape, smooth surface and within a size range of 250-400 nm which fulfills the primary requirements for efficient drug delivery to the target site as large particles (more than 150 nm) are mainly accumulated in liver.[41] A lower PDI value suggests a narrow range of size distribution of particles.[42] Nanoparticles with zeta potential ranging from −30 mV to +30 mV, have a tendency to settle down quickly as compared to those having zeta potential range >+30 mV or <−30 mV which generally form colloidal dispersion. [43, 44] But the particles with zeta potential values ranging from −30 mV to +30 mV never settle down so quickly that they would not be administered intravenously. They should be stored in a powder from (at 4-8 °C) and suspended in saline solution or water for injection and shaken well before administration. ApNp3 had 19.14% drug loading and was found to be stable at least for 90 days (period of study) at 4-8 °C.

A variable hydrolytic degradation of nanoparticles was observed in different pH buffers. Nanoparticles were found to

be more stable in bicarbonate buffer (pH 10) and PBS (pH 7.4) in comparison with acetate (pH 5) and citrate (pH 3) buffers. ApNp3 was stable in mouse serum at least for 24 h.

ApNp3 had an initial burst release of apigenin (24% in 6 h) in PBS (pH. 7.4) followed by a sustained drug release pattern (52% in 60 days). Burst release might have occurred due to a comparatively faster release of drug molecules present close to the surface of the nanoparticles and a subsequent sustained release of drug occurred due to the release of drug molecules from the deeper region of the matrix as the drug molecules had to traverse more distance through the tortuous complex network pathways through the polymeric matrix.[19] A good linearity (as assessed by R^2 value) has favored that drug diffusion followed Korsmeyer–Peppas kinetics with an anomalous diffusion pattern.[3] Drug release was affected and altered by different pH values of the medium. Apigenin released fast in acidic pH (both in pH 3 and 5) due to the degradation of PLGA in acidic media.

FITC labeled ApNp3 showed much higher cytotoxicity in Hep-G2 and Huh-7 cells in comparison to free apigenin due to higher cellular uptake and a sustained release of drug over time as supported by confocal microscopic data, flow cytometric images and quantification by LC-MS/MS. Concisely, the nanoparticles were internalized more by the hepatocellular carcinoma cells in a time-dependent manner.

^{99m}Tc-ApNp3 was found to accumulate predominantly in liver (the targeted organ in this study). The findings support the fact that there was a preferential hepatic distribution of ApNp3 than free apigenin (API). Further, apigenin loaded radiolabeled nanoparticles were also found to reach the livers of animals with HCC due to their nano-size and predominantly accumulated in hepatic tissue. Although the average particle sizes were 200 nm (ApNp3) and 400 nm (FITC-ApNp5) respectively, for two different formulations, they had size distribution ranges that varied from 30 to 500 nm. Hence some of the smaller particles might have eliminated faster which were visualized in the figure. However, numbers of published reports also showed that various nanocarriers size ranging from 150 to 250 nm and labeled with ^{99m}Tc, were detected in kidney and urinary bladder as well as in urine.[45, 46]

The biodistribution data obtained from radiolabeled ApNp3/apigenin were further supported by the data obtained by LC-MS/MS determination. Various pharmacokinetic parameters in mice plasma and liver (up to 72 h) showed much higher AUC and lower clearance rate of ApNp3 in comparison with API in both plasma and liver. This could be possibly responsible for more bioavailability of apigenin from ApNp3 than API. Difference in half-lives also suggests that apigenin from nanoparticles (half-life of apigenin from ApNp3 in plasma and hepatic circulation were 70.7±4.3 and 25.1±1.1 h respectively), followed a sustained release pattern. Plasma and hepatic clearance values reveal that ApNp3 caused reduction of apigenin clearance predominantly and assisted its longer presence in the body. Plasma protein binding of apigenin is predominantly long and release of drug from the plasma protein is comparatively much slower.[17, 18] Hence $t_{1/2}$ of the drug in the blood was comparatively more than its value in liver. Initially nanoparticles taken up by the liver maintained the hepatic level of the drug. However, faster hepatic metabolism and elimination of larger nanoparticles and very slow distribution of plasma protein bound drug to liver at the extended period could be responsible for shorter hepatic half-life of the drug in animals.

Significant anti-cancer potential of the optimized nanoparticles containing apigenin (ApNp3) in rats bearing HCC was observed. The efficiency of this formulation was achieved in controlling the tumor incidence and HAF. Predominant lower incidence of HCC development and a gross reduction of HAF upon ApNp3 treatment showed potential antitumor effect of apigenin loaded in nanoparticles on HCC development *in-vivo*.[47, 48] Free apigenin also improved the tissue structure, but not to the extent of ApNp3 mediated improvement. ApNp3 could have acted either on delaying the progress of development of HCC or on regenerating the damage of hepatic tissue towards normal, clearly seen in histopathology study. Presence of apigenin in the tumor area thus could be beneficial for controlling the proliferation of preneoplastic and neoplastic cells, hindering tumor formation.[47, 48] Apigenin has a significant role in tumor suppression by maintaining level of tumor suppressor gene p^{53} in humans.[10] Apigenin loaded nanoparticles and free-apigenin had no noticeable effect on normal liver. Blank nanoparticles also had no effect on normal liver, suggesting that PLGA has no toxic effect in liver at all. Longer availability of apigenin as it released slowly from the nanoparticles and had a much lower clearance rate than free apigenin may be a responsible factor for such potential role of apigenin from ApNp3 than the free drug.

Cyt P-450, GST and UDPGT are well known tumor markers and have been extensively used to evaluate the progress of hepatic tumor development.[26, 28, 48, 49] Hence we have selected these markers to identify any biochemical changes occurred in tumors and the surrounding non-tumor hepatic tissue upon the treatment of ApNp3, as we found that the apigenin content varied in tumor and non-tumor surrounding tissues upon ApNp3 application. Interestingly, we found that modulation of these enzyme activities and iso-enzyme (cyt P-450) content predominantly varied in the tumor area upon nanoparticle treatment as compared to free apigenin treatment. This may be due to the enhanced permeability and retention (EPR) effect of ApNp3 in the solid tumors.[50] Thus, apigenin nanoparticles may serve as a successful line of treatment against HCC or as an adjuvant strategy to improve this disease state and can provide us a new therapeutic option to treat hepatocellular carcinoma patients. Further investigation in the area is warranted.

Appendix A. Supplementary data

Supplementary data to this article can be found online at https://doi.org/10.1016/j.nano.2018.05.011.

References

1. Li HL, Ji WB, Zhao R, Duan WD, Chen YW, Wang XQ, et al. Poor prognosis for hepatocellular carcinoma with transarterial chemoembolization pre-transplantation: retrospective analysis. *Gastroenterol* 2015;**21**(12):3599-606.
2. Weledji EP, Orock GE, Ngowe MN, Nsagha DS. How grim is hepatocellular carcinoma? *Ann Med Surg* 2014;**3**:71-6.
3. Torre LA, Bray F, Siegel RL, Ferlay J, Tieulent JL, Jemal A. Global cancer statistics, 2012. *Clin* 2015;**65**(2):87-108.

4. Jarnagin W, Chapman WC, Curley S, D'Angelica M, Rosen C, Dixon E, et al. Surgical treatment of hepatocellular carcinoma: expert consensus statement. *HPB* 2010;**12**:302-10.
5. Sanyal AJ, Yoon SK, Lencionic R. The etiology of hepatocellular carcinoma and consequences for treatment. *Oncologist* 2010;**15** (4):14-22.
6. Smith RJ. Nutrition and metabolism in hepatocellular carcinoma. *Hepatobiliary Surg Nutr* 2013;**2**(2):89-96.
7. Hootegem AV, Verslype C, Steenbergen WV. Sorafenib-induced liver failure: a case report and review of the literature. *Case Rep Hepatol* 2011;**2011**:1-4, https://doi.org/10.1155/2011/941395.
8. ZhouY Li Y, Zhou T, Zheng S, Li S, Li HB. Dietary natural products for prevention and treatment of liver cancer. *Nutrients* 2016;**8**:1-23.
9. Sung B, Chung HY, Kim ND. Role of apigenin in cancer prevention *via* the induction of apoptosis and autophagy. *J Cancer Prev* 2016;**21** (4):216-26.
10. Chinembiri TN, du Plessis LH, Gerber M, Hamman JH, du Plessis J. Review of natural compounds for potential skin cancer treatment. *Molecules* 2014;**19**:11679-721.
11. Das S, Das J, Samadder A, Paul A, Khuda-Bukhsh AR. Strategic formulation of apigenin-loaded plga nanoparticles for intracellular trafficking, DNA targeting and improved therapeutic effects in skin melanoma in vitro. *Toxicol Lett* 2013;**223**:124-38.
12. Qin Y, Zhao D, Zhou HG, Wang XH, Zhong WL, Chen S, et al. Apigenin inhibits nf-κb and snail signaling, emt and metastasis in human hepatocellular carcinoma. *Oncotarget* 2016;**7**(27):41421-31.
13. Chiang LC, Ng LT, Lin IT, Kuo PL, Lin CC. Anti-proliferative effect of apigenin and its apoptotic induction in human hep g2 cells. *Cancer Lett* 2006;**237**:207-14.
14. Takagaki N, Sowa Y, Oki T, Nakanishi R, Yogosawa S, Sakai T. Apigenin induces cell cycle arrest and p21/waf1 expression in a p53-independent pathway. *Oncol* 2005;**26**:185-9.
15. Cai J, Zhao XL, Liu AW, Nian H, Zhang SH. Apigenin inhibits hepatoma cell growth through alteration of gene expression patterns. *Phytomedicine* 2011;**18**:366-73.
16. Lefort EC, Blay J. Apigenin and its impact on gastrointestinal cancers. *Mol Nutr Food Res* 2013;**57**:126-44.
17. Cao H, Chen L, Xiao J. Binding citrus flavanones to human serum albumin: effect of structure on affinity. *Mol Biol Rep* 2011;**38**:2257-62.
18. Gradolatto A, Basly JP, Berges R, Teyssier C, Chagnon MC, Siess MH, et al. Pharmacokinetics and metabolism of apigenin in female and male rats after a single oral administration. *Drug Metab Dispos* 2004;**33**:49-54.
19. Das PJ, Paul P, Mukherjee B, Mazumder B, Mondal L, Baishya R, et al. Pulmonary delivery of voriconazole loaded nanoparticles providing a prolonged drug level in lungs: a promise for treating fungal infection. *Mol Pharm* 2015;**12**:2651-64.
20. Mirakabad MST, Koshki KN, Akbarzadeh A, Yamchi MR, Milani M, Zarghami N, et al. PLGA-based nanoparticles as cancer drug delivery systems. *Cancer Prev* 2014;**15**(2):517-35.
21. Maji R, Dey NS, Satapathy BS, Mukherjee B, Mondal S. Preparation and characterization of tamoxifen citrate loaded nanoparticles for breast cancer therapy. *Nanomed* 2014;**9**:3107-18.
22. Abouelmagd SA, Sun B, Chang AC, Ku YJ, Yeo Y. Release kinetics study of poorly water-soluble drugs from nanoparticles: are we doing it right? *Mol Pharm* 2015;**12**(3):997-1003.
23. Mandal D, Shaw TK, Dey G, Pal MM, Mukherjee B, Bandyopadhyay AK, et al. Preferential hepatic uptake of paclitaxel-loaded poly-(D-L-lactide-co-glycolide) nanoparticles — a possibility for hepatic drug targeting: Pharmacokinetics and biodistribution. *Biol Macromol* 2018;**112**:818-30.
24. Shaw TK, Mandal D, Dey G, Pal MM, Paul P, Chakraborty S, et al. Successful delivery of docetaxel to rat brain using experimentally developed nanoliposome: a treatment strategy for brain tumor. *Drug Deliv* 2017;**24**(1):346-57.
25. Gaonkar RH, Gangul S, Dewanjee S, Sinha S, Gupta A, Ganguly S, et al. Garcinol loaded vitamin E TPGS emulsified PLGA nanoparticles: preparation, physicochemical characterization, *in vitro* and *in vivo* studies. *Sci Rep* 2016;**7**:1-14.
26. Satapathy BS, Mukherjee B, Baishya R, Debnath MC, Dey NS, Maji R. Lipid nanocarrier-based transport of docetaxel across the blood brain barrier. *RSC Adv* 2016;**6**:85261-74.
27. Dong X, Lan W, Yin X, Yang C, Wang W, Ni J. Simultaneous determination and pharmacokinetic study of quercetin, luteolin, and apigenin in rat plasma after oral administration of matricaria chamomilla l. extract by HPLC-UV. *Evid Based Complement Alternat Med* 2017:1-7.
28. Ghosh MK, Patra F, Ghosh S, Hossain CM, Mukherjee B. Antisense oligonucleotides directed against insulin-like growth factor-II messenger ribonucleic acids delay the progress of rat hepatocarcinogenesis. *J Carcinog* 2014;**13**(2):1-17.
29. Hu XY, Liang JY, Guo XJ, Liu L, Guo YB. 5-Fluorouracil combined with apigenin enhances anticancer activity through mitochondrial membrane potential ($\Delta\Psi$m)-mediated apoptosis in hepatocellular carcinoma. *Clin Exp Pharmacol Physiol* 2015;**42**(2):146-53.
30. Das T, Patra F, Mukherjee B. Effect of antisense oligomer in controlling c-raf.1 overexpression during diethylnitrosamine-induced hepatocarcinogenesis in rat. *Cancer Chemother Pharmacol* 2010;**65**:309-18.
31. Omura T, Sato R. The carbon monoxide-binding pigment of liver microsomes. I. Evidence for its hemoprotein nature. *J Biol Chem* 1964;**239**:2370-8.
32. Ahn D, Putt D, Kresty L, Stoner GD, Fromm D, Hollenberg PF. The effects of dietary ellagic acid on rat hepatic and esophageal mucosal cytochromes P450 and phase II enzymes. *Carcinogenesis* 1996;**17** (4):821-8.
33. Singhvi G, Sing M. Review: in-vitro drug release characterization models. *Pharm Stud Res* 2011;**2**(1):77-84.
34. Kim EY, Yu JS, Yang M, Kim AK. Sub-toxic dose of apigenin sensitizes HepG2 cells to TRAIL through ERK-dependent up-regulation of TRAIL receptor DR5. *Mol Cells* 2013;**35**(1):32-40.
35. Kim BR, Jeon YK, Nam MJ. A mechanism of apigenin-induced apoptosis is potentially related to anti-angiogenesis and anti-migration in human hepatocellular carcinoma cells. *Food Chem Toxicol* 2011;**49**:1626-32.
36. Mathai AM, Alexander J, Kuo FY, Torbenson M, Swanson PE, Yeh MM. Type II ground-glass hepatocytes as a marker of hepatocellular carcinoma in chronic hepatitis B. *Hum Pathol* 2013;**44**(8):1665-71.
37. Madunić J, Madunić IV, Gajski G, Popić J, Garaj-Vrhovac V. Apigenin: A dietary flavonoid with diverse anticancer properties. *Cancer Lett* 2018, https://doi.org/10.1016/j.canlet.2017.
38. Jeyabal PVS, Syed MB, Venkataraman M, Sambandham JK, Sakthisekara D. Apigenin inhibits oxidative stress-induced macromolecular damage in N-nitrosodiethylamine (NDEA)-induced hepatocellular carcinogenesis in Wistar albino rats. *Mol Carcinog* 2005;**44**:11-20.
39. Singh JP, Selvendiran K, Banu SM, Padmavathi R, Sakthisekaran D. Protective role of apigenin on the status of lipid peroxidation and antioxidant defense against hepatocarcinogenesis in Wistar albino rats. *Phytomedicine* 2004;**11**(4):309-14.
40. Shukla S, Gupta S. Apigenin: A promising molecule for cancer prevention. *Pharm Res* 2010;**27**(6):962-78.
41. Blanco E, Shen H, Ferrari M. Principles of nanoparticle design for overcoming biological barriers to drug delivery. *Nat Biotechnol* 2015;**33** (9):941-51.
42. Masarudin MJ, Cutts SM, Evison BJ, Phillips DR, Pigram PJ. Factors determining the stability, size distribution, and cellular accumulation of small, monodisperse chitosan nanoparticles as candidate vectors for anticancer drug delivery: application to the passive encapsulation of [^{14}C]-doxorubicin. *Nanotechnol Sci Appl* 2015;**8**:67-80.
43. Meißner T, Potthoff A, Richter V. Suspension characterization as important key for toxicological investigations. *J Phys Conf Ser* 2009;**170** (1):1-6.
44. Basu S, Mukherjee B, Chowdhury SR, Paul P, Choudhury R, Kumar A, et al. Colloidal gold-loaded, biodegradable, polymer-based stavudine

nanoparticle uptake by macrophages: AN in vitro study. *Nanomed* 2012;**7**:6049-61.
45. Yu M, Zheng J. Clearance pathways and tumor targeting of imaging nanoparticles. *ACS Nano* 2015;**9**:6655-74.
46. Polyak A, Palade EA, Balogh L, Posteny Z, Haasz V, Janoki G, et al. In vitro and biodistribution examinations of Tc-99m-labelled doxorubicin-loaded nanoparticles. *Nucl Med Rev* 2011;**14**:55-62.
47. Schlageter M, Terracciano ML, D'Angelo S, Sorrentino P. Histopathology of hepatocellular carcinoma. *Gastroenterol* 2014;**20**(43):15955-64.
48. Yan X, Qi M, Li P, Zhan Y, Shao H. Apigenin in cancer therapy: anti-cancer efects and mechanisms of action. *Cell Biosci* 2017;**7**:1-16.
49. Yan T, Lu L, Xie C, Chen J, Peng X, Zhu L, et al. Severely impaired and dysregulated cytochrome P450 expression and activities in hepatocellular carcinoma: implications for personalized treatment in patients. *Mol Cancer Ther* 2015;**14**(12):2874-86.
50. Kobayashi H, Watanabe R, Choyke PL. Improving conventional enhanced permeability and retention (EPR) effects; what is the appropriate target. *Theranostics* 2014;**4**(1):81-9.

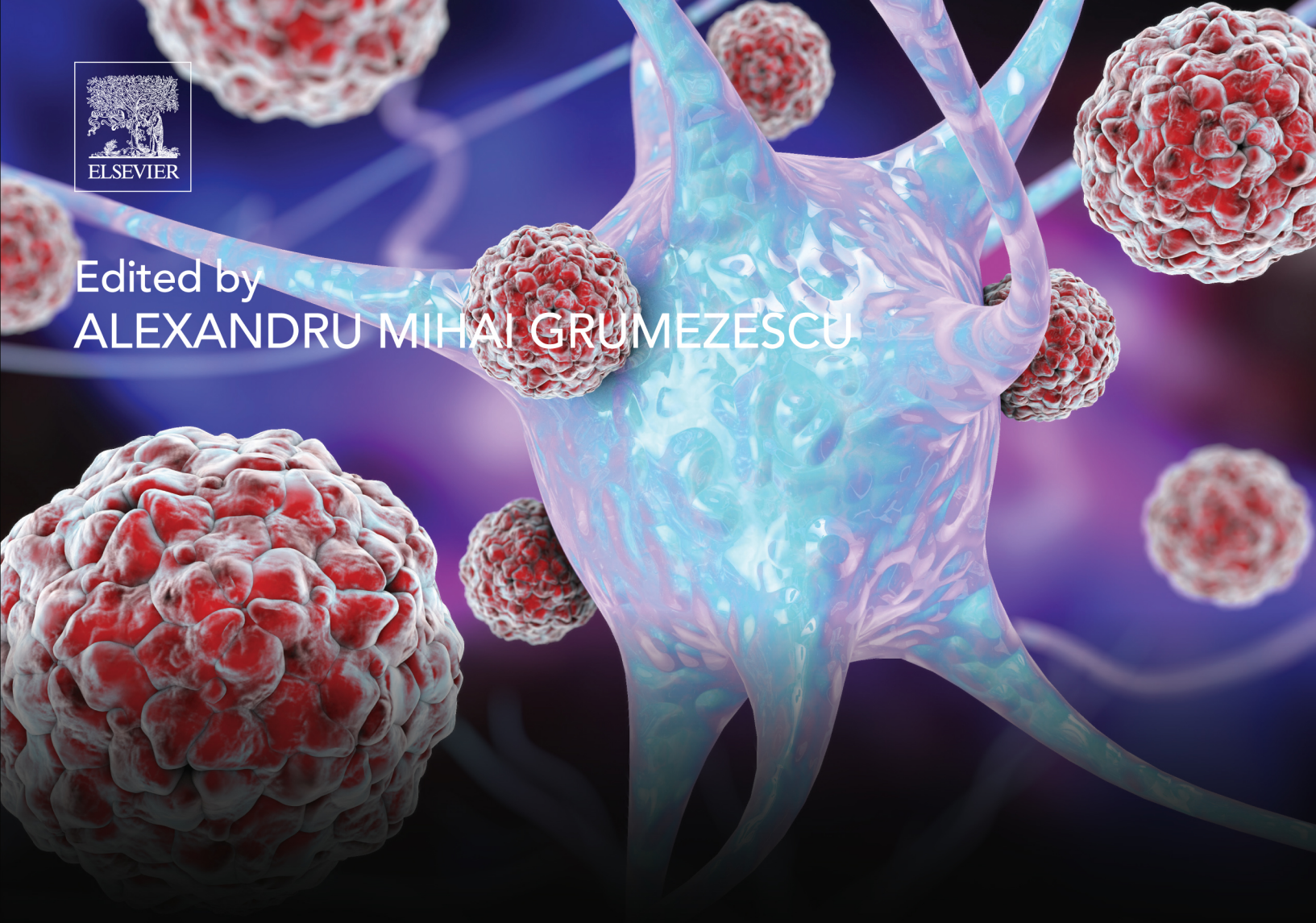

Edited by
ALEXANDRU MIHAI GRUMEZESCU

MULTIFUNCTIONAL SYSTEMS FOR COMBINED DELIVERY, BIOSENSING AND DIAGNOSTICS

Chapter 14

Pulmonary Administration of Biodegradable Drug Nanocarriers for More Efficacious Treatment of Fungal Infections in Lungs: Insights Based on Recent Findings

Biswajit Mukherjee, Paramita Paul, Lopamudra Dutta, Samrat Chakraborty, Moumita Dhara, Laboni Mondal and Soma Sengupta

Jadavpur University, Kolkata, West Bengal, India

Chapter Outline

1 INTRODUCTION

Ever since BC 2000, the inhalation route was exploited for the treatment of diseases. Especially Chinese and Indian people used to inhale the smoke from burned herbal preparations, such as *Ephedra sinica* or *Datura stramonium*, to treat asthma. Pedanius Dioscorides, the eminent Greek pharmacologist, botanist, and surgeon, came up with *De Materia* (first pharmacopoeia) (Andrade et al., 2013). He and Aelius Galenus (127–199/217 AD) treated their patients with sulfur vapor by inhalation route. The word *inhaler* was first coined by English physician John Mudge, in 1778 (Anderson, 2005) while

Multifunctional Systems for Combined Delivery, Biosensing and Diagnostics. http://dx.doi.org/10.1016/B978-0-323-52725-5.00014-9

describing his invention. However, Hippocrates is recognized as the pioneer for designing the first therapeutic inhalation device. Since then, a plethora of compounds and mixtures, such as solution of picric acids, tar, iodine, have been utilized for the treatment of an array of diseases, for example, tuberculosis and other infectious diseases, by using a wide variety of methods, such as ceramic inhalers, combustible papers, burning papers, liquid atomizers, etc. During 19th and 20th centuries, asthma cigarettes became one of the popular ways to deliver drugs, but these were withdrawn in 1992 (Dessanges, 2001). According to the reports published in the literatures (Anderson, 2005; Andrade et al., 2013; Dessanges, 2001), it has been the well-known fact that antibiotic, such as penicillin, was administered by nebulization for the treatment of pulmonary infections. At the present time, inhalation devices are categorized into three different types, such as nebulizers, pressurized metered dose inhalers (pMDI), and dry powder inhalers (DPI). The inhalation route has started its journey for the treatment of diseases primarily confined into the respiratory tract. However, significant scientific and technological advances have led to a change in the paradigm and, in modern times, this route has found its potential for the treatment of a battery of local and systemic diseases, such as asthma, tuberculosis, and other bacterial infections, fungal infections, cystic fibrosis, chronic obstructive pulmonary disease, diabetes, or cancer, as well as being investigated for noninvasive vaccination (Andrade et al., 2013).

The lungs and airways, acting as principal sites of gas exchange, are exposed to a wide variety of organic, inorganic, and biological components, causing as a location for wide varieties of diseases. Therefore, the lung is very prone to an array of bacterial, fungal, and viral infections, and often it promotes systemic infections as a result. As per the mortality rate, the infections of lower respiratory tract stand on the third position globally, but they stand at the first position in developing countries, being responsible for approximately 3.5 million deaths annually (Mansour et al., 2009). This has instigated a lot of interests among the researchers around the globe to exploit the lungs for the pulmonary administration of active pharmaceutical ingredients in the form of various delivery systems. Moreover, this route offers a significant promise due to its potential advantages over peroral administrations, such as avoidance of first-pass metabolism, allowing targeted delivery to the site of action, resulting in a decrease in the side effects of the drug, high surface area responsible of local drug action, as well as systemic absorption of drugs, etc. (Yang et al., 2008a).

Among many of the existing delivery systems to become ideal carriers for pulmonary delivery, colloidal carriers (nanocarriers) have instigated a lot of interest among the researchers around the globe, due to their enormous potential as drug delivery vehicles (Andrade et al., 2013; Mansour et al., 2009; Marianecci et al., 2011; Patton and Byron, 2007; Yang et al., 2008a). A few of them are:

1. They are very much capable of maintaining relatively uniform distribution of drugs among the alveoli.
2. They have the potential to enhance the solubility of drugs, as compared to the inherent aqueous solubility of chemical entities.
3. They provide sustained release of drugs that improves the pharmacokinetic profile of drugs, reduces dosing frequency and side effects, resulting in better therapeutic outcome and patient compliance.
4. They are biocompatible, biodegradable, as well as being able to deliver macromolecules.

Particle size solely determines the deposition of particles in different regions of lungs and, based on it, the three different mechanisms of drug deposition, namely, impaction, sedimentation, and diffusion have been proposed. In the impaction process, particles collide with the walls of the respiratory walls under the influence of the centrifugal force, and are deposited in the oropharynx region. Generally the DPI and MDI with a particle size larger than 5 μm follow this mechanism. For DPI, deposition of particles primarily depends on the inspiratory capability of patients and, if it is insufficient, dry powders deposit in the upper airways due to the mass of the particles and the inertial forces. Similarly, larger particles of MDI tend to deposit mostly in the upper respiratory tract, even under the influence of high speeds of the generated aerosols. In the case of sedimentation, the gravitational force is solely responsible, and particles with a size in the range of 1–5 μm follow this mechanism and deposit slowly in the smaller airways and bronchioles (Paranjpe and Goymann, 2014). Therefore, breathing pattern has a strong impact on the sedimentation, as it is evident that slow breathing provides sufficient duration span for sedimentation (Andrade et al., 2013; Mansour et al., 2009; Paranjpe and Goymann, 2014).

In diffusion process, Brownian motion is considered to be the major player and, due to this motion, particles move randomly, resulting in the dissolution of API in alveolar fluid upon contact with lungs surfactant, and finally deposit into deeper alveolar tissue (Yang et al., 2008a).

Nanoparticulate drug delivery systems (DDSs) deliver their therapeutic payloads through the process of sedimentation. Upon being released from the aerosol, they form aggregates that are found to have sufficient mass to sediment and deposit in the bronchiolar region.

Results obtained from many studies involving the development of nanoconstructs for pulmonary delivery, encapsulating a plethora of therapeutic payloads, are of great promise, requiring the establishment of clinical relevance in clinical trials. Apart from that, numerous other parameters, such as large-scale production, batch-to-batch reproducibility, variable lung

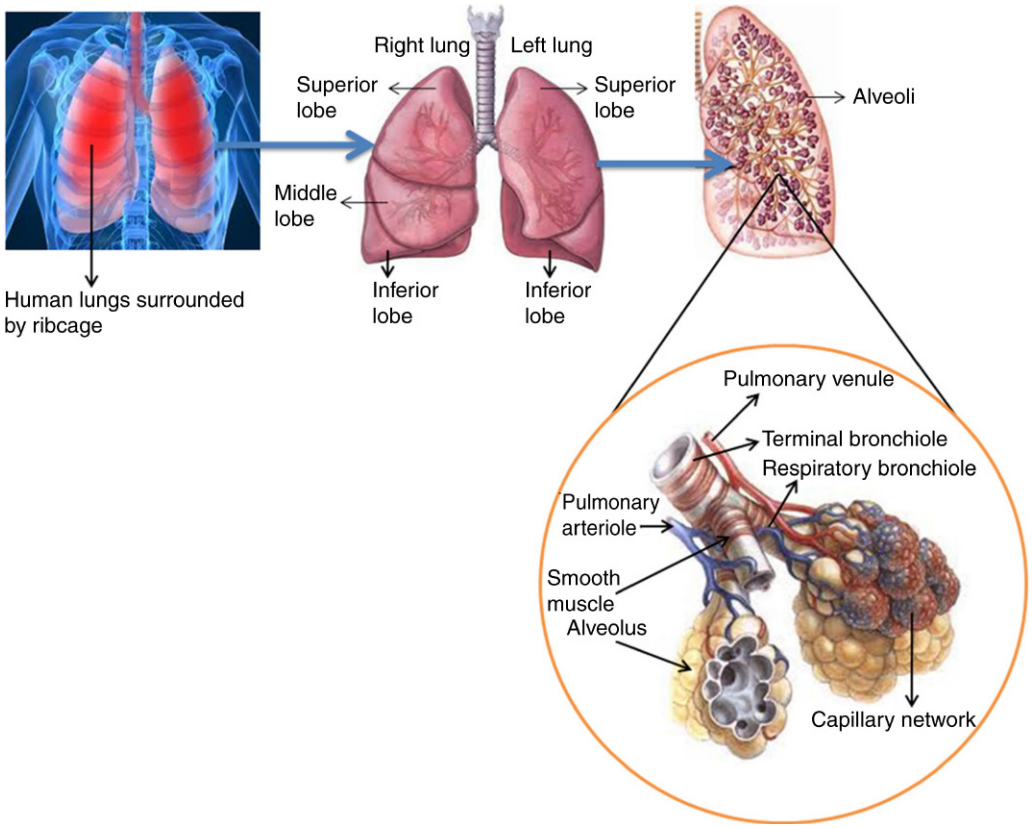

FIGURE 14.1 Diagrammatic representation of lung morphology and anatomy, showing structure of bronchioles.

deposition pattern, and cost effectiveness should be addressed properly, to ease the translation for pulmonary delivery of drug nanocarrier from laboratories to clinic.

Therefore, the focus of the present chapter is to establish the rationale and potentials of the pulmonary route for the treatment of fungal infections in lungs, for a better therapeutic management, and improved patient compliance. The chapter describes the advantages of various pulmonary delivery systems, with a special emphasis on nanocarriers.

2 LUNG MORPHOLOGY

The lungs, the gaseous exchange center of the human body, are surrounded by the chest wall, and separated by the mediastinum from the heart and other organs (positioned in the thoracic cavity) (Fig. 14.1). The left lung is constituted with two lobes, namely superior and inferior, separated by an oblique fissure, while the right lung has three lobes, that is, superior, middle, and inferior lobes, divided by oblique and horizontal fissures (Sahasrabudhe et al., 2013). The tube-like air pipe trachea acts as the passage for the air to the chest and neck; it is divided in two main branches, bronchi, each of which enters into each lung. Outside the lungs, the pleura (a balloon-like structure), the covering membrane, protects the lungs (Lai-Fook, 2004), and at the same time it produces a lubricating fluid that causes the smooth movement of lungs in the chest cavity. The main bronchi are branched into smaller bronchi that again are divided into smaller branchings known as bronchioles. The bronchi contain small glands and cartilage, while bronchioles do not contain the same. Outside the bronchi, there is a lining of cells having tiny hairs called cilia (American Lung Association, 2015). This part executes the first line of defense of lungs in fighting against bacterial or viral infection. Bronchi gradually form a tree-like branching, and become smaller. At the end part of this there is formed a grape-like structure, known as alveoli. These are small, thin air sacs that are normally surrounded by a "hair net" of capillaries. The alveolar walls are mostly constituted with type I alveolar squamous cell through which exchange of gas occurs.

3 LUNG FUNGAL INFECTION

Lungs are susceptible to fungal infections, as it is a primary passage of fungi causing deep mycosis (Panda, 2004). Several types of lung fungal infections are described further.

3.1 Aspergillosis

In recent years, aspergillus infection in lungs is very predominant. The reason may be primarily due to various factors, such as random use of corticosteroids and various immunomodulating drugs, increasing human immunodeficiency virus infection, large number of immunosuppressed patients caused by solid organs and bone marrow transplantation, etc. *Aspergillus* species are the main causative agent of aspergillosis (Thompson and Patterson, 2008). Its pathological reactions can be manifested in humans in different ways, such as allergic bronchopulmonary aspergillosis (ABPA), allergic alveolitis, aspergilloma, invasive aspergillosis, etc. (Davies and Saros, 1994; Fraser et al., 1994; Panda, 2004).

3.1.1 Allergic Bronchopulmonary Aspergillosis

ABPA, a hypersensitive reaction as aspergillus forms colonies in the bronchi, is the most common manifestation of aspergillus pulmonary disease (Greenberger, 2002). The main cause of its occurrence is due to abrupt inhalation of a large amount of aspergillus spores. Prolonged contact to aspergillus spores may exaggerate immune-mediated bronchial pathology, and often this may lead to asthma. This is generally known as ABPA. It is found that more than 20% of asthma cases exhibit ABPA (Panda, 2004).

3.1.2 Allergic Alveolitis

As described earlier, this is also caused by rapid inhalation of a huge quantity of aspergillus spores, and it is mostly manifested among the people working in moldy hay or managing compost dumps. The symptoms of allergic alveolitis, likely in form of influenza and dry cough, may appear 4–9 days later (Davies and Saros, 1994; Fraser et al., 1994; Panda, 2004).

3.1.3 Aspergillomas

Aspergillomas, also known as fungal balls, are normally found in injured or scarred lung tissue, such as bronchiectatic areas or preexisting cavities. These cavities are the very productive zone for mycelia growth, and eventually they produce a ball-like structure that maneuvers independently without entering into the blood vessel or viable tissue. Some predictive factors of this disease are growing size or number of aspergillomata, higher *Aspergillus*-specific IgG titers, immunosuppression, human immunodeficiency virus infection, lung transplantation, etc. (Addrizzo-Harris et al., 1997; Panda, 2004; Zmeili and Soubani, 2007). Aspergillomas may be the reason of hemoptysis, and this may be lethal in rare cases (Denning et al., 2003).

3.1.4 Invasive Aspergillosis

Invasive aspergillosis, the main reason of immunosuppressed patients' morbidity and death, is caused by the invasion of aspergillus fungus into viable tissue, causing tissue necrosis (Panda, 2004; Patterson et al., 2000). Mostly four types of *Aspergillus* species are liable for invasive aspergillosis, such as: *A. fumigatus*, *A. terreus*, *A. flavus*, and *A. niger*. Among all, *A. fumigatus* is the causative organism of more than 90% of such disease (Patterson et al., 2000). Examples of some invasive aspergillosis types are mentioned further.

3.1.4.1 Invasive Pulmonary Aspergillosis

One of the most prevalent forms of the invasive disease is invasive pulmonary aspergillosis (IPA). Usually after 10–14 days of hematopoietic stem cell transplantation, IPA is manifested and is normally coupled with intense granulocytopenia. Fever, pleuritic chest pain, dry cough, dyspnea, and hemoptysis are the common symptoms of IPA (Smith and Kauffman, 2012; Thompson and Patterson, 2008).

3.1.4.2 Tracheobronchial Aspergillosis

Typically tracheobronchial aspergillosis is noticeable among the patients of AIDS, or who have undergone lung transplants. Cough, fever, chest pain, and hemoptysis are few nonspecific symptoms of such aspergillosis (Thompson and Patterson, 2008).

3.1.4.3 Chronic Forms of Pulmonary Aspergillosis

Semiinvasive pulmonary aspergillosis and/or chronic necrotizing pulmonary aspergillosis are found at the lower respiratory tract, as aspergillosis spectrum. Chronic necrotizing pulmonary aspergillosis refers to chronic respiratory symptoms, cavitary lung disease, and serum precipitating antibodies to *Aspergillus* species (Hope et al., 2005; Thompson and Patterson, 2008).

3.2 Fusariosis

Out of nearly hundred species of *Fusarium*, only few of them, such as *F. solani*, *F. moniliforme*, and *F. oxysporum* are the sources of about 90% of human fungal fusariosis infection. The symptoms of fusariosis are quite similar with *Aspergillus*, such as fever, chest pain, cough, dyspnea, and pleurisy (Nucci and Anaissie, 2002; Torres and Kontoyiannis, 2011).

3.3 Mucormycosis

Mucormycosis is a fungal infection caused by Mucorales. Among three genera, such as *Rhizopus*, *Rhizomucor*, and *Mucor*, they cause 75% of mucormycosis (Kontoyiannis et al., 2010). The infection occurs in upper airways in the form of granulomatous invasion, and may gradually move forward into sinuses and/or brain tissue. A mortality rate of approximately 80% has been reported due to this infection (Panda, 2004). Mucorales species are very much susceptible to angioinvasion that may turn into tissue necrosis, and impaired immunity. Patients suffering from hematological malignancy with neutropenia, hematopoietic cell transplant recipients, diabetics, and immunocompromised hosts are vulnerable to pulmonary mucormycosis infection. The most common symptoms of mucormycosis are cough, chest pain, dyspnea, and hemoptysis (Roden et al., 2005; Smith and Kauffman, 2012).

3.4 Scedosporiosis

Scedosporium boydii complex consisting in *S. boydii*, *S. apiospermum*, and *S. aurantiacum*, and *S. prolificans* are very common fungi among *Scedosporium* species (Gilgado et al., 2009). Hematopoietic cell transplant recipients, solid organ transplant recipients, and patients suffering from hematological malignancies are prone to scedosporiosis. *S. prolificans* is able to sporulate in vivo, possibly causing greater risk of antifungal drug resistance. This phenomenon makes *S. prolificans* very unique from most other fungi (Husain et al., 2003; Rodriguez-Tudela et al., 2009).

3.5 Blastomycosis

Blastomyces dermatitidis, a dimorphic fungus, causes blastomycosis (Saccente and Woods, 2010). In case of acute pulmonary infection due to *B. dermatitidis*, patients may remain asymptomatic or may suffer from fever, dyspnea, dry cough, and mild chest pain (Smith and Kauffman, 2010). Chronic pulmonary blastomycosis may result in upper lobe cavitary lesions that may look similar to tuberculosis or histoplasmosis, or mass-like lesions. The lesions may often look like a cancerous lesion. In the infection, symptoms, such as fever, fatigue, night sweats, cough with purulent sputum and hemoptysis, weight loss, and dyspnea, may persist for weeks. The most familiar appearance of disseminated extrapulmonary blastomycosis is observed as cutaneous lesions (Smith and Kauffman, 2012). Less severe pulmonary infection by this fungus comprises mass lesions, single or multiple nodules, lobar pneumonia, and chronic fibrocavitary or fibronodular infiltrates (Limper et al., 2011).

3.6 Cryptococcosis

Cryptococcus neoformans causes cryptococcosis. However, *Cryptococcus gattii* is also responsible for cryptococcosis. *Cryptococcus* (that remains in nature in an encapsulated form) randomly produces a polysaccharide capsule while entering in the pulmonary region (Byrnes et al., 2009; Limper et al., 2011). Cryptococcosis is restricted to the lungs in immunocompetent host, and it commonly exists in patients with chronic ailments of lungs. Immunocompetent host with cryptococcosis infection may not always show symptoms. However, it may exhibit as dry cough, fever, and dyspnea that may lead to acute respiratory distress syndrome in case of immunocompromised patients (Baddley et al., 2008; Chang et al., 2006; Pappas et al., 2001).

3.7 Coccidioidomycosis

Normally two species of *Coccidioidomyces*, such as *C. immitis* and *C. posadasii*, are most commonly found. In the environment, coccidioides that are present as mold form are simply inhaled into the alveoli. These molds convert into spherules consisting of endospores in the lungs and, after maturation, these spherules split and discharge the endospores that cause coccidioidomycosis infection (Ampel, 2011; Smith and Kauffman, 2012). *Coccidioides* infections usually are asymptomatic. However, fever, dry cough, fatigue, dyspnea, and anterior chest pain may be manifested for coccidioidomycosis. For about 5%–10% of the patients, acute pneumonia complication occurs (Ampel, 2011; Anstead and Graybill, 2006). Acute

pulmonary coccidioidomycosis can be different from community-acquired pneumonia due to limited response to antibacterial treatment, as well as peripheral blood eosinophilia, hilar adenopathy, and existence of erythema nodosum, and erythema multiforme (Valdivia et al., 2006).

3.8 Histoplasmosis

Histoplasma capsulatum, the cause of histoplasmosis, is found as a mold in nature, and as yeast inside tissues. Inhalation of *H. capsulatum* into the alveoli causes infection into humans. Pulmonary histoplasmosis may lead to acute self-limited pneumonia that may appear in the form of dry cough, mild chest discomfort, fever, and fatigue. Often in the case of immunosuppressed patients, severe pneumonia may appear and, in some cases, it may lead to acute respiratory distress syndrome. One of the exceptional difficulties of pulmonary histoplasmosis is mediastinal fibrosis. Symptoms of this pulmonary histoplasmosis are cough, wheezing, dyspnea, and hemoptysis. But symptoms that persist for a month may vary in case of chronic cavitary pulmonary histoplasmosis. Examples of such symptoms are fever, anorexia, fatigue, weight loss, hemoptysis, and cough with purulent sputum, etc. (Kauffman, 2007; Wheat et al., 2004).

4 TREATMENT OF LUNG FUNGAL INFECTION

Voriconazole is used as first-line treatment for pulmonary aspergillosis (Herbrecht et al., 2002; Limper et al., 2011; Walsh et al., 2008). Posaconazole is also considered as an effective treatment of aspergillosis, however not approved as primary agent (Walsh et al., 2007). Echinocandins are used as second-line therapy, and/or echinocandins with voriconazole combination are applied to increase antifungal action for this purpose (Limper et al., 2011; Walsh et al., 2008).

Posaconazole and voriconazole are considered as the primary drugs for the treatment of fusariosis (Lortholary et al., 2010; Raad et al., 2006). Besides, some physicians also use lipid formulations of amphotericin B (AmB) or combination of AmB lipid formulation with voriconazole (Ho et al., 2007).

AmB is considered as the preferred drug for mucormycosis. Lipid-based formulations of AmB show better drug efficacy, as compared to the original deoxycholate formulation. Besides azole groups, posaconazole is used for step-down therapy (Lewis et al., 2010).

Voriconazole is used as a primary drug for the treatment of *S. apiospermum* and *S. prolificans* (Troke et al., 2008), and posaconazole is also considered to be effective (Torres et al., 2005).

AmB is applied to treat patients with severe blastomycosis, and it is also used for immunosuppressed patients. Once they are stable, azole is used for a few weeks. Itraconazole (ITZ) may be considered as primary agent. On the other hand, voriconazole or fluconazole can be used as second-line treatment (Chapman et al., 2008; Smith and Kauffman, 2010).

In case of cryptococcosis, AmB with flucytosine is used for a few weeks, and fluconazole is used as step-down treatment. Fluconazole is also used for a few months to treat mild to moderate cryptococcosis (Perfect et al., 2010).

AmB can be used to treat severe coccidioidomycosis, and azoles can be used to treat less severe cases (Galgiani et al., 2005). ITZ or fluconazole is used as step-down therapy for long-term treatment of coccidioidomycosis. If azoles fail as the first-line drug, posaconazole and/or voriconazole can be used in that case (Smith and Kauffman, 2012).

AmB is utilized as the preferred therapy for histoplasmosis. For mild to moderate infection, azoles are used as first-line drug and, if AmB produces a positive result as first-line therapy, azoles can be used as step-down therapy in that case. ITZ, voriconazole, and posaconazole are also preferred drugs to treat histoplasmosis (Freifeld et al., 2009; Wheat et al., 2007).

5 CLINICAL STATUS TO TREAT FUNGAL INFECTION BY PULMONARY ROUTE

Local delivery of medications to the lungs is highly desirable, especially in patients with specific pulmonary diseases, such as invasive fungal infection in the lung, cystic fibrosis, asthma, chronic pulmonary infections, or lung cancer. There are many dosage regimens available that are given orally or intravenously to treat these diseases (Table 14.1). But unfortunately till now there is no therapy available through pulmonary route, in spite of having added advantages of directly delivering the drug to the infected lungs.

6 IMPORTANCE OF PULMONARY ROUTE FOR DRUG ADMINISTRATION

The desired efficacy of a therapy mostly depends on the delivery strategy by which a drug is delivered with an optimum concentration. Above or below the maximum and minimum concentrations of a drug at its therapeutic window, it can produce moderate to severe side effects, or provide a subtherapeutic or no effect. Different DDSs already available or currently

TABLE 14.1 Drugs and Dosage Forms Used by the Routes Other Than the Pulmonary Route of Administration to Treat Lung Fungal Infection

Drug	Trade Name of the Formulation	Dosage Form and Route	Manufacturer
AmB	Amphotec	Complex; i.v.	Kadmon Pharmaceuticals, LLC
	Anolip	Lipid Complex; i.v.	Actiza Pharmaceutical
	Ampholip	Lipid Complex; i.v.	Farma glow
	Amphocil	Colloidal dispersion; i.v. infusion	Wintac Ltd.
	Abelcet	Lipid Complex; i.v.	Sigma-Tau Pharmaceuticals, Inc.
	AmBisome	Liposome; i.v. infusion	Mercury Medicare
Natamycin	Natacyn	Suspension; ophthalmic	Alcon Laboratories, Inc.
Nystatin	Nyotran	Lyophilized liposomal formulation; i.v.	Aronex Pharmaceuticals
Terconazole	Terazol 7	0.4% Cream; vaginal application	Janssen Pharmaceuticals, Inc.
Voriconazole	Vfend	Tablets; oral	Pfizer
		Suspension; oral	
		Infusion; i.v.	
ITZ	Sporanox	Solution; oral	Janssen Pharmaceuticals, Inc.
		Capsules; oral	
Tioconazole	Vagistat-1	Ointment; vaginal application	Novartis Consumer Health
Butoconazole nitrate	Gynazole 1	Cream; vaginal application	Ther-Rx and Perrigo Company
Oxiconazole nitrate	Oxistat	Cream; topical application	GlaxoWellcome
Econazole nitrate	Spectazole	Cream; topical application	Janssen Biotech, Inc.
Ketoconazole	Nizoral	2% Shampoo; application in scalp	Janssen-Cilag
	Xolegel	Gel; topical application	Aqua Pharmaceuticals
Fluconazole	Diflucan	Tablets; oral	Pfizer
		Suspension; oral	
		Infusion; i.v.	
Posaconazole	Noxafil	Suspension; oral	Merck
		Delayed-release tablets; oral	
Anidulafungin	Eraxis	Lyophilized product; i.v. infusion	Pfizer
Caspofungin acetate	Cancidas	Lyophilized product; i.v. infusion	Merck & Co., Inc.
Micafungin sodium	Mycamine	Lyophilized product; i.v.	Astellas Pharma Ltd.
Flucytosine	Ancobon	Capsules; oral	Valeant Pharmaceuticals, Inc.
Butenafine HCl	Mentax	Cream; topical application	Mylan Bertek Pharmaceuticals, Inc.
Naftifine hydrochloride	Naftin	Gel; topical application	Merz Pharmaceuticals, LLC
		Cream; topical application	
Terbinafine hydrochloride	Lamisil	Tablets; oral	Novartis
		Granules; oral	
		Gel; topical application	

AmB, Amphotericin B; ITZ, itraconazole; i.v., intravenous.

under development can be efficiently used to minimize drug degradation, prevent toxic adverse effects, and increase the bioavailability of the drugs. The developmental strategy of new formulation involves interdisciplinary approaches coordinating various branches of science and technology, for example, polymer science, pharmaceutical sciences, clinical medicine, molecular biology, etc.

Pulmonary infections caused by *Aspergillus* species are associated with significant morbidity and mortality in immunocompromised patients (Walsh et al., 2008). Although systemic drug delivery is used popularly in the treatment

of pulmonary infections, aerosolized delivery is an attractive option in the prevention of pulmonary fungal infections because the drug can act locally in a site-specific manner, with a higher local concentration, and a minimal systemic exposure.

Growing interest has given to the potential of pulmonary route as a noninvasive administration for both the systemic and local drug delivery of therapeutic agents, because of the high permeability and large area for absorption in lungs (approximately 70–140 m^2 in adult humans, having enormously thin mucosal membrane for absorption), and good blood supply (Groneberg et al., 2001, 2002, 2003). The alveolar epithelium of the distal lung has been shown to be a major absorption site for many of the therapeutics and various macromolecules (Sangwan et al., 2001; Scheuch and Siekmeier, 2007; Tuncer and Nevin, 2007). Further, advantages of pulmonary route of administration over peroral application are the comparatively low enzymatic activity and rapid drug absorption, with a capacity for overcoming hepatic "fast-pass metabolism." Although for a prolonged period drugs have been administered through pulmonary route, current pulmonary drug delivery has become an attractive choice with a remarkable scientific and biomedical interest in the area of healthcare research. It has been already reported that the local respiratory disorders, such as asthma, pulmonary infection, pulmonary hypertension, and some systemic disorders (e.g., diabetes) can be well treated by pulmonary route (Gangurde et al., 2012).

7 PRINCIPAL MECHANISMS OF RESPIRATORY DEPOSITION

The respiratory deposition of inhaled drug particles in the lung is very complex, and deposition is based on many factors. Some of the influencing factors include:

- Breathing rate
- Lung volume
- Respiration volume
- Health of the subject
- Airway bifurcations leading to constant changing of hydrodynamic flow of fluid

Depending on the particle size, respiratory airflow, and structural position in the respiratory system, lung deposition occurs via one of the following principal mechanisms.

7.1 Impaction

The airways bifurcate each time, and suspended particles travel along their original path due to inertia, and impact on the airway walls.

7.2 Sedimentation

Sedimentation is the settling down of particles in the smaller airways. The rate of sedimentation is based on the low airflow rate, mainly in the small airways. Low airflow rate tends to change terminal velocity, and ultimately sedimentation occurs.

7.3 Interception

Interception occurs when a drug particle contacts on airway surface, depending on its physical size and shape.

7.4 Diffusion

Diffusion is a primary mechanism of deposition where the particles go from a region of higher concentration to a lower concentrated region, due to Brownian motion. Diffusional depositions occur mostly in the nasopharynx, and most likely in the smaller airways.

7.5 Absorption

The lung is more permeable to macromolecules, including many more therapeutic peptides and proteins than any other portal of entry into the body. Particularly, peptides that have been chemically altered to inhibit peptidase enzyme exhibit very high bioavailability by the pulmonary route. Small molecules that are highly soluble and cationic can exhibit prolonged absorption.

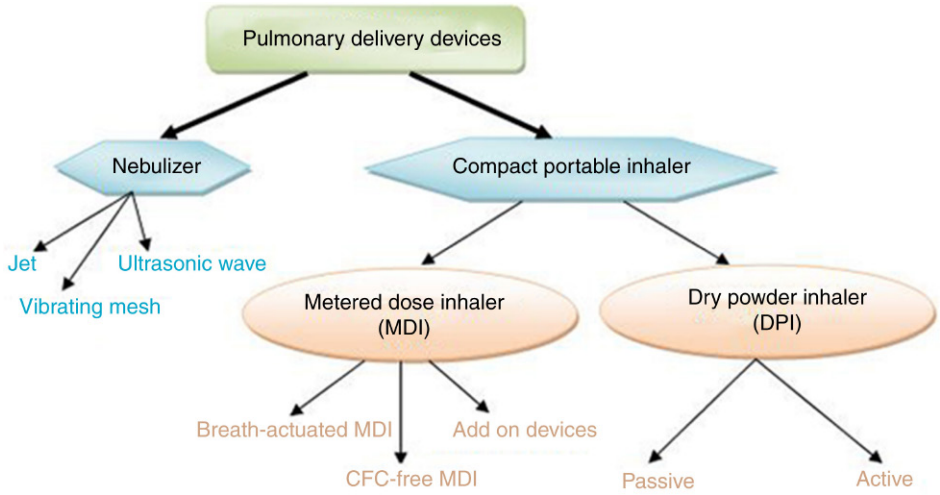

FIGURE 14.2 Evolution of pulmonary delivery devices. *CFC*, Chlorofluorocarbons; *DPI*, dry powder inhalers; *MDI*, metered dose inhalers.

8 PULMONARY DRUG DELIVERY DEVICES

The development of modern inhalation devices can be broadly divided into two categories with various varieties (Fig. 14.2):

1. Nebulizer
2. Compact portable inhaler

8.1 Nebulizer

Nebulizers have been used to treat respiratory diseases for many years. The working principle of jet nebulizer is based on Bernoulli principle by which compressed gas (air or oxygen) is passed through a narrow orifice, creating a low-pressure area at the adjacent liquid feed tube (Fig. 14.3). This evacuates the solution, with the drug being drawn up from the fluid reservoir and shattered in the gas stream through fine droplets. In an ultrasonic nebulizer, a piezoelectric crystal is used with a high vibrating frequency (usually 1–3 MHz) to generate a fountain of liquid in the mobilizing chamber.

The physical properties of pulmonary drug formulations may have an outcome based on particle size and nebulization rates. The viscosity, osmolarity, ionic strength, pH, and surface tension may also affect the nebulization of some formulations.

Constant output jet nebulizer can aerosolize most of the drug solution, and provides a large dose with very little patient coordination skill. Treatment by using a nebulizer can be time consuming, and also less effective, where there is 50% loss

FIGURE 14.3 Nebulizer and its components.

with a continuously operated nebulizer. On average, only 10% of the total dose loaded in a nebulizer is in reality deposited in the lungs (Giraud and Roche, 2002).

Recently, technically advanced novel nebulizers have been developed to reduce drug wastage and improve delivery efficacy. In a nebulizer, the aerosol output is increased by directing auxiliary air entrained at the time of inspiration by enhanced delivery designs. Adaptive aerosol delivery monitors a patient's breathing pattern in the first three breaths, and then targets the aerosol delivery into the first 50% of inhalation of each time. This commits that the aerosol is delivered to the patient during inspiration only, thereby eliminating loss during expiration that occurs with a continuous output nebulizer (Ashurst et al., 2000; Borgstrom et al., 1996).

8.2 Compact Portable Inhaler

8.2.1 Metered Dose Inhaler

It is the revolutionary invention of MDI that overcomes the problem of the hand-bulb nebulizer, and serves portability to outpatients for the first time. This inhalation device is currently the most widely used aerosol delivery device (Fig. 14.4). MDI provides a drug aerosol driven by propellants, such as chlorofluorocarbons (CFC) and hydrofluoroalkanes. MDI emits only a small portion of the drug dose to the lung. On average, only 10%–20% of the delivered dose is deposited in the lung. The high velocity and large particle size of the spray cause around 50%–80% of deposition of drug in the oropharyngeal region. Hand and mouth discoordination is another barrier in the optimal use of an MDI system.

The efficacy of an MDI device depends on a patient's breathing pattern, inspiratory flow rate (IFR), and hand and mouth coordination. Increased IFR results in a decrease in total pulmonary dose deposition and diffusion into the peripheral airway. Fast inhalations (>60 L/min) result in a less peripheral deposition, since deposition of the aerosol takes place by inertial impaction in the oropharyngeal region and the conducting airways. When aerosol is inhaled slowly, drug deposition by gravitational sedimentation in the peripheral region of the lung is improved. Peripheral drug deposition has also been shown to improve with an increase in tidal volume, and a decrease in respiratory frequency. As the inhaled volume is enhanced, aerosols are able to diffuse more into the lung peripheral region. An increased breath-holding period on completion of inhalation enables particles that penetrate the periphery to deposit in that region, instead of being exhaled during the expiratory phase. Thus, the best conditions for inhaling MDI aerosols include a starting volume equivalent to the functional residual capacity, actuation of the device at the start of inhalation, IFR of <60 L/min followed by a 10-s breathhold at the end of inspiration (Norwood et al., 1995).

8.2.2 Pressurized Metered Dose Inhalers

The pMDI is not available for all drugs or dosages, making it difficult for clinicians to prescribe the same type of device for diverse inhaled medications. This is exacerbated by the trend of many pharmaceutical companies not to release newer inhaled drugs as pMDIs. The design of the CFC-propellant pMDI requires initial and frequent priming of the device. Failure to prime the device results in the administration of a substantially lower dose than that prescribed. Unfortunately, frequent priming tends to waste drug in the atmosphere (Dalby and Suman, 2003).

8.2.3 Dry Powder Inhalers

Interest in DPIs as an effective, efficient, and environmentally friendly way of delivering drugs to the lung has accelerated in recent years. A fundamental difficulty with developing solid state aerosols or DPIs is managing both the ubiquitous and

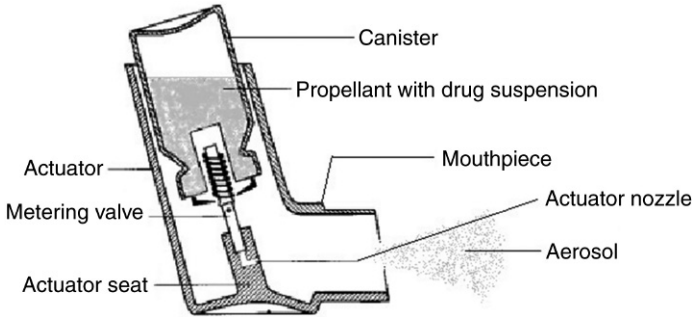

FIGURE 14.4 MDI and its components.

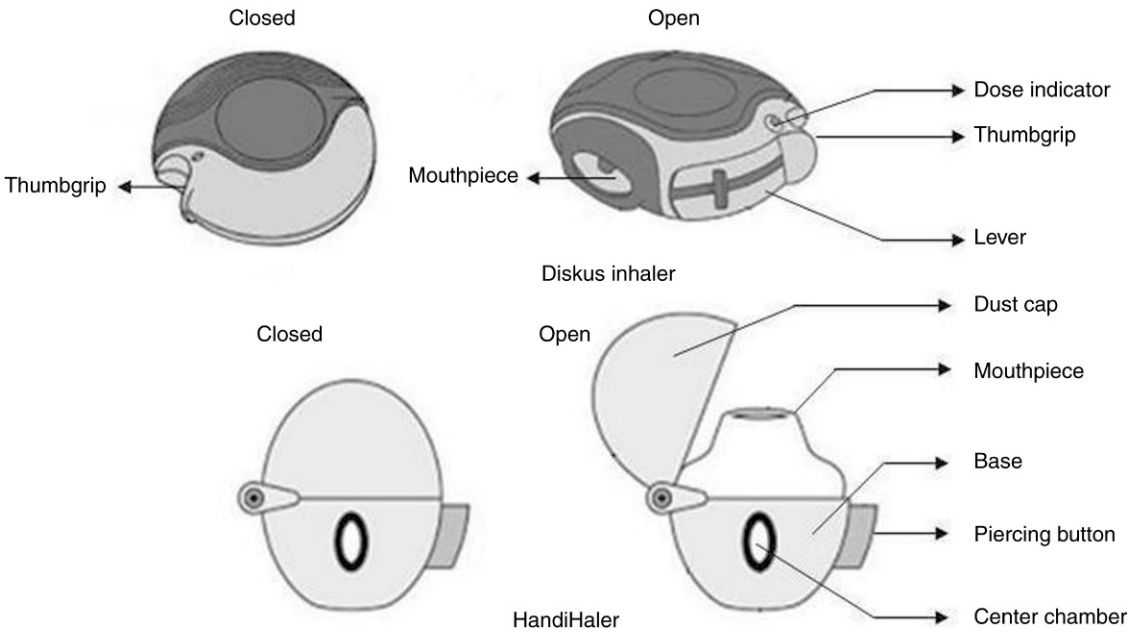

FIGURE 14.5 Schematic diagram of some currently available DPIs and their components.

the transient forces contained in powder beds. Indeed, managing such particulate forces, for example, via particle engineering techniques, is now considered central to successful DPI formulation and production (Fig. 14.5).

In consequence, much attention is currently focused on producing smart formulations, where it may be possible to achieve excellent powder flow and low cohesive forces.

Pharmaceutical scientists too frequently meet major obstacles when they engage in the world of DPI product design, because of the complications of this area resulting from the plethora of DPI device designs. There is tremendous variation in the methods used to store and meter powders, and to generate the aerosol cloud. In the case of DPI aerosol generation, there is a great deal of variation between different types of device, as well as in the fluid dynamic and electrostatic environment that the powder formulation experiences (Ashurst et al., 2000).

The drug aerosol is created in a DPI by directing air through loose powder. Most drug particles from DPIs are too large to penetrate into the lungs because of either large powder agglomerates, or the presence of large carrier particles (e.g., lactose). Thus, dispersion of the powder into fine respirable particles depends on the creation of turbulent air flow that causes the aggregates to break up into particles small enough to be carried into the lower airways, and also to separate carrier from the drug in the device chamber. Each DPI has a different airflow resistance that regulates the required inspiratory effort. The higher the resistance of the device, the more difficult it is to generate an inspiratory flow great enough to attain the maximum dose from the inhaler device. However, deposition in the lung tends to be augmented when using high-resistance inhalers (Yu and Chien, 1997). However, an efficient and robust formulation technology can provide more acceptable use of DPI products (Begat et al., 2004).

9 PULMONARY FORMULATIONS TO TREAT LUNG FUNGAL INFECTION

Targeted drug delivery to the lungs has evolved to be one of the most widely investigated systemic or local drug delivery approaches (Le and Schiller, 2010). The evolution of novel DDSs for the treatment of pulmonary fungal infections is increasing day by day because of the recurrence of fungal infection, even after the conventional therapy occurred, due to the live spores in the lungs remaining there due to the absence of long-term drug availability at the site of infection. Pulmonary route in particular also makes it possible to deposit drugs in a more site-specific manner at high concentrations within the infected lung, thereby reducing the overall amount of drug given to patients (10%–20% of the peroral quantity), as well as increasing local drug activity while reducing systemic side effects, and avoiding first-pass metabolism.

To further exploit the other advantages presented by the lungs, as well as to overcome some challenges encountered, scientists developed interests in DDS for pulmonary administration. These systems can be broadly classified into immediate release (e.g., lactose–drug mixtures for DPI application) and controlled release systems (such as liposomes, micelles, nano- and microparticles based on polymers).

Nanodrug carriers, such as liposomes, nanoparticles (NPs), micelles, etc., have been used to improve the therapeutic index of new or established drugs by modifying drug absorption, reducing metabolism, prolonging biological half-life, or reducing cytotoxicity. Drug distribution is then controlled primarily by properties of the drug nanocarriers, and no longer by physicochemical characteristics of the drug substance only. A careful design of DDS for pulmonary route requires thorough knowledge of players, such as lung architecture, appropriate selection of the carrier materials, production process, and device for successful delivery of drug to lungs (Maji et al., 2014).

Most of the drugs are administered intravenously for the treatment of fungal infection in lung to avoid degradation in the gastrointestinal tract. Patients, however, avoid injections and i.v. treatments, because they are painful, inconvenient, and expensive. Pulmonary drug delivery offers a noninvasive alternative to injections, and can also be more efficient and effective to deliver the drug, and achieves patient compliance (Raja Kumar et al., 2014) (Table 14.2).

9.1 Liposomes

Polyene antibiotic AmB is regarded as a gold standard for the treatment of deep-seated systemic fungal infections in lung (Gulati et al., 1998; Stamm and Dismukes, 1983). Liposomal formulation of AmB was introduced in the market in the year 1990 (Katz et al., 1990) under the brand name of AmBisome (NeXstar Pharmaceuticals, San Dimas, United States), given intravenously to treat *Candida* spp., *Aspergillus* spp., *Fusarium* spp., and other fungi infections in neutropenic, visceral leishmaniasis, and methylmalonic acidemia patients (Kelsey et al., 1999; Stockler et al., 1993; Walsh et al., 2001).

To get a substantial lung tissue concentration and low systemic exposure of AmB, Fungizone (AmB desoxycholate) or AmBisome (liposomal AmB) was delivered by nebulization (Ruijgrok et al., 2000). AmBisome was found to show greater pharmacokinetics than free drug, including prolonged systemic circulation half-life, reduced plasma clearance rate, decreased renal toxicity, and most importantly, enhanced therapeutic efficacy (Walsh et al., 1998).

Aerosolized liposomal AmB was found to be more effective for the prevention of IPA in a placebo-controlled trial in patients with prolonged neutropenia (Rijnders et al., 2008).

Becker et al. (2002) concluded that efficacy of AmBisone therapy can be enhanced by the addition of Fungizone at the start of the treatment, due to the availability of the drug in the lung at start of treatment.

In another study, the surface was modified by coating with alveolar macrophage-specific ligands (O-palmitoyl mannan or OPM), and also with monoclonal antibody EBA-2 in AmB-loaded aerosolized liposomes and emulsomes (core composed of solid lipid surrounded by phospholipid bilayers), respectively for their selective presentation to lungs (alveolar macrophages) in aspergillosis infection. Further, ^{99m}Tc-labeled liposomes could be used for in vivo imaging of the infection site, as depicted by scintigraphy imaging (Vyas et al., 2009).

Systemic delivery of voriconazole for two months, followed by ITZ for one month, was ineffective; liposomal AmB was transbronchially administered directly into the pulmonary aspergilloma using a transbronchial aspiration cytology needle, resulting in the aspergilloma disappearing by seven and a half months after the first treatment (Takeda et al., 2014).

9.2 Lipid Complex

Mucormycosis have documented successful outcomes with either liposomal AmB or AmB lipid complex. Nevertheless, based on the combination of these retrospective clinical data, the historically poor success rates with AmB deoxycholate, and the animal data, show superiority of aerosolized liposomal AmB over AmB deoxycholate (Lowry et al., 2007; Spellberg et al., 2005).

9.3 Nanoparticles

ITZ has been strategically encapsulated into chitosan-based NPs using a modified ionic gelation method; drugs were fabricated as inhalable microparticles using spray-drying technique. Different ratios of chitosan:tripolyphosphate were used, and its 55% encapsulation was found at a 1:3 ratio of chitosan:tripolyphosphate. In vitro inhalation parameters, including fine particle fraction and emitted dose percentage, were measured by a twin stage impinge. The data of in vitro deposition specify that processing of NPs with mannitol and leucine could improve the aerosolization properties significantly (Jafarinejad et al., 2012).

Although AmB was investigated as desoxycholate salt, liposomal, or lipid complex form, PLGA–dimercaptosuccinic acid polymeric NPs loaded with desoxycholate AmB for sustained delivery of the drug was found to reduce the number

TABLE 14.2 Comparative Study of Pulmonary Versus Other Routes (i.v., Oral, etc.)

Drug	Spectrum/Activity	Dosage Form	Route of Administration	Conclusions	References
AmB	Aspergillosis, cryptococcosis, systemic candidiasis, histoplasmosis, blastomycosis, coccidioidomycosis, and zygomycosis	AmB deoxycholate, liposome, and lipid complex	i.v.	Less nephrotoxicity in lipid formulations	Limper et al. (2011)
	Aspergillosis	Liposomes coated with alveolar macrophage-specific ligands (OPM and OPP)	Aerosol	The ligand-anchored liposomal aerosols are very effective in rapid attainment of high drug concentration in lungs with high population of alveolar macrophages and maintain the same over prolonged period of time	Vyas et al. (2009)
	Paracoccidioidomycosis, candidiasis, aspergillosis, and cryptococcosis	NPs	i.v.	The approach was able to reduce the dosing frequency by threefold without causing renal or hepatic toxicity and avoid any increase in plasma lipid levels	Amaral et al. (2009)
Voriconazole	Invasive aspergillosis	NPs	Pulmonary	Pulmonary deposition of the NPs was studied using a customized inhalation chamber; drug was detectable in lungs until 7 and 5 days after administration, for porous and nonporous particles, respectively; porous NPs with lower MMADs showed better pulmonary deposition in deep lung regions and sustained presence in lungs than the nonporous particles	Sinha et al. (2013)
		Infusion	Aerosol	An inhaled aqueous solution of voriconazole and sulfobutyl ether-β-cyclodextrin is capable of producing high lung tissue, as well as plasma concentrations was observed following single and multiple inhaled doses in a pharmacokinetics study	Tolman et al. (2009)
ITZ	Invasive pulmonary aspergillosis caused by *A. fumigatus*	Nanostructured particles by SFL formulation	Aerosol	Aerosolized administration of SFL ITZ was effective as prophylaxis in improving survival in this murine model of IPA due to *A. fumigatus*; the survival benefit can be explained by the ability of aerosolized SFL ITZ to limit disease progression and angioinvasion, both of which were markedly reduced, in comparison to mice that received control or ITZ oral solution by oral gavage	Alvarez et al. (2007)
	Invasive pulmonary aspergillosis	Nanostructured particles (less than 1 μm in diameter) by EPAS and SFL	Aerosolized with the nebulizer	The prolonged survival and limited systemic exposure with aerosolized delivery of EPAS and SFL ITZ are encouraging	Hoeben et al. (2006)
	Pulmonary aspergillosis	Nanostructured particles (less than 1 μm in diameter) by EPAS and SFL	Aerosolized with the nebulizer	An effective method of targeted delivery of ITZ to the deep lung for the treatment and prevention of acute fungal infections	McConville et al. (2006)
	Invasive pulmonary fungal infection	Chitosan-based polymeric micelles as a nanocarrier system	Nebulized	In vitro nebulization study of the ITZ-loaded formulations showed that the SA chitosan–based polymeric micelles had adequate capability as nanocarriers to deliver ITZ, and can remain their stability during nebulization	Moazeni et al. (2012)

(*Continued*)

TABLE 14.2 Comparative Study of Pulmonary Versus Other Routes (i.v., Oral, etc.) (*cont.*)

Drug	Spectrum/Activity	Dosage Form	Route of Administration	Conclusions	References
Caspofungin	Invasive aspergillosis	Caspofungin in 0.9% NaCl solutions 10 and 30 mg/mL	Aerosolized with disposable and reusable type of nebulizer	Two types of commercial nebulizing systems efficiently aerosolize the drug, the choice of which depends on whether a disposable or reusable type of jet nebulizer is most suitable for the particular patient care setting; the therapeutic potential of aerosolized caspofungin in preventing invasive aspergillosis in immunocompromised hosts warrants further evaluation in animal and human trials	Wong-Beringer et al. (2005)
Pneumocandins	*Candida*, *Aspergillus* spp, and *Pneumocystis carinii*	Solution in water for aerosol and solution in normal saline for intraperitoneal administration	Aerosol	The pneumocandins are highly active against *Aspergillus* species, and dramatic improvement in survival was found with aerosolized form	Kurtz et al. (1995)

EPAS, Evaporative precipitation into aqueous solution; MMAD, mass median aerodynamic diameter; NP, nanoparticle; OPM, O-palmitoyl mannan; OPP, O-palmitoyl pullulan; SA, stearic acid; SPL, spray-freezing into liquid.

of AmB administrations, with fewer undesirable effects and a favorable extended dosing interval required to treat mycosis intraperitoneally (Amaral et al., 2009).

Later on, AmB NPs were prepared through liquid antisolvent precipitation for oral administration. The AmB NPs exhibited 2.1 times faster dissolution rates, and 13 times equilibrium solubility, compared with the raw drug; this could be of beneficial for aerosol delivery (Zu et al., 2014).

Patients receiving oral prophylaxis of voriconazole has shown to provide a better intrapulmonary penetration into the pulmonary epithelial lining fluid in lung transplant patients (Capitano et al., 2006). Nevertheless, the suitability of an aqueous solution of voriconazole solubilized with sulfobutyl ether-β-cyclodextrin for targeted drug delivery to the lungs via nebulization has been established (Tolman et al., 2009). Another interesting study depicts that polylactide-*co*-glycolide NPs containing voriconazole made porous using an effervescent mixture for improved pulmonary delivery for sustained drug release for over 15 days. Pulmonary deposition of the particles was studied using a customized inhalation chamber (Sinha and Mukherjee, 2012) for experimental mice. Porous particles had a lower mass median aerodynamic diameter (MMAD), and the highest initial drug deposition than nonporous particles. VNPs with improved drug loading were successfully delivered to murine lungs (Sinha et al., 2013). The most recent studies involve the development of PLGA NPs containing voriconazole, radiolabeling with technetium-99m to investigate the effect on their blood clearance, biodistribution, and in vivo gamma imaging. In vivo deposition of the drug in the lobes of the mice lung, and accumulation in various major organs, has also been observed. Drug accumulation was more pronounced in the lung, in the case of administration of the NPs than that of the free drug. The free drug was found to be excreted faster than the NPs containing drug, following the inhalation route, as assessed by gamma scintigraphy study (Das et al., 2015).

Other antifungals, such as pneumocandin, have been shown to be more effective for prophylaxis against IPA in rats, when given through aerosolization, compared to parenteral treatment of the same (Kurtz et al., 1995).

The in vitro suitability of caspofungin for aerosol administration by characterizing factors that influence efficacy and airway tolerance of aerosol delivery, such as physicochemical properties, the aerodynamics of drug particles, and efficiency of nebulizing systems, etc. (Wong-Beringer et al., 2005). Aerosolization of caspofungin has been evaluated by using three different jet nebulizer and compressor systems. The ability of the drug to achieve favorable physiochemical properties for nebulization requires dilution in normal saline, and a more concentrated (30 mg/mL) solution.

ITZ DPI composed of NPs using high-pressure homogenization with tocopherol polyethylene 1000 succinate as a stabilizer has been prepared, and was embedded in carrier microparticles of mannitol and/or sodium taurocholate, by spray-drying. There followed impaction studies using a multistage liquid impactor to determine the aerodynamic performance and fine-particle fraction that is theoretically able to reach the lung (Duret et al., 2012).

A recent study shows germination of inhaled fungal spores initiates infection, causing severe pneumonia and even mortality. It has been observed that nebulized AmB–polymethacrylic acid NP prophylaxis prevents invasive aspergillosis. It was not toxic to lung epithelial cells or monocyte-derived macrophages in vitro, or in an in vivo transplant immunosuppression mouse model of life-threatening invasive aspergillosis. Three days of nebulizer based prophylaxis delivered the NP effectively to lung, and prevented both fungal growth and lung inflammation (Shirkhani et al., 2015).

Self-assembled AmB-loaded polyglutamic acid NPs were prepared and characterized, and in vitro potential against *Candida albicans* was determined. The biodegradable polyglutamic acid–based formulation of AmB showed potent antimicrobial activity similar to that of Fungizone against *C. albicans*. Interestingly, AmB-bearing PGA NPs were found to inhibit biofilm formation to a considerable extent. In summary, AmB−PGA NPs showed highly attenuated toxicity when compared with Fungizone, while retaining equivalent active antifungal properties (Zia et al., 2015)

9.4 Nanosuspension

It has been found that when nanostructured crystalline ITZ formulations were aerosolized, high lung tissue concentrations were achieved, while the systemic exposure was reduced (Hoeben et al., 2006).

Another study shows high and sustained lung tissue concentrations were achieved after inhalation of ITZ in mice, following oral and pulmonary dosing of amorphous nanoparticulate ITZ compositions, as well as the ITZ oral solution (Sporanox/Janssen) (Vaughn et al., 2006).

Administration of nanoparticulate ITZ containing polysorbate 20 as a nebulized suspension of evaporative precipitation into aqueous solution (EPAS) ITZ provided for targeted high lung concentrations in a murine model (McConville et al., 2006).

Administered as a nebulized suspension of URF, ITZ nanostructured powder agglomerates with enhanced dissolution properties, as well as high bioavailability. These engineered powders have been nebulized as dispersions to rodents to evaluate the pharmacokinetic parameters following inhalation (Yang et al., 2008b).

Nanoparticulate nystatin was found to show better in vitro and in vivo antifungal activities against *C. albicans*. A nystatin nanosuspension was prepared by wet-media milling. Immunosuppressed DBA/2 mice were orally infected with *C. albicans*, and treated with conventional nystatin suspension, nystatin nanosuspension, or saline control for 14 days. Beginning on day 3 of treatment, lower oral burdens of *C. albicans* were found in the nanosuspension group, compared with the suspension and control groups. Mouse survival was also superior in the nanosuspension group (Melkoumov et al., 2013).

9.5 Micelles

There are only few reports investigating the application of inhalable polymeric micelles for delivery of antifungals for inhalation route. Water-soluble chitosan was grafted to stearic acid (SA) chains via 1-ethyl-3-(3-dimethylaminopropyl) carbodiimide mediated coupling reaction that was determined by ^{1}H NMR. Chitosan–SA conjugate nanomicelles of AmB of 101–248 nm was evaluated for the antifungal activity, aggregation state of the drug, nebulization efficiency, and retention of AmB in the micelles after nebulization (Gilani et al., 2011).

Another study reveals that ITZ was entrapped into the hydrophobically modified chitosan micelles (120–200 nm). The in vitro pulmonary profile of polymeric micelles was studied by an air-jet nebulizer connected to a twin stage impinger. The nebulization efficiency was up to 89%, and the fine particle fraction varied from 38% to 47%. The micelles had enough stability to remain in the encapsulation of the drug during the nebulization process (Moazeni et al., 2012).

10 WHY PULMONARY ROUTE?

In recent years, pulmonary drug delivery is an attractive route of administration of drugs due to various beneficial effects. In fact, the lungs are a competent entry point for drugs to the bloodstream due to the huge surface area for absorption (about 100 m^2), the very thin absorption membrane (0.1–0.2 μm), and outstanding blood flow (5 L/min) capability that rapidly allocates molecules all over the body. Moreover, the lungs reveal fairly low local metabolic activity and, in contrast to the oral route of drug administration, pulmonary inhalation is not subjected to first-pass metabolism (Goel et al., 2013). The various advantages of pulmonary DDSs are listed here (Banker and Rhodes, 2002; Cole and Mackay, 1990; Hillery et al., 2001; Sciarra and Cutie, 1991):

1. Straight delivery of the medicament to the affected area is possible.
2. Reduced dose is required for the desired pharmacological action that results in reduced systemic side effects.
3. Quick onset of drug action.
4. Intestinal and hepatic first-pass metabolism can be avoided.
5. Much reduced hostile environment is present in the lungs than in the oral route to most drugs, including proteins and peptides.
6. While administering a dose, sterility of the product can be maintained.
7. There is better protection against drug degradation by oxygen and moisture, thus the stability is augmented for labile substances.

11 LIMITATIONS OF PULMONARY ROUTE (IF ANY)

There are not only advantages, but also some limitations of the pulmonary rote of delivery. The limitations of the delivery of drugs to lungs (Sciarra and Cutie, 1991) are very important in the design of effective pulmonary DDSs. Some of them are mentioned here;

1. The oropharyngeal settlement may give local adverse effects.
2. Patients may have trouble using the delivery devices correctly.
3. Various aspects affect the reproducibility of drug delivery to the lungs, including physiological (respiratory scheme) and pharmaceutical (tool, formulation) variables. For the systemic delivery of drugs with a small therapeutic index, such deviations may be undesirable.
4. Drug absorption may be limited due to the barrier action of the mucus and the drug–mucus interactions.
5. Mucociliary clearance diminishes the retention time of drugs within the lungs that may affect the pharmacological efficacy of the slowly absorbed drugs.
6. The lungs are not an easily reachable surface for drug delivery, and complex delivery devices are required for targeted drug delivery.

12 CONCLUSIONS

Due to rapid blood turnover and fast blood flow, it is hard to maintain persistent therapeutic drug levels in lung. This causes an inability of drug molecules to kill the live fungi in totality, and the fungal spores survive. To maintain the drug concentration in lung, high dose of drug is to be given, often causing high level of toxicity in patients, and inability of the patients to continue the treatment. Fungal infection in lungs is, therefore, difficult to treat by conventional DDSs. Pulmonary drug delivery has a great potential for successful delivery of drug to the lung for effective treatment locally, and even for systemic fungal infections, resulting in a better therapeutic outcome. There are numbers of pulmonary drug delivery devices and DDSs available. Extensive research in the area is in progress. However, existing pulmonary DDSs are not effective enough, and designing the appropriate delivery strategy may explore a new avenue for pulmonary drug delivery to improve the pharmacokinetic profile of the therapeutic payloads.

REFERENCES

Addrizzo-Harris, D.J., Harkin, T.J., McGuinness, G., Naidich, D.P., Rom, W.N., 1997. Pulmonary aspergilloma and AIDS: a comparison of HIV infected and HIV-negative individuals. Chest 111, 612–618.

Alvarez, C.A., Wiederhold, N.P., McConville, J.T., Peters, J.I., Najvar, L.K., Graybill, J.R., et al., 2007. Aerosolized nanostructured itraconazole as prophylaxis against invasive pulmonary aspergillosis. J. Infect. 55, 68–74.

Amaral, A.C., Bocca, A.L., Ribeiro, A.M., Nunes, J., Peixoto, D.L., Simioni, A.R., et al., 2009. Amphotericin B in poly(lactic-co-glycolic acid) (PLGA) and dimercaptosuccinic acid (DMSA) nanoparticles against paracoccidioidomycosis. J. Antimicrob. Chemother. 63, 526–533.

Ampel, N.M., 2011. Coccidioidomycosis. In: Kauffman, C.A., Pappas, P.G., Sobel, J.D. et al., (Eds.), Essentials of Clinical Mycology. Springer, New York, NY, pp. 349–366.

Anderson, P.J., 2005. History of aerosol therapy: liquid nebulization to MDIs to DPIs. Respir. Care 50, 1139–1150.

Andrade, F., Diana, R., Videira, M., Ferreira, D., Sosnik, A., Sarmento, B., 2013. Nanotechnology and pulmonary delivery to overcome resistance in infectious disease. Adv. Drug Deliv. Rev. 65, 1816–1827.

American Lung Association, 2015. How lungs work. Available from: http://www.lung.org/lung-health-and-diseases/how-lungs-work/

Anstead, G.M., Graybill, J.R., 2006. Coccidioidomycosis. Infect. Dis. Clin. North Am. 20, 621–643.

Ashurst, I.I., Malton, A., Prime, D., Sumby, B., 2000. Latest advances in the development of dry powder inhalers. Pharm. Sci. Technol. 3, 246–256.

Baddley, J.W., Perfect, J.R., Oster, R.A., Larsen, R.A., Pankey, G.A., Henderson, H., et al., 2008. Pulmonary cryptococcosis in patients without HV infection: factors associated with disseminated disease. Eur. J. Clin. Microbiol. Infect. Dis. 27, 937–943.

Banker, G.S., Rhodes, T.R., 2002. Modern PharmaceuticsMarcel Dekker, New York, NY, (pp. 529–586).

Becker, M.J., de Marie, S., Fens, M.H., Hop, W.C., Verbrugh, H.A., Bakker-Woudenberg, I.A., 2002. Enhanced antifungal efficacy in experimental invasive pulmonary aspergillosis by combination of AmBisome with Fungizone as assessed by several parameters of antifungal response. J. Antimicrob. Chemother. 49, 813–820.

Begat, P., Morton, D.A.V., Staniforth, J.N., Price, R., 2004. The cohesive adhesive balances in dry-powder inhaler formulations II: influence on fine particle delivery characteristics. Pharm. Res. 21, 1826–1833.

Borgstrom, L., Derom, E., Stahl, E., Wahlin-Boll, E., Pauwels, R., 1996. The inhalation device influences lung deposition and bronchodilating effect of terbutaline. Am. J. Respir. Crit. Care Med. 153, 1636–1640.

Byrnes, III, E.J., Bildfell, R.J., Frank, S.A., Mitchell, T.G., Marr, K.A., Heitman, J., 2009. Molecular evidence that the range of the Vancouver Island outbreak of *Cryptococcus gattii* infection has expanded into the Pacific northwest in the United States. J. Infect. Dis. 199, 1081–1086.

Capitano, B., Potoski, B.A., Husain, S., Zhang, S., Paterson, D.L., Studer, S.M., et al., 2006. Intrapulmonary penetration of voriconazole in patients receiving an oral prophylactic regimen. Antimicrob. Agents Chemother. 50, 1878–1880.

Chang, W.C., Tzao, C., Hsu, H.H., Lee, S.C., Huang, K.L., Tung, H.J., et al., 2006. Pulmonary cryptococcosis: comparison of clinical and radiographic characteristics in immunocompetent and immunocompromised patients. Chest 129, 333–340.

Chapman, S.W., Dismukes, W.E., Proia, L.A., Bradsher, R.W., Pappas, P.G., Threlkeld, M.G., et al., 2008. Clinical practice guidelines for the management of blastomycosis: 2008 update by the Infectious Diseases Society of America. Clin. Infect. Dis. 46, 1801–1812.

Cole, R.B., Mackay, A.D., 1990. Concepts of pulmonary physiology. Essentials of Respiratory DiseaseChurchill Livingstone, New York, NY, pp. 49–60.

Dalby, R., Suman, J., 2003. Inhalation therapy: technological milestones in asthma treatment. Adv. Drug Deliv. Rev. 55, 779–791.

Das, P.J., Paul, P., Mukherjee, B., Mazumder, B., Mondal, L., Baishya, R., et al., 2015. Pulmonary delivery of voriconazole loaded nanoparticles providing a prolonged drug level in lungs: a promise for treating fungal infection. Mol. Pharm. 12, 2651–2664.

Davies, S.F., Saros, G.A., 1994. Fungal Infection. In: Nadel, J.A., Murray, J.G. (Eds.), Textbook of Respiratory Medicine. WB Saunders Co., Philadelphia, PA, pp. 1161–1170.

Denning, D.W., Riniotis, K., Dobrashian, R., Sambatakou, H., 2003. Chronic cavitary and fibrosing pulmonary and pleural aspergillosis: case series, proposed nomenclature change, and review. Clin. Infect. Dis. 37, S265–S280.

Dessanges, J.F., 2001. A history of nebulization. J. Aerosol Med. 14, 65–71.

Duret, C., Wauthoz, N., Sebti, T., Vanderbist, F., Amighi, K., 2012. New inhalation-optimized itraconazole nanoparticle-based dry powders for the treatment of invasive pulmonary aspergillosis. Int. J. Nanomed. 7, 5475–5489.

Fraser, R.S., Pare, J.A.P., Eraser, R.G., Pare, P.D., 1994. Infectious diseases of lungs in synopsis of diseases of chest, second ed. WB Saunders & Co., Philadelphia, PA.

Freifeld, A., Proia, L., Andes, D., Baddour, L.M., Blair, J., Spellberg, B., et al., 2009. Voriconazole use for endemic fungal infections. Antimicrob. Agents Chemother. 53, 1648–1651.

Galgiani, J.N., Ampel, N.M., Blair, J.E., Catanzaro, A., Johnson, R.H., Stevens, D.A., et al., 2005. Coccidioidomycosis. Clin. Infect. Dis. 41, 1217–1223.

Gangurde, H.H., Chordiya, M.A., Baste, N.S., Tamizharasi, S., Upasan, C.D., 2012. Approches and devices used in pulmonary drug delivery system: a review. Asian J. Pharmaceut. Res. Health Care 4, 11–27.

Gilani, K., Moazeni, E., Ramezanli, T., Amini, M., Fazeli, M.R., Jamalifar, H., 2011. Development of respirable nanomicelle carriers for delivery of amphotericin B by jet nebulization. J. Pharm. Sci. 100, 252–259.

Gilgado, F., Cano, J., Gené, J., Serena, C., Guarro, J., 2009. Different virulence of the species of the *Pseudallescheria boydii* complex. Med. Mycol. 47, 371–374.

Giraud, V., Roche, N., 2002. Misuse of corticosteroid metered-dose inhaler is associated with decreased asthma stability. Eur. Respir. J. 19, 246–251.

Goel, A., Baboota, S., Sahni, J.K., Ali, J., 2013. Exploring targeted pulmonary delivery for treatment of lung cancer. Int. J. Pharm. Invest. 3, 8–14.

Greenberger, P.A., 2002. Allergic bronchopulmonary aspergillosis. J. Allergy Clin. Immunol. 110, 685–692.

Groneberg, D.A., Eynott, P.R., Döring, F., Dinh, Q.T., Oates, T., Barnes, P.J., et al., 2002. Distribution and function of the peptide transporter PEPT2 in normal and cystic fibrosis human lung. Thorax 57, 55–60.

Groneberg, D.A., Nickolaus, M., Spinger, J., Doring, F., Daniel, H., Fischer, A., 2001. Localization of peptide transporter PEPT2 in the lung: implications of pulmonary oligopeptide uptake. Am. J. Pathol. 158, 707–714.

Groneberg, D.A., Witt, C., Wagner, U., Chung, K.F., Fischer, A., 2003. Fundamentals of pulmonary drug delivery. Resp. Med. 97, 382–387.

Gulati, M., Bajad, S., Singh, S., Ferdous, A.J., Singh, M., 1998. Development of liposomal amphotericin B formulation. J. Microencapsul. 15, 137–151.

Herbrecht, R., Denning, D.W., Patterson, T.F., Bennett, J.E., Greene, R.E., Oestmann, J.W., et al., 2002. Voriconazole versus amphotericin B for primary therapy of invasive aspergillosis. N. Engl. J. Med. 347, 408–415.

Hillery, A.M., Lloyd, A.W., Swarbrick, J., 2001. Pulmonary drug delivery in drug delivery and targeting for pharmacists and pharmaceutical scientists. Taylor and Francis, London; New York.

Ho, D.Y., Lee, J.D., Rosso, F., Montoya, J.G., 2007. Treating disseminated fusariosis: amphotericin B, voriconazole, or both? Mycoses 50, 227–231.

Hoeben, B.J., Burgess, D.S., McConville, J.T., Najvar, L.K., Talbert, R.L., Peters, J.I., et al., 2006. In vivo efficacy of aerosolized nanostructured itraconazole formulations for prevention of invasive pulmonary aspergillosis. Antimicrob. Agents Chemother. 50, 1552–1554.

Hope, W.W., Walsh, T.J., Denning, D.W., 2005. The invasive and saprophytic syndromes due to *Aspergillus* spp. Med. Mycol. 43, S207–S238.

Husain, S., Alexander, B.D., Munoz, P., Avery, R.K., Houston, S., Pruett, T., et al., 2003. Opportunistic mycelia fungi in organ transplant recipients: emerging importance of non-*Aspergillus* mycelial infections. Clin. Infect. Dis. 37, 221–229.

Jafarinejad, S., Gilani, K., Moazeni, E., Ghazi-Khansari, M., Najafabadi, A.R., Mohajel, N., 2012. Development of chitosan-based nanoparticles for pulmonary delivery of itraconazole as dry powder formulation. Powder Technol. 222, 65–70.

Katz, N.M., Pierce, P.F., Anzeck, R.A., Visner, M.S., Canter, H.G., Foegh, M.L., 1990. Liposomal amphotericin B for treatment of pulmonary aspergillosis in a heart transplant patient. J. Heart Transplant 9, 14–17.

Kauffman, C.A., 2007. Histoplasmosis: clinical and laboratory update. Clin. Microbiol. Rev. 20, 115–132.

Kelsey, S.M., Goldman, J.M., McCann, S., Newland, A.C., Scarffe, J.H., Oppenheim, B.A., et al., 1999. Liposomal amphotericin (AmBisome) in the prophylaxis of fungal infections in neutropenic patients: a randomised, double-blind, placebo-controlled study. Bone Marrow Transplant. 23, 163–168.

Kontoyiannis, D.P., Marr, K.A., Park, B.J., Alexander, B.D., Anaissie, E.J., Walsh, T.J., et al., 2010. Prospective surveillance for invasive fungal infections in hematopoietic stem cell transplant recipients, 2001-2006: overview of the transplant-associated infection surveillance network (TRANSNET) database. Clin. Infect. Dis. 50, 1091–1100.

Kurtz, M.B., Bernard, E.M., Edwards, F.F., Marrinan, J.A., Dropinski, J., Douglas, C.M., et al., 1995. Aerosol and parenteral pneumocandins are effective in a rat model of pulmonary aspergillosis. Antimicrob. Agents Chemother. 39, 1784–1789.

Lai-Fook, S.J., 2004. Pleural mechanics and fluid exchange. Physiol. Rev. 84, 385–410.

Le, J., Schiller, D.S., 2010. Aerosolized delivery of antifungal agents. Curr. Fungal Infect. Rep. 4, 96–102.

Lewis, R.E., Albert, N.D., Liao, G., Hou, J., Prince, R.A., Kontoyiannis, D.P., 2010. Comparative pharmacodynamics of amphotericin B lipid complex and liposomal amphotericin B in a murine model of pulmonary mucormycosis. Antimicrob. Agents Chemother. 54, 1298–1304.

Limper, A.H., Knox, K.S., Sarosi, G.A., Ampel, N.M., Bennett, J.E., et al., 2011. An official american thoracic society statement: treatment of fungal infections in adult pulmonary and critical care patients. Am. J. Respir. Crit. Care Med. 183, 96–128.

Lortholary, O., Obenga, G., Biswas, P., Caillot, D., Chachaty, E., Bienvenu, A.L., Antonino, C., et al., 2010. International retrospective analysis of 73 cases of invasive fusariosis treated with voriconazole. Antimicrob. Agents Chemother. 54, 4446–4450.

Lowry, C.M., Marty, F.M., Vargas, S.O., Lee, J.T., Fiumara, K., Deykin, A., et al., 2007. Safety of aerosolized liposomal versus deoxycholate amphotericin B formulations for prevention of invasive fungal infections following lung transplantation: a retrospective study. Transpl. Infect. Dis. 9, 121–125.

Maji, R., Dey, N.S., Satapathy, B.S., Mukherjee, B., Mondal, S., 2014. Preparation and characterization of Tamoxifen citrate loaded nanoparticles for breast cancer therapy. Int. J. Nanomed. 9, 3107–3118.

Mansour, H.M., Rhee, Y.S., Wu, X., 2009. Nanomedicine in pulmonary delivery. Int. J. Nanomed. 4, 299–319.

Marianecci, C., Marzio, L.D., Rinaldi, F., Carafa, M., Alhaique, F., 2011. Pulmonary delivery: innovative approaches and perspectives. J. Biomater. Nanobiotechnol. 2, 567–575.

McConville, J.T., Overhoff, K.A., Sinswat, P., Vaughn, J.M., Frei, B.L., Burgess, D.S., et al., 2006. Targeted high lung concentrations of itraconazole using nebulized dispersions in a murine model. Pharm. Res. 23, 901–911.

Melkoumov, A., Goupil, M., Louhichi, F., Raymond, M., de Repentigny, L., Leclair, G., 2013. Nystatin nanosizing enhances in vitro and in vivo antifungal activity against *Candida albicans*. J. Antimicrob. Chemother. 68, 2099–2105.

Moazeni, E., Gilani, K., Najafabadi, A.R., Reza Rouini, M., Mohajel, N., Amini, M., et al., 2012. Preparation and evaluation of inhalable itraconazole chitosan based polymeric micelles. Daru 20, 85.

Norwood, D.L., Prime, D., Downey, B.P., Creasey, J., Sethi, S.K., Haywood, P., 1995. Analysis of polycyclic aromatic hydrocarbons in metered dose inhaler drug formulations by isotope dilution gas chromatography/mass spectrometry. J. Pharm. Biomed. Anal. 13, 293–304.

Nucci, M., Anaissie, E., 2002. Cutaneous infection by *Fusarium* species in healthy and immunocompromised hosts: implications for diagnosis and management. Clin. Infect. Dis. 35, 909–920.

Panda, B.N., 2004. Fungal infections of lungs: the emerging scenario. Indian J. Tuberc. 51, 63–69.

Pappas, P.G., Perfect, J.R., Cloud, G.A., Larsen, R.A., Pankey, G.A., Lancaster, D.J., et al., 2001. Cryptococcosis in human immunodeficiency virus-negative patients in the era of effective azole therapy. Clin. Infect. Dis. 33, 690–699.

Paranjpe, M., Goymann, C.C.M., 2014. Nanoparticle-mediated pulmonary drug delivery: a review. Int. J. Mol. Sci. 15, 5852–5873.

Patterson, T.F., Kirkpatrick, W.R., White, M., Hiemenz, J.W., Wingard, J.R., Dupont, B., 2000. Invasive aspergillosis. Disease spectrum, treatment practices, and outcomes. I3 *Aspergillus* Study Group. Medicine 79, 250–260.

Patton, J.S., Byron, P.R., 2007. Inhaling medicines: delivering drugs to the body through the lungs. Nat. Rev. Drug Discov. 6, 67–74.

Perfect, J.R., Dismukes, W.E., Dromer, F., Goldman, D.L., Graybill, J.R., Hamill, R.J., et al., 2010. Clinical practice guidelines for the management of cryptococcal disease: 2010 update by the Infectious Diseases Society of America. Clin. Infect. Dis. 50, 291–322.

Raad, I.I., Hachem, R.Y., Herbrecht, R., Graybill, J.R., Hare, R., Corcoran, G., et al., 2006. Posaconazole as salvage treatment for invasive fusariosis in patients with underlying hematologic malignancy and other conditions. Clin. Infect. Dis. 42, 1398–1403.

Raja Kumar, J., Muralidharan, S., Parasuraman, S., 2014. Antifungal agents: new approach for novel delivery systems. J. Pharm. Sci. Res. 6, 229–235.

Rijnders, B.J., Cornelissen, J.J., Slobbe, L., Becker, M.J., Doorduijn, J.K., Hop, W.C., et al., 2008. Aerosolized liposomal Amphotericin B for the prevention of invasive pulmonary Aspergillosis during prolonged neutropenia: a randomized, placebo-controlled trial. Clin. Infect. Dis. 46, 1401–1408.

Roden, M.M., Zaoutis, T.E., Buchanan, W.L., Knudsen, T.A., Sarkisova, T.A., Schaufele, R.L., et al., 2005. Epidemiology and outcome of zygomycosis: a review of 929 reported cases. Clin. Infect. Dis. 41, 634–653.

Rodriguez-Tudela, J.L., Berenguer, J., Guarro, J., Kantarcioglu, A.S., Horre, R., de Hoog, G.S., et al., 2009. Epidemiology and outcome of *Scedosporium prolificans* infection: a review of 162 cases. Med. Mycol. 47, 359–370.

Ruijgrok, E.J., Vulto, A.G., Van Etten, E.W., 2000. Aerosol delivery of amphotericin B desoxycholate (Fungizone) and liposomal amphotericin B (AmBisome): aerosol characteristics and in-vivo amphotericin B deposition in rats. J. Pharm. Pharmacol. 52, 619–627.

Saccente, M., Woods, G.L., 2010. Clinical and laboratory update on blastomycosis. Clin. Microbiol. Rev. 23, 367–381.

Sahasrabudhe, N., Gosney, J.R., Hasleton, P., 2013. The normal lung: histology, embryology, development, aging and function. In: Hasleton, P., Flieder, D.B. (Eds.), Spencer's Pathology of the Lung. Cambridge University Press, Cambridge, UK, pp. 1–40.

Sangwan, S., Agosti, J.M., Bauer, L.A., Otulana, B.A., Morishige, R.J., Cipolla, D.C., et al., 2001. Aerozolized protein delivery in asthma: gamma camera analysis of regional deposition and perfusion. J. Aerosol. Med. 14, 185–195.

Scheuch, G., Siekmeier, R., 2007. Novel approaches to enhance pulmonary delivery of proteins and peptide. J. Physiol Pharmacol. 58, 615–625.

Sciarra, J.J., Cutie, A.J., 1991. Pharmaceutical aerosols, second ed. Varghese Publishing House, Bombay, India, (pp. 589–618).

Shirkhani, K., Teo, I., Armstrong-James, D., Shaunak, S., 2015. Nebulised amphotericin B-polymethacrylic acid nanoparticles prophylaxis prevents invasive aspergillosis. Nanomedicine 11, 1217–1226.

Sinha, B., Mukherjee, B., 2012. Development of an inhalation chamber and a dry powder inhaler device for administration of pulmonary medication in animal model. Drug Dev. Ind. Pharm. 38, 171–179.

Sinha, B., Mukherjee, B., Pattnaik, G., 2013. Poly-lactide-*co*-glycolide nanoparticles containing voriconazole for pulmonary delivery: in vitro and in vivo study. Nanomedicine 9, 94–104.

Smith, J.A., Kauffman, C.A., 2010. Blastomycosis. Proc. Am. Thorac. Soc. 7, 173–180.

Smith, J.A., Kauffman, C.A., 2012. Pulmonary fungal infections. Respirology 17, 913–926.

Spellberg, B., Edwards, Jr., J., Ibrahim, A., 2005. Novel perspectives on *Mucormycosis*: pathophysiology, presentation, and management. Clin. Microbiol. Rev. 18, 556–569.

Stamm, A.M., Dismukes, W.E., 1983. Current therapy of pulmonary and disseminated fungal diseases. Chest 83, 911–917.

Stockler, S., Lackner, H., Ginter, G., Schwinger, W., Plecko, B., Muller, W., 1993. Liposomal amphotericin-B (AmBisome) for treatment of cutaneous widespread candidosis in an infant with methylmalonic acidaemia. Eur. J. Pediatr. 152, 981–983.

Takeda, T., Itano, H., Kakehashi, R., Fukita, S., Saitoh, M., Takeda, S., 2014. Direct transbronchial administration of liposomal amphotericin B into a pulmonary aspergilloma. Respir. Med. Case Rep. 11, 7–11.

Thompson, III, G.R., Patterson, T.F., 2008. Pulmonary aspergillosis. Semin. Respir. Crit. Care Med. 28, 103–110.

Tolman, J.A., Nelson, N.A., Son, Y.J., Bosselmann, S., Wiederhold, N.P., Peters, J.I., et al., 2009. Characterization and pharmacokinetic analysis of aerosolized aqueous voriconazole solution. Eur. J. Pharm. Biopharm. 72, 199–205.

Torres, H.A., Kontoyiannis, D.P., 2011. Hyalohyphomycoses (hyaline molds). In: Kauffman, C.A., Pappas, P.G., Sobel, J.D. et al., (Eds.), Essentials of Clinical Mycology. second ed. Springer, New York, NY, pp. 281–304.

Torres, H.A., Hachem, R.Y., Chemaly, R.F., Kontoyiannis, D.P., Raad, I.I., 2005. Posaconazole: a broad spectrum triazole agent. Lancet Infect. Dis. 5, 775–785.

Troke, P., Aguirrebengoa, K., Arteaga, C., Ellis, D., Heath, C.H., Lutsar, I., et al., 2008. Treatment of scedosporiosis with voriconazole: clinical experience with 107 patients. Antimicrob. Agents Chemother. 52, 1743–1750.

Tuncer, D.I., Nevin, C., 2007. Controlled delivery of peptides and proteins. Curr. Pharm. Des. 13, 99–117.
Valdivia, L., Nix, D., Wright, M., Lindberg, E., Fagan, T., Lieberman, D., et al., 2006. Coccidioidomycosis as a common cause of community-acquired pneumonia. Emerg. Infect. Dis. 12, 958–962.
Vaughn, J.M., McConville, J.T., Burgess, D., Peters, J.I., Johnston, K.P., Talbert, R.L., et al., 2006. Single dose and multiple dose studies of itraconazole nanoparticles. Eur. J. Pharm. Biopharm. 63, 95–102.
Vyas, S.P., Khatri, K., Goyal, A.K., 2009. Functionalized nanocarrier(s) to image and target fungi infected immune cells. Med. Mycol. 47, S362–S368.
Walsh, T.J., Anaissie, E.J., Denning, D.W., Herbrecht, R., Kontoyiannis, D.P., Marr, K.A., et al., 2008. Treatment of aspergillosis: clinical practice guidelines of the Infectious Diseases Society of America. Clin. Infect. Dis. 46, 327–360.
Walsh, T.J., Goodman, J.L., Pappas, P., Bekersky, I., Buell, D.N., Roden, M., et al., 2001. Safety, tolerance, and pharmacokinetics of high-dose liposomal amphotericin B (AmBisome) in patients infected with *Aspergillus s*pecies and other filamentous fungi: maximum tolerated dose study. Antimicrob. Agents Chemother. 45, 3487–3496.
Walsh, T.J., Raad, I., Patterson, T.F., Chandrasekar, P., Donowitz, G.R., Graybill, R., et al., 2007. Treatment of invasive aspergillosis with posaconazole in patients who are refractory to or intolerant of conventional therapy: an externally controlled trial. Clin. Infect. Dis. 44, 2–12.
Walsh, T.J., Yeldandi, V., McEvoy, M., Gonzalez, C., Chanock, S., Freifeld, A., et al., 1998. Safety, tolerance, and pharmacokinetics of a small unilamellar liposomal formulation of amphotericin B (AmBisome) in neutropenic patients. Antimicrob. Agents Chemother. 42, 2391–2398.
Wheat, L.J., Conces, D., Allen, S.D., Blue-Hnidy, D., Loyd, J., 2004. Pulmonary histoplasmosis syndromes: recognition, diagnosis, and management. Semin. Respir. Crit. Care Med. 25, 129–144.
Wheat, L.J., Freifeld, A.G., Kleiman, M.B., Baddley, J.W., McKinsey, D.S., Loyd, J.E., et al., 2007. Clinical practice guidelines for the management of patients with histoplasmosis: 2007 update by the Infectious Diseases Society of America. Clin. Infect. Dis. 45, 807–825.
Wong-Beringer, A., Lambros, M.P., Beringer, P.M., Johnson, D.L., 2005. Suitability of caspofungin for aerosol delivery: physicochemical profiling and nebulizer choice. Chest 128, 3711–3716.
Yang, W., Peters, J.I., Williams, 3rd, R.O., 2008a. Inhaled nanoparticles—a current review. Int. J. Pharm. 356, 239–247.
Yang, W., Tam, J., Miller, D.A., Zhou, J., McConville, J.T., Johnston, K.P., et al., 2008b. High bioavailability from nebulized itraconazole nanoparticle dispersions with biocompatible stabilizers. Int. J. Pharm. 361, 177–188.
Yu, J., Chien, Y.W., 1997. Pulmonary drug delivery: physiologic and mechanistic aspects. Crit. Rev. Ther. Drug Carrier Syst. 14, 395–453.
Zia, Q., Khan, A.A., Swaleha, Z., Owais, M., 2015. Self-assembled amphotericin B-loaded polyglutamic acid nanoparticles: preparation, characterization and in vitro potential against *Candida albicans*. Int. J. Nanomed. 10, 1769–1790.
Zmeili, O.S., Soubani, A.O., 2007. Pulmonary aspergillosis: a clinical update. QJM 100, 317–334.
Zu, Y., Sun, W., Zhao, X., Wang, W., Li, Y., Ge, Y., et al., 2014. Preparation and characterization of amorphous amphotericin B nanoparticles for oral administration through liquid antisolvent precipitation. Eur. J. Pharm. Sci. 53, 109–117.

FURTHER READING

Peng, H.S., Liu, X.J., Lv, G.X., Sun, B., Kong, Q.F., Zhai, D.X., et al., 2008. Voriconazole into PLGA nanoparticles: improving agglomeration and antifungal efficacy. Int. J. Pharm. 352, 29–35.

Edited by
ALEXANDRU MIHAI GRUMEZESCU

NANOBIOMATERIALS IN CANCER THERAPY

APPLICATIONS OF NANOBIOMATERIALS

Volume 7

CHAPTER

7

Multifunctional drug nanocarriers facilitate more specific entry of therapeutic payload into tumors and control multiple drug resistance in cancer

Biswajit Mukherjee, Samrat Chakraborty, Laboni Mondal, Bhabani Sankar Satapathy, Soma Sengupta, Lopamudra Dutta, Ankan Choudhury and Dipika Mandal

Department of Pharmaceutical Technology, Jadavpur University, Kolkata, India

7.1 INTRODUCTION

Cancer has instigated lots of interest among researchers around the globe due to its high mortality, unique nature, and inadequate treatment strategies. As per the published report of American Cancer Society, it is expected that by 2030 about 21.4 million new cancer cases will impose a serious global concern and cancer related death toll may reach up to 13.2 million due to the growth and aging of population. Despite the remarkable breakthroughs that have been achieved in understanding the disease, especially mapping and profiling of specific tumor biomarkers, characterization of cancer cells and the understanding of signal cascades involved in pathogenesis of cancer, the development of an appropriate treatment strategy is still in its infancy. This may be due to our inability to deliver the cargo of drug(s) specifically to the target site without imparting any adverse effect on healthy tissues and organs. Therefore, it would be very much essential to develop a smarter and more efficient carrier system that can overcome the biological barriers, distinguish between normal and cancerous cells, capable enough to exploit the heterogeneous and complex microenvironment to deliver cargo within an optimal dosage range (Mukherjee et al., 2014; Karra and Benita, 2012).

Traditional treatment options for cancer include surgical intervention, radiation, and chemotherapeutic drugs, which produce adverse effects on healthy cells, thus imparting toxicity to the patients. Moreover, most of the potent anticancer agents possess limited solubility in the biological environment, which has greatly

Nanobiomaterials in Cancer Therapy. DOI: http://dx.doi.org/10.1016/B978-0-323-42863-7.00007-4

reduced their pharmacokinetic properties. Therefore, attention has been paid not only to develop the new drugs but also on the development of novel therapeutic strategies, such as photodynamic therapy and gene therapy. The most important fact is that the success of these techniques depends on delivery of therapeutic agents (drugs, photosensitizers, and genes) into the target tumor sites for better therapeutic outcome. In this context, nanoscaled drug delivery systems offer significant promise owing to their size, surface charge, flexibility for decoration with ligands of diverse nature for specific targeting to tumors, better protection of drugs from harsh environment (highly acidic environment in the stomach, lysosomes of cells and high level of protease or other enzymes in the bloodstream) before they can reach the target site, resulting in improvements in biodistribution and pharmacokinetics of drugs in the systemic circulation, controlled release of the drugs over a longer period of time at desired doses, co-delivery of multiple types of drugs, and/or diagnostic agents to combat multiple drug resistance (MDR) (Ang et al., 2014).

Basically, nanocarriers are submicron colloidal systems (1−1000 nm) of diverse chemical compositions, shape, and physiochemical properties which decide their *in vivo* fate along with their smooth translation from laboratories to clinics. Nanocarriers that are most commonly used for cancer treatment include liposomes, nanoparticles (NPs), nanoemulsion, polymeric micelles, dendrimers, etc.

The advantages of using NPs as a drug delivery system include the following:

1. NPs allow easy manipulation and alteration of their particle size and surface characteristics for achieving both passive and active drug targeting after parenteral administration.
2. NPs can control and sustain release of drug, both during the transportation of the particle and at the site of localization. This alters the organ distribution of the drug and, subsequently, the clearance of the drug so that increased drug therapeutic efficacy and reduced side effects can be achieved.
3. By altering the constituents of the NP matrix, controlled release and degradation characteristics of the particles can be modulated. NPs allow relatively higher drug loading and also allow incorporation of drug into the delivery system without any chemical reaction; which is an important factor for preserving drug activity.
4. NP surfaces can be modified by attaching targeting ligands or be guided magnetically to achieve site-specific targeting.
5. NPs are versatile enough to be used via various routes of administration including oral, nasal, parenteral, intraocular, and others (Ang et al., 2014; Sun et al., 2014).

Many strides have been made to develop nanocarriers specifically targeted to tumors (Sun et al., 2014). The advancements in molecular biology and improved understandings of signaling pathways have led to the development of nanocarriers to potentially enhance the treatment efficiency as well as to overcome the hurdles associated with conventional therapies. More importantly, targeted

delivery should be designed in such a way that it substantially increases the fraction of systemic administered dose that reaches the target sites by tuning the biodistribution of drug and thus producing high local drug concentration at the tumor site while minimizing collateral damage to healthy cells. Ideally, effective targeted delivery systems must have four important characteristics: retain, evade, target, and release. In the case of intravenously (IV) administered nanoformulations this means efficient loading of drug into specific delivery vehicles, optimum residence in the circulation to reach the specific site of the body where it will act and finally release drug at the site within a time period that allows the drug to exert its function (Karra and Benita, 2012). There are two main types of targeting strategies which are largely exploited for the delivery of nanocarriers, known as active and passive targeting. As discussed earlier, tumors are characterized by defective vasculature and poor lymphatic drainage, which facilitate the accumulation of nanocarriers within the target tissues. The phenomenon is known as the enhanced permeability and retention (EPR) effect. The success of EPR-based tumor targeting is heavily dependent on the size of the NPs. Depending on the type and stage of the tumor, cut-off size typically varies between 100 and 800 nm. Nanocarriers smaller than the cut-off size can gain entry into the tumor interstitium from the blood vessels (Mukherjee et al., 2014; Sun et al., 2014).

In the case of liposome, the cut-off size was found to be 400 nm, whereas for particles smaller than 200 nm for effective targeting. The penetration of nanocarriers within the tumor tissues was found to be diffusion-mediated and inversely proportional to their size. In most of the literature, it has been mentioned that carriers within the size range of 30−200 nm are believed to be optimal for exploiting EPR due to certain features, such as overcoming obstacles provided by the tumors and ability to rapidly establish the equilibrium toward extravasation (Aruna et al., 2013; Yuan et al., 1995). Apart from that, tumor interstitium also plays a determining role in delivering drug through passive targeting. The transport of nanocarriers into the interstitium is a result of net force between extravasation and interstitial pressure along with the concentration gradient (Haley and Frenkel, 2008; Heldin et al., 2004). Moreover, the shape of the NPs is also found to be crucial in determining the efficiency of passive targeting. The results of many experiments have shown that spherical particles were found to be better candidate compared to rod- and bar-shaped nanocarriers (Yoo et al., 2012). This is because spherical particles tend to follow the laminar flow pattern and those particles that move near the surface of the vascular wall generally extravasate into the tumors, whereas rod- and bar-shaped particles are hydrodynamically unstable and fail to follow the flow pattern as they travel in the bloodstream. Lastly, the surface properties of nanocarriers also play a crucial role in EPR-mediated targeting. Nanocarriers with prolonged circulation half-life and stealth capability adsorb less protein, leading to a significant reduction in clearance by the mononuclear phagocytic system (MPS).

Despite the fact that intensive research is on-going into the targeting of nanocarriers to tumors, the efficiency of translation from laboratories to clinics is very low. Therefore, researches should be engineered and tuned in such a way that they may overcome the shortcomings to potentiate the translation of formulations. Therefore in this chapter our focus is on the key issues which should be overcome by the nanocarriers for better therapeutic outcome.

7.2 CANCER AND ITS MICROENVIRONMENT

Cancer is a group of diseases which cause abnormal and uncontrolled cell division coupled with malignant behaviors such as tissue invasion, angiogenesis, and metastasis. A malignant tumor is a neoplasm occurring from a failure in the regulation of tissue growth. This abnormal proliferation of tissues is caused by mutations of genes like the oncogenes (that promote cell growth and reproduction) and tumor suppressor genes (that inhibit cell division and survival) (Blanco et al., 2012). Researchers have identified the potential role of various components of tumor microenvironments that strongly influence the cellular phenotypes along with the susceptibilities of tumor toward chemical entities by a range of mechanisms. The tumor microenvironment is composed of numerous components, such as cells (cancer-associated fibroblasts or macrophages), extracellular matrix (ECM), signaling molecules, and mechanical signals that act in a paracrine manner to influence various functions such as tumor initiation, supportive role for tumor growth and proliferation, protection of tumor from host immunity, induction and potentiation of drug resistance, and providing a suitable environment for dormant metastases to thrive. During the early stages of development, cancer cells are heavily dependent on a tumor-supportive microenvironment, whereas at the later stages (i.e., metastatic stage) they become biologically self-sufficient. This acquired self-sufficiency reduces the dependency of cancer cells toward the microenvironment and this is probably one of the prime factors that explains the insensitivity to chemotherapy as they act by blocking the paracrine acting stimuli (Mukherjee et al., 2014; Sun et al., 2014).

7.3 CHARACTERISTIC FEATURES OF TUMOR

7.3.1 ANGIOGENESIS

The ability of cancer cells to spread into the adjacent or distant organs makes them more deadly. The process known as metastasis is the ability of cancer cells to penetrate into blood and lymphatic vessels, circulate through the intravascular stream and finally proliferate at other site(s). Therefore, metastatic spread of cancer tissue is very much dependent on the vascular network and is triggered by chemical signals from tumor cells in a state of rapid growth. The process of

formation of new blood and lymphatic vessels is known as angiogenesis and lymphangiogenesis, respectively. A group of researchers conducted a study which was found to be very useful in providing strong evidence regarding the dependency of cancer cells on the vascular network. In this study, they compared the behavior of cancer cells infused into iris rich in blood vessels and into the anterior chamber devoid of circulation. The larger growth of cancer cells (beyond 2 mm^3) in the area where angiogenesis is possible clearly indicates that angiogenesis plays a crucial role in the progression of cancer. Angiogenesis basically consists of four steps (Nishida et al., 2006) and the process is initiated through local injury in the basement membrane of the tissues leading to immediate destruction and hypoxia (Dameron et al., 1994). After that, activation and migration of endothelial cells occur under the influence of angiogenic factors. In the next step, proliferated endothelial cells will be stabilized and finally the influences of angiogenic factors still continue to control the process of angiogenesis. The requirements for nutrients and oxygen are the key to initiate the process of angiogenesis and occurs due to the imbalance of interplay between diffusible pro- and antiangiogenic molecules that are released by cancer cells and other cells, such as endothelial cells, stromal cells, and the cellular components of ECM. In other words, the "switch on" angiogenesis means simultaneous upregulation of activity of angiogenic factors as well as downregulation of inhibitors. Researchers have identified more than a dozen varieties of proteins as angiogenic activators which include vascular endothelial growth factors (VEGFs), basic fibroblast growth factors (bFGF), angiogenin, transforming growth factor (TGF)-α, TGF-β, tumor necrosis factor (TNF)-α, platelet-derived endothelial growth factor, granulocyte colony-stimulating factor, placental growth factor, interleukin-8, cell/tissue-specific growth factor (e.g., hepatocyte growth factor), and epidermal growth factor (Dameron et al., 1994). Among them VEGF is found to have a profound influence on the process of angiogenesis in normal and neoplastic tissues. It is also known as fibroblast growth factor (FGF-2) and expressed in five spliced isoforms (Narang and Varia, 2011). It acts by interactions with tyrosine kinase receptors such as Flt-1 and Flk-1; and appears in the cancerous tissue and tumor stroma under the influence of cytokines and other growth factors. Endothelial cells activated by VEGF produce matrix metalloproteinases (MMPs) (Nelson et al., 2000). The ECM is made up of proteins and polysaccharides which are broken down by MMPs, accelerating the migration of endothelial cells. The migration of endothelial cells into the surrounding tissues takes place through multiplication and finally they organize into hollow tubes enriched with a mature network of blood vessels with the help of adhesion factors such as integrin-α or -β (Dameron et al., 1994; Narang and Varia, 2011). The newly formed blood vessels are stabilized by angiotensin 1, 2 and their receptor Tie-2 (Tournaire et al., 2004). As mentioned above, activators alone are not potent enough to initiate angiogenesis, it is equally important that inhibitors such as angiostatin, endostatin, interferon, platelet factor 4, thorombospondin, prolactin, and tissue inhibitors of metalloproteinase-1, -2, and -3 for the vessel growth need to be downregulated. In addition to angiogenesis,

vascular growth of tumor is also dependent on *de novo* generation of vascular endothelial cells. This process of neovascularization is also known as postnatal vasculogenesis that involves mesenchymal/mesodermal progenitor cells. There may be three types of progenitor stem cells, such as endothelial progenitor cells (EPCs), hematopoietic progenitor cells (HPCs), as well as local EPCs residing within the vascular wall. The literature suggests that the vascular wall harboring the EPCs and HPCs in the perivascular space provides a microenvironment where cells can exist as well as mobilize on the basis of the needs of the tissue (Erguen et al., 2008; Zengin et al., 2006). Thus EPCs and HPCs can aid the processes of angiogenesis and vasculogenesis.

7.3.2 ABNORMAL TUMOR VASCULATURE

Tumor vasculature differs drastically from normal tissue vasculature. Tumor vasculature has certain unique features such as lack of smooth muscle cells and pericytes in the vessel wall, lack of lymphatic drainage, distorted basement membrane, discontinuous endothelial lining, and lack of sinusoidal vessel plexuses. Despite the fact that factors regulating the growth of the vasculature of tumor and normal tissues are the same, the growth of the tumor vasculature is ill-regulated. The presence of angiogenic factors in tumor is plentiful but the gradient in growth factors is either random or scarce, leading to vigorous disorderly growth in all possible directions at all junctures (Sun et al., 2014; Danquah et al., 2011). This type of growth is known as invasive percolation, where invading blood vessels percolate the tissue in all possible directions resulting in inefficient penetration of the blood supply into solid tumor, thus causing intratumoral differences in vascularization of tumor. Therefore, solid tumors possess avascular central regions whereas the periphery is rich in leaky vasculature (Mukherjee et al., 2014; Maeda et al., 2009). The permeability of lymphatic vessels for solutes and liquids is more than in blood capillaries. They help in the movement of the macromolecules such as protein from interstitial space back into the circulation. Lymphatic vessels also potentiate the metastases by carrying the detached tumor cells from a primary tumor site to lymph nodes. An impaired lymphatic system is a hallmark of a tumor. It leads to retention of macromolecules for longer periods of time and contributes to EPR effect along with chaotic and defective vasculature observed in tumors. The lack of lymphatic system also contributes to increased tumor interstitial fluid pressure (IFP). The interstitium, rich in collagen, acts as a biological scaffold for tissues. It occupies the space between cells and tissues; and is lined by cell membranes and blood vessel walls. Within the matrix, a hydrophilic gel composed of interstitial fluid and macromolecular constituents, such as proteoglycan and hyaluronate, is present. Tumor interstitium differs significantly from normal tissues which include three to five times larger interstitial space, high interstitial hydraulic conductivity and diffusivity, a comparatively larger amount of mobile fluid and finally, faster spread of hydrophilic agents resulting from significant extravascular convection (Sun et al., 2014).

The interstitial pressure and capillary pressure in normal tissues are 0 mmHg and 1−3 mmHg, respectively, and the pressure gradient enhances the convective transport of macromolecules from vascular compartments to the interstitium. The pressure gradient in tumor is opposite that of normal tissues. The combined effect of three factors, presence of osmotic force drawing solutes into the tumor, functionally deficient blood and lymphatics, and finally, contractile ability of tumor stroma, are of prime importance for the existence of high IFP. Recent data from several literatures report that IFP can reach upto 100 mmHg in the tumor core, whereas the periphery exhibits pressure almost equal to atomospheric pressure or slightly negative (Danquah et al., 2011). Multiple effects, such as reduced convection across the walls of tumor vessels and movement of the interstitial fluid into surrounding tissues resulting in flushing out of therapeutic agents from the tumor, have been observed due to the existence of high IFP. These factors impose obstacles that hamper the potency of systemic therapy to tumor, especially the transport of macromolecules as they rely on convective transvascular transport for their migration through the interstitium after crossing the endothelial barrier (Sun et al., 2014).

7.3.3 TUMOR pH

In the last few decades, the perception was that tumors possess acidic pH due to the conversion of glucose to lactic acid. The recent data from the literature suggest that intracellular pH in tumor is neutral or alkaline, whereas the extracellular compartment exhibits slightly acidic pH. The ion-pumps responsible for transport of ions into the extracellular compartment are of vital importance for maintaining the established pH gradients. Moreover, other pathogenic mechanisms, such as ATP hydrolysis, glutaminolysis, ketogenesis, and CO_2/carbonic acid production are found to play crucial roles in maintaining the pH gradients besides aerobic and anaerobic glycolysis. The established pH gradients favor the accumulation of weakly acidic drugs such as mitoycin C (Sun et al., 2014).

7.3.4 HYPOXIA

Hypoxia refers to a condition where tissues receive a suboptimal amount of oxygen or the partial pressure of oxygen has decreased below the critical level that leads to defective clinical and biological functioning of cells or organs. Tumors are characterized by high-rate proliferation leading to high cell density that creates a huge local demand for oxygen. Moreover, distorted tumor vasculature limits the delivery of oxygen throughout the tumor, resulting in regions of hypoxia. It is of different types with unique characteristic features, such as inadequate perfusion (ischemic or acute hypoxia), increased diffusion distances (chronic hypoxia), anemia (anemic hypoxia), and hypoxemia (hypoxemic hypoxia). Hypoxic regions are heterogeneously distributed in 50−60% of solid tumors. Hypoxia in tumors induces hypoxia inducible factor-1 (HIF-1) which has profound influence

in regulating the gene transcription of ATP-binding cassette (ABC) transporters in cancer cells, thus playing a crucial role in tumor progression. The most important consequence of tumor hypoxia is that tumor becomes insensitive to chemotherapy due to the overexpression of ABC transporters which are involved in effluxing of anticancer drug from the tissue (Danquah et al., 2011; Iyer et al., 2013).

7.4 DIFFERENT TYPES OF NANOCARRIERS

7.4.1 POLYMERIC 'NPs'

In general, the term 'NPs' denotes a wide range of submicron colloidal systems that include organic polymeric nanostructures of synthetic polymers, natural polymers, metals, nonmetals, etc. A few examples include polymeric NPs, protein base NPs, solid lipid nanoparticles (SLNs) comprising of physiological lipid, inorganic NPs, such as semiconductor NPs, iron oxide NPs, quantum dots (QDs), gold NPs, and nonmetal NPs such as carbon nanorods (Figure 7.1).

Among them, polymeric NPs have gained significant interest due to the huge advancement in polymer science in the last few decades. Polymeric NPs usually have a core-shell structure and based on their method of preparation, they usually possess two types of morphology that include nanocapsules (NCs) and nanospheres. NCs are delivery systems where a polymeric membrane encapsulates the drug in a central cavity, while nanospheres are matrix-like systems with the drug being physically dispersed throughout the matrix. The important factors in designing NPs as an efficient delivery system are controlling the size of the NP, surface properties, and release characteristics of the therapeutically active agents from

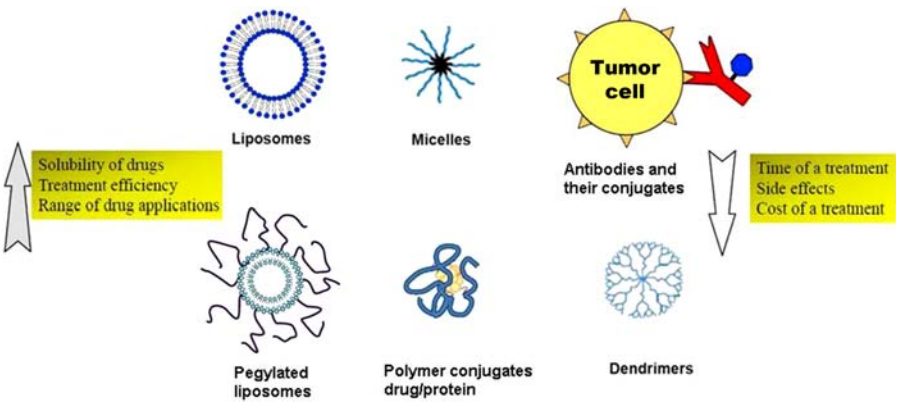

FIGURE 7.1

Different nanocarriers for chemotherapy and their advantages (shaded arrow indicates advantages of NPs and clear arrow indicates disadvantages of NPs).

them. Although liposomal delivery systems are also versatile systems, they have certain drawbacks regarding low encapsulation efficiency, rapid leakage of water-soluble drug in the presence of blood components, and poor storage stability. Polymeric NPs offer some specific advantages over liposomes on such issues by increasing the stability of encapsulated endrug/proteins and possess useful controlled-release properties (Sun et al., 2014).

Polymeric NPs are known to be the most effective nanocarriers for cancer chemotherapy (Alexis et al., 2008). Polymeric NPs are nanosized (size less than 1 μm in diameter) colloidal structures, and they are prepared from both natural polymers, such as dextran, heparin, chitosan, alginates, gelatin, and collagen, and synthetic polymers, such as polyethylene glycols (PEGs), polycaprolactone (PCL), polylactic acid (PLA), *N*-(2-hydroxypropyl)-methacrylamide copolymer, poly-L-glutamic acid (PGA), and polystyrene-maleic anhydride copolymer. Among them, poly(lactic-*co*-glycolic acid) (PLGA) has been exploited most because it is the only polymer approved by US FDA for systemic application. Apart from the polymeric systems, protein-based platforms have also established their potential as drug delivery carriers due to their biodegradability, biocompatibility, and low toxicity. These platforms comprise of naturally self-assembled protein subunits of the same protein or a combination of proteins making up a complete system. The proteins which are usually investigated for the development of drug delivery systems include ferritin/apoferritin protein cage, plant-derived viral capsids, the small heat-shock protein cage, albumin, collagen, gelatin, etc.

The polymer constitutes the hydrophobic core which acts as a container for the anticancer drug, where the drug is either entrapped, dissolved, encapsulated, or attached to the NP matrix (Reddy et al., 2011; Bajpai et al., 2008). These polymers are biodegradable and so generally fragmented into monomers which are metabolized and removed from the body through metabolic pathways. By modifying polymer side chain to develop novel polymers or by synthesizing copolymers, the rate of polymer degradation and subsequent drug release may be controlled. The most common biocompatible polymers which are used in many pharmaceutical applications are PGA and PLA (Alexis et al., 2008a). Based upon the method of preparation, NPs can have different characteristics and different release properties (Bajpai et al., 2008; Rawat et al., 2006). The drug is entrapped in NPs due to the hydrophobic interaction between the drug molecule and polymeric NP core. The stability of linker between the drug−polymer conjugate influences the release of drug from a NP. Hence, drug release is delayed if the linker is too stable and if the linker is too unstable drug may be released before the NP reaches the tumor (Reddy et al., 2011). Due to small size, NPs are able to penetrate capillaries and are taken up by the cells. As a result, the accumulation of drug at the site of action increases (Ochekpe et al., 2009). This makes them significant for drug delivery as they increase the specificity of action of drug by altering their pharmacokinetic profile and tissue distribution. NPs can be used for targeting antitumor drugs to the malignant tumor cells, in order to increase therapeutic efficacy and decrease systemic toxicity. Depending on the pathophysiological condition of tumor, such as

overexpressed receptors and angiogenesis, the strategy of NP targeting may be decided (Haley and Frenkel, 2008; Fonseca et al., 2002; Hans and Lowman, 2002; Sanvicens and Marco, 2008; Tanaka et al., 2004; Sandhiya et al., 2009).

7.4.2 NANOLIPOSOMES

Liposomes were discovered by Alec Bangham and colleagues in 1961 as a swollen spherical phospholipid system. Later, their potential as carriers for drugs, nutrients, and other bioactive agents was established. They have potential to deliver drug cargo to tumors because of their ability to protect the drug from degradation as well as improving the pharmacokinetics of encapsulated drug while reducing the adverse effects associated with bolus administration. Moreover, they are flexible enough for ligand modification, and modification of their size. They have the ability to encapsulate a plethora of drug molecules to make them very attractive delivery systems for cancer therapy.

Nanoliposomes are nanosized versions of liposomes. They are self-assembling closed colloidal structures of spherical shape and composed of unilamellar or multilamellar lipid bilayer vesicles with a central aqueous core (Haley and Frenkel, 2008; Cho et al., 2008). Liposomes are composed of phospholipids, such as phosphatidylglycerol, phosphatidylcholine, phosphatidylserine, and phosphatidylethanolamine and other molecules such as cholesterol. The hydrophilic head of lipid remains on the surface, while the hydrophobic tail is positioned inwards, inside the bilayer. Liposomes are very versatile with respect to lipid composition, surface charge, and size, and are capable of incorporating both hydrophilic and hydrophobic drugs. For this reason they are used widely in drug delivery as efficient nanocarriers (Ochekpe et al., 2009; Solaro et al., 2010; Abreu et al., 2011; Khosravi-Darani and Mozafari, 2010). There are, however, certain limitations. For example, liposomes administered through intravenous route are quickly removed by reticuloendothelial system (RES) due to opsonization. Besides, liposomes are disintegrated by hydrophobic, electrostatic, and van der Waals forces in the system. Therefore, to avoid such a scenario steric stabilization is required and this may be obtained through surface modification (e.g., by attaching PEG, dextran, or poly-*N*-vinylpyrrolidones to the lipid bilayer), which reduces immediate RES clearance (Fattal et al., 2004). Additionally, their tissue specificity can be increased through conjugation with targeting ligands, such as monoclonal antibody or aptamer (Haley and Frenkel, 2008; Cuong and Hsieh, 2009; Mishra et al., 2010).

Due to encapsulation of drugs in liposomes, liposomal chemotherapeutic formulations have reduced side effects compared to conventional medication such as cardiotoxicity produced by doxorubicin or peripheral neurotoxicity produced by cisplatin and vincristine. Nanoliposomes are used in cancer because, due to their nanosize, they are capable of extravasating from blood circulation through the leaky vasculature of tumor and increasing the therapeutic efficacy of chemotherapeutics at the site of action of tumor (Khan, 2010).

7.4.3 POLYMERIC MICELLES

Micelles are nanosized colloidal dispersions prepared from amphiphilic molecules, with a hydrophobic tail and a hydrophilic head. The hydrophobic core acts as a reservoir for hydrophobic drugs and the hydrophilic shell stabilizes the hydrophobic core. Polymeric micelles are prepared by increasing the concentration of the molecules above the corresponding critical micelle concentration. Micelles are preferred due to easy surface manipulation and easy encapsulation of drug. Due to these properties they are considered as a suitable nanocarrier for poorly water-soluble anticancer drugs such as paclitaxel and docetaxel. By physical encapsulation and/or chemical covalent attachment drug can be loaded into polymeric micelles and the drug release from micelles may be controlled by an external stimulus such as pH, temperature, enzymes, and ultrasound. Polymeric micelles are preferentially stored in tumor tissue due to the EPR effect. Cancerous tissues are more permeable and leaky than healthy tissues and lack proper lymphatic drainage. Accumulation of micelles is greater in such tissues and the free micelles which are present in blood circulation are cleared by the kidneys (Wiradharma et al., 2009; Huh et al., 2008; Liu et al., 2008; Rapoport, 2007; Kagaya et al., 2012; Drbohlavova et al., 2013). Particle size, drug loading capability, stability, and drug release kinetics of polymeric micelles may be altered by altering the physicochemical properties and structures of polymers (Chen, 2010).

7.4.4 NIOSOMES

Niosomes are comparatively more stable than liposomes due to the presence of nonionic surfactant on their surface. They can also be developed in the nano range. They are composed of hydrated nonionic surfactant with or without incorporation of cholesterol and other fats. Both hydrophilic and lipophilic drugs are encapsulated by niosomes, in which the former remains in the vesicular aqueous core and the latter is in the lipophilic shell. They are significant due to their low toxicity, reduced side effects, increased therapeutic effectiveness, and enhanced stability. The nonionic surfactants are chemically stable against oxidation and temperature but are physically unstable during dispersion due to aggregation, fusion, leakage, or hydrolysis of drugs (Zarei et al., 2013; Pardakhty and Moazeni, 2013; Mehta et al., 2013). Niosome's properties depend on vesicle composition, lamellarity, size, surface charge, tapped volume, concentration of drug, etc. (Kazi et al., 2010). Zarei et al. (2013) established the efficacy of paclitaxel-loaded niosomes as chemotherapeutic.

7.4.5 SOLID LIPID NANOPARTICLES

SLNs have a spherical shape with an average diameter of 10−1000 nm. They are used as a colloidal NP drug delivery system in which lipid drug carrier solidifies at room temperature as well as at body temperature. SLN consists of solid lipid,

such as triglycerides, fatty acids, waxes, partial glycerides, and polyethylene glycosylated lipid; emulsifiers, such as polysorbates, poloxamer and lecithin; and water. They have outstanding physical stability and are able to deliver lipophilic drugs with high loading capacity. SLNs are applied for some of their significant features such as enhancement of drug solubility, increased bioavailability, controlled drug release, better targeting of drug, and ease of administering through various routes such as parenteral, peroral, pulmonary, and topical (Mathur et al., 2010; Lim et al., 2013; Anajwala et al., 2010; Yassin et al., 2013). Kang et al. (2010) developed doxorubicin-loaded SLNs and established their *in vivo* effect on P-glycoprotein (P-gp) overexpressing MCF-7/ADR cells, a representative of a breast cancer cell line that has adrinamycin resistance. The SLNs acted by overcoming the chemoresistance of adrinamycin-resistant breast cancer. Yuan and his coworkers prepared docetaxel-loaded SLNs that reduced systemic toxicity but maintained proper anticancer activity (Yuan et al., 2014).

7.4.6 VIRAL NANOPARTICLES

Viral nanoparticles (VNPs) are a developing field with a prospective impact in pharmaceutical technology. VNPs, which carry both genomic and nongenomic cargo, enter a new host cell by binding to deliver that cargo. They are mainly based on bacteriophages and plant viruses such as cowpea mosaic virus, cowpea chlorotic virus, red clove necrotic mottle virus, chlorotic ringspot virus, because they are considered to be safer in human compared to mammalian viruses. VNPs are immunogenic and genetically encoded. They exist in various shapes and sizes and are changeable with atomic precision. To develop the procedure and method of high precision, VNP tailoring and self-gathering of mutant and chimeric particles for numeral viral systems are created after knowing the structures of viruses at atomic resolution (Wen et al., 2013; Cheng et al., 2013). VNPs are utilized in drug and gene delivery, diagnostics, and cellular imaging (Liu et al., 2014). VNPs are also applied to target tumors *in vivo*, such as the transferrin conjugated to cowpea mosaic virus to regulate the uptake of iron by tumor cells. The development of vascularization in the tumor can be visualized by applying fluorescent cowpea mosaic virus injection into major vessels of chorioallantoic membrane (Manchester and Singh, 2006). Steinmetz and coworkers worked on cowpea mosaic virus-based NPs which interact with surface vimentin on tumor cells and detected the tumor cells *in vitro* and *in vivo* (Steinmetz et al., 2011).

7.4.7 QUANTUM DOTS

QDs are inorganic colloidal fluorescent semiconductor NPs composed of 10−50 atoms of elements from groups II−IV or III−V of the periodic table, with a diameter ranging from 2 to 10 nm. QD can be used for various biosensing purposes. They consist of two main parts—the metalloid crystalline core and the shell which protects the core. QD can be conjugated with bioactive moieties or

specific ligands, such as receptors, antibodies, and ligands. The shape and size of QD, which decide their absorption and light emission, can be controlled and QD-producing electromagnetic waves in the fluorescence spectrum can be used for biomedical imaging. A probe consisting of a combination of different-sized QDs within a single bead emits a prominent spectrum of a variety of colors and light intensity can be used as a spectral bar code. Due to their long-term stability, high sensitivity, long-term and multicontrast imaging agents QDs are preferable for *in vivo* cancer detection and diagnosis. However, toxicity of QDs is considerable due to hazardous heavy metals. Therefore, systemic toxicity should be investigated before *in vivo* application in humans (Reddy et al., 2011; Cai and Chen, 2007; Kim, 2007; Walling et al., 2009; Diaz and Vivas-Mejia, 2013).

7.4.8 DENDRIMERS

Dendrimers (Greek word *dendron*, meaning a tree), discovered in 1980 by Donald Tomalia and his colleagues, have a characteristic hyperbranched structure with monodispersed macromolecules (Dilnawaz et al., 2011). They acquire nearly perfect 3-D, geometrical architecture and growth of the chain length results in more branched and longer core producing ultimately in the globular structure of the dendrimers. They adopt a closely packed dense structure which extends to the periphery, having diameter ranges between 1.4 nm and 1.9 nm. Drug can be loaded into dendrimers by adopting various approaches, such as through electrostatic interaction and covalent conjugations to the surface of the dendrimer. The surface of the dendrimers is generally rich in functional moieties, such as amine or carboxyl groups, that are used as binding sites for drug molecules equipped with relevant functional groups through electrostatic or covalent interaction.

Dendrimers are prepared by using different types of polymers, such as polyamidoamine (PAMAM), PGA, PEG, polypropyleneimine, and polyethyleneimine. Dendrimers which can be synthesized by divergent synthesis or convergent synthesis, consist of three different parts, namely the focal core, monotonous units of numerous interior layers, and multiple peripheral functional groups. The nanocavity environment and drug solubility properties are determined by the focal core and internal parts, while the functional groups maintain the solubility and chemical properties of polymers. The molecular properties such as shape, dimension, size, and polarity may be controlled as they are synthesized in a stepwise way (Rawat et al., 2006; Drbohlavova et al., 2013; Diaz and Vivas-Mejia, 2013). They are capable of solubilizing hydrophobic drugs and may be conjugated or modified with targeting moieties, such as antibody and biotin (Hussain et al., 2004). Dendrimers are mainly used as a coating agent for protection of drug molecules and site-specific delivery of drugs to minimize drug toxicity. Choi and his group prepared DNA-assembled PAMAM dendrimer clusters for specific targeting of cancer cells (Choi et al., 2005). On the other hand, PAMAM dendrimers

also showed successful gene transfection and transepithelial transport efficacy (Choi et al., 2005; Rawat et al., 2006).

7.4.9 FULLERENE

Fullerene, a nanoscale structure, is composed of carbon atoms in various shapes, such as hollow spheres, ellipsoids, or tubes. Among them, fullerenes having soccer-ball-like architecture are known as buckyballs. They are not broken up in the body and are excreted intact after they are administered inside the human body. A highly symmetrical C_{60} molecule contains 20 hexagons and 12 pentagons of carbon atoms may be entrapped within fullerene and surface modification may be done by conjugating ligands or antibody for targeting. Chemically and physically they act as electron-lacking alkenes in spite of their extreme conjugation (Reddy et al., 2011; Bakry et al., 2007). Functionalized fullerene can be used for cancer diagnosis and therapy. Gd^{3+} can maintain its property, prevent leakage and its dissociation *in vivo* after encapsulation in fullerene and is used as a magnetic resonance contrast agent for detecting abnormal tissues like tumor. After conjugation with PEG C_{60} shows a strong tumor-suppressive property when administered IV in tumor-bearing mice coupled with light irradiation (Chen et al., 2012).

7.4.10 CARBON NANOTUBES

Carbon nanotubes are cylinders of nanosize diameter consisting of one or several coaxial graphite layers. Depending on their structure, they are mainly categorized into two types, single-walled nanotubes comprising of a single cylindrical carbon wall, and multiwalled carbon nanotubes in which multiple cylindrical carbon walls are nested within other cylinders (Shvedova et al., 2009; Lacerda et al., 2006). They are used as sensors for protein and DNA detection, carriers for proteinaceous drug delivery, and diagnostic devices for serum sample analysis. Though they are absolutely insoluble in every solvent, the chemical modification of their surfaces makes them water-soluble and a functionalized linker with a wide variety of active molecules such as nucleic acid, proteins, peptides, and therapeutic agents can be used for targeting. In cancer treatment carbon nanotubes can play a vital role as they can carry several molecules at once due to their multiple covalent functionalizations with tumor-specific ligands and antibody attached to the surface of the sidewalls or tips of the tubes (Cho et al., 2008). Due to their optical properties and thermal conductivity, carbon nanotubes kill cancer cells by way of local hyperthermia. However, toxicity, therapeutic efficacy, pharmacokinetic profile, and biodistribution parameters should be thoroughly examined before *in vivo* application of carbon nanotubes (Sharma and Chen, 2009; Kam et al., 2005; Zhang et al., 2009).

7.4.11 NANOFIBERS

Polymeric nanofibers, which can be prepared by three different techniques, namely electrospinning, phase separation, and self-assembly, have nanosize diameter. Among these three techniques, electrospinning is a largely accepted technique to manufacture nanofibers because this technique is simple, cost-effective, flexible, and possible to scale up. Further, various natural polymers, such as collagen, chitosan, gelatin, silk fibroin, and synthetic polymers, such as PLA, PLGA, polyethylene oxide, PCL can be used in this technique. Nanofibers are used in tissue regeneration and drug delivery applications due to their significant characteristics, such as high interconnected porosity with adjustable pore size, high surface area to volume ratio, capability of surface functionalization, structural similarity with ECM, modifiable surface morphology. The properties of nanofibers can be changed simply by various manufacturing parameters such as flow rate of polymer, distance between capillaries and collectors, voltage, viscoelasticity of solution, and surface tension (Diaz and Vivas-Mejia, 2013; Zamani et al., 2013; Wang et al., 2005; Xu et al., 2008). Ringel et al. (2014) established that carbon nanofibers have the ability to enhance cellular accumulation of carboplatin by about 28% compared to single treatment of carboplatin used as chemotherapeutics and Liu and coworkers showed that self-assembled peptide nanofibers are efficient for targeted delivery of hydrophobic drug in cancer (Liu et al., 2014).

7.5 TUMOR TARGETING THROUGH NANOCARRIERS

The conventional chemotherapeutic agents have nonspecific biodistribution and poor pharmacokinetic profiles leading to systemic toxicity associated with severe side effects (Park et al., 2008). Therefore, the development of tumor-targeted drug delivery systems has been a real challenge for the formulation scientists all over the world. The concept of tumor targeting is mostly based on two factors, one is the tumor microenvironment and the other is tumor angiogenesis. By understanding these two factors only, it is possible to design drug delivery systems to target tumors. In the present scenario, nanomedicines have been found to exploit the above two factors successfully to gain access to the tumor site. They can enter tumor passively through the defective vasculature surrounding the tumors using their nanosize and also remain there for a prolonged period of time. Alternatively, specific ligands grafted at the surface of nanocarriers allow them to bind to the receptors exclusively expressed or overexpressed by cancer cells or angiogenic endothelial cells for active targeting (Danhier et al., 2010). Thus, tumor-targeting strategies can be broadly explained by these two processes.

7.5.1 EPR-MEDIATED PASSIVE TARGETING

Passive targeting involves the transport of drug-loaded nanocarriers through the hyperpermeable tumor capillaries by simple passive diffusion. It fully relies on the defective tumor biology and size of the carrier system for the delivery of chemotherapeutics, which can be overall explained by the term EPR effect (Maeda et al., 2009). For passive targeting, the EPR effect is the sole guiding principle for all nanocarriers. Rapid growth of tumor cells coupled with rapid vascularization led to increased production of many mediators and enzymes, which make the tumor blood vessels more hyperpermeable than normal (Dong and Mumper, 2010) (Figure 7.2). Along with this, the lack of a proper lymphatic drainage system leads to passive accumulation and retention of drug-loaded nanocarriers in the tumor resulting in the EPR effect.

For passive targeting mechanism, size and surface properties of drug delivery nanocarrier systems are important factors. The size must be controlled to avoid early recognition and uptake by the RES. It has been found that nanocarriers of greater size than 200 nm are frequently attacked by macrophages, whereas drug delivery systems of size less than 10 nm also suffer from untimed clearance by kidneys (Bae and Park, 2011). Thus the optimal size to maximize blood circulation time and targetability of the nanocarrier system is usually considered 10–100 nm, with a hydrophilic surface to circumvent RES uptake and clearance (Alexis et al., 2008a).

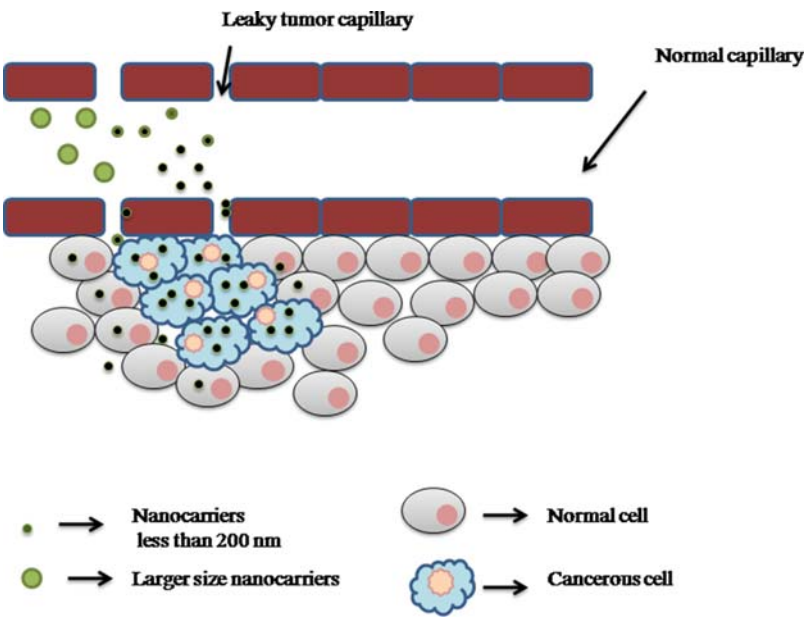

FIGURE 7.2

Passive tumor targeting of nanocarriers by the EPR effect (Mukherjee et al., 2013).

In order to reach the target solid tumor site in the desired concentration, the circulation time of nanocarriers in the blood should be increased to a reasonable extent. This is achieved by hydrophilic surface modification with different macromolecules, such as PEG and polyethyleneimine. Due to the steric effect of such hydrophilic polymers, the binding of nanocarriers to opsonins, which actually promotes RES clearance, is significantly reduced, resulting in enhanced blood circulation time (Federico and Vladimir, 2013). This in turn increases the accumulation and retention of drug-loaded nanocarriers at the tumor sites via EPR.

However, passive targeting does not offer specific biodistribution of chemotherapeutics to tumors only. Rather, it is a type of nanospecfic tumor-targeting strategy. In this case, the majority of administered nanocarriers are known to accumulate in other organs, particularly in the liver, spleen, and lungs. Hence, the pharmacological actions of the drugs are not limited to selective tumor sites within the body (Saini et al., 2012). The healthy cells also have the greatest chance of cytotoxic drug exposure. Again, passive targeting facilitates the efficient localization of nanocarriers in the tumor interstitium but cannot promote their uptake by cancer cells. Also, the EPR effect is not a homogeneous phenomenon in all tumors or even different regions of the same tumor due to the highly complex nature of tumors, particularly in the case of humans (Lammers et al., 2012). Thus, to achieve effective drug delivery to tumors, ligand-mediated active targeting strategies are now heavily investigated in nanotechnology-based cancer research.

7.5.2 SPECIFIC LIGAND-MEDIATED ACTIVE TARGETING

Active targeting relies on the fact that tumors are an assembly of wide varieties of cells which carry unique molecular markers. The majority are either not expressed in normal cells or expressed at much lower levels than in tumor cells (Danhier et al., 2010). Therefore, a successful drug-targeting approach requires the identification of a unique molecular target from antigenic landscapes. Generally, biomarkers are known as a repository of a plethora of molecules such as mutant genes, RNAs, proteins, lipid, and even small metabolite molecules. Advancements in molecular biology have led to the utilization of modern techniques. cDNA microarrays, tissue microarray, and immunohistochemical techniques play vital roles in molecular profiling of tumor and identification of biomarkers, which further provide useful information on the behavior of tumor along with its stage, grade, clinical course, and treatment efficiency. Principles of active targeting are dependent on a multitude of factors, as discussed here. The number of cell surface receptors and their availability on their surface are important as they govern the number of targeting moieties that will eventually bind specifically to the tumor. Apart from that, binding affinity of the targeting ligand is also very important because low binding affinity may limit the efficiency of the targeting approach (Kakde et al., 2011). However, multivalent binding characters of targeted NPs somehow compensate for this pitfall. It should also be kept in mind in

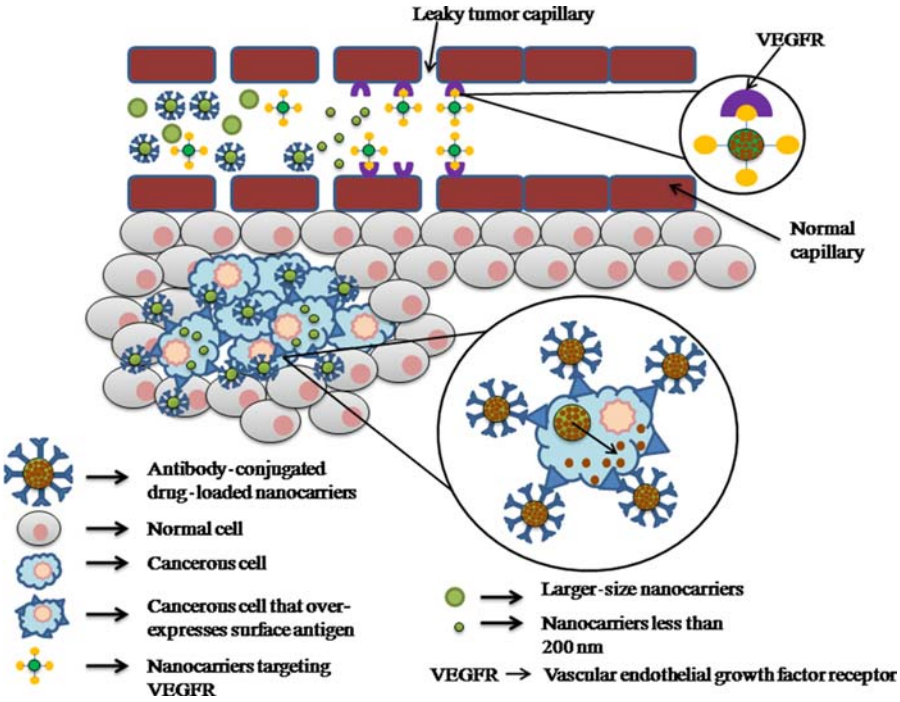

FIGURE 7.3

Ligand-mediated active tumor targeting of engineered nanocarriers (Mukherjee et al., 2013).

designing the multivalent NPs, as it may also increase the probability of recognition by MPS. Finally, the chosen targeting ligands must have an innate ability to induce receptor-mediated endocytosis as this is essential for internalization of drug carriers into the desired cells, which in turn decides the efficiency of uptake of nanocarriers within the tumors. The ligands used for tumor targeting mostly involve antibody, antibody fragments, aptamers, polysaccharide, peptide, small biomolecules like folic acid, etc. (Yinan et al., 2014; Figure 7.3).

7.6 TYPES OF TARGETING LIGANDS

7.6.1 MONOCLONAL ANTIBODIES AND ANTIBODY FRAGMENTS

The overexpression of receptors or antigens in many cancers lends to efficient drug uptake via receptor-mediated endocytosis. Antibodies and antibody fragments, an important class of targeting ligands with a high degree of specificity for cellular receptors and a wide range of binding affinities, are being keenly

investigated in targeted drug delivery (Karra and Benita, 2012). Over the last decade, the feasibility of antibody-mediated tumor targeting has been clinically demonstrated following the commercial approval of several mAb (monoclonal antibody)-mediated nanocarriers by the FDA. The recent advances in hybridoma technology have led to the development of chimeric, and fully humanized, mAbs to reduce their immunogenicity significantly (Byrne et al., 2008). The ability of engineered mAbs to target disease processes has been demonstrated by the success of several monoclonal antibody therapeutics, including cetuximab, rituximab, trastuzumab, and bevacizumab (Karra and Benita, 2012).

The success of mAb-functionalized nanocarriers as compared to conventional chemotherapeutics has been well evidenced by numerous recent research studies (Mukherjee et al., 2014; Karra and Benita, 2012). A recent study by Acharya et al. (2009) showed that epidermal growth factor receptor (EGFR) mAb-conjugated rapamycin-loaded PLGA/Poly vinyl alcohol (PVA) NPs resulted in 17 times higher internalization by MCF-7 cells than the corresponding nontargeting NPs. The IC50 value for mAb-conjugated nanocarriers (26.11 ng/ml) was significantly lower than those for free rapamycin (268.9 ng/ml) and nontargeting drug-loaded nanocarriers (1.734 μg/ml). Another study reported the targeted delivery of doxorubicin, utilizing chitosan nanocarriers surface-modified with anti-HER2 trastuzumab. The study demonstrated an enhanced and selective uptake of trastuzumab-decorated nanocarriers by HER2-positive cancer cells compared with nontargeted nanocarriers and free drug (Yousefpour et al., 2011).

Though mAbs have been largely used to direct the nanocarriers in a tumor-specific manner as compared to mAbs, antibody fragments have now demonstrated higher potential for the engineering of targeted NPs as they are smaller in size and lack the complement activation region of mAbs, while retaining the antigen-binding specificity. In many research investigations, antibody fragment-conjugated nanocarriers have been shown to improve the therapeutic efficacy of encapsulated drug significantly through targeted delivery (Karra and Benita, 2012). For example, MCC-465, a $F(ab')_2$ fragment-decorated doxorubicin-encapsulated liposome is currently in a phase I clinical trial. It has demonstrated much superior cytotoxic activity against several human stomach cancer cells than conventional therapeutics and free drug (Matsumura et al., 2004). In another work, EGFR targeted scFv (single-chain variable fragment) conjugated heparin-*cis*-diamminedichloroplatinum (DDP) (EHDDP) NPs encapsulating cisplatin significantly enhanced antitumor activity of DDP without weight loss or damage to the kidneys and spleen in nude mice bearing H292 cell tumors (Peng et al., 2011).

7.6.2 PEPTIDES

Peptide ligands have shown attractive targeting potential due to their small size, higher stability, relative ease of large-scale synthesis, etc. The development of phage display techniques and other screening methods has enabled the discovery of new peptide-targeting domains and the isolation of new cell-specific peptide

ligands. The SP5-52 peptide-linked liposome has been shown to greatly enhance the therapeutic effect of doxorubicin, decrease the growth of tumor blood vessels, and enable high survival rates among human lung and oral cancer-bearing xenograft mice (Lee et al., 2007). In another study, a novel targeting peptide coupled to liposomes carrying doxorubicin showed an increased therapeutic index of the chemotherapeutics with significant enhancement in survival rates of mice with human lung cancer xenografts as compared to conventional formulations. The peptide conjugated formulation demonstrated enhanced drug accumulation in tumor tissues by 5.7-fold compared with free drug (Chang et al., 2009). Cys-Arg-Glu-Lys-Ala (CREKA), Asn-Gly-Arg (NGR), and Ile-Thr-Asp-Gly-Glu-Ala-Thr-Asp-Ser-Gly (LABL) are a few examples of peptides used to develop targeted NPs (Kamaly et al., 2012). Here we will only discuss the common peptides used for tumor endothelium and tumor lymph node targeting.

7.6.2.1 Cyclic arginyl-glycyl-aspartic acid

Cyclic arginyl-glycyl-aspartic acid (cRGD) peptides have now been explored as a specific targeting moiety owing to their high affinity for $\alpha_v\beta_3$ integrin receptors. These receptors are highly expressed on cancer endothelial cell surface, playing a crucial role in tumor angiogenesis and cancer cell metastasis (Prokopiou et al., 2013). Thus, conjugation of nanocarriers with cRGD sequence leads to the targeted delivery of chemotherapeutics at tumor endothelial cells, blocking the crucial angiogenesis process.

In a recent study, novel $\alpha_v\beta_3$ integrin-targeted superparamagnetic iron oxide (SPIO) NPs were developed and evaluated for their specific uptake by endothelial cells *in vitro* and *in vivo*. The nanocarriers were coated with 3-aminopropyltrimethoxysilane and conjugated with Arg-Gly-Asp (RGD) peptides. Uptake of RGD nanoparicles by human umbilical vein endothelial cells (HUVEC) was significantly higher when compared with unlabeled NPs and could be competitively inhibited by addition of unbound RGD (Karra and Benita, 2012). In another study, RGD peptide-conjugated chitosan-based polymeric micelles encapsulating doxorubicin could significantly increase the doxorubicin concentration in integrin-overexpressing human hepatocellular carcinoma cell line (BEL-7402), but not in human epithelial carcinoma cell line (HeLa). The competitive cellular-uptake test showed that the cellular uptake of RGD-modified micelles in BEL-7402 cells was significantly inhibited in the presence of excess free RGD peptides. *In vitro* cytotoxicity tests demonstrated doxorubicin-loaded RGD-modified micelles could specifically enhance the cytotoxicity against BEL-7402 compared with nontargeted micelles and free drug (Cai et al., 2011).

7.6.2.2 LyP-1 peptide

Recently LyP-1, a nine-amino-acid cyclic peptide, has been recognized as targeting ligands for specifically targeting tumors and tumor lymphatics that are nonspecific to other peptides such as F3, CREKA peptide, and RGD peptides (Çevik and Gürsoy, 2011). This peptide can accumulate in high concentration at the

tumor and can also induce apoptosis in the cell after internalization. In a study by Yan et al. (2012), LyP peptide was conjugated to the doxorubicin-loaded PEGylated liposomes to target the lymphatic metastatic tumors. The peptide-conjugated nanoliposomes were shown to be taken up by the tumor cells and metastatic lymph nodes without disturbing the normal lymph nodes which ultimately enhanced the *in vitro* inhibition and controlled the progress of *in vivo* lymphatic metastatic tumors. Additionally, liposomal doxorubicin showed reduction in tissue damage to the injection site that was much less than the damage observed after IV doxorubicin solution. In a study, Luo et al. (2010) have demonstrated target-specific NPs for drug delivery to lymphatic metastases. They conjugated LyP-1 peptide to the PEG-PLGA NPs for specifically targeting to the lymph nodes. The study concluded eight times higher uptake of peptide conjugated NPs in metastasis lymph nodes, establishing the ability of LyP-1-modified nanocarriers as a promising targeting vehicle to metastatic tumors.

7.6.3 TRANSFERRIN

Transferrin is a serum glycoprotein which transports iron through the blood and into cells by binding to the transferring receptor and subsequently being taken up through receptor-mediated endocytosis. Thus, the transferrin receptor is a vital protein involved in regulation of iron uptake and cell growth. This receptor is highly expressed on cancer cells (maybe up to 100-fold higher) than its normal expression on healthy cells, which can be thus taken as an important cancer cell marker to design targeted delivery systems (Cho et al., 2008). Its extracellular accessibility, higher ability to internalize, and its central role in the cellular pathology of human cancer make this receptor one of the attractive targets for active tumor targeting. Many nanocarrier-based drug delivery systems conjugated with transferrin have already been reported by several researchers (Mukherjee et al., 2014). In one study, Maruyama (2011) showed that PEGylated oxaliplatin-loaded nanoliposomes conjugated with transferrin exhibited much higher tumor accumulation over untargeted nanoliposomes. A remarkable tumor growth inhibition was observed for transferrin-conjugated targeted nanoliposomes against C26 colon carcinoma-bearing mice than free drug and unconjugated nanocarriers. In another study, conjugation of transferrin to doxorubicin-loaded liposomes resulted in enhanced delivery of doxorubicin to tumors and tumor growth inhibition over conventional doxorubicin-loaded liposomes (Li et al., 2009). Recently, another novel liposome formulation, MBP-426, conjugated to the human transferrin (T_f) ligand, has been reported to improve the safety and efficacy of oxaliplatin by specifically targeting transferrin receptors on tumor cells (Sankhala et al., 2009).

7.6.4 APTAMERS

Over the past few years, aptamers have become a popular class of targeting ligand for anticancer drug delivery. Though monoclonal antibodies were previously the

primary targeting tools, but with the developing knowledge on biotechnological research, novel targeting agents, such as aptamers, are now gaining importance as a new generation of targeting molecules.

Aptamers are small, single-stranded DNA/RNA oligonucleotides of 5−40 kDa with well-defined three-dimensional structures (Cao et al., 2009). Sizes of the aptamers are somewhat intermediate between larger antibodies (150 kDa) and smaller peptides (1−5 kDa), which makes them the ideal candidate for tumor cell targeting. They bind to their target molecules with high affinity and specificity like mAbs, and simultaneously possess many superior desirable properties to mAbs, such as ease of selection, low cost of production, and low immunogenicity. Aptamers of wild-type RNA and DNA molecules have a short *in vivo* lifespan since they are mostly degraded by several nucleases. Thus different strategies, such as the use of chemically modified oligonucleotides (Rusconi et al., 2002), unnatural internucleotide linkages (King et al., 2007), and hydrophilic polymer modification, are now being adopted to synthesize aptamers, with improved stability.

Aptamers enjoy many superior qualities than monoclonal antibodies or other similar targeting ligands. They exhibit much better thermal stability than mAbs. They can be denatured and renatured several times without significant loss of activity (Zhang et al., 2011). The synthesis of aptamers does not rely on biological systems unlike mAbs. Again, as compared to mAbs, the production cost is much less and also they are easier to scale up. Furthermore, the smaller size of aptamers compared with intact antibodies (∼150 kDa) is assumed to have better tissue penetration in solid tumors. The lack of immunogenicity is another added advantage in favor of aptamers for targeted tumor therapy over antibodies.

However, aptamers also have some limitations, such as pharmacokinetic instability and quick systemic clearance. The small size and polyanionic nature of aptamers are mostly responsible for their rapid blood clearance. To improve this, aptamers are conjugated with hydrophilic polymers, such as PEG, which can alter their pharmacokinetics (Watson et al., 2000).

7.6.5 SMALL BIOMOLECULES

Small molecules have also attracted considerable attention as potential targeting ligands due to their low molecular weights (MWs), low production costs, and easy conjugation with NPs. The small size of this kind of targeting ligand allows the functionalization of multiple ligand molecules on single NPs. Among the small biomolecules, folic acid has been investigated extensively in designing targeted nanocarriers.

Folic acid has emerged as an alternative targeting ligand for the tumor-specific drug delivery system due to its high binding affinity for folate receptors (FRs). FRs serve as an excellent cellular surface marker for many types of solid tumors, such as breast, colon, kidney, lung, and ovary, pharmacokinetics (Mahato et al., 2011).

Targeting to FRs is based on the fact that the expression of FRs in normal tissue usually remains low, but is highly upregulated in many human cancers. Furthermore, many investigations suggest that the density of FRs increases as the stage of cancer advances (Mahato et al., 2011). Thus folic acid conjugated nanocarriers have the ability to deliver the loaded cargo specifically to pathologic cells without causing much harm to normal tissues. Being a vitamin B2 family, folic acid can be taken up by the epithelial cells through receptor-mediated endocytosis. Folic acid or its conjugates reversibly bind with the FRs heavily present on the surface of cancer cells and are internalized to intracellular compartments to form endosomes (Song et al., 2013). Subsequently, this conjugation between FR and folic acid-conjugated nanocarriers separates in acidic environment at a pH nearly 5.0−5.5. After dissociation, FRs return back to the cell surface for fresh uptake and the drug-loaded carrier releases the contents in the cytosol.

Many drugs have been used to prepare folate drug conjugate including paclitaxel, docetaxel, platinum complexes, alkylating agents, 5-fluorouracil, mitomycin C, etc. Many nanocarrier-based drug delivery systems such as liposomes, NPs, and polymeric micelles have already been investigated in recent years using folic acid as targeting moiety and showed superior efficacy both *in vitro* and *in vivo* as compared to unconjugated nanoformulations.

A recent work by Song et al., 2013 showed a much higher cellular uptaking ability of folic-acid-conjugated doxorubicin-loaded chitosan NPs in FR-positive SMMC-7221 cells than unmodified NP formulations, which is due to the folate-receptor-mediated endocytosis.

7.7 CHALLENGES ASSOCIATED WITH TARGETING

A passive targeting strategy has certain shortfalls as the vessels formed through angiogenesis are not evenly distributed in solid tumor and all the regions of tumor do not have homogeneous permeability. In other words, the EPR effect is highly heterogeneous and exhibits wide variance not only in different tumors but also among the patients with the same type of tumor. Furthermore, small tumors or metastatic lesions do not exhibit strong angiogenesis and thus efficiency of passive targeting in these situations is a highly debatable issue which has to be addressed properly to take maximum benefit of passive targeting.

Extravasation of nanocarriers within the tumor is absolutely dependent on EPR, active targeting approaches can only potentiate the uptake and retention of nanocarriers by augmenting the receptor-mediated endocytosis. Therefore the problems associated with a passive targeting strategy are partially overcome by increasing the probability of intracellular drug accumulation. Active targeting involves efficient ligand−receptor interaction, which is dependent on a variety of factors including the extent of target-cell-specific expression of the receptor related to normal cells, availability of the receptors on the tumor cell surface, the rate of

internalization of nanocarriers following saturation of receptors, etc. Furthermore, the expression of a specific tumor targeting receptor may not be homogeneously distributed within a tumor or may change in its surface expression over time (Jain and Stylianopoulos, 2010). Tumor cells exhibit high heterogeneity and high probability of mutation frequency even among the same cancer patient. Furthermore, most of the solid tumors are not the result of a single gene but are the product of multiple gene defects (Shervington and Lu, 2008). Therefore, designing of mAb-mediated nanocarriers against tumor-specific antigen is not an easy task. Owing to the highly complex nature of tumors, particularly in spontaneous human tumors, promising outcomes from initial *in vitro* studies may be quite different from outcomes from cancer patients (Kwon et al., 2012). Such complexities are related to identifying an effective ligand−receptor interaction. It should be noted that tumor target ability is intimately dependent on type and position of ligands. Some ligands, like antibodies, are highly specific. But other ligands, such as cRGD and FAs, are not specific to cancer cells only, since their corresponding receptors are not solely expressed on the tumor cell surface, but are also present on normal healthy cells all over, which again puts a question mark on the success of targeted chemotherapy. In a recent review by Mukherjee et al. (2013), most of the challenges in the development of targeted nanomedicines have been addressed along with the obstacles in successful translation of the targeted nanocarrier-based delivery systems from laboratories to clinics.

7.8 DRUG RESISTANCE AND HOW TO COMBAT IT WITH DIFFERENT NANOCARRIERS

Treatment of cancer patients varies depending upon a range of individual factors including the specific pathological and molecular characteristics of the cancer, its position, degree of severity, and the health condition of the patient (Chorawala et al., 2012). The ultimate intention is to obliterate all the cancer cells with minimal harm to the normal tissue. The drug resistance in cancer patients is one of the foremost challenges for anticancer drug treatment (Gottesman, 2002), as cancer cells develop resistance against the anticancer drugs. Many cases at the beginning of the treatment with chemotherapeutics promise a favorable response. However, with time, recurrence of the disease occurs in patients. Incompetent drug delivery causes a low concentration of drug at the site of neoplasia leading to drug resistance to the cancer cells. The presence of anticancer drug at the surrounding tissue further causes deadly toxicity to healthy cells. It is, therefore, important to design a proper and effective drug carrier system which specifically delivers the drug to the site of neoplasia avoiding their lethal side effects to the surrounding normal cells. Inadequate circulation time, improper biodistribution, nonspecific cellular uptake, etc., can limit the access of the drug to tumor (Jain, 1994), resulting in repetitive courses of chemotherapy. Such repetitive treatments lead to

genetic mutation to stop the cancer cells from responding to the drug which might have acted potentially at the initial phases of treatment. Once the cancer cells become resistant to a drug they can be less or nonresponsive to the structurally and functionally similar chemical agents. Phenomena such as increasing self-repairing capacity, expression of misleading altered drug targets, enhancing drug metabolism, or overexpressing drug efflux pumps are some of the mechanisms of cancer cells to provide chemoresistance (Gottesman, 2002). Multidrug therapy rather than single-drug treatment has proven more effective as the combination of drugs may provide more hindrance for the cancer cells to develop drug resistance (Bonadonna et al., 1975; Scheithauer et al., 1993). However, multidrug treatment in many cases does not prevent the cancer cells from gaining resistance against those or similar drugs. Such an incident is known as MDR.

NP drug delivery improves therapeutic effectiveness and diminishes the side effects of the drugs by improving their pharmacokinetics. The advancements in nanotechnology and biotechnology have contributed immensely to the development of biocompatible nanocarriers adapted to specific needs and they have the ability to deliver therapeutic payloads specifically to the target tissue(s) (Couvreur and Vauthier, 2006; Davis et al., 2008; Zhang et al., 2008). Nanocarriers also possess the potential to deliver multiple drugs directed against different molecular targets, which may result in suppression of MDR phenotypes as well as a decrease in MDR-based drug efflux.

Hypoxia has been considered one of the major contributors in developing MDR in tumor. It is recognized as a state of unresponsiveness of tumor tissue toward functionally and structurally unrelated chemotherapeutic agents. In addition to hypoxia, selection pressure such as mutations in oncogenes and tumor suppressor genes are found to play a crucial role in the development of MDR by disrupting the cell cycle check points which help the tumor cells to escape apoptosis. It has been reported that inactivating mutations in pRb (retinoblastoma) and p53 tumor suppressor protein cascade are enough to induce MDR in pretumorigenic cells that express telomerase (Bonanno et al., 2014). The downstream effects of p53 inactivation are associated with tumor progression by inhibiting the proapoptotic factors, such as *Bax* and *Bak*, along with activation of antiapoptotic *Bcl-2* proteins. Many researchers reported that cancer cell plasticity has a strong influence in the persistence of disease in the presence of therapeutic interventions (Olaussen et al., 2006). It is the ability of one cell type to attain the properties of another cell type that can potentially be coupled to regenerate specific cell types affected by disease condition. For example, a subpopulation of tumor cells has cancer stem cells (CSCs) that are actively involved in tumor development by producing the bulk population of nontumorigenic cancer cell progeny through differentiation. Drug resistance imposes a huge obstacle toward the potency of the chemotherapeutic regimen. Ideally MDR has been implicated in elevated expression of drug efflux transporter, changes in the kinetics of drugs or amplification of drug targets. According to the CSC hypothesis, tumors are composed of a small population of cells which are known as tumor-initiating cells bearing

tumorigenic potential (Vinogradov and Wei, 2012). The ability of these cells to undergo self-renewal by cell division to form diverse types of cells is responsible for malignancy. CSCs are found to possess certain features, such as self-renewal and differentiation as normal tissue stem cells. The CSC hypothesis suggests functional heterogeneity in solid tumors is found to be hierarchically arranged, with CSCs present at the apex of the hierarchy. The CSC model has also paved the way to exploit the cellular mechanisms responsible for therapeutic refractoriness and dormant behavior displayed by many solid tumors (Bonanno et al., 2014; Olaussen et al., 2006).

MDR is the one of the biggest hurdles faced by scientists from different arenas dealing with development of an effective delivery system in cancer for better therapeutic outcomes. Mechanisms responsible for inducing MDR can be categorized under five classes, such as induction of drug transporters, DNA repair, changes in drug metabolism, gene amplification, or mutation of the target protein and changes in the apoptotic/signaling pathway. The mechanisms are distinctly different from each other, even though the MDR is the synergistic effect of combined MDR mechanisms, such as blocked apoptosis (decreased ceramide) and increased efflux (upregulated P-gp). Apart from the transporters, the other nonpump-mediated factors are responsible for inducing MDR as mentioned. One of them is the overexpression of drug-metabolizing enzymes, such as cytochrome P450 and gluconaryl transferase, resulting in a sharp decrement in the effective concentration of drugs by potentiation of their metabolism. The balance between the proapoptotic and antiapoptotic pathways is extremely vital since defects in apoptotic machinery results in overproduction of antiapoptotic proteins leading to a hindrance in programmed cell death without interference with cellular mechanisms. Finally, ceramide (CER) which has been recognized as a second messenger signaling molecule has potential in differentiation, proliferation, immune response, and apoptosis, and thus it becomes one of the potent inducers of MDR. They are very effective in activating apoptotic inducers such as ceramide-activated protein kinase, which acts as a negative modulator of RAS (KSR), cRaf, protein kinase C, cathepsin D, and ceramide-activated protein phosphatases.

7.9 MAJOR MECHANISMS OF DRUG RESISTANCE

7.9.1 DRUG INACTIVATION

To obtain clinical efficacy most of the chemotherapeutic agents require metabolic activation. Drug activation is a complex mechanism inside the body where substances interact with different proteins (Housman et al., 2014). As a result of these interactions drugs become partially degraded or a complex formation occurs leading to their inactivation. Cancer cells also develop resistance toward treatment due to decreased drug activation. For example, the physiological response to the presence of drug is the overexpression of drug-metabolizing enzymes or carrier

molecules (e.g., the increased production of glutathione (Gamcsik et al., 2002) or ubiquitin which leads to inactivation of the drug by forming conjugate that is excreted. On the other hand, underexpression of drug-metabolizing enzymes can decrease drug effectiveness in situations where an administered dormant prodrug has to undergo catalytic adaptation to an active form. For example, rabinoside is required to be transformed by the action of deoxycytidine kinase; loss or mutation of this enzyme will leave this drug less effective (Chorawala et al., 2012). Cytochrome p450 monooxygenases (cyp450) are a group of enzymes that modify the chemical structure of drugs, for removal from the body. These enzymes are present in the cells of the intestinal wall, endothelium, liver, and other tissues. Genetic variations leading to cyp450 structure and its expression result in functional diversities in drug and nutrient absorption and clearance (Lamba et al., 2002).

7.9.2 ALTERATION OF DRUG TARGETS

Due to mutations leading to variation in expression levels of target proteins/other molecules, molecular targets of drugs may change and thereby hamper the efficacy of therapeutic agents. These alterations ultimately result in drug resistance in chemotherapy. A very common instance of this happened with antiestrogen (e.g., tamoxifen) therapy of breast cancer due to transition to an endocrine-resistant in which there is an apparent loss of function of estrogen receptors in the resistant tumor cells (Housman et al., 2014). Most probably, the existing cancer cells are no longer dependent on estrogen for growth. Cytotoxic drugs are designed to hinder a constituent which is absolutely necessary for cell survival. The surviving cells may mutate in such a manner that it produces a protein that preserves its activity but no longer fastens to the drug, for stereochemical reasons, and is therefore not inhibited by it (Chorawala et al., 2012). For example, imatinib (Gleevac; STI571) is a tyrosine kinase inhibitor that stimulates apoptosis by preventing cell growth in cancerous cells by disabling the damaged bcr-abl receptors, preventing ATP binding (Gorre et al., 2001). Reachability of drug to the intended site of action is also a problem that develops a form of resistance. The inner portions of large tumors are likely to have a poor blood supply and drugs generally have inadequate access to this area. Treatment of brain tumors has such problems caused by the blood−brain barrier (BBB) (Ramakrishnan, 2003).

7.9.3 DRUG EFFLUX

Probably one of the most important forms of resistance against the antineoplastic agents is by the action of a group of membrane proteins which extrude cytotoxic molecules causing drug efflux and reducing the intracellular drug concentration below the effective threshold. The transporter systems which are responsible for MDR belong to the family of ABC and consist of about 13 members. P-gp is an example of such a transporter which has been extensively exploited by scientists.

This 170 kDa protein consists of 12 transmembrane spanning domains and 2 cytoplasmic binding domains. It is capable of effluxing a plethora of substances of diverse chemical nature and effluxing requires hydrolysis of two ATP molecules. Apart from its potential role in MDR, it is a vital component of the BBB, providing neuroprotection and is also found in liver, kidneys, placenta, and intestines (Fukuda and Schuetz, 2012). Other than P-gp, the other members of ABC family transporters include multidrug-resistance protein 1 (*Mrp-1, Abcc-1*), breast cancer resistance protein (*BCRP, ABCG1*), mitoxantrone resistance protein (*MXR1/BCRP, ABCG2*), and *ABCB4*. *MRP-1* is widely distributed in normal tissues, including the BBB, and is closely associated with poor prognosis and broad-spectrum efflux. *BCRP* provides resistance to classical chemotherapeutic agents, such as mitoxantrone, and may also have a potential role in effluxing tyrosine kinase inhibitors. In addition to exploring the 13 members of ABC transporters actively involved in MDR, researchers are now trying to exploit the newer member(s) of ABC transporters. A few years ago, researchers explored the cellular localization, structure, and function of two different forms of ABCB6 in human cell lines (Selvakumaran et al., 2003; Sui et al., 2013). They distinctly differ with respect to MW and distribution. Both of them (high MW, 104 kDa and low MW, 79 kDa) have localized into the mitochondrial outer membrane while nucleotide binding domains of transporters are oriented toward the cytoplasm. The interesting fact is that high MW is only present in the plasma membrane. Although they are very much effective in effluxing the cisplatin and paclitaxel, they prefer effluxing of porphyrins. The noteworthy aspect is that the potential role of transporters in MDR is well characterized, however not enough data are available to establish the benefits of these effluxing pumps to achieve better therapeutic outcome and therefore they require much more attention from researchers.

7.9.4 DNA DAMAGE REPAIR

Another important factor of drug resistance in chemotherapy is the repair of damaged DNA. In this mechanism, DNA damage response mechanisms can undo the drug-induced damage. For example, cisplatin resistance occurs by developing an enhanced ability to eliminate cisplatin−DNA adducts and restoring cisplatin-induced lesions, through the action of DNA repair proteins (Bonanno et al., 2014; Olaussen et al., 2006; Selvakumaran et al., 2003). Inhibition of repair pathways used in combination with DNA-damaging chemotherapy could stimulate cancer cells and could therefore augment the effectiveness of the therapy.

7.9.5 CELL DEATH INHIBITION

Stimulation of cell death and inhibition of cell endurance are the core principles of cancer therapy. Cell death occurs by two antagonistic regulatory events, apoptosis and autophagy. Genes such as *H-ras* and *Bcl-2/Bax* are involved in the

apoptotic pathway. This type of resistance will influence a variety of ranges (possibly all) of anticancer drugs. It also potentially increases the fraction of surviving mutant cells, which leads to larger tumor heterogeneity (Chorawala et al., 2012). *Bcl-2* family protein inhibitors are successful in inducing apoptosis in cancer cells, but its extended use can produce resistance. Autophagy, a vital homeostatic cellular recycling mechanism, is a key player in response to metabolic and therapeutic stresses, makes efforts to retain metabolic homeostasis through the catabolic lysis of excessive proteins and injured or aged organelles (Sui et al., 2013). Autophagy is based on phagolysosomal death in an acidic lysosomal pH. Drugs such as chloroquine and its derivatives check this process by raising the pH to inactivate digestive enzymes in lysosomes. Fluorouracil along with chloroquine is more efficient at treating cancer cells (Sasaki et al., 2010).

7.9.6 EPITHELIAL–MESENCHYMAL TRANSITION AND METASTASIS

By the process of epithelial–mesenchymal transition (EMT) solid tumors become metastatic. It also comprises angiogenesis, that is, the formation of new blood vessels around metastatic tumors (Shang et al., 2013; Singh and Settleman, 2010). Various factors play significant roles in the development of drug resistance in EMT, but these depend on the metastatic grade of the tumor, which is the level of differentiation and degree of EMT. For example, in ERBB2 (HER2)-positive breast cancer, tumors that express high levels of β_1 integrins are more resistant to antibody inhibitors such as trastuzumab (Lenisak et al., 2009). Resistance in cancer cells may also develop in the signaling processes of differentiation, which are vital for EMT. For example, β_3 integrin and src regulate TGFβ-mediated EMT in mammary cancer (Galliher and Schiemann, 2006).

7.10 ADVANTAGES OF NP-BASED DRUG DELIVERY FOR EFFECTIVE CANCER THERAPY

Nanocarriers have established advantages as they may provide a prolonged circulation time and controlled drug release. They also show drug-targeting ability and specificity in the cellular uptake. They can be used for encapsulating a number of drugs for multidrug treatment (Markman et al., 2013). NPs (size 50–100 nm) have proven to be a promising drug carrier for cancer therapy (Che-Ming and Liangfang, 2009). Some of the NP-based drug carriers are available in the market or are in clinical trials. Commercially available NPs and the NPs in clinical trials have been well reviewed by Peer et al. (2007). Schematic representations of different nanoparticulate drug carriers and their advantages are given in Figure 7.1.

7.10.1 PROLONGED SYSTEMIC CIRCULATION

Patel and Rothenberg hypothesized that a permissible high dose of the anticancer drugs could fight against MDR mechanisms of the cancer cells (Patel and Rothenberg, 1994). Highly porous tumor vessels play a fundamental role in EPR effect (Shang et al., 2013; Matsumura et al., 2004). Anticancer drugs of small molecular size and nanosize drug carriers are selectively retained in the ECM within the tumor after they escape from the blood capillaries at the tumor site. However, many anticancer drugs are rapidly eliminated from the body by renal and hepatic clearance, biochemical degradation in plasma, immune opsonization, and by nonselective cellular uptake (Park et al., 2001) and the EPR effect shows no advantage in those cases. Nanosize drug carriers generally provide significantly longer plasma retention time. For this, drug nanocarriers may be an attractive option for cancer therapy. For instance, liposomes were found to be partially successful (Torchilin, 2005). Monocytes and macrophages of the RES generally remove them, but drug remains protected, escaping plasma degradation and glomerular filtration. Stealth liposomes or pegylated (PEG) liposomes showed a predominant increase in circulation half-life (Couvreur and Vauthier, 2006). Pegylated liposome containing doxorubicin (Doxil) showed a favorable and improved pharmacokinetic profile compared with free doxorubicin (Dox) (Gabizon et al., 2003).

7.10.2 TARGETED DRUG DELIVERY

Nonuniform drug distribution and incomplete cancer treatment occur due to poor vascularization and vessel permeability in solid tumors (Matsumura and Maeda, 1986). NPs with targeting ligands, such as antibodies and peptides, are being used to encounter these problems through ligand−receptor interactions (Lammers et al., 2012). Many tumor cells overexpress some antigens and antibodies (against those specific antigens)—conjugated NPs accumulate predominantly at those tumor sites. For instance, anti-HER2 antibody conjugated liposomes showed about 700-fold higher drug accumulation compared to the nonantibody-conjugated liposomes in HER2-overexpressing breast cancer cells (Park et al., 2001). However, the large size of the antibodies often limits their use. Fab fragments have been used as successful targeting ligands (Maruyama et al., 1999). Fab-liposome ameliorated circulation half-life by six fold compared to the antibody-conjugated liposome which showed a twofold increase compared with the nonantibody/Fab-conjugated liposome (Maruyama et al., 1999).

7.10.3 STIMULI-RESPONSIVE DRUG RELEASE

NPs may be suitable to fight MDR in cancer cells. Quick drug release from a formulation may cause rapid drug loss from the circulation. On the other hand, slow drug release may cause drug resistance due to less drug efflux in the tumor. Thus, optimal and balanced drug release may achieve maximum therapeutic efficacy for treating

tumor. Longer circulation time and rapid drug release in tumor may be optimally efficacious in tumor therapy. Stimulus-mediated destabilization of the formulation may provide such characteristics for the formulations. The pH-sensitive activation is an example of such a phenomenon. The tumor environment is generally characteristically acidic (pH 6−6.8) (Kraus and Wolf, 1996). Liposomes are stable at neutral or low alkaline pH (7.0−7.4) of blood. However, liposomal membrane destabilization occurs at acidic pH and the structure becomes permeable in the acidic surroundings of tumors (Kraus and Wolf, 1996). The pH-sensitive micelles are also used due to collapse the micellar structure in acidic conditions (Lee et al., 2008).

7.10.4 DRUG EFFLUX AND DRUG ENDOCYTOSIS

In MDR, before functioning, drug molecules are forced to come out from the tumor site to the surrounding tissue area by a drug efflux mechanism, but drug nanocarriers can partially escape the efflux pumps and are internalized through an endocytotic mechanism (Koval et al., 1998; Rejman et al., 2004).

7.10.5 CO-DELIVERY OF DRUG AND CHEMO-SENSITIZING AGENTS

Anticancer drug along with a chemo-sensitizing agent effectively controls the MDR effect. Chemo-sensitizing agents are P-gp modulators, such as cyclosporine and verapamil, and they typically reduce P-gp activity or expression. The P-gp modulators also regulate transmembrane pumps (of the healthy tissues) which serve as a defensive barrier against foreign molecules (Thiebaut et al., 1987) thus limiting their clinical use. Coencapsulation of P-gp modulators and drug to nanocarriers reversed the MDR effect by reducing the activity of the drug efflux pumps (Soma et al., 2000). Administration of polyalkylcyanoacrylate NPs loaded with Dox and cycloporine A (CyA) restricted MDR as CyA directly binds to P-gp and inhibits its activity (Soma et al., 2000). Ceramide, a secondary messenger in the apoptotic signaling process, when encapsulated in drug-loaded NPs and administered, has successfully overcome MDR (van Vlerken et al., 2007). Liposome has a unique structure for combination therapy. Hydrophilic drug partitions to the aqueous core, whereas the hydrophobic drug separates into the lipid bilayered membrane (Zhang et al., 2009).

Development of drug resistance in cancer cells hinders successful cancer therapy. Inadequate access of drug to the tumor is a predominant cause of drug resistance. Drug nanocarriers such as NPs and nanoliposomes may be one of the possible alternatives as they are mostly capable of providing prolonged circulation time with a specificity to deliver the drug to the target site of action. Besides, they undertake endocytotic internalization and may undergo stimulus-mediated drug release. Furthermore, a number of therapeutic agents can be loaded into the nanocarriers which makes them suitable for combination therapy. These attractive properties of the carrier vehicles may allow them to combat the challenges of drug resistance in the neoplastic cells more effectively.

7.10.6 RECENT TRENDS IN NANOCARRIERS FOR TARGETED CANCER THERAPY

Target specificity of nanoformulations for cancer therapy is more important than any other therapies that currently employ nanotechnology since the anticancer drugs involve more deleterious side effects than any other drugs used in any therapy. More than 30 years ago a phenomenon was observed involving preferential accumulation of certain macromolecules in the tumorous environment (Bertrand et al., 2014; Matsumura and Maeda, 1986). This was later named EPR. This led to the emergence of the possibility of NPs being passively targeted toward cancerous tissues, bypassing the other inert cells depending upon the combination of many complex biological processes such as angiogenesis, enhanced vascular permeation, change in hemodynamic regulation, heterogeneities in tumor genetic profile, irregularities in the tumor microenvironment, and lymphangiogenesis involved with the EPR (Bertrand et al., 2014), since these factors are largely variable and highly irregular when idiosyncracies of different types of cancer, tumor, and patients are taken into account. Also, the tendencies of distribution and accumulation of nanomaterials in tumorous sites are variably influenced by the biological and physicochemical properties of each material (Bertrand et al., 2014). For these reasons the exploitation of EPR as an effective and productive approach for passive targeting may be obsolete, even though the body of works depicting this phenomenon is still being comprehensibly documented (Rabanel et al., 2012). In the last few years, EPR and passive targeting have been molded into work that incorporates the strategies of steric stabilization of nanocarriers beginning with monosialogangliosides (GM1) in the 1990s (Mori et al., 1991) and presently with PEG (Zamboni et al., 2011; Noguchi et al., 1992). The latter works, done by Zamboni et al. (2011), involved liposomes of CKD-602 with surface pegylation of nanocarriers and showed that the nanocarriers were stable and safe from the attack of blood components and internalized by the MPS, increasing their circulation time and subsequently increasing the chances of these carriers encountering and entering the tumor site. The nanocarriers have higher propensity of being accumulated in the tumor interstitium when there is a higher number of phagocytotic and dendritic cells in the tumor microenviroment due to some intrinsic interactions of these cells with the encapsulated materials (Zamboni et al., 2011). PEGylation has been profusely adopted as a suitable strategy for passive targeting as it prevents the recognition of nanocarriers by blood opsonins and enhances the circulation time, which often enforces the EPR effect. This fact has been evidenced previously from the studies of Han et al. (2006) and Harrington et al. (2001b). The animal model they used for studying tumor accumulation of liposomes containing doxorubicin and radiolabels respectively, produced a very high tumor to blood ratio of the aforementioned components. Recently, Esfahani et al. (2014) prepared paclitaxel-loaded nanoliposomes that were pegylated and used against breast cancer cells. While the mean diameter, encapsulation efficiency and *in vitro* drug release profile for both the pegylated and nonpegylated

formulations did not differ very much, the cytotoxicity of pegylated nanoliposomal paclitaxel was higher than nonpegylated species with statistical significance enough to conclude that the pegylated nanoliposomes might be the superior candidate (Esfahani et al., 2014). But perhaps the most important work on pegylation was done during the trials of pegylated doxorubicin liposomes which demonstrated the efficacy of first-generation anticancer nanomedicines in decreasing the mortality rate in humans (Liu et al., 2012; Gabizon et al., 1994; Northfelt et al., 1996; Symon et al., 1999; Harrington et al., 2001a; Koukourakis et al., 2000).

The doxorubicin levels in the tumor sites were usually 4- to 16-fold higher with the liposomes than free doxorubicin, 3−7 days after administration (Gabizon et al., 1994; Northfelt et al., 1996). Other surface modifiers, such as detergents and fusogenic lipids, that either disrupt or fuse with the cell membrane lining also enhance the passive targeting of nanocarriers which may sometimes be translated into superior efficacy of the formulations in cancer therapy. Sharma et al. (2013) investigated surface-modified NPs that had greater interactions with the cancer cell lipids to improve tumor targeting and delivery of recombinant pCEP4 vector containing cytomegalovirus-driven wild-type human p53 cDNA. The surface modifiers used were the surfactants and didodecyldimethyl ammonium bromide (DMAB) and cetyltrimethyl ammonium bromide (CTAB), which led to increased biophysical interaction with the membrane lipids of cancer cells. They found that NPs surface-modified with DMAB and CTAB-modified species produced increased uptake with human prostate cancer cell culture (PC-3) (6.7-fold) and HUVEC (5.5-fold) than with unmodified NPs due to greater interaction of the modified NPs. The DMAB-modified NPs specifically showed higher affinity ($>$ twofold) toward the cancerous PC-3 cells than the endothelial cells, which was evident on increasing the incubation time. This certainly establishes the chance of using such surfactants for passive targeting purposes since the surfactants were more successful in targeting cancerous cell lipids than common epithelial cells due to the intrinsic biophysical characteristics which are unique to tumor microenvironments.

The use of magnetic NPs and ultrasound-guided nanocarriers are gaining importance as compatible methods for enhancing passive targeting in cancer therapies. Momtazi et al. (2014) designed and synthesized a magnetic nanocarrier consisting of a SPIO core and biocompatible and biodegradable poly(sebacic anhydride)-block-methyl ether poly(ethylene glycol) (PSA-mPEG) polymer matrix for targeting cancer cells. *In vitro* cell viability and cellular uptake of SPIO-polymeric NPs with MDA-MB-231 breast cancer cells were investigated and the MDA-MBA-231 cells showed internalization of SPIO-polymeric NPs within a size range of 150−200 nm after 24 h. This has led to the suggestion that SPIO-polymeric NPs may have the required properties for passive targeting and could be useful for future studies of targeted cancer therapy. Using ultrasound may not alter the formulation step but may act as an adjuvant to the passive targeting capabilities of nanocarriers. Oh et al. (2014) developed docetaxel-loaded pluronic NPs and investigated their viability using high-intensity focused

ultrasound (HIFU) as an external stimulus-induced clinical system for enhancement of tumor targeting. Maximum accumulation of NPs was observed at an HIFU exposure of 20 W/cm^2 and above this value tumor tissue and blood vessels were destroyed. Thus, tumor targeting and effective extravasation of pluronic NPs into the interior cells of tumor tissue were confirmed with HIFU exposure which might increase the pore size of tumor tissue and enhanced permeability of pluronic NPs through a nonthermal mechanism and thereby increase the effectiveness of the therapy. Another recent study threw up an interesting approach of exploiting the microenviroment of the epithelial cells in the tumor site. Voigt et al. (2014) experimented with polyelectrolyte-modified NPs that were preferentially taken up by endothelial or epithelial cells. This was achieved through the interaction of the polyelectrolytes with the clathrin- and caveolin-mediated endocytosis. Anionic polyelectrolytes of varying lipophilicity were found to influence endothelial and epithelial cell uptake of NPs including a synthetic polyelectrolyte called polyvinyl sulfonic acid, composed of an aromatic sulfonic acid backbone, which exhibited specific affinity for the caveolae of endothelial cells. By exploiting the fact that higher expression of caveolae occurs in endothelial cells (e.g., HUVEC) than the epithelial cells (e.g., HeLa culture), a purely physiochemical approach for passive targeting of NPs to endothelial cells may be suggested. Thus, by altering the charge and lipophilic characteristics of the NP surface, one can evolve a strategy of achieving targeted delivery without the need for receptor−ligand-type targeting strategies.

Active targeting or ligand-mediated targeting (Bertrand et al., 2014) of nanocarriers to cancerous cells or tumorous endothelial cells (Ku et al., 2014) has gained more popularity over passive targeting recently because it provides a window of increasing specificity of the therapy as these strategies strive to enhance the cellular uptake of nanocarriers, rather than accumulation in the tumor site (Ku et al., 2014). As of the time of writing, only a few targeted liposomes and polymeric NPs have seen the light of clinical studies (Sanna et al., 2014). Among liposomes, one of the prototypes that was studied extensively was MCC-465, a novel pegylated liposomal doxorubicin formulation conjugated with antigen-binding fragments F(ab′)2 from the Goat Antihuman IgG (GAH) antibody (Matsumura et al., 2004). The formulation utilized pegylation to confer immune shielding and the antigen-binding fragments for targeting, respectively, against the endothelial cells of human stomach cancer (Matsumura et al., 2004). Another liposomal nanocarrier under clinical trial is MBP-426, a transferrin-conjugated liposome that contains the platinum-based cytotoxic drug oxaliplatin. The formulation has been targeted against human gastroesophageal adenocarcinoma and has progressed into phase II trials (Sanna et al., 2014). Another such liposomal formulation was SGT53-01, which was surface-functionalized with antitransferrin receptor single-chain antibody fragment (TfRscFv) as the targeting ligand. The liposome contained the p53 tumor suppressor gene to cancer cells, and is currently undergoing phase I clinical trials in combination with doxorubicin as a multifunctional nanoformulation for the treatment of solid tumors (Sanna et al.,

2014). More recently, a new nanoimmunoliposomal formulation containing doxorubicin, called C225-ILS-DOX, gained entry into phase I investigation against solid tumor type cancers expressing anti-EGFRs (Sanna et al., 2014; Mamot et al., 2012). The ligands used for this purpose were antigen-binding fragments of the chimeric monoclonal antibody cetuximab (C225, Erbitux), which were covalently conjugated to the liposome (Mamot et al., 2011, 2012). Antibody fragment of anti-Her2 antibody (AbscFv) has also been used as a targeting ligand for a liposomal formulation MM-302 for delivering doxorubicin in Her2-expressing breast cancer cell lines and is also undergoing clinical evaluation in phase I (Wickham and Futch, 2012).

Among targeted polymeric nanocarriers, CALAA-01 was the first to reach clinical development. The formulation was designed as cyclodextrin-based pegylated NPs tailored to deliver anti-RRM2, an siRNA which is capable of reducing expression of the M2 subunit of ribonucleotide reductase (Sanna et al., 2014) using transferrin as the targeting ligand. The safety of the formulation CALAA-01 was evaluated in a phase I clinical trial by conducting IV administration to adults with solid tumors (Davis, 2009). Another such formulation under phase I trials is Atu027 tailored for siRNA delivery into solid tumor cells with the ligand protein kinase N3 conjugated on its surface (Sanna et al., 2014). Also in phase I trials is the formulation C-VISA-BikDD that uses proapoptotic genes as targeting ligands for delivering BikDD plasmid DNA into cells of pancreatic cancer (Sanna et al., 2014). A new docetaxel-loaded targeted nanomedicine, BIND-014 (Hrkach et al., 2012) has been developed by a team led by Langer and Farokhzad at the Massachusetts Institute of Technology, Harvard Medical School, and BIND Therapeutics and recently entered phase II clinical trial for the treatment of solid tumors such as prostate cancer. The formulation consisted of a biodegradable copolymeric core (PLA or PLGA and PEG) and a pseudomimetic dipeptide as a prostate-specific membrane antigen (PSMA)-targeting ligand (Hrkach et al., 2012).

Besides them, a large body of on-going work contributes regularly to the development of nanocarriers using varying ligands like antibody, aptamers, proteins, peptides, and other small molecules targeted toward cancer cells. Jang et al. (2014) synthesized silica (SiO_2)-core-shell iron oxide (Fe_3O_4) magnetic NPs conjugated with human monoclonal antibody trastuzumab and encapsulated in liposomes to target the Her2/*neu* antigen-expressing breast cancer cells. The resultant particles had good biological stability and trastuzumab-conjugation increased specific targeting on Her2/*neu*-positive human SKBR-3 breast cancer cells against unmodified liposome-encapsulated magnetic NPs. Another work on targeting of nanocarriers with antibody conjugation was done by Maya et al. (2013). They developed cetuximab conjugated O-carboxymethyl chitosan NPs containing paclitaxel (PTXL) for targeting EGFR overexpressing cancer cells. *In vitro* study showed that the modified formulation induced significant cytotoxicity against cancer cell lines like A549, A431, and SKBR3, which expressed EGFR, compared to MIAPaCa-2 cells that did not express the receptor, thus underlining the

target specificity of the formulation, which delivered paclitaxel and induced cytotoxicity only to the desired target cells. Choi et al. (2015) synthesized inhalable self-assembled human serum albumin (HSA) NPs containing doxorubicin with TNF-related apoptosis-inducing ligand (TRAIL) protein as a targeting ligand that specifically binds to death receptors 4 and 5 (DR 4/5) expressed by various cancer cells. The TRAIL-HAS-doxorubicin formulation exhibited an antitumor effect through a synergistic cytotoxicity/apoptotic activity in H226 lung cancer cells (since H226 cells are resistant to TRAIL-induced apoptosis) significantly reduced the tumor size of H226-implanted BALB mice. Works involving aptamer-mediated targeting are also becoming prominent since the pioneering works of Farokhzad et al. (2006) and Dhar et al. (2008), which used RNA aptamers A10 to target and bind with the PSMA for prostate cancer tumors. Xu et al. (2013) prepared unimolecular micelles consisting of a hydrophobic core of Boltron H40 with PLA branches and a hydrophilic shell of PEG containing doxorubicin. The micelle was surface-modified using A10 aptamer that exhibited preferential cytotoxicity in PSMA expressing CWR22Rn1 Prostate carcinoma cells and equally significant tumor reduction in CWR22Rn1 Prostate carcinoma induced mice when compared against nontargeted formulations. Another study employed chitosan NPs conjugated with aptamers targeting MUC1 glycoproteins expressed by human colon cancer cells. The formulation delivered anticancer molecule SN38, an active metabolite of natural product irinotecan, to HT-29 cell lines and the efficacy of the targeting ligands in enhancing cellular uptake was evaluated through cytotoxicity assay, which proved the aptamer-conjugated formulation to be more toxic than the nontargeted ones (Sayari et al., 2014). Peptide sequences can also act as targeting ligands as is evident from extensive use of RGD (arginine−glycine−aspartic acid) peptide which can strongly and specifically bind to $\alpha_v\beta_3$ integrin receptors (Kamaly et al., 2012; Shi et al., 2011). But the applicability of RGD in targeting cancer cells may be limited as $\alpha_v\beta_3$ integrin is also widely expressed on normal or inflamed tissues (Bertrand et al., 2014). Structure−activity relationship studies revealed that a change of molecular geometry of linear RGD peptides to its cyclic form increased antitumor efficiency 10-fold compared with that of its linear counterpart (Colombo et al., 2002). Xiao et al. (2012) prepared multifunctional unimolecular micelle made of a hyperbranched amphiphilic block copolymer H40-poly(L-glutamate-hydrazone-doxorubicin)-*b*-poly(ethylene glycol) for delivering doxorubicin with cyclic RGD as a targeting ligand for cancer therapy. The prepared cRGD-conjugated unimolecular micelles exhibited more prominent cellular uptake and cytotoxicity in U87MG human glioblastoma cells than nontargeted unimolecular micelles and also reduced tumor size in U87MG tumor-bearing mice, measured by noninvasive PET imaging. The role of cyclic RGD in targeting was further established by them through an initial blocking dose of cyclic RGD which reduced the cytotoxic and antitumor effect of subsequent RGD-conjugated formulations due to saturation of the receptor sites. Valetti et al. (2014) worked with another peptide sequence as their targeting ligand—CKAAKN—conjugated on squalene

monodisperse NPs for delivering the anticancer drug gemcitabine (in its squalenoyl prodrug form). The CKAAKN interacts specifically with the Wnt-2 mimetic pathway involving the Frizzled receptor 5 (FZD-5), that promotes vascular anomalies and angiogenesis in tumor vessels found in the RIP-Tag2 transgenic mice, a prototypical mouse model used for studying multistage pancreatic islet cell carcinoma. The formulation was also found to promote pericyte coverage, which resulted in normalization of the vasculature and improvement of the tumor accessibility for further therapy, as measured through quantification assay of α-smooth muscle actin (α-SMA) and of antibody rabbit anti-NG2 (chondroitin sulfate proteoglycan polyclonal) co-localized with tumor endothelial cells. Folic acid has been another popular candidate for targeting ligand which binds with the FR overexpressed on the surface of a variety of human tumors, including ovarian, brain, breast, colon, renal, and lung cancers (Hilgenbrink and Low, 2005; Markert et al., 2008). Yu et al. (2014) synthesized NPs from cholesterol-modified glycol chitosan with dual functionalization, one through conjugation of folic acid and another through the conjugation of a peptide sequence CGYGPKKKRKVGG (an SV40 large-T antigen with the primary sequence KKKRK), which acts as a nuclear localization signal so that the particle is recognized by the nuclear transport proteins, that is, importin α and importin β. The targeted formulation containing doxorubicin as cytotoxic agent and coumarin-6 as imaging agent, showed efficient intracellular trafficking and nucleus transportation in FR-expressing human nasopharyngeal epidermoid carcinoma (KB) cells and also exhibited lower IC_{50} than other nontargeted formulations. The doxorubicin formulations also showed the strongest antitumor efficacy against KB tumor xenograft models in female BALB/c nude mice. The specificity of the formulations toward the FRs were established by the reduced intracellular uptake of the targeted formulations by the human lung carcinoma cells (A549) which do not express FRs. Another recent study was done by Li et al. (2014) who prepared folic-acid-conjugated poly(ethylene glycol)−chitosan oligosaccharide lactate NPs for delivering siRNAs targeting against human HIF-1α, which has been reported to inhibit angiogenesis and tumor cellular energy production resulting in growth suppression in ovarian cancer. An *in vitro* study was done using human ovarian endometrioid carcinoma OVK18#2 cells, which expressed FRs and an *in vivo* study was done using OVK18#2 xenograft in nude BALB mice. The targeted NPs showed higher preferences toward the folate-receptor-expressing carcinoma cell line than the ones devoid of such receptors like mouse macrophage RAW 264.7 cells. This result was also seen in the tumor reduction efficiency in xenografted mice acted upon by targeted formulations. A unique strategy in active targeting that came forward recently was promulgated by You et al. (2014) in their experiment of targeting cancer cells with a molecularly assembled logic robot, called the Nano-Claw built by using aptamers as building blocks, which can recognize the expression levels of multiple cell membrane markers expressed as surface antigens by cancer cells and induce therapeutic operations as an automation. The logic robot comprised an oligonucleotide backbone as the scaffold, several structure-switchable aptamers as capture

toes, which targeted each cell-surface marker and then generated the respective barcode oligonucleotide for activation of the last component of the robot (the effector toe), which is a logic-gated DNA duplex that analyzes these barcode oligonucleotides and autonomously makes decisions in generating a diagnostic signal (such as fluorescence) or a therapeutic effect. This particular study involved three aptamers for three cell lines Sgc8c, Sgc4f, and TC01 that overexpressed markers commonly found on cancer cells, such as human acute lymphoblastic leukemia cells (CCRF-CEM). The programmable nature of nucleic acids makes this particular strategy susceptible to further scale-up and amplification through covalently linking these probes with other visual reporting systems, drugs, or NPs with anticancer effect.

7.11 CONCLUSIONS

The platform provided by multifunctional drug nanocarriers has shown their potential in drug targeting, as well as in cancer diagnosis and therapy. Nanocarriers also hold a major role in delivering multiple drugs directed against different molecular targets, probably resulting in suppression of multiple-drug-resistant phenotypes as well as decreasing MDR-based drug efflux. The cancer targeting concept through active targeting considering the complex nature of tumor and the tumor-surrounding microenvironment has described the optimal conditions for future therapeutic tools in cancer therapy. The payload of the targeted nanocarriers may be drug, a gene silencing sequence, a radioisotope, or a combination type, and thus provides unlimited possibilities in cancer therapeutics. Based on the pharmaceutical and physiological factors, the appropriate approach may be chosen for designing and scaling-up nanocarriers to clinics. Several such engineered therapies are already in clinical practice. Thus, nanocarrier systems which specifically target different portions of tumors by using different targeting moieties may eliminate the problems of multidrug-resistant tumors.

REFERENCES

Abreu, A.S., Castanheira, E.M., Queiroz, M.J.R., Ferreira, P.M., Vale-Silva, L.A., Pinto, E., 2011. Nanoliposomes for encapsulation and delivery of the potential antitumoral methyl 6-methoxy-3-(4-methoxyphenyl)-1H-indole-2-carboxylate. Nanoscale Res. Lett. 6, 482.

Acharya, S., Dilnawaz, F., Sahoo, S.K., 2009. Targeted epidermal growth factor receptor nanoparticle bioconjugates for breast cancer therapy. Biomaterials 30, 5737–5750.

Alexis, F., Pridgen, E., Molnar, L.K., Farokhzad, O.C., 2008. Factors affecting the clearance and biodistribution of polymeric nanoparticles. Mol. Pharm. 5, 505–515.

Alexis, F., Rhee, J.W., Richie, J.P., Radovic-Moreno, A.F., Langer, R., Farokhzad, O.C., 2008a. New frontiers in nanotechnology for cancer treatment. Urol. Oncol. 26, 74–85.

American Cancer Society, 2011. Global Cancer Facts & Figures, second ed. American Cancer Society, Atlanta. Available from: <http://www.cancer.org/acs/groups/content/@epidemiologysurveilance/documents/document/acspc-027766.pdf> (Last citation on 1st Dec, 2015).

Anajwala, C.C., Jani, G.K., Swamy, S.M.V., 2010. Current trends of nanotechnology for cancer therapy. Int. J. Pharm. Sci. Nanotech. 3, 1043–1056.

Ang, C.Y., Tan, S.Y., Zhao, Y., 2014. Recent advances in biocompatible nanocarriers for delivery of chemotherapeutic cargoes towards cancer therapy. Org. Biomol. Chem. 12, 4776–4806.

Aruna, U., Rajalakshmi, R., Muzib, Y.I., Vinesha, V., Sushma, M., Vandana, K.R., et al., 2013. Formulation and evaluation of Felodipine mouth dissolving tablets by using solubility enhancing technique. Int. J. Inn. Pharm. Res. 4, 318–324.

Bae, Y.H., Park, K., 2011. Targeted drug delivery to tumors: myths, reality and possibility. J. Control. Rel. 153, 198–205.

Bajpai, A.K., Shukla, S.K., Bhanu, S., Kankane, S., 2008. Responsive polymers in controlled drug delivery. Prog. Polym. Sci. 33, 1088–1118.

Bakry, R., Vallant, R.M., Najam-ul-Haq, M., Rainer, M., Szabo, Z., Huck, C.W., et al., 2007. Medicinal applications of fullerenes. Int. J. Nanomed. 2, 639–649.

Bertrand, N., Wu, J., Xu, X., Kamaly, N., Farokhzad, O.C., 2014. Cancer nanotechnology: the impact of passive and active targeting in the era of modern cancer biology. Adv. Drug Deliv. Rev. 66, 2–25.

Blanco, M.D., Teijón, C., Olmo, R.M., Teijón, J.M., 2012. In: Sezer, A.D. (Ed.), Recent Advances in Novel Drug Carrier Systems. InTech, Croatia.

Bonadonna, G., Zucali, R., Monfardini, S., De Lena, M., Uslenghi, C., 1975. Combination chemotherapy of Hodgkin's disease with adriamycin, bleomycin, vinblastine, and imidazole carboxamide versus MOPP. Cancer 36, 252–259.

Bonanno, L., Favaretto, A., Rosell, R., 2014. Platinum drugs and DNA repair mechanism in lung cancer. Anticancer Res. 34, 493–502.

Byrne, J.D., Betancourt, T., Brannon-Peppas, L., 2008. Active targeting schemes for nanoparticle systems in cancer therapeutics. Adv. Drug Deliv. Rev. 60, 1615–1626.

Cai, W., Chen, X., 2007. Nanoplatforms for targeted molecular imaging in living subjects. Small 3, 1840–1854.

Cai, L.L., Liu, P., Li, X., Huang, X., Ye, Y.Q., Chen, F.Y., 2011. RGD peptide mediated chitosan-based polymeric micelles targeting delivery for integrin-over expressing tumor cells. Int. J. Nanomed. 6, 3499–3508.

Cao, Z., Tong, R., Mishra, A., Xu, W., Wong, G.C., Cheng, J., et al., 2009. Reversible cell-specific drug delivery with aptamer-functionalized liposomes. Angew. Chem. Int. Ed. Engl. 48, 6494–6498.

Çevik, Ö., Gürsoy, R.N., 2011. Analytical method development and validation for the anticancer peptide, Lyp-1. Hacettepe Uni. J. Faculty Pharm. 31, 97–108.

Chang, D.K., Lin, C.T., Wu, C.H., Wu, H.C., 2009. A novel peptide enhances therapeutic efficacy of liposomal anti-cancer drugs in mice models of human lung cancer. PLos One 4, e4171.

Che-Ming, J.H., Liangfang, Z., 2009. Therapeutic nanoparticles to combat cancer drug resistance. Curr. Drug Metab. 10, 836–841.

Chen, Z.G., 2010. Small-molecule delivery by nanoparticles for anticancer therapy. Trends Mol. Med. 16, 594–602.
Chen, Z., Ma, L., Liu, Y., Chen, C., 2012. Applications of functionalized fullerenes in tumor theranostics. Theranostics 2, 238–250.
Cheng, F., Tsvetkova, I.B., Khuong, Y.-L., Moore, A.W., Arnold, R.J., Goicochea, N.L., 2013. The packaging of different cargo into enveloped viral nanoparticles. Mol. Pharm. 10, 51–58.
Cho, K., Wang, X., Nie, S., Chen, Z., Shin, D.M., 2008. Therapeutic nanoparticles for drug delivery in cancer. Clin. Cancer Res. 14, 1310–1316.
Choi, Y., Thomas, T., Kotlyar, A., Islam, M.T., Baker Jr., J.R., 2005. Synthesis and functional evaluation of DNA-assembled polyamidoamine dendrimer clusters for cancer cell-specific targeting. Chem. Biol. 12, 35–43.
Choi, S.H., Byeon, H.J., Choi, J.S., Thao, L., Kim, I., Lee, E.S., et al., 2015. Inhalable self-assembled albumin nanoparticles for treating drug-resistant lung cancer. J. Control Rel. 197, 199–207.
Chorawala, M.R., Oza, P.M., Shah, G.B., 2012. Mechanisms of anticancer drugs resistance: an overview. Int. J. Pharm. Sci. Drug Res. 4, 1–9.
Colombo, G., Curnis, F., Mori, G.M.S.D., Gasparri, A., Longoni, C., Sacchi, A., et al., 2002. Structure–activity relationships of linear and cyclic peptides containing the NGR tumor-homing motif. J. Biol. Chem. 277, 47891–47897.
Couvreur, P., Vauthier, C., 2006. Nanotechnology: intelligent design to treat complex disease. Pharm. Res. 23, 1417–1450.
Cuong, N.V., Hsieh, M.F., 2009. Recent advances in pharmacokinetics of polymeric excipients used in nanosized anti-cancer drugs. Curr. Drug Metab. 10, 842–850.
Dameron, K.M., Volpert, O.V., Tainsky, M.A., et al., 1994. Control of angiogenesis in fibroblasts by p53 regulation of thorombospongin-1. Science 265, 1582–1584.
Danhier, F., Feron, O., Preat, V., 2010. To exploit the tumor microenvironment: passive and active tumor targeting of nanocarriers for anti-cancer drug delivery. J. Control. Rel. 148, 135–146.
Danquah, M.K., Zhang, X.A., Mahato, R.I., 2011. Extravasation of polymeric nanomedicines across tumor vasculature. Adv. Drug Deliv. Rev. 63, 623–639.
Davis, M.E., 2009. The first targeted delivery of siRNA in humans via a self-assembling, cyclodextrin polymer-based nanoparticle: from concept to clinic. Mol. Pharm. 6, 659–668.
Davis, M.E., Chen, Z.G., Shin, D.M., 2008. Nanoparticle therapeutics: an emerging treatment modality for cancer. Nature Rev. Drug Discov. 7, 771–782.
Dhar, S., Gu, F.X., Langer, R., Farokhzad, O.C., Lippard, S.J., 2008. Targeted delivery of cisplatin to prostate cancer cells by aptamer functionalized Pt(IV) prodrug-PLGA–PEG nanoparticles. Proc. Nat. Acad. Sci. 105, 17356–17361.
Diaz, M.R., Vivas-Mejia, P.E., 2013. Nanoparticles as drug delivery systems in cancer medicine: emphasis on RNAi-Containing nanoliposomes. Pharmaceuticals 6, 1361–1380.
Dilnawaz, F., Acharya, S., Misra, R., Singh, A., Sahoo, S.K., 2011. Nanotechnology and drug delivery. In: Sattler, K.D. (Ed.), Hand Book of Nanophysics: Nanomedicine and Nanorobotics. CRC Press Taylor and Francis Group, Boca Raton, FL, p. 27.4.
Dong, X., Mumper, R.J., 2010. Nanomedicinal strategies to treat multidrug-resistant tumors: current progress. Nanomedicine (Lond) 5, 597–615.
Drbohlavova, J., Chomoucka, J., Adam, V., Ryvolova, M., Eckschlager, T., Hubalek, J., et al., 2013. Nanocarriers for anticancer drugs—new trends in nanomedicine. Curr. Drug Metab. 14, 547–564.

Erguen, S., Hohn, H.P., Kilic, N., Singer, B.B., Tilki, D., 2008. Endothelial and hematopoietic progenitor cells (EPCs and HPCs): hand in hand fate determining partners for cancer cells. Stem Cell Rev. 4, 169–177.

Esfahani, M.K.M., Alavi, S.E., Akbarzadeh, A., Ghassemi, S., Saffari, Z., Farahnak, M., et al., 2014. Pegylation of nanoliposomal paclitaxel enhances its efficacy in breast cancer. Trop. J. Pharm. Res. 13, 95.

Farokhzad, O.C., Cheng, J., Teply, B.A., Sherifi, I., Jon, S., Kantoff, P.W., et al., 2006. Targeted nanoparticle-aptamer bioconjugates for cancer chemotherapy *in vivo*. Proc. Nat. Acad. Sci. 103, 6315–6320.

Fattal, E., Couvreur, P., Dubernet, C., 2004. "Smart" delivery of antisense oligonucleotides by anionic pH-sensitive liposomes. Adv. Drug Deliv. Rev. 56, 931–946.

Federico, P., Vladimir, P.T., 2013. Recent trends in multifunctional liposomal nanocarriers for enhanced tumor targeting. J. Drug Del.32, Article ID 705265.

Fonseca, C., Simoes, S., Gaspar, R., 2002. Paclitaxel-loaded PLGA nanoparticles: preparation, physicochemical characterization and *in vitro* anti-tumoral activity. J. Control. Rel. 83, 273–286.

Fukuda, Y., Schuetz, J.D., 2012. ABC transporters and their role in nucleoside and nucleotide drug resistance. Biochem. Pharmacol. 83, 1073–1083.

Gabizon, A., Catane, R., Uziely, B., Kaufman, B., Safra, T., Cohen, R., et al., 1994. Prolonged circulation time and enhanced accumulation in malignant exudates of doxorubicin encapsulated in polyethylene-glycol coated liposomes. Cancer Res. 54, 987–992.

Gabizon, A., Shmeeda, H., Barenholz, Y., 2003. Pharmacokinetics of pegylated liposomal doxorubicin: review of animal and human studies. Clin. Pharmacokinet. 42, 419–436.

Galliher, A.J., Schiemann, W.P., 2006. β3 integrin and Src facilitate transforming growth factor-β mediated induction of epithelial-mesenchymal transition in mammary epithelial cells. Breast Cancer Res. 8, R42.

Gamcsik, M.P., Dubay, G.R., Cox, B.R., 2002. Increased rate of glutathione synthesis from cystine in drug-resistant MCF-7 cells. Biochem. Pharmacol. 63, 843–851.

Gorre, M.E., Mohammed, M., Ellwood, K., Hsu, N., Paquette, R., Rao, P.N., et al., 2001. Clinical resistance to STI-571 cancer therapy caused by BCRABL gene mutation or amplification. Science 293, 876–880.

Gottesman, M.M., 2002. Mechanisms of cancer drug resistance. Annu. Rev. Med. 53, 615–627.

Haley, B., Frenkel, E., 2008. Nanoparticles for drug delivery in cancer treatment. Urol. Oncol. 26, 57–64.

Han, H.D., Lee, A., Song, C.K., Hwang, T., Seong, H., Lee, C.O., et al., 2006. *In vivo* distribution and antitumor activity of heparin-stabilized doxorubicin-loaded liposomes. Int. J. Pharm. 313, 181–188.

Hans, M.L., Lowman, A.M., 2002. Biodegradable nanoparticles for drug delivery and targeting. Curr. Opin. Solid State Mater. Sci. 6, 319–327.

Harrington, K.J., Mohammadtaghi, S., Uster, P.S., Glass, D., Peters, A.M., Vile, R.G., et al., 2001a. Effective targeting of solid tumors in patients with locally advanced cancers by radiolabeled PEGylated liposomes. Clin. Cancer Res. 7, 243–254.

Harrington, K.J., Rowlinson-Busza, G., Syrigos, K.N., Uster, P.S., Vile, R.G., Peters, A.M., et al., 2001b. The effect of irradiation on the biodistribution of radiolabeled pegylated liposomes. Int. J. Radiat. Oncol. Biol. Phys. 50, 809–820.

Heldin, C.H., Rubin, K., Pietras, K., Ostman, A., 2004. High interstitial fluid pressure—an obstacle in cancer therapy. Nat. Rev. Cancer 4, 806–813.
Hilgenbrink, A.R., Low, P.S., 2005. Folate receptor-mediated drug targeting: from therapeutics to diagnostics. J. Pharm. Sci. 94, 2135–2146.
Housman, G., Byler, S., Heerboth, S., Lapinska, K., Longacre, M., Snyder, N., et al., 2014. Drug resistance in cancer: an overview. Cancers (Basel) 6, 1769–1792.
Hrkach, J., Hoff, V.D., Ali, M.M., Andrianova, E., Auer, J., Campbell, T., et al., 2012. Preclinical development and clinical translation of a PSMA-targeted docetaxel nanoparticle with a differentiated pharmacological profile. Sci. Transl. Med. 4, 1–11.
Huh, K.M., Min, H.S., Lee, S.C., Lee, H.J., Kim, S., Park, K., 2008. A new hydrotropic block copolymer micelle system for aqueous solubilization of paclitaxel. J. Control Rel. 126, 122–129.
Hussain, M., Shchepinov, M., Sohail, M., Benter, I.F., Hollins, A.J., Southern, E.M., et al., 2004. A novel anionic dendrimer for improved cellular delivery of antisense oligonucleotides. J. Control Rel. 99, 139–155.
Iyer, K.A., Singh, A., Ganta, S., Amiji, M.M., 2013. Role of integrated cancer nanomedicine in overcoming drug resistance. Adv. Drug Deliv. Rev. 65, 1784–1802.
Jain, R.K., 1994. Barriers to drug delivery in solid tumors. Sci. Am. 271, 58–65.
Jain, R.K., Stylianopoulos, T., 2010. Delivering nanomedicine to solid tumors. Nat. Rev. Clin. Oncol. 7, 653–664.
Jang, M., Yoon, Y.I., Kwon, Y.S., Yoon, T.J., Lee, H.J., Hwang, S.I., 2014. Trastuzumab-conjugated liposome-coated fluorescent magnetic nanoparticles to target breast cancer. Korean J. Radiol. 15, 411–422.
Kagaya, H., Oba, M., Miura, Y., Koyama, H., Ishii, T., Shimada, T., 2012. Impact of polyplex micelles installed with cyclic RGD peptide as ligand on gene delivery to vascular lesions. Gene Ther. 19, 61–69.
Kakde, D., Jain, D., Shrivastava, V., Kakde, R., Pati, A.T., 2011. Cancer therapeutics-opportunities, challenges and advances in drug delivery. J. Appl. Pharm. Sci. 1, 1–10.
Kam, N.W.S., O'Connell, M., Wisdom, J.A., Dai, H., 2005. Carbon nanotubes as multifunctional biological transporters and near-infrared agents for selective cancer cell destruction. Proc. Nat. Acad. Sci. USA 102, 11600–11605.
Kamaly, N., Xiao, Z., Valencia, P.M., Radovic-Moreno, A.F., Farokhzad, O.C., 2012. Targeted polymeric therapeutic nanoparticles: design, development and clinical translation. Chem. Soc. Rev. 41, 2971–3010.
Kang, K.W., Chun, M.K., Kim, O., Subedi, R.K., Ahn, S.G., Yoon, J.H., et al., 2010. Doxorubicin-loaded solid lipid nanoparticles to overcome multidrug resistance in cancer therapy. Nanomed. Nanotech. Biol. Med. 6, 210–213.
Karra, N., Benita, S., 2012. The ligand nanoparticle conjugation approach for targeted cancer therapy. Curr. Drug Metab. 13, 22–41.
Kazi, K.M., Mandal, A.S., Biswas, N., Guha, A., Chatterjee, S., Behera, M., et al., 2010. Niosome: a future of targeted drug delivery systems. J. Adv. Pharm. Technol. Res. 1, 374–380.
Khan, D.R., 2010. The use of nanocarriers for drug delivery in cancer therapy. J. Cancer Sci. Ther. 2, 58–62.
Khosravi-Darani, K., Mozafari, M.R., 2010. Nanoliposome potentials in nanotherapy: a concise overview. IJNN 6, 3–13.

Kim, K.Y., 2007. Nanotechnology platforms and physiological challenges for cancer therapeutics. Nanomed. Nanotech. Biol. Med. 3, 103–110.

King, D.J., Safar, J.G., Legname, G., Prusiner, S.B., 2007. Thioaptamer interactions with prion proteins: sequence-specific and non-specific binding sites. J. Mol. Biol. 369, 1001–1014.

Koukourakis, M.I., Koukouraki, S., Fezoulidis, I., Kelekis, N., Kyrias, G., Archmandritis, S., et al., 2000. High intratumoural accumulation of stealth liposomal doxorubicin (Caelyx®) in glioblastomas and in metastatic brain tumours. Br. J. Cancer 83, 1281–1286.

Koval, M., Preiter, K., Adles, C., Stahl, P.D., Steinberg, T.H., 1998. Size of IgG-opsonized particles determines macrophage response during internalization. Exp. Cell Res. 242, 265–273.

Kraus, M., Wolf, B., 1996. Implications of acidic tumor microenvironment for neoplastic growth and cancer treatment: a computer analysis. Tumour Biol. 17, 133–154.

Ku, S.H., Kim, K., Choi, K., Kim, S.H., Kwon, I.C., 2014. Tumor-targeting multifunctional nanoparticles for siRNA delivery: recent advances in cancer therapy. Adv. Healthcare Mater. 3, 1182–1193.

Kwon, K., Lee, S.C., Han, B., Park, K., 2012. Analysis on the current status of targeted drug delivery to tumors. J. Control Rel. 164, 108–114.

Lacerda, L., Bianco, A., Prato, M., Kostarelos, K., 2006. Carbon nanotubes as nanomedicines: from toxicology to pharmacology. Adv. Drug Deliv. Rev. 58, 1460–1470.

Lamba, J.K., Lin, Y.S., Schuetz, E.G., Thummel, K.E., 2002. Genetic contribution to variable human CYP3A-mediated metabolism. Adv. Drug Deliv. Rev. 54, 1271–1294.

Lammers, T., Kiessling, F., Hennink, E.W., Storm, G., 2012. Drug targeting to tumors: principles, pitfalls and (pre-) clinical progress. J. Control Rel. 161, 175–187.

Lee, T.Y., Lin, C.T., Kuo, S.Y., Chang, D.K., Wu, H.C., 2007. Peptide-mediated targeting to tumor blood vessels of lung cancer for drug delivery. Cancer Res. 67, 10958–10965.

Lee, E.S., Gao, Z., Bae, Y.H., 2008. Recent progress in tumor pH targeting nanotechnology. J. Control Rel. 132, 164–170.

Lenisak, D., Xu, Y., Deschenes, J., Lai, R., Thoms, J., Murray, D., et al., 2009. Beta1-integrin circumvents the antiproliferative effects of trastuzumab in human epidermal growth factor receptor-2-positive breast cancer. Cancer Res. 69, 8620–8628.

Li, T.S.C., Yawata, T., Honke, K., 2014. Efficient siRNA delivery and tumor accumulation mediated by ionically cross-linked folic acid–poly(ethylene glycol)–chitosan oligosaccharide lactate nanoparticles: for the potential targeted ovarian cancer gene therapy. Eur. J. Pharm. Sci. 52, 48–61.

Li, X., Ding, L., Xu, Y., Wang, Y., Ping, Q., 2009. Targeted delivery of doxorubicin using stealth liposomes modified with transferrin. Int. J. Pharm. 373, 116–123.

Lim, E.K., Jang, E., Lee, K., Haam, S., Huh, Y.M., 2013. Delivery of cancer therapeutics using nanotechnology. Pharmaceutics 5, 294–317.

Liu, B., Yang, M., Li, R., Ding, Y., Qian, X., Yu, L., et al., 2008. The antitumor effect of novel docetaxel-loaded thermosensitive micelles. Eur. J. Pharm. Biopharm. 69, 527–534.

Liu, Y., Tseng, Y.C., Huang, L., 2012. Biodistribution studies of nanoparticles using fluorescence imaging: a qualitative or quantitative method? Pharm. Res. 29, 3273–3277.

Liu, J., Liu, J., Xu, H., Zhang, Y., Chu, L., Liu, Q., et al., 2014. Novel tumor-targeting, self-assembling peptide nanofiber as a carrier for effective curcumin delivery. Int. J. Nanomed. 9, 197–207.

Luo, G., Yu, X., Chen, J., Yang, F., Fu, D., Long, J., et al., 2010. LyP-1-conjugated nanoparticles for targeting drug delivery to lymphatic metastatic tumors. Int. J. Pharm. 385, 150–156.

Maeda, H., Bharate, G.Y., Daruwalla, J., 2009. Polymeric drugs for efficient tumor-targeted drug delivery based on EPR-effect. Eur. J. Pharm. Biopharm. 71, 409–419.

Mahato, R., Tai, W., Cheng, K., 2011. Prodrugs for improving tumor targetability and efficiency. Adv. Drug Deliv. Rev. 63, 659–670.

Mamot, C., Ritschard, R., Vogel, B., Dieterle, T., Bubendorf, L., Hilker, C., et al., 2011. A phase I study of doxorubicin-loaded anti-EGFR immunoliposomes in patients with advanced solid tumors. J. Clin. Oncol. 29, S3029.

Mamot, C., Ritschard, R., Wicki, A., Stehle, G., Dieterle, T., Bubendorf, L., et al., 2012. Tolerability, safety, pharmacokinetics, and efficacy of doxorubicin-loaded anti-EGFR immunoliposomes in advanced solid tumours: a phase 1 dose-escalation study. Lancet Oncol. 13, 1234–1241.

Manchester, M., Singh, P., 2006. Virus-based nanoparticles (VNPs): platform technologies for diagnostic imaging. Adv. Drug Deliv. Rev. 58, 1505–1522.

Markert, S., Lassmann, S., Gabriel, B., Klar, M., Werner, M., Gitsch, G., et al., 2008. Alpha-folate receptor expression in epithelial ovarian carcinoma and non-neoplastic ovarian tissue. Anticancer Res. 28, 3567–3572.

Markman, J.L., Rekechenetskiy, A., Holler, E., Ljubimova, J.Y., 2013. Nanomedicine therapeutic approaches to overcome cancer drug resistance. Adv. Drug Deliv. Rev. 65, 1866–1879.

Maruyama, K., 2011. Intracellular targeting delivery of liposomal drugs to solid tumors based on EPR effects. Adv. Drug Deliv. Rev. 63, 161–169.

Maruyama, K., Ishida, O., Takizawa, T., Moribe, K., 1999. Possibility of active targeting to tumor tissues with liposomes. Adv. Drug Deliv. Rev. 40, 89–102.

Mathur, V., Satrawala, Y., Rajput, M.S., Kumar, P., Shrivastava, P., Vishvkarma, A., 2010. Solid lipid nanoparticles in cancer therapy. Int. J. Drug Del. 2, 192–199.

Matsumura, Y., Maeda, H., 1986. A new concept for macromolecular therapeutics in cancer chemotherapy: mechanism of tumoritropic accumulation of proteins and the antitumor agent smancs. Cancer Res. 46, 6387–6392.

Matsumura, Y., Gotoh, M., Muro, K., Yamada, Y., Shirao, K., Shimada, Y., et al., 2004. Phase I and pharmacokinetic study of MCC-465, a doxorubicin (DXR) encapsulated in PEG immunoliposome, in patients with metastatic stomach cancer. Ann. Oncol. 15, 517–525.

Maya, S., Kumar, L.G., Sarmento, B., Sanoj Rejinold, N., Menon, D., Nair, S.V., et al., 2013. Cetuximab conjugated O-carboxymethyl chitosan nanoparticles for targeting EGFR overexpressing cancer cells. Carbohydr. Polym. 93, 661–669.

Mehta, A.K., Dubal, A.P., Mane, P.D., Deshmukh, H., 2013. Recent trends in niosomes as nanocarriers. Unique J. Pharm. Biol. Sci. 1, 12–17.

Mishra, B., Patel, B.B., Tiwari, S., 2010. Colloidal nanocarriers: a review on formulation technology, types and applications toward targeted drug delivery. Nanomed. Nanotech. Biol. Med. 6, 9–24.

Momtazi, L., Bagherifam, S., Singh, G., Hofgaard, A., Hakkarainen, M., Glomm, W.R., et al., 2014. Synthesis, characterization, and cellular uptake of magnetic nanocarriers for cancer drug delivery. J. Colloid Interface Sci. 433, 76–85.

Mori, A.M., Klibanov, A.L., Torchilin, V.P., Huang, L., 1991. Influence of the steric barrier activity of amphiphatic poly (ethylene glycol) and ganglioside GM1 on the circulation time of the liposomes and on the target binding of immunoliposomes *in vivo*. FEBS Lett. 284, 263–266.

Mukherjee, B., Satapathy, B.S., Mondal, L., Dey, N.S., Maji, R., 2013. Potentials and challenges of active targeting at the tumor cells by engineered polymeric nanoparticles. Curr. Pharm. Biotechnol. 14, 1250–1263.

Mukherjee, B., Das, S., Chakraborty, S., Satapathy, B.S., Das, P.J., Mondal, L., et al., 2014. Potentials of polymeric nanoparticle as drug carrier for cancer therapy: with a special reference to pharmacokinetic parameters. Curr. Drug Metab. 15, 565–580.

Narang, A.S., Varia, S., 2011. Role of tumor vascular architecture in drug delivery. Adv. Drug Deliv. Rev. 63, 640–658.

Nelson, A.R., Fingleton, B., Rothenberg, M.L., Matrisian, L.M., 2000. Matrix metalloproteinases: biologic activity and clinical implications. J. Clin. Oncol. 18, 1135–1149.

Nishida, N., Yano, H., Nishida, T., Kamura, T., Kojiro, M., 2006. Angiogenesis in cancer. Vasc. Health Risk Manag. 2, 213–219.

Noguchi, T., Takahashi, T., Yamaguchi, K., Kitamura, A., Noguchi, H., Tsurumi, K., et al., 1992. Enhanced tumor localization of monoclonal antibody by treatment with kinase II inhibitor and angiotensin II. Jpn. J. Cancer Res. 83, 240–243.

Northfelt, D.W., Martin, F.J., Working, P., Volberding, P.A., Russell, J., Newman, M., et al., 1996. Doxorubicin encapsulated in liposomes containing surface-bound polyethylene glycol: pharmacokinetics, tumor localization, and safety in patients with AIDS-related Kaposi's sarcoma. J. Clin. Pharmacol. 36, 55–63.

Ochekpe, N.A., Olorunfemi, P.O., Ngwuluka, N., 2009. Nanotechnology and drug delivery part 2: nanostructures for drug delivery. Trop. J. Pharm. Res. 8, 275–287.

Oh, K.S., Han, H., Yoon, B.D., Lee, M., Kim, H., Seo, D.W., et al., 2014. Effect of HIFU treatment on tumor targeting efficacy of docetaxel-loaded Pluronic nanoparticles. Colloids Surf. B Biointerfaces 119, 137–144.

Olaussen, K., Dunant, A., Fouret, P., Brambilla, E., Andre, F., Haddad, V., et al., 2006. DNA repair by ERCC1 in non-small-cell lung cancer and cisplatin-based adjuvant chemotherapy. New Engl. J. Med. 355, 983–991.

Pardakhty, A., Moazeni, E., 2013. Nano-niosomes in drug, vaccine and gene delivery: a rapid overview. Nanomed. J. 1, 1–12.

Park, J.W., Kirpotin, D.B., Hong, K., Shalaby, R., Shao, Y., Nielsen, U.B., et al., 2001. Tumor targeting using anti-her2 immunoliposomes. J. Control. Rel. 74, 95–113.

Park, J.H., Lee, S., Kim, J.H., Park, K., Kim, K., Kwon, I.C., 2008. Polymeric nanomedecine for cancer therapy. Prog. Polym. Sci. 33, 113–137.

Patel, N.H., Rothenberg, M.L., 1994. Multidrug resistance in cancer chemotherapy. Invest. New Drugs 12, 1–13.

Peer, D., Karp, J.M., Hong, S., Farokhzad, O.C., Margalit, R., Langer, R., 2007. Nanocarriers as an emerging platform for cancer therapy. Nat. Nanotechnol. 2, 751–760.

Peng, X.H., Wang, Y., Huang, D., Wang, Y., Shin, H.J., Chen, Z., et al., 2011. Targeted delivery of cisplatin to lung cancer using scFvEGFR-heparin-cisplatin nanoparticles. ACS Nano 5, 9480–9493.

Prokopiou, E.M., Ryder, S.A., Walsh, J.J., 2013. Tumour vasculature targeting agents in hybrid/conjugate drugs. Angiogenesis 16, 503–524.

Rabanel, J.M., Aoun, V., Elkin, I., Mokhtar, M., Hildgen, P., 2012. Drug-loaded nanocarriers: passive targeting and crossing of biological barriers. Curr. Med. Chem. 19, 3070–3102.
Ramakrishnan, P., 2003. The role of P-glycoprotein in the blood–brain barrier. Einstein Q. J. Biol. Med. 19, 160–165.
Rapoport, N., 2007. Physical stimuli-responsive polymeric micelles for anti-cancer drug delivery. Prog. Polym. Sci. 32, 962–990.
Rawat, M., Singh, D., Saraf, S., Saraf, S., 2006. Nanocarriers: promising vehicle for bioactive drugs. Biol. Pharm. Bull. 29, 1790–1798.
Reddy, A.K., Rathinaraj, B.S., Prathyusha, P., Bhargav, T.A., Rajani, T., Rajamanickam, V., et al., 2011. Emerging trends of nanotechnology in cancer therapy. Int. J. Pharm. Biol. Sci. Arch. 2, ISSN 0976–3333.
Rejman, J., Oberle, V., Zuhorn, I.S., Hoekstra, D., 2004. Size-dependent internalization of particles via the pathways of clathrin- and caveolae-mediated endocytosis. Biochem. J. 377, 159–169.
Ringel, J., Erdmann, K., Hampel, S., Kraemer, K., Maier, D., Arlt, M., et al., 2014. Carbon nanofibers and carbon nanotubes sensitize prostate and bladder cancer cells to platinum-based chemotherapeutics. J. Biomed. Nanotechnol. 10, 463–477.
Rusconi, C.P., Scardino, E., Layzer, J., Pitoc, G.A., Ortel, T.L., Monroe, D., et al., 2002. RNA aptamers as reversible antagonists of coagulation factor IXa. Nature 419, 90–94.
Saini, R.K., Chouhan, R., Bagri, L.P., Bajpai, A.K., 2012. Strategies of targeting tumors and cancers. J. Cancer Res. Updates 1, 129–152.
Sandhiya, S., Dkhar, S.A., Surendiran, A., 2009. Emerging trends of nanomedicine-an overview. Fundam. Clin. Pharmacol. 23, 263–269.
Sankhala, K.K., Mita, A.C., Adinin, R., Wood, L., Beeram, M., Bullock, S., et al., 2009. A phase I pharmacokinetic (PK) study of MBP-426, a novel liposome encapsulated oxaliplatin. J. Clin. Oncol. 27 (15S), 2535.
Sanna, V., Pala, N., Sechi, M., 2014. Targeted therapy using nanotechnology: focus on cancer. Int. J. Nanomed. 9, 467–483.
Sanvicens, N., Marco, M.P., 2008. Multifunctional nanoparticles-properties and prospects for their use in human medicine. Trends Biotechnol. 26, 425–433.
Sasaki, K., Tsuno, N.H., Sunami, E., Tsurita, G., Kawai, K., Okaji, Y., et al., 2010. Chloroquine potentiates the anticancer effect of 5-fluorouracil on colon cancer cells. BMC Cancer 10, 1–11.
Sayari, E., Dinarvand, M., Amini, M., Azhdarzadeh, M., Mollarazi, E., Ghasemi, Z., et al., 2014. MUC1 aptamer conjugated to chitosan nanoparticles, an efficient targeted carrier designed for anticancer SN38 delivery. Int. J. Pharm. 473, 304–315.
Scheithauer, W., Rosen, H., Kornek, G.V., Sebesta, C., Depisch, D., 1993. Randomised comparison of combination chemotherapy plus supportive care with supportive care alone in patients with metastatic colorectal cancer. BMJ 306, 752–755.
Selvakumaran, M., Pisarcik, D.A., Bao, R., Yeung, A.T., Hamilton, T.C., 2003. Enhanced cisplatin cytotoxicity by disturbing the nucleotide excision repair pathway in ovarian cancer cell lines. Cancer Res. 63, 1311–1316.
Shang, Y., Cai, X., Fan, D., 2013. Roles of epithelial-mesenchymal transition in cancer drug resistance. Curr. Cancer Drug Targets 13, 915–929.
Sharma, R., Chen, C.J., 2009. Newer nanoparticles in hyperthermia treatment and thermometry. J. Nanopart. Res. 11, 671–689.

Sharma, B., Peetla, C., Adjei, I.M., Labhasetwar, V., 2013. Selective biophysical interactions of surface modified nanoparticles with cancer cell lipids improve tumor targeting and gene therapy. Cancer Lett. 334, 228–236.

Shervington, A., Lu, C., 2008. Expression of multidrug resistance genes in normal and cancer stem cells. Cancer Invest. 26, 535–542.

Shi, J., Xiao, Z., Kamaly, N., Farokhzad, O.C., 2011. Self-assembled targeted nanoparticles: evolution of technologies and bench to bedside translation. Acc. Chem. Res. 44, 1123–1134.

Shvedova, A.A., Kisin, E.R., Porter, D., Schulte, P., Kagan, V.E., Fadeel, B., et al., 2009. Mechanisms of pulmonary toxicity and medical applications of carbon nanotubes: two faces of Janus? Pharmacol. Ther. 121, 192–204.

Singh, A., Settleman, J., 2010. EMT, Cancer stem cells and drug resistance: an emerging axis of evil in the war on cancer. Oncogene 29, 4741–4751.

Solaro, R., Chiellini, F., Battisti, A., 2010. Targeted delivery of protein drugs by nanocarriers. Materials 3, 1928–1980.

Soma, C.E., Dubernet, C., Bentolila, D., Benita, S., Couvreur, P., 2000. Reversion of multidrug resistance by co-encapsulation of doxorubicin and cyclosporin A in polyalkylcyanoacrylate nanoparticles. Biomaterials 21, 1–7.

Song, H., Su, C., Cui, W., Zhu, B., Liu, L., Chen, Z., et al., 2013. Folic acid-chitosan conjugated nanoparticles for improving tumor-targeted drug delivery. Biomed. Res. Int. 2013, 1–6.

Steinmetz, N.F., Cho, C.F., Ablack, A., Lewis, J.D., Manchester, M., 2011. Cowpea mosaic virus nanoparticles target surface vimentin on cancer cells. Nanomedicine (Lond) 6, 351–364.

Sui, X., Chen, R., Wang, Z., Huang, Z., Kong, N., Zhang, M., et al., 2013. Autophagy and chemotherapy resistance: a promising therapeutic target for cancer treatment. Cell. Death Dis. 4, e838.

Sun, T., Zhang, Y.S., Pang, B., Hyun, D.C., Yang, M., Xia, Y., 2014. Engineered nanoparticles for drug delivery in cancer therapy. Angew. Chem. Int. Ed. 53, 12320–12364.

Symon, Z., Peyser, A., Tzemach, D., Lyass, O., Sucher, E., Shezen, E., et al., 1999. Selective delivery of doxorubicin to patients with breast carcinoma metastases by stealth liposomes. Cancer 86, 72–78.

Tanaka, T., Shiramoto, S., Miyashita, M., Fujishima, Y., Kaneo, Y., 2004. Tumor targeting based on the effect of enhanced permeability and retention (EPR) and the mechanism of receptor-mediated endocytosis (RME). Int. J. Pharm. 277, 39–61.

Thiebaut, F., Tsuruo, T., Hamada, H., Gottesman, M.M., Pastan, I., Willingham, M.C., 1987. Cellular localization of the multidrugresistance gene product P-glycoprotein in normal human tissues. Proc. Nat. Acad. Sci. U.S.A 84, 7735–7738.

Torchilin, V.P., 2005. Recent advances with liposomes as pharmaceutical carriers. Nat. Rev. Drug Discov. 4, 145–160.

Tournaire, R., Simon, M.P., Noble, F., Eichmann, A., England, P., Pouysségur, J., 2004. A short synthetic peptide inhibits signal transduction, migration and angiogenesis mediated by Tie2 receptor. EMBO Rep. 5, 262–267.

Valetti, S., Maione, F., Mura, S., Stella, B., Desmaële, D., Noiray, M., et al., 2014. Peptide-functionalized nanoparticles for selective targeting of pancreatic tumor. J. Control. Rel. 192, 29–39.

van Vlerken, L.E., Duan, Z., Seiden, M.V., Amiji, M.M., 2007. Modulation of intracellular ceramide using polymeric nanoparticles to overcome multidrug resistance in cancer. Cancer Res. 67, 4843–4850.

Vinogradov, S., Wei, X., 2012. Cancer stem cells and drug resistance: the potential of nanomedicine. Nanomedicine 7, 597–615.

Voigt, J., Christensen, J., Shastri, V.P., 2014. Differential uptake of nanoparticles by endothelial cells through polyelectrolytes with affinity for caveolae. Proc. Nat. Acad. Sci. 111, 2942–2947.

Walling, M.A., Novak, J.A., Shepard, J.R.E., 2009. Quantum dots for live cell and *in vivo* imaging. Int. J. Mol. Sci. 10, 441–491.

Wang, M., Hsieh, A.J., Rutledge, G.C., 2005. Electrospinning of poly(MMA-co-MAA) copolymers and their layered silicate nanocomposites for improved thermal properties. Polymer 46, 3407–3418.

Watson, S.R., Chang, Y.F., O'Connell, D., Weigand, L., Ringquist, S., Parma, D.H., 2000. Anti-L-selectin aptamers: binding characteristics, pharmacokinetic parameters, and activity against an intravascular target *in vivo*. Antisense Nucleic Acid Drug Dev. 10, 63–75.

Wen, A.M., Rambhia, P.H., French, R.H., Steinmetz, N.F., 2013. Design rules for nanomedical engineering: from physical virology to the applications of virus-based materials in medicine. J. Biol. Phys. 39, 301–325.

Wickham, T., Futch, K., 2012. A phase I study of MM-302, a HER2-targeted liposomal doxorubicin, patients with advanced, HER2-positive breast cancer. Cancer Res. 72 (24 Suppl), P5–18-09.

Wiradharma, N., Zhang, Y., Venkataraman, S., Hedrick, J.L., Yang, Y.Y., 2009. Self-assembled polymer nanostructures for delivery of anticancer therapeutics. Nano Today 4, 302–317.

Xiao, Y., Hong, H., Javadi, A., Engle, J.W., Xu, W., Yang, Y., et al., 2012. Multifunctional unimolecular micelles for cancer-targeted drug delivery and positron emission tomography imaging. Biomaterials 33, 3071–3082.

Xu, X., Chen, X., Ma, P., Wang, X., Jing, X., 2008. The release behavior of doxorubicin hydrochloride from medicated fibers prepared by emulsion-electrospinning. Eur. J. Pharm. Biopharm. 70, 165–170.

Xu, W., Siddiqui, I.A., Nihal, M., Pilla, S., Rosenthal, K., Mukhtar, H., et al., 2013. Aptamer-conjugated and doxorubicin-loaded unimolecular micelles for targeted therapy of prostate cancer. Biomaterials 34, 5244–5253.

Yan, Z., Wang, F., Wen, Z., Zhan, C., Feng, L., Liu, Y., et al., 2012. LyP-1-conjugated PEGylated liposomes: a carrier system for targeted therapy of lymphatic metastatic tumor. J. Control. Rel. 157, 118–125.

Yassin, A.E.B., Albekairy, A., Alkatheri, A., Sharma, R.K., 2013. Anticancer-loaded solid lipid nanoparticles: high potential advancement in chemotherapy. Dig. J. Nanomater. Bios. 8, 905–916.

Yinan, Z., Fenghua, M., Chao, D., Zhiyuan, Z., 2014. Ligand-directed active tumor-targeting polymeric nanoparticles for cancer chemotherapy. Biomacromolecules 15, 1955–1969.

Yoo, J.W., Elizabeth, C., Samir, M., 2012. Factors that control the circulation time of nanoparticles in blood: challenges, solution and future prospect. Curr. Pharm. Des. 16, 2298–2307.

You, M., Peng, L., Shao, N., Zhang, L., Qiu, L., Cui, C., et al., 2014. DNA "Nano-Claw": logic-based autonomous cancer targeting and therapy. J. Am. Chem. Soc. 136, 1256–1259.

Yousefpour, P., Atyabi, F., Vasheghani-Farahani, E., Movahedi, A.M., Dinarvand, R., 2011. Targeted delivery of doxorubicin-utilizing chitosan nanoparticles surface-functionalized with anti-Her2 trastuzumab. Int. J. Nanomed. 6, 1977–1990.

Yu, J., Xie, X., Xu, X., Zhang, L., Zhou, X., Yu, H., et al., 2014. Development of dual ligand-targeted polymeric micelles as drug carriers for cancer therapy *in vitro* and *in vivo*. J. Mater. Chem. B 2, 2114.

Yuan, F., Dellian, M., Fukumura, D., Leunig, M., Berk, D.A., Torchilin, V.P., et al., 1995. Vascular permeability in a human tumor xenograft: molecular size dependence and cut-off size. Cancer Res. 55, 3752–3756.

Yuan, Q., Han, J., Cong, W.S., Ge, Y., Ma, D.D., Dai, Z.X., et al., 2014. Docetaxel-loaded solid lipid nanoparticles suppress breast cancer cells growth with reduced myelosuppression toxicity. Int. J. Nanomed. 9, 4829–4846.

Zamani, M., Prabhakaran, M.P., Ramakrishna, S., 2013. Advances in drug delivery via electrospun and electrosprayed nanomaterials. Int. J. Nanomed. 8, 2997–3017.

Zamboni, W.C., Eiseman, J.L., Strychor, S., Rice, P.M., Joseph, E., Zamboni, B.A., et al., 2011. Tumor disposition of pegylated liposomal CKD-602 and the reticuloendothelial system in preclinical tumor models. J. Liposome Res. 21, 70–80.

Zarei, M., Norouzian, D., Chiani, M., Ebrahimi, H., Mohammadi, M., Akbarzadeh, A., 2013. Advantages of paclitaxel-loaded nano niosomes to nanoliposomal formulation: an *in vitro* study. Int. J. Life Sci. Biotechnol. Pharma Res. 2, 335–342.

Zengin, E., Chalajour, F., Gehling, U.M., Ito, W.D., Treede, H., Lauke, H., et al., 2006. Vascular wall resident progenitor cells: a source for postnatal vasculogenesis. Development 133, 1543–1551.

Zhang, L., Gu, F.X., Chan, J.M., Wang, A.Z., Langer, R.S., Farokhzad, O.C., 2008. Nanoparticles in medicine: therapeutic applications and developments. Clin. Pharmacol. Ther. 83, 761–769.

Zhang, X.K., Meng, L.J., Lu, Q.H., Fei, Z.F., Dyson, P.J., 2009. Targeted delivery and controlled release of doxorubicin to cancer cells using modified single wall carbon nanotubes. Biomaterials 30, 6041–6047.

Zhang, Y., Hong, H., Cai, W., 2011. Tumor-targeted drug delivery with aptamers. Curr. Med. Chem. 18, 4185–4194.

Send Orders for Reprints to reprints@benthamscience.ae

Current Drug Metabolism, **2016,** *17,* **000-000**

Variation of Pharmacokinetic Profiles of Some Antidiabetic Drugs from Nanostructured Formulations Administered Through Pulmonary Route

Biswajit Mukherjee*, Paramita Paul, Ankan Choudhury, Sanchari Bhattacharya, Ruma Maji and Lopamudra Dutta

Department of Pharmaceutical Technology, Jadavpur University, Kolkata-700032, West Bengal, India

Biswajit Mukherjee

Abstract: Diabetes is a chronic disease that occurs when the pancreas does not produce enough insulin, or when the body cannot effectively use the insulin it produces. WHO projects that diabetes death will be doubled between 2005 and 2030, where 347 million people worldwide had diabetes as per the report of 2013. The increase in the prevalence of diabetes is due to three influences - lifestyle, ethnicity, and age. Current challenges in diabetes management include optimizing the use of the already available therapies to ensure adequate glycemic condition, blood pressure, lipid control and to reduce complications. At present, several pieces of research have been focusing on new management options for diabetes. Among these options, the use of nanomedicine is becoming an eye catching and most promising one. Currently, nanoparticles and nanoliposomes are thrust areas of research to treat any deadly disease like diabetes. These drug delivery systems ultimately result in longer circulation half-lives, improved drug pharmacokinetics, and reduced side effects of therapeutically active substances that may be insulin and non-insulin. Moreover, the pulmonary route is the most promising alternative route of drug delivery since it is non-invasive and lungs have a large surface area for absorption of drugs, richly supplied by the capillary network. The present review summarizes the pharmacokinetic parameters and challenges in the field of nanoparticles and nanoliposomes of insulin and other antidiabetic drugs given through pulmonary route to treat diabetes effectively.

Keywords: Diabetes, nanoparticles, nanoliposomes, pulmonary, insulin, antidiabetics.

INTRODUCTION

Diabetes mellitus is caused by the insufficient production of insulin in pancreatic islet cells, leading to an increase in blood glucose level or hyperglycemia. Diabetes mellitus has been classified as insulin-dependent diabetes (type 1) and non-insulin-dependent diabetes (type 2) [1].

As on today, the subcutaneous route has widely been the primary mode for insulin delivery. Nevertheless, clinical studies showed that a significant percentage of patients had failed to attain this long- term glycemic control with this treatment [2,3]. Few well-recognized reasons for this failure are the poor patient compliance due to the fear of injection and the other physiological reasons such as pain, discomfort *etc.* [4]. Several novel approaches like supersonic injectors, infusion pumps, sharp needles, pens etc. have been developed to increase the compatibility of diabetic patients. Oral delivery is the most convenient and acceptable route but the antidiabetic drugs specially insulin is degraded by intestinal enzymes and is not absorbed intact across the gastrointestinal mucosa [5].

The pulmonary delivery route for antidiabetic medication has shown a huge hope and expectation and is receiving a lot of scholastic interests. Few main reasons behind it are the non-invasive nature of the method, providing a large area for absorption (75-150 m^2) [6, 7, 8, 9], avoidance of hepatic first-pass metabolism, enhanced solubility of the drug in alveolar fluid and rapid onset of action due to the presence of a very thin (0.1-0.2 μm) monolayer epithelial diffusion path [1,10] from the airspaces into the blood in the alveoli [10,11,12]. Additionally, the alveolar environment has limited degradative activity by enzymes in both the extra and intracellular compartments as compared to gastrointestinal tract (GIT) [1,9,10,13], thus making it an attractive path for delivering peptides and protein-based therapeutics including insulin [14].

Despite many advantages of the pulmonary route, a frequent and long-term inhalation is necessary to achieve satisfactory efficacy because the therapeutic effects of most of the protein drugs are short [15].

The objective of pharmaceutical formulations is the transformation of drug compounds into active products with the desired therapeutic effect. Accordingly, a delivery system that allows the long-term release of drugs after a single inhalation is required. In this context, nanoformulations developed for pulmonary delivery of drugs have numerous benefits. The alveolar delivery ensures efficient and uniform distribution of drug. The lung environment and alveolar surface enhance the solubility of the drug, more so than its intrinsic aqueous solubility. Moreover, alveolar retention mimics sustained release pattern and hence decreases dosing frequency. These features decrease the dose related side-effects, enhance cellular internalization of drugs and improve patient compliance [10,16]. Thus, the pulmonary route of delivery of insulin or other peptides and protein brings special attention to the drug delivery researchers.

There are numerous applications for nanotechnology but the branch involving treatment, diagnosis, monitoring and control of physiological systems is broadly termed as “nanomedicine” by the National Institutes of Health (Bethesda, MD, USA) [17]. The two main types of nanomedicine products currently in clinical trials are: diagnostic agents and drug delivery devices [18]. Over the past few decades, research efforts have been focused on developing nanoformulations such as nanoparticles, liposomes, nanoemulsions, dendrimers etc. to ensure efficient delivery of drugs to the target tissues. Insulin nanoliposomes are one of the recent approaches in the controlled release aerosol preparation. Intratracheal delivery of insulin liposomes has shown to produce the desired insulin effect [19].

In this review article, we will mainly focus on the various approaches taken to deliver conventional antidiabetic drugs in the

*Address correspondence to this author at the Division of Pharmaceutics, Department of Pharmaceutical Technology, Jadavpur University, Kolkata-700032, India; Tel: +91-33-2457 2588; Fax: +91-33-2414 6677; E-mail: biswajit55@yahoo.com

1389-2002/16 $58.00+.00

nanoformulations via the pulmonary route and their advantages or limitations over the concurrent traditional therapies from the pharmacokinetic viewpoint.

Respiratory system: The respiratory area and the conducting airways are two important regions of the human respiratory system. The first region includes respiratory bronchioles, alveolar ducts, and alveolar sacs; and the later comprises of nasal cavity, associated sinuses, nasopharynx, oropharynx, larynx, trachea, bronchi, and bronchioles. A major portion (90%) of drug particles are removed in the upper airways as it has a higher filtering capacity. In the wall of the conducting airways, mucus containing the glycosylated protein called mucin forms a gel-like covering and has a ciliary action which washes drug molecules away. The main components of lungs are bronchi, alveoli, small air passage, lymph tissues and blood vessels of which bronchi are further divided into bronchioles and alveoli (approx 300 million). The maximum transepithelial (i.e., through the blood-gas barrier) drug transport uses the smaller airways and alveolar spaces which comprise more than 95% of lung's surface area and are directly connected with systemic circulation through dense capillary network [20,21], making them ideal for non-invasive drug administration. The various advantages and disadvantages are listed in Table **1**.

Significance of Delivery of Drug Nanocarriers by Pulmonary Route

Pulmonary route of drug delivery via nanocarriers offers well maintained systemic as well as local delivery of drugs in various ways such as using dry powder inhaler (DPI), nebulizers *etc*. It is also a convenient method for delivery of protein/peptide drug molecules encapsulated in those nanocarriers for treating respiratory as well as non-respiratory diseases [23]. Nanomedicine imparts more specificity to the treatments compared to the other modes of drug delivery, resulting in higher bioavailability and minimum dose related toxicity. The common nanocarriers used for this purpose are described below [22,23]:

- *Liposome*: It is a phospholipid vesicle composed of one or more concentric phospholipid bilayer(s) encapsulating an aqueous core and is often helpful for achieving sustained systemic release of drugs and efficient encapsulation of both hydrophilic and hydrophobic drugs [22].
- *Nanoparticles:* Nanoparticles are colloidal particles where the drug molecules are either encapsulated or dissolved or entrapped or attached chemically to the main matrix. Nanoparticles provide some advantages which include sustained release of drugs, minimal risk of adverse effects, increased patient compliance *etc.* [22].
- *Polymeric Micelles:* Micelles in nanoscale range (10-400 nm) are promising carriers for various drug molecules for pulmonary administration. Drugs are incorporated in the core of these structures. Such formulations often result in a better stability, prolonged *in vivo* retention time and enhanced capability of drug action on the target organs [23].

Pulmonary Deposition of Inhaled Nanocarriers

The mass median aerodynamic diameter (MMAD) of nanoparticles, along with the breathing pattern determine the deposition of the particles in the lungs [9, 10, 12]. The aerodynamic diameter of a particle is the combined function of its shape, size and density of the particle given by the formula [24]:

$$d_{aer} = \sqrt{\frac{\rho}{\rho_0 \chi}} d_g$$

Where, d_{aer} is the aerodynamic diameter, d_g is the geometric diameter, χ is the shape factor and $\frac{\rho}{\rho_0}$ is the specific gravity of the particle.

The particles deposit along the pulmonary pathway by inertial impact, interception, sedimentation, and diffusion [24,25]. The alveolar deposition is a bimodal phenomenon in which two types of particles (in terms of their size ranges) are involved. One kind involves particles between 1000 nm and 5000 nm and another one involves particles below 100 nm [9]. Only the two aforementioned size ranges penetrate deeper into the central and distal tracts of the lungs [12,26] through sedimentation and diffusion. The highest alveolar diffusion occurs for particles below 100 nm [7] as shown in Fig. (**1**). Though the size ranges are not always consensual and pulmonary delivery of nanoparticles for therapeutic purposes may supersede such limits. Depending on their size and shape, the particles usually deposit by following the fundamental mechanisms as mentioned below.

Impaction: Impaction is the physical phenomenon by which the particles of an aerosol tend to follow a trajectory movement due to inertia while travelling through the airways of the respiratory tract. This mainly happens in the first 10 bronchial generations, where the velocity of the air is high and the flow pattern is turbulent. The particles >5000 nm impact inertially in the nasopharyngeal region and are swallowed [10]. Particles above 100 nm and below 1000 nm are either deposited in the inert tracheobronchial region or are exhaled out [7, 16], especially if the drug is given through dry powder inhalers (DPI) or metered-dose inhalers (MDI).

Table 1. Advantages and limitations of pulmonary drug delivery

Advantages	Limitations	Reference
• Non-invasive in nature • Less toxic/ negligible side effects • Requires less and infrequent dosage • Quick onset of action • Avoids gastro intestinal tract related problems like gastric irritation, low bioavailability, protein binding, enzymatic degradation, etc. • Avoids first pass metabolism • High bioavailability • Minimum exposure to other vital organs. • Suitable for long-term treatments in asthma, diabetes *etc*,	Less stable *in vivo* Difficulty in transportation through the alveolar cells for certain types of molecules. Pulmonary irritation and toxicity. Poor drug retention.	[1, 9, 12, 22]

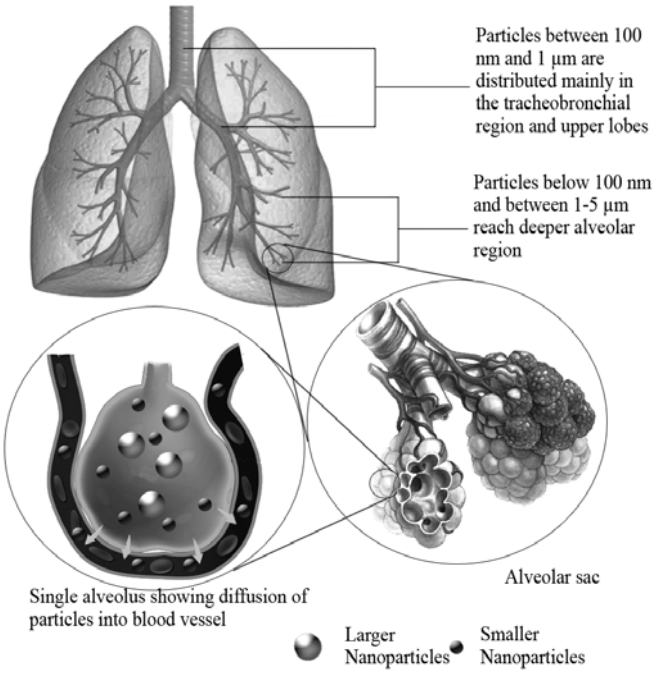

Fig. (1). Distribution and absorption of formulations in the respiratory system on the basis of the sizes of the inhaled particles.

Interception: Interception occurs mainly in the case of fibers. Due to their elongated shape, they are deposited on the wall of the airways as soon as they come in contact with it.

Sedimentation: Sedimentation is the physical phenomenon by which particles having sufficient mass are deposited due to gravity when they remain in the airways for a sufficient period of time. This occurs predominantly in the last 5 bronchial generations, where the air velocity is slow with a long residence time.

Diffusion: This occurs mainly for the particles below 100 nm where the clouds of nanoparticles remain suspended in the alveolar spaces in a fluidic motion. This phenomenon is guided by the concentration and/or pressure gradient, which facilitates the flow of the particles into the alveolar sacs for further absorption into the capillary network.

Besides, size and other factors such as composition, surface charges etc. are also crucial. Polymeric nanoparticles of 400 nm diameter [27] and lipid nanoparticles of 300 nm diameter [28] produced alveolar deposition in the magnitude of 75% and 45% respectively of the initial dose delivered. Nanoparticle aggregates with an aerodynamic diameter between 1 and 5 μm may enhance alveolar deposition provided they segregate on contact with the alveolar fluid [29].

Pharmacokinetics of Inhaled Nanocarriers Containing Antidiabetic Drugs

Hypoglycemic agents, be it insulin or other oral anti-diabetic agents, act primarily when they reach the systemic circulation. They mainly sensitize various receptors on the cell membrane either by acting as secretagogues for insulin or by improving insulin resistance [30,31]. Hence rapid absorption of an antidiabetic drug through alveolar surface and subsequent rapid onset of action with a longer residence time in the systemic circulation ensure efficient hypoglycemic action of that agent from a nanoformulation delivered through pulmonary route. However, residence time of a formulation in blood depends on the combined effect of bypassing the hepatic portal system and sustained drug-releasing capability of a nanocarrier [32]. Drug permeability through alveolar epithelium is found to be predominantly more than that of other noninvasive routes. As an example, the bioavailability of insulin administered via pulmonary route has been reported to be 20-100 times greater than that of other noninvasive routes. The reason may be the higher permeability of the drug through the alveolar epithelium and less volume of local fluid, resulting in high concentrations of drug near the bloodstream [23,33]. Out of the three main types of alveolar cells, other than the Type I and Type II pneumocytes, macrophages are mainly responsible for the immunogenic phagocytotic response to foreign substances such as drug nanocarriers [34]. Particles between 300-500 nm are more susceptible to phagocytosis [35], but small particles (<260 nm) [7] are capable of escaping phagocytosis [10,36]. Particles with size around 100 nm are widely considered as desirable for the purpose of delivering drugs [11,37]. Though anything below 1000 nm is considered as the nanoparticle, but all submicron sizes are not considered for pulmonary delivery due to safety concerns [11]. Inconsistent or uncontrolled dosing of inhalable nanoparticles induces inflammatory responses, epithelial damage in lungs, and extrapulmonary effects, such as oxidative stress or increased blood clotting, as well [9,36,38,39]. But these studies mostly relied on inorganic nanoparticles of very high doses. Generally, these threats do not correspond entirely to the homogenized and metered dosage of polymeric or lipid nanoparticles used in the therapeutic purpose, with a care taken during their administration [40].

Alveolar Absorption

Drug absorption through alveolar epithelium is very high due to its large surface area and all lipophilic and non-ionised molecules are readily permeated through it into the circulation [12]. The alveolar epithelium is composed of specialized cells with apparent structural polarity and the cells are permeable to water, gases and lipophilic molecules [9]. Hydrophilic molecules have a mean half-life value of about an hour whereas the similar size lipophilic molecules have half-lives less than a minute [41] in the alveoli. Many molecules undergo parallel transportation via the transcellular and paracellular pathways [42], with tight junctions between Type I pneumonocytes allowing diffusion of molecules only below 0.6 nm diameter. Besides, macromolecules above 40 kDa are absorbed very slowly over several hours but smaller peptides such as insulin (5.8 kDa) reach the circulation within minutes [43]. This inverse relation is more strongly demonstrated for proteins and peptides as they are primarily absorbed through the paracellular pathways where size/molecular weight acts as a major barrier [9]. Still there are many instances where proteins and peptides of higher molecular weight crossed transcellular barrier through receptor-mediated transcytosis and non-specific pinocytosis [12]. Peptides and similar molecules can be absorbed by active transport using a high-affinity peptide transporter (PEPT-2) present in alveolar Type II cells and in capillary endothelium [8,44]. This possibility is further enforced by the presence of the protein Caveolin in alveolar Type I cells and endothelial cells of the lung. Clathrin (another adjuvant protein) in alveolar Type I and II pneumonocytes also attribute to active transportation and absorption of protein through the alveolar pinocytosis [45]. Transcellular passive diffusion occurs only for the lipophilic molecules [4]. Since most of the antidiabetic drugs have low lipophilicity, they are absorbed mainly through the paracellular pathway into the system [4]. However, drug encapsulation within a hydrophobic scaffold and a large area for absorption in the alveoli compensate for this problem [7,16,46].

Clearance from the Lungs

The mucociliary escalator mechanism causes a major obstacle for nanoparticles deposited in the airways against penetration into alveolar region [47] by decreasing pulmonary retention and enhancing elimination of nanoparticles [12]. The cells secreting mucous exist in the region from the trachea to the terminal bronchiole. This

mucous creates a blockade for many particles to reach the alveolar site of action [48]. Drug particles held in this mucus layer are removed by the mucociliary clearance mechanism where the constantly beating cilia push the entrapped drug back towards the pharynx [49]. The alveolar Type II cells synthesize lung surfactants that are primarily made of phospholipids (mainly dipalmitoylphosphatidylcholine), cholesterol and surfactant-associated proteins [50]. Insoluble or poorly soluble particles in the mucus and the surfactant are not readily absorbed [9]. Since the nanocarrier scaffolds are mostly hydrophobic, they undergo dissolution in both intracellular and extracellular fluids including mucus.

Hydrophobic nanocarriers allow hydrophilic hypoglycemic molecules to be absorbed by passive diffusion across the alveolar epithelium [7]. However, the level and duration of retention and elimination of such nanoparticles vary with the nature of the nanoparticles [9] and physiological condition of lungs [12]. For instance, the thickness of the mucus layer increases from 2 to 30 μm in healthy lungs whereas even more than 250 μm in cases of cystic fibrosis and other obstructive airway diseases [51]. The nuisance of mucociliary and alveolar clearance can be controlled by keeping the particle diameter around 100 nm as seen by an experiment by Möller *et al*. (2008) [38] using ^{99m}Tc labeled carbon nanoparticles. In this experiment the mucociliary clearance resulted in elimination of just 25% of the deposited nanoparticles after 1 day, while clearance from the periphery of lungs is only about 3% of the deposited nanoparticles as explored by a radioactive probe. Pharmacokinetic (PK) data gathered after administering Cyclosporine-A loaded liposome in mice showed that the liposome was retained 16.9 times longer than the free Cyclosporine-A in healthy lungs and 7.5 times longer than the lungs with inflamed epithelial lining and increased mucociliary build-up, upon the administration of the same formulation [52].

Although phagocytosis is the predominant mechanism in the clearance of solid particles from pulmonary passages, the percentage of nanoparticles present in macrophages after inhalation has been found to decrease [9]. This may be due to a certain inefficiency of macrophages in recognition and elimination of particles below a certain size [33,53]. As mentioned earlier, particles below 260 nm undergo less phagocytosis [7,54,55] and below 70 nm are not recognized by macrophages [7]. This may be attributed to the absence or reduced promotion of the chemotactic signal from the smaller nanoparticles [36]. This further ensures the important role played by endocytosis in epithelial translocation of nanoparticles at the cellular level. There are several existing transcellular endocytotic pathways such as pinocytosis, adsorptive endocytosis (nonspecific binding to receptors) and receptor-mediated endocytosis exhibited by both the types of alveolar pneumocytes [45, 56]. The abundance of Caveolin 1 protein in alveolar type 1 pneumocytes and in the pulmonary capillary endothelium may establish the possibility of Caveolin-mediated endocytosis as an important pathway in epithelial translocation of nanoparticles [51, 57]. The hypothesis has been further supported by an experiment by Brandenberger *et al*. (2010) where inhibition of Caveolin and Clathrin-mediated endocytosis by methyl-β-cyclodextrin resulted in a significant reduction in uptake of gold nanoparticles by human alveolar epithelial cells and inhibition was more extenuated when the nanoparticles were coated with polyethylene glycol (PEG) [58]. These factors are often helpful in delivering peptides and peptidomimetic molecules such as insulin [59], exendin-4 [15] etc. in the form of nanoparticles for inducing hypoglycemia through pulmonary routes.

In vivo Fate of Insulin and non-Insulin Nanoformulations: A Pharmacokinetic View

Once the nanoparticles cross the physiological barrier and enter the systemic circulation, nature of the drug molecules governs their ultimate fate. Antidiabetic formulations can be divided broadly into two classes- insulin and non-insulin agents (oral hypoglycemic agents) [60].

Insulin

Insulin is probably the most studied antidiabetic drug for developing nanoformulations to deliver through pulmonary routes [9]. Insulin is generally used for patients suffering from diabetes mellitus type 1, the subtype of the disease which is caused by the lack of insulin secretions by β cells of islets of Langerhans in the pancreas. Insulin is a dipeptide molecule where the two polypeptidic chains of 21 and 30 amino acids long respectively are joined by two disulfide linkages [1]. Insulin has gathered so much interest solely for being a peptide but unfit for oral administration due to its degradation by the proteolytic/peptidolytic enzymes (pepsin in stomach; trypsin, chymotrypsin, and carboxypeptidases in the duodenum) of the gastro-intestinal tract [61, 62]. Parenteral administration, in particular subcutaneous route, is accepted widely and unanimously for insulin delivery [1]. But there are problems such as patient noncompliance due to painful injections and episodes of acute hypoglycemia due to inconsistent and careless dosing since the delivery route is irreversible [63,64]. Transdermal route acts as a popular alternative as a non-invasive parenteral delivery route but the peptidic (ionized) nature, molecular weight and size of insulin make it a poor candidate for transdermal absorption and hence, even though it reduces the pain problem, it produces incomplete and inconvenient results [1]. This led to further investigation with other routes among which pulmonary route has become a very prominent choice [14] and has been in use since 1925 [9,14,65]. This even culminated in a pulmonary antidiabetic product called Exubera® which came to the market in 2006 after the approval of the United States Food and Drug Administration and European Medical Agency, but was withdrawn in 2007. The product was developed by Nektar/Pfizer as a dry powder formulation [1,9,14]. Another aerosol-based product for the delivery of insulin was developed jointly by Aradigm and Novo Nordisk but was discontinued from 2008 while it was in Phase III trials [9].

Many experimental formulations have been developed for pulmonary delivery of insulin through nanocarriers. The main goal for such delivery is to allow the nano-encapsulated insulin molecules to enter the systemic circulation through a non-invasive route and release insulin through a gradual biodegradation of the polymeric scaffold [10]. Insulin molecules in the blood bind with the insulin receptors present on the cell membrane and initiate a phosphorylation reaction on the Insulin Receptor Substrate 1 (IRS1) [66]. Phosphorylated IRS1 then initiates the activation of phosphoinositol-3-kinase (PI3K) which in turn converts phosphatidylinositol 4,5-bisphosphate (PIP2) into phosphatidylinositol 3,4,5-triphosphate (PIP3). This reaction activates the protein kinase B which functions bimodally [67] by upregulating glycogen synthesis through inactivation of glycogen synthase kinase, and results in migration of glucose transporter-4 (GLUT4) towards the plasma membrane [68]. This migration of GLUT4 causes increased uptake of free glucose from the blood into the cells. Glucose then either undergoes glycolysis or gets stored as glycogen in the cells [68]. But these physiological reactions require a steady blood insulin content of 8–11 μIU/mL (57–79 pmol/L) [69]. The product Exubera® had to be withdrawn [9] because the Pfizer found it to be commercially nonfeasible even though it produced patient comfort and convenience and showed similar postprandial glycemic control and similar values of glycated haemoglobin (HbA1c) to that of subcutaneous insulin injections [70]. The main reason is that it was a short-term insulin formulation and failed to maintain the required physiological insulin level for a longer duration, which again necessitates further injection of long-term insulin [71]. Strategies were taken to prolong the duration of action by modification of the structure of the insulin molecules by attaching biodegradable molecules such as PEG to it (PEGylation). PEGylated insulin were delivered via pulmonary routes in rats and dogs and it was seen that PEGylated insulin were

systemically absorbed from the lungs [12, 72]. The extent of absorption was decreased following PEGylation on multi-protein sites as well as the use of large PEGs (5–12 kDa). In the circulation, PEGylated proteins maintain a sustained plasma level of insulin as they would do when injected subcutaneously at regular intervals. PEGylation also protects peptides from local proteolysis in the lungs and thereby increases the systemic absorption of the intact molecule from the alveoli [48,73,74].

As mentioned before, nanocarriers address the problem of degradation of proteins or peptides by nano-encapsulation which enables the drug to remain in the circulation for a longer time and drug release remains sustained for such longer duration. They also protect the encapsulated material from phagocytosis and enzymatic degradation. Bi *et al*. (2008) encapsulated insulin into liposomal carriers to increase drug retention time and control the drug release in the lungs [75]. Nanoliposomes with an average diameter of 295 nm and an encapsulation efficiency of 43% were administered through intratracheal instillation in diabetic rats, causing a decrease in systemic levels of glucose for 12 h after its administration [75]. It resulted in successful hypoglycemic effect with low blood glucose level for a prolonged period and a relative pharmacological bioavailability as high as 38.38% in the group of 8 IU/kg dosage. These data were compared against the results shown by the traditional subcutaneous insulin injection and naked insulin solution given through pulmonary route. Another study by Chono *et al.* (2009) showed that liposome of dipalmitoylphosphatidylcholine containing insulin reduced serum glucose to a greater extent than insulin solution when both were administered via intratracheal routes to the experimental rats [76]. This study also showed the relationship between the size of liposomes and their macrophagic uptake. Liposomes of mean diameter 100 nm showed elevated serum insulin level and those of 1000 nm size were preferentially retained by alveolar macrophages. A parallel *in vitro* study in the same experiment using Calu-3 cell cultures showed that liposomal encapsulation enhanced absorption of insulin through the opening of the tight junctions of alveolar cells. Insulin encapsulated lecithin nanoparticles of an average diameter 300 nm not only produced a deposition of 45% of the delivered dose in the alveolar level but also retained the primary, secondary and tertiary polypeptide structures of the insulin molecule [28]. Liu *et al.* (1993) studied the effects of oligomerization and liposomal entrapment on pulmonary insulin. Pulmonary absorption was investigated in rats using an intratracheal instillation method. Their study confirmed that the intratracheal administration of insulin liposomes led to the facilitated pulmonary uptake of insulin and enhanced the hypoglycemic effect [77]. Liu *et al* (2008) also produced solid lipid nanoparticles of phosphatidylcholine having an average diameter of 115 nm, which showed a prolonged hypoglycemic effect in diabetic mice by lowering the plasma glucose level to 39% within 8 h and elevating insulin level to 170 μIU/ml within 4 h of pulmonary administration of the nanoparticles containing weight equivalent in insulin of about 20 IU/kg of formulation [78]. The nanoparticles continued the hypoglycemic effect up to 12 h and the basal glucose level returned only after 24 h. The formulation achieved a mean residence time (MRT) approximately 7.7 h.

Polylactide-co-glycolic acid (PLGA) nanosphere of 400 nm loaded with insulin was administered to guinea pig through nebulization for 20 minutes and recorded a significant alveolar deposition (75%) and a considerable reduction in blood glucose level with a prolonged effect over 48 h as compared to aqueous native insulin solution [27]. In a follow-up study, the same research group later modified the PLGA nanoparticles with chitosan but this time with a different peptide ecaltonin (a calcitonin analogue) so as to utilize the properties of the coating to adhere the particles for a longer period in the mucociliary environment of the lungs in guinea pigs [79]. This strategy was used by Lee *et al.* (2013) for antidiabetic action in delivering a palmitic acid derivative of exendin-4 (exenatide), a glucagon-like peptide (GLP) receptor agonist which decreased the release of plasma glucagon [15]. The retention of the particles in lungs over 72 h with a sustained release prolonged the hypoglycemic action for over 4 days in mice. Huang *et al*. (2009) developed nanoparticles of insulin using low molecular weight chitosan, of an average diameter of approximately 400 nm and an encapsulation efficiency of 95.5% which gave a characteristic release profile of insulin beginning with a burst effect followed by prolonged release for 24 h. The nanoparticles demonstrated a hypoglycemic effect similar to subcutaneous insulin injection but prolonged in time in diabetic mice [80]. The biphasic release of insulin, also seen by Kawashima *et al.* (1999), can mimic the actions of available insulin mixtures of short and long duration of action [27]. Yamamoto *et al*. (2007) produced PLGA nanoparticles which showed an *in vitro* and *in vivo* alveolar deposition of approximately 45% (w/w) of emitted dose and a more prolonged pharmacological effect (over 12 h) compared to the solutions of insulin administered via pulmonary and *i.v.* routes [81]. In another study, chitosan nanoparticles (average diameter 380-450 nm) were produced with [46] and without lipid coating [82] obtained by ionic gelation with tripolyphosphate ion. The resultant nanoparticles had encapsulation efficiency between 65 and 81%. A rapid release of insulin from nanoparticles without lipid coating was observed while the formulations with the lipid coating showed a prolonged release of insulin [46, 82]. Poly(n-butyl cyanoacrylate) (PBCA)/dextran nanoparticles with an average diameter of 255 nm showed that insulin release (*in vitro*) had a biphasic characteristic of an initial burst effect followed by prolonged release of insulin, while *in vivo* studies showed a more prolonged therapeutic effect when compared with insulin solution administered via lungs [83]. Further, there was insulin bioavailability of 57% from the nanoparticles as compared to the subcutaneous injection of insulin solution [83]. The minimum blood glucose concentration reached 46.9%, 30.4% and 13.6% respectively of the initial level after pulmonary delivery of 5, 10 and 20 IU Kg^{-1}insulin-loaded nanoparticles to normal rats. The time to reach the minimum blood glucose level (T_{min}) was 4, 4 and 8 h for three doses, respectively.

Non-Insulin

The non-insulin antidiabetics include the classical oral antidiabetics and the peptide analogues which act primarily in diabetes mellitus type 2 where the insulin secretion is normal, but the cells become desensitized to insulin. The predominant classes of oral antidiabetics include biguanides, sulfonylureas, thiazolidinediones and α-glucosidase inhibitors [84]. The peptide analogues include incretin mimetic insulin secretagogues such as glucagon-like peptide-1 (GLP-1) and gastric inhibitory peptide analogues [85]. These molecules have warranted far fewer attentions than insulin in terms of pulmonary delivery, but there have been some noteworthy works involving such drugs. These drugs act mainly via subsidiary pathways that help insulin secretion or that manipulate glucose metabolism in the body through enzymatic inhibition/upregulation. Since all these drugs have poor lipophilicity, encapsulation in a nanolipoidal or polymeric scaffold enhances their absorption through the highly lipophilic cellular membranes [4]. Pulmonary route can be a highly preferable route as it provides a very large surface for the absorption of drug, something that may compensate for the poor penetration factor as it is seen in the highly folded epithelium of the intestine where larger surface area of the cell overcomes the difference in partitioning between the cell membrane and the extracellular fluid [4].

Sulfonylureas act as insulin secretagogues by inhibiting the K^+ ATP channel in the β cells of the pancreas, thereby stopping the K^+ efflux and leading to subsequent depolarization of the cells which initiate a Ca^{2+} influx and a protein activation cascade. This ends in exocytosis of insulin-loaded vesicles and hence increases plasma insulin level [86]. Non-sulfonyl urea insulin secretagogues include

meglitinide and repaglinide, which follow the same mechanism but differ in their binding site with the sulfonylureas [87]. They are fast, but short-acting insulinotropic drugs which have been employed in chitosan-alginate nanocomplexes for inhalation purpose [88]. In this study they used repaglinide as the hypoglycemic agent and prepared nanocomplexes of sizes in the 300-400 nm range and utilized the mucoadhesive properties of chitosan-alginate gel to achieve a gradual sustained hypoglycemic effect which lowered the blood glucose level to 47% within 8 h and up to 38% in 24 h post-treatment [88].

Biguanides, such as metformin and phenformin, and thiazolidinediones, such as pioglitazone and rosiglitazone [86], act by reducing insulin resistance in diabetes mellitus type 2 (DMT2). The biguanides are usually the first-line drugs given in DMT2 though their mechanisms are not fully understood. Metformin decreases hyperglycemia primarily by suppressing hepatic gluconeogenesis and may decrease insulin resistance by activation of AMP-activated protein kinase (AMPK) [89]. The thiazolidinediones are dependent on the presence of insulin for activity, but they themselves do not affect insulin secretion. The thiazolidinediones are highly selective and potent agonist for the peroxisome proliferator activated receptor-gamma (PPAR-γ). Activation of PPAR-γ regulates the transcription of insulin-responsive genes involved in the control production, transport, and utilization of glucose through increased production of GLUT 1 and GLUT 4 receptors [84].

Peptide analogues include GLP-1 and GLP-1 agonist such as exenatide (Ex4), which bind with the GLP receptors to inhibit the release of glucagon and increase the release of insulin, thus lowering blood glucose level. They have been extensively investigated through strategies such as PEGylation and nano-encapsulation for administration via pulmonary route. Both the strategies resulted in nanoscale formulations capable of protecting them from the proteolytic enzymes of the alveolar epithelium and mucociliary passage [12,48]. PEGylated versions of GLP-1 were studied for pulmonary delivery in diabetic rats where GLP-1 was conjugated with PEG (molecular weight 1, 2, or 5 kDa) [90]. The PEG-2000 conjugate had the greatest hypoglycemic response as the PEGylation of GLP-1 prolonged the half-life of GLP-1 and decreased renal clearance rate [90]. Although the study showed that the half-life directly depended on the length of the PEG chain, but the length was inversely related to the rate of absorption and biological activity of the peptide [90]. This may be due to larger PEG chains which might effectively prevent proteolysis of the peptide molecules and hence increased their bioavailability. Another study investigated Ex4 in type 2 diabetic mice [91] where Ex4 was conjugated with PEG (molecular weight 1, 2, or 5 kDa) showing prolonged half-life and hypoglycemia. Ex4 was also studied in nanoparticle formulation in its palmitic acid derivative form. The mucoadhesive nature of chitosan-coated PLGA nanoparticles ensured that the drug was released over three days *in vitro* and produced hypoglycemia over four days in mice. The above-mentioned findings may encourage formulation scientists to explore new strategies to receive more success in the field in near future.

CONCLUSION

The review highlights that the pulmonary drug delivery is a highly prospective field of drug administration in the near future. Pulmonary drug delivery also offers a huge opportunity for systemic administration of antidiabetic drug molecules such as insulin or non-insulin agents. The large surface area, good vascularization, solute exchange capacity and ultra-thin membranes of alveolar epithelia are unique features that facilitate pulmonary drug delivery. Further large lung surface area and thin alveolar epithelium permit rapid drug absorption and the first-pass metabolism can be avoided, too.

Pulmonary drug delivery depends upon several factors including particle size, shape, density, charge and pH of delivery entity, velocity of entry, quality of aerosol deposition, character of alveoli, binding characteristics of aerosol on the alveolar surface, quality of alveolar capillary bed and its subsequent vascular tree. Those parameters ultimately reflect the pharmacokinetic modulation of the administered therapeutic agent using the pulmonary route. However, the defense mechanism of lungs against foreign particle should not be ignored. The defense can be by either mucosal clearance or degradation by macrophages and enzymes. The lung can also develop immunological reactions against unwanted entities such as viruses. As per the safety concern, depending on the size of the nanocarriers it is possible to escape the phagocytosis by delivering the nanoparticles generally of small sizes (i.e. <260 nm) to the lungs. However, particles > 5000 nm to 3 μm are generally phagocytosed by macrophages. The large particles (i.e. >5000 nm) are not suitable for the pulmonary delivery as they tend to deposit in the nasopharyngeal region and are swallowed. The particles above 100 nm and below 1000 nm also have a tendency to get deposited in the tracheobronchial region or exhaled. Again, particles having a size below 100 nm reach the lungs efficiently and show the highest alveolar diffusion. From the different experimental studies it was observed that antidiabetic drug such as insulin can be easily encapsulated to the nanostructured systems for pulmonary delivery which gave results similar or sometimes better than the conventional delivery routes such as subcutaneous injection. Evidence shows that this strategy improves the therapeutic efficacy and reduces the systemic toxicity of the drug by improving its pharmacokinetic profile.

It is expected that the continued research interest in the pulmonary route of administration will lead to more breakthroughs in several areas of formulation and device designs for pulmonary drug delivery, resulting in an improved patients' acceptance and compliance.

CONFLICT OF INTEREST

The authors confirm that this article content has no conflicts of interest.

ACKNOWLEDGEMENTS

All the authors contributed in writing of the manuscript. All the authors jointly developed the structure and arguments for the paper. Biswajit Mukherjee made critical revisions and approved final version. All authors reviewed and approved the final manuscript.

REFERENCES

[1] Elçioğlu, H. K.; Sezer A. D. Nanoparticle Insulin Drug Delivery — Applications and New Aspects**.** *Application of Nanotechnology in Drug Delivery*, INTECH publishing, **2014.**

[2] Petitti, D. B.; Klingensmith, G. J.; Bell, R. A.; Andrews, J. S.; Dabelea, D.; Imperatore, G.; Marcovina, S.; Pihoker, C.; Standiford, D.; Waitzfelder, B.; Mayer-Davis, E. Glycemic control in youth with diabetes: the SEARCH for diabetes in Youth Study. *J. Pediatr.*, **2009**, *155*, 668–672.

[3] Mortensen, H. B.; Robertson, K. J.; Aanstoot, H. J.; Danne, T.; Holl, R. W.; Hougaard, P.; Atchison, J. A.; Chiarelli, F.; Daneman, D.; Dinesen, B.; Dorchy, H.; Garandeau, P.; Greene, S.; Hoey, H.; Kaprio, E. A.; Kocova, M.; Martul, P.; Matsuura, N.; Schoenle, E. J.; Søvik, O.; Swift, P. G.; Tsou, R. M.; Vanelli, M.; Aman, J. Insulin management and metabolic control of type 1 diabetes mellitus in childhood and adolescence in 18 countries. Hvidore Study Group on Childhood Diabetes. *Diabet. Med.*, **1998**, *15*, 752–759.

[4] Gundogdu, E.; Yurdasiper, A. Drug transport mechanism of oral antidiabetic nanomedicines. *Int. J. Endocrinol. Metab.*, **2014,** *12*, e8984.

[5] Pandey Shivanand, ChoudharyAmruta, Patel Binal, R. Mahalaxmi, Devmurari Viral, N. P. Jivani. Pulmonary Delivery as a Route for Insulin. *International Journal of Pharm. Tech. Research*, 2009, 1, 1190-1197.

[6] Iazzetti, G.; Rigutti, E. *Atlas of Anatomy*. Taj Books, Surrey, UK, **2005**.

[7] Yang, W.; Peters, J.; Williams, R. R. Inhaled nanoparticles – a current review. *Int. J. Pharm.*, **2008**, *356*, 239–247

[8] Groneberg, D.; Fischer, A.; Chung, K.; Daniel, H. Molecular mechanisms of pulmonary peptidomimetic drug and peptide transport. *Am. J. Respir. Cell Mol. Biol.*, **2004**, *30*, 251–260.

[9] Andrade, F.; Videira, M.; Ferreira, D.; Sarmento, B. Nanocarriers for Pulmonary Administration of Peptides and Therapeutic Proteins. *Nanomedicine*, **2011**, *6*, 123-141.

[10] Sung, J. C.; Pulliam, B. L.; Edwards, D. A. Nanoparticles for drug delivery to the lungs. *Trends Biotechnol.*, **2007**, *25*, 563–570.

[11] Mansour, H. M.; Rhee, Y; Wu, X. Nanomedicine in pulmonary delivery. *Int. J. Nanomedicine*, **2009**, *4*, 299–319.

[12] Loira-Pastoriza, C.; Todoroff, J.; Vanbever, R. Delivery strategies for sustained drug release in the lungs. *Adv. Drug Deliv. Rev.*, **2014**, *75*, 81-91.

[13] Cryan, S.; Sivadas, N.; GarciaContreras, L. *In vivo* animal models for drug delivery across the lung mucosal barrier. *Adv. Drug Deliv. Rev.*, **2007**, *59*, 1133–1151.

[14] Henkin, R. I. Inhaled insulin-Intrapulmonary, intranasal and other routes of administration: Mechanisms of action. *Nutrition*, **2010**, *26*, 33-39.

[15] Lee, C.; Choi, J.S.; Kim, I.; Oh, K.T.; Lee, E.S.; Park, E.S.; Lee, K.C.; Youn, Y.S. Long-acting inhalable chitosan-coated poly(lactic-co-glycolic acid) nanoparticles containing a hydrophobically modified exendin-4 for treating type 2 diabetes, *Int. J. Nanomedicine*, **2013**, *8*, 2975–2983.

[16] Bailey, M. M.; Berkland, C. J. Nanoparticle formulations in pulmonary drug delivery. *Med. Res. Rev.***2009**, *29*, 196–212.

[17] Park, J. H.; Lee, S.; Kim, J. H.; Park, K.; Kim, K.; Kwon, I. C. Polymeric nanomedicine for cancer therapy. *Prog. Polym. Sci.* **2008**, *33*, 113–137.

[18] Resnik, D. B.; Tinkle, S. S. Ethical issues in clinical trials involving nanomedicine. *Contemp. Clin. Trials*. **2007**, *28*, 433–441.

[19] Huang, Y. Y.; Wang, C. H. Pulmonary delivery of insulin by liposomal carriers. *J. Control. Release.* **2006**, *113*, 9-14.

[20] Patil, J. S.; Sarasija, S. Pulmonary drug delivery strategies: A concise, systematic review, *Lung India*, **2012**, *29*, 44–49.

[21] Paranjpe, M.; Müller-Goymann, C. C. Nanoparticle-mediated pulmonary drug delivery: a review, *Int. J. Mol. Sci.*, **2014**, *15*, 5852-5873.

[22] Chaturvedi, N.P.; Solanki, H. Pulmonary drug delivery system: review *Int. J. App. Pharm.*, **2013**, *5*, 7-10.

[23] Smola, M.; Vandamme, T.; Sokolowski, A. Nanocarriers as pulmonary drug delivery systems to treat and to diagnose respiratory and non respiratory diseases. *Int. J. Nanomedicine*, **2008**, *3*, 1-19.

[24] Hinds, W.C. (ed.) *Aerosol technology: properties, behavior, and measurement of airborne particles* (2nd ed.), Wiley, **1999.**

[25] Crowder, T.; Rosati, J.; Schroeter, J.; Hickey, A.; Martonen, T. Fundamental effects of particle morphology on lung delivery: predictions of stokes' law and the particular relevance to dry powder inhaler formulation and development. *Pharm. Res.*, **2002**, *19*, 239–245.

[26] Usmani, O. S.; Biddiscombe, M. F.; Barnes, P. J. Regional lung deposition and bronchodilator response as a function of beta2-agonist particle size. *Am. J. Respir. Crit. Care Med.*, **2005**, *172*, 1497–1504.

[27] Kawashima, Y.; Yamamoto, H.; Takeuchi, H.; Fujioka, S.; Hino, T. Pulmonary delivery of insulin with nebulized DL-lactide/glycolide copolymer (PLGA) nanospheres to prolong hypoglycemic effect. *J. Control. Release*, **1999**, *62*, 279–287.

[28] Nyambura, B.; Kellaway, I.; Taylor, K. Insulin nanoparticles: stability and aerosolization from pressurized metered dose inhalers. *Int. J. Pharm.*, **2009,** *375*, 114–122.

[29] Grenha, A.; CarriónRecio, D.; TeijeiroOsorio, D.; Seijo, B.; RemuñánLópez, C. (Eds) *Nano and Microparticulate Carriers for Pulmonary Drug Delivery*. American Scientific Publishers, Valencia, CA, USA, **2008**.

[30] Rodbard, H. W.; Jellinger, P. S.; Davidson, J. A. Statement by an American Association of Clinical Endocrinologists/American College of Endocrinology consensus panel on Type 2 diabetes mellitus: an algorithm for glycemic control. *Endocr. Pract.*, **2009**, *15*, 540–559.

[31] Ramesan, R. M.; Sharma, C. P. Challenges and advances in nanoparticles based oral insulin delivery. *Expert Rev. Med. Devices*, **2009**, *6*, 665–676.

[32] Mosser, D. M.; Edwards, J. P. Exploring the full spectrum of macrophage activation. *Nature reviews. Immunology*, **2008,** *8*, 958–69.

[33] Tomoda, K.; Ohkoshi, T.; Nakajima, T.; Makino, K. Preparation and properties of inhalable nanocomposite particles: effects of the size, weight ratio of the primary nanoparticles in nanocomposite particles and temperature at a spray dryer inlet upon properties of nanocomposite particles. *Colloids Surf. B Biointerfaces*, **2008,** *64*, 70–76.

[34] Lambrecht, B. N. Alveolar Macrophage in the Driver's Seat. *Immunity*, **2006,** *24*, 366–368.

[35] Chono, S.; Tanino, T.; Seki, T.; Morimoto, K. Influence of particle size on drug delivery to rat alveolar macrophages following pulmonary administration of ciprofloxacin incorporated into liposomes. *J. Drug Target.*, **2006**, *14*, 557–566.

[36] Oberdörster, G.; Oberdörster, E.; Oberdörster, J. Nanotoxicology: an emerging discipline evolving from studies of ultrafine particles. *Environ. Health Perspect*., **2005**, *113*, 823–839.

[37] Shekunov, B. Nanoparticle technology for drug delivery – From nanoparticles to cutting-edge delivery strategies – Part I. *Idrugs*., **2005,** *8*, 399–401.

[38] Möller, W.; Felten, K.; Sommerer, K. Deposition, retention, and translocation of ultrafine particles from the central airways and lung periphery. *Am. J. Respir. Crit. Care Med.*, **2008**,*177*, 426–432.

[39] Renwick, L.; Brown, D.; Clouter, A.; Donaldson, K. Increased inflammation and altered macrophage chemotactic responses caused by two ultrafine particle types. *Occup. Environ. Med.*, **2004,** *61*, 442–447.

[40] Chang, C. The immune effects of naturally occurring and synthetic nanoparticles. *J. Autoimmun.*, **2010**, *34*, J234–J246.

[41] Patton, J. S.; Fishburn, C. S.; Weers, J. G. The lungs as a portal of entry for systemic drug delivery. *Proc. Am. Thorac. Soc*., **2004,** *1*, 338–344.

[42] Pezron, I.; Mitra, R.; Pal, D.; Mitra, A. Insulin aggregation and asymmetric transport across human bronchial epithelial cell monolayers (Calu3). *J. Pharm. Sci.*, **2002,** *91*, 1135–1146.

[43] Patton, J. S.; Byron, P. R. Inhaling medicines: delivering drugs to the body through the lungs. *Nat. Rev. Drug Discov*., **2007**, *6*, 67–74.

[44] Islam, N.; Gladki, E. Dry powder inhalers (DPIs) – a review of device reliability and innovation. *Int. J. Pharm.*, **2008,** *360*, 1–11.

[45] Kim, K.; Malik, A. Protein transport across the lung epithelial barrier. *Am. J. Physiol. Lung Cell. Mol. Physiol.*, **2003,** *284*, L247–L259.

[46] Grenha, A.; Remuñán-López, C.; Carvalho, E.; Seijo, B. Microspheres containing lipid/chitosan nanoparticles complexes for pulmonary delivery of therapeutic proteins. *Eur. J. Pharm. Biopharm.*, **2008,** *69*, 83–93.

[47] Beck-Broichsitter, M.; Merkel, O.M.; Kissel, T. Controlled pulmonary drug and gene delivery using polymeric nano-carriers. *J. Control. Release*, **2012**, *161*, 214–224.

[48] Muralidharan, P.; Mallory, E.; Malapit, M.; Hayes, D.; Mansour, H. M. Inhalable PEGylated Phospholipid Nanocarriers and PEGylated Therapeutics for Respiratory Delivery as Aerosolized Colloidal Dispersions and Dry Powder Inhalers.*Pharmaceutics*, **2014**, *6*, 333-353.

[49] Har-el, Y.; Fiegel, J.; Dawson, M.; Hanes, J. Chapter 16: Gene Delivery to the Lung. In *Pharmaceutical Inhalation Aerosol Technology*; Hickey, A.J., Ed.; Marcel Dekker Inc.: New York, NY, USA, Volume 134, pp. 498–505, **2004**.

[50] Hills, B. A. An alternative view of the role(s) of surfactant and the alveolar model. *J Appl. Physiol*., **1999,** *87*, 1567–1583.

[51] Roy, I.; Vij, N. Nanodelivery in airway diseases: challenges and therapeutic applications. *Nanomedicine*, **2010**, *6*, 237–244.

[52] Arppe, J.; Vidgren, M.; Waldrep, J. C. Pulmonary pharmacokinetics of cyclosporin a liposomes. *Int. J. Pharm.*, **1998**, *161*, 205–214.

[53] SemmlerBehnke, M.; Takenaka, S.; Fertsch, S. Efficient elimination of inhaled nanoparticles from the alveolar region: Evidence for interstitial uptake and subsequent reentrainment onto airways epithelium. *Environ. Health Perspect.*, **2007**, *115*, 728–733.

[54] Dailey, L.; Jekel, N.; Fink, L. Investigation of the proinflammatory potential of biodegradable nanoparticle drug delivery systems in the lung. *Toxicol. Appl. Pharmacol.* **2006**, *215*, 100–108.

[55] Azarmi, S.; Roa, W.; Löbenberg, R. Targeted delivery of nanoparticles for the treatment of lung diseases. *Adv. Drug Deliv. Rev.*, **2008,** *60*, 863–875.

[56] Hartig, S.; Greene, R.; Dasgupta, J. Multifunctional nanoparticulate polyelectrolyte complexes. *Pharm. Res.*, **2007**, *24*, 2353–2369.

[57] Kathuria, H.; Cao, Y.; Ramirez, M.; Williams, M. Transcription of the caveolin1 gene is differentially regulated in lung type I epithelial and endothelial cell lines. A role for ETS proteins in epithelial cell expression. *J. Biol. Chem.*, **2004,** *279*, 30028–30036.

[58] Brandenberger, C.; Mühlfeld, C.; Ali, Z. Quantitative evaluation of cellular uptake and trafficking of plain and polyethylene glycol-coated gold nanoparticles. *Small,* **2010**, *6*, 1669–1678.

[59] Lassmann-Vague, V.; Raccah, D. Alternatives routes of insulin delivery, *Diabetes & Metabolism*, **2006**, *32*, 513-522.

[60] Moses, R. G. Combination Therapy for Patients with Type 2 Diabetes: Repaglinide in Combination with Metformin. *Expert Rev. Endocrinol. Metab*. **2010,** *5*, 331-342.

[61] Damge, C.; Reis, C. P.; Maincent, P. Nanoparticle strategies for the oral delivery of insulin. *Expert Opin. Drug Deliv.*, **2008,** *5*, 45–68.

[62] Card, J. W.; Magnuson, B. A.A review of the efficacy and safety of nanoparticle-based oral insulin delivery systems. *Am. J. Physiol. Gastrointest. Liver. Physiol.* **2011**, *301*, G956–G967

[63] Hermansen, K.; Rönnemaa, T.; Petersen, A. H.; Bellaire, S.; Adamson, U. Intensive therapy with inhaled insulin via the AERx® insulin diabetes management system: A 12-week proof-of-concept trial in patients with type 2 diabetes. *Diabetes Care*, **2004**, *27*, 162-167.

[64] Rolla, A. R.; Rakel, R. E. Practical approaches to insulin therapy for type 2 diabetes mellitus with premixed insulin analogues. *Clinical Therapeutics*, **2005**, *27*, 1113-1125.

[65] *G*ä*n*sslen, M. About inhalation of insulin. KlinWochenschr, *4*, 71, **1925.**

[66] Sun, X.J.; Rothenberg, P.; Kahn, C. R.; Backer, J. M.; Araki, E.; Wilden, P. A.; Cahill, D. A.; Goldstein, B. J.; White, M. F. Structure of the insulin receptor substrate IRS-1 defines a unique signal transduction protein. *Nature*, **1991**, *352*, 73–77.

[67] Fang, X.; Yu, S.X.; Lu, Y.; Bast, R. C.; Woodgett, J.R.; Mills, G.B. Phosphorylation and inactivation of glycogen synthase kinase 3 by protein kinase A. *Proc. Natl. Acad. Sci. U.S.A.* **2000**, *97*, 11960–11965.

[68] McManus, E. J.; Sakamoto, K.; Armit, L.; Ronaldson, L.; Shpiro, N.; Marquez, R.; Alessi, D. R. Role that phosphorylation of GSK3 plays in insulin and Wnt signalling defined by knocking analysis. *EMBO J*. **2005,** *24*, 1571–1583.

[69] Iwase, H.; Kobayashi, M.; Nakajima, M.; Takatori, T. The ratio of insulin to C-peptide can be used to make a forensic diagnosis of exogenous insulin overdosage. *Forensic Sci. Int.***2001**, *115*, 123–127.

[70] Wolzt, M.; De La Peña, A.; Berclaz, P.; Tibaldi, F.; Gates, J.; Muchmore, D. Air inhaled insulin versus subcutaneous insulin: pharmacokinetics, glucodynamics, and pulmonary function in asthma. *Diabetes Care*, **2008,** *31*, 735–740.

[71] Karathanasis, E.; Bhavane, R.; Annapragada, A. Glucosesensing pulmonary delivery of human insulin to the systemic circulation of rats. *Int. J. Nanomedicine,* **2007,** *2*, 501–513.

[72] Leach, C.; Kuo, M.; Bueche, B.; Fishburn, S.; Viegas, T.; Bossard, M.; Guo, L.; Bentley, M.; Hobbs, C.; Cherrington, A. Modifying the pulmonary absorption and retention of proteins through PEGylation. *Respir. Drug Deliv. IX,* **2004**, *1*, 69–78.

[73] Lee, K.C.; Chae, S.Y.; Kim, T.H.; Lee, S.; Lee, E.S.; Youn, Y.S. Intrapulmonary potential of polyethylene glycol-modified glucagon-like peptide-1s as a type 2 anti-diabetic agent. *Regul. Pept.* **2009**, *152*, 101–107.

[74] Insulin inhalation—Pfizer/Nektar therapeutics: Hmr 4006, inhaled peg-insulin—Nektar, PEGylated insulin—Nektar. *Drugs R&D* **2004**, *5*, 166–170.

[75] Bi, R.; Shao, W.; Wang, Q.; Zhang, N. Spray freeze dried dry powder inhalation of insulin loaded liposomes for enhanced pulmonary delivery. *J. Drug Target,* **2008,** *16*, 639–648.

[76] Chono, S.; Fukuchi, R.; Seki, T.; Morimoto, K. Aerosolized liposomes with dipalmitoylphosphatidylcholine enhance pulmonary insulin delivery. *J. Control. Release,* **2009**,*137*, 104–109.

[77] Liu, F. Y.; Shao, Z.; Kildsig, D. O.; Mitra, A. K. Pulmonary delivery of free and liposomal insulin. *Pharm. Res.,* **1993,** *10*, 228-232.

[78] Liu, J.; Gong, T.; Fu, H. Solid lipid nanoparticles for pulmonary delivery of insulin. *Int. J. Pharm.*, **2008**, *356*, 333–344.

[79] Yamamoto, H.; Kuno, Y.; Sugimoto, S.; Takeuchi, H.; Kawashima, Y. Surface modified PLGA nanosphere with chitosan improved pulmonary delivery of calcitonin by mucoadhesion and opening of the intercellular tight junctions. *J. Control. Release,* **2005**, *102*, 373–381.

[80] Huang, X.; Du, Y.; Yuan, H.; Hu, F. Preparation and pharmacodynamics of low molecular weight Chitosan nanoparticles containing insulin. *Carbohydr. Poly.*, **2009,** *76*, 368–373.

[81] Yamamoto, H.; Hoshina, W.; Kurashima, H. Engineering of poly(dl-lactic-co-glycolic acid) nanocomposite particles for dry powder inhalation dosage forms of insulin with the sprayfluidized bed granulating system. *Adv. Powder Technol.*, **2007,** *18*, 215–228.

[82] Grenha, A.; Seijo, B.; Remunan-Lopez, C. Microencapsulated chitosan nanoparticles for lung protein delivery. *Eur. J. Pharm. Sci*., **2005**, *25*, 427–437.

[83] Zhang, Q.; Shen, Z.; Nagai, T. Prolonged hypoglycemic effect of insulin loaded polybutylcyanoacrylate nanoparticles after pulmonary administration to normal rats. *Int. J. Pharm*., **2001,** *218*, 75–80.

[84] DeRuitter, J. *Overview of the Antidiabetic Agents*. Endocrine Pharmacotherapy Module, Spring, **2003.**

[85] Reddy, V. S.; Sahay, R. K.; Bhadada,S. K.; Agrawal J.K.; Agrawal, N. K. Newer Oral Antidiabetic Agents. *J. Indian Acad. Clin. Med*., **2000,** *1*, 245-251.

[86] Agabegi, E. D.; Agabegi, S. S. *Step-Up to Medicine (Step-Up Series)*. Hagerstwon, MD: Lippincott Williams & Wilkins, **2008.**

[87] Rendell, M. Advances in diabetes for the millennium: drug therapy of type 2 diabetes. *MedGenMed*., **2004**, *6*, 9.

[88] Elmowafy, E.; Osman, R.; El-Shamy, A. H.; Awad, G. A. Nanocomplexes of an insulinotropic drug: optimization, microparticle formation, and antidiabetic activity in rats. *Int. J. Nanomedicine*, **2014**, *9*, 4449–4465.

[89] Zhou, G.; Myers, R.; Li, Y.; Chen, Y.; Shen, X.; Fenyk-Melody, J.; Wu, M.; Ventre, J.; Doebber, T.; Fujii, N.; Musi, N.; Hirshman, M.; Goodyear, L., Moller, D. Role of AMP-activated protein kinase in mechanism of metformin action. *J. Clin. Invest*., **2001,** *108*, 1167–1174.

[90] Youn, Y.S.; Jeon, J.E.; Chae, S.Y.; Lee, S.; Lee, K.C. PEGylation improves the hypoglycaemic efficacy of intranasally administered glucagon-like peptide-1 in type 2 diabetic *db*/*db*mice. *Diabetes Obes. Metab.*, **2008**, *10*, 343–346.

[91] Kim, T. H.; Park, C. W.; Kim, H. Y.; Chi, M. H.; Lee, S. K.; Song, Y. M.; Jiang, H. H.; Lim, S. M.; Youn, Y. S.; Lee, K. C. Low molecular weight (1 kDa) polyethylene glycol conjugation markedly enhances the hypoglycemic effects of intranasally administered exendin-4 in type 2 diabetic *db*/*db*mice. *Biol. Pharm. Bull*., **2012**, *35*, 1076–1083.

Received: January 30, 2015 Revised: September 22, 2015 Accepted: October 9, 2015

Send Orders for Reprints to reprints@benthamscience.ae

Current Pharmaceutical Design, 2015, *21*, 000-000

Nanoscale Formulations and Diagnostics With Their Recent Trends: A Major Focus of Future Nanotechnology

Biswajit Mukherjee*, Lopamudra Dutta, Laboni Mondal, Niladri Shekhar Dey, Samrat Chakraborty, Ruma Maji and Tapan Kumar Shaw

Department of Pharmaceutical Technology, Jadavpur University, Kolkata-700032, India

Biswajit Mukherjee

Abstract: Nanomedicine is an emerging and rapidly growing field, possibly exploring for high expectation to healthcare. Nanoformulations have been designed to overcome challenges due to the development and fabrication of nanostructures. Unique size-dependent properties of nanoformulations make them superior and indispensable in many areas of human activity. Nano drug delivery systems are formulated and engineered to carry and deliver a number of substances in a targeted and controlled way. The vision of nanocarriers can be designed that will serve a dual purpose, allowing both treatment and diagnosis to be contained in an 'all-in-one' package. Nanoscale drug-delivery systems efficiently regulate the release, pharmacokinetics, pharmacodynamics, solubility, immuno-compatibility, cellular uptake and biodistribution of chemical entities (drug). Their cellular uptake takes place by various mechanisms such as micropinocytosis, phagocytosis and receptor mediated endocytosis. These phenomena cause longer retention in blood circulation resulting in the release of the encapsulated materials in a sustained manner thus minimize the plasma fluctuations and toxic side effects. In this manner, the therapeutic index of conventional pharmaceuticals is efficiently increased. They can be used to deliver both micro and macro biomolecules such as peptides, proteins, plasmid DNA and synthetic oligodeoxynucleotides. In this present review, several recent developing and modifying nano-products for the detection, analysis, and treatment of diseases with their US and world patents along with various diagnostic kits have been discussed.

Keywords: Nanotechnology, nanoformulations, patents, diagnostic kits, diseases, nanoparticles.

INTRODUCTION

In pharmaceutical industries, a new molecular entity (NME) with potent biological activity but poor water solubility generally faces significant challenges to be formulated. Nanotechnology is an emerging discipline which may address some of the drawbacks associated with potential NMEs [1]. It involves the science and engineering of producing objects smaller than one hundred nanometers [2]. It also covers an extended area of drug delivery and targeting. Though it seems to be a mysterious concept to many people, nanotechnology is influencing our present lives and in combination with biotechnology and information technology, it is going to determine the way we live in future. In the present world, research of every field is involved in getting utmost benefits from the latest technology at lower cost which creates a necessity to bring nanotechnology based therapeutic approaches and products from the very core laboratory to clinic [3].

Nanomedicine provides various opportunities in health care system. In biomedical fields, nanotechnology is the study of nanoparticles, nano liposome, nanocapsules, nanospheres, nanosuspensions, nanoemulsions, nanorobots, *etc*.

Early detection and/or treatment of cancers, increased biocompatibility, active and passive disease targeting and multi-functionality about therapeutic capability are the potential benefits to medical applications offered by nanotechnology to allow simultaneous disease monitoring and treatment [4]. It also greatly influences the treatment of a huge number of diseases, including diabetes, Alzheimer's disease, several inflammatory conditions, such as arthritis, rheumatism and asthma *etc*.

In more defined terms, nanomedicine in the area of healthcare involves the development of specific new drugs and delivery systems with encapsulation and liberation of drugs, diagnostic kits, biosensors, testing devices with images, materials for implants, artificial bone and skin, bone substitutes, regeneration of neurons, dental products, orthopedic, cardiac and retina implants [5], *etc*.

In this review, the main focus is on different aspects of nanotechnology, its application in drug delivery and several fields of prospect, where current and emerging nanotechnologies could facilitate novel classes of therapeutics. However, this article can only provide a glimpse into this rapidly evolving field at present and in the future.

NANOTECHNOLOGY

Nanotechnology involves with the development of materials at atomic, molecular and macromolecular level (like human bone, tennis and badminton racquets, racing bicycle, hockey stick, golf ball, *etc*.) being recognised as a game-changer in future. The Greek word "nano" means dwarf. Adopting this technology, scientists are able to comprehend and maneuver materials by the scale of atoms and molecules, having properties such as at least 1 to 100 nm dimension, can be designed using methodologies, which control the physical and chemical attributes of molecular-scale structures, and able to combine to make large structures [6,7]. The properties of material change while converting it to its nanoscale size [8,9]. Predominant changes in properties, such as increase in surface area, dominance of quantum effects associated with minute sizes, higher surface area to volume ratio *etc*. and variation in materials magnetic, thermal and electrical properties are observed due to the conversion from macro to nano size. For example, at macro scale copper is opaque; however at the nanoscale, it is transparent [8,9]. Similarly, inert platinum becomes a catalyst at nanoscale. Various examples of nanodimensions such as water molecules, DNA, red blood corpuscles (RBC), virus *etc*. are present in nature. The inception of nanotechnology is believed to have been founded in 1959 by Nobel Laureate physicist Richard Feynman in a post-dinner speech titled "There is plenty of room at the bottom". He gave an idea about the capabilities of an atom by atom assembly and considered nano-engineering could lead to new materials and pathways. In

*Address correspondence to this author at the Department of Pharmaceutical Technology, Jadavpur University, Kolkata-700032, India;
Tel/Fax: +91-33-24146677; E-mail: biswajit55@yahoo.com

1381-6128/15 $58.00+.00

ancient time Indian craftsmen and artisan used nanotechnology to design weapons. At first in 1902, Richard Zsigmondy observed and measured the size of nanoparticle using the ultra microscope. The term nanotechnology was first coined by Norio Taniguchi, a researcher at the University of Tokyo in 1974. In 1980s, the inventions which facilitated the imaging of individual atoms or molecules, as well as their manipulation, contributed to major progress in the field of nanotechnology. A significant progress of nanotechnology was observed due to the discovery of fullerene C_{60} by Kroto's and Smalley's research team. In 1991, the discovery of carbon nanotubes by Saumiolijima and later the National Nanotechnology Initiative (NNI) and the United State Government led the further development in the field of nanotechnology [8, 9].

ADVANTAGES OF NANOTECHNOLOGY

Some advantages of nanotechnology are mentioned below:

a. Using this technology, stronger, tougher and lighter materials are being produced for construction and engineering purposes. Some such applications include low maintenance coating, reducing the thermal transfer rate of fire retardant and insulation, improvement of cementitious materials' property, significant changes in the sound absorption of acoustic absorber, glass reflectivity improvement, *etc*. [10].

b. Significant changes are being made in healthcare and drug delivery systems. Drug delivery, tissue engineering, diagnostics, nanosurgery, nano nephrology, *etc*. are some areas of use of nanomaterials in nanomedicine [11].

c. Improvement is made in transport system such as adding nano size silicon carbide into tyre manufacturing elastomers to increase the wet skid resistance and decrease abrasion of the tyre about 50 % [12].

d. Significant products (such as nanonutrients and neutraceuticals) have been achieved in nutrition using nanotechnology [13].

e. Nanotechnology also plays a huge role in maintaining a sustainable environment. In this regard, few applications are in air monitoring by solid state gas sensors, automated water analyzer computer supported system for water monitoring, nanoscale zero-valent iron (NZVI) for water remediation and nano filters using carbon nanotubes or nanocapillary arrays to remove impurities and reactives [14].

f. Quantum dots, a newer nanotechnological invention, is playing a crucial role in biological field such as cell labeling, *in vivo* imaging, biosensing, diagnostics (as diagnostic fluorophores in nucleic acid detection and immunolabeling) and bimodal magnetic-luminescent imaging [15].

SIGNIFICANCE OF NANOTECHNOLOGY IN PHARMACEUTICAL FIELD

Nanotechnology has flourished pharmaceutical research by developing the potential site-specific delivery system with minimum drug toxicity and better efficacy. The applications of pharmaceutical nanotechnology are largely shown in nanomedicine and they include development of drug delivery system, diagnostic kits, material for implantation, neuron regeneration, cardiac and retina implantation, biosensors, artificial bone and skin, bone substitute material, dental product, testing device with images *etc*. for monitoring, diagnosis, treatment and controlling biological systems [7, 16]. The drug delivery system has been revolutionized due to pharmaceutical nanotechnology research in the form of nanoparticles, nanoliposomes, nanopores, quantum dots, nanospheres, nanocapsules, nanoshells, nanotubes, dendrimers, nanocrystals, nanovaccines, *etc*. Nanorobotics, nanosize empty viral capsids, nanomaterials on chips, magnetic nanoparticles and magnetic immunoassay have also a significant role in nanomedicine [9] (Fig. **1**).

NANOMATERIALS IN NANOMEDICINE

Nanoparticles

Nanoparticles are the submicron size spherical particles composed of natural or synthetic biodegradable polymers which can provide controlled and targeted delivery of the drug with better efficacy and fewer side-effects. Antibody conjugation with nanoparticles can be used to bind selectively with specific antigens and enhanced cellular uptake as well as intracellular stability. The monoclonal antibodies (mAbs), however, require achieving maximum response for long half-life, the power to penetrate to the target tissue, not to induce an immune response, and to provide a maximum cytotoxic effectiveness in target cells [17]. Antibodies conju-

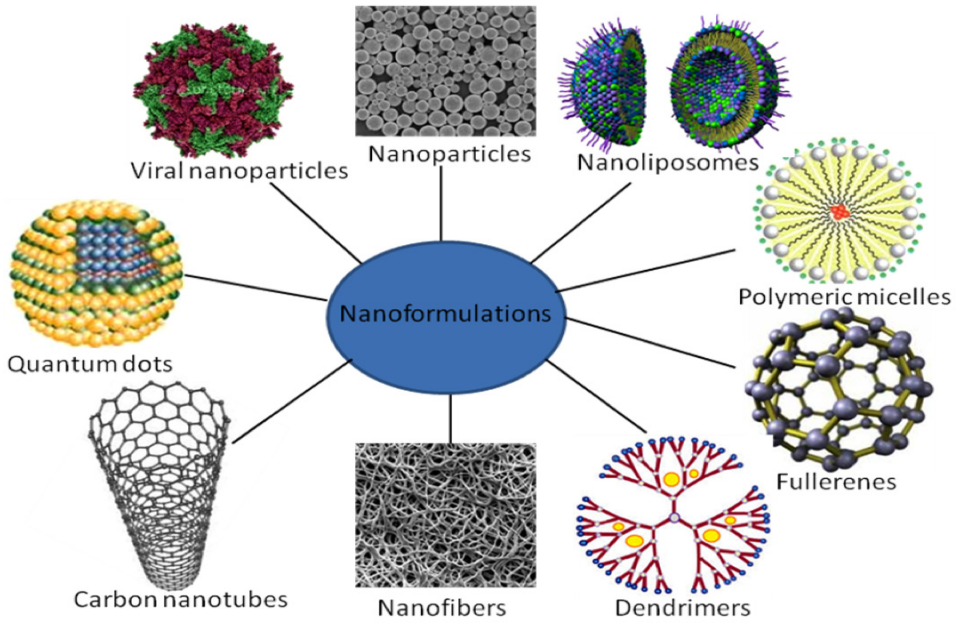

Fig. (1). Different types of nanoformulations.

gated magnetic nanoparticles show magnetic signal on introduction to a magnetic field [18]. Use of magnetic nanoparticles conjugated with specific antibodies along with super conducting quantum interference device sensors for breast cancer has shown uniqueness in terms of ultra-sensitive detection for diagnostic as well as drug delivery [19]. Nanoparticles can be coated with various functional groups like aldehyde, amino, sulfate, hydroxyl, and carboxyl groups on their surfaces. Depending on these properties humanized anti her2/neu monoclonal antibody (Herceptin) was conjugated with superparamagnetic iron oxide (nanomag-D-SPIO 20nm) with COOH group on the surface of nanoparticles for cancer targeting [19]. Synthetic molecules of DNA/ RNA/ aptamers are also used to recognize specific proteins. The main advantage of using aptamers compared to antibodies is avoidance of immunogenic reactions. On the other hand, aptamers possess the disadvantages due to their high cost for manufacturing in bulk quantities and vulnerability to enzymatic degradation compared to antibodies [20]. The antibody-conjugated nanoparticles can be used for two biomedical applications: such as therapy and diagnosis [21]. In therapy, the applications can be divided into *in vivo* use and *in vitro* experimentation that comprises contrast agents for cell sorting, magnetic resonance imaging, sensing, enzyme immobilization, bioseparation, purification transfection, immunoassays, *etc*. Nanoparticles have been utilized as carriers for siRNA, oligonucleotides, plasmid DNA, to transfect cells for using the cellular machinery to generate therapeutic proteins, to distinguish the cells into specific ones or to trigger a cellular response [22]. The nanoparticle can act as a defensive coating to the moiety. Hence, synthetic siRNAs are used for therapeutic intervention as a valuable tool. However, it is essential to develop their cellular target specificity, their efficient cellular delivery (particular into primary cells) along with their stability [23]. Aptamers are short, synthetic, single-stranded oligonucleotides which selectively bind with various molecular targets (such as nucleic acids, proteins), cells and tissues with high likeliness and specificity. Aptamers demonstrate advantages for low immunogenicity, low toxicity, a small size to enable solid tumor penetration and high affinity to bind with the target and these characters make aptamers one of the ideal candidates for targeted cancer therapy compared with traditional ligands, including antibodies, peptides and small molecules [20]. Smart multifunctional nano-structure (SMN) was developed with porous hollow magnetite nanoparticles containing the anticancer drug doxorubicin, a hetero- bifunctional PEG ligand and sgc8 aptamer for targeted chemotherapy and magnetic resonance imaging in cancer cells. Conjugation of aptamers on the outer surface of SMN resulted in enhanced specific binding and intake of SMNs to targeted cancer cells. Immobilization of aptamers on silica nanoparticles has been reported for drug delivery, targeted recognition and stimuli-sensitive release. For targeted drug delivery sgc8 aptamer-modified mesoporous silica nanoparticles were developed by Zhu *et al*. [22]. Polyelectrolyte multilayers coating was done on mesoporous silica nanoparticles to prevent untimely leakage of the drug during the delivery process but to provide controllable drug release under reducing conditions [22]. The few above mentioned distinguishable studies thus focus on the future role of nanoparticles in nanomedicine.

Viral Nanoparticles

Development of virus-derived materials in the medical sector is becoming a growing area of pharmaceutical as well as medicinal fields [24]. Virus capsid is tried for use in drug delivery as nanocarriers. Viruses used in viral nanoparticle (VNP) development are well known because of their genomic sequence, organization, virion structure and expression strategies [25]. Main advantages of VNPs include biodegradability, biocompatibility, and mono-dispersibility. Virus-like particles (VLPs) and VNPs have combined chemists, biologists, medical researchers and engineers in single platform [26]. VLPs can be regarded as a subclass of VNPs which are the genome-free counterparts of VNPs. Being derived from natural sources VNPs are valuable because of their biocompatibility and biodegradability, as well as nonhazardous and non-infectious in humans and other mammals [27]. Various designs of VNPs are available where the internal cavity can be composed of imaging reagents, drug molecules, quantum dots and other nanoparticles. On the other hand, the external surface of VNPs can be modified with targeting ligands to allow cell-specific delivery [28]. The administration of engineered VNPs to animal model systems has discovered that altering the surface charge of particles influences their plasma clearance and tissue distribution [29]. Surface charge plays an important role in interaction and uptake processes of target cells which has also been demonstrated. The primary function of virions is to transport, encapsidate, release nucleic acids, and in some cases proteins, among different environments [30]. Assembly in the presence of high concentrations of foreign molecules and the application of pH shock are the two techniques available for loading VNPs with low molecular weight substances, nucleic acids and proteins. DNA entrapment by *in vitro* association has been accomplished using various VNPs [31]. Functional groups present in the side chain of genetically introduced amino acids of structural proteins of the VNPs can be utilized for chemical conjugation. Carboxylic acids, thiol groups, amines and side chains of tyrosines can interact with activated conjugates. Using this approach, different molecules can be covalently combined at specific positions of a variety of structurally diverse VNPs [32].

Liposomes

Liposomes are spherical concentric nanostructured vesicles containing lipid bilayers and aqueous core that can encapsulate hydrophilic therapeutic molecules in their internal core or hydrophobic agents into their lipid bilayers. Liposomes are capable of enhancing the blood circulation time of the drug by avoiding renal clearance and reticuloendothelial system, and increase the drug deposition in the tumor via the EPR effect [33].

Development of liposomes with targeting vectors attached to the bilayer surface is a great deal of effort in the modern medicinal field. These vectors have included ligands such as oligosaccharides, peptides, proteins, and vitamins [34]. Conjugation of highly specific monoclonal antibodies (MAbs) is well established. Challenges have been taken up as well by many researchers for antibody-conjugated nanoliposomal carriers. Numerous procedures such as amine modification, carbohydrate modification, disulfide modification, and noncovalent conjugation for the conjugation of antibodies to nanoliposomes have been developed [35]. The size differences may be significant when conjugating the antibody to liposomes, particularly when molecules, such as polyethylene glycol (PEG)-lipids, are incorporated on or into the liposome membrane. Size may affect conjugation efficiency and liposome aggregation. Different antibodies may be more sensitive to some procedures than others and, therefore, it may be necessary to attempt a number of protocols. Commonly procedures involve either the thiolation of antibodies with 3-(2-pyridyldithio) propionic acid-N-hydroxysuccinimide ester (SPDP), followed by deprotection with dithiothreitol (DTT) or antibody conjugation to maleimide-derivatized 1,2-distearoyl-sn-glycero-3-phosphoethanolamine(DSPE) or 1,2-dipalmitoyl-sn-glycero-3-phosphoethanolamine (DPPE) *etc*. on liposomal membrane [36].

Two vital approaches may enhance the *in vivo* stability and efficacy of the drug carriers. One such approach is to diminish membrane fluidity by incorporation of cholesterol to hinder lipid extraction by high-density lipoproteins in the blood which causes liposome breakdown. Some approved formulations of this kind are DaunoXome, Myocet, Depocyt, Mariqibo, Doxil, *etc*. [35]. The second approach is the inclusion of flexible hydrophilic molecules. An example is PEG, permitted by the United States Food and Drug Administration, is widely used in several approved formulations, such as Doxil, SPI-077, S-CDK602, *etc*. Nevertheless, polyvinyl

pyrrolidones or Poly [N-(2-hydroxypropyl)methacrylamide] are also potentially significant. Inclusion of flexible hydrophobic inert and biocompatible PEG with lipid anchor in liposomes forms the hydrated steric barrier by reducing liposome interaction with blood-borne component, decreasing their spleen and liver binding and enhancing their blood circulation time. Superior interaction of 'cell penetrating peptide'- attached PEGylated liposomes with the cells was confirmed after coupling of the peptide *in vitro* with PEG1000 as compared to their coupling with PEG750 or PEG 3400 and was interrelated with the construction of ligand arrangement [34]. The lengthy placement of PEGylated liposomes in blood has been associated with their lower elimination by the mononuclear phagocyte system (MPS) and correlated with their increased tumor accumulation and efficacy [37]. Albumin conjugation to drug-loaded PEGylated liposomes has been reported to enhance their circulation time and resulting therapeutic activity [38]. Radiolabeled liposomes were shown to mount up in cancerous cells as well as in normal organs in patients; revealing the need of tumor targeting. Internalization of antibodies on the surface of doxorubicin loaded PEGylated liposomes noticeably enhanced their therapeutic effectiveness for cancer chemotherapy [39]. Similarly, Bartlett *et al*. showed that although untargeted and transferrin-targeted siRNA nanoparticles were identical to tumor distribution, the latter achieved superior *in vivo* silencing [40]. Liposomes are the most widely used nanocarriers for drug delivery. Kang *et al.* established the high specificity and efficacy of aptamer-guided liposome as a delivery approach by modification of the liposome with sgc8 aptamer to deliver drug to the target cells [41]. The sgc8 aptamer-liposome conjugate could target leukemia CCRF-CEM cells specifically as revealed from the flow cytometry results after 30 min of incubation time [20]. Thiolated oligonucleotide aptamer (thioaptamer) against E-selectin (EST-Apt) after intravenous administration resulted in their gathering at the tumor site of breast cancer xenografts with similar circulation half-time [34, 36].

Thiophosphate-backbone modified oligonucleotide aptamer also called "thio"aptamer was reported to bind E-selectin expressed on endothelial cells with high affinity and specificity [42]. The above findings show the potential of nanosize liposome in drug delivery and drug targeting and claim for their enormous utility in the field in near future.

Quantum Dots

Quantum dots are 1-10 nm in size tiny semiconductor crystals made up of compounds of the elements belonging to the group III to V and II to VI of the periodic table. Examples of the elements are Hg, Cd, Ag, P, Pb, Ln, Zn, Se, Te *etc.* Quantum dots can be conjugated with tumor-specific targeting agent that can bind to the active binding sites to attach the quantum dots to cancerous cells for active targeting purpose [43]. Consecutively, immunofluorescent probes are developed with antibodies to recognize these tumors. The quantum dot probes are lacking the tumor-specific active binding agents for passive targeting [44]. DNA-interacting drug like doxorubicin for cancer chemotherapy was immobilized onto quantum dots [45]. Many studies have revealed that quantum dot-conjugated oligonucleotide sequences (attached via surface carboxylic acid groups) may be targeted to bind with DNA or mRNA [46]. Binding of quantum dots with molecular structures is exclusive to the cell as well as virus coat. Early detection of respiratory syncytial virus (RSV) is vital for controlling the disease and drug development. Quantum dots conjugated with antibody identify RSV quickly and delicately [47]. These nanostructures may pave to a new avenue in drug delivery and drug targeting along with a fast diagnosis.

Gene Delivery

Gene delivery is an area of considerable current interest. Genetic materials (DNA, RNA, and oligonucleotides) have been used as molecular medicines and are delivered to specific cell types to either inhibit some undesirable gene expression or express therapeutic proteins. Different types of targeting molecules such as peptides, antibodies, saccharine *etc*. have been verified for modulation of nanocarriers to achieve active targeting [48]. Recently, ultrafine silica nanoparticles, with surfaces functionalized by cationic-amino groups that assist to bind nanoparticles on the cell surface, have been shown to not only protect plasmid DNA from enzymatic digestion but also transfect into the cultured cells that express encoded proteins [49]. During the past decades, the studies of nanocarriers for target-specific gene delivery have gained immense attention. In current field of research, the bioadhesive PLGA nanoparticles established a promising area of therapy for a number of critical diseases. Kong *et al.* investigated the efficacy of Mannan modified DNA loaded bioadhesive PLGA nanoparticles for targeting the Kupffer cells by gene therapy. They also studied Mannan-based PE-grafted ligands for the alteration of nanocarrier's surface. [48]. A technology for brain disorders, such as Alzheimer's disease and Parkinson's disease, constitutes an unmet medical help. Short interference RNA (siRNA) mediated gene therapy is an attractive approach for meeting these. This can be fulfilled efficiently by the delivery of plasmid DNA and siRNA through nanocarriers targeting brain parenchymal cells. One of the rational approaches in treating Alzheimer's disease, Parkinson's disease *etc*. involves topical administration. At present, the adeno-associated virus encoding L-amino acid decarboxylase, which is under phase I clinical trial, is being focused on the treatment of Parkinson's disease as gene therapy [50] though as a safe gene carrier for brain disorders, an efficient nonviral carrier would still be desirable for use.

From the previous discussion, it is found that multifunctional envelope-type nanoliposome may be used to deliver plasmid DNA and siRNA to various organs like lungs, liver and adipose tissue [49]. Magnetic nanoparticles, composed of an iron oxide core and polymeric shell, present a particularly promising carrier for enhanced tumor delivery of therapeutic to many brain disorders, including Alzheimer's disease and Parkinson's disease. The delivery of the nanoparticles to tumor vasculature is an important prerequisite for their magnetic entrapment within the glioma lesion [50]. Nanoparticles as gene carriers become popular in the mammalian cultured cells, whereas its application in plant cells is still limited. Although several nanoparticles including mesoporous silica, starch (such as hydroxyethyl starch, propyl starch, potato starch *etc*.), poly(amidoamine) dendrimer polyethyleneimine and chitosan were used as gene carriers to deliver gene into plant materials, no stable genetically modified plant-mediated by nanoparticles have been obtained so far. ZnS nanoparticles have the advantages such as small size, good biocompatibility and controllable preparation coupled with rationally designed functionalizations. ZnS nanoparticles may be a desirable gene carrier to deliver DNA into intact plant cells with the aid of an ultrasound-mediated method as reported [51].

Polymeric Micelles

Polymeric micelles are colloidal particles of nano dimensions (usually 5-100 nm) that are composed of an amphiphilic polymer having both hydrophilic and hydrophobic units. At low concentration in an aqueous medium, the amphiphiles usually exist as monomers. However, at a certain concentration range, these amphiphiles tend to aggregate and self-assembled to form unique structures, called micelles [52]. The narrow concentration range at which micelle formation takes place commonly referred as critical micelle concentration (CMC). Due to the presence of two distinct regions i.e. a hydrophilic head-group with a hydrophobic core, micelles are used as a drug delivery system for delivery of hydrophobic anticancer drugs [53]. Since the majority of anticancer drugs are hydrophobic with a low aqueous solubility and bioavailability, solubilization of these hydrophobic drugs in the core of micelles can overcome the problem of the aqueous solubility and can improve drug bioavailability. Currently, many polymeric micelles for

anticancer therapy are under clinical trials. SP1049C, Genexol-PM, NK012, NK105 *etc*. are few examples of them [53].

Conjugations of an aptamer with micelles are recently a new concept for drugs delivery. For example, micelles synthesized from diacyl lipid can be conjugated with DNA aptamer to get a DNA-micelle aggregate which is much biocompatible and stable [54]. In another case, to attain a targeted drug delivery by Tan group, aptamer-micelle which is self- assembled quite easily is also possible when a lipid end is attached to a TD05 aptamer [34, 36]. Thus, the nanosize polymeric micelles are being explored as new drug delivery vehicles capable of drug targeting also.

Fullerenes

Fullerenes, the third carbon allotrope, are defined as a family of carbon molecules with cage like structure with hollow spheres [55]. In September 1985, Robert F. Curl, Jr., Richard E. Smalley, and Harold W. Kroto discovered fullerene C_{60} during laser spectroscopy experiments at Rice University [56]. Fullerenes were named after Richard Buckminster Fuller. After their discovery, these nanomaterials have been investigated for drug delivery purposes. But the main obstacle of using fullerenes for drug delivery application is their poor solubility. Therefore, they reported to be modified chemically or by some supramolecular approaches and these functionalized fullerenes have been used as a promising carrier for drug delivery [57].

It is reported that a metal moiety can be easily entangled into the inner hollow sphere of the fullerenes molecule, which have been investigated to be utilized for MRI technology [55]. A dramatic increase of production and use related to such diagnostic materials is expected over the next many decades. Due to their unique physical and chemical properties fullerene-based nanomaterials are considered to be promising for novel nanotechnology applications [58]. While the toxicity of C_{60} nanoparticles (nC_{60}) and carbon nanotubes (CNTs) in aqueous suspensions has been studied in detail, our current understanding of their fate and transport in subsurface environments is quite limited [59]. The distinctive chemical structure of C_{60} nanoparticles, rendered them to acquire the unique photophysical properties to use them in photodynamic therapy (PDT) for biological applications. The production of reactive oxygen species (ROS), when they are irradiated with light in visible wavelength region is the key mechanism in this case [56, 60, 61].

Photosensitizing nanomaterials are offering a substitute platform to effective PDT in place of traditional organic photosensitizer. Liu *et al.* developed aptamer-fullerene photosensitizer to obtain a photodynamic effect [20]. For example, R13 aptamer conjugated fullerene can be used for PDT of A549 lung cancer in the presence of serum with a very good and effective result. Thus, the aptamer-fullerene conjugate moiety may be a good alternative treatment strategy for tumor targeted PDT applications and the photodynamic efficacy and biocompatibility of this conjugate are reported to be improved in the absence of light [34, 36].

Carbon Nanotubes

Carbon nanotubes (CNTs) are allotropes of carbon, discovered by Japanese scientist Sumio Iijiama of Nippon Electric Company Limited' in 1991 and are made of graphite with a cylindrical structure, just like a honeycomb structure [62]. The CNTs due to their unique mechanical, electrical and surface properties can be a very good choice for a variety of applications in the field of biotechnology, biomedical engineering and drug delivery purposes [63, 64]. The pure CNTs are insoluble in most of the solvent system when considering for drug delivery application and also seem to be cytotoxic [65-67]. But for biological application, it should be soluble in some solvent system and should also be biocompatible and it is done by functionalization of CNTs. Furthermore, during functionalization bioactive molecules can be conjugated to the surface of CNTs and this conjugated complex can be a good carrier for delivery of drugs, antigens and gene delivery [68]. Thus, functionalized CNTs recently attracting much more interest for delivering varieties of biomolecules such as genes, proteins, DNA, antibodies, vaccines, biosensors, cells *etc*. and have also been assessed for gene therapy, immunotherapy, tissue regeneration and diagnosis of different diseases [69].

The unique structures of CNTs render them to functionalize so that they can adsorb or covalently bind to a different type of molecules of therapeutic interest and also help to target to particular sites. The use of functionalized CNTs is a promising vehicle for cancer therapy as reported by most of the researchers because the CNTs have shown much unexpected advantage over other means of drug delivery such as targeted drug delivery system based on functionalized CNTs with some bioactive moieties are very less toxic and also very much effective for easy permeation through cell membrane and as carbon is a constituent of human body so they are seemed to be very much biocompatible material also. Thus functionalized CNTs can be a promising carrier for delivering therapeutic drugs, vaccines, and nucleic acids and other moieties where cellular penetration is required to be better for effective treatment. They also help to increase the solubility of the drugs in some cases during attachment of the drug to functionalized CNTs and thus provide better efficacy and safety of the drug [70-73].

The lymph node cancer may be targeted with the help of CNTs by entrapping magnetic nanoparticles loaded with cisplatin folic-acid-functionalized multiwalled carbon nanotubes (MWNTs) [74-77]. In another study, gemcitabine, can be loaded into magnetic MWNTs can be targeted to lymph node metastasis [78]. Camptothecin loaded MWNTs functionalized by polyvinyl alcohol were found to be very much effective for the treatment of breast cancer and carcinoma of skin cancers [79].

CNTs have also been shown to be a powerful tool for enantiomer separation of chiral drugs and chemicals in pharmaceutical industry as well as in laboratory and for extraction of drugs and pollutants in different media by solid phase extraction before analysis [70].

The resultant moiety during hybridization of gold nanomaterials and CNTs is reported to exhibit better and strong optical absorption in the near infrared region. This unique property of hybrid nanomaterial facilitates production of a higher amount of temperature and thus helps a photo-thermal process during treatment to be more effective and speedy. For example, gold nano popcorn and single walled carbon nanotubes hybrid moiety when conjugated with S6 aptamer can be used for targeting breast cancer. Here the recognition of SK-BR-3 breast cancer cells of this moiety is reported through interaction with the aptamer only. Now irradiation with near infrared light helps to increase the temperature of the hybrid molecule, leads to selective death of the cancer cell [80]. Another photothermal hybrid nanomaterial is reported to be possible with A9 aptamer-conjugated gold nanocage with single-walled carbon nanotubes by Khan *et al.* for getting a targeted imaging of cancer site and also photothermal damage of prostate cancer cells [81]. These hybrid nanomaterials thus can be used for imaging therapy and are very effective to separate target and non-target cancer cells. So it may be concluded that these hybrid nanomaterials are far better than a single nanomaterial due to their better photothermal destruction power of the cancer cell and better target-ability and may be very proficient treatment strategy for getting an effective *in vivo* photothermal cancer treatment [34,36].

Dendrimers

Dendrimers are the another new class of branched, synthetic polymeric macromolecular nanocarriers with layered tree-like architectures, reported to be an effective carrier system in the field of pharmaceutical nanotechnology and nanomedicines due to their distinct structural properties with a high degree of molecular uniformity, low polydispersity and having size in the range of 1-10 nm

[82, 83]. A classical dendrimer generally has three components: a central initiator core, the repeating units, and terminal groups at the periphery. They are synthesized from repeating unit of monomers and unlike conventional polymerization reaction, they are made by a step by step repetition of the monomer units, leading to a highly defined 3-D structure [84]. Thus the production of dendrimers consists of a sequence of repetitive steps starting with a central initiator core and each growth step called as "generation", and represented by "G"; and each step makes the polymer twice in a number of reactive surface sites, and also approximately double the molecular weight of the preceding generation, leading to a polymer of larger molecular diameter [85]. There are two types of synthesis methods of dendrimers such as divergent and convergent method of synthesis. In divergent method, the development starts from the central core and it is directed towards the edge radially and in convergent method of synthesis, the growth begins at the edge directing the production of synthesis towards the centre. The generation type, chemical composition of the core and the surface functionalities of the dendritic structure, determine the size, shape and reactivity of these macromolecules and a proper control of these parameters makes them a very interesting and innovative nanocarrier in drug delivery application.

The delivery of a drug with the help of dendrimers can be done either by physically entrapping the drug inside dendrimeric cavities or by conjugating the drug covalently at the peripheral terminal group(s). So dendrimers for the drug delivery purpose can serve as an excellent vehicle for delivering a number of hydrophilic and also hydrophobic drugs. The hydrophobic drugs are generally incorporated into the nonpolar cavities of the dendrimers. However, suitable modifications of the internal dendrimeric cavities are also able to deliver a hydrophilic drug. Dendrimers are also able to deliver different positively/negatively charged drugs by proper selection of an opposite charged functional group at the terminal structure during synthesis and these non-covalent inclusions or complexes offer advantages such as enhancement of aqueous solubility of drug, its stability, improvement of drug pharmacokinetic and pharmacodynamic behaviors, time-dependent controlled release of the drug.

The delivery of different antibodies and other bioactive moieties is achieved by conjugating them with suitably modified terminal groups of dendrimers and this also helps to improve solubility, reactivity and miscibility of these molecules also in the cellular system. The dendrimers are also having the ability to bypass different efflux transporters in the cellular system and thus this carrier system may be used to deliver drug(s) across the cellular barriers [83, 86].

Dendrimers based on poly amidoamines, polyamines, polyamides (polypeptides), poly(aryl ethers), polyesters, carbohydrate, DNA *etc*. are currently widely used for different biological applications and among them, the dendrimers based on poly amidoamine (PAMAM dendrimers) are available commercially with a wide range of generations and peripheral functionalities (SigmaAldrich and Dendritic Nanotechnologies) [82].

The peptide and saccharide-conjugated dendrimers are reported to deliver the drug in a targeted manner [87]. The conjugation of these biologically active peptide and saccharides via reactive chemical group(s) at the dendrimer periphery usually turned into nanoparticles and these nanoparticles selectively can be targeted to particular cell of interest [87]. In a study, the peptide dendrimer was conjugated with doxorubicin (DOX), the drug of choice for treating breast cancer, to obtain an enzyme responsive drug delivery carrier [88]. Here, DOX has been reported to conjugate at the periphery of the mPEGylated peptide dendrimers via an enzyme responsive tetrapeptide linker Gly-Phe-Leu-Gly (GFLG) and the conjugated structure of the drug and dendrimers were self-assembled into nanoparticles. This nanoparticle was found to increase the antitumor activity at the breast tumor site in a 4T1 breast tumor model with minimizing the dose-related cytotoxicities and other side effects to the normal tissues [88]. This dendrimers-GFLG-DOX conjugate based nanoparticle was found to be very effective in patients suffering from ovarian cancer. Zhang *et al*. demonstrated higher accumulation and retention within SKOV-3 ovarian tumor tissue [89]. PAMAM dendrimers having generations 4 and 5 (G4, G5) and plasmid DNA have been reported to prepare dendrimeric nanoparticles for gene delivery to liver and colon cancer [89].

Dendrimers may be used for gene therapy after the conjugation of targeting peptide. For example PAMAMs dendrimers with generation 5 and 6 can be modified with RGD (a cyclic arginine-glycine-aspartic Acid) ligands with different densities (i.e. by varying the number of RGDs per dendrimers). Now conjugating of this resultant molecule with plasmid DNA can be used for specific targeting of gene to mesenchymal stem cells which are derived from bone marrow. The cellular uptake of the nucleic acid may be improved by this way and the expression of target genes can be unregulated [90].

Nanofibers

Nanofibers are important materials because of their large surface area. In the field of nanotechnology, fibers having size in between 100 to 200 nm and generally obtained from both natural and synthetic biocompatible polymers are known as nanofibers and have proven to be promising materials for application in the medical and pharmaceutical fields [91]. There are several methods for the production of nanofibers such as drawing, template synthesis, phase separation, self-assembly, electrospinning, melt-blown, *etc*. [92]. Drug delivery system (DDS) that includes the method of drug loading and different release mechanism further deals with the different applications of nanofibers as a drug delivery vehicle. A wide range of polymers such as polyvinyl alcohol, gelatin, collagen, chitosan, and carboxymethylcellulose can be subjected to electrospinning technique to produce nanofibers.

Nanofibers, for their application in drug delivery and others medical purposes must be made from biocompatible polymers of natural or synthetic origin. Poly(ethylene oxide), poly(vinyl alcohol) and poly(caprolactone) are the few names of such synthetic polymers, while poly(L-lactic acid), chitin, chitosan, cellulose and other compounds derived from cellulose are the few amongst naturally originated polymers which may often be tried for this purpose [92].

NANOTECHNOLOGY IN DIAGNOSIS OF DISEASES

The conjugation of nanotechnology with biology has driven the development of newer diagnostic approaches, devices for various analysis, contrast agents and different vehicles for drug delivery. Nanoparticle-based technologies represent an unparallel latest progress that may cause the revolution in the field of medicine and biology. Nanotechnology has high potential in the diagnosis of diseases as well as to novel therapeutic applications. During last few years, nanomaterials have shown their efficacy in the field of *in vitro* and *in vivo* research and application, due to their nano-size that resembles the various biomolecules and structures [93].

The surface of the nanoparticles is compatible with the modification with different modes such as polymers, different functional groups, serum proteins, antibodies aptamers or peptides so that the nanodevice can target and attach to particular organ, cell, protein, or a particular gene *in vivo*.

Nanoparticles are useful devices as they hold some characteristic properties such as some optical or magnetic parameters that are manipulatable for the purpose of getting a detectable signal output. The assay based on a nanoparticulate diagnostic system depends generally on the binding of the nanoscale probe to the target biomaterials and generation of a detectable signal that signifies the target molecules. Nanotechnology in the pharmaceutical field has provided various newer approaches and invention of ideas in designing

and developing quick, accurate, cost effective and sensitive diagnostic techniques.

Polynucleotide target (such as sequence-specific DNA) can be easily detected by using nanoparticulate system especially with gold nanoparticles fabricated with 3'- and 5'-(alkanethiol) oligonucleotides, as reported by Storhoff *et al.* (1998) [94]. In this colorimetric detection technique oligonucleotide capped-Au nanoparticles are subjected to form complex with a target of 24-base polynucleotide and cause the change in colour of the solution (from red to purple) which shows the enhanced color differentiation in the reverse phase thin layer chromatography. This simple extraordinary probe system utilizes the distance-dependent optical properties of Au nanoparticle aggregate and provides easy one pot colorimetric detection of a target sequence in the presence of other oligonucleotides even differing in one nucleotide in their sequence.

Driskell *et al.* (2011) reported the easy and simple detection of influenza "A" virus by using antibody conjugated gold nanoparticles and dynamic light scattering method of detection [95]. The probe of gold nanoparticles form aggregates with the influenza virus and this extent of aggregation is measured in term of the mean hydrodynamic diameter correlated with virus concentration. After optimization, this assay method provided the better virus detection (in the limit of less than 100 tissue culture infectious dose/mL than the commercial diagnostic kits. Additionally this assay not only improves the assay time, but is also equally applicable to the influenza virus from different biological matrices [95].

Liu *et al.* (2007) developed a disposable diagnosis device consisting of conventional immunochromatographic strip tests with nanoparticle probe such as quantum dots [96]. The electrochemical immunoassay was conducted for the purpose of detection of different protein biomarkers. This device can be effective in detecting and identifying different infectious diseases, cardiovascular problems, in cancer detection, and last but not the least biological warfare agents. When optimized, this sensitive and low-cost tool is able to detect a minimum 30 pg /mL IgG model analyte within 7 min which demonstrates the detection speed of the device [96].

An immunochromatographic assay kit was developed by Toriyama *et al,* 2015, consisting of fluorescent silica nanoparticles fabricated with anti-Acanthamoeba antibodies [97] and evaluated its efficacy for the detection of Acanthamoeba and diagnosis of Acanthamoeba keratitis (AK). After the evaluation the kit provided better sensitivity and response than the conventional one in diagnosing the disease condition [97].

Magnetic nanoparticles (MNPs) possess several physical and chemical properties that make them a promising synthetic platform for the creation of novel chemical, biological and analytical detection systems [98]. Jangpatarapongsa *et al.* (2011) described the utilization of magnetic nanoparticles as a novel device to detect BCR/ABL fusion gene in chronic myelogenous leukemia (CML) [99]. The surface of carboxyl-functionalized nanoparticulate probes was conjugated covalently with amine-functionalized primers which were capable to separate PCR products. This technique showed high sensitivity and specificity in separation and presented an alternative way out for both CML patients treatment monitoring and also for the purpose of prevention [99].

A study by Ye *et al.* (2009) described the use of single base (guanosine, cytidine, thymidine and adenosine) coded CdS nanoparticles as diagnostic probe for the detection of DNA point mutation [100]. They have used piezoelectric quartz crystal microbalance (QCM) monitoring system for the evaluation of hybridization between target DNA and nanoparticles (Fe_3O_4/Au magnetic nanoparticles). Another study of similar type was performed by Pang *et al.* 2007 that demonstrated the detection method for DNA point mutation using QCM based on Fe_3O_4/Au core/shell nanoparticle and DNA ligase reaction [100]. This approach efficiently represented the recognition and type of a single-base mutation in -28 sites of artificial β-thalassemia gene successfully [100].

To overcome the difficulties of treating the patients with infectious disease, it is obvious to have an effectivetool for the identification of pathogens for the purpose of prevention of this mortal disease. During the last fifty years, there is little improvement in the field of diagnosis of infectious disease.

Pham *et al.* (2012), developed a rapid diagnostic kit to detect the H5N1 influenza virus by utilizing gold nanoparticles specific to the virus [101]. The colloidal gold nanoparticles were conjugated with single chain antibodies (scFv7 and scFv24) specific to the H5N1 virus. The reactivity and capability of these nanodevices were tested qualitatively which ensured the effectiveness and reliability of these nanoprobes as a potential component of developing the kit of H5N1 virus diagnosis [101].

RECENT PATENTS IN NANOFORMULATIONS

The application of nanotechnology in the field of medicine has led to the emergence of newest member of molecular nanotechnology known as nanomedicine. Despite the fact, that the application of nanomedicine in the healthcare is still in infancy, this branch already has established its versatile potential for monitoring, repairing, building and control of biological systems on the molecular level. The advancement of nanotechnology has resulted in the development of a smarter biodegradable delivery system capable of delivering the cargo of drugs to the target site as well as is flexible enough for tagging with ligands of varied nature. Moreover, it provides better pharmacokinetic profiling of drugs leading to a better therapeutic outcome. Although theoretically, it sounds good but the development of such delivery systems and the translation of them from laboratories to clinics come across numbers of obstacles which have not yet been overcome. Till date, there are near about 30 drug delivery products in the market, which constitute total annual income of US$ 33 billion with an annual growth rate of 15%. Most of them are designed to deliver the drugs to several types of cancer [102]. Few examples of such products are Doxil® (Caleyx® in Europe), DaunoXome®, Abraxane®, Depocyt®, Genexol-PM®, Oncospar® *etc*. In recent years, number of patents filed on nanoformulations has increased dramatically. Nanoparticle-based targeted delivery systems in cancer have experienced 185% of growth rate in a span of last 4-5 years whereas only 110 patents were registered between 1987 and 2008. In this section, we will discuss some of the recent patents filed on nanocarrier systems [102]. However, many discrepancies exist as some of them are not filed in English, lack of detailed information is missing except title and summary while filing the patents in offices *etc*. It is a serious drawback which should be rectified as it affects inventors as well as the scientific community by limiting the diffusion of potentially interesting and valid approaches. Moreover, much more uniformity, flexibility is required to form regulatory authorities in framing the rules that bridge the gap between the scientific and industrial forum for granting and applications of patents especially at the level of the International, European and US patent offices. Another interesting fact is that patent filed by inventors with the claim of new method of preparation lacks either detailed information or does not shed light on all of the technological aspects that would be required to establish the originality of the developed method. Here we will focus on some recent patents on different types of nanocarriers [103] (Table **1**).

PATENTS ON POLYMER BASED NANOPARTICLES

Polymeric nanoparticles offer significant assurance for delivering a drug to a target site and are found to be advantageous due to their biocompatibility, biodegradability, ease of formulation and tunable sustained release characteristics. Significant numbers of patents have been filed on polymeric nanoparticles. Albumin-bound nanoparticulate delivery system of paclitaxel is approved by the

Table 1. Available marketed products, clinical trials and patented products.

Available Marketed Products				
Types of Nanoformulation	**Product**	**Use**		**References**
Nanoparticles	Oncospar (Sigma Tau Pharmaceuticals Ltd., Germany)	Acute lymphoblastic leukemia		[104]
	Mircera (Hoffmann-La-Roche, Switzerland)	Symptomatic anemia associated with chronic kidney disease		[104]
	Adagenise (Sigma Tau Pharmaceuticals Ltd., Germany)	Severe combined immunodeficiency disease		[104]
	Pegasys (Hoffmann-La-Roche, Switzerland)	Hepatitis C		[104]
	Abraxane (American Biosciences, USA)	Breast Cancer		[104]
	PegIntron (Schering Corporation, USA)	Hepatitis C		[104]
Nanoliposomes	Abelcet™ (Liposome Company NJ, USA)	Fungal infection		[105]
	Doxil™ (Sequus Pharmaceuticals,Inc., C.A .)	Kaposi's sarcoma , Refractory ovarian cancer		[106-108]
	Epaxel™ (Swiss Serum Institute, Switzerland)	Hepatitis A		[109-111]
Fullerene	Radical Sponge® (Vitamin C60 BioResearch Corporation, Japan)	Cosmetics		[112]
	EGF Complex Cocktail, BellaPelle™, USA	Cosmetics		[112]
	Zelens® Fullerene C-60 Day Cream, Zelens®, UK	Cosmetics		[112]
Gene delivery	Glybera® (alipogene tiparvovec), UniQure B.V, Netherlands (It has been approved by the European Commission for commercialization in the European Union.)	Lipoprotein lipase deficiency		[113]
	Rexin-G, Epeins Biotechnologies Corp., US U.S. FDA approved Phase 3 product	Breast cancer, Hormone refractory Prostate cancer, Ovarian cancer, Squamous cell carcinoma		[114]
Dendrimer	Superfect®, Qiagen, Natherlands	Plasmid transfection, protein overex-pression		[115]
	PAMAM (polyamidoamine) dendrimer, Dendritech, Inc. Midland, Mich.	Diagnostics and drug delivery		[116]
Products in Clinical Trials				
Types of Nanoformulation	**Product**	**Use**	**Phase of Clinical Trials**	**References**
Nanoparticles	BIND-014 (PEG-PLA Docetaxel)	Solid tumors	I	[104]
	CRLX101 (Cyclodextrin-PEG Camptothecin)	Several types of cancers	II	[104]
	CALAA-01 (Cyclodextrin-PEG-Transferrin)	Solid tumors	I	[104]
	ProLindac™ (HPMA-DACH containing Oxaliplatin)	Solid tumors	II	[104]
	Opaxio™ (Poliglutamic acid Paclitaxel)	Lung and ovarian cancer	III	[104]
	MTX- HAS (Methotrexate)	Kidney cancer	II	[104]
Nanoliposomes	ThermoDox® (Doxorubicine)	Liver and breast cancer	III	[117,118]

(Table 1) Contd….

Products in Clinical Trials				
Types of Nanoformulation	**Product**	**Use**	**Phase of Clinical Trials**	**References**
Gene delivery	LEP-ETU (Paclitaxel)	Advanced cancer	I	[119,120]
	Arikace (Amikacin)	Pulmonary infection	III	[121,122]
	ProSavin®	Parkinson's disease	I/II	[123]
	RetinoStat® (Sanofi)	Age-related macular degeneration	I	[123]
	StarGen™ (Sanofi)	Stargardt disease	I/II	[123]
	GeneTherapy product CYL-02	Pancreatic adenocarcinoma	I	[123]
	Autologous PBL and/or autologous HSC transduced with the normal human ADA gene	Severe combined immunodeficiency syndrome	I, II	[124]
	Ad5yCD/mutTKSR39rep-ADP	Cancer	II	[124]
	AAV1-gamma-sarcoglycan vector injection	Limb girdle muscular dystrophy Type 2C; Gamma-sarcoglycanopathy	I	[124]
	VEGF-D gene transfer	Angina pectoris, Myocardial infarction	I	[124]
	HSV-TK adenovirus gene therapy	Brain and central nervous system tumors	I	[124]
	Adeno-associated Virus Serotype 8 Factor IX Gene Therapy	Hemophilia B	I, II	[124]
	Gene Therapy for Gyrate Atrophy	Gyrate atrophy	I	[124]
	Autologous CD34 positive cells transduced with WAS encoding lentiviral vector	Wiskott-aldrich syndrome	II	[124]
Dendrimers	Dendrimer-Docetaxel (Taxotere®)	Cancer	I	[124]
Polymeric micelles	Genexol-PM (Paclitaxel), Samyang, Korea	Cancer	III, IV	[125]
	NK105 (Paclitaxel) Nanocarrier/Nippon Kayaku, Japan	Cancer	II, III	[125]
	SP1049C (Doxorubicin), Supprateck, Canada	Cancer	III	[125]
	DTXL-TNP (Docetaxel), BIND Biosciences	Cancer	I	[125]
	NC6004 (Cisplatin), Nanocarrier, Japan	Cancer	I, II	[125]
	NK012 (SN-38), Nippon Kayaku, Japan	Cancer	II	[125]
	NK911 (Doxorubicin), Nippon Kayaku, Japan	Cancer	II	[125]

(Table 1) Contd….

Patented Nanoformulations				
Types of product	**Product**	**Patent Publication Number**	**Approved Year and Place**	**References**
Nanoparticles	Nanoparticles with covalently bound surfactant for drug delivery	US 8414926 B1	2013 (Virginia)	[126]
	Process for preparing therapeutic compositions containing nanoparticles	US 5510118 A	1996 (Ireland, Massachusetts)	[127]
Nanoliposomes	Preparation of nanoliposome-encapsulating proteins and protein-encapsulated nanoliposome	US 7951396 B2	2011 (Korea, Republic of)	[128]
	Nanoliposome using esterified lecithin and method for preparing the same, and composition for preventing or treating skin diseases comprising the same	US 8685440 B2	2014 (Korea, Republic Of)	[129]
Gene delivery	Polymeric gene delivery system	US 6262034 B1	2001(US)	[130]
	Cationized polysaccharide nanoparticle gene delivery systems and manufacturing method thereof	CN 102154352 B	2012 (China)	[131]
	Nanoparticle gene delivery system of cationized lycium barbarum polysaccharides and preparation method thereof	CN 102154350 B	2012 (China)	[132]
	Cationic angelica polysaccharide nanoparticle gene delivery system and preparation method thereof	CN 102154351 B	2012 (China)	[133]
	Use of targeted cross-linked nanoparticles for *in vivo* gene delivery	US 7514098 B2,	2009 (US)	[134]
	Crosslinked PEI nanoparticle transfection agents for delivery of biomolecules with increased efficiency	US 8513206 B2,	2013 (India)	[135]
	Double-stranded RNA-based nanoparticles for insect gene silencing	US 8841272 B2	2014 (Kansas)	[136]
Dendrimer	Use of dendrimer nanotechnology for delivery of biomolecules into plant cells	US 8686222 B2	2014 (India)	[137]
	Dendrimer conjugates	US 8252834 B2	2012 (US)	[138]
	Targeted polylysine dendrimer therapeutic agent	US 8420067 B2	2013(Australia)	[139]
Polymeric micelles	Polymeric micelles for drug delivery	US 7638558 B2	2009 (Florida)	[140]
	Stable polymeric micelle-type drug composition and method for the preparation thereof	US 7217770 B2	2007(Korea, Republic Of)	[141]
	Preparation of sterile stabilized nanodispersions	US 6780324 B2	2004 (Canada)	[142]

United States Food and Drug Administration (US-FDA) and the European Medical Agency for the treatment of breast cancer unresponsive to conventional chemotherapy or has relapsed. This is also known as nab-paclitaxel and sold under the trade name "Abraxane". This nanoparticulate system has also exhibited positive results in phase III clinical trial as a first line drug in non-small-cell-lung-cancer (NSCLC) as compared to solvent-based paclitaxel [102]. In September 2013, Abraxane was approved by FDA for use in treating advanced pancreatic cancer as a less toxic (although less effective) alternative to Folfirinox (chemotherapy regimen consisting of folinic acid, 5-flurouracil, irinotecan and oxaliplatin). Abraxane® was developed by Abraxis Biosciences and was acquired by Celgene. Besides, many researchers around the globe have paid considerable attention to the development of targeted polymeric nanocarriers and filed patents on the basis of their invention. Some of them are mentioned below [102].

Sanofi-Aventis has filed a French patent (WO2013127949 A1) on the work that has dealt with the design of nanoparticles composed of functional polylactic acid - polyethyleneglycol (PLA-PEG) copolymers for targeted delivery and imaging. According to

the invention, a clickable copolymer platform of PLA-PEG- azide compound may be used to couple a number of functional alkyne-ligands including cell penetration enhancing agent, homing device, detoxifying agent, imaging agent, drug, stimuli-responsive agent, docking agent *etc*. [143].

Jiansong *et al.* developed epirubicin hydrochloride and gadopentetate dimeglumine loaded polylactic-co-glycolic acid (PLGA) nanoparticles and filed a patent (CN102525936A) for their design. The invention was designed to overcome the problem associated with short *in vivo* retention time of the drugs. They claimed that the developed nanocarrier would remain at the tumor site for a long period of time and release the drug in a controlled manner resulting in better therapeutic outcome [144].

Yiyi *et al.* have filed a Chinese patent (CN102697795A) on the design and development of PLGA nanoparticles containing a combination of epirubicin and quercitin. The invention discloses simultaneous encapsulation of a hydrophilic drug (epirubicin) and hydrophobic drug (quercitin). Nanoparticle was prepared by multiple emulsion-solvent evaporation technique. Inventors claimed that the combination was found to be effective against multiple drug resistant cancer cells and produce less toxicity to normal cells [145].

Jessie *et al.* have filed a Chinese patent (CN102697737 A) on an invention that uses paclitaxel loaded nano and micro particles comprising of gelatin and PLGA. The idea behind the invention is to target the tumor with a fast-release formulation of a tumor apoptosis-inducing agent, a slow-release formulation of a tumor therapeutic agent, and a pharmaceutically acceptable carrier. The inventors claimed that the drug would release from microparticle rapidly to induce apoptosis whereas nano-sized particle would provide sustained delivery of drugs for prolonged periods of time [146].

PATENTS ON LIPID NANOCARRIERS

Among the different nanoscale size drug delivery systems, lipid nanocarriers such as emulsions, micelles, liposomes and lipid nanoparticles have gained attention of researchers due to their biocompatibility, biodegradability, easy industrial scale-up and administration through multiple routes. The number of patents filed on solid lipid nanoparticles has emphasized the preparation and characterization of solid lipid nanoparticles.

Lipotec SA has filed a patent (WO201116963 and US20130017239) that deals with the production of polymer-coated nanostructured lipid carriers (NLC) and solid lipid nanoparticles (SLN) intended for pharmaceutical, food, and cosmetic use. The carrier exists in the form of an aqueous dispersion. The active ingredients can be lipophilic, hydrophilic or amphiphilic and incorporated into the carrier by various methods such as dissolution, dispersion, and adsorption. The addition of surfactants or cyclodextrins can increase the dissolution of active ingredients in the lipid [147, 148].

A patent (CN101972229 B) has been filed on the basis of a Chinese invention to encapsulate the enzyme catalase in SLN. The inventors have proposed two-steps water/oil/water (w/o/w) emulsion methods in which an aqueous solution of the enzyme is emulsified in an organic solution of solid lipid by ultrasound treatment. This initial w/o emulsion is dispersed in an outer aqueous phase by means of hydrophilic surfactant [149].

A recent patent (US20090214663 A1) describes the development of simple and cost-effective preparation method for the production of stabilized nanoparticles to encapsulate proteins. The freeze-dried nanoparticles may be formed by sonicating soybeans lecithin in an aqueous solution of poloxamer containing a trehalose as cryoprotectant. The developed nanocarrier can encapsulate proteins having different charges depending on their isoelectric points in physiological conditions. The positively charged protein can be absorbed on the surface of the lipid core through ionic interaction whereas negatively charged protein can be absorbed into the lipid core through chitosan of low molecular weight [150].

Further, nanoscaled liposomal formulations have established their potential to deliver a cargo of drugs specifically to target site. Doxil® is the first FDA approved PEGylated liposomal formulation encapsulating doxorubicin for the treatment of cancer. The successful translation of Doxil from laboratory to clinic instigated a great deal of interest on liposome among the researchers and subsequently DaunoXome® and Myocet® have followed the path of Doxil® and have been clinically approved for the treatment of metastatic breast cancer and AIDS-related Kaposi's sarcoma. Apart from that Depocyt® (liposomal Cytarabine) has also got approval from FDA for cancer of white blood cells such as acute myeloid leukemia and non-Hodgkin lymphoma. Significant numbers of patents have been proposed in liposomal formulations [102].

A patent (US20130115269 A1) describes the use of anti-tumor necrosis factor α (TNF-α) as a targeting ligand intended for arthritis and other inflammatory diseases. A variety of steroidal, non-steroidal drugs, disease modifying drugs, as well as other anti-inflammatory compounds, may be incorporated into the anti-TNF-α coated liposomes. The anti-TNF-α coated drug liposomes can accumulate at the inflamed site for maximum therapeutic effect [151].

A patent was filed (WO2013105101 A1) on the invention to specifically deliver the drugs into monocyte. The developed liposome comprising of lipid, among which, one is cationic. The liposome exhibits net positive charge that would help them to adhere to the monocyte in a freshly drawn blood and the developed liposome has the potential for the treatment of monocyte associated prophylaxis, treatment and amelioration [152].

Rochlitz *et al.* have filed a patent (WO2010103118 A1) on the developed immuno-liposome comprising of antibody or antibody fragment, which recognizes vascular endothelial growth factor receptor (VEGFR) on the surface of tumor cells or tumor-associated endothelial cells to deliver specifically to the tumor cells. The approach applied in present invention is that the EGFR-targeting cannot only be used against antigen-presenting tumor cells but alternatively, can also be used against the tumor stroma, including the tumor-associated vasculature, which offers some potential advantages [153].

INORGANIC NANOPARTICLES

Magnetic nanoparticles found for their potential biomedical applications have an inorganic nanoparticle core and are coated with by suitable coating materials. Magnetic nanoparticles can be dispersed in aqueous and lipid phases. Such newly developed patented nanoparticles (US0264199) possess a core surrounded by oleic acid and stabilized by block copolymer based on ethylene oxide and propylene oxide. The developed lipophilic magnetic nanoparticles have the potential to target the drug (doxorubicin) deeply into the brain tissue [154]. Recently a patent (US0206146) has been filed on the design of an internal magnet capable of drug attachment. The internal layer is coated with a polymeric layer of dextran or silicon which in turn is coated with an extra layer of polysorbate 80. It helps the nano-magnet to penetrate through the blood-brain barrier [155].

A patent (US7530940) was filed on the methods of utilizing the metal nanoparticles to potentiate the dose and effectiveness of x-rays in a therapeutic regimen to destroy the target tumor tissue. The metal nanoparticles can be tagged with chemical and/or biological moiety that would enhance the chances of binding with the target tissue. These types of nanoparticles are made up of metal core surrounded by the surface layer. The metal core is formed by heavy metals such as gold, iron, copper, tin, tantalum, tungsten, osmium, bismuth, *etc*. [156].

CONCLUSION

The expanding progress of nanotechnology in the area of biomedicine can be endorsed to the technological advantages, including improved biodistribution profiles of drug and targeting drug delivery to the specific organs, which reduce the number of doses, dosing frequency and consequently, the toxicity and adverse effects.

In addition, controlled release of therapeutic agents makes therapy far more efficient and convenient for users, with better patient compliance, particularly those with chronic diseases that require continued administration and repeated doses of medicines.

This review has highlighted recent drug carriers with a promising set of technologies, which have great potential for diseases such as cancer, diabetes and many other chronic diseases and they likely have a strong impact in this field in the future.

Nanomedicine has a significant impact in the future advancement in therapeutic approach that may overcome the limitations of conventional therapies for better therapeutic outcome on both global and individual levels.

CONFLICT OF INTEREST

The authors confirm that this article content has no conflict of interest.

ACKNOWLEDGEMENTS

Declared none.

REFERENCES

[1] Shi J,Votruba AR, Farokhzd OC, *et al*. Nanotechnology in drug delivery and tissue engineering: From discovery to applications. Nano Lett 2010; 10: 3223-30.

[2] Sajja HK, East MP, Mao H, *et al*. Development of multifunctional nanoparticles for targeted drug delivery and noninvasive imaging of therapeutic effect. Curr Drug Discov Technol 2009; 6: 43-51.

[3] Nagaich U. Nanomedicine: revolutionary trends in drug delivery and diagnostics. J Adv Pharm Technol Res 2014; 5: 1.

[4] Mc Neil SE. Nanoparticle therapeutics: a personal perspective. Wiley Interdiscip Rev Nanomed Nanobiotechnol 2009; 1: 264-71.

[5] The Freedonia Group [home page on the Internet]. Nanotechnology in Health Care: US Industry Study with Forecasts to 2011, 2016 & 2021. [cited 2015 Mar 22]. Available from: (http: //www.freedoniagroup.com/brochure/21xx/2168smwe.pdf)

[6] Safari J, Zarnegar Z. Advanced drug delivery systems: nanotechnology of health design a review. J Saudi Chem Soc 2014; 18: 85-99.

[7] Martis EA, Badve RR, Degwekar MD. Nanotechnology based devices and applications in medicine: an overview. Chron Young Sci 2012; 3: 68-73.

[8] Ochekpe NA, Olorunfemi PO, Ngwuluka NC. Nanotechnology and drug delivery Part 1: background and applications. Trop J Pharm Res 2009; 8: 265-74.

[9] Mukherjee B, Dey NS, Maji R, *et al*. Current status and future scope for nanomaterials in drug delivery. In: Demir AS, Eds. Application of nanotechnology in drug delivery. USA: Intech 2014; pp: 525-44.

[10] Vigneshkumar C. Study on nanomaterials and application of nanotechnology and its impacts in construction. Discovery 2014; 23: 8-12.

[11] Reddy JRK, Sagar EG, Prathap SBC, *et al*. Nanomedicine and drug delivery-revolution in health system. JGTPS 2011; 2: 21-30.

[12] Steyn WJ, Vd M. Research and application of nanotechnology in transportation. Proceeding of the 27th Southern African Transport Conference (SATC 2008). Pretoria, South Africa, 2008; pp. 345-53.

[13] Raliya R, Tarafdar JC, Gulecha K, *et al.* Scope of nanoscience and nanotechnology in agriculture. J Appl Biol Biotechnol 2013; 1: 41-4.

[14] Hristozov D, Ertel J. Nanotechnology and sustainability: benefits and risks of nanotechnology for environmental sustainability. Forum der Forschung 2009; 22: 161-8.

[15] Medintz IL, Mattoussi H, Clapp AR. Potential clinical applications of quantum dots. Int J Nanomed 2008; 3: 151-67.

[16] Antunes A, Fierro I, Guerrante R, *et al*. Trends in nanopharmaceutical patents. Int J Mol Sci 2013; 14: 7016-31.

[17] Wang K, Ruan J, Qian Q, *et al.* BRCAA1 monoclonal antibody conjugated fluorescent magnetic nanoparticles for *in vivo* targeted magnetofluorescent imaging of gastric cancer. J Nanobiotechnol 2011; 9: 23.

[18] Kumar S, Siethoff LT, Persson M, *et al*. Magnetic capture from blood rescues molecular motor function in diagnostic nanodevices. J Nanobiotechnol 2013; 11: 14.

[19] Arruebo M, Valladares M, González-Fernández Á. Antibody-conjugated nanoparticles for biomedical applications. J Nano Mat 2009; 2009: 1-24.

[20] Liu Q, Jin C, Wang Y, *et al.* Aptamer-conjugated nanomaterials for specific cancer cell recognition and targeted cancer therapy. NPG Asia Mater 2014; 6: e95.

[21] Shamsipour F, Zarnani AH, Ghods R, *et al.* Conjugation of monoclonal antibodies to super paramagnetic iron oxide nanoparticles for detection of her2/neu antigen on breast cancer cell lines. Avicenna J Med Biotechnol 2009; 1: 27-31.

[22] Hathaway HJ, Butler KS, Adolphi NL, *et al.* Detection of breast cancer cells using targeted magnetic nanoparticles and ultrasensitive magnetic field sensors. Breast Cancer Res 2011, 13: R108.

[23] Powell RD, Hainfeld JF. Preparation and high-resolution microscopy of gold cluster labeled nucleic acid conjugates and nanodevices. Micron 2011; 42: 163-74.

[24] Zhang Q, Li Y, Shi Y, *et al.* HVJ envelope vector, a versatile delivery system: Its application, and perspectives. Biochem Biophys Res Commun 2008; 373: 345-9.

[25] Garcea RL, Gissmann L. Virus-like particles as vaccines and vessels for the delivery of small molecules. Curr Opin Biotechnol 2004; 15: 513-7.

[26] Grasso S, Santi L. Viral nanoparticles as macromolecular devices for new therapeutic and pharmaceutical approaches. Int J Physiol Pathophysiol Pharmacol 2010; 2: 161-78.

[27] Ma Y, Nolte RJM, Cornelissen JJLM. Virus-based nanocarriers for drug delivery. Adv Drug Deliv Rev 2012; 64: 811-25.

[28] Lee LA, Wang Q. Adaptations of nanoscale viruses and other protein cages for medical applications. Nanomed Nanotech Biol Med 2006; 2: 137-49.

[29] Lima ST, Airavaara M, Harvey BK. Viral vectors for neurotrophic factor delivery: A gene therapy approach for neurodegenerative diseases of the CNS. Pharmacol Res 2010; 61: 14-26.

[30] Wu Z, Chen K, Yildiz I, *et al*. Development of viral nanoparticles for efficient intracellular delivery. Nanoscale 2012; 4: 3567-76.

[31] Yildiz I, Shukla S, Steinmetz NF. Applications of viral nanoparticles in medicine. Curr Opin Biotechnol 2011; 22: 901-8.

[32] Zeng Q, Wen H, Wen Q, *et al.* Cucumber mosaic virus as drug delivery vehicle for doxorubicin. Biomaterials 2013; 34: 4632-42.

[33] Peer D, Karp JM, Hong S. Nanocarriers as an emerging platform for cancer therapy. Nat Nanotechnol 2007; 2: 751-60.

[34] Shigdar S, Luczo J, Ming Q, *et al.* Aptamer therapeutics: the 21st century's magic bullet of nanomedicine. Open Conf Proc J 2010; 1: 118-24.

[35] Perche F, Torchilin VP. Recent trends in multifunctional liposomal nanocarriers for enhanced tumor targeting. J Drug Deliv 2013; 2013: 1-32.

[36] Mann AP, Bhavane RC, Somasunderam A. Thioaptamer conjugated liposomes for tumor vasculature targeting. Oncotarget 2011; 2: 298-304.

[37] Bae YH, Park K. Targeted drug delivery to tumors: myths, reality and possibility. J Control Release 2011; 153: 198-205.

[38] Yokoe J, Sakuragi S, Yamamoto K, *et al*. Albumin-conjugated PEG liposome enhances tumor distribution of liposomal doxorubicin in rats. Int J Pharm 2008; 353: 28-34.

[39] Wang R, Xiao R, Zeng Z, *et al.* Application of poly (ethylene glycol) distearoylphosphatidylethanolamine (PEG-DSPE) block copolymers and their derivatives as nanomaterials in drug delivery. Int J Nanomed 2012; 7: 4185-98.

[40] Bartlett DW, Su H, Hildebrandt IJ, *et al.* Impact of tumor-specific targeting on the biodistribution and efficacy of siRNA nanoparticles measured by multimodality *in vivo* imaging. Proc Natl Acad Sci 2007; 104: 15549-54.

[41] Kang H, O'Donoghue MB, Liu H, *et al.* A liposome-based nanostructure for aptamer directed delivery. Chem Commun 2010; 46: 249-51.
[42] Mann AP, Somasunderam A, Nieves-Alicea R, *et al.* Identification of thioaptamer ligand against E-selectin: Potential application for inflamed vasculature targeting. PLoS One 2010; 5: 1-12.
[43] Mishra P, Vyas G, Harsoliya MS, *et al.* Quantum dot probes in disease diagnosis. Int J Pharm Pharm Sci Res 2011; 1: 42-6.
[44] Modani S, Kharwade M, Nijhawan M. Quantum dots: a novelty of medical field with multiple applications. Int J Curr Pharm Res 2013; 5: 55-9.
[45] Wang X, Ma XL, Feng X, *et al.* Controlled synthesis and characterization of ZnSe quantum dots. J Nanosci Nanotechnol 2010; 10: 7812-5.
[46] Pandurangan DK, Sravya MK. Quantum dot aptamers-an emerging technology with wide scope in pharmacy. Int J Pharm Pharm Sci 2012; 4: 24-31.
[47] Mukherjee S, Das U. Quantum dots: An optimistic approach to novel therapeutics. Int J Pharm Sci Rev Res 2011; 7: 59-64.
[48] Kong F, Ge L, Liu X, *et al.* Mannan-modified PLGA nanoparticle for targeted gene delivery. Int J Photoenergy 2012; 2012: 1-7.
[49] Roy I, Ohulchanskyy TY, Bharali DJ, *et al.* Optical tracking of organically modified silica nanoparticle as DNA carriers: a nonviral nanomedicine approach for gene delivery. Proc Natl Acad Sci USA 2005; 102: 279-84.
[50] Chertok B, David AE, Yang VC. Polyethylenemine-modified iron oxide nanoparticle for brain tumor drug delivery using magnetic targeting and intra-carotid administration. Biomaterials 2010; 31: 6317-24.
[51] Yu-qin F, Lu-hua L, Pi-wu W, *et al.* Delivering DNA in plant cell by gene carrier of nanoparticle. Chem Res Chin Univ 2012; 28: 672-6.
[52] Oerlemans C, Bult W, Bos M, *et al*. Polymeric micelles in anticancer therapy: targeting, imaging and triggered release. Pharm Res 2010; 27: 2569-89.
[53] Tan C, Wang Y, Wei F, *et al*. Exploring polymeric micelles for improved delivery of anticancer agents: recent developments in preclinical studies. Pharmaceutics 2013; 5: 201-19.
[54] Liu H, Zhu Z, Kang H, *et al*. DNA-based micelles: synthesis, micellar properties and size-dependent cell permeability. Chemistry 2010; 16: 3791-7.
[55] Bakry R, Vallant RM, Haqe MN, *et al.* Medicinal applications of fullerenes. Int J Nanomed 2007; 2: 639-49.
[56] Pikhurov DV, Zuev VV. The effect of fullerene C60 on the mechanical and dielectrical behavior of epoxy resins at low loading. Nanosist Fiz Him Mat 2013; 4: 834-43.
[57] Saeedfar K, Heng LY, Ling TL, *et al.* Potentiometric urea biosensor based on an immobilised fullerene-urease bio-conjugate. Sensors 2013; 13: 16851-66.
[58] Kumar CSSR. Nanomaterials for biosensors. Nanotechnologies for the life sciences. Weinheim: Wiley 2007.
[59] Kovács B, Nagy G, Dombi R, *et al.* Optical biosensor for urea with improved response time. Biosens Bioelectron 2003; 18: 111-8.
[60] Hsieh TH, Kinloch AJ, Masania K, *et al.* The mechanisms and mechanics of the toughening of epoxy polymer modified with silica nanoparticles. Polymer 2010; 51: 6284-94.
[61] Ogasawa T, Ishida Y, Kasai T. Mechanical properties of carbon fiber/ fullerene dispersed epoxy composites. Comp Sci Technol 2009; 69: 2002-7.
[62] Iijima S. Helical microtubules of graphitic carbon. Nature 1991; 354: 56-8.
[63] Karchemski F, Zucker D, Barenholz Y, *et al.* Carbon nanotubes-liposomes conjugate as a platform for drug delivery into cells. J Control Release 2012; 160: 339-45.
[64] Zhang R, Olin H. Carbon nanomaterials as drug carriers: real time drug release investigation. Mat Sci Eng C 2012; 32: 1247-52.
[65] Tasis D, Tagmatarchis N, Georgakilas V, *et al.* Soluble carbon nanotubes. Chem Eur J 2003; 9: 4000-8.
[66] Colvin VL. The potential environmental impact of engineered nanomaterials. Nat Biotechnol 2003; 21: 1166-70.
[67] Warheit DB, Laurence BR, Reed KL, *et al.* Comparative pulmonary toxicity assessment of single-wall carbon nanotubes in rats. Toxicol Sci 2004; 77: 117-25.
[68] Tran PA, Zhang L, Webster TJ. Carbon nanofibers and carbon nanotubes in regenerative medicine. Adv Drug Deliv Rev 2009; 61: 1097-114.
[69] Hua H, Lien APH, Pierre D, *et al.* Carbon nanotubes: Applications in pharmacy and medicine. Bio Med Res Int 2013; 2013: 12.
[70] Elhissi AMA, Ahmed W, Hassan IU, *et al.* Carbon nanotubes in cancer therapy and drug delivery. J Drug Deliv 2012; 2012: 1-10.
[71] Singh P, Tripathi RM, Saxena A. Synthesis of carbon nanotubes and their biomedical application. J Optoelectron Biomed Mater 2010; 2: 91-8.
[72] Kumar SP, Prathibha D, Shankar NL, *et al*. Pharmaceutical applications of Carbon nanotubes mediated drug delivery systems. IJPSN 2012; 5: 1685-96.
[73] Bianco A, Kostarelos K, Prato M. Applications of carbon nanotubes in drug delivery. Curr Opin Chem Biol 2005; 9: 674-9.
[74] Reddy ST, Rehor A, Schmoekel HG, *et al. In vivo* targeting of dendritic cells in lymph nodes with poly (propylene sulfide) nanoparticles. J Control Release 2006; 112: 26-34.
[75] Yang F, Fu DL, Long J, *et al.* Magnetic lymphatic targeting drug delivery system using carbon nanotubes. Med Hypotheses 2008; 70: 765-7.
[76] Yang F, Hu J, Yang D, *et al.* Pilot study of targeting magnetic carbon nanotubes to lymph nodes. Nanomedicine 2009; 4: 317-30.
[77] Yang L, Ng KY, Lillehei KO. Cell-mediated immunotherapy: A new approach to the treatment of malignant glioma. Cancer Control 2003; 10: 138-47.
[78] Yang F, Jin C, Yang D, *et al.* Magnetic functionalised carbon nanotubes as drug vehicles for cancer lymph node metastasis treatment. Eur J Cancer 2011; 47: 1873-82.
[79] Sahoo NG, Bao H, Pan Y, *et al*. Functionalized carbon nanomaterials as nanocarriers for loading and delivery of a poorly water-soluble anticancer drug: a comparative study. Chem Commun 2011; 47: 5235-7.
[80] Beqa L, Fan Z, Singh AK, *et al.* Gold nano-popcorn attached SWCNT hybrid nanomaterial for targeted diagnosis and photothermal therapy of human breast cancer cells. ACS Appl Mater Interfaces 2011; 3: 3316-24.
[81] Khan SA, Kanchanapally R, Fan Z, *et al.* A gold nanocage-CNT hybrid for targeted imaging and photothermal destruction of cancer cells. Chem Commun 2012; 48: 6711-3.
[82] Cameron C, John AM, Jean MJF, *et al.* Designing dendrimers for biological applications. Nat Biotechnol 2005; 23: 1517-26.
[83] Madaan K, Kumar S, Poonia N, *et al.* Dendrimers in drug delivery and targeting: drug-dendrimer interactions and toxicity issues. J Pharm Bioallied Sci 2014; 6: 139-50.
[84] Caminade AM, Turrin CO. Dendrimers for drug delivery. J Mater Chem B 2014; 2: 4055-66.
[85] Kesharwani P, Jain K, Jain NK. Dendrimer as nanocarrier for drug delivery. Prog Polym Sci 2014; 39: 268-307.
[86] Samad A, Alam MI, Saxena K. Dendrimers: A class of polymers in the nanotechnology for the delivery of active pharmaceuticals. Curr Pharm Des 2009; 15: 2958-69.
[87] Liu J, Gray WD, Davis ME, *et al.* Peptide and saccharide-conjugated dendrimers for targeted drug delivery: a concise review. Interface Focus 2012; 2: 307-24.
[88] Zhang C, Pan D, Luo K, *et al.* Peptide dendrimer-doxorubicin conjugate-based nanoparticles as an enzyme-responsive drug delivery system for cancer therapy. Adv Healthcare Mater 2014; 3: 1299-308.
[89] Zhang C, Pan D, Luo K, *et al.* Dendrimer-doxorubicin conjugate as enzyme-sensitive and polymeric nanoscale drug delivery vehicle for ovarian cancer therapy. Polym Chem 2014; 5: 5227-35.
[90] Pandita D, Santos JL, Rodrigues J, *et al.* Gene delivery into mesenchymal stem cells: A biomimetic approach using RGD nanoclusters based on poly (amidoamine) dendrimers. Biomacromolecules 2011; 12: 472-81.
[91] Peresin MS, Habibi Y, Zoppe JO, *et al.* Nanofiber composites of polyvinyl alcohol and cellulose nanocrystals: manufacture and characterization. Biomacromolecules 2010; 11: 674-81.
[92] Vasita R, Katti DS. Nanofibers and their applications in tissue engineering. Int J Nanomed 2006; 1: 15-30.
[93] Alharbi KK, Al-sheikh YA. Role and implications of nanodiagnostics in the changing trends of clinical diagnosis. Saudi J Biol Sci 2014; 21: 109-17.
[94] Storhoff JJ, Elghanian R, Mucic RC, *et al.* One-pot colorimetric differentiation of polynucleotides with single base imperfections using gold nanoparticle probes. J Am Chem Soc 1998; 120: 1959-64.

[95] Driskell JD, Jones CA, Tompkins SM, *et al.* One-step assay for detecting influenza virus using dynamic light scattering and gold nanoparticles. Analyst 2011; 136: 3083-90.

[96] Liu G, Lin YY, Wang J, *et al.* Disposable electrochemical immunosensor diagnosis device based on nanoparticle probe and immunochromatographic strip. Anal Chem 2007; 79: 7644-53.

[97] Toriyama K, Suzuki T, Inoue T, *et al.* Development of an immunochromatographic assay kit using fluorescent silica nanoparticles for rapid diagnosis of acanthamoeba keratitis. J Clin Microbiol 2015; 53: 273-7.

[98] Niemirowicz K, Markiewicz KH, Wilczewska AZ, *et al.* Magnetic nanoparticles as new diagnostic tools in medicine. Adv Med Sci 2012; 57: 196-207.

[99] Jangpatarapongsa K, Polpanich D, Yamkamon V, *et al.* DNA detection of chronic myelogenous leukemia by magnetic nanoparticles. Analyst 2011; 136: 354-8.

[100] Ye M, Zhang Y, Li H, *et al.* A novel method for the detection of point mutation in DNA using single-base-coded CdS nanoprobes. Biosens Bioelectron 2009; 24: 2339-45.

[101] Pham VD, Hoang H, Phan TH, *et al*. Production of antibody labeled gold nanoparticles for influenza virus H5N1 diagnosis kit development. Adv Nat Sci Nanosci Nanotechnol 2012; 3: 045017.

[102] Jin SE, Jin HE, Hong SS. Targeted delivery system of nanobiomaterials in anticancer therapy: from cells to clinics. Biomed Res Int 2014; 2014: 1-23.

[103] Carbone C, Cupri S, Leonardi A, *et al.* Lipid-based nanocarriers for drug delivery and targeting: a patent survey of methods of production and characterization. Pharm Pat Analyst 2013; 2: 665-77.

[104] Martins P, Rosa D, Fernandes AR, *et al.* Nanoparticle drug delivery systems: Recent patents and applications in nanomedicine. Recent Pat Nanomed 2013; 3: 105-18.

[105] Wasan KM, Lopez-Berestein G. Characteristics of lipid-based formulations that influence their biological behavior in the plasma of patients. Clin Infect Dis 1996; 23: 1126-38.

[106] Immordino ML, Dosio F, Cattel L. Stealth liposomes: Review of the basic science, rationale, and clinical applications, existing and potential. Int J Nanomed 2006; 1: 297-315.

[107] Park JW. Liposome-based drug delivery in breast cancer treatment. Breast Cancer Res 2002; 4: 95-9.

[108] Hoarau D, Delmas P, David S, *et al.* Novel long-circulating lipid nanocapsules. Pharm Res 2004; 21: 1783-9.

[109] Stegmann T, Morselt HW, Booy FP, *et al.* Functional reconstitution of influenza virus envelopes. EMBO J 1987; 6: 2651- 9.

[110] Glück R, Mischler R, Brantschen S, *et al.* Immunopotentiating reconstituted influenza virus virosome vaccine delivery system for immunization against hepatitis A. J Clin Invest 1992; 90: 2491-5.

[111] D'Acremont V, Herzog C, Genton B. Immunogenicity and safety of a virosomal hepatitis A vaccine (Epaxal) in the elderly. J Travel Med 2006; 13: 78-83.

[112] Nanomaterials. Sunscreens and Cosmetics: Small Ingredients Big Risks [homepage on the Internet]. Friends of the Earth Report [cited 2015 Apr 10]. Available from: (www.foe.org/sites/default/files/final_USA_web.pdf).

[113] Unique [home page on the internet]. Glybera [cited 2015 Apr 12]. Available from: (http: //www.uniqure.com/pipeline/glybera/)

[114] Gordon EM, Hall FL. Rexin-G, a targeted genetic medicine for cancer. Expert Opin Biol Ther 2010; 10: 819-32.

[115] Qiagen [homepage on the Internet]. SuperFect Transfection Reagent [cited 2015 Apr 12]. Available from: (https: //www.qiagen.com/in/products/catalog/assay-technologies/transfection-reagents/superfect-transfection-reagent/)

[116] Dendritech [homepage on the Internet]. PAMAM Dendrimers [cited 2015 Apr 12]. Available from: (http: //www.dendritech.com/pamam.html)

[117] Yarmolenko PS, Zhao Y, Landon C, *et al.* Comparative effects of thermosensitive doxorubicin-containing liposomes and hyperthermia in human and murine tumours. Int J Hyperthermia 2010; 26: 485-98.

[118] Dromi S, Frenkel V, Luk A, *et al*. Pulsed high intensity focused ultrasound and low temperature-sensitive liposomes for enhanced targeted drug delivery and antitumor effect. Clin Cancer Res 2007; 13: 2722-7.

[119] Zhang JA, Anyarambhatla G, Ma L. Development and characterization of a novel cremophor EL free liposome-based paclitaxel (LEP-ETU) formulation. Eur J Pharm Biopharm 2005; 59: 177-87.

[120] Fetterly GJ, Grasela TH, Sherman JW. Pharmacokinetic/pharmacodynamic modeling and simulation of neutropenia during phase I development of liposome-entrapped paclitaxel. Clin Cancer Res 2008; 14: 5856-63.

[121] Li Z, Zhang Y, Wurtz W. Characterization of nebulized liposomal amikacin (Arikace) as a function of droplet size. J Aerosol Med Pulm Drug Deliv 2008; 21: 245-54.

[122] Okusanya OO, Bhavnani SM, Hammel J. Pharmacokinetic and pharmacodynamic evaluation of liposomal amikacin for inhalation in cystic fibrosis patients with chronic pseudomonal infection. Antimicrob Agents Chemother 2009; 53: 3847-54.

[123] Oxford Biomedica [Home page on the internet]. Products [cited 2015 Apr 12]. Available from: (http: //www.oxfordbiomedica.co.uk/products/)

[124] Clinical Trial.gov [homepage on the Internet]. Gene therapy [cited 2015 Apr 12]. Available from: (https: //clinicaltrials.gov)

[125] Lu Y, Park K. Polymeric micelles and alternative nanosized delivery vehicles for poorly soluble drugs. Int J Pharm 2013; 453: 198-214.

[126] Turos E, Greenhalgh KR, Garay JC, inventor; University of South Florida, assignee. Nanoparticles with covalently bound surfactant for drug delivery. United States Patent US 8414926 B1. 2013.

[127] Bosch HW, Marcera DM, Mueller RL, Swanson JR, Mishra JS, inventor; Nanosystems Llc, assignee. Process for preparing therapeutic compositions containing nanoparticles. United States Patent US 5510118 A. 1996.

[128] Kyun OHD, Lee KY, inventor; Regeron, Inc., assignee. Preparation of nanoliposome-encapsulating proteins and protein-encapsulated nanoliposome. United States Patent US 7951396 B2. 2011.

[129] Hong JP, Lee SK, Kim WC, *et al*. Nanoliposome using esterified lecithin and method for preparing the same, and composition for preventing or treating skin diseases comprising the same. United States Patent US 8685440 B2. 2014.

[130] Mathiowitz E, Shik Jong Y, Boekelheide K, inventor; Neurotech S.A., assignee. Polymeric gene delivery system. United States Patent US 6262034 B1. 2001.

[131] Jiangnan Y, Ximing X, Cao X, *et al*. Cationized polysaccharide nanoparticle gene delivery systems and manufacturing method thereof. Chinese Patent CN 102154352 B. 2012.

[132] Jiangnan Y, Ximing X, Cao X, Miao W, Wen TW, inventor; Jiangsu University, assignee. Nanoparticle gene delivery system of cationized lycium barbarum polysaccharides and preparation method thereof. Chinese Patent CN 102154350 B. 2012.

[133] Ximing X, Miao W, Jiangnan Y, Wen DW, Cao X, inventor; Jiangsu University, assignee. Cationic angelica polysaccharide nanoparticle gene delivery system and preparation method thereof. Chinese Patent CN 102154351 B. 2012.

[134] Bednarski MD, Guccione S, Li KC, inventor; The Board of Trustees of The Leland Stanford Junior University, assignee. Use of targeted cross linked nanoparticles for *in vivo* gene delivery. United States Patent US 7514098 B2. 2009.

[135] Gupta KC, Kumar P, Shami A, Pathak A, inventor; Council of Scientific and Industrial Research, assignee. Cross linked PEI nanoparticle transfection agents for delivery of biomolecules with increased efficiency. United States Patent US 8513206 B2. 2013.

[136] Zhu KY, Zhang X, Zhang J, inventor; Kansas State University Research Foundation, assignee. Double-stranded RNA-based nanoparticles for insect gene silencing. United States Patent US 8841272 B2. 2014.

[137] Samuel JP, Samboju NC, Yau KY, Webb SR, Burroughs F, inventor; Dow Agrosciences, Llc., assignee. Use of dendrimer nanotechnology for delivery of biomolecules into plant cells. United States Patent US 8686222 B2, 2014.

[138] Baker JR, Cheng XM, Thomas TP, Huang BM, inventor; The Regents of the University of Michigan, assignee. Dendrimer conjugates. United States Patent US 8252834 B2. 2012.

[139] Krippner GY, Williams CC, Kelly BD, *et al*. Targeted polylysine dendrimer therapeutic agent. United States Patent US 8420067 B2. 2013.

[140] Breitenkamp K, Sill KN, Skaff H, Breitenkamp R, inventor; Intezyne Technologies, Inc., assignee. Polymeric micelles for drug delivery. United States Patent US 7638558 B2. 2009 Dec.

[141] Seo MH, Yi YW, Yu JW, inventor; Samyang Corporation, assignee. Stable polymeric micelle-type drug composition and method for the preparation thereof. United States Patent US 7217770 B2. 2007.

[142] Garrec DL, Kabbaj M, Leroux JC, inventor; Labopharm, Inc., assignee. Preparation of sterile stabilized nanodispersions. United States Patent US 6780324 B2. 2004.

[143] Bazile D, Couvreur P, Lakkireddy HR, Mackiewicz N, Nicolas J, inventor; Sanofi, applicant. Functional PLA-PEG copolymers, the nanoparticles thereof, their preparation and used for targeted drug delivery and imaging. European Patent WO201312794 A1, 2013.

[144] Song J, Hongxing F, Jingjing S, Hui L, Ying L, inventor; Lishui Central Hospital, assignee. Compound epirubicin hydrochloride polylactic-co-glycolic acid (PLGA) nanoparticles and preparation method thereof. Chinese Patent CN102525936A. 2014.

[145] Yiyi S, Ling Z, Dong L, Jia Y, inventor; Chengdu Medical College, assignee. Anti-tumor combined medicament. Chinese Patent CN102697795A. 2014.

[146] Jessie LSA, Guillaume WM, Si T, inventor; Jessie LSA, Guillaume WM, Si T, assignee. Tumor- targeting drug-loaded particles. Chinese Patent CN102697737A, 2014.

[147] Sabel BA, Schroeder U, inventor; Nanodel Technologies Gmbh, assignee. Drug targeting system, method of its preparation and its use. United States Patent US 7025991B2. 2006.

[148] Sill KN, Skaff H, Breitenkamp K, Breitenkamp R, inventor; Intezyne Technologies, Inc., assignee. Polymeric micelles for drug delivery. United States Patent US8263665B2. 2012.

[149] Johansen LM, Lee MS, Nichols MJ, Zimmermann GR, inventor; Combinatorx Inc., assignee. Compositions and methods for treatment for neoplasms. European Patent EP1883407A4. 2009.

[150] Albrecht TB, Davey RA, inventor; Albrecht Thomas B, Davey Robert A, assignee. Virus coated nanoparticles and uses thereof. United States Patent US 20090214663A1, 2009.

[151] Smith HJ, Smith JR, inventor; Smith HJ, Smith JR, assignee. Anti-tumor necrosis factor alpha (TNF-a) antibody used as a targeting agent to treat arthritis and other diseases. United States Patent US 20130115269A1, 2013.

[152] Jensen SS, inventor; Bioneer A/S, Dtu Nanotech, assignee. Cationic liposomal drug delivery system for specific targeting of human cd 14+ monocytes in whole blood. France Patent WO2013135800A1. 2013.

[153] Rochlitz C, Mamot C, Wicki A, Christofori G, inventors; Universitätsspital Basel, assignee. Chemotherapeutic composition for the treatment of cancer. France Patent WO2010103118A1, 2010.

[154] Vinod DL, Tapan KJ, Diandra LP, inventors; University of Nebraska, assignee. Magnetic nanoparticle composition and methods for using the same. United States Patent US264199, 2007.

[155] Akhtari M, Engel J, inventors; University of California, assignee. Functionalized magnetic nanoparticle use thereof and methods. United States Patent US 0206146, 2008.

[156] Hainfeld JF, Slatkin DN, inventors; Nanoprobes, Inc., assignee. Methods of enhancing radiation effects with metal nanoparticles. United States Patent US 7530940B2. 2009.

Received: July 18, 2015 **Accepted: September 22, 2015**